Table of Contents

Acknowledgments……..iv
Abstract……v
Table of contents……..x
List of Figures……..xvi
List of Schemes……..xxvi
List of Tables……..xxviii
List of Abbreviations……..xxxi

1 Chapter 1 Introduction 1

1.1 Clean Energy Through Photovolatics 2
1.2 Photoinduced Electron Transfer in Photosynthesis 3
1.3 Photoinduced Electron Transfer for Solar Energy Conversion 4
1.4 Porphyrins 5
1.5 Porphyrins as Sensitizers and Electron Donors 7
1.6 Fullerenes 8
1.7 Fullerenes as Electron Acceptors 10
1.8 Marcus Theory of Electron Transfer 13
1.9 Endohedral Metallofullerenes 16
1.10 Photoinduced Multistep Energy and Electron Transfer 18
1.10.1 Porphyrin-Fullerene Triads for Multistep Electron Transfer 18
1.10.2 Porphyrin-Fullerene Tetrad and Pentads for Multistep Electron Transfer 20
1.11 Supramolecular Bonding for Molecular Assembly 21
1.12 Self-Assembled Supramolecular Porphyrin-Fullerene Dyads 22
1.12.1 Dyads Prepared by Base-Paired Hydrogen Bonding. 22
1.12.2 Dyads Prepared by Crown Ether- Ammonium Cations 23
1.12.3 Dyads and Triads Prepared by Axial Co-ordination 24

1.13 Supramolecular Porphyrin-Fullerene Chemistry 26
1.13.1 The Nature of the Porphyrin- Fullerene Interaction 28
1.14 Supramolecular Bis-Porphyrins Hosts for Fullerenes 29
1.14.1 Cyclic Bis-Porphyrins as Hosts for Fullerenes 29
1.14.2 Acyclic bis-porphyrins as hosts for Fullerenes 33
1.15 Calix[n]arenes 34
1.15.1 Conformations of Calixarenes 34
1.15.2 Chemistry of Calixarenes Wide and Narrow Rim 35
1.16 Wide Rim Calixarene Linked Bis-Porphyrins 36
1.17 Narrow Rim Calixarene Linked Bis-Porphyrins 37
1.17.1 Fullerene Binding of Narrow Rim Calixarene Linked Bis-Porphyrins 37
1.17.2 Computational Modeling of Calixarene Bis-Porphyrins 40
1.17.3 Photophysical Measurements of Calixarene Bis-Porphyrin 41
1.18 Aims of this Research 43

2 Chapter 2 Synthesis and Modification of Porphyrins for Calixarene Bis-Porphyrin Hosts 49

2.1 Introduction 50
2.1.1 Direct Porphyrin Synthesis versus Modification 51
2.1.2 Palladium and Nickel Catalyzed Reactions for Porphyrin Modification 52
2.2 Aim and Strategy 55
2.3 Computational Modeling of Bis-Porphryins 56
2.3.1 Computational Modeling of Bis-Porphyrins 2.1-2.3 57
2.3.2 Computational Modeling of Bis-porphyrins 2.4 and 2.5 62
2.4 Synthesis of Bis-Porphyrins 66
2.4.1 Synthesis of Porphyrin 2.7 66
2.4.2 Synthesis of Brominated Porphyrin 2.8 67

2.4.3 Synthesis of Amino Porphyrins via Suzuki Coupling 69
2.4.4 Synthesis of Bis-Porphyrins 2.1-2.3 71
2.4.5 Synthesis of Bis-Porphyrin 2.4 72
2.4.6 Synthesis of Bis-Porphyrin 2.5 74
2.5 Fullerene Binding studies with Bis-Porphyrins 75
2.5.1 Fullerene Binding Studies with Bis-Porphyrins 2.1-2.3 77
2.5.2 Fullerene Binding Studies of Bis-porphyrins 2.4 and 2.5 80
2.6 Porphyrin-Fullerene Co-Crystallates 83
2.6.1 Porphyrin-Fullerene Co-Crystallates Zn2.11.C_{60}.toluene and Zn2.11.2C_{70} 83
2.6.2 Porphyrin-Fullerene Co-Crystallate Zn2.14.3C_{60}.3toluene 86
2.6.3 Porphyrin-Fullerene Co-Crystallate 2.7.C_{60} 87
2.7 Charge Transfer Bands 89
2.8 Summary 92
2.9 Experimental 94
2.9.1 General Experimental 94
2.9.2 General Procedure for UV-Visible Titrations 94
2.9.3 Computational Modeling Software and Calculations. 95
2.9.4 Synthetic Procedures for Porphyrin Modification Via Suzuki Coupling 96
2.9.5 Synthetic Procedure for Porphyrin Modification Via Nickel Coupling 112
2.9.6 General Information and Crystallographic Tables for Single Crystal X-ray Diffraction 119

3 Chapter 3 Tetra-alkylated and Extended Linker Calixarene Bis-Porphyrins 125

3.1 Introduction 126
3.1.1 Linker Flexibility versus Binding 126
3.1.2 Calixarenes as Scaffolds for Wide Rim Bis-Porphyrins 129
3.1.3 Synthesis and Conformation of Tetra-Alkylated Calixarenes 130

3.2 Aim and Strategy 132
3.3 Computational Modeling of Bis-Porphyrins 134
3.3.1 Computational Modeling of Bis-Porphyrin 3.8 134
3.3.2 Computational Modeling of Bis-porphyrins 3.9 and 3.10 136
3.4 Synthesis of Bis-Porphyrins 141
3.4.1 Synthesis on Bis-Porphyrin 3.8 141
3.4.2 Synthesis of Bis-Porphyrin 3.9 143
3.4.3 Synthesis of Bis-Porphyrin 3.10 146
3.5 Fullerene Binding Studies 148
3.5.1 Fullerene Binding Studies with Bis-Porphyrin 3.8 148
3.5.2 Fullerene Binding Studies with Bis-Porphyrin 3.9 and 3.10 in Toluene 150
3.5.3 Fullerene Binding Studies with Bis-Porphyrins 3.9 and 3.10 in Acetonitrile/Toluene (1:1) 153
3.6 Variable Temperature NMR studies 157
3.6.1 NMR Spectra of Bis-Porphyrin Hosts 2.1, 3.9 and 3.10 at 300 K 157
3.6.2 Variable Temperature ^{1}H NMR Studies of Bis-porphyrin 3.9 160
3.6.3 Variable Temperature NMR Studies of Bis-porphyrin 2.1 162
3.6.4 Variable Temperature NMR Studies of Bis-Porphyrin 3.10 163
3.7 X-Crystal structures 164
3.7.1 X-Crystal structure of Bis-Porphyrin 3.8 164
3.7.2 X-Crystal Structure of Calixarene 3.21 167
3.8 Charge Transfer Bands of 3.9 and 3.10 in Toluene. 168
3.9 Summary 170
3.10 Experimental 171
3.10.1 Synthetic Procedure for Bis-Porphyrin 3.8 171
3.10.2 Synthetic Procedure for Bis-Porphyrin 3.9 and 3.10 173
3.10.3 General Information and Crystallographic Tables for Single Crystal X-ray Diffraction 179

4 Chapter 4 Wide Rim Ferrocene Appended Bis-Porphyrins Prepared by Palladium Coupling Reactions. 183

4.1 Photoinduced Multistep Electron Transfer in Porphyrin-Fullerene Triads 184
4.1.1 Porphyrin Appended Ferrocene Calixarene Bis-Porphyrin 185
4.2 Aims and Strategy..... 187
4.2.1 Computational Modeling of Bis-Porphyrins 190
4.2.2 Modeling of Bis-Porphyrins 4.2 and 4.3 with C_{60} 190
4.2.3 Computational Modeling of Bis-Porphyrins 4.5 and 4.6 with C_{60} 193
4.3 Synthesis of Ferrocene Appended Bis-Porphyrins 196
4.3.1 Synthesis of Bis Porphyrin 4.2 196
4.3.2 Synthesis of Bis-Porphyrin 4.3 198
4.3.3 Attempted Synthesis of Bis-Porphyrin 4.4 199
4.3.4 Synthesis of Bis-Porphyrin 4.5 201
4.3.5 Synthesis of Bis-Porphyrin 4.6 203
4.4 Fullerene Binding Studies with Bis-Porphyrins 207
4.4.1 Fullerene Binding Studies with Bis-Porphyrins 4.2 and 4.3 208
4.4.2 Fullerene Binding Studies of Bis-porphyrins 4.5 and 4.6 in Toluene 210
4.4.3 Fullerene Binding studies of Bis-porphyrins 4.5 and 4.6 Acetonitrile/Toluene (1:1) 212
4.5 Fluorescence of Bis-Porphyrins..... 214
4.5.1 Fluorescence of Bis-porphyrins 2.1, 4.2 and 4.3 214
4.5.2 Fluorescence of Bis-porphyrins 3.10, 4.5 and 4.6 215
4.6 X-Ray Crystal Structures..... 216
4.6.1 X-Ray Crystal Structure of Calixarene 4.9 216
4.6.2 X-Ray Crystal Structure of Calixarene 4.23 218
4.6.3 X-ray Structure of Calixarene 4.24 219
4.7 Porphyrin-Fullerene Charge Transfer Bands..... 220

4.7.1 Charge Transfer and Electronic Coupling in Bis-Porphyrins 4.2 and 4.3 220
4.7.2 Charge Transfer and Electronic Coupling in Bis-Porphyrins 4.5 and 4.6 221
4.8 Summary 222
4.9 Experimental 225
4.9.1 Synthetic Procedure for Bis-Porphyrins 4.2 and 4.3 225
4.9.2 Synthetic Procedure for Bis-Porphyrins 4.5 and 4.6 236
4.9.3 General Information and Crystallographic Tables for Single Crystal X-ray Diffraction 244

5 Chapter 5 Wide Rim Appended Ferrocene Bis-Porphyrins Prepared by Amide Coupling 253

5.1 Introduction 254
5.2 Aims and Strategy 255
5.3 Computational Modeling of Bis-Porphyrins 5.6 and 5.7 256
5.4 Synthesis of Ferrocene Appended Bis-Porphyrins 259
5.4.1 Attempted Synthesis of Bis-Porphyrin 5.5 259
5.4.2 Synthesis of Bis-porphyrin 5.6 261
5.4.3 Synthesis of Bis-Porphyrin 5.7 264
5.5 Fullerene Binding Studies with Bis-Porphyrins 5.6 and 5.7 269
5.5.1 Fullerene Binding studies with Bis-porphyrins 5.6 and 5.7 in Toluene 270
5.5.2 Fullerene Binding studies with Bis-porphyrins 5.6 and 5.7 Acetonitrile/Toluene (1:1) 272
5.6 Fluorescence of Bis-Porphyrins 3.10, 5.6 and 5.7 274
5.7 Charge Transfer Bands 275
5.8 Summary 276
5.9 Experimental 277
5.9.1 Synthetic Procedure for Bis-Porphyrins 5.6 and 5.7 277

List of Figures

1.1: Representation of the photosynthetic membrane in purple bacteria adapted from Gust. 4

1.2: Energy level diagram for photoexcitation followed by a) Donor-Acceptor electron transfer system and b) Donor–Acceptor energy transfer. 5

1.3: Core of structure and IUPAC numbering system of an unsubstituted porphyrin. 6

1.4: The Gouterman Four-Orbital model adapted from Anderson and the UV-visible spectra of a typical porphyrin showing the intense Soret Band and the four Q bands magnified.[17] 7

1.5: Porphyrin-quinone dyads 1.1and 1.2. 7

1.6: Three-dimensional and partial wire frame of C_{60} and C_{70}. 8

1.7: Example of well established C_{60} functionalization. 9

1.8: Molecular orbital diagram for C_{60}. 10

1.9: Early porphyrin-fullerene dyads 1.3 and 1.4. 11

1.10: Systematic variation of amide linked porphyrin-fullerene dyads 1.5. 12

1.11: Covalently linked porphyrin-fullerene parachute dyads, 1.6 and 1.7. 13

1.12: Marcus diagram showing the comparative rates of charge separation $k_{ET(CS)}$ and charge recombination $k_{ET(CR)}$ for C_{60} and quinone Q, due to the reorganisation energy adapted from Imahori. 15

1.13: Drawing of several endohedral fullerenes; a) typical trimetallic nitride fullerene, b) metal carbide unit and c) metal oxide cluster, reproduced from Fortea. 17

1.14: Endohedral fullerenes-porphyrin dyads 1.8 and 1.9. 17

1.15: Covalently linked ferrocene-porphyrin-fullerene triad 1.10 and zinc porphyrin-freebase porphyrin-fullerene dyad 1.11. 19

1.16: Covalently linked ferrocene-porphyrin-fullerene tetrad 1.12, and tetrad and pentad 1.13 and 1.14. 21

1.17: Base-paired hydrogen bonding dyad 1.15. 23

1.18: Crown ether-ammonium cation dyad 1.16. 24

1.19: Axial coordinated porphyrin-fullerene dyads 1.17 and 1.18. 25

1.20: Dissociation of the 1.17 radical pair $ZnP^{\bullet+}$ $PyC_{60}^{\bullet-}$ upon photoexcitation and electron transfer. 25

1.21: Axially linked triads 1.19. 26

1.22: Pyrrolidine linked porphyrin-fullerene dyad 1.4 and X-ray crystal structure of 1.4 showing close contact between the C_{60} and the porphyrin (phenyl rings omitted for clarity).[35] 27

1.23: a) Zigzag Co-crystallate Structures of C_{60} and $H_2TPP.C_{60.}$ b) The co-crystallate structure of $Co(II)OEP_{2.}C_{60.}$ 27

1.24: Close association of the 6:6 ring junction of C_{60} (purple) and H_2TPP (grey). 28

1.25: Cyclic bis-porphyrin hosts 1.20 and 1.21 and the X-ray structure of cyclic zinc bis-porphyrin 1.21 with $C_{60.}$ 30

1.26: Cyclic bis-porphyrins 1.22 and 1.23 and the X-ray structure of 1.23 with $Sc_3N@C_{80}$. ¨ 31

1.27: Pyridyl functionalized cyclic bis-poprhyrin.Ni1.24 and the self assembled X-ray crystal structure of Ni1.24. 31

1.28: X-ray structures of cyclic bis-porphyrins Ni1.24 and 1.24 with C_{60}. 32

1.29: Palladium linked bis-porphyrin 1.25a and the X-ray structure of 1.25b with C_{60} 33

1.30: (a) Flat and (b) three-dimensional representation of *p-tert* calix[4]arene. 34

1.31: The conformations of calixarene. 35

1.32: Wide rim appended calixarene bis-porphyrins 1.30, 1.31 and 1.32. 36

1.33: Calix- and thiocalixarene narrow rim bis- and tetra-porphyrins 1.33a-h. 37

1.34: Narrow rim functionalized calixarene bis-porphyrins. 38

1.35: Structure of the host–guest complex of the palladium derivative of 1.38, calculated using molecular mechanics (UFF Force Field) and 1.36, calculated using two layer ONIOM modeling (/B3LYP/6-31G(d);UFF) for the Nickel(II) Derivative and C_{60} ... 40

1.36: Differential absorption spectra (visible and near-infrared) obtained upon femtosecond flash photolysis (420 nm) of 1.36 (4.1 x 10^{-6} M) and C_{60} (2.0x 10^{-5} M) in argon-saturated toluene with a time delay of 50 ps at room temperature. 42

1.37: Examples of hosts made in Chapter Two. 44

1.38: Examples of hosts made in Chapter Three. 45

1.39: Examples of ferrocene functionalized hosts made in Chapter Four. 46

1.40: An example of ferrocene amide functionalized hosts made in Chapter Five. 46

2.1: Narrow rim functionalized calixarene bis-porphyrins. 50

2.2: New calixarene linked bis-porphyrin hosts prepared in Chapter Two via Suzuki coupling of porphyrins. 55

2.3: Calixarene linked bis-porphyrin hosts prepared in Chapter Two via nickel catalyzed coupling. 56

2.4: Calculated structures (ONIOM/B3LYP/6-31G(d);UFF) for the nickel(II) derivative of a) host–guest complex 2.1 with C_{60} and b) host 2.1 without C_{60}. 59

2.5: a) Calculated structures (ONIOM/B3LYP/6-31G(d);UFF) for the nickel(II) derivative of a) host–guest complex 2.2 with C_{60} and b) host 2.2 without C_{60}. 60

2.6: Calculated structures (ONIOM/B3LYP/6-31G(d);UFF) for the nickel(II) derivative of a) host–guest complex 2.3 with C_{60} and b) host 2.3 without C_{60}. 61

2.7: Calculated structures (ONIOM/B3LYP/6-31G(d);UFF) for the palladium (II) derivative of host–guest complex 2.4 with C_{60}. 63

2.8: Front and side views of structures (ONIOM/B3LYP/6-31G(d);UFF) for the palladium (II) derivative of host 2.4. 63

2.9: Calculated structures (ONIOM/B3LYP/6-31G(d);UFF) for the palladium (II) derivative of host–guest complex 2.5 with $C_{60.}$ 64

2.10: Calculated structure (ONIOM/B3LYP/6-31G(d);UFF) for the palladium (II) derivative of host 2.5..... 65

2.11: The thermodynamic equilibrium process for a host-guest complex. 75

2.12: UV-visible titration of 2.1 ($1.22x10^{-6}$ M) in toluene upon addition of C_{60} (0-95 Eq). Inset; plot of the non-linear least square fit for the change in absorption at the Soret of 2.1 upon addition of fullerene. 77

2.13: UV-visible titration of 2.1 ($1.22x10^{-6}$ M) in toluene upon addition of a) C_{70} (0-20 Eq) and b) $Lu_3N@C_{80}$ (0-6 Eq). Insets; plot of the non-linear least square fit for the change in absorption at the Soret of 2.1 upon addition of fullerene. 78

2.14: UV-visible titration of 2.4 ($1.27x10^{-6}$ M) in toluene with addition of C_{60} (0-134 Eq.) and b) C_{70} (0-40 Eq.)..... 81

2.15 UV-visible titration of 2.5 ($1.51x10^{-6}$ M) in toluene with addition of C_{60} (0-120 Eq) and b) addition C_{70} (0-35 Eq)..... 82

2.16: Co-crystallate packing structure (hydrogen atoms omitted for clarity) and the side view of the close contacts between the porphyrin and fullerene in Zn2.11.$C_{60.}$toluene. Represented with atomic displacement parameters shown as thermal ellipsoids at 50% probability. 84

2.17: Co-crystallate packing structure (hydrogen atoms omitted for clarity) and the top view of the close contact between the porphyrin and fullerene for Zn2.11.C_{70} represented with atomic displacement parameters shown as thermal ellipsoids at 50% probability. 85

2.18: Co-crystallate packing structure for Zn2.14.C_{60}.toluene. Represented with atomic displacement parameters shown as thermal ellipsoids at 50% probability (hydrogens omitted for clarity). 86

2.19: Side view of the close contacts between the porphyrin and fullerene for Zn2.14.C_{60}.toluene. Represented with atomic displacement parameters shown as thermal ellipsoids at 50% probability 87

2.20: The zigzag arrangement between the porphyrins and fullerenes for 2.7.C_{60}. Represented with atomic displacement parameters shown as thermal ellipsoids at 50% probability. 88

2.21: Co-crystallate packing structures of 2.7.C_{60}, showing the linear packing of C_{60} and porphyrins. Represented with atomic displacement parameters shown as thermal ellipsoids at 50% probability (hydrogen atoms omitted for clarity). 88

2.22: UV-visible absorption spectra of 2.1 [1.8 x10^{-5} M] in toluene upon addition of C_{60} (0-7 Eq.) showing the Q bands of the porphyrin and the emergence of the charge transfer band (inset magnified section of charge transfer band) 89

2.23: UV-visible absorption spectra of 2.1 [1.8 x10^{-5}] with C_{60} (0-7 Eq.) with the spectra of free 2.1 subtracted showing charge transfer band in toluene. 90

2.24: HOMO-LUMO gap of a porphyrin and fullerene. 91

3.1: Directly substituted bis-porphyrin 3.1 and the methylene extended bis-porphyrin 1.35. 127

3.2: Wide rim calixarene bis-porphyrin hosts 1.35, 1.36 and 1.37. 130

3.3: Different isomers of tetra-alkylated calixarene: cone; 1,3 alternate; partial cone (carbonyl up) and partial cone (butyl up). 131

3.4: Hosts prepared in Chapter Three: 3.8, 3.9 and 3.10. 133

3.5: a) Front and b) side view of the calculated structure (ONIOM/B3LYP/6-31G(d);UFF) for the nickel(II) derivative of host–guest complex 3.8 with C_{60}. 135

3.6: a) Front and b) side views of the calculated structure (ONIOM/B3LYP/6-31G(d);UFF) for the nickel(II) derivative of host 3.8. 136

3.7: Calculated structures (ONIOM/B3LYP/6-31G(d);UFF) for the nickel(II) derivative of hosts–guest complex 3.9 with C_{60} and b) 3.10 with C_{60} 139

3.8: Calculated structures (ONIOM/B3LYP/6-31G(d);UFF) for the nickel(II) derivative of a) 3.9 and b) 3.10. 140

3.9: UV-visible titration of 3.8 (1.95 x10^{-6}M) in toluene with a) addition C_{60} (0-110 Eq.) and b) C_{70} (0-45 Eq.)..... 149

3.10 : UV-visible titration of 3.9 (1.2x10^{-6} M) in toluene with a) addition C_{60} (0-250 Eq.) and b) UV-visible titration of 3.9 with C_{70} (0-95 Eq.). Insets; plot of the non-linear least square fit for the change in absorption at the Soret of 3.9 upon addition of fullerene. 151

3.11 : UV-visible titration of 3.10 (1.2x10^{-6} M) in toluene with a) addition C_{60} (0-240 eq.) and b) C_{70} (85 Eq.). Insets; plot of the non-linear least square fit for the change in absorption at the Soret of 3.10 upon addition of fullerene. 152

3.12: UV-visible spectra of titrations of 3.9 (1.2x10^{-6} M) in toluene/acetonitrile (1:1) with a) C_{60} (0-39 Eq.)and b) C_{70} (0-20 Eq.). Inset; plot of the non-linear least square fit for the change in absorption at the Soret of 3.10 upon addition of fullerene. 155

3.13: UV-visible spectra of titrations of 3.10 (1.2x10^{-6} M) in toluene/acetonitrile (1:1) with a) addition C_{60} (0-37 Eq.) and b) C_{70} (0-18 Eq.) Inset; plot of the non-linear least square fit for the change in absorption at the Soret of 3.10 upon addition of fullerene. 156

3.14: Calixarene and porphyrin with ^{1}H NMR markings. 158

3.15: ^{1}H NMR spectra of 2.1 in D_8 toluene (solvent and *tert*-butyl protons signals omitted for clarity). 158

3.16: ^{1}H NMR Spectra of bis-porphyrin 3.9 in D_8 toluene (solvent and *tert*-butyl protons signals omitted for clarity). 159

3.17: ^{1}H NMR spectra of bis-porphyrin 3.10 in D_8 toluene (solvent and *tert*-butyl protons signals omitted for clarity). 160

3.18: Variable temperature ^{1}H NMR of bis-porphyrin 3.9 ranging from 220-365K, illustrating the proton signals of the bridging methylenes (*), the amide linker methylene (♦), the methoxy CH_3 group (○) and the central porphyrin NH (♥). 161

3.19: Variable temperature ^{1}H NMR of bis-porphyrin 3.9 ranging from 220-365K illustrating the broadening and shifting of the porphyrin proton signals, β pyrrole (β) and the aromatic substituents (▼). 162

3.20: Variable temperature ^{1}H NMR spectra of bis-porphyrin 2.1 ranging from 220-300K illustrating the chemical shifts and broadening of the methylene bridges (*), the methylene amide linker (♦) and the porphyrin central NH protons (♥). 163

3.21: Variable temperature ^{1}H NMR of 3.10 showing the chemical shifts and broadening of the methylene bridges (*), the methylene amide linker (♦) and the porphyrin central NH protons (♥). 164

3.22: Side view of the X-ray crystal structures of bis-porphyrin 3.8, represented with atomic displacement parameters shown as thermal ellipsoids at 50% probability (hydrogen atoms omitted for clarity). 165

3.23: Top view of the X-ray crystal structures of bis-porphyrin 3.8, represented with atomic displacement parameters shown as thermal ellipsoids at 50% probability (hydrogen atoms omitted for clarity). 166

3.24: The recalculated model of the 3.8 based off the X-ray crystal structure. (ONIOM/B3LYP/6-31G(d);UFF) for the nickel(II) 166

3.25: Crystal structure of the methyl and ethyl esters derivatives of 3.21 represented with atomic displacement parameters shown as thermal ellipsoids at 50% probability (hydrogen atoms omitted for clarity). 167

3.26: UV-visible spectra of a) 3.10 and b) Zn3.10 in toluene displaying the emergence of the charge transfer band at 690 and 760 nm respectively with increasing concentration of C_{60} (Left). The absorption spectra of 3.1 and Zn3.1 with the free host subtracted giving a better visualization of the charge transfer band (right). 168

4.1: Covalent triads 1.13 and 1.14[72,77] and supramolecular triad 1.22. 185

4.2: Host 4.1 and the calculated structure (ONIOM/B3LYP/6-31G(d);UFF) for the nickel(II) derivative of hosts–guest complex 4.1 with C_{60} 186

4.3: a)Photoexcitation (1) and primary electron transfer (2) followed by secondary electron transfer (3). b) Reaction scheme and energy level diagram for ferrocene functionalized calixarene bis-porphyrin. 187

4.4: Hosts 4.2 and 4.3 prepared via Sonogashira coupling in Chapter Four. 188

4.5: Attempted ferrocene functionalized bis-porphyrin host 4.4 and hosts made 4.5 and 4.6 in Chapter Four. 189

4.6: Calculated structures (ONIOM/B3LYP/6-31G(d);UFF) for the nickel(II) derivative of hosts–guest complexes a) 4.2 and b) 4.3 with C_{60}. 192

4.7: Calculated structures (ONIOM/B3LYP/6-31G(d);UFF) for the nickel(II) derivative of hosts–guest complex 4.5 with C_{60}. 194

4.8: Calculated structures (ONIOM/B3LYP/6-31G(d);UFF) for the nickel(II) derivative of hosts–guest complex 4.6 with C_{60}. 195

4.9: ^{1}H NMR of bromocalixrenes a) 4.23 and b) 4.19, showing proton signals of the phenyl rings (●), the methylene linker ethyl ester (♦), the methylene bridges (*)and the *n*-butyl chains (○). 205

4.10: ^{1}H NMR of ferrocene functionalized calixarenes 4.24 and 4.20; showing proton signals of the ferrocene (ɔ), the phenyl rings (●), methylene linker ethyl ester (♦),methylene bridges (*) and n-butyl chain (○). 206

4.11 ^{1}H NMR of ferrocene functionalized bis-porphyrin a) 4.6 and b) 4.5, showing proton signals of the phenyl rings (●),the ferrocene (ɔ) the methylene linker ethyl ester (♦), methylene bridges (*) and *n*-butyl chains(○). 207

4.12: UV-visible titration of 4.2 (1.75×10^{-6} M) in toluene with a) addition C_{60} (0-120 Eq.) and b) C_{70} (0-45 Eq.). Insets; plot of the non-linear least square fit for the change in absorption at the Soret of 4.2 upon addition of fullerene. 209

4.13: UV-visible titration of 4.2 (1.75×10^{-6} M) in toluene with addition $Lu_3N@C_{80}$ (0-4.9 Eq.). Inset; plot of the non-linear least square fit for the change in absorption at the Soret of 4.2 upon addition of fullerene. 210

4.14: UV-visible titration of 4.5 ($1.28x10^{-6}$ M) in toluene with a) addition C_{60} (0-550 Eq.) and b) C_{70} (0-95 Eq.) Insets; plot of the non-linear least square fit for the change in absorption at the Soret of 4.5 upon addition of fullerene..... 211

4.15: UV-visible titration of 4.5 ($1.28x10^{-6}$ M) in acetonitrile/toluene (1:1) with a) addition C_{60} (0-20 Eq.) and b) C_{70} (0-5 Eq.). Insets; plot of the non-linear least square fit for the change in absorption at the Soret of 4.5 upon addition of fullerene 213

4.16 Fluorescence spectra of the free base (1.2×10^{-6} M) and zinc derivatives of 4.4 and 4.5 compared to the non ferrocene functionalized bis-porphyrin 3.10. 215

4.17: Fluorescence Quenching of 4.5 and 4.6 compared to the non ferrocene functionalized bis-porphyrin 3.10. 216

4.18: X-ray structure of 4.9 represented with atomic displacement parameters shown as thermal ellipsoids at 50% probability (hydrogen atoms omitted for clarity). 217

4.19: X-ray structure of 4.23 represented with atomic displacement parameters shown as thermal ellipsoids at 50% probability (hydrogen atoms omitted for clarity). 218

4.20: X-ray structure of 4.24 represented with atomic displacement parameters shown as thermal ellipsoids at 50% probability (protons omitted for clarity)..... 219

4.21: a) UV- visible spectra of 4.2 in toluene displaying the emergence of the charge transfer band at 715 nm with increasing concentration of C_{60} and b) the absorption spectra of 4.2 with the free host subtracted giving a better visualization of the charge transfer band. 220

4.22: a) UV- visible spectra of 4.5 in toluene displaying the emergence of the charge transfer band at 710 nm with increasing concentration of C_{60} and b) the absorption spectra of 4.5 with the free host subtracted giving a better visualization of the charge transfer band. 222

5.1: Various wide rim ferrocene amide functionalized calixarenes prepared for anion and cation sensing 255

5.2: Attempted ferrocene functionalized bis-porphyrin host 5.5 and the hosts 5.6 and 5.7 made in Chapter Five 256

5.3: Calculated structures (ONIOM/B3LYP/6-31G(d);UFF) for the nickel(II) derivative of host–guest complex 5.6 with C_{60} 258

5.4: Calculated structures (ONIOM/B3LYP/6-31G(d);UFF) for the nickel(II) derivative of host–guest complex 5.7 with C_{60} 259

5.5: ^{1}H NMR of nitro functionalized calixarenes a) 5.15 and b) 5.10, showing proton signals of the phenyl rings (●), methylene linker ethyl ester (♦), methylene bridges (*) and the n-butyl chain (○). 266

5.6: ^{1}H NMR of amino functionalized calixarenes a) 5.16 and b) 5.11 showing proton signals of the phenyl rings(●), the methylene linker ethyl ester (♦), methylene bridges (*) and *n*-butyl chains(○). 267

5.7: ^{1}H NMR of ferrocene functionalized calixarenes a) 5.17 and b) 5.12 showing proton signals of the phenyl rings (●), the ferrocene (ɔ) the methylene linker ethyl ester (♦), methylene bridges (*) and *n*-butyl chains (○). 268

5.8: ^{1}H NMR of ferrocene functionalized bis-porphyrin a) 5.7 and b) 5.6, showing proton signals of the phenyl rings (●), the ferrocene (ɔ), the methylene linker ethyl ester (♦), methylene bridges (*) and *n*-butyl chains (○). 269

5.9: UV-visible titration of 5.6 $1.28\text{x}10^{-6}$ M) in toluene with a) addition C_{60} (0-490 Eq.) and b) C_{70} (0-95 Eq.): Insets; plot of the non-linear least square fit for the change in absorption at the Soret band of 5.6 upon addition of fullerene. 271

5.10: UV-visible titration of 5.6 ($1.28\text{x}10^{-6}$ M) in acetonitrile/toluene (1:1) with a) addition C_{60} (0-20 Eq.) and b) C_{70} (0-5 Eq.) Insets; plot of the non-linear least square fit for the change in absorption at the Soret band of 5.6 upon addition of fullerene. 273

5.11: Fluorescence emission spectra of 5.6 and 5.7, compared to the non ferrocene functionalized bis-porphyrin 3.10 (1.2x10-4 M) 274

5.12: a) UV-visible spectra of 5.6 in toluene displaying the emergence of the charge transfer band at 700nm with increasing concentration of C_{60} and b) the absorption spectra of 5.6 with the free host subtracted giving a better visualization of the charge transfer band. 275

List of Schemes

2.1: Lindsey's original procedure for A_3B substituted porphyrin. 51

2.2: Various palladium catalyzed reactions for modifying the porphyrin core. 53

2.3: Nickel catalyzed reactions with phenols, carbonyls and amines to prepare modified porphyrins. 54

2.4: Synthesis of porphyrin 2.7 66

2.5: Synthesis of mono and dibrominated porphyrins 2.8 and 2.9 67

2.6: Synthesis of A_2BC substituted porphyrins; 2.10 and 2.13 and amide hydrolysis to 2.15 and 2.16 69

2.7: Synthesis of 2.17 via Suzuki coupling and hydrolysis of the amide to corresponding amine 2.18 71

2.8: Synthesis of free base and zinc analogs of bis-porphyrins 2.1-2.3 71

2.9: Synthesis of bis-porphyrin 2.4 73

2.10: Synthesis of bis-porphyrin 2.5 75

3.1: Attempted synthesis of dicarboxyethoxy-calixarene 127

3.2: Synthesis of three methylene spaced bis-porphyrin 3.7 128

3.3: Synthesis of bis-porphyrin 3.8 141

3.4: Synthesis of porphyrin acid 3.16 via a statistical mixture; 142

3.5: Synthesis of bis-porphyrin 3.9 144

3.6: Synthesis of bis-porphyrin 3.10 146

4.1: Synthesis of bis-porphyrin 4.2 and Zn4.2 197

4.2: Synthesis of 4-ethynyl phenyl ferrocene. 198

4.3: Synthesis of bis-porphyrin 4.3 and Zn4.3. 199

4.4: Attempted synthesis of bis-porphyrin 4.4; 200

4.5: Synthesis of bis-porphyrin 4.5 201

4.6: Synthesis of bis-porphyrin 4.6 204

5.1: Original synthesis of amide functionalized bis-porphyrin 5.11. 260

5.2: Synthesis of bis-porphyrin 5.6..... 262

5.3: Synthesis of bis-porphyrin 5.7..... 265

List of Tables

1.1: Association constants for various metallated derivatives of bis-porphyrin.1.21 with C_{60} and C_{70} in toluene. 30

1.2: Association constants for wide rim functionalized calixarene bis-porphyrins 1.30-1.32 37

1.3: Association constants for narrow rim functionalized calixarene bis-porphyrins 1.33a-1.38. 39

1.4: Binding constants of the zinc and freebase derivatives of 1.36 with fullerenes in 1,2-dichlorobenzene. 40

1.5: Photophysical properties of 1.36 and Zn1.36 with fullerenes C_{60}, $Lu_3N@C_{80}$ and $Sc_3N@C_{80}$ obtained by femtosecond flash photolysis measurements for the studied assemblies. 43

2.1: Key geometric features of the molecular modeling (ONIOM/B3LYP/6-31G(d);UFF) for the nickel(II) derivative of host-guest complexes of 2.1, 2.2 and 2.3 with C_{60} 58

2.2: Key geometric features of the molecular modeling (ONIOM/B3LYP/6-31G(d);UFF) for the nickel(II) derivative of hosts of 2.1, 2.2 and 2.3. 58

2.3: Association constants for free base and zinc derivatives of host 2.1, 2.2 and 2.3 with fullerenes C_{60}, C_{70} and $Lu_3N@C_{80}$. 80

2.4: Estimation of electronic coupling constants between the free base and zinc derivatives of bis-porphyrin hosts 2.1-2.3 and C_{60} 92

2.5: Crystal data and structure refinement for Zn2.11.C_{60}. 120

2.6: Crystal data and structure refinement for Zn2.11.2C_{70}. 121

2.7: Crystal data and structure refinement for Zn2.14.3C_{60}.3toluene 122

2.8: Crystal data and structure refinement for 2.7.C_{60}. 123

3.1: Binding constants of bis-porphyrins with different flexibility.[122,128] 128

3.2: ^{13}C and ^{1}H NMR data for the bridging methylene and ester methylene groups.[182] 132

3.3: Key geometric features of the molecular modeling (ONIOM/B3LYP/6-31G(d);UFF) for the nickel(II) derivative of host-guest complexes of A, 3.9 and 3.10 with C_{60} 137

3.4: Key geometric features of the molecular modeling (ONIOM/B3LYP/6-31G(d);UFF) for the nickel(II) derivative of tetra-alkylated bis-porphyrins 3.9, 3.10 and dialkylated porphyrin 2.1. 138

3.5: Association constants of hosts 3.9 and 3.10 with C_{60} and C_{70} in toluene. 150

3.6: Association constants of bis-porphyrins 3.9 and 3.10 with C_{60} and C_{70} in toluene/acetonitrile (1:1). 154

3.7: Estimation of electronic coupling between the bis-porphyrin and fullerene based on the charge transfer band for 3.10 and Zn 3.10. 169

3.8: Crystal data and structure refinement for 3.8. 180

3.9: Crystal data and structure refinement for 3.21. 181

4.1: Key geometric features of the computational modeling (ONIOM/B3LYP/6-31G(d);UFF) for the nickel(II) derivative of host-guest complexes of 2.1, 4.2 and 4.3 with C_{60}. 191

4.2: Key geometric features of the computational modeling (ONIOM/B3LYP/6-31G(d);UFF) for the nickel(II) derivative of host-guest complexes of 3.10, 4.5 and 4.6 with C_{60}. 194

4.3: Association constants of free base and zinc(II)derivatives of 4.2, 4.3 and 2.1 with C_{60}, C_{70} and $Lu_3@C_{80}$ in toluene. 208

4.4: zAssociation constants of hosts 4.5, 4.6 and 3.10 with C_{60} and C_{70} in toluene. 212

4.5: Association constants of hosts 4.4, 4.5 and 3.10 with C_{60} and C_{70} in acetonitrile/toluene (1:1). 212

4.6: Estimation of electronic coupling constants between free base and zinc bis-porphyrin hosts 4.2, 4.3 and 2.1 and C_{60}. 221

4.7: Estimation of electronic coupling constants between bis-porphyrin host 3.10, 4.5 and 4.6 with C_{60}. 222

4.8: Crystal data and structure refinement for 4.9. 245

4.9: Crystal data and structure refinement for4.23. 246

4.10: Crystal data and structure refinement for 4.24 247

5.1: Key geometric features of the molecular modeling (ONIOM/B3LYP/6-31G(d);UFF) for the nickel(II) derivative of functionalized bis-porphyrin hosts of 5.6 and 5.7 and non functionalized bis-porphyrin host 3.10. 258

5.2: Association constants for bis-porphyrins 5.6, 5.7 and 3.10 in toluene..... 270

5.3: Association constants for bis-porphyrins 5.6, 5.7 and 3.10 in acetonitrile/toluene (1:1)... 272

List of Abbreviations

A	acceptor
ADP	adenosine diphosphate
ATP	adenosine triphosphate
B3LYP	Beck, 3-parameter, Lee – Yang Parr hybrid functioal
C_{60}	fullerene
$CHCl_3$	chloroform
$CDCl_3$	deuterochloroform
CH_3CN	acetonitrile
CT	charge transfer
CS	charge separated/separation
CR	charge recombination
D	donor
DCC	N,N'-Dicyclohexylcarbodiimide
DIC	N,N'-Diisopropylcarbodiimide
DFT	density functional theory
DMF	dimethylformamide
DNA	deoxyribonucleic acid
ESI-TOF	electrospray ionization with time of flight
ET	electron transfer
Fc	ferrocene
FAB	fast atom bombardment
IR	infrared
HOMO	highest occupied molecular orbital
HATU	2-(7-Aza-1H-benzotriazole-1-yl)-1,1,3,3-tetramethyluronium hexafluorophosphate
LUMO	lowest unoccupied molecular orbital
MM	molecular mechanics
MS	mass spectrometry
NBS	*N*-bromosuccinimide
NMR	nuclear magnetic resonance
OEP	octaethyl porphyrin

ONIOM	our own n-layers integrated molecular orbital and molecular mechanics
P/2HP/ZnP	porphyrin/ freebase porphyrin/ zinc porphyrin
PPM	parts per million
PRC	photosynthetic reaction centre
Q	quinone
QM	quantum mechanics
S	sensitizer
TLC	thin layer chromatography
TPP	tetraphenyl porphyrin
THF	tetrahydrofuran
TMS	tetramethylsilane
UFF	universal force field
UV	ultraviolet

Chapter 1

Introduction

1.1 Clean Energy Through Photovolatics

At present 80% of our global energy requirements are provided by fossil fuels such as natural gas, coal and oil,[1] however these are non-renewable resources and stockpiles have only a finite lifetime. There is also a growing consensus that the burning of fossil fuels is leading to dangerous accumulation of green house gases in the atmosphere and air pollution.[2] Recent scientific reports point out a higher mean planetary surface temperature which is resulting in climate change.[3] Global energy consumption is projected to increase at a staggering rate as developing countries such as China and India become larger economic powers.[4]

In order to protect and maintain the quality of human life and the global environment, cleaner and renewable energy resources must be employed. Natural renewable resources such as hydroelectric and geothermal power have already been employed to reduce our dependence on fossil fuels but there are only a finite number of locations where power plants can be constructed and as such these methods of energy production are nearing the point of saturation.

Solar energy can be converted into several different forms of useful energy; heat, fuel and electricity. The amount of solar energy that hits the earth each day is more than enough to power the entire planet for a year.[5] Solar energy is one of the few alternate energy supplies that can be scaled up to meet our demands and as such represents a highly promising sustainable energy source. Nature has evolved photosynthesis as a highly effective means of harnessing solar power, one which humanity hopes to match. Research initiatives are underway to discover a way in which to tap into this renewable resource.

Conventional solar cells using semiconducting materials such as silicon have contributed greatly to modern society. They are not, however, satisfactory in terms of economic cost and energy conversion efficiency. Efficiencies of these solar cells have reached 34% in multijunction cells.[6,7] The photovoltaic effect in inorganic cells involves the direct production of free electrons and holes by photon absorption. The resulting electrons and holes are separated with the electrons collecting at one end of the electrode and holes at the other, owing to the internal electric field created by the two layers of the semiconductor. Some of these same strategies have been applied to organic solar cells in which two organic semiconductors are laminated with some limited success.

Photovoltaic systems which have attracted much attention are dye sensitized solar cells developed by Grätzel.[8] These cells are made of optically transparent semiconducting titanium oxide doped with a light absorbing dye, immersed in an I_3/I^- electrolyte. These devices have shown exceptional promise as they could potentially be made of low-cost materials, being less expensive than older solid-state cells. Currently conversion efficiencies are lower than the better thin-film cells but they have the potential for future development through improvement of the dye and electrolyte efficiencies.[9] The appeal of Grätzel cells lies in their ability to use dyes that mimic the efficient process of photosynthesis to increase the overall efficiency of the solar cell. A number of different dyes have been explored for use in Grätzel Cells including porphyrin complexes.[10]

1.2 Photoinduced Electron Transfer in Photosynthesis

Photosynthesis is the process by which plants and some bacteria convert light energy into chemical energy in the form of adenosine triphosphate (ATP). The core of natural photosynthesis is a cascade of photoinduced energy and electron transfers among donors and acceptors in the light harvesting antenna complexes and reaction centre.[11,12] Photosynthesis is much simpler in purple bacteria than it is green plants and a basic representation is shown in Figure 1.1. Light is harvested by the "special pair" bacteriochlorophyll which are tuned to collect in the infrared and visible spectrum. The Antenna complex is excited to a higher energy state (1). The collected energy is funneled into the reaction centre, where a special pair of bacteriochlorophyll dimer (BChl) is raised to a higher energy state by the absorption of light. Within 2-4 ps of excitation an electron is passed to a pheophytin unit (BPhe) with a quantum yield of near unity. The radical pheophytin anion passes its electron to a quinone (Q_A) with a lifetime of 200 ps followed by the terminal quinone (Q_B) with lifetime of 10 μs (2). This multi-step electron transfer sequence results in charge separated state with a long lifetime.

The reduction of the quinone to hydroquinone involves the uptake of two protons split from water and from there it is passed onto a proton pump cytochrome bc_1 (3). The hydroquinone is oxidized back to quinone and releasing energy which is used to pump protons across the membrane to create a charge imbalance (4). The special pair is reduced by cytochrome C (Cyt C) to its original oxidation state. Finally the enzyme ATP synthase allows the protons to flow back across the membrane (5) driving the formation of ATP from adenosine diphosphate

(ADP) and inorganic phosphate (Pi). ATP is then used by the bacterium for the majority of its energy needs.

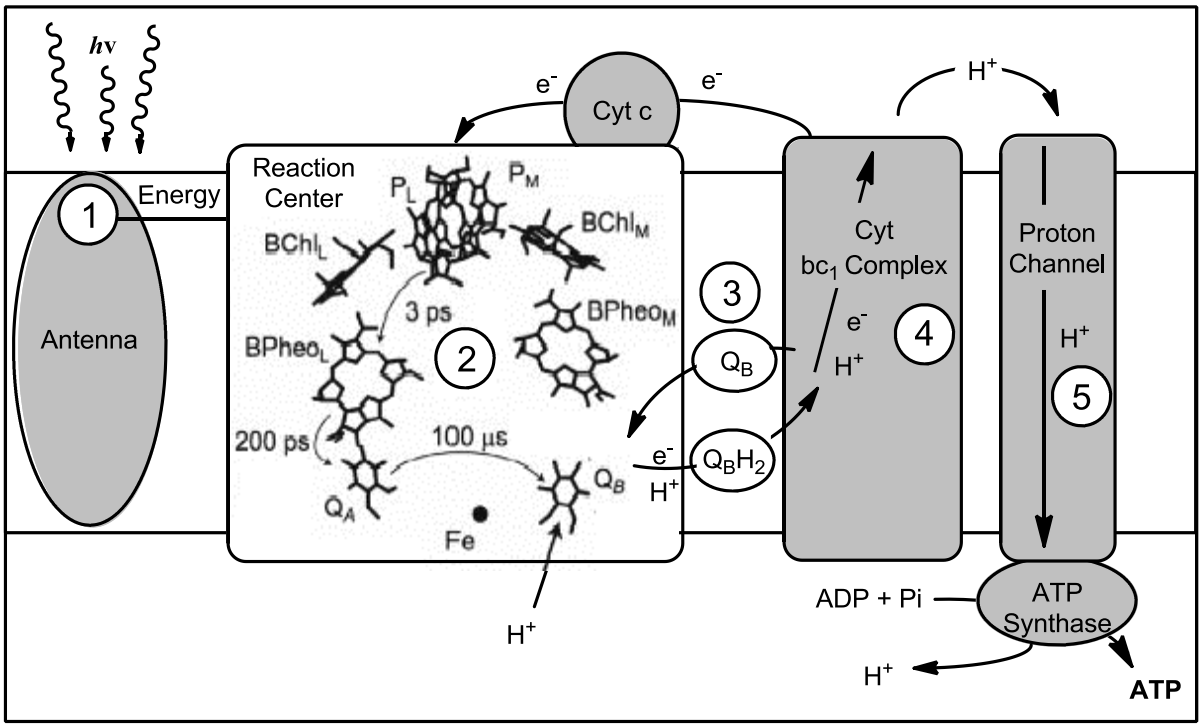

Figure 1.1: Representation of the photosynthetic membrane in purple bacteria adapted from Gust.[13]

1.3 Photoinduced Electron Transfer for Solar Energy Conversion

The importance of the photoinduced electron transfer in photosynthesis has caught the attention of chemists as these primary principles can be applied to the construction of solar energy conversion systems. In order to operate efficiently, certain features are required by these solar energy conversion systems. These systems must be able to capture light by a sensitizer or antenna molecule to a give an excited energy state. From the excited state the molecule must then transfer an electron to an acceptor molecule to form a charge separated state. The lifetimes of the charge separated state must be long enough to make use of the electron without recombination taking place.

There are two main mechanisms by which an excited donor (D*) can interact with an acceptor molecule upon photoexciation; (a) electron transfer and (b) energy transfer. A schematic representation of these processes using energy level diagrams is presented in Figure 1.2. Electron transfer occurs when the excited electron in the donor molecule is transferred to the vacant LUMO energy level of the acceptor, thus creating a donor-acceptor pair with the donor

as a radical cation $D^{\bullet+}$ and the acceptor a radical anion $A^{\bullet-}$. Energy transfer occurs when the energy of the excited donor molecule is donated to the acceptor, exciting the acceptor (A*). The donor is returned to the ground state. This type of reaction is likely to occur if the acceptor molecule has a low-energy excited state and is not amenable to oxidation or reduction.

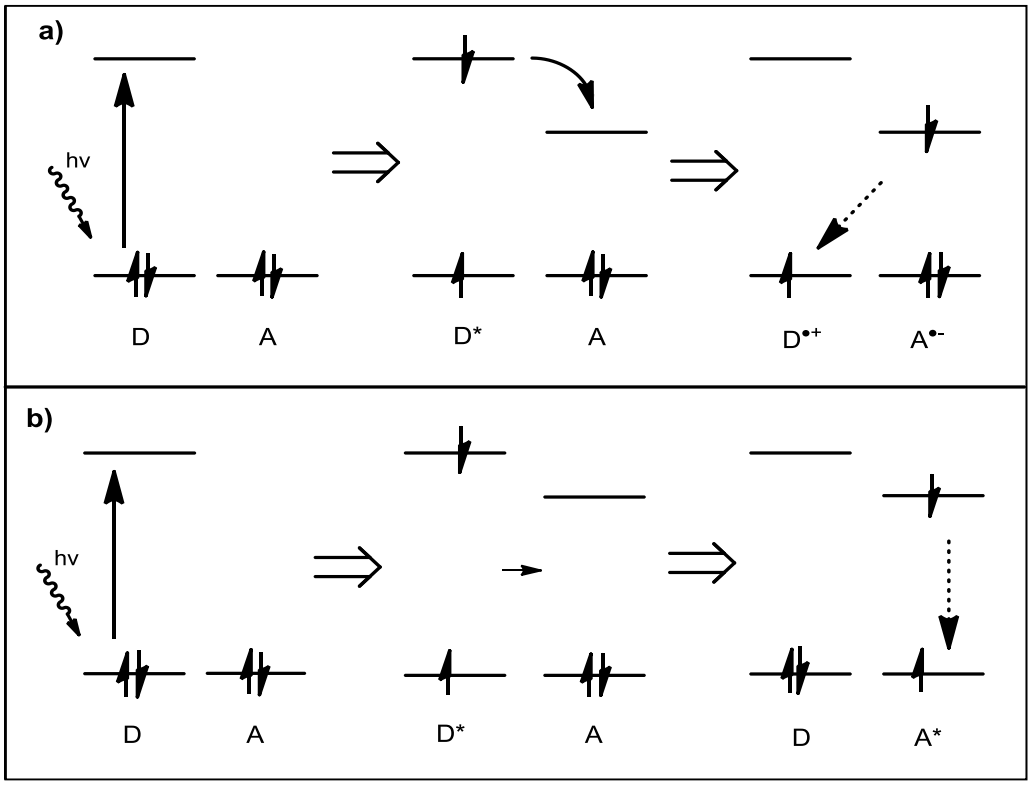

Figure 1.2: Energy level diagram for photoexcitation followed by a) Donor-Acceptor electron transfer system and b) Donor–Acceptor energy transfer.

Upon electron transfer the absorbed energy can be utilized to drive electrical current or promote chemical reactions before the back electron transfer leads to the initial states of donor and acceptor species. Researchers have been trying to mimic the primary steps in photosynthesis, where light is absorbed and charge separation occurs. There have been a number of simple two component systems developed to try and mimic this photoinduced electron transfer process.

1.4 Porphyrins

Porphyrins are large aromatic macrocycles consisting of four pyrrole rings that are joined by four methine bridges (Figure 1.3).[14] They are of central importance in biology for electron transfer. The iron porphyrin heme is the central core unit in blood hemoglobin. It reversibly

coordinates molecular oxygen and transports it around the body. Chlorophyll, a reduced magnesium chlorin, captures light energy in the near-ultraviolet and red regions of the visible spectrum and uses it to create chemical energy and molecular oxygen.

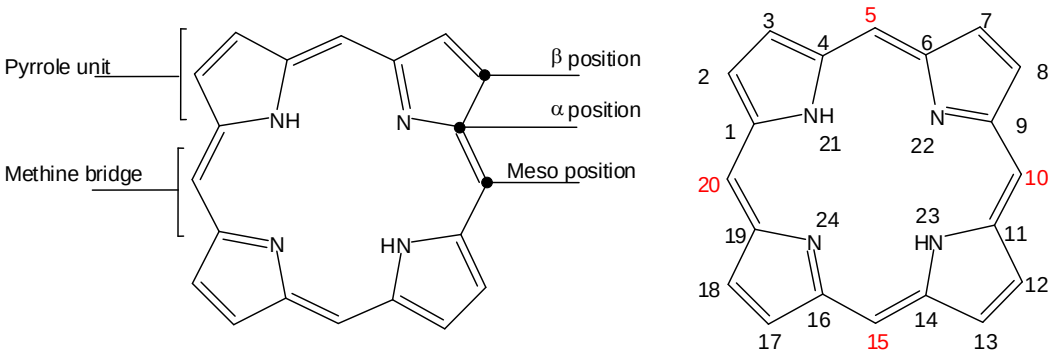

Figure 1.3: Core of structure and IUPAC numbering system of an unsubstituted porphyrin.

Porphyrins and their analogues offer a variety of desirable features such as; a rigid and planar geometry, high stability, intense electronic absorption, strong fluorescence and a small HOMO-LUMO energy gap. These features make them particularly attractive chromophores to use in solar energy conversion as sensitizers and electron transfer agents. The macrocycle can also be readily modified at both the β-pyrrole and meso positions making them versatile for a wide range of applications.

The UV-visible spectrum of porphyrins shown in Figure 1.4 consists of a strong transition to the second excited state ($S_0 \rightarrow S_2$) at about 400 nm (the Soret band) and a weak transition to the first excited state ($S_0 \rightarrow S_1$) at about 550 nm (the Q band). Conversion from S_2 to S_1 is rapid so fluorescence is only detected from S_1. These bands both arise from π–π* transitions in the large aromatic system and can be explained by considering the Gouterman four orbitals,[15,16] two π orbitals (a_{1u} and a_{2u}) and a degenerate pair of π* orbitals (e_{gx} and e_{gy}). The two highest occupied π orbitals have about the same energy and rather than two almost coincident absorption bands due to $a_{1u} \rightarrow e_g$ and $a_{2u} \rightarrow e_g$ transitions, the two transitions mix together by a process known as configurational interaction. This process results in two bands with very different intensities and wavelengths: Constructive interference leads to the intense short-wavelength Soret band, while the weak, long-wavelength Q band results from destructive combinations.

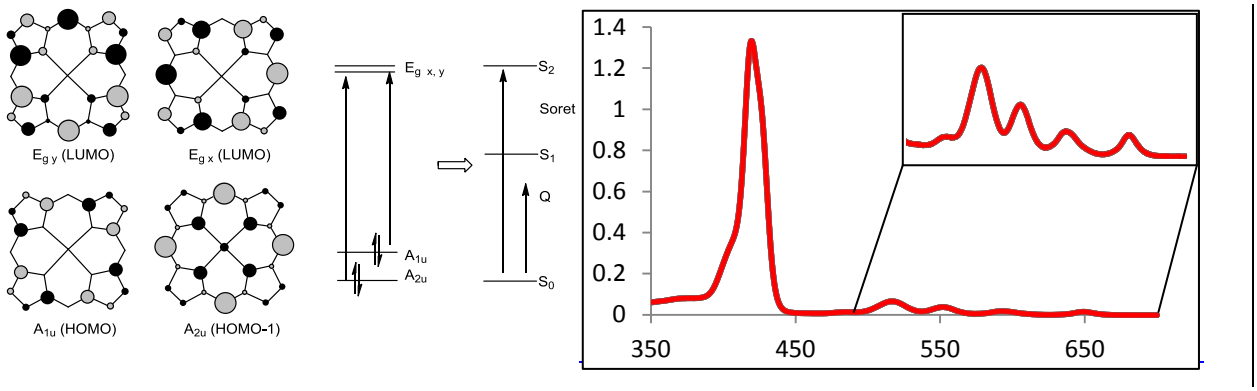

Figure 1.4: The Gouterman Four-Orbital model adapted from Anderson and the UV-visible spectra of a typical porphyrin showing the intense Soret Band and the four Q bands magnified.[17]

1.5 Porphyrins as Sensitizers and Electron Donors

A number of dyads for solar energy conversion have been prepared using porphyrins as the donor. Osuka and Tsue *et al.*[18,19] have made use of planar electron acceptors such as quinones/benzoquinones, **1.1** and **1.2** respectively. These have been thoroughly reviewed by Wasielewski.[20] Even in the most sophisticated structures, lifetimes of the charge separated state for these dyads are quite short-lived in the range of 10-100's of ps. Solvent also plays a significant role in determining both the rates and energetics of electron transfer events in these systems.

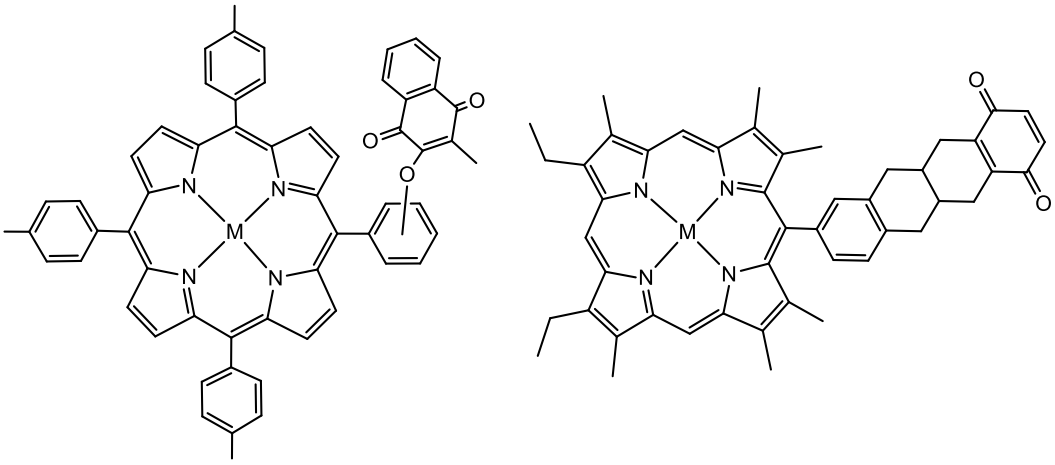

1.1 **1.2**

Figure 1.5: Porphyrin-quinone dyads **1.1**and **1.2**.[18,19]

1.6 Fullerenes

Fullerenes, an allotrope of carbon, were discovered in the early 1980's by laser vaporization of graphite.[21,22] Fullerenes are large three-dimensional closed cage spheres built from slightly pyramidal sp^2-hybridised carbons arranged in pentagons surrounded by hexagons. Fullerenes come in a wide range of sizes and shapes (C_{60}, C_{70}, C_{76} C_{78}, and C_{84} amongst higher fullerenes). The most common fullerene is $C_{60,}$ which made up of 60 chemically equivalent carbon atoms and is highly symmetrical (icosahedral I_h). C_{70} is the second most common fullerene. C_{70} is ellipsoidal in shape, composed of two hemispheres connected by a ring of hexagons. All Fullerenes were initially thought of as aromatic molecules, however X-ray diffraction studies revealed they are actually a polyenic structure, possessing two different bond types: i) Those joining two hexagons (6,6 junctions) display a shorter double bond length of 1.38 Å and ii) those joining a pentagon and hexagon (5,6 junction) show more single bond character and bond length of 1.45 Å. [23,24]

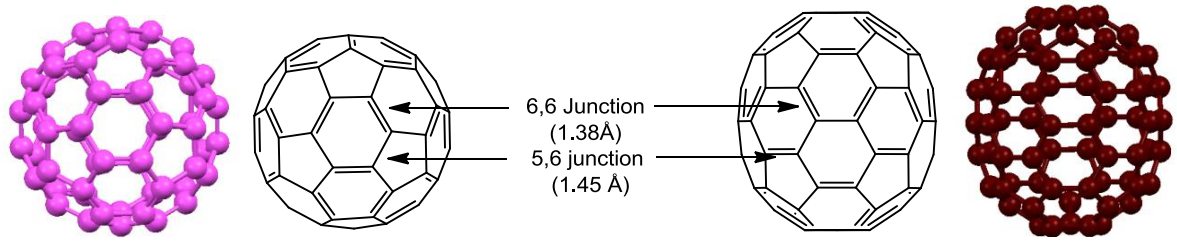

Figure 1.6:Three-dimensional and partial wire frame of C_{60} and C_{70}.

The chemical modification of fullerenes, specifically C_{60}, has been extensively studied and found to possess reactivity that matches the that of alkenes.[25] The main driving force for the reactivity of fullerenes is the deviation of planarity of the double bonds due to the spherical shape.[26] Functionalization reactions typically take place on the 6,6 junctions, resulting a relief of strains associated with the rigidity of the sp^2 hybridized bonds. Functionalization reactions are widely employed by chemist as a means to address problematic physical properties of fullerenes such as poor solubility while maintaining or enhancing their core properties. Cycloaddition or nucleophilic additions are the most common reactions employed. Several reactions examples are depicted in Figure 1.7 below.

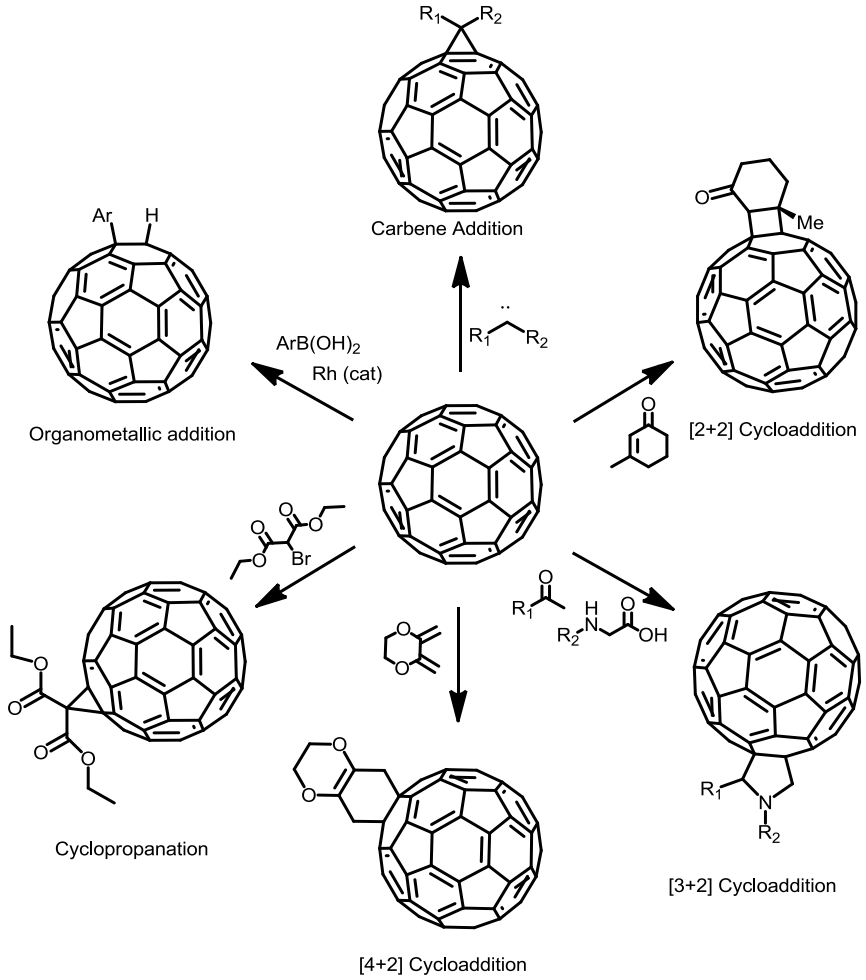

Figure 1.7: Example of well established C_{60} functionalization.[25]

The molecular orbital diagram of C_{60}, shown in Figure 1.8, has 30 filled π- orbitals where the HOMO (h_u) is a five-fold degenerate orbital.[27] The LUMO (t_{1u}) is a low lying triply degenerate orbital which allows for six reversible one-electron reductions of C_{60}.[28,29] as is evidenced by six reduction potentials in the cyclic volatmmetry of C_{60}.[30] The first of these is seen to be similar to that of quinones. C_{70} exhibits analogous behavior, with six reductions at comparable potentials.

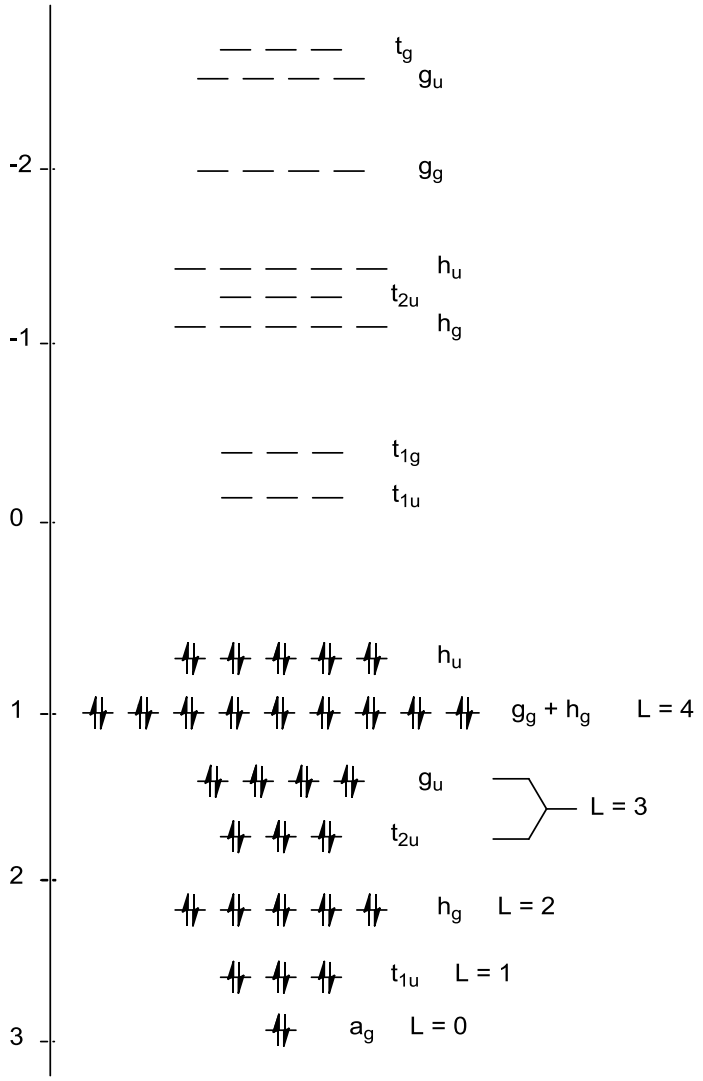

Figure 1.8: Molecular orbital diagram for C_{60}.[27]

1.7 Fullerenes as Electron Acceptors

Fullerenes are attractive chromophores for use as electron acceptors in solar energy conversion.[31,32] Consequently a number of porphyrin-fullerene based systems have been prepared via a variety of different covalent bonding types. An early example of a covalently connected porphyrin fullerene dyad **1.3** was prepared by Gust,[33] via Diels-Alder[4+2] cycloaddition reaction of a diene substituted porphyrin to C_{60} (Figure 1.9). Steady state luminescence spectroscopy revealed that the porphyrin excited state was significantly quenched compared to the parent porphyrin. Time resolved fluorescence measurements showed that a charge separated state ($ZnP^{\cdot+}$-$C_{60}^{\cdot-}$) was produced from an electron transfer of the porphyrin photoexcited state to the fullerene with a lifetime of 9 ps in benzonitrile.

Simultaneously Boyd and Reed prepared a short linked porphyrin fullerene dyad **1.4** by direct attachment of a fullerene to the β-pyrrole position of a tetraphenyl porphyrin using a Prato [3+2] cycloaddition to C_{60}.[34,35] This dyad displayed a longer lifetime of 290 ps for the free base porphyrin and 50 ps for the zinc porphyrin. These resulting charge-separated states are relatively long lived compared with similarly linked porphyrin-quinone dyads.

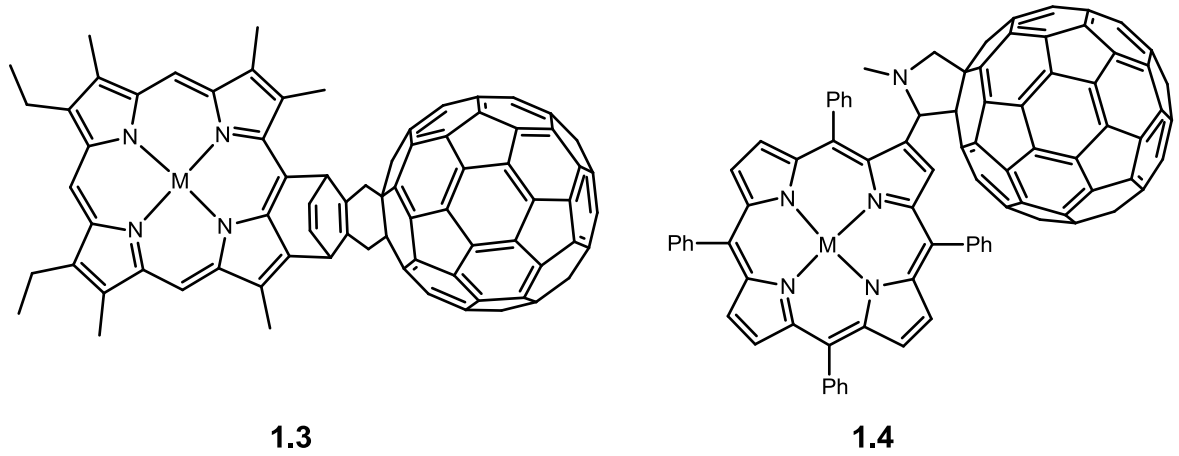

1.3 **1.4**

Figure 1.9: Early porphyrin-fullerene dyads **1.3**[33] and **1.4**.[34]

This key discovery has prompted the synthesis of other porphyrin fullerene linked systems.[36-40] It was hoped that by controlling the nature of the linker as well as the orientation and spatial separation of the two chromophores, it would be possible to gain control of the electron recombination process and to maximize the charge separated state lifetime. Imahori and Sakata reported the synthesis of amide linked porphyrin fullerene dyads **1.5a-d** (Figure 1.10).[41,42] The orientation of the amide linker was systematically varied with the bonds between the porphyrin phenyl group arranged *para* (**1.5a** and **1.5b**), *meta* (**1.5c**) and *ortho* (**1.5d**). In addition the cyclohexane fused to C_{60} was also attached to the 3,4 position on the aromatic spacer (**1.5a, 1.5c** and **1.5d**) and the 2,3 position (**1.5b**). Photoexcitation of the dyads showed that the *meta*-substituted linker showed the longest lifetime for the charge separated state. This has been attributed to the stronger electronic coupling interactions between the porphyrin and fullerene moieties in the *ortho* and *para* linkages compared to the *meta* structure.

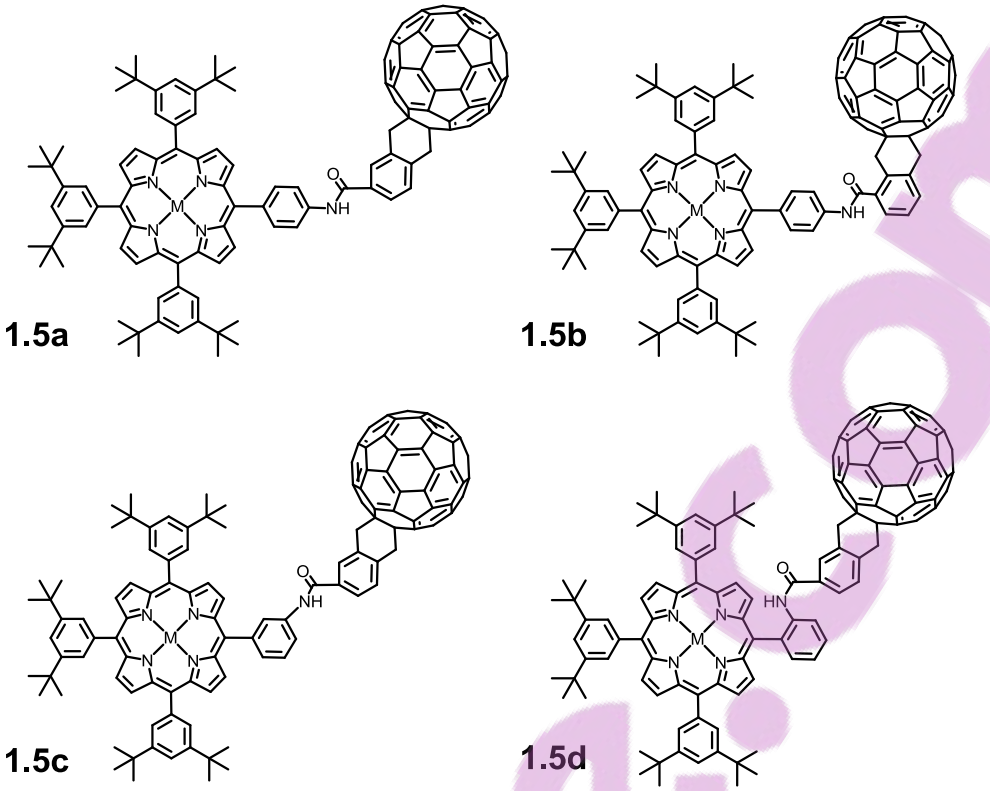

Figure 1.10: Systematic variation of amide linked porphyrin-fullerene dyads **1.5**.[41,42]

Parachute shaped porphyrin fullerene dyad **1.6** has also been prepared by Diederich *et al*. via a double cyclopropanation reaction (Figure 1.11).[43,44] In these dyads there is a close face to face arrangement between the porphyrin and C_{60}. Photophysical measurements indicate that electron transfer dominates over energy transfer in both polar and non-polar solvents, generating the charge separated state ($ZnP^{\cdot+}$-$C_{60}^{\cdot-}$). In contrast to other non-parachute dyads, which only show charge separation in polar solvents. Lifetimes for the charge separated state of **1.6** were 619 ps in toluene, 385 ns in THF and 38ps in benzonitrile[45].

Schuster *et al*. reported the same trend with a C_{60} porphyrin parachute dyad **1.7** prepared by a single cyclopropanation addition.[46,47] Dyad **1.7** exhibited a slower charge recombination producing a $ZnP^{\cdot+}$-$C_{60}^{\cdot-}$ radical pair lifetime of 99 ps in THF and 69 ps in benzonitrile. The shorter charge separated state lifetime compared to **1.6** has been attributed to the looser stacking arrangement between the two chromophores.

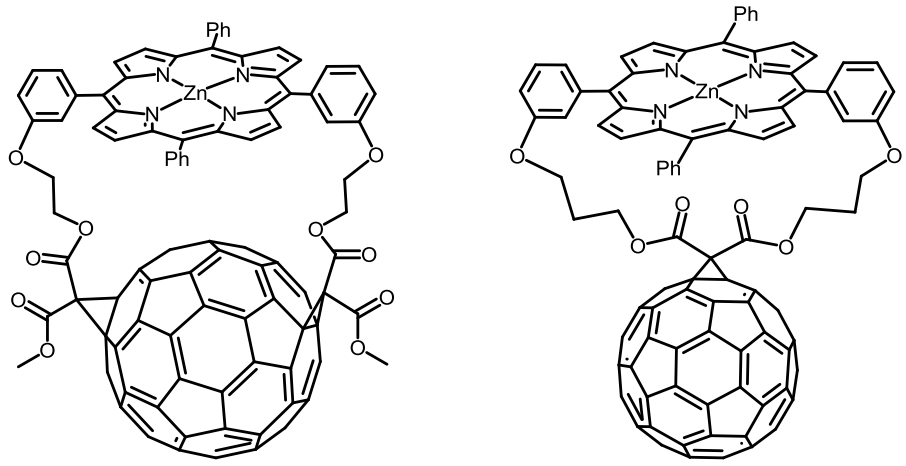

1.6 **1.7**

Figure 1.11: Covalently linked porphyrin-fullerene parachute dyads, **1.6**[44] and **1.7**. [46,47]

1.8 Marcus Theory of Electron Transfer

Lifetimes of the charge separated state for porphyrin-fullerene dyads are observed to be longer than that of similarly linked porphyrin-quinone dyads. These dyads demonstrate more rapid photoinduced charge separation and retarded charge recombination. In the natural photosynthetic reaction center, transfer is optimized with regard to the reorganization energy (λ) associated with electron transfer. This is done by embedding the donor and acceptor chromophores in a transmembrane protein. Marcus theory of electron transfer provides a valuable guide for certain key aspects involved in photoinduced electron transfer reaction, such as the efficiency of forward electron transfer versus back electron transfer.[48,49] To quantify the driving force dependence on the electron transfer rate constant (k_{ET}), are employed.

$$k_{ET} = \left(\frac{4\pi^3}{h^2 \lambda k_B T} \right)^{1/2} V^2 \exp\left[- \frac{\left(\Delta G^\circ_{ET} + \lambda \right)^2}{4\lambda k_B T} \right]$$

Equation 1.1

$$\Delta G\ddagger = \frac{\left(\Delta G^\circ_{ET} + \lambda \right)^2}{4\lambda}$$

Equation 1.2

(ΔG°_{ET}) is the free energy change, ($\Delta G‡$) is the activation barrier for the electron transfer reaction, (*V)* is the electronic coupling, (k_B) the Boltzmann constant, (*h*) the Planck constant and (*T*) the absolute temperature.

The electronic coupling, *V* is dependent on the separation and distance of the spacer between the donor and acceptor. λ is composed of two components, the vibrational component or solvent independent component (λ_i), and a solvent dependent component which depends on polarization changes in the solvent environment (λ_s). These parameters have different values before and after the electron transfer occurs, therefore the energy associated with these rearrangements defines λ.

$$\lambda = \lambda_s + \lambda_i$$

Equation 1.3

λ plays an important role in the determining rates and energetics of the electron transfer, which can be realized upon examination of the Marcus parabolic curve. In the 'normal region' of the Marcus curve, as G°_{ET} become more negative, the electron transfer rate increases until it reaches a maximum point where $G^{\circ}_{ET} = \lambda$ (top region). Here the reaction rate is mostly governed by electronic coupling between the donor and the acceptor. However, as G°_{ET}, becomes further negative and $G^{\circ}_{ET} > \lambda$, the electron transfer rate decreases (inverted region).

In principal smaller λ values assist in reaching the maximum of the Marcus parabola at a reduced G^{0}_{ET}, in turn shifting the energy wasting charge recombination though into the Marcus 'inverted region'. In natural photosynthesis, the λ-value is optimized for each electron transfer process. This allows the forward electron transfer processes to proceed under optimal conditions towards the top region of the Marcus parabola, whereas the highly exergonic and energy-wasting back electron transfer process is shifted into the 'inverted' region. Consequently, in each process the forward electron transfer is remarkably faster compared to the corresponding reverse process, extending the long-lived charge separation with a quantum yield near unity.

It was proposed that the reorganization energy of fullerenes is much smaller than that of typical two-dimensional acceptors.[50] Imahori and Sakata suggested that the reason C_{60} has a lower reorganization energy is due to the unit charge of the fullerene radical anion, $C_{60}^{\bullet-}$ being delocalized over its entire three dimensional framework, while the charge over the quinone radical anion ($Q^{\bullet-}$) is centralized over the oxygen atoms.[51,52] Thus the charge density of each carbon atom is smaller in $C_{60}^{\bullet-}$ than $Q^{\bullet-}$, making the solvent reorganization energy λ_s of the fullerene smaller. The Marcus parabolic curves shown in Figure 1.12 compares the efficiency of electron transfer for a porphyrin-C_{60} and a porphyrin-quinone based donor acceptor system. For the C_{60} dyad the forward electron transfer lies at the top of the Marcus curve while the quinone dyad lies in the normal region. As a result the forward reaction accelerates when using C_{60} as an acceptor compared to quinone. The back electron transfer for the porphyrin-C_{60} dyad lies deep in the inverted region of the curve while the quinone dyad lies near the top of the curve. Consequently, back electron transfer is retarded when using C_{60} as an electron transfer agent.

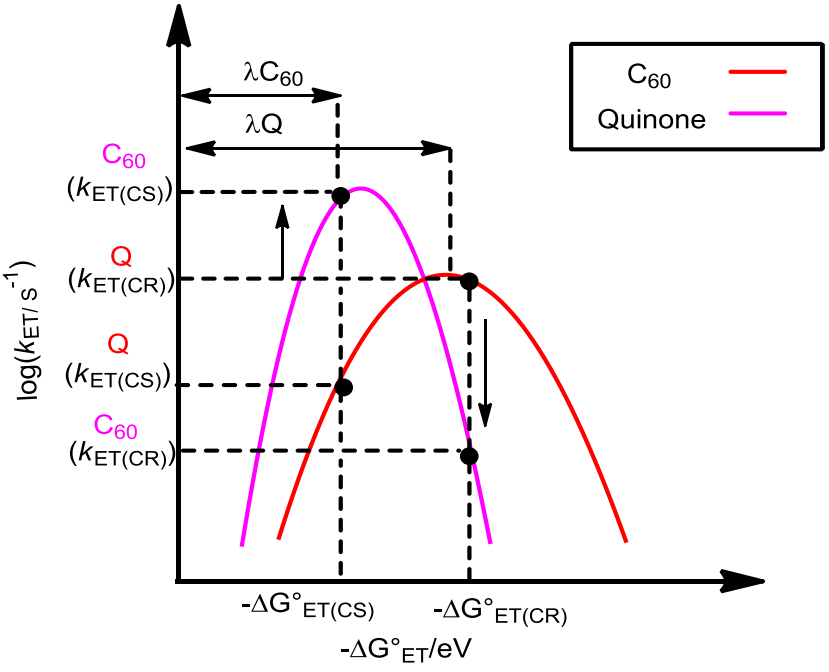

Figure 1.12: Marcus diagram showing the comparative rates of charge separation $k_{ET(CS)}$ and charge recombination $k_{ET(CR)}$ for C_{60} and quinone Q, due to the reorganisation energy adapted from Imahori.[53]

1.9 Endohedral Metallofullerenes

Empty fullerenes, C_{60} in particular, exhibit many of the qualities that are found in natures solar energy conversion/storage systems. Empty fullerenes are also capable of encapsulating a variety of chemical entities to form endohedral fullerenes.[54,55] Recently methods have been developed for synthesis of endohedral fullerenes encapsulating a variety of different atoms and polyatomic molecules in high purity and sufficient quantities. This has allowed further studies on their physical and chemical nature through spectroscopic methods and chemical modification.[56]

A vast array of endohedral fullerenes have now been prepared through variation of the number of carbons that form the cage and the types of atoms and molecules trapped in the interior of the cage. These trapped species include: chemically inert gas atoms, chemically reactive nitrogen or phosphorus atoms, electropositive metal atoms and diatomic molecules. Endohedral fullerenes containing metal clusters have been prepared. These clusters include metal carbides, metal nitrides and metal oxides and sulfides (Figure 1.13). Of major interest have been the more abundant trimetallic nitride clusters $M_3N@-C_n$, where n = 76-96.[57] The metal determines the size and the symmetry of thee fullerene cage with larger metals favoring larger cages. A variety of different metals have been used to make endohedral fullerenes with the some of the more common being scandium, lanthanum and yttrium. In general the trimetallic M_3N is planar and can freely rotate inside the fullerene.[58] This is the origin of disorder in the X-ray crystal structures of endohedral fullerenes.

Chemically, endohedral fullerenes have similar chemical behavior to empty cage fullerenes, undergoing Diels Alder cycloadditions and Prato reactions.[59] Endohedral fullerenes are characterized by their capacity to allow for electron transfer from the metal atom to the fullerene cage. Endohedral fullerenes have different electrochemical properties due to displaying higher LUMO orbital energies compared to empty cage fullerenes.[60] This property provides a path toward higher voltages and hopefully higher efficiencies for molecular electronic and organic photovoltaic devices. Several polymer hetrojunction solar cells have been developed with modified trimetallic nitride endohedral fullerenes showing increased voltages.[61,62]

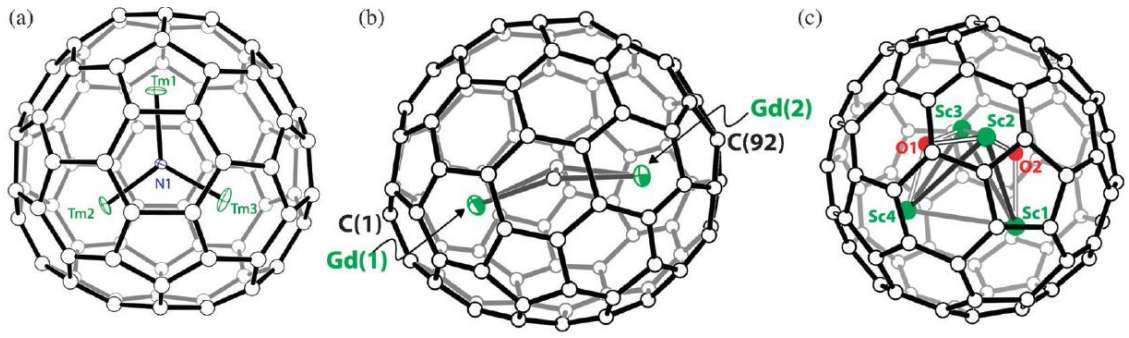

Figure 1.13: Drawing of several endohedral fullerenes; a) typical trimetallic nitride fullerene, b) metal carbide unit and c) metal oxide cluster, reproduced from Fortea.[63]

Endohedral fullerenes covalently coupled to zinc tetraphenyl porphyrin, have been prepared by a [1+ 2] cycloaddition.[64] Dyad **1.8** employs a $La_2N@I_h\text{-}C_{80}$ and **1.9** $Sc_3N@\ I_h\text{-}C_{80}$ as the electron acceptor. Transient absorption studies on these two dyads demonstrated significant differences in their electronic properties compared to empty fullerenes. Upon photoexcitation of **1.8**, a fast charge separation process yields the radical ion pairs namely $La_2N@I_h\text{-}C_{80}^{\bullet+}\text{-}ZnP^{\bullet-}$ or $La_2N@I_h\text{-}C_{80}^{\bullet-}\text{-}ZnP^{\bullet+}$ depending on the solvent polarity. On the other hand regardless of the solvent used, **1.9** forms the radical ion pair $Sc_3N@I_h\text{-}C_{80}^{\bullet-}\text{-}ZnP^{\bullet+}$. Such a change in photoreactivity has been rationalized when considering the energy levels of **1.8** and **1.9** in different solvents from electrochemical assays. The lifetimes of radical porphyrin cation-fullerene anion pairs were short-lived at 230 and 43ps in toluene for **1.8** and **1.9** respectively.

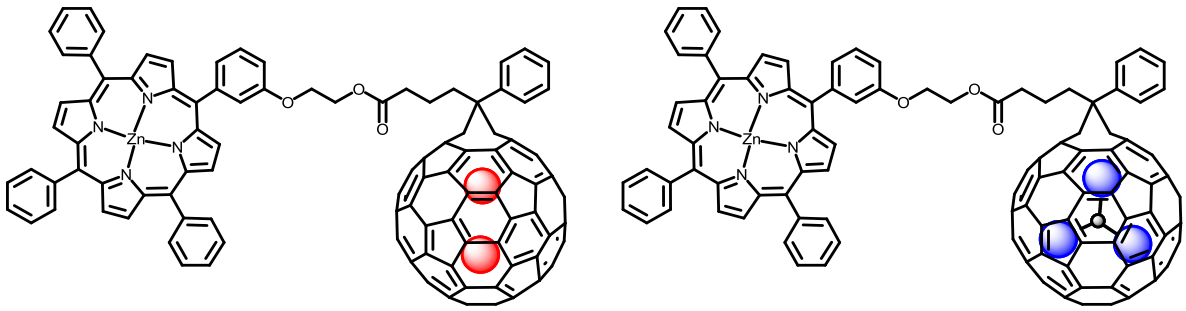

1.8 **1.9**

Figure 1.14: Endohedral fullerenes-porphyrin dyads **1.8** and **1.9**.[64]

1.10 Photoinduced Multistep Energy and Electron Transfer

In order to prolong the charge separated state lifetime, a multistep electron transfer is required. This has been observed in natural photosynthetic systems, where multiple chromophores are imbedded in a transmembrane protein. Although multistep electron transfer results in a loss of energy at each step, the spatial distance separating the radical ion pair prolongs the lifetime of the final charge-separated state.[65] Organic synthesis allows us to manipulate the energy and electron transfer processes by linking donors and acceptors with covalent and non-covalent bonds instead of using proteins.

1.10.1 Porphyrin-Fullerene Triads for Multistep Electron Transfer

There are two models of molecular triads have been proposed for multistep electron transfer.[53] One is the sensitizer-acceptor-acceptor (S-A_1-A_2), where the electrons are moved down progressive acceptor chromophores to increase the CS state while the electron hole remains on the sensitizer. The electron gradient for each state in the triad is designed in the order S*-A_1-A_2 > $S^{\bullet+}$-$A_1^{\bullet-}$-A_2 > $S^{\bullet+}$-A_1-$A_2^{\bullet-}$. Therefore the second electron transfer must compete with the energy wasting charge recombination to produce $S^{\bullet+}$-A_1-$A_2^{\bullet-}$. An example of this type of system is has been prepared by Imahori *et al*.[66] Several porphyrin (S), pyromellitimide (A_1), C_{60} (A_2) triads have been reported. These triads provide the appropriate energy gradients for electron transfer and exhibit longer charge separated states than dyads composed of porphyrins and pyromellitimides or fullerenes.

The second model for molecular triads is the donor-sensitizer-acceptor (D-S-A) model, where the electron hole is moved by the transfer of an electron from a secondary donor to the sensitizer, and the electron charge remains on the acceptor. A number of different authors have prepared a variety of these molecular triads with the addition of secondary donors such as ferrocene (Fc),[66-71] secondary metallatated porphyrins,[72] carotenoids[73,74] and other reducing species.[75,76]

A fullerene-porphyrin-ferrocene triad **1.10** prepared by Imahori and co-workers displays a lifetime extension without a decrease in efficiency (Figure 1.15a).[66,67] Photoexcitation of porphyrin, ZnP results in a charge separated state from the porphyrin to $C_{60,}$ generating

$C_{60}^{\bullet-}$-$Zn^{\bullet+}$-Fc in high quantum yield. The charge separated state undergoes a secondary electron transfer process between the $ZnP^{\bullet+}$ and the ferrocene to a long lived $C_{60}^{\bullet-}$-Zn-$Fc^{\bullet+}$ charge separated state. A lifetime of up to 16 μs was observed for the charge separated state in deoxygenated benzonitrile. Electron transfer rate constants for charge recombination were also determined in solvent of different polarity. It was observed that the charge recombination rates decrease with increasing solvent polarity, implying that recombination is in the normal region of the Marcus curve.

Imahori has also described the synthesis of triad **1.11,** consisting of a fullerene moiety covalently linked by two porphyrins (zinc and free base porphyrin), shown in Figure 1.15.[72,77] This triad utilizes the zinc porphyrin as an energy transferring antennae molecule. Upon excitation, the zinc porphyrin, ZnP, transfers its singlet energy to the energetically lower lying free base porphyrin , H_2P. This energy transfer is then followed by sequential electron transfer from the singlet excited state of the free base porphyrin to the fullerene yielding ZnP-$H_2P^{\bullet+}$-$C_{60}^{\bullet-}$. Subsequent electron transfer from the ZnP to the $H_2P^{\bullet+}$ occurs to yield $ZnP^{\bullet+}$-H_2P-$C_{60}^{\bullet-}$. A lifetime of 21μs was determined for the final charge separated state with a quantum yield of 0.4 in deoxygenated benzonitrile.

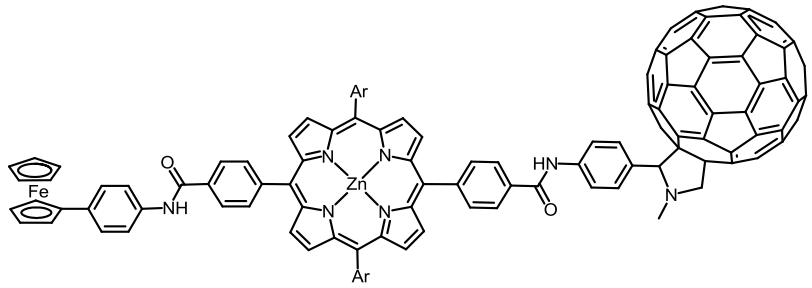

1.10

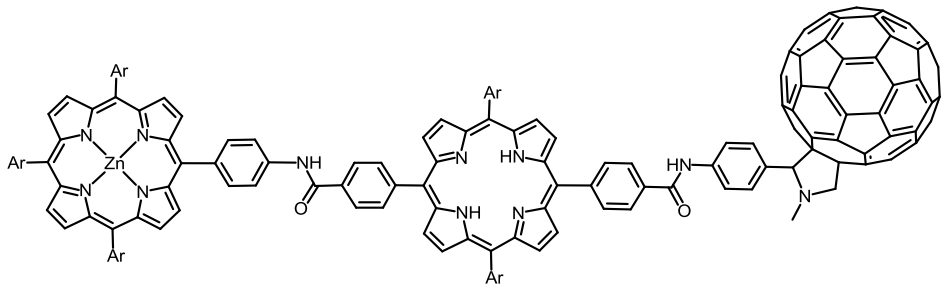

1.11

Figure 1.15: Covalently linked ferrocene-porphyrin-fullerene triad **1.10**[66,67,78] and zinc porphyrin-freebase porphyrin-fullerene dyad **1.11**.[72,77]

1.10.2 Porphyrin-Fullerene Tetrad and Pentads for Multistep Electron Transfer

Tetrads and pentads further prolong the lifetime of the final charge separated state through photoinduced electron transfer and multiple electron transfers within the molecule. The ferrocene-zinc porphyrin-freebase porphyrin-fullerene (Fc-ZnP-H_2P-C_{60}) molecular tetrad **1.12** covalently connected through amide bonds was designed and prepared by Imahori *et al*.[67] This tetrad displayed an extremely long lived charge separated state in frozen media and in solution. Upon excitation of the zinc porphyrin, energy transfer takes place to the free base porphyrin followed by an electron transfer to generate Fc-ZnP-$H_2P^{\bullet+}$-$C_{60}^{\bullet-}$. Immediate electron transfer from the zinc porphyrin to free base porphyrin then generates the Fc-$ZnP^{\bullet+}$-H_2P-$C_{60}^{\bullet-}$. The ferrocene moiety further separates the overall charges by reducing the zinc porphyrin to yield a long range charge separated state $Fc^{\bullet+}$-ZnP-H_2P-$C_{60}^{\bullet-}$. The lifetime of the tetrad was determined to be 380 ms in frozen benzonitrile, comparable with the bacterial photosynthesis.

A *meso* linked zinc porphyrin dimer $(ZnP)_2$ and trimer $(ZnP)_3$ were coupled with fullerene and a ferrocene donor to form molecular tetrad and pentad **1.13** and **1.14** and their photoinduced charge separation studied.[67,77-80] Photoirradiation of the tetrad results in an electron transfer from the singlet excited state of the zinc porphyrin pair $(ZnP)_2^*$ to C_{60} to produce the porphyrin fullerene radical pair Fc-$(ZnP)_2{}^{\bullet+}C_{60}^{\bullet-}$. Subsequent electron transfer from the ferrocene to the $(ZnP)_2^{\bullet+}$ leads to the final charge separated state $Fc^{\bullet+}$-$(ZnP)_2$- $C_{60}^{\bullet-}$ with a lifetime of 19 μs in benzonitrile at 295 K before decaying back to the ground state with an quantum yield of 0.8. In the case of pentad **1.14**, the photoirradiation results in a similar photoinduced charge transfer process yielding a final charge separated state of Fc-$(ZnP)_3{}^{\bullet+}C_{60}^{\bullet-}$. The lifetime of the charge separated state was 0.53 s in DMF at 163 K, with a high quantum yield of 0.83 in benzonitrile. The increased light harvesting efficiency was attributed to the efficient charge separation through the porphyrin trimer and the delocalization of the radical cation over the porphyrin trimer.

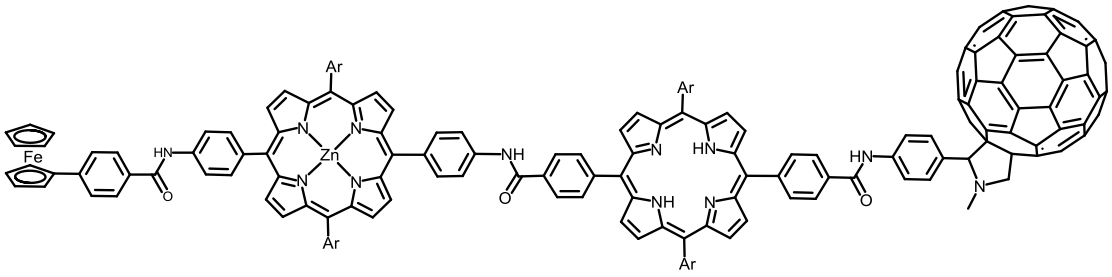

1.12

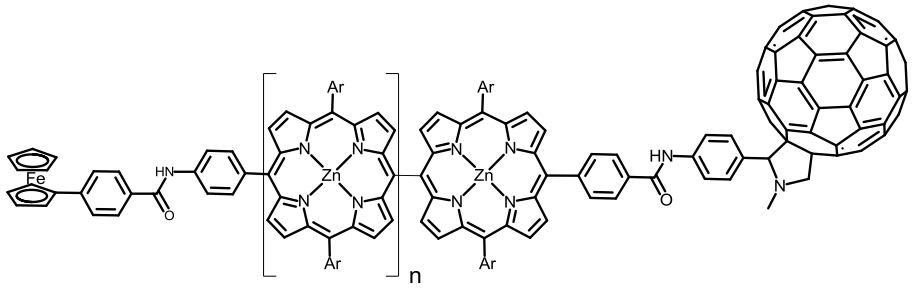

1.13 n=1
1.14 n=2

Figure 1.16: Covalently linked ferrocene-porphyrin-fullerene tetrad **1.12**,[67,78,79] and tetrad and pentad **1.13** and **1.14**.[80]

1.11 Supramolecular Bonding for Molecular Assembly

Although covalently linked multi-component systems exhibit excellent results in regard to charge separation lifetimes, they do have synthetic limitations such as decreased solubility and yield, which can arise with an increasing number of chromophores. In bacterial photosynthesis the redox-active components are arranged in a non-covalent manner within a protein matrix. The nature of the medium between the components can also help control the electronic coupling between the donor and acceptor.

Supramolecular chemistry is the chemistry of non-covalent bonds. These systems involve aggregates of molecules or ions, which are held together by weak interactions or recognition elements, such as electrostatic interactions, hydrogen bonding, dispersion interactions and solvation effects.[81,82] Supramolecular chemistry can be split into two broad categories, 'self assembly' and 'host-guest chemistry'. The primary difference between the two areas is a question of size and shape. In self assembly, two or more molecules which are similar in size can spontaneously and reversibly associate with each other to form a larger, non-covalent

bound aggregate. DNA is an example of self assembly in nature. Two strands can self assemble via hydrogen bonds and aromatic stacking interactions to form a double helical structure. In 'host-guest chemistry', a large molecule termed the 'host', is capable of enclosing smaller 'guest' molecules via non-covalent interactions in a binding site. Normally the binding site region of the molecule is said to have the necessary size, geometry and functionalities to accept and bind a guest molecule via non-covalent interactions.

Non-covalent interactions are considerably weaker compared to covalent interactions, however, the power of supramolecular chemistry lies in the combination of a number of weak interactions co-operating to form stable complexes and the ability to associate and disassociate by changing equilibrium conditions.

Ionic and dipole interactions also called electrostatic interactions are based on the coulombic attractions between opposite charges. They can be split into three main categories; ion-ion, ion-dipole and dipole-dipole interactions. The strongest of these is ion-ion, which is comparable in strength to covalent bonds. Ion-ion interactions are non-directional in nature meaning that they can occur in any orientation. Ion-dipole interactions which occur between ions and polarisable molecules are weaker than ion-ion and are orientation dependant, meaning that they must be suitably aligned for optimal binding efficiency. Dipole-dipole interactions are the weakest electrostatic interactions as ions have a higher charge density than dipoles and are also directional. They are extremely useful for bringing species into alignment.

1.12 Self-Assembled Supramolecular Porphyrin-Fullerene Dyads

Several non-covalently linked porphyrin-fullerene dyads have been developed employing different self assembly methods. These dyads have been studied in order to assess how the photoinduced electron transfer changes in comparison to covalently linked dyads.

1.12.1 Dyads Prepared by Base-Paired Hydrogen Bonding.

Use of Watson-Crick hydrogen bonding has been employed by Sessler *et al*. as a method for preparation of a self assembled donor-accepter complex **1.15** (Figure 1.17).[83] A cytidine appended porphyrin (ZnP-Cy) and a guanosine functionalized fullerene (Gs-C_{60}) were

synthesized. These two components self assembled in dichloromethane to give a new donor-acceptor ensemble (ZnP-Cy:Gs-C_{60}). Evidence of self assembly between the guanosine-cytidine base pair couple was established by the decrease in fluorescence intensity of the ZnP-Cy in dichloromethane as a function of increasing concentration of the Gs-C_{60}. A binding constant of 5.1 ± 0.5 x 10^4 M^{-1} in dichloromethane was determined, consistent with guanosine-cytidine dyads.

Time resolved fluorescence and transient absorption measurements were undertaken to support the conclusion of dyad formation and intra-molecular quenching, observed in steady state experiments. The transient spectra revealed that dyads underwent photoinduced electron transfer through the formation of the zinc porphyrin cation radical $ZnP^{\bullet+}$ and the fullerene anion radical $C_{60}^{\bullet-}$, with a long lived lifetime of 2.02 μs.

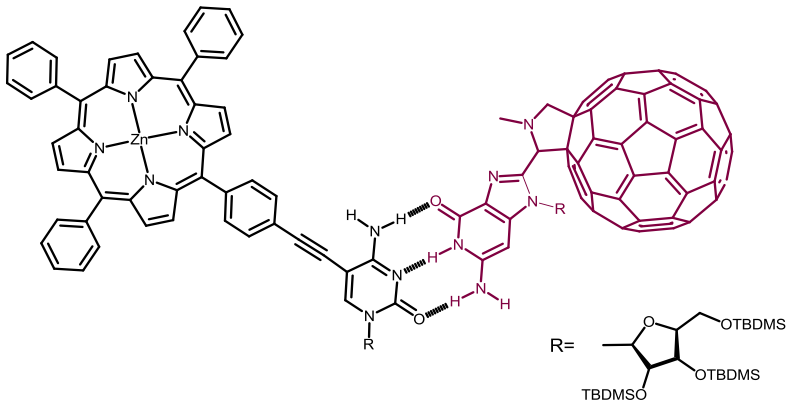

1.15

Figure 1.17: Base-paired hydrogen bonding dyad **1.15**.[83]

1.12.2 Dyads Prepared by Crown Ether- Ammonium Cations

Crown ethers have been shown to be one of the most effective groups for selective binding to cationic, anionic and neutral analytes. Benzo-18-crown-6 is of major importance because of its ability to bind quaternary alkyl ammonium cations. A number of self assembled porphyrin-fullerene dyads have been prepared using this supramolecular coupling method.[84] Nierengarten and co-workers prepared a supramolecular donor-acceptor assembly **1.16** by combining a fullerene functionalized with a ammonium subunit NH_3-C_{60} and a porphyrin crown ether conjugate ZnP-18-crown-6.[85] The porphyrin and fullerene subunits self assemble in solution to

form a very stable ZnP-18-Crown-6:NH_3-C_{60} dyad. The association constant for the assembly was studied by both NMR and UV-visible binding studies and was determined to be 375,000 M^{-1}, two orders of magnitude higher than that of NH_3-C_{60} with 18-crown-6 (2,100 M^{-1} in $CDCl_3$). The additional stabilization of the supramolecular complex was attributed to an additional intramolecular interaction of. π-π stacking between the fullerene and the porphyrin (Figure 1.18)

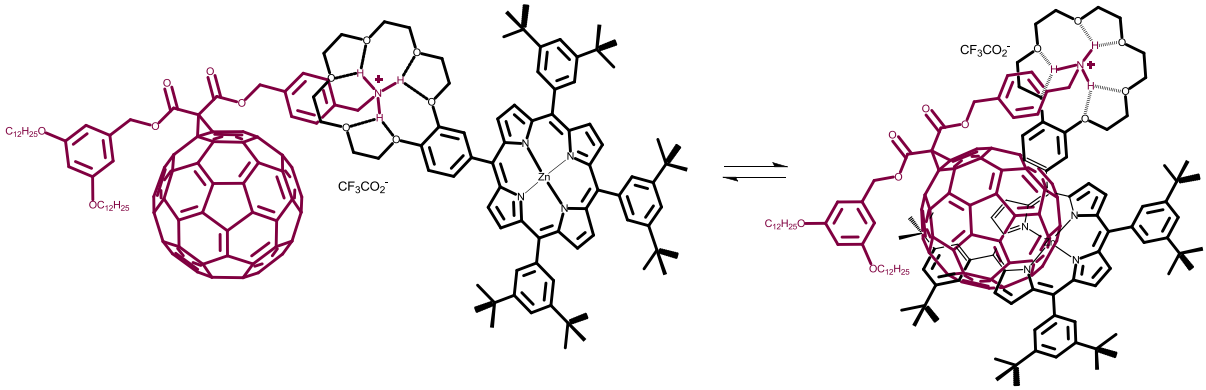

1.16

Figure 1.18: Crown ether-ammonium cation dyad **1.16**.[85]

1.12.3 Dyads and Triads Prepared by Axial Co-ordination

A number of models for photoinduced electron transfer have been reported in which porphyrin attached with axial ligands. Numerous metals such as zinc, aluminum and ruthenium have been inserted into the porphyrin core and have the ability to form five- and six- coordinated complexes. Variable coordination has been explored by several groups to design in the preparation of donor-acceptor systems which undergo photoinduced electron transfer.

The first examples of axial coordination with donor-acceptor assemblies were undertaken simultaneously by several research groups. Pyridine and imadazole functionalized fullerenes, (Pyr-C_{60}/ Im-C_{60}) were coordinated to a zinc porphyrin (ZnP) it give **1.17** and **1.18** respectively.[86-89] In these complexes the reversible coordination of the Pyr-C_{60}/Im-C_{60} to the square planar zinc center constitutes a labile but measurable association (5 x 10^3 and 11 x 10^3 M^{-1} for Pyr-C_{60} and Im-C_{60} respectively).

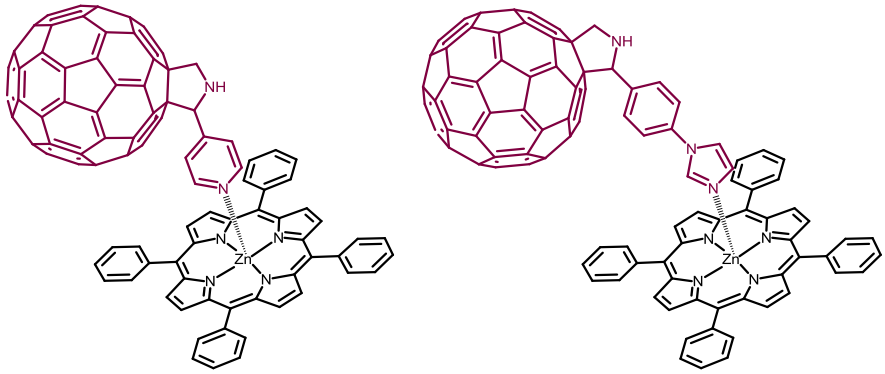

Zn1.17 **Zn1.18**

Figure 1.19: Axial coordinated porphyrin-fullerene dyads **1.17**[86,89] and **1.18**.[87,88]

Transient absorption studies have shown that the excited state zinc porphyrin rapidly transfers an electron to the C_{60} moiety within the ZnP:Pyr-C_{60} complex. The weak equilibrium between dissociation and association of the zinc-pyridine bond facilitate the break-up of the radical pair before the competing charge recombination can occur. The charge separated state of the assembly lasts 10 μs in THF and several hundred microseconds in benzonitrile. Although the quantum yield of the radical pair is quite low, the lifetimes of radical pairs in covalently linked dyads is in the order of nanoseconds. The enhancing effect of the dissociation between chromophores is demonstrated by a ruthenium porphyrin RuP.[90] The ruthenium porphyrin-C_{60} complex is more stable due to strong π back-bonding in the metal pyridine bond compared to the zinc analog. As a result the $RuP^{\bullet+}$:Pry-$C_{60}^{\bullet-}$ radical pair does not dissociate in polar solvents, and so the charge recombines much more rapidly with a lifetime of less than 4 ns.

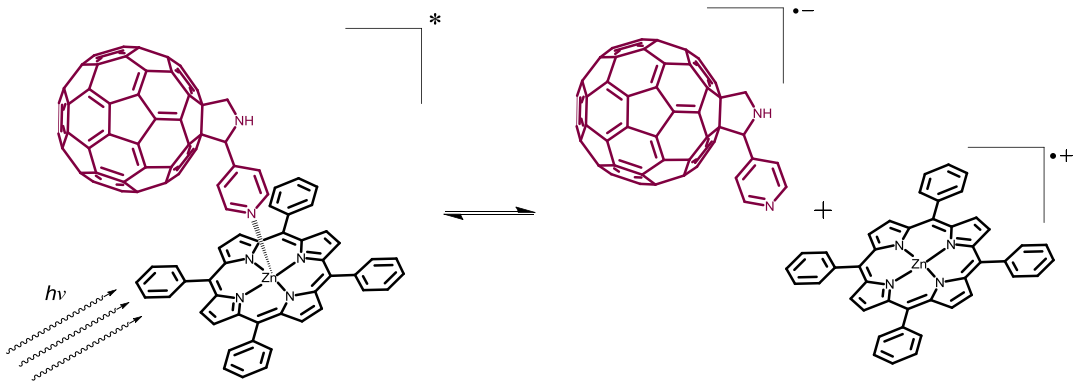

Figure 1.20: Dissociation of the **1.17** radical pair $ZnP^{\bullet+}$ $PyC_{60}^{\bullet-}$ upon photoexcitation and electron transfer. [86]

The concept of axial coordination was extended to supramolecular triads comprising of a fullerene axially coordinated to a porphyrin with a covalently bound secondary donor. The group of D'Souza has constructed many supramolecular triads using co-ordination chemistry.[91] A ferrocene-porphyrin-fullerene supramolecular triad, assembled by axial co-ordination of the imadazole functionalized fullerene **1.18** to a zinc porphyrin covalently attached to ferrocene **1.19**.[92] Photoexcitation of the zinc porphyrin was followed by electron transfer to the fullerene to yield Fc-ZnP$^{\bullet+}$-Im$C_{60}^{\bullet-}$. Subsequent transfer of an electron from the ferrocene to the zinc porphyrin resulting in Fc$^{\bullet+}$-ZnP-Im$C_{60}^{\bullet-}$. a charge separated state lifetime of 10 ns. While longer than the co-ordinate porphyrin fullerene dyads, the lifetimes were, approximately 100 times shorter that covalently linked ferrocene porphyrin fullerene triads, this has been attributed due to the close proximity of the radical charges on the $C_{60}^{\bullet-}$ and the Fc$^{\bullet+}$ observed in molecular modeling of the complex.

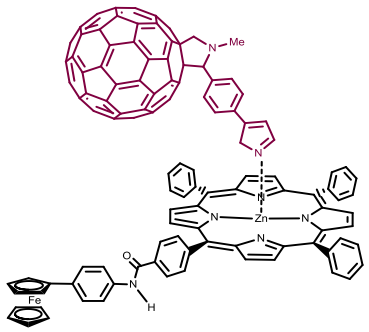

1.19

Figure 1.21: Axially linked triads **1.19.**[91]

1.13 Supramolecular Porphyrin-Fullerene Chemistry

The supramolecular recognition between fullerenes and porphyrins was first recognized in the crystal structure of a pyrrolidine linked porphyrin-fullerene dyad reported by Sun.[35] The molecular packing of the dyads shown in Figure 1.22 displayed a distance of 2.75 Å between the closest carbon atom of fullerene and the mean 16 atom plane of a neighbouring porphyrin. This distance was clearly shorter than the seperation of typical π-π systems in the solid state, such as inter-layer graphite (3.35 Å), interfacial porphyrin-porphyrin (>3.2 Å), fullerene to fullerene (>3.2 Å) and fullerene-arene interactions (3.3-3.5 Å).[93]

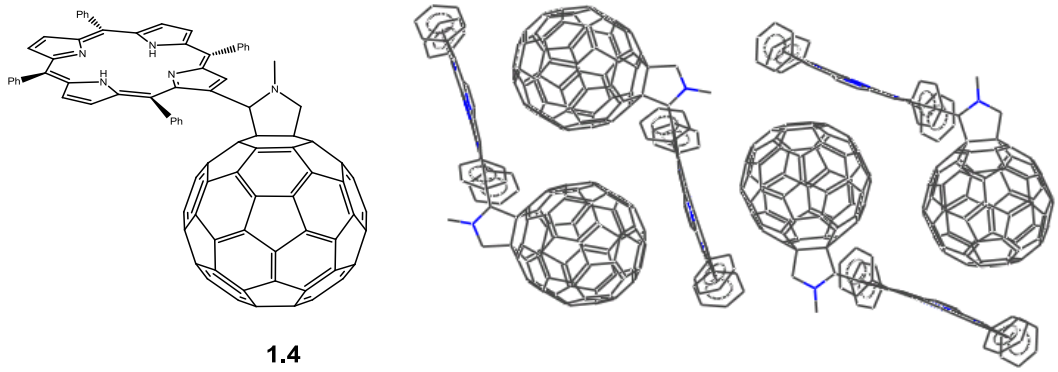

1.4

Figure 1.22: Pyrrolidine linked porphyrin-fullerene dyad **1.4** and X-ray crystal structure of **1.4** showing close contact between the C_{60} and the porphyrin (phenyl rings omitted for clarity).[35]

The attractive interaction between fullerenes and porphyrins, derived from the close porphyrin/fullerene distance observed in **1.4,** has also been observed in untethered porphyrin fullerene co-crystallates. Boyd and Reed showed that the association continues in co-crystallates of C_{60} and C_{70} with tetra-phenyl porphyrin H_2-TPP and Zn-TPP producing a zigzag 1:1 packing motif (Figure 1.23).[94] An important aspect of the packing was that C_{70} molecules were aligned sideways, parallel to the porphyrin rather than end on. This interaction is thought to maximize π- π interactions. Octaethylporphyrins (OEP) have also been co-crystallized with fullerenes as shown in Figure 1.23.[95] These molecules are less sterically hindered and adopt a face-to-face porphyrin-porphyrin architecture which is commonly seen in the structures of porphyrins.

a)

b)

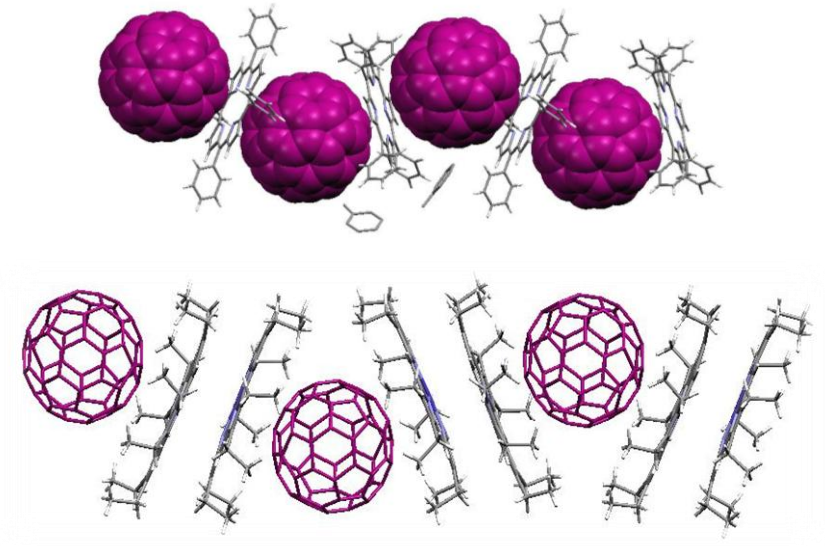

Figure 1.23: a) Zigzag Co-crystallate Structures of C_{60} and $H_2TPP.C_{60}$.[94,95] b) The co-crystallate structure of $Co(II)OEP_2.C_{60}$.[95]

This structural pattern of alternating porphyrins and fullerenes is common in many co-crystallate structures, although the packing motifs can vary due to steric differences between the porphyrins. Porphyrins have also been observed in domed or warped conformations. This departure from planarity is believed to enhance π-π interactions. In general solid state structures of porphyrin-C_{60} co-crystallates show close contact between the fullerene and the centre of the porphyrins.[94] However, examples of fullerene-fullerene contacts are also recorded. In the absence of steric effects the order of interaction strengths is porphyrin-porphyrin > porphyrin-fullerene > fullerene-fullerene.[93]

1.13.1 The Nature of the Porphyrin- Fullerene Interaction

The main contributors to the molecular recognition between fullerenes and porphyrins are π-π attraction and electrostatic interactions. The primary attraction is the π-π interaction; this is highlighted by the fact that in co-crystallates of porphyrins with the ellipsoidal C_{70}, the fullerene aligns sideways, parallel to the porphyrin rather than end on to maximize the interaction. The attraction improved by weak electrostatic interactions between the two chromophores. In crystal structures, the electron rich 6:6 ring junction of the fullerene, is aligned with the electropositive center of the porphyrin, rather than the less electron rich 6:5 ring junctions interact with the electron rich nitrogens of the porphyrin core.[94]

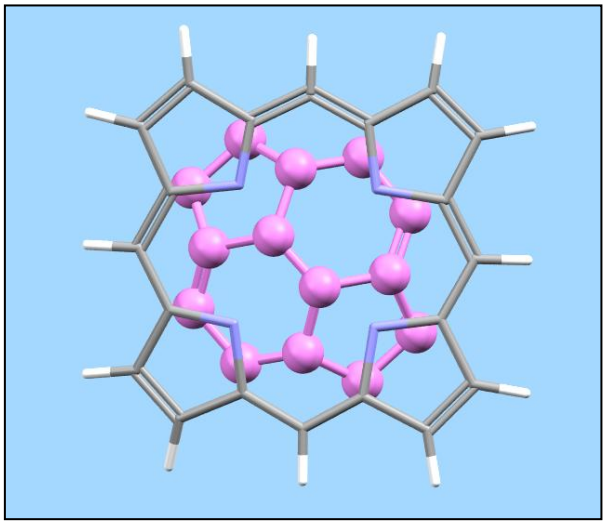

Figure 1.24: Close association of the 6:6 ring junction of C_{60} (purple) and H_2TPP (grey).[94]

NMR studies demonstrate that the porphyrin-fullerene interaction also exists in solution. Significant upfield shifts were detected in both the ^{1}H NMR spectrum of H_2TPP and the ^{13}C NMR spectrum of C_{60} when the two components in toluene solution.[94]

1.14 Supramolecular Bis-Porphyrins Hosts for Fullerenes

Singular porphyrin-fullerene interactions are not strong enough to form a stable complex at micromolar concentrations. Bis-porphyrins do however form stable complexes due to multivalency effects. A significant number of new bis-porphyrin hosts for fullerenes have been developed. Two different classes of bis-porphyrin architectures have been designed and synthesized for the inclusion and encapsulation of fullerenes and are generally classified as cyclic and acyclic bis-porphyrins.

1.14.1 Cyclic Bis-Porphyrins as Hosts for Fullerenes

Aida *et al*. prepared macrocyclic bis-porphyrin hosts **1.20** and **1.21** (Figure 1.25) designed to bind fullerenes.[96] The first host **1.20**, had rigid, diacetylenic spacers between the two porphyrin units and displayed no interaction with $C_{60,}$ where the more flexible dihexyl-linked bis-porphyrin **1.21**, showed strong association for C_{60}. The cyclic dimer has the highest known binding for fullerenes C_{60} and C_{70}. Further studies focusing on porphyrin metallation (Table 1.1) showed a noticeable influence on the complexation of fullerenes in particular with group 9 metals Co(II) and Rh(III) which increase association by an order of magnitude.[97] When inserted into the porphyrin unit group 10 and 11 metals ions, Cu(II), Ni(II) and Ag(I). display lower binding affinities for both fullerenes. The association of C_{70} was also observed to be an order of magnitude greater than C_{60}, attributed to the ellipsoidal shape of the C_{70}. The observed side on attraction versus end on packing in co-crystallate structures of porphyrin and C_{70} is also evident in solution through ^{13}C NMR. Five non-chemically equivalent carbons are observed for C_{70} as different ^{13}C NMR signals, three signals corresponding to the equatorial band of C_{70} and two for the poles. When complexed with **1.21** all signals experience upfield chemical shift but the equatorial carbon atoms demonstrate the greatest changes, supporting C_{70} complexation in a side on conformation in solution as well as solid state in order to maximize π-π interactions.

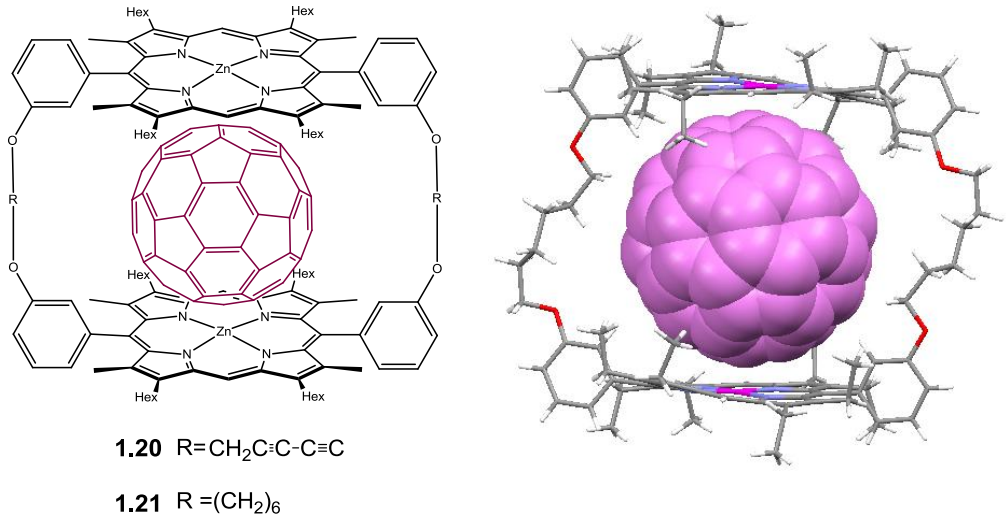

Figure 1.25: Cyclic bis-porphyrin hosts **1.20** and **1.21** and the X-ray structure of cyclic zinc bis-porphyrin **1.21** with C_{60}. [96]

Table 1.1: Association constants for various metallated derivatives of bis-porphyrin**.1.21** with C_{60} and C_{70} in toluene. [97]

1.20	**2H**	**Co(II)**	**Rh(III)**	**Ni(II)**	**Cu(II)**	**Ag(II)**	**Zn(II)**
C_{60}(M^{-1})	7.95×10^5	1.99×10^6	2.5×10^7	2.50×10^5	5.01×10^5	1.25×10^6	6.30×10^5
C_{70} (M^{-1})	1.52×10^7	1.25×10^7	1.00×10^8	1.95×10^6	5.01×10^6	3.16×10^6	1.95×10^7

Analogously, linked cyclic dyads **1.22** and **1.23** have recently been prepared by Ballester and are shown in Figure 1.26.[98] These hosts utilize the same rigid, diacetylenic and flexible dihexyl- spacers but employed a modified porphyrin with unsubstituted β-pyrroles and mesityl groups at the *meso* positions. Both of these cyclic hosts form complexes with the trimetallic nitride endohedral fullerene $Sc_3N@C_{80}$. UV-visible titration experiments confirmed the existence of a strong π-π interaction between the fullerene and the dimer bearing hexyl spacers producing a association constants of $K_a = 2.6 \pm 0.3 \times 10^5\ M^{-1}$. Complexes of **1.22** and **1.23** with $Sc_3N@C_{80}$ were characterized by X-ray diffraction analysis. In the 1:1 porphyrin to fullerene complex of **1.22:C_{60}**. The host adopts a scoop shaped conformation having a dihedral angle of 87.3° between the porphyrin planes. The hexyl analog **1.23** adopts a similar conformation but forms a 2:1 bis-porphyrin to fullerene ratio, with the fullerene encapsulated and completely isolated by the bis-porphyrins.

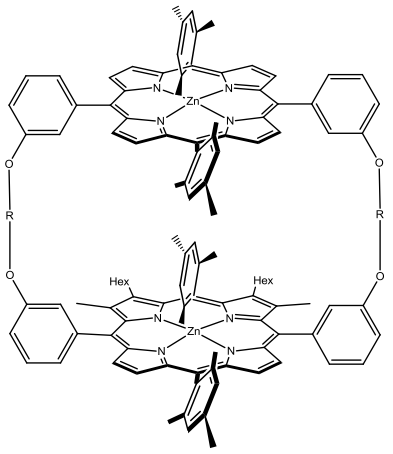

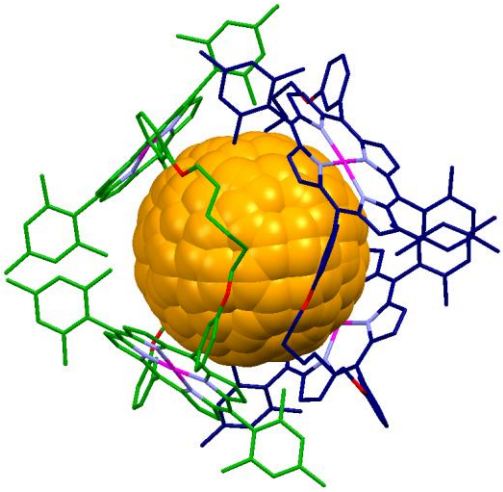

1.22 R=$CH_2C{\equiv}C{-}C{\equiv}C$

1.23 R = $(CH_2)_6$

Figure 1.26: Cyclic bis-porphyrins **1.22** and **1.23** and the X-ray structure of **1.23** with $Sc_3N@C_{80}$. [98]

Tani and coworkers have reported a cyclic nickel bis-porphyrin dimer **Ni1.24** linked by shorter butadiyne spacers and bearing 4-pyridyl groups.[99] The aim of this work was to construct a tubular assembly with cyclic hosts capable engaging in hydrogen bonding interactions with a donor or metal ion. The dimer was seen to self assemble through non classical C-H···N hydrogen bonds between the pyridyl groups and the β-pyrrole CH as well as π-π interactions between the pyridyl groups (Figure 1.27).

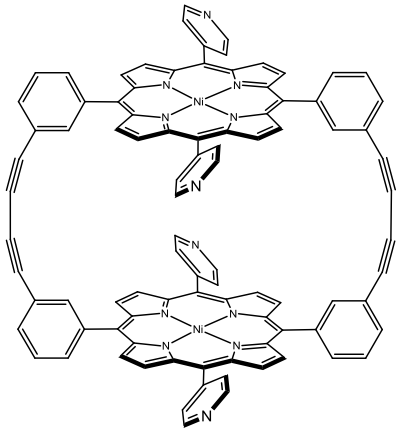

Ni 1.24

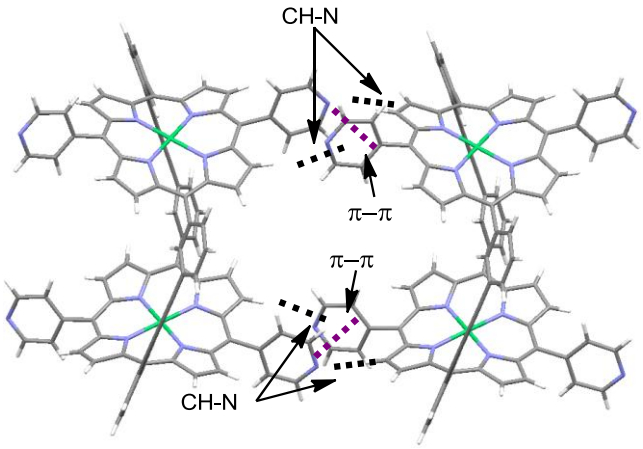

Figure 1.27: Pyridyl functionalized cyclic bis-poprhyrin.**Ni1.24** and the self assembled X-ray crystal structure of **Ni1.24**. [99]

The cyclic bis-porphyrin presented the appropriate cavity size to include C_{60} and UV-visible titrations gave an association for a 1:1 complex with C_{60} of 2.0 x 10^5 M^{-1}, comparable to the Aida cyclic host.[97] X-ray crystal structures show that C_{60} sits slightly off center and the porphyrin buckle as the cavity of the host is too small for the comfortable inclusion of C_{60}.[100] The pyridyl supramolecular bonding motif is maintained. Time resolved transient absorption studies were carried out, however the expected charge transfer was not observed due to intersystem crossing of the excited porphyrin singlet to a triplet excited state which results in energy transfer instead of electron transfer to C_{60}.

Removal of the metal to yield the corresponding free base host **1.24** lowers the association of the cyclic dimer with C_{60} to 9.6 x 10^4 M^{-1}.[101] The structure of the **1.24:C_{60}** complex was also determined by X-ray crystallography (Figure 1.28). This structures show displayed a 1:1 complex with a planar porphyrin ring and a small cavity size for C_{60}. In the crystal structure of **Ni1.24**, the dimer includes a C_{60} molecule in a clamshell-like conformation, in which the porphyrin rings are tilted with respect to each other. The dihedral angle of the two porphyrin planes is 52.4°, and the center to center distance between the two porphyrins of 11.13 Å bears a strong resemblance to that of acyclic hosts. Time resolved transient absorption spectra were obtained with femtosecond laser flash photolysis demonstrates the formation of a charge separated state with a lifetime of 470 ps.

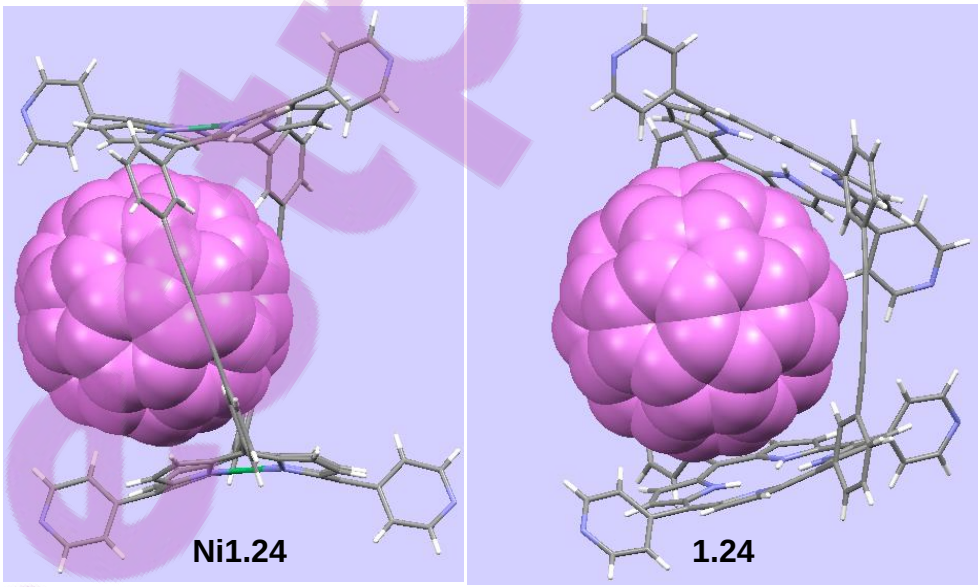

Figure 1.28: X-ray structures of cyclic bis-porphyrins **Ni1.24** and **1.24** with C_{60}.[99,101]

1.14.2 Acyclic bis-porphyrins as hosts for Fullerenes

The first acyclic porphyrin hosts designed to bind fullerenes were palladium linked bis-porphyrins prepared by Sun *et al.*[102] These "Jaws" bis-porphyrins **1.25a** and **1.25b** were synthesized by co-ordination of two A_3B type porphyrins bearing *meta* pyridyl nitrogens to a bischloro-palladium linker. This bis-porphyrin host shows the formation of a 1:1 complex with both C_{60} and C_{70} by FAB/MALDI mass spectroscopy and by variable temperature ^{13}C NMR. Association constants in toluene with C_{60} estimated by ^{1}H NMR titrations were 5.2 $x10^3$ M^{-1}. Single crystal X-ray diffraction analysis of **1.25b** with C_{60} revealed a clam shaped porphyrin dimer with C_{60} sandwiched between the porphyrin units. The dimer demonstrated a centre to centre porphyrin distance of 11.94 Å with an interplanar porphyrin angle of 41.6° This arrangement is commonly seen in co-crystallate structures of untethered tetraphenyl porphyrins and fullerenes and is consistent with calculations.

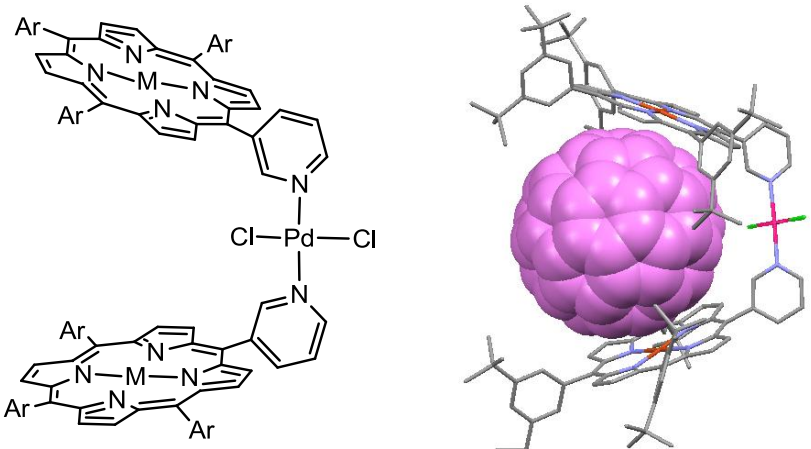

1.25a Ar = p-Tolyl

1.25b Ar = 3,5-di-*tert*-butyl phenyl

Figure 1.29: Palladium linked bis-porphyrin **1.25a** and the X-ray structure of **1.25b** with C_{60}.[102]

Sun *et al*. similarly investigated metallated analogues of **1.25b**, and their affinity to fullerenes. Binding constants in toluene were found to increase in the order Fe(II) < Pd(II) < Zn(II) < Mn(II) < Co(II) < Cu(II) < 2H. The reason for the higher binding of C_{60} with the free base **1.29b**, was attributed to the favorable electrostatic forces that occur between the electronegative 6:6 ring junction of the fullerene and the electron poor central NH of the porphyrins.

1.15 Calix[n]arenes

Calix[n]arenes are [1n] metacyclophanes first reported by Zinke and Ziegler.[103,104] They have acquired their name from the Greek vase called a calix crater. Calix[n]arenes come in a variety of different ring sizes ranging from n=3 to n=12, and are generally synthesized by base induced condensation reaction of para-*tert*-butyl phenol with formaldehyde.[105] The most common is the cyclotetramer, calix[4]arene consisting of four phenolic units connected by methylene bridges. Calix[4]arenes have been used for a variety of molecular recognition, and supramolecular applications. These include as sensors for anions,[106] cations[107-109] and neutral organics. They can also be readily functionalized on both the narrow and wide rims, making them attractive as scaffoldsdue to their preorganised cavity.[110-112] In the remainder of this thesis the name calixarene will be used in reference to calix[4]arene, with the narrow rim referring to the phenolic rim and the wide rim referring to the *para* substituents.

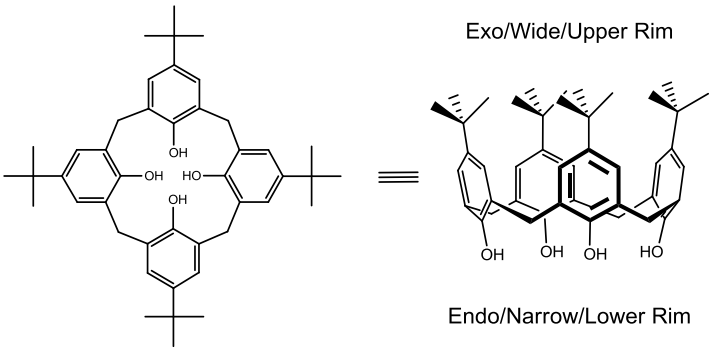

Figure 1.30: (a) Flat and (b) three-dimensional representation of *p-tert* calix[4]arene.

1.15.1 Conformations of Calixarenes

Calixarenes are conformationally mobile molecules due to the two possible rotational positions available to the phenol units. Rotation of the aryl ring allows either the oxygen on the narrow rim, or the para-substituent on the wide rim to pass through the centre of the macrocycle.[113] This mobility creates four possible isomers for the calixarene. The orientation of the aryl rings can either be upward or downward relative to the average plane defined by the methylene groups. When all four of the oxygen atoms point in the same direction, the macrocycle exhibits a bowl shaped structure called the 'cone' conformation. Inversion of one of the phenol rings

yields the 'partial cone' configuration. Whereas inversion of two of the phenol rings can give either '1,2 alternate' or '1,3 alternate' conformations (Figure 1.31).[103,104] The conformational preference for unsubstituted calixarene is the cone form, due to strong intramolecular hydrogen bonding from the four hydroxyl groups.

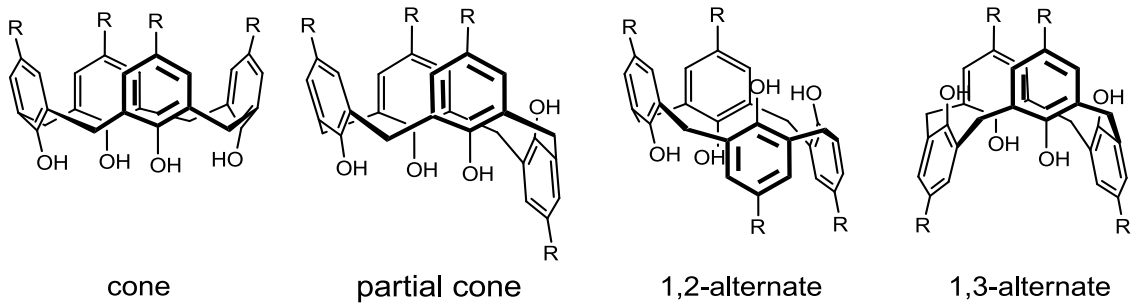

Figure 1.31: The conformations of calixarene.

^{1}H NMR spectra can be used to deduce the conformation of calixarenes. The cone conformation produces the simplest spectrum due to the higher symmetry of the calixarene scaffold. An AB splitting pattern of two sets of doublets is exhibited for the diastereotopic methylene bridge protons with a coupling constant of *J*= 13.1-13.4 Hz. The 1,3 alternate conformation displays one singlet for the methylene bridges, whereas the 1,2 alternate and partial cone present more complex ^{1}H NMR spectra which may vary depending on the substituents on the calixarene ring.

1.15.2 Chemistry of Calixarenes Wide and Narrow Rim

Calixarene may be readily derivatized along the narrow rim by alkylation of the phenolic groups.[114] Calixarene can be fully or selectively alkylated in a 1,3 alternate method with the use of a alkyl halides and an appropriate base. Smaller groups such as methyl, ethyl allow for interconversion between conformers, whereas larger groups prevent interconversion.

Functionalization on the wide rim has been thoroughly explored and can occur at either the *para* or *meta* positions, although modification at the *para* position dominates this class of functionalization as the position is heavily activated by the presence of the oxygen atom on the narrow rim. Examples of the types of functional groups employed include a variety of carbon

containing fragments as well as SO_3^-, $-NO_2$, $-NH_2$, -N=NR, PPh_2 and halides. These may be mono, di or tetra-substituted.

1.16 Wide Rim Calixarene Linked Bis-Porphyrins

Calixarene have been used as a molecular scaffold for the attachment of various chromophores. Dudic and co-workers synthesised a bis-porphyrins **1.30** and **1.31** that were originally designed to bind anions by appending porphyrins to the wide rim of calixarenes (Figure 1.32).[115] These bis-porphyrins displayed an affinity for both C_{60} and C_{70} demonstrating higher selectivity for C_{70}.[116]

Arimura *et al* synthesised bis-porphyrin host **1.32**.[117] This bis-porphyrin did not exhibit association with C_{60} but did show form a host-guest complex with. C_{70}. Computational modelling reveal that the larger cavity size between the wide rim porphyrins accommodates C_{70} in a pole to pole orientation but is too large to incorporate C_{60}. Intramolecular hydrogen bonding of the hydroxyl groups with the ethers on the narrow rim induces pinched cone conformation commonly observed in di-substituted calixarenes.

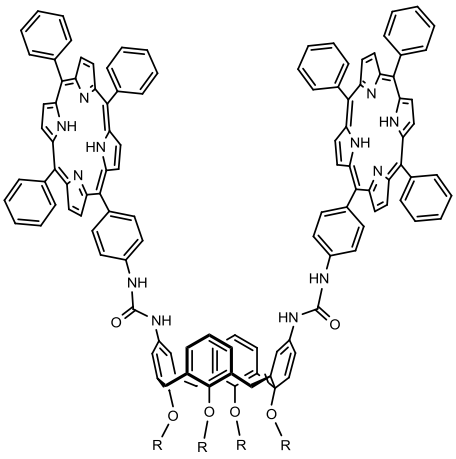

1.30 R = $(CH_2)_2CH_3$
1.31 R = $CH_2C(O)OEt$

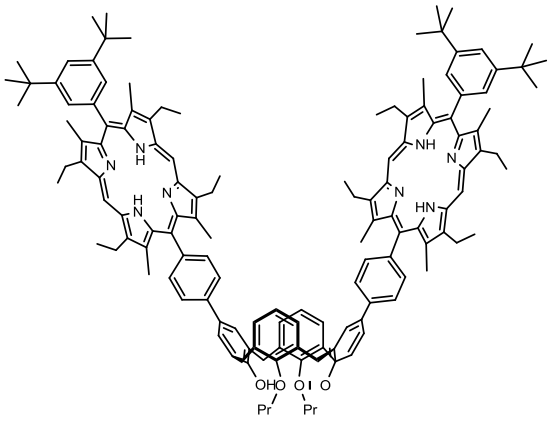

1.32

Figure 1.32: Wide rim appended calixarene bis-porphyrins **1.30, 1.31**[115,116] and **1.32**[117]

Table 1.2: Association constants for wide rim functionalized calixarene bis-porphyrins **1.30**-**1.32**.

K_a (M^{-1})	C_{60}	C_{70}
1.30	3,500	7,200
1.31	1,460	14,500
1.32	-	5,000

1.17 Narrow Rim Calixarene Linked Bis-Porphyrins

1.17.1 Fullerene Binding of Narrow Rim Calixarene Linked Bis-Porphyrins

Dudic and co-workers also prepared a series of the narrow rim appended calix- and thiocalixarene linked bis- and tetra-porphyrins that were originally designed to bind cations through hydrogen bonding with ester oxygens.[118] These bis and tetra-porphyrins displayed an affinity for fullerene binding.[119] Thiocalixarene hosts **1.33e-h** showed lower association of both C_{60} and C_{70} relative to calixarene linked bis-porphyrins **1.33a-d**. The tetra substituted calixarenes **1.33b** and **1.33d** had a reduction in the association of both C_{60} and C_{70} compared to the bis-porphyrin **1.33a** and **1.33c**. The tetra substituted thiocalixarene **1.33f** on the other hand revealed an increase in the association of both C_{60} and C_{70} compared to the bis-porphyrin **1.33e**.

a-d: X = CH3
e-f: X = S
a,c,e,g: R = H,
b,d,f,h: R = Porph

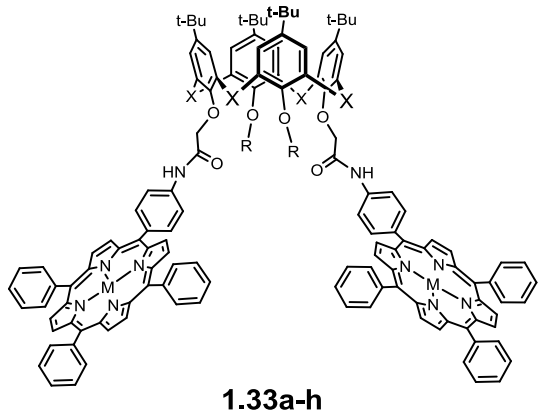

1.33a-h

Figure 1.33: Calix- and thiocalixarene narrow rim bis- and tetra-porphyrins **1.33a-h**.[119,120]

Work on narrow rim calixarene linked bis-porphyrins has similarly been carried out by Hosseini.[121,122] Comparison between the free base phenyl bis-porphyrin **1.33a** prepared by

Dudic and the tolyl porphyrin bis-porphyrin derivative **1.34** reveals a significant increase in the binding for both C_{60} (4.8 - 8.7 x 10^3 M^{-1}) and C_{70} (21 - 38 x 10^3 M^{-1})

A systematic study was carried by investigating the effect of porphyrin type and substituents. Bis-porphyrin **1.35** was substituted with pentafluorophenyl units at the *meso* position in order to investigate whether improvements in fullerene association could be garnered from the close approach observed in X-ray crystal structures of tetrakis(pentafluorophenyl) porphyrin and C_{60}.[123] These structures display close contacts between the *ortho*-F and the center of a 6-membered rings of the fullerene with a distances of 2.93-3.16 Å. Bis-porphyrin **1.36** was substituted with 3,5-*tert*-butylphenyl groups in the *meso* positions of the porphyrin. These substituents were selected based on co-crystallate structures of Co(II) 5,10,15,20-tetra-(3,5-*tert*-butyl phenyl)porphyrin with C_{60} which demonstrate number of close contacts between the porphyrin and the fullerene via CH-π interactions and C_{60} encapsulation by the *tert*-butyl groups.[124] Bis-porphyrin **1.37** was derivatised with *n*-butyls believed to enhance association by wrapping around the fullerene. Bis-porphyrin **1.38** is the 3,5-di-*tert*-butyl phenyl porphyrin but the *tert*-butyl groups have been removed from the wide rim of the calixarene scaffold.[125]

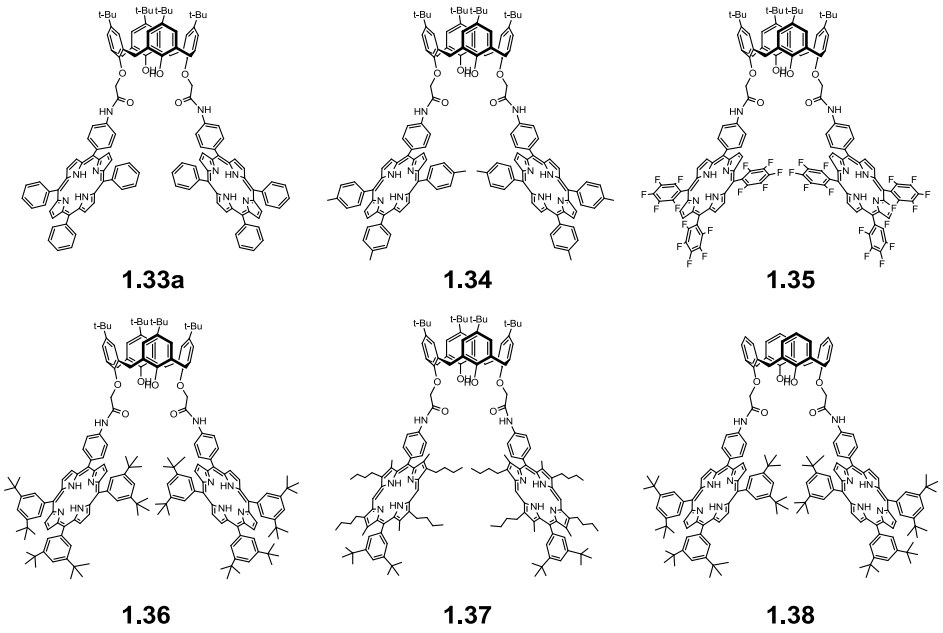

Figure 1.34: Narrow rim functionalized calixarene bis-porphyrins. [119,122]

Table 1.3: Association constants for narrow rim functionalized calixarene bis-porphyrins **1.33a-1.38**.[119,122]

Host	K_a C_{60} (M^{-1})	K_a C_{70} (M^{-1})
1.33a	4,900	21,000
1.34	8,700	38,600
1.35	7,000	13,000
1.36	26,000	234,000
1.37	2,750	-
1.38	32,000	370,000

The largest fullerene association was observed with bis-porphyrin hosts **1.36** and **1.38.** This has been attributed to the number of close contacts between the porphyrin and the fullerene via CH-π interactions by the *tert*-butyl methyls, compared to the phenyl and tolyl substituted porphyrins. Host **1.38** is larger due to the removal of the sterically bulky *tert*-butyl groups on the wide rim of the calixarene. This allows the calixarene scaffold to adopt a more energetically stable conformation.

The pentafluorophenyl host **1.35** did not demonstrate any enhanced binding of fullerenes. This has been attributed to the unfavorable interactions between the electron withdrawing fluorine and the electron deficient fullerenes compared to the more electron donating 3,5-di-*tert*-butyl groups.[126] The host displaying the lowest association for fullerenes was the octaalkyl derivative **1.37**, which may be explained by co-crystallates structures of octaalkyl porphyrins and fullerenes which form porphyrin dimers. Dimerisation is inhibited for the aryl systems especially in more bulky 3,5-*tert*-butyl phenyl porphyrins.

The association of endohedral fullerenes $Sc_3N@C_{80}$ and $Lu_3N@C_{80}$ with **1.36** and **Zn1.36** in 1,2-dichlorobenzene have also been measured.[127] Association constants for both endohedral fullerenes increased by two orders of magnitude compared to $C_{60.}$ The calixarene linked bis-porphyrins are suitable for the purification of endohedral metallofullerenes.

Table 1.4: Binding constants of the zinc and freebase derivatives of **1.36** with fullerenes in 1,2-dichlorobenzene.[127]

	1.36 (M^{-1})	**Zn1.36** (M^{-1})
C_{60}	1.87E+03	1.40E+03
$Sc_3N@C_{80}$	1.34E+05	1.68E+05
$Lu_3N@C_{80}$	1.57E+05	1.77E+05

1.17.2 Computational Modeling of Calixarene Bis-Porphyrins

Computational modeling of the host–guest complex **1.36** with C_{60} has been performed.[121,122,127] Several features of this host contribute to effective fullerene binding. **1.36** adopts a pinched cone conformation with angles between opposing phenyl rings of 44.4 and 85.1° as is observed in similar di-substituted calixarenes. There are two sets of hydrogen bonds between the amide N–H and the calixarene phenol oxygen (NH···O) and between the calixarene phenol hydroxyl and an adjacent calixarene ether oxygen (OH···O). The two planar porphyrin molecules bind to C_{60} via van der Waals attractions with an interplaner angle of 50.1°. The C_{60} is arranged with 6:6 ring junctions centered over the porphyrin at distances of 2.76, 2.67, 2.71 and 2.70 Å, as expected from arrangements in co-crystallate structures. In addition to van der Waals attractions, there are a significant number of CH-π interactions between either the *ortho*-protons of the porphyrin *meso* phenyl groups or the methyl protons of *tert*-butyl groups adjacent to the fullerene C–H to six-membered ring centroids of C_{60} (2.7-3.2 Å).

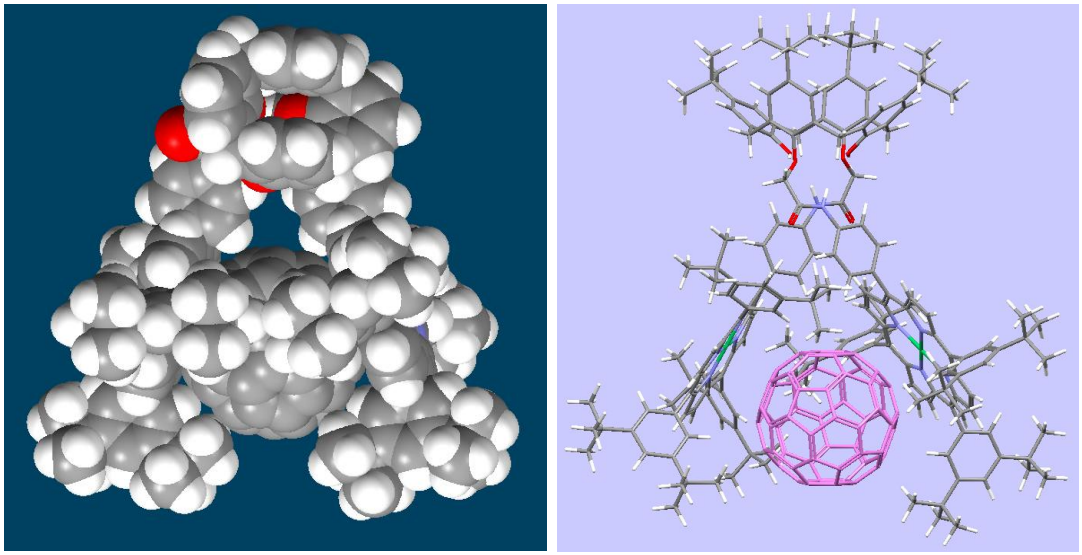

Figure 1.35: Structure of the host–guest complex of the palladium derivative of **1.38,** calculated using molecular mechanics (UFF Force Field)[125] and **1.36,** calculated using two layer ONIOM modeling (/B3LYP/6-31G(d);UFF) for the Nickel(II) Derivative and C_{60}[127]

Host **1.38** has similarly been modeled using molecular mechanics.[125] These models show a variation of the relative orientation of the calixarene scaffold, which appear to be due to removal of the steric crowding caused by the *tert*-butyl groups on the wide rim of the calixarene. This decreased steric effect may allow for better hydrogen bonding on the narrow rim.

1.17.3 Photophysical Measurements of Calixarene Bis-Porphyrin

Femtosecond transient absorption spectroscopy was used to obtain further insights into the excited-state interactions between the bis-porphyrins (**1.36** and **Zn1.36**) and the fullerenes C_{60}, $Sc_3N@C_{80}$ and $Lu_3N@C_{80}$. All of the systems were probed with 150 fs laser pulses. Bis-porphyrins displayed a singlet excited state immediately after the laser pulse as a result of instantaneously deactivating excited state. The singlet-singlet transition include characteristic absorption changes at 500-810 nm, namely a quenching of the spectrum at 540 nm and the appearance of two new bands at 660 and 730 nm. These features correlate with what would be expected for singlet–singlet transitions for ground state bis-porphyrins. The lifetime of the photoexcited state decay within 9.8 ns and 2.4 ns for **1.36** and **Zn1.36** respectively to a triplet excited state, giving a new maxima at 780 and 860 nm for **1.36** and **Zn1.36**. The triplet excited state returns to ground state slowly over tens to hundreds of μs.

In the case of the fullerenes C_{60}, $Lu_3N@C_{80}$ and $Sc_3N@C_{80}$, excitation at 420 nm gives rise to transient absorption changes that are dominated by marked singlet–singlet absorptions in the near-infrared. C_{60} displays a fingerprint absorption at 920 nm. Fullerenes are then subject to a rapid intersystem crossing process to the energetically lower lying triplet excited state. The trimetallic cluster enclosed exerts a dramatic effect on the intersystem crossing, shortening the lifetime of the singlet state.

Transient absorption spectroscopy of bis-porphyrin **1.36** and C_{60} confirmed the charge transfer to form the **1.36**$^{\bullet+}$**-C$_{60}$**$^{\bullet-}$ species. After subjecting the species to 150 fs laser pulse, the formation of a porphyrin excited state was observed, as seen in the spectral signatures of free **1.36**. in contrast to the free host the spectra transforms rapidly ($\tau_{1/2}$ = 100 ps) indicative of two new species. Spectral signatures characteristic of the one-electron oxidized form of **1.36** and the one-electron reduced form of $C_{60}^{\bullet-}$, are observed at 600–800 and 1080 nm, respectively

consistent with a process of intramolecular charge transfer that yields a **1.36**$^{\bullet+}$ **-C$_{60}$**$^{\bullet-}$ radical-ion-pair state.

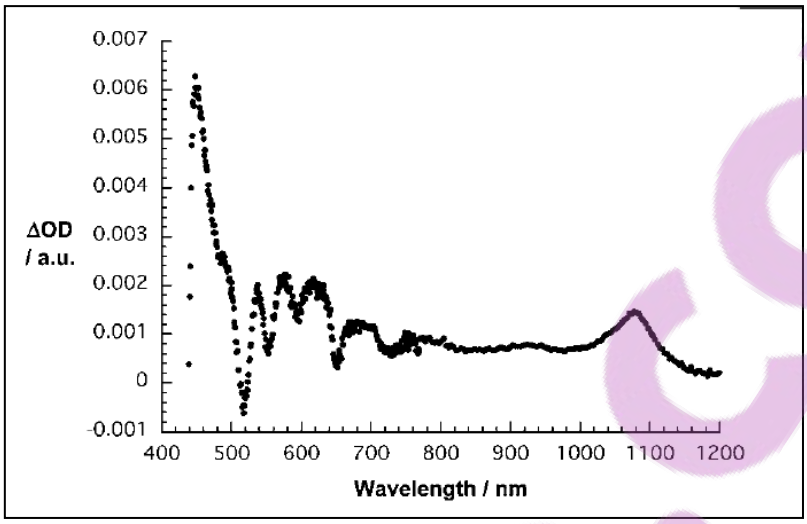

Figure 1.36: Differential absorption spectra (visible and near-infrared) obtained upon femtosecond flash photolysis (420 nm) of **1.36** (4.1 x 10^{-6} M) and C_{60} (2.0x 10^{-5} M) in argon-saturated toluene with a time delay of 50 ps at room temperature.[127]

In toluene solutions the charge separation in **1.36-C$_{60}$** and **Zn1.36- C$_{60}$** are fast, with lifetimes of 100 ps and 85 ps, respectively (Table 1.1). The charge recombination step displayed lifetimes of 1458 ps for **1.36-C$_{60}$** and 535 ps for **Zn1.36-C$_{60}$**. Using a solvent mixture of acetonitrile/toluene (5:1) increases the association of the bis-porphyrin and fullerenes,[122] as well as increasing the solvent polarity, results in decreased lifetime of the charge separated state accelerating the charge recombination from 1458 to 535 ps for **1.36-C$_{60}$** and 535 to 350 ps for **Zn1.36-C$_{60}$**.

Table 1.5: Photophysical properties of **1.36** and **Zn1.36** with fullerenes C_{60}, $Lu_3N@C_{80}$ and $Sc_3N@C_{80}$ obtained by femtosecond flash photolysis measurements for the studied assemblies.[127]

Host guest	τ_{CS}/ps	τ_{CR}/ps	Solvent
C_{60}-1.36	100	1458	Toluene
C_{60}-1.36	80	914	Toluene – acetonitrile (5:1)
C_{60}-Zn1.36	85	535	Toluene
C_{60}-Zn1.36	60	350	Toluene – acetonitrile (5:1)
$Lu_3N@C_{80}$-1.36	22	229	*o*-Dichlorobenezene
$Lu_3N@C_{80}$-Zn1.36	51	779	*o*-Dichlorobenezene
$Sc_3N@C_{80}$-43	49	284	*o*-Dichlorobenezene

The endohedral fullerenes exhibit a charge transfer state which is reversed and it is the one-electron reduced form of **1.36** and the one-electron oxidized form of $Lu_3N@C_{80}$ and$Sc_3N@C_{80}$ that develop. This $Lu_3N@C_{80}^{\bullet+}$ **1.36**$^{\bullet-}$ radical-ion-pair state formation has been attributed to the lower HOMO-LUMO orbitals of the endohedral fullerene.

1.18 Aims of this Research

The research described in this thesis has two aims. First is to prepare new bis-porphyrins hosts for the binding of fullerenes C_{60}, C_{70}, and $Lu_3N@C_{80}$ and investigate their association properties through UV-visible titration studies. Several new hosts have been developed through modification of the calixarene scaffold, the linkers appending the porphyrins as well as the porphyrin substituents themselves.

The geometry of the calixarene scaffold provides a level of preorganisation that is ideal for the construction of bis-porphyrins with the correct distance and arrangement for the formation of host guest complexes with fullerenes. Large fullerene binding constants are necessary for meaningful photophysical studies because such measurements must be done at low concentrations where undesired dissociation becomes favored. The interaction of the bis-porphyrin hosts with fullerenes is investigated by computational modeling.

The second objective of this research is to prepare molecular triads for the purpose of mimicking the primary events of natural photosynthesis, namely photoexcitation and electron

transfer. Ferrocene is a suitable secondary electron donor for a photoactive system. After photoinduced charge separation between the porphyrin and the fullerene occurs, the ferrocene can reduce the porphyrin radical cation. This process allows for a greater spatial separation between charges and can increase the lifetime of the charge separated state. Ferrocene can be covalently attached to the wide rim of the calixarene scaffold by a variety of different methods.

Throughout this thesis computational modeling has been utilized to estimate energies of optimization and the geometric and electronic structures of the hosts as well as the host-guest complexes. Modeling has also been used to examine structural differences due to the introduction of ferrocene to the wide rim. Association constants with fullerenes have been measured and charge transfer bands have been observed using UV-visible absorption spectroscopy. Charge transfer bands can be used as an estimation of the electronic coupling between the porphyrins and fullerenes.

The contents of the remainder of this thesis are as follows:

Chapter two discusses the synthesis of, and modification of the porphyrin substituents for calixarene linked bis-porphyrin hosts. New methods for the synthesis and modification of porphyrins with different *meso*-substituted via transition metal coupling are presented. The first is a "mixed" Suzuki coupling for preparation of porphyrins with different substituents at the 15-position. The second is a nickel catalyzed reaction to prepare phenoxyporphyrins.

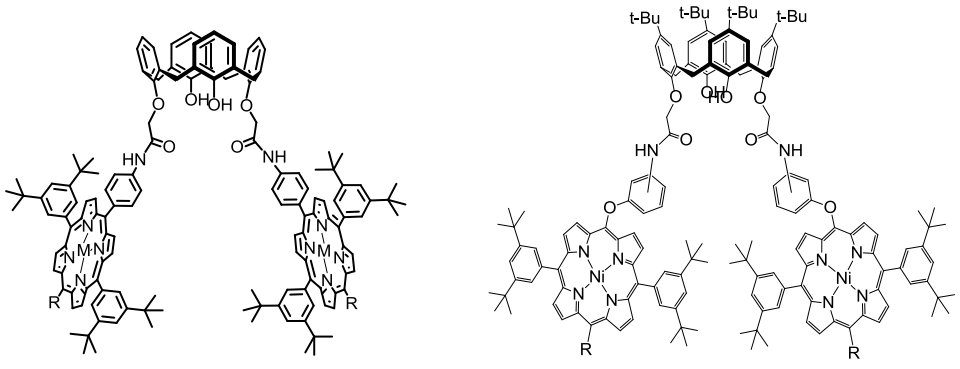

Figure 1.37: Examples of hosts made in Chapter Two.

In Chapter three, the modification of the calixarene scaffold and the methylene linkers is described. An extended linker has been prepared by selective alkylation of the narrow rim

hydroxyl groups, in order to investigate the increased flexibility on the host-guest association. The calixarene scaffold has also been modified by tetra alkylation of all the hydroxyl groups on the narrow rim to remove the hydrogen bonding between the hydroxyl groups and the ether oxygen. Removal of this hydrogen bonding motif allows increased flexibility of the scaffold. Variable temperature ^{1}H NMR studies have also been employed to help describe the differences in binding though changes to the conformation of the calixarene.

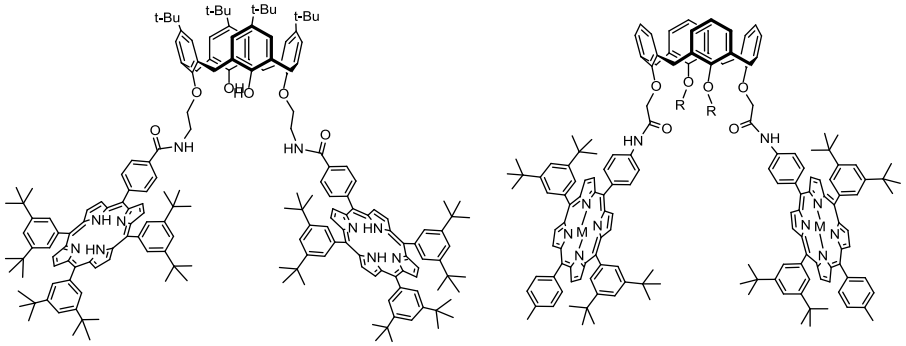

Figure 1.38: Examples of hosts made in Chapter Three.

Chapter Four discusses ferrocene functionalization of bis-porphyrin hosts on the wide rim of the calixarene scaffold via palladium catalyzed coupling reactions. Derivatization of this type is expected to increase the lifetime of the charge separated state.

Two palladium catalyzed reactions have been used to append ferrocene to the wide rim of the calixarene. The first type of palladium coupling is Sonogashira coupling, which has been used to couple both ethynyl ferrocene and ethynyl phenyl ferrocene to the wide rim. These new hosts have secondary donors with different spatial geometries and distances from the porphyrins on the narrow rim. The second form of palladium coupling used is Suzuki coupling. This method has been used to couple ferrocene phenyl boronic acid to the wide rim of the calixarene. Two different isomers of a ferrocene functionalized bis-porphyrin have been prepared via tetra-alkylation of the calixarene, with ferrocene groups to be appended to the phenyl rings both *para* to the porphyrin amide as well as *para* to the n-butyl groups. Fluorescence spectroscopy of these hosts have carried out in order to determine whether the ferrocene units are at situated to allow electron transfer to the porphyrin sensitizers.

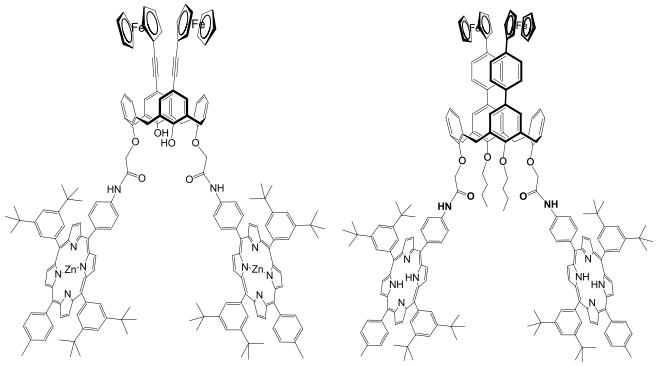

Figure 1.39: Examples of ferrocene functionalized hosts made in Chapter Four.

Chapter five discusses the functionalization of calixarene bis-porphyrin hosts on the wide rim of the calixarene scaffold with ferrocene via amide coupling reactions. A brief summary of attempted methods for the reduction of the wide rim nitro groups to amines is presented for dialkylated calixarenes. Tetra-alkylation of the calixarene scaffold results in two isomers of a ferrocene functionalized bis-porphyrin, depending on the order of alkylation. The ferrocene groups have been appended to the phenyl rings *para* to the porphyrin amide and *para* to the *n*-butyl groups. Fluorescence spectroscopy of these hosts has been carried out in order to determine if the ferrocene units are at a significant distance from the porphyrins for electron transfer.

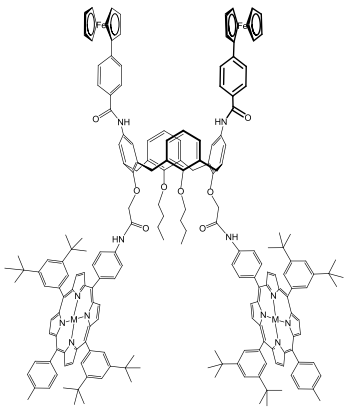

Figure 1.40: An example of ferrocene amide functionalized hosts made in Chapter Five.

Chapter 2

Synthesis and Modification of Porphyrins for Calixarene Bis-Porphyrin Hosts

2.1 Introduction

Narrow rim appended calixarene bis-porphyrins, prepared by attachment of amino porphyrins to carboxylic acid functionalized calixarene have been shown to bind fullerenes. Variation of the substituents on the porphyrin at both the *meso* and β-pyrrole positions have been explored and have been shown to have a significant effect on the association with fullerenes.[128,129] The bis-porphyrin host **1.36** with three bulky 3,5-di-*tert*-butyl phenyl groups at the *meso* positions of the porphyrin displays the highest association for both C_{60} and C_{70}. The significant increase in association of **1.36** has been attributed to the numerous of CH-π close contacts of the *tert*-butyl methyl groups with the fullerene. The *tert*-butyl methyls at the 10 and 20-positions of the porphyrin show the closest contacts with the fullerenes with distance ranging from 2.79-3.28 Å. There seems to be lesser influence however, for the CH-π interactions with the *tert*-butyl methyl groups attached to the phenyl group at the 15-position of the porphyrin due to the angle of the porphyrin planes.

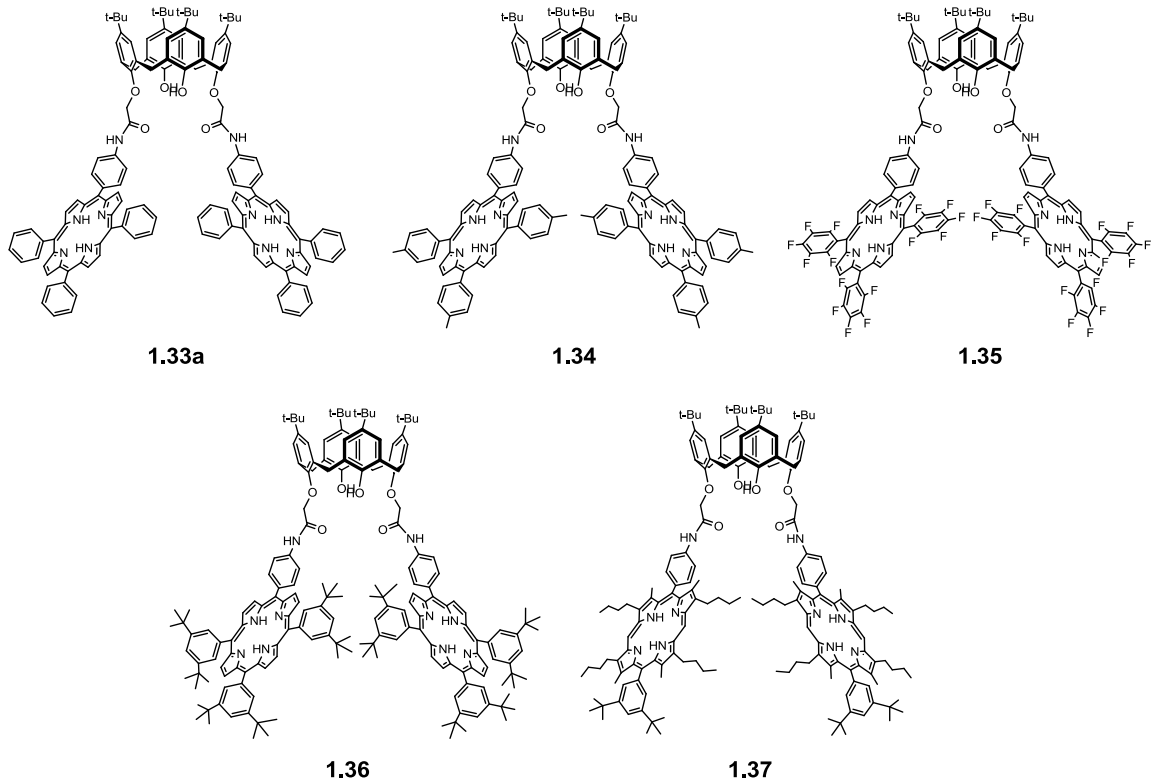

Figure 2.1: Narrow rim functionalized calixarene bis-porphyrins.[120,128,129]

Advances in catalysis with porphyrins have given porphyrin chemists an elaborate set of tools for the preparation of porphyrins bearing multiple functionalities. In this chapter the synthesis and modification of porphyrins bearing different substituents are reported. These new porphyrins have been appended to calixarenes to make new bis-porphyrins, which are to be employed as hosts for fullerenes.

2.1.1 Direct Porphyrin Synthesis versus Modification

There are two main methods for the synthesis of porphyrins. The method developed by Adler and Longo involves the addition of a benzaldehyde and pyrrole refluxing in propionic acid.[130] Although this reaction gives reasonable yields with simple benzaldehydes and can be performed on a large scale, it cannot be performed with sensitive functional groups. Modern alternative described by Lindsey employs milder conditions that allow porphyrins to be prepared with more sensitive aldehydes in high yield.[131] These methods have been thoroughly exploited and have been modified to prepared porphyrins with different substituents by using a statistical mixture of different aldehydes. The preparation of 5-(*para*-aminophenyl)-10,15,20-tris(3,5-di-*tert*-butylphenyl)porphyrin has been reported by Imahori *et al.*[41] is shown in Scheme 2.1. Yields of these substituted porphyrins are low, especially if the reacting aldehydes have differing reactivities. These reactions may lead to the formation of scrambled, statistical mixtures containing non-substituted or disubstituted porphyrins. These mixtures can be difficult to separate chromatographically or by recrystallization. A contemporary method for the preparation substituted porphyrins is to modify an existing porphyrin core.

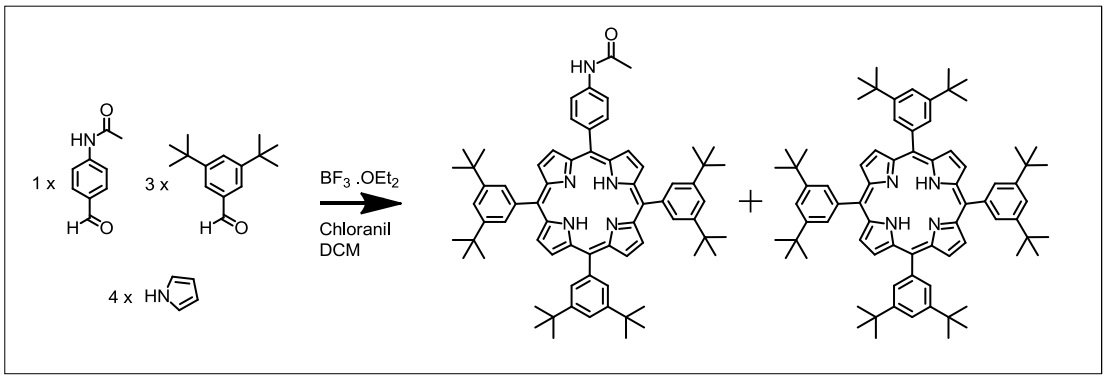

Scheme 2.1: Lindsey's original procedure for A_3B substituted porphyrin.[131]

The development of efficient strategies leading to diverse substitution patterns of porphyrin rings is of great importance as they can provide an accurate method for tailoring porphyrins for a specific application. Different chemical strategies leading to A_2B_2 and A_2BC have been demonstrated. The simplest preparation for a A_2B_2 system involves the acid catalyzed condensation of dipyrromethane with aldehyde.[132,133] Other methods involve condensation of dipyrromethane-1-carbinols or the elaborate acyl-dipyrromethane route by Lindsey *et al.*[134] Alternate substitution patterns may be accessed via a stepwise modification of a preformed 5,15-A_2 compound which is then subjected to further functionalization.[135]

2.1.2 Palladium and Nickel Catalyzed Reactions for Porphyrin Modification

Organometallic and transition metal coupling reactions play an important role in modern synthetic chemistry, allowing one step carbon-carbon or carbon-hetroatom bond formation.[136] Many transition metal catalysts have been developed for the preparation of elaborate and multifunctional chromophores. In most cases organometallic reagents and metal catalysts were initially developed for small aromatic molecules and subsequently have been adapted for specific applications in porphyrin chemistry.

Palladium catalyzed reactions are favored for the modification of porphyrins. They require relatively mild reaction conditions, are accessible from commercially avaliable starting materials, are high yielding and are suitable for many functional groups. Bromoporphyrins are the key starting materials for palladium catalyzed reactions and are readily prepared using *N*-bromosuccinimide (NBS) to prepare porphyrin brominated at both the *meso*- and β-positions. A number of different types of palladium catalyzed reactions are available for the preparation of different types of carbon-carbon bonds and are shown in Scheme 2.2.

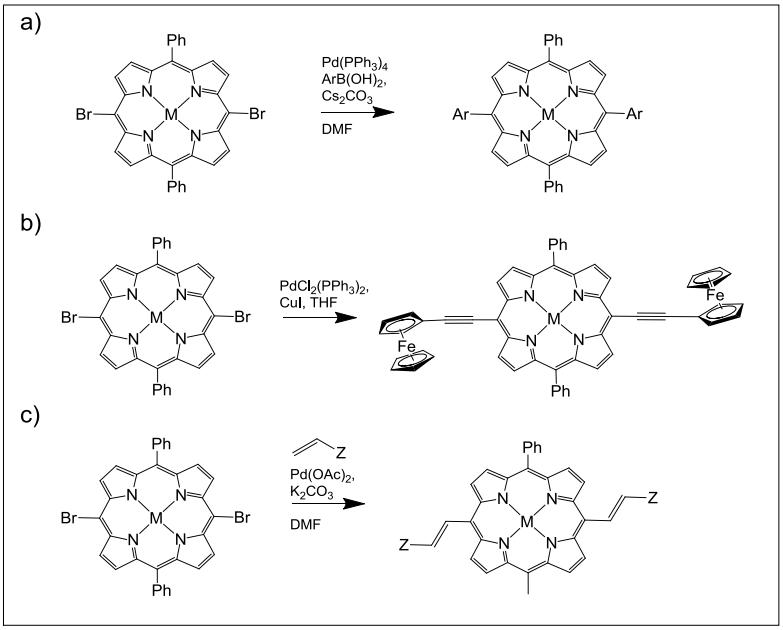

Scheme 2.2: Various palladium catalyzed reactions for modifying the porphyrin core.[137]

Suzuki reactions (Scheme 2.2a) are used to couple vinyl or aryl boronic acids to halides, catalyzed by a palladium(0) complex and an appropriate base.[138] Recent catalyst and method developments have broadened the possible applications enormously. Organoboranes or boronate esters may be used in place of boronic acids for example.[139] Borylated porphyrins can be obtained via palladium catalyzed reaction of bromo porphyrin with pinacolborane.[140] Typically, mild conditions and various aryl groups can be used to prepare A_3B A_2B_2 and A_2BC forms.

Sonogashira reactions (Scheme 2.2b) are used for the coupling of terminal ethynyl substituted chromophores with an aryl or vinyl halide.[141] The reaction is achieved with a palladium(II) catalyst, a copper(I) co-catalyst and an appropriate base. Typically iodo or bromo porphyrins are reacted with terminal acetylenes to give acetylene substituted porphyrin.[142] Ethynyl bridges have strong π conjugation and allow effective electronic interactions within systems. Sonogashira coupling has been used to construct large assemblies of porphyrin units and has recently been used to incorporate ferrocene units by connection to porphyrins through an ethylene linker.[143-145] Typically Sonogashira reactions require the presence of copper iodide as a co-catalyst. Therefore metallated porphyrins must be used in order to avoid undesired metallation by copper.

Alternative approaches involving palladium mediated coupling are Heck[146] and Stille[147] reactions (Heck coupling shown in Scheme 2.2c only). The Heck method is used for coupling

of unsaturated halides with an alkene in the presence of base and palladium(II) catalyst to form substituted alkenes. Heck coupling has been used to introduce alkenyl functionality into both *meso* and β position of the porphyrin. Stille is used for coupling of an organotin compound and an organic halide with palladium(0) catalyst. Tin compounds may be prepared from their corresponding bromides and are also commercially available and cheaper than boronates used for Suzuki coupling. Generally C-C bond formation is performed on haloporphyrins and non-porphyrin tin reagents; although it has been shown that stannyl porphyrins can be prepared via Stille reactions using organostannanes.[148]

Nickel demonstrates similar activity as a catalyst in the carbon-carbon coupling of *meso* dibromoporphyrin nickel with carbonyls compounds.[149] The catalytic system operates under mild conditions and allows access to a series of potentially useful *meso*-functionalized porphyrins on large scale. The porphyrins can also be functionalized by way of nickel catalyzed C-O and C-N bond forming reactions by reaction of the *meso*-dibrominated nickel porphyrin with oxygen and nitrogen based nucleophiles under mild reaction conditions (Scheme 2.3).

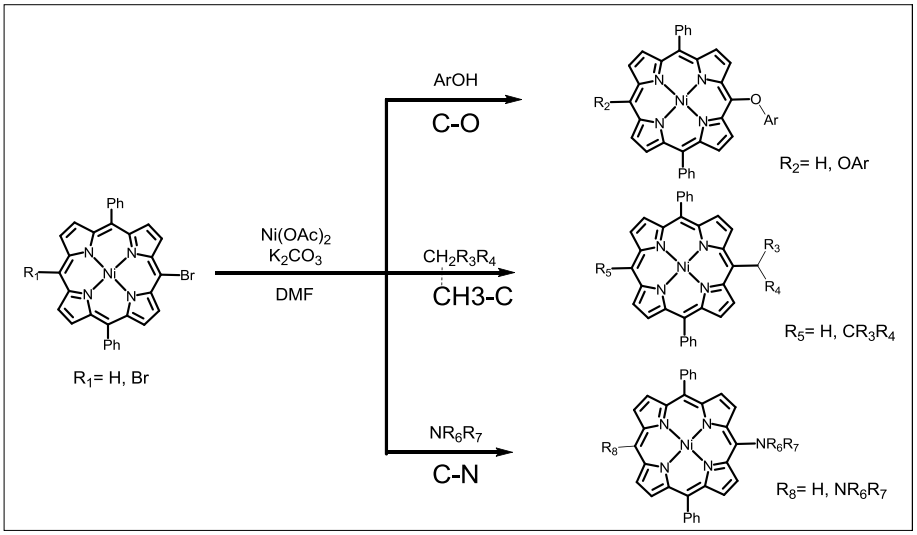

Scheme 2.3: Nickel catalyzed reactions with phenols, carbonyls and amines to prepare modified porphyrins.[149]

2.2 Aim and Strategy

The aim of this chapter is to synthesize and modify porphyrins for attachment to calixarenes and to explore the effect of the porphyrin modification on the binding of fullerenes. Suzuki coupling has been employed for the preparation of A_2BC substituted porphyrins for coupling to the calixarene scaffold. Experimental data and computational modeling studies, porphyrins substituted with 3,5 di-*tert*-butyl phenyl at the 10 and 20-*meso* position display the highest association for fullerenes. Therefore these structures have been retained in the synthesis and modification of the porphyrins. Coupling of the porphyrin to the calixarene scaffold at the 5–position of the porphyrin was achieved with an amide bond. A 4-amidophenyl boronic acid, which may be hydrolyzed to the corresponding amine upon coupling, was employed. The porphyrin substituent at the 15-position can be changed to investigate the influence on this substituent on fullerene binding.

New bis-porphyrins **2.1**-**2.3** have been prepared and the effect of different substituents on fullerene association explored by UV-visible titrations. Porphyrin to fullerene charge transfer band for these host-guest complexes have been used to estimate the electronic coupling between the porphyrins and fullerene. X-ray crystal structures of co-crystallate porphyrins and fullerene are discussed as a method of explaining differences between the fullerene association of hosts **2.1**-**2.3.**

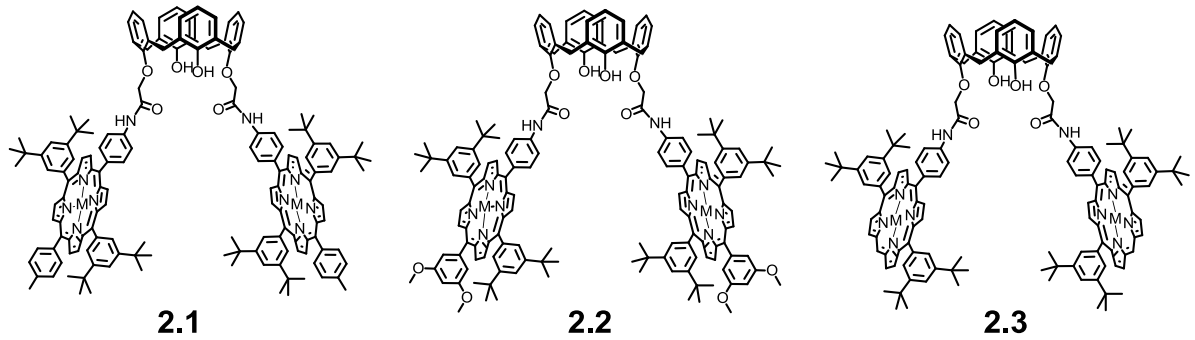

Figure 2.2: New calixarene linked bis-porphyrin hosts prepared in Chapter Two via Suzuki coupling of porphyrins.

A nickel catalyzed reaction has been employed to form porphyrin phenyl ethers. These ether porphyrins were appended to the calixarenes scaffold via amide coupling to give bis-porphyrins **2.4** and **2.5**. These bis-porphyrins offer increased flexibility within the porphyrin

substituents that may aid the host's ability to accommodate fullerenes. Both the 3-aminophenoxy porphyrin as well as the 4-aminophenoxy porphyrin were prepared and coupled to calixarenes in an attempt to investigate the effect of the ether functional groups and the angular arrangement of the porphyrins with respect to the calixarene. The effect on fullerene association was explored using UV-visible titrations.

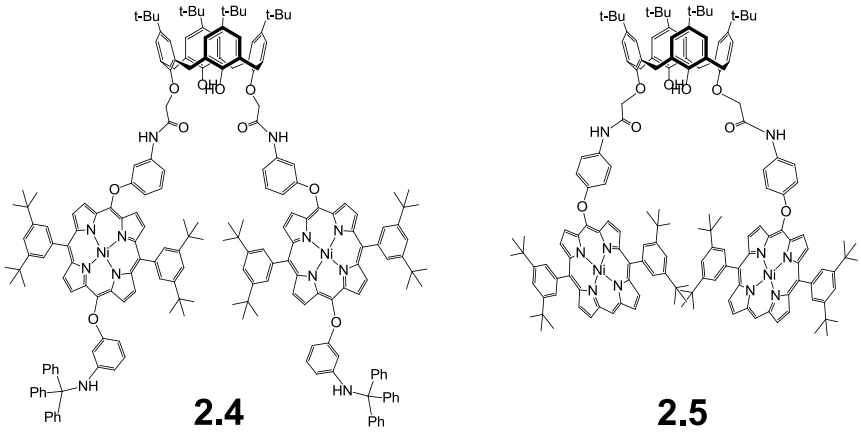

Figure 2.3: Calixarene linked bis-porphyrin hosts prepared in Chapter Two via nickel catalyzed coupling.

2.3 Computational Modeling of Bis-Porphryins

Computational molecular modeling has been employed to study the structure of the calixarene linked bis-porphyrin hosts and the supramolecular interaction between the hosts and fullerenes C_{60} and $C_{70.}$ Molecular models of the complexes have been calculated using GAUSIAN 09 with a two layer ONIOM method.[150,151] The ONIOM method (Our Own N-layered Integrated Orbital and Molecular mechanics) developed by Morokuma and co-workers uses different computational approaches to describe layers of the molecule.[150] This allows more accurate yet computationally demanding calculations to be carried out on key areas of the molecule, in tandem with less demanding calculations. This results in significantly reduced computational times whilst maintaining accuracy of calculations.

The calixarene linked bis-porphyrin host-guest complexes have been modeled in two layers The calixarene scaffold and the amide linkers have been modeled in high layer using density functional theory (DFT)[152] with a B3LYP hybrid functional[153] using a 6-31G basis set.[154,155] This method allows for adequate determination of bond lengths and angles in organic systems to be made.[156] The porphyrins and fullerene were modeled in the low layer by Molecular

Mechanics (MM)[157] using a universal force field (UFF).[158] Molecular mechanics can be used to adequately model both the van der Waals interaction between the curved π surface of the fullerene and the planar π surface of the porphyrin as well as the bond lengths and angles of the two molecules. Bis-porphyrins were modeled with nickel or palladium metalloporphyrins, which results in better approximation of planarity of the porphyrin moiety compared to free base porphyrins. For the computational modeling of **2.4** and **2.5** the amines and trityl phenyls were removed to simplify optimizations.

2.3.1 Computational Modeling of Bis-Porphyrins 2.1-2.3

Models of the host:C_{60} complexes **2.1-2.3** have similar structural characteristics. The calixarene adopts the same pinched cone conformation observed in **1.36** and **1.38,** due to the hydrogen bonding motif adopted by the phenolic groups of the narrow rim. The angle of the phenol rings are all approximately 78° and the angle of the alkylated phenyl rings are approximately 23°. The hydrogens of the hydroxyl groups point toward the ether oxygen of an adjacent phenyl and the hydrogen bonding distance between the phenol hydroxyl and ether oxygen are consistent between each host, ranging from 1.90-1.95 Å. Hydrogen bonding distances between the N-H of amide and the oxygen of the neighboring ether are 2.44 and 2.28 Å. The porphyrins are tilted slightly towards each other due to CH-π interactions between the methyl groups of one *tert*-butyl phenyl and the phenyl ring on the second porphyrin. The center to center distance between the porphyrin metal centers is 9.88-9.93 Å, with an angle between the two 24-atom porphyrin mean planes of 72.4°. The C_{60} is arranged with 6:6 ring junctions centered over the porphyrin at a distance of 2.76-3.21 Å. For each host the number of CH-π interactions varies. For **2.1** and **2.2** there are six CH-π interactions from *ortho*-protons of the phenyl on the 10, 20 and 15-position of the porphyrin. In **2.3** there are no substituents on the 15-position and the number of CH-π interactions available is reduced to four. All hosts are substituted at position 10 and 20 with 3,5 di-*tert*-butyl phenyls which provide up to four CH-π interactions between the terminal C-Hs of the *tert*-butyl groups and the fullerene ranging from 2.7-3.3 Å. Host **2.2,** which is substituted with 3,5-di-methoxyphenyls at the 15-position has an additional two CH-π interactions spanning between the methyl groups and fullerene unit which to further enhance interactions. A table of key structural characteristics for hosts **2.1-2.3** with C_{60} is given in Table 2.2.

Table 2.1: Key geometric features of the molecular modeling (ONIOM/B3LYP/6-31G(d);UFF) for the nickel(II) derivative of host-guest complexes of **2.1**, **2.2** and **2.3** with C_{60}.

Host:C_{60}	**2.1**	**2.2**	**2.3**
Calixarene ester functionalized phenyl ring angle (°)	23.8	23.1	23.6
Calixarene phenol ring angle (°)	78.2	77.7	78.5
Hydrogen bonding distance phenol O-H ether O (Å)	1.90, 1.90	1.90,1.95	1.90, 1.94
Hydrogen bonding distance amide N-H ether O (Å)	2.27, 2.40	2.41, 2.29	2.27, 2.40
Porphyrin center to center distance (Å)	9.94	9.88	9.88
Interplanar angle for the 24-atom porphyrin mean plane(°)	74.2	72.0	72.4
Porphyrin metal to fullerene 6:6 junction distance (Å)	2.81, 3.36 2.96, 3.03	2.76 3.17 2.90, 3.16	2.75, 3.22 2.87, 3.17
Total number of CH-π interactions from *o*-protons, *tert*-butyls methyl and methoxy methyls	10	12	8
CH-π distances between methyl groups on the *tert*-butyl and *tert*-butyl phenyl second porphyrin. (Å)	2.94	2.97	2.93

The fullerene was removed and the models of **2.1-2.3** recalculated. All the reoptimized models show that the 24-atom porphyrin mean planes decreases to an angle of 55-57° and a porphyrin to porphyrin distance of 8.2-8.3Å. As the porphyrins approach one another, the angle between the functionalized calixarene phenyls decreases and the distance in the hydrogen bonding motif increases. The close approach of porphyrins allows stronger CH-π interaction between the porphyrin 3,5-di *tert*-butyl phenyls. The calculated structures of the host-guest complexes and the hosts **2.1-2.3** are shown in Figure 2.4-2.5 respectively. A table of key structural characteristics for hosts **2.1-2.3** are given in Table 2.2.

Table 2.2: Key geometric features of the molecular modeling (ONIOM/B3LYP/6-31G(d);UFF) for the nickel(II) derivative of hosts of **2.1**, **2.2** and **2.3**.

Free host	**2.1**	**2.2**	**2.3**
Calixarene ester functionalized phenyl ring angle (°)	21.2	18.9	17.6
Calixarene phenol ring angle (°)	77.4	75.9	75.5
Hydrogen bonding distance phenol O-H ether O (Å)	1.94,1.95	1.97,1.97	1.99,2.00
Hydrogen bonding distance amide N-H ether O (Å)	2.44,2.48	2.48,2.51	2.55,2.51
Porphyrin center to center distance (Å)	8.35	8.58	8.35
Interplanar angle for the 24-atom porphyrin mean plane (°)	55.9	56.2	57.4
CH-π interaction between methyl groups on the *tert*-butyl and *tert*-butyl phenyl second porphyrin (Å)	2.77	2.85	2.93

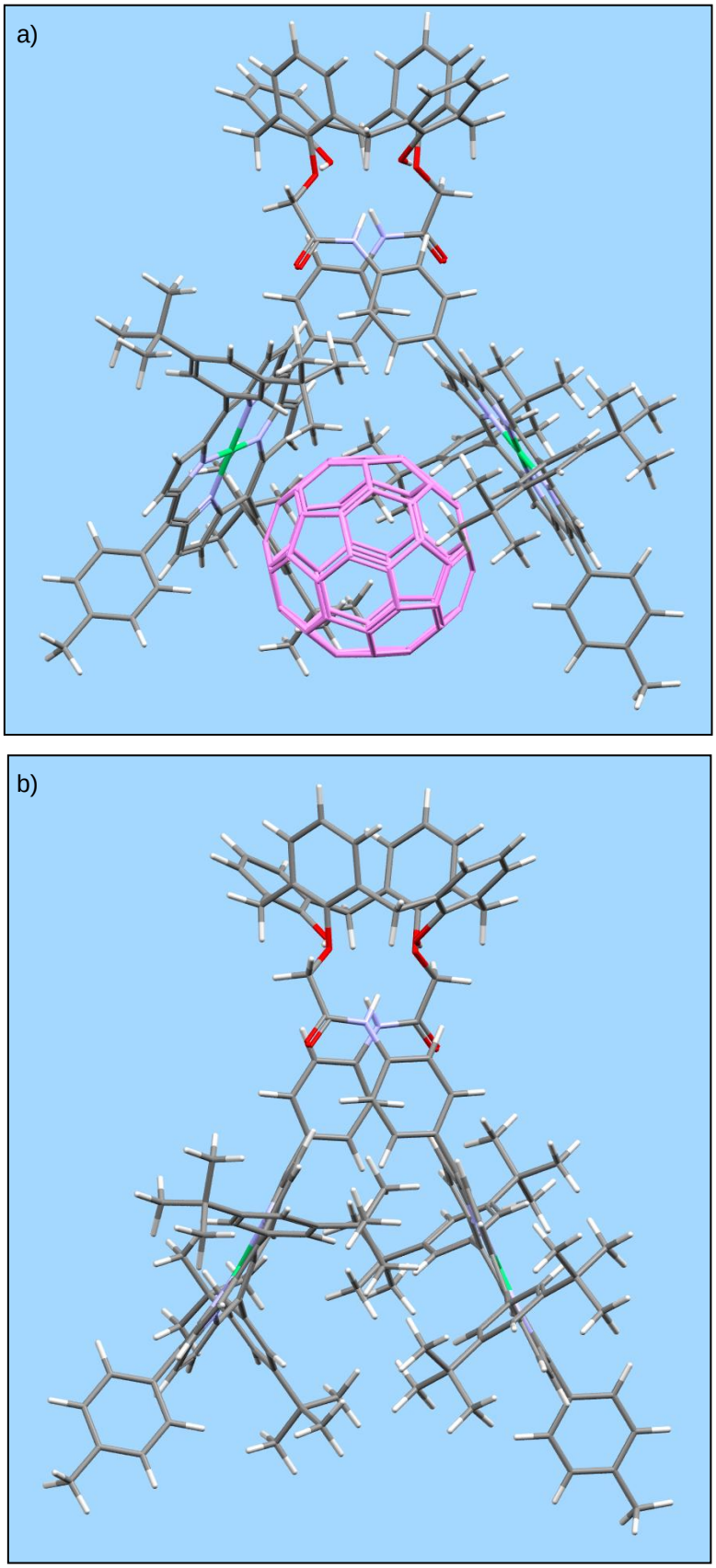

Figure 2.4: Calculated structures (ONIOM/B3LYP/6-31G(d);UFF) for the nickel(II) derivative of a) host–guest complex **2.1** with C_{60} and b) host **2.1** without C_{60}.

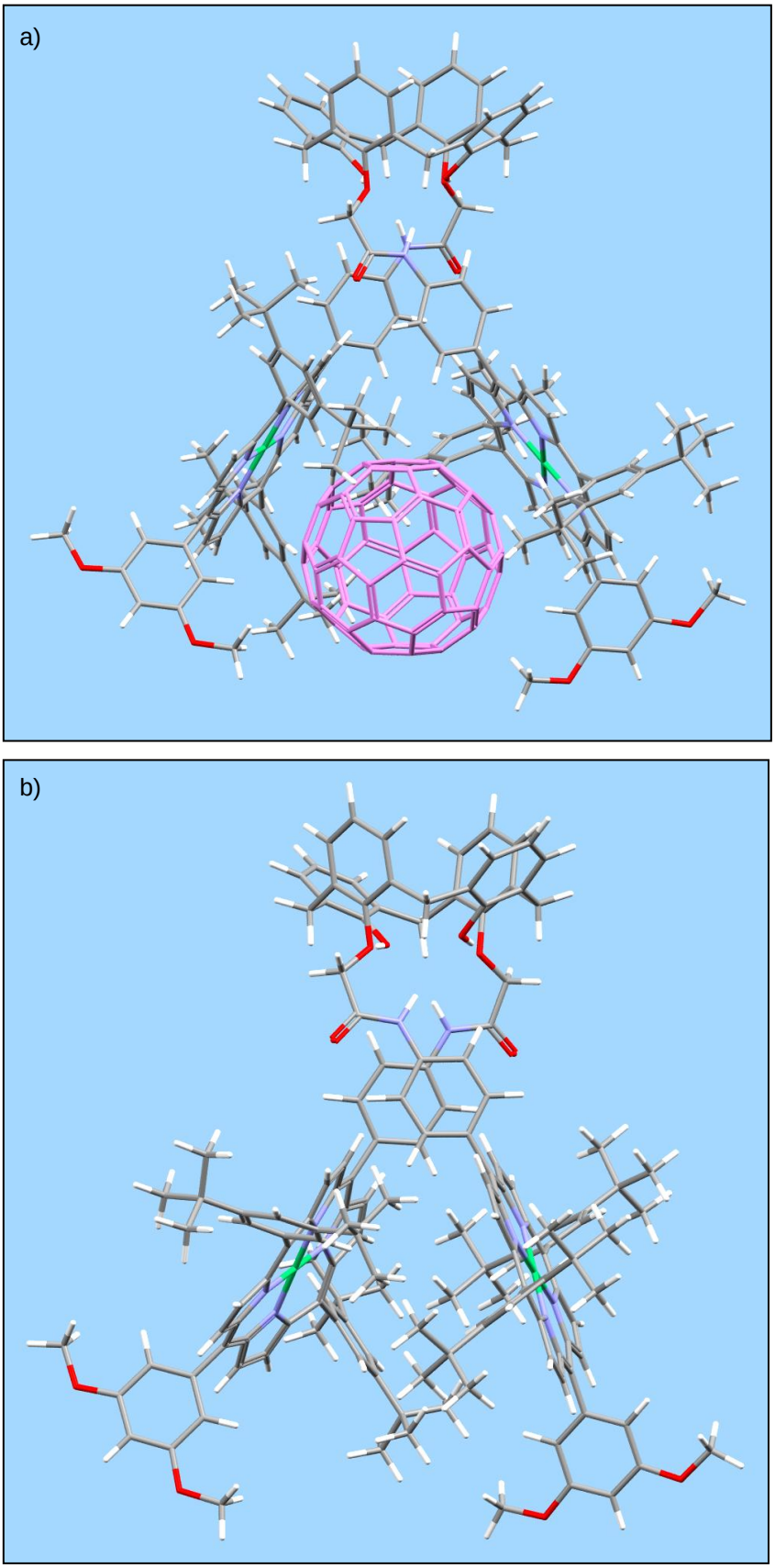

Figure 2.5: a) Calculated structures (ONIOM/B3LYP/6-31G(d);UFF) for the nickel(II) derivative of a) host–guest complex **2.2** with C_{60} and b) host **2.2** without C_{60}.

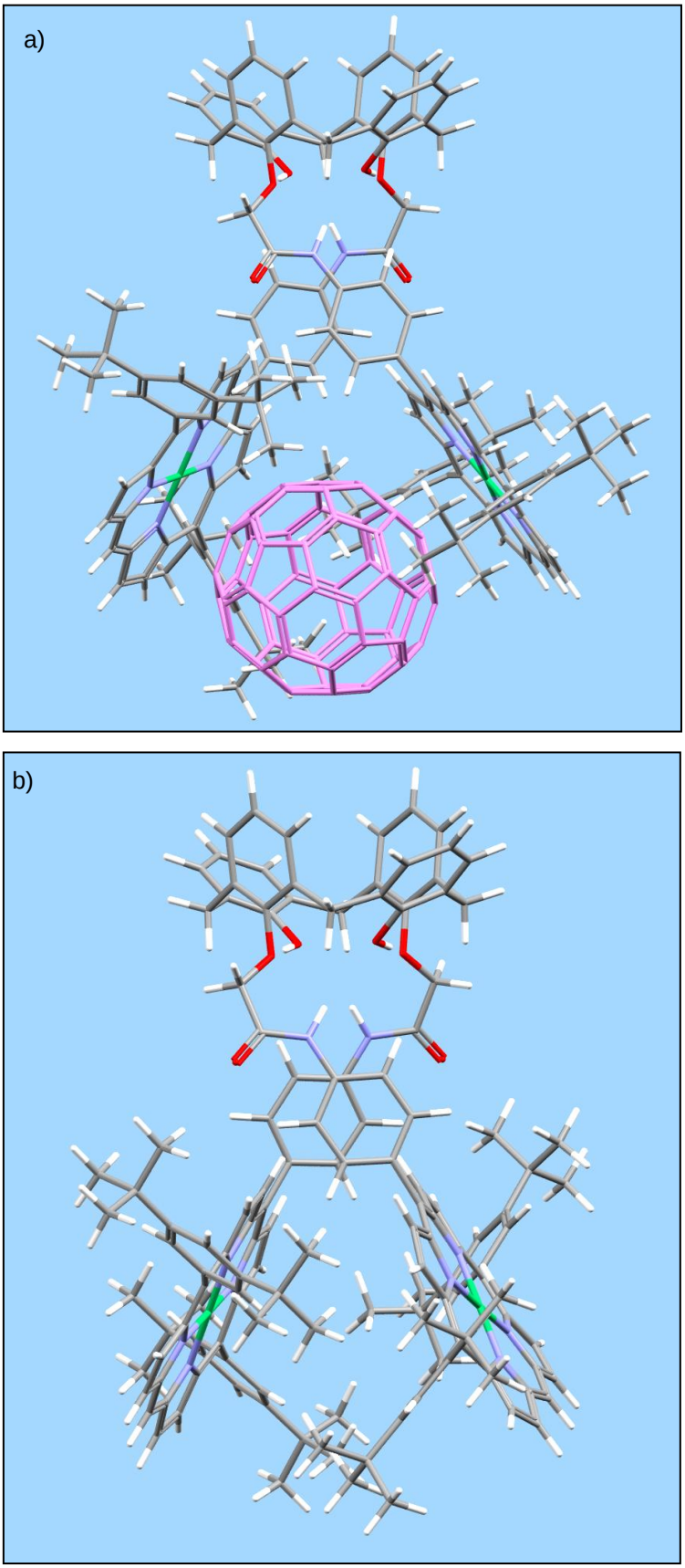

Figure 2.6: Calculated structures (ONIOM/B3LYP/6-31G(d);UFF) for the nickel(II) derivative of a) host–guest complex **2.3** with C_{60} and b) host **2.3** without C_{60}.

2.3.2 Computational Modeling of Bis-porphyrins 2.4 and 2.5

Computational modeling of bis-porphyrins **2.4** and **2.5** reveals several insights about the suitability of these hosts for fullerenes. In the optimized structures of bis-porphyrin **2.4** the calixarene maintains a pinched cone conformation due to the hydrogen bonding motif between the hydroxyl and ether. There is also hydrogen bonding between the amide NH and the oxygen of the hydroxyl groups. The porphyrins show the correct orientation to accommodate fullerenes due to the *meta*-amide groups to the ether oxygen. The center to center porphyrin distances is 10.97 Å, with an interplanar angle for the 24-atom porphyrin mean planes of 44.6°. While the *meta*-position of the amide orientates the porphyrin planes away from the calixarene in a similar manner as observed for **2.1-2.3**, it also means that the phenyls of the ether substituent occupy a position in the cleft of the binding sites closer to the ideal binding position of the fullerene. The distances of the metal center to closest carbon of the fullerene are long at 3.38-3.48 Å. The CH-π distances from the ether phenyls to fullerene centroids are 2.65 and 2.81 Å. It is possible that these groups impose steric constraints on accommodation of the fullerene into the binding site.

With the removal of the fullerene from host **2.4** and reoptimization of the host structure, the bis-porphyrin maintains the same basic structure as the host-guest complex. The bis-porphyrin shows subtle changes to the calixarene scaffold, whereas significant changes are observed in between the porphyrins. The porphyrin cavity widens, giving a center to center distance of 12.11 Å. The interplanar angle of the two 24-atom porphyrin mean planes widen to 55.8°.

The analogous geometries of the host-guest complex and the free host support the suitability of **2.4** as fullerene host. Computational studies suggest that binding may be adversely affected by the phenyl ether which imposes steric constraints on the binding cavity of the bis-porphyrin. The calculated structures of the host-guest complex of **2.4** with C_{60} and the free host are shown in Figure 2.7 and Figure 2.8 respectively.

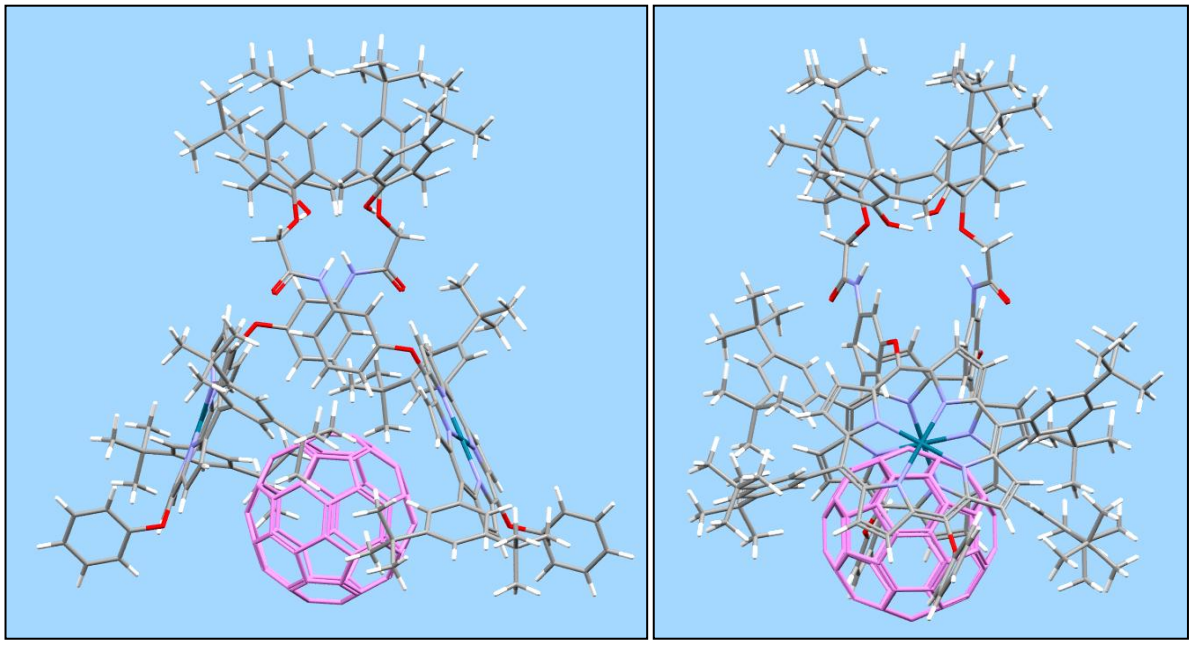

Figure 2.7: Calculated structures (ONIOM/B3LYP/6-31G(d);UFF) for the palladium (II) derivative of host–guest complex **2.4** with C_{60}.

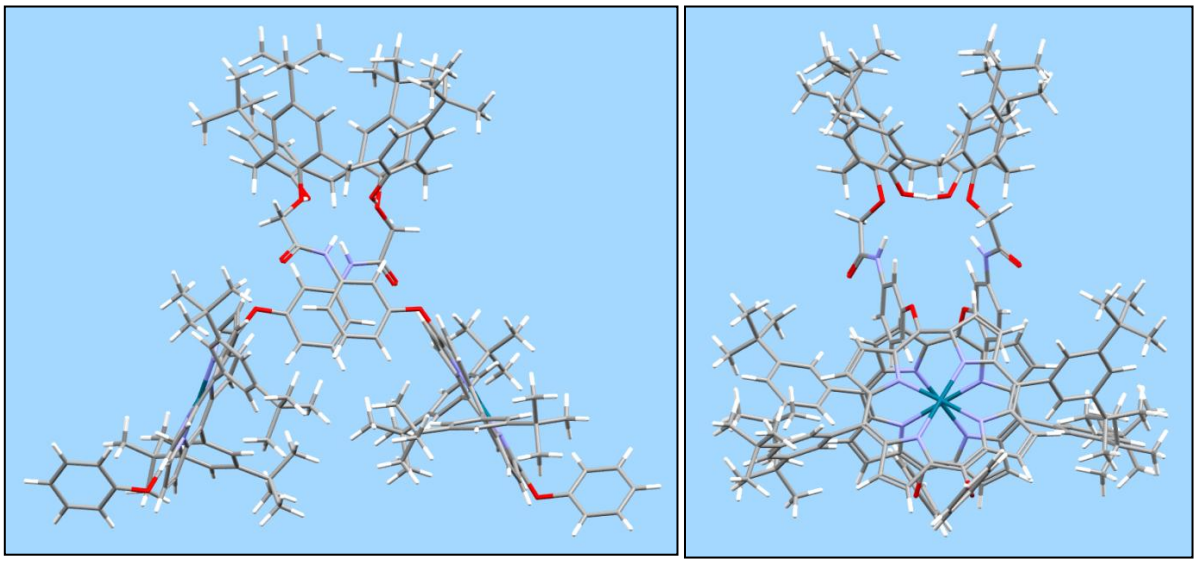

Figure 2.8: Front and side views of structures (ONIOM/B3LYP/6-31G(d);UFF) for the palladium (II) derivative of host **2.4.**

In host **2.5** the amide groups at the *para*-positions of the phenyl ethers are not appropriately positioned for the binding of fullerenes. This fact is reflected in the geometry of the host-guest complex, where the linkers, amides and the ether phenols are required to twist so that the two porphyrin planes can adopt a geometry suitable for binding fullerenes. The metal center to center distance of the porphyrins is longer for **2.5** at 11.98 Å and the interplanar angle between

the two 24-atom porphyrin mean planes 41.3°. The fullerene does not sit directly over the porphyrin center but is slightly offset.

With removal of C_{60} and reoptimization of the host, there is a significant change in structure of the bis-porphyrin. The ether oxygens of the porphyrin rotate to orientate the porphyrins away from each other and toward the calixarene. Such a significant change in the geometry of the host can be explained in terms of the energy levels of the optimized structures. To form a stable complex, the free energy of the complex must be sufficiently lower than that of the combined free host and the guest in order to offset the energy required institute geometry changes complementary to fullerene binding. In bis-porphyrin **2.5,** the energy of the free host is lower than that required to institute geometry changes complementary to fullerene binding and form a stable host guest complex. The calculated structures of the host-guest complex of **2.5** with C_{60} and the free host are shown in Figure 2.9 and Figure 2.10 respectively.

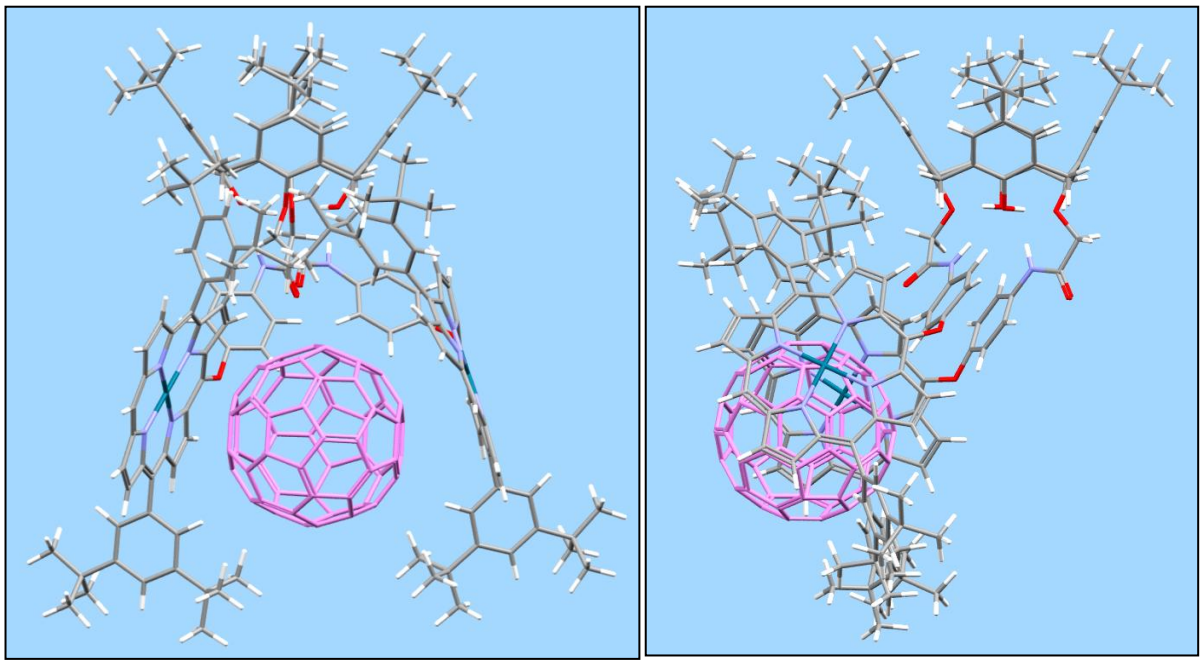

Figure 2.9: Calculated structures (ONIOM/B3LYP/6-31G(d);UFF) for the palladium (II) derivative of host–guest complex **2.5** with C_{60}.

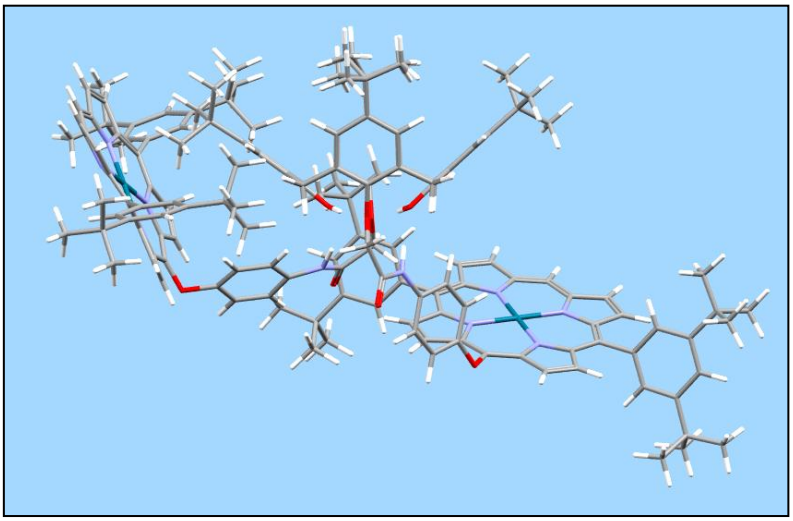

Figure 2.10: Calculated structure (ONIOM/B3LYP/6-31G(d);UFF) for the palladium (II) derivative of host **2.5.**

Computational models of bis-porphyrin host **2.1-2.3** display a suitable geometry for the binding of fullerenes with the appropriate interplanar porphyrin angles and distances to accommodate fullerenes. Upon removal of the fullerene and reoptimization of the free host, the change in geometry is small, with slight reduction of the interplanar porphyrin angles and distance. The key differences between the hosts are the number of CH-π interactions from the porphyrin to the fullerene. Bis-porphyrin **2.2** offers the most CH-π interactions due to the presence of the methoxy groups. Host **2.3** which lacks a phenyl group at the 15-position, offers the least. It is expected that the order of association may follow **2.2** > **2.1** > **2.3**.

Bis-porphyrin host **2.4** shows potential to bind fullerenes, possessing appropriate interplanar porphyrin angles and distances to accommodate fullerenes. It is anticipated that the presence of the ether substituted phenyl may sterically reduce the association strength of fullerene binding site.

Based on the optimized structure of **2.5** with and without C_{60}, the host does not appear to be suitable for the formation on a host-guest complex. The geometry of the free host is lower when the porphyrin planes orientate away from each other. The host must undergo a structural shift in order to form a host-guest complex which is energetically unfavorable.

2.4 Synthesis of Bis-Porphyrins

Traditional methods for the synthesis of porphyrins are limited with regard to forming selective mixed functionality. Statistical mixtures of all possible products are usually formed. These mixtures give low yield for desired products and can be difficult to separate chromatographically.

Dipyrromethane was prepared by the method reported by Lindsey.[159] Previous methods for dipyrromethane have been synthetically difficult with some requiring highly toxic reagents such as phosgene.[160] These methods may result in crude mixtures of oils, which would require purification via distillation or chromatography.[161,162] Lindsey's method has been used to prepare a variety of differently substituted porphyrins and shows little formation of other condensation fragments. Heating paraformaldehyde in excess pyrrole with indium trichloride forms dipyrromethane **2.6** as an off white crystalline solid in a 90% yield.

2.4.1 Synthesis of Porphyrin 2.7

Porphyrin **2.7** was prepared by the [2+2] condensation reaction reported by Bonifazi.[163] Dipyrromethane **2.6** and 3,5-di-*tert*-butyl benzaldehyde, with a catalytic amount of trifluoracetic acid, was stirred in degassed dichloromethane for 16 hours. Chloranil was added and the reaction refluxed for two hours to oxidize the porphyrinogen to the porphyrin in 35% yield. The porphyrin was purified by passing the reaction mixture through a plug of silica and eluting the porphyrin from the polypyrrole with a mixture of dichloromethane and hexane.

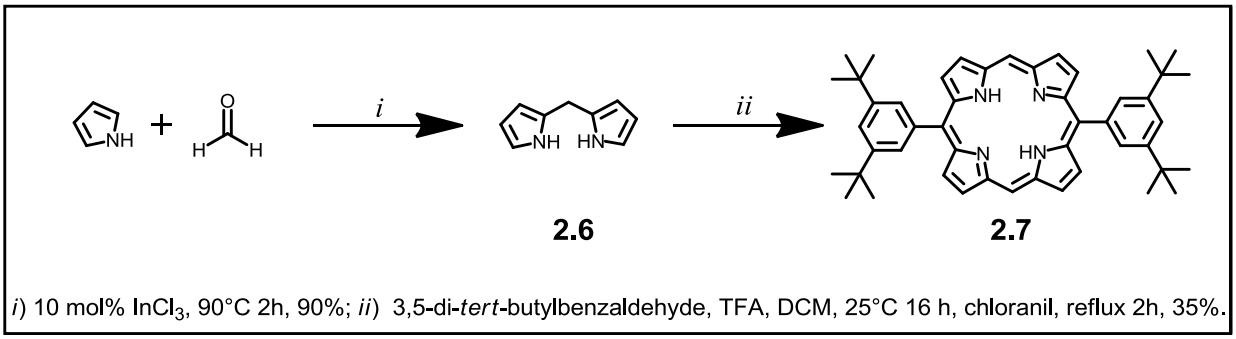

Scheme 2.4: Synthesis of porphyrin **2.7**

2.4.2 Synthesis of Brominated Porphyrin 2.8

Bromination of porphyrins has been reported by several research groups.[163,164] The use of NBS as a brominating agent can result in the bromination of porphyrins at not only the *meso* position of the porphyrin but also the β-pyrrole positions. For the bromination of 5,15-diphenyl porphyrin low temperatures and short reaction times are required to prevent over bromination of the β-pyrrole positions. Reactions performed with a stoichiometric amount of NBS and excess pyridine formed a mixture of unreacted, monobrominated and dibrominated products which can be easily separated by column chromatography. Using a 10-fold excess of NBS forms the dibrominated product in high yield.

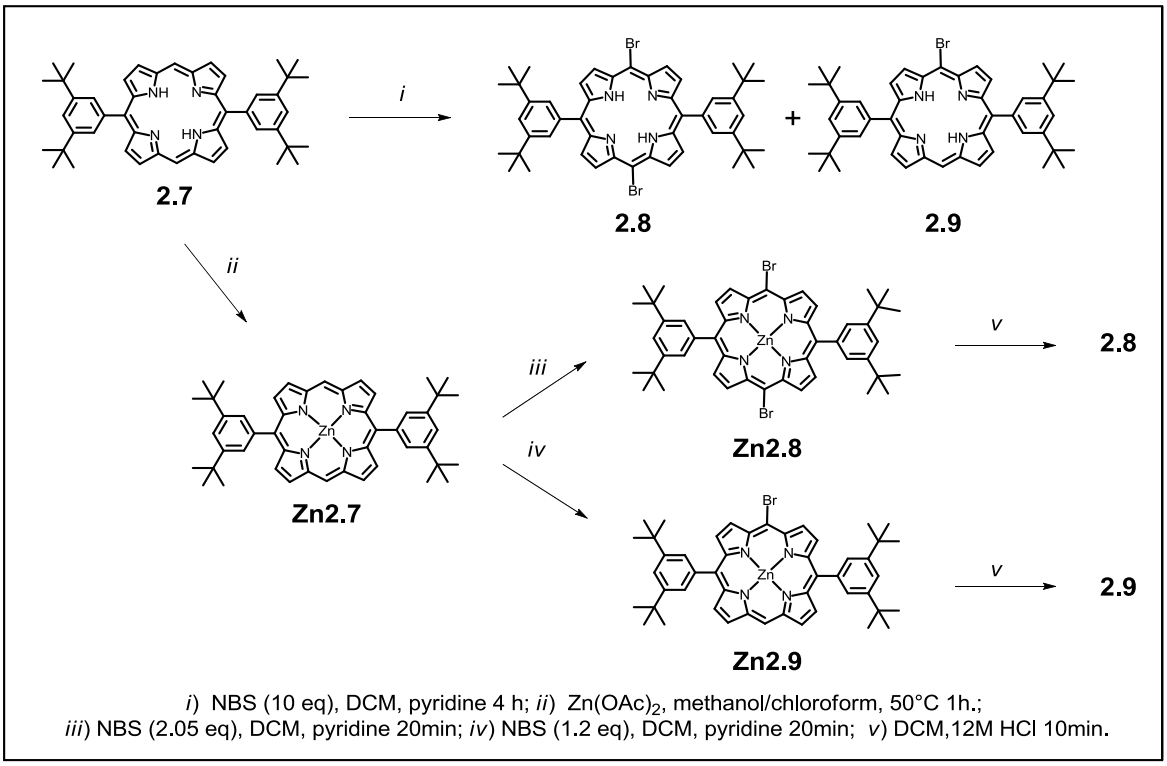

Scheme 2.5: Synthesis of mono and dibrominated porphyrins **2.8** and **2.9**

Following Arnold's method, bromination of **2.7** proved more difficult than initially expected.[164] Unlike the diphenyl porphyrin analog, the mono and dibrominated 3,5-*tert*-butylphenyl porphyrins **2.8** and **2.9** were found to be insoluble in chloroform, precipitating out of solution as a purple solid.[165] This is unusual as 3,5-di-*tert*-butyl porphyrins are considered more soluble than the phenyl analogues in non-polar and halogenated solvents. The solid was soluble enough to confirm the formation of the dibrominated porphyrin **2.8** via ^{1}H NMR

spectroscopy, however the mono brominated porphyrin **2.9** was also present. The ^{1}H NMR of mono brominated porphyrin **2.9** is identified by two singlets at 10.15 and 2.91 ppm, corresponding to the free *meso* proton and the central NH protons respectively. A doublet at 8.08 ppm corresponds to the *ortho*-protons of the 3,5 di-*tert*-butylphenyl groups. Integral comparison between this doublet and the analogous signal for **2.8** can be used to determine the relative ratio these species. Over several reactions the percentage of the mono product was between 0 and 30%. Due to low solubility of both **2.8** and **2.9**, purification of the products proved difficult by chromatography or recrystallization. Variation of several factors for bromination conditions was explored in an attempt to selectively form the dibrominated product **2.8**. These variations included the amount of NBS used (2-20 equivalents), temperature (-4 to 25°C), solvent (dichloromethane and chloroform) and ratio of pyridine to solvent (1:50 - 1:4). The increased quantity of pyridine appeared to reduce the amount of **2.9** formed - possibly due to increasing the solubility of the product but the amount of **2.9** was generally above 10%. Metallation of the porphyrin with zinc was examined as a means to increase solubility and promote dibromination.

Cheng *et al*. reported a method for the dibromination of the zinc derivative of the 5,15 *meso*-porphyrin **Zn2.7** in high yield.[166] Bromination of **Zn2.7** was attempted again with two equivalents of NBS and 3% pyridine at 0°C in dichloromethane. The reaction in this case went a deep green colour and displayed no sign of any precipitate. Presumably the pyridine can coordinated to the zinc porphyrin, thereby increasing the solubility of the brominated porphyrin. After ten minutes the reaction was quenched with acetone. The red product was precipitated out by addition of methanol and removal of the dichloromethane solvent. The resulting red solid was less soluble in $CDCl_3$ than the free base and ^{1}H NMR was inconclusive in regard to the extent of the bromination in due to a high signal to noise ratio. Upon addition of pyridine to the NMR sample, the solution turned a deep green colour and precipitate dissolved. The resultant ^{1}H NMR gave no indication of mono brominated porphyrin present but broadened proton signals indicate the co-ordination pyridine. The zinc was removed from the porphyrin by treatment with concentrated HCl. No mono bromoporphyrin was detected in the subsequent products. It was found that a slight excess of NBS (2.05 equivalents) leads to full bromination of the zinc porphyrin **Zn2.8,** with no detectable signals for **Zn2.9**. A large excess of NBS resulted in bromination of the porphyrin at the β-pyrrole positions. Reaction of **Zn2.7** with 1.2 equivalents of NBS and 3% pyridine at 0°C in dichloromethane for ten

minutes, results the mono brominated porphyrin **Zn2.9** in 70% yield. A small amount of **Zn2.8** was also detected.

2.4.3 Synthesis of Amino Porphyrins via Suzuki Coupling

Employing the method reported by Lyons for coupling of ferrocene phenyl boronic acid and 4-acetamidophenyl boronic acid to **2.8**,[165] Suzuki coupling of the dibrominated porphyrin **2.8** was accomplished with eqimolar amounts of two different boronic acids. This resulted in the formation of a statistical mixture of three differently substituted porphyrins (A_2B_2, A_2BC, A_2C_2 type porphyrins). These porphyrins were separable via column chromatography using silica and dichloromethane/ethyl acetate.

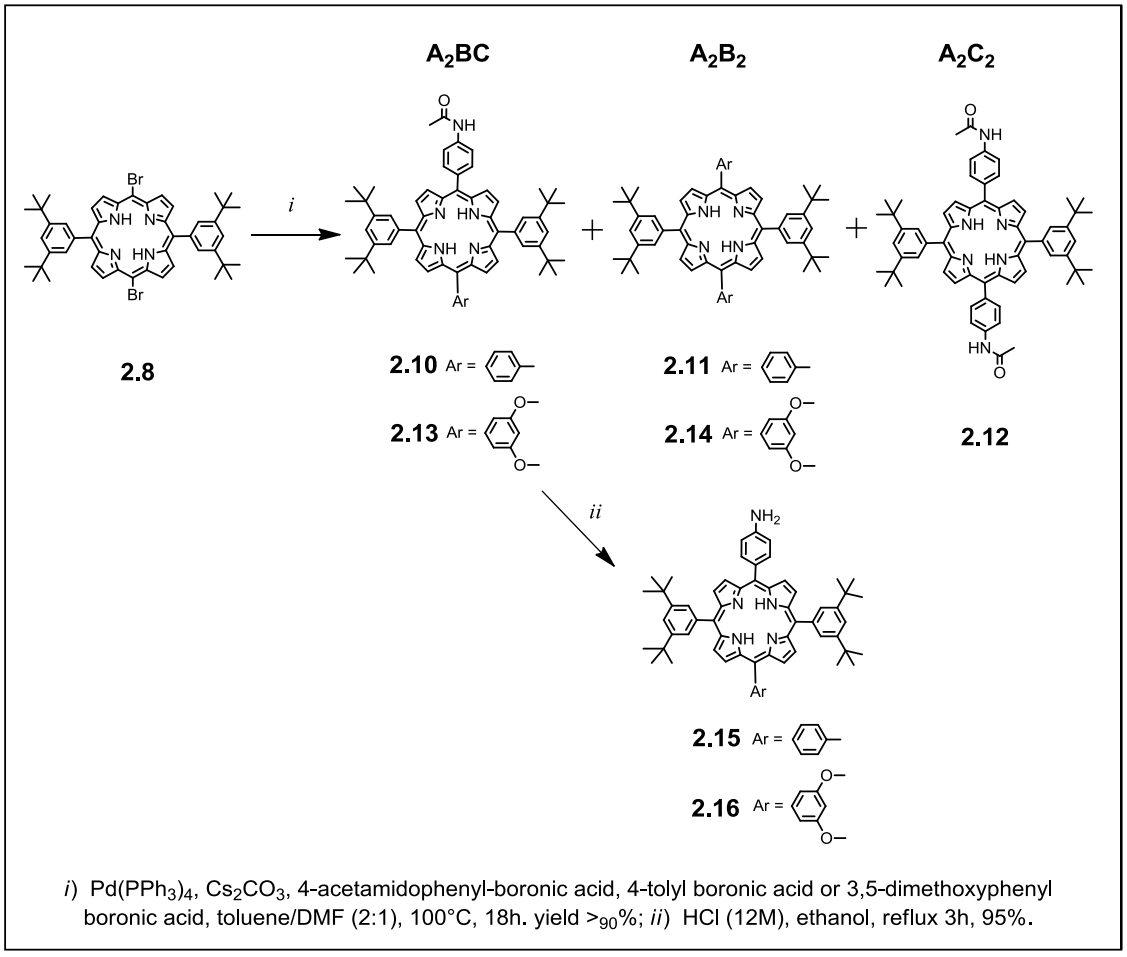

Scheme 2.6: Synthesis of A_2BC substituted porphyrins; **2.10** and **2.13** and amide hydrolysis to **2.15** and **2.16**

Bromoporphyrin **2.8** was heated at 100°C for 16 hours with a mixture of 4-acetamidophenyl boronic acid and either 4-tolyl boronic acid or 3,5-dimethoxyphenyl boronic acid using caesium carbonate as a base and 10% tetrakis(triphenylphospine) palladium(0) in thoroughly degassed 4:1 toluene/DMF (Scheme 2.6). DMF was necessary to aid the solubility of **2.8** and caesium carbonate in the reaction. The product mixture was then purified by column chromatography, eluting with dichloromethane and increasing percentages of ethyl acetate. The A_2BC porphyrins **2.10** and **2.13** were major products with smaller fractions of the disubstituted A_2C_2, di-4-acetamidophenyl porphyrin **2.12** and the A_2B_2 porphyrin (being either the ditolyl **2.11** or bis-3,5-dimethoxyphenyl porphyrin **2.14**). It was determined that the yield of the A_2BC porphyrins **2.10** and **2.13** could be increased to 60% by using 1.3 equivalents of the 4-acetamidophenyl boronic acid and 0.7 equivalents of either the tolyl or 3,5-dimethoxypheyl boronic acid with a total porphyrin yield of 95%. Hydrolysis of the porphyrin amides to the corresponding amines was performed by refluxing the porphyrins in 12 M hydrochloric acid with 20% ethanol for three hours. The acidic solutions were neutralized by slow addition of solid sodium bicarbonate and subsequently purified via flash chromatography.

Purification of the A_2BC Suzuki porphyrins was complicated by the presence of mono-4-acetamidophenyl porphyrin **2.17** (A_2B). The acetamido porphyrin **2.17** was formed when the dibrominated porphyrin **2.8** contained significant amounts (≥5%) of the mono-brominated porphyrin **2.9**. It was noted that freeze-pump-thaw degassing of the solvent is necessary in order to prevent cleavage of the bromide. **2.17** was found to be inseparable from both **2.10** and **2.13** by column chromatography due to the porphyrins having similar polarities. The amino-porphyrins **2.15** and **2.16** were also found to be inseparable from **2.18**.

The mono-4-acetamidopheneyl porphyrin **2.17** was prepared by Suzuki coupling of the free base mono bromoporphyrin **2.9** with three equivalents of 4-acetamidophenyl boronic acid, caesium carbonate and 5% tetrakis(triphenylphosphine) palladium(0) in thoroughly degassed toluene/DMF (Scheme 2.7). **2.17** was prepared in 90% yield with trace diacetamidophenyl porphyrin **2.12** present. These two compounds have differing polarities and are easily separated by column chromatography eluting with dichloromethane/ethyl acetate (9:1) to separate **2.17** from **2.12**. The amide product was converted into the corresponding amine **2.18** by refluxing in ethanol with 12 M hydrochloric acid.

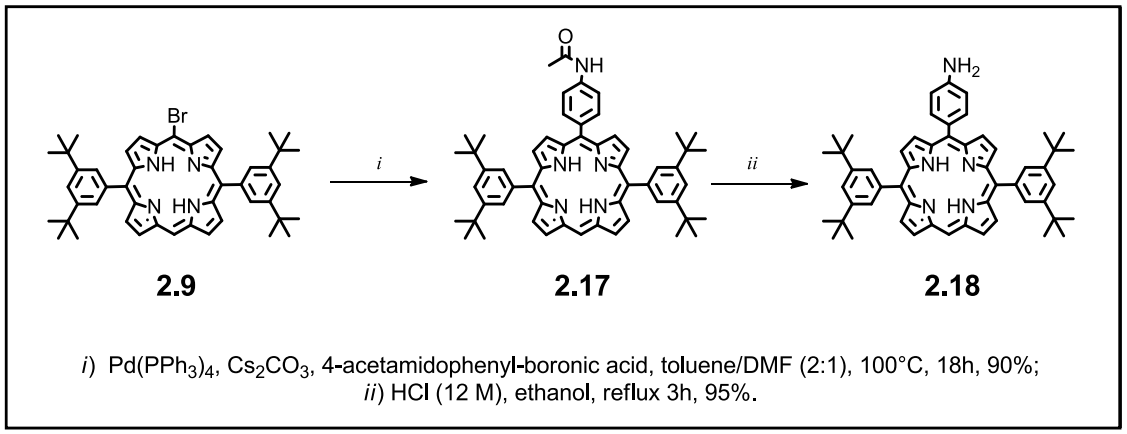

Scheme 2.7: Synthesis of **2.17** via Suzuki coupling and hydrolysis of the amide to corresponding amine **2.18**

2.4.4 Synthesis of Bis-Porphyrins 2.1-2.3

The alkylation of the calixarene scaffold was achieved by the method outlined by Collins *et al.*[167] by refluxing calixarene and ethyl bromoactetate with potassium carbonate in anhydrous acetonitrile. Subsequent hydrolysis of the ester functional groups was carried out to form the corresponding acid **2.19**. The amino porphyrins were coupled to the calixarene diacid using the procedure described by Dudic shown in Scheme 2.8.[120]

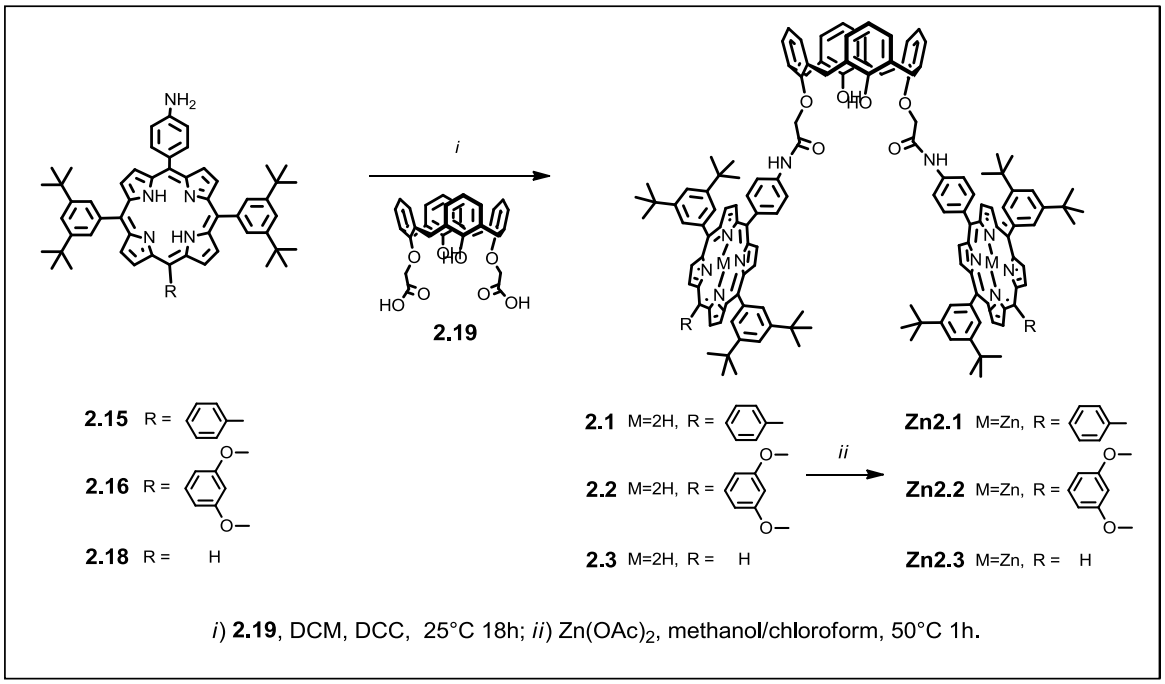

Scheme 2.8**:** Synthesis of free base and zinc analogs of bis-porphyrins **2.1-2.3**

Calixarene diacid **2.19** was stirred at room temperature with excess DCC and two equivalents amino porphyrin (either **2.15**, **2.16** or **2.18)** for 18 hours. The resultant bis-porphyrins were former in approximately 50% yield. The bis-porphyrin hosts were purified by column chromatography eluting with dichloromethane/hexane. Mass spectrometry confirmed the formation of the bis-porphyrin hosts **2.1-2.3**, which were detected as both the mono and dication. The ^{1}H NMR spectra of **2.1-2.3** display clear proton signals corresponding to both the calixarene and the porphyrins, integrating in a ratio of 2:1. The methylene bridges of the calixarene were shown as two sets of doublets corresponding to the cone conformation. Bis-porphyrins **2.1-2.3** were recrystallized from chloroform/ethanol to prepare an analytically pure sample for titration measurements.

2.4.5 Synthesis of Bis-Porphyrin 2.4

Nickel-porphyrin **Ni2.7** was prepared from the free base bis(3,5-*tert*-butylphenyl)porphyrin **2.7** by refluxing the porphyrin with nickel acetate in DMF for one hour, during which time the reaction mixture became deep red in colour. The solution was reduced in volume and purified by passing the porphyrin through a short plug of silica. The porphyrin was then dibrominated with 10 equivalents of NBS in dichloromethane and 10% pyridine at 0° for ten minutes.[164] During this time the nickel dibromoporphryin precipitated out of solution. Unlike the corresponding free base, the ^{1}H NMR analysis of the precipitate showed no detectable traces of undesirable products.

The reaction developed by Chen was followed for the preparation of **2.20**.[149] Dibromoporphyrin **Ni2.8** with four equivalents of 3-acetamidophenol, potassium carbonate and 10 mol% of nickel acetate was heated to 100°C in DMF under nitrogen for one hour. The reaction was monitored by thin layer chromatography (TLC). Over three hours the reaction showed little evidence of any product formation. This seems due to the relative insolubility of the dibrominated porphyrin **Ni2.8** compared to the phenyl analog used by Chen. The temperature was increased to reflux and the reaction continued for a further 16 hours. Analysis of the final mixture showed the presence of **2.20** product in moderate yield. Hydrolysis of the acetamide was carried out by refluxing **2.20** with concentrated hydrochloric acid in ethanol for

three hours to yield the subsequent diamino **2.21** without removal of the nickel metal form the porphyrin core.

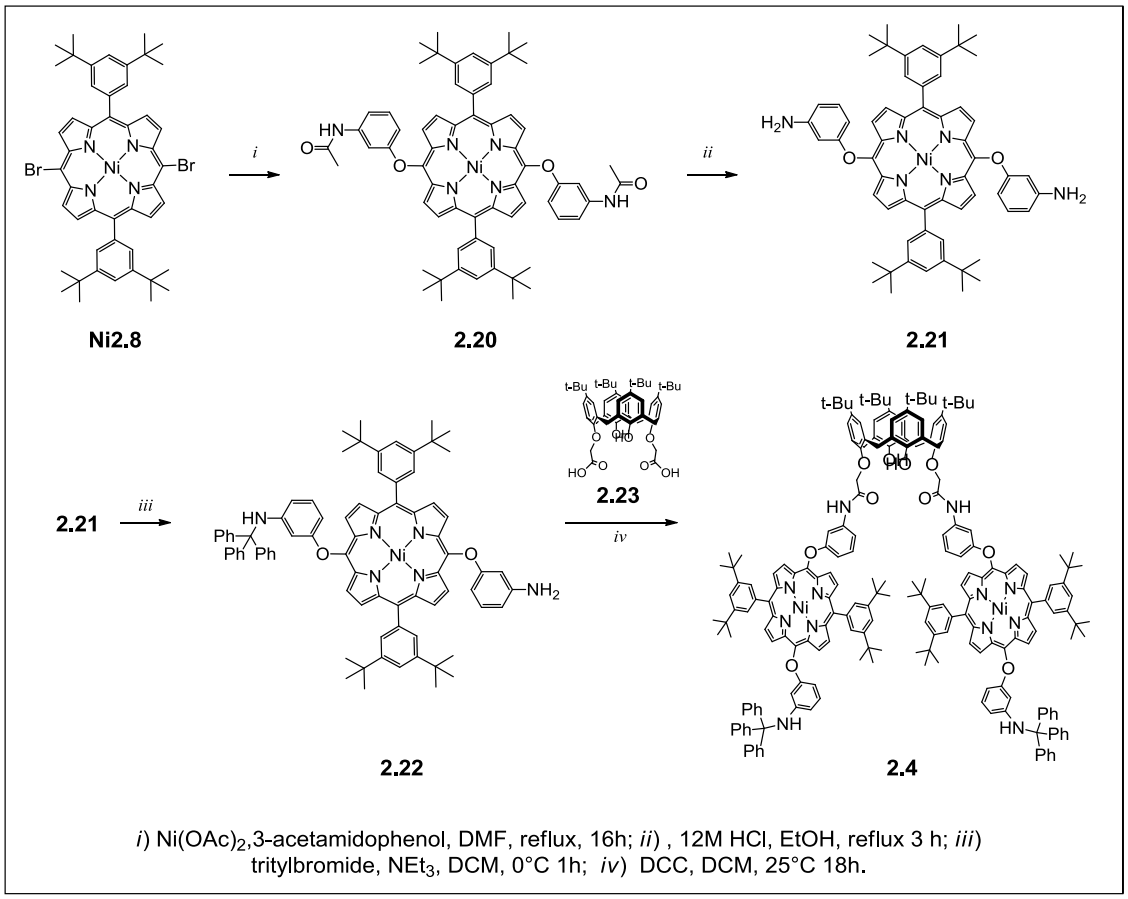

Scheme 2.9: Synthesis of bis-porphyrin **2.4.**

Mono protection of diamine was then carried out by standard protection methods.[168] Drop wise addition of trityl bromide to a solution of **2.21** in dichloromethane with triethylamine resulted in a mixture of the mono-trityl, mono-amino porphyrin **2.22,** as well as ditrityl porphyrin and unreacted **2.21**. The statistical mixture was purified by column chromatography (silica, dichloromethane). Porphyrin **2.22** was then coupled with the calixarene diacid **2.23** with DCC in dichloromethane to give the bis-porphyrin **2.4** in high yield. The ^{1}H NMR spectrum of **2.4** displayed proton signals integrating to one calixarene and two porphyrins. The methylene bridges of the calixarene were shown as two sets of doublets corresponding to the cone conformation. Mass spectrometry confirmed the formation of the bis-porphyrin host **2.4**.

2.4.6 Synthesis of Bis-Porphyrin 2.5

The preparation of the 4-aminophenoxy analog of porphyrin **2.20** was less straight forward (shown in Scheme 2.10). Dibromo porphyrin **Ni2.8** was reacted with 4-acetamidophenol, but the reaction failed to proceed or resulted in the cleavage of the bromine groups to give **Ni2.7**. Chen *et al.* performed a coupling reaction study involving various substituted phenols. While acetamidophenols were not investigated in the study, both 3-nitrophenol and 4-nitrophenol were examined. The coupling reaction with 3-nitrophenol proceeded in high yield and reacted over two hours, however the reaction with 4-nitrophenol took ten times as long and formed only moderate yields, due to degradation of the porphyrin.

In an attempt to prepare the 4-amino-analog, 4-nitrophenol was used with the aim or reducing the nitro group to an amine. Refluxing **Ni2.8** with 4-acetamidophenol for 18 hours gave the mono substituted 4-nitrophenylether-porphyrin **2.25** in 50% yield, while the di-4-nitrophenylether-porphyrin, **2.24** was only obtained in 13% yield. The synthesis was extended to the mono-substituted porphyrin, **2.25.** Reduction of the nitro functionality to the amine was performed by refluxing **2.25** with tin(II)chloride and hydrochloric acid in ethanol. The reaction proceeded cleanly and in high yield to give mono amine **2.26** which was then coupled with the calixarene diacid **2.23** to give the bis-porphyrin **2.5** in 70% yield. The ^{1}H NMR spectrum of **2.5** displayed proton signals integrating to one calixarene and two porphyrins with an amide NH proton signal at 8.02 ppm. The methylene bridges of the calixarene were shown as two sets of doublets corresponding to the cone conformation. Mass spectrometry confirmed the formation of the bis-porphyrin host **2.5**.

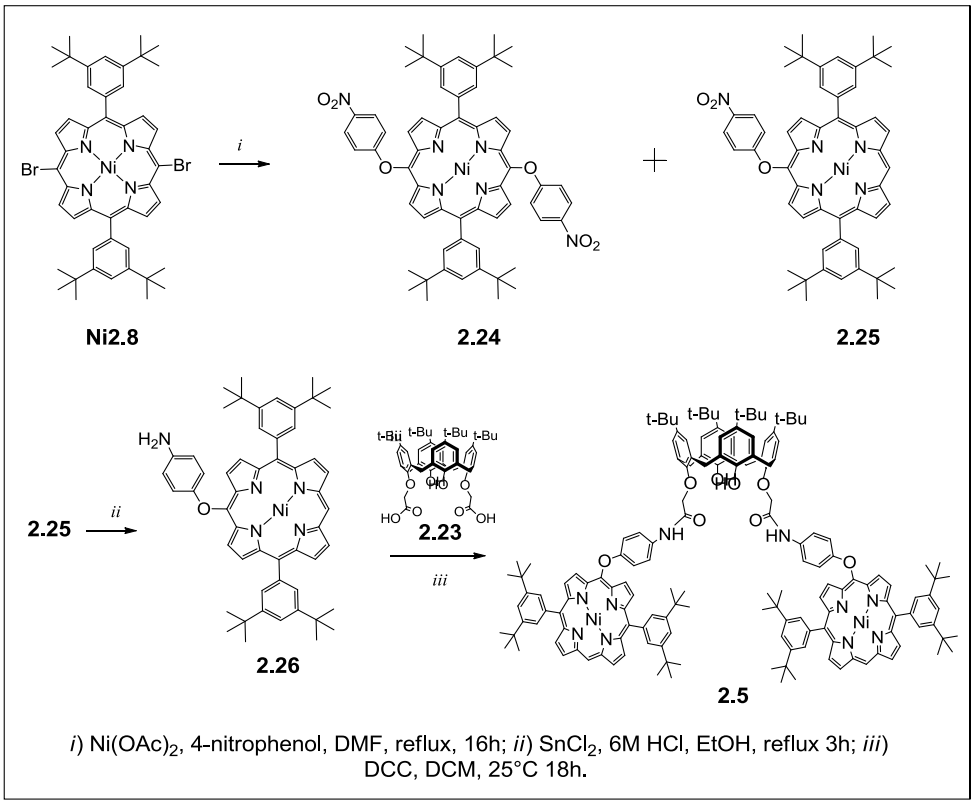

Scheme 2.10: Synthesis of bis-porphyrin **2.5**

2.5 Fullerene Binding studies with Bis-Porphyrins

The affinity of a host for a particular guest is measured by the binding constant K_a, which represents the thermodynamic equilibrium constant for the process Host + Guest ⇄ Complex.

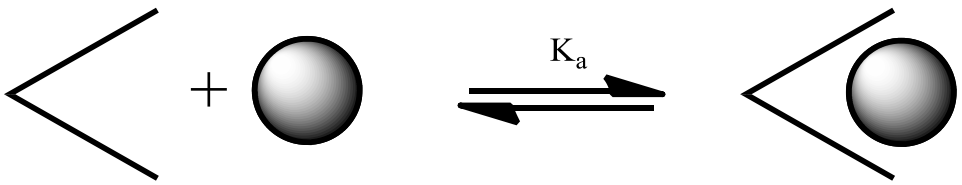

$$K_a = \frac{[Complex]}{[Host][Guest]}$$

Figure 2.11: The thermodynamic equilibrium process for a host-guest complex.

The equilibrium depends on a number of factors such as size and shape of the host binding site, the type and strength of the interactions between the host and the guest, as well as steric interactions. It has been shown that solvation of the host, guest and the complex is a determining factor for association.

Binding constants can be measured by titration methods using ^{1}H NMR, fluorescence and UV-visible spectroscopy. ^{1}H NMR spectroscopy is the least sensitive method and requires higher concentrations of both host and guest to make measurable determination of the association. Titrations using this method monitor the chemical shifts in the central NH porphyrin signal as a function of C_{60}. This method is problematic with respect to the solubility of C_{60} and C_{70} in toluene (2.8 mg/mL and 0.7 mg/mL respectively).

Fluorescence is the most sensitive spectroscopic method for the determination of binding constants. Porphyrins are typical fluorescence molecules. As the host-guest complex is formed by the addition of fullerene, quenching of the porphyrin fluorescence occurs due to energy and charge transfer reactions. The degree of quenching can be used to determine the concentration of the host-guest complex and hence the binding constant in titration experiments. The decrease in porphyrin fluorescence can then be fitted to a non-linear least square method described by Valeur.[169] Binding constants for C_{70} cannot be obtained by this method as C_{70} has a stronger absorption at the Soret and Q-bands wavelength. This higher absorption results in absorptive losses and leads to an over estimation of the association, as the fluorescence quenching is not completely due to complexation. Various methods are available to correct the inner filter effect though reproducibility is poor.

Association constants for the bis-porphyrin hosts were estimated by UV-visible spectroscopy. UV-Visible titrations were performed using a dual beam spectrometer running a spectrum of the host solution in toluene and a blank of the corresponding solvent. Titrating equal quantities of fullerene into both solutions allows for the subtraction of absorbance due to free fullerene. The maximum absorption at the Soret Band wavelength was recorded and C_{60}, C_{70} or $Lu_3N@C_{80}$ was added into each solution. After each addition of guest the UV-visible spectrum was obtained and the change in absorbance measured at the Soret wavelength of the free host. The titration data was then analyzed and the association constant (K_α) for the host guest complex can be determined from Equation 2.1.

$$Y = \frac{L(1 + K_a X + K_a A) - \sqrt{L^2(1 + K_a X + K_a A)^2 - 4K_a AXL^2}}{2K_a A}$$

Equation 2.1

X is the guest concentration, A is the host concentration, Y is the measured change in absorbance at a given wavelength and L is the maximum change in absorbance when the entire host is bound with the guest.

2.5.1 Fullerene Binding Studies with Bis-Porphyrins 2.1-2.3

Upon addition of fullerene to a solution of bis-porphyrin there is a significant decrease in absorbance of the Soret band and a red shifting of this band compared to pristine bis-porphyrin. A clear isosbestic point is observed, which is an indication of the formation of a 1:1 complex.

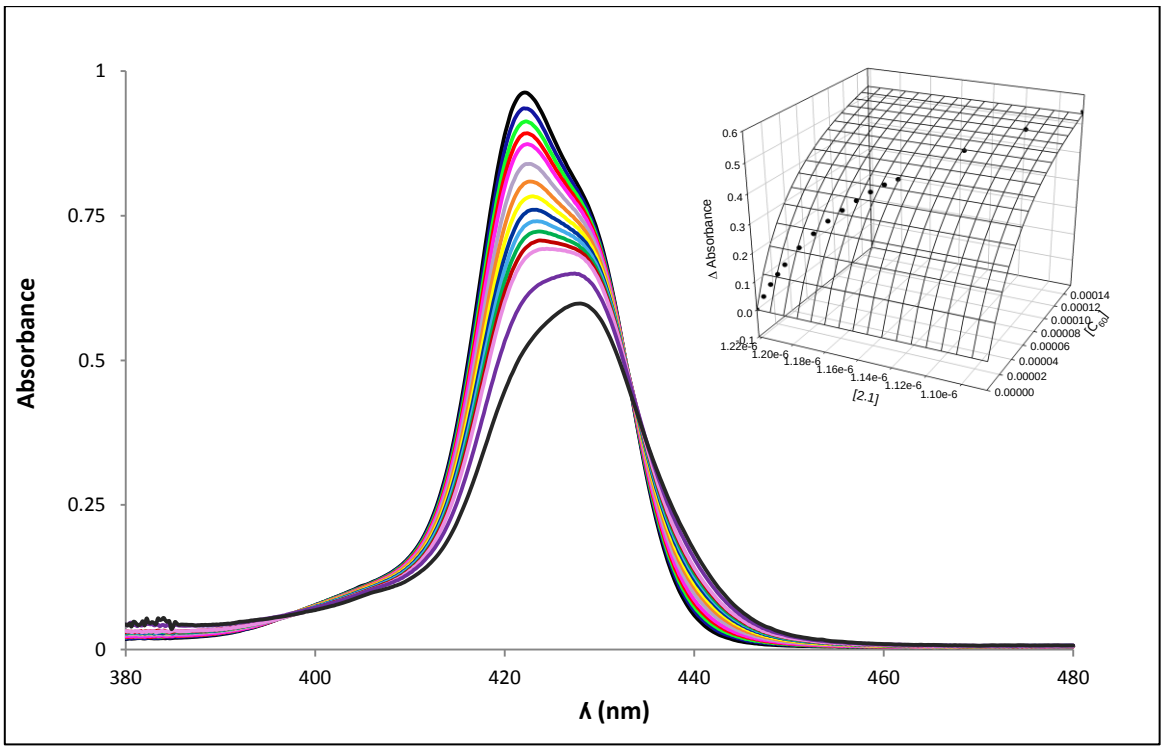

Figure 2.12: UV-visible titration of **2.1** (1.22x10^{-6} M) in toluene upon addition of C_{60} (0-95 Eq). Inset; plot of the non-linear least square fit for the change in absorption at the Soret of **2.1** upon addition of fullerene.

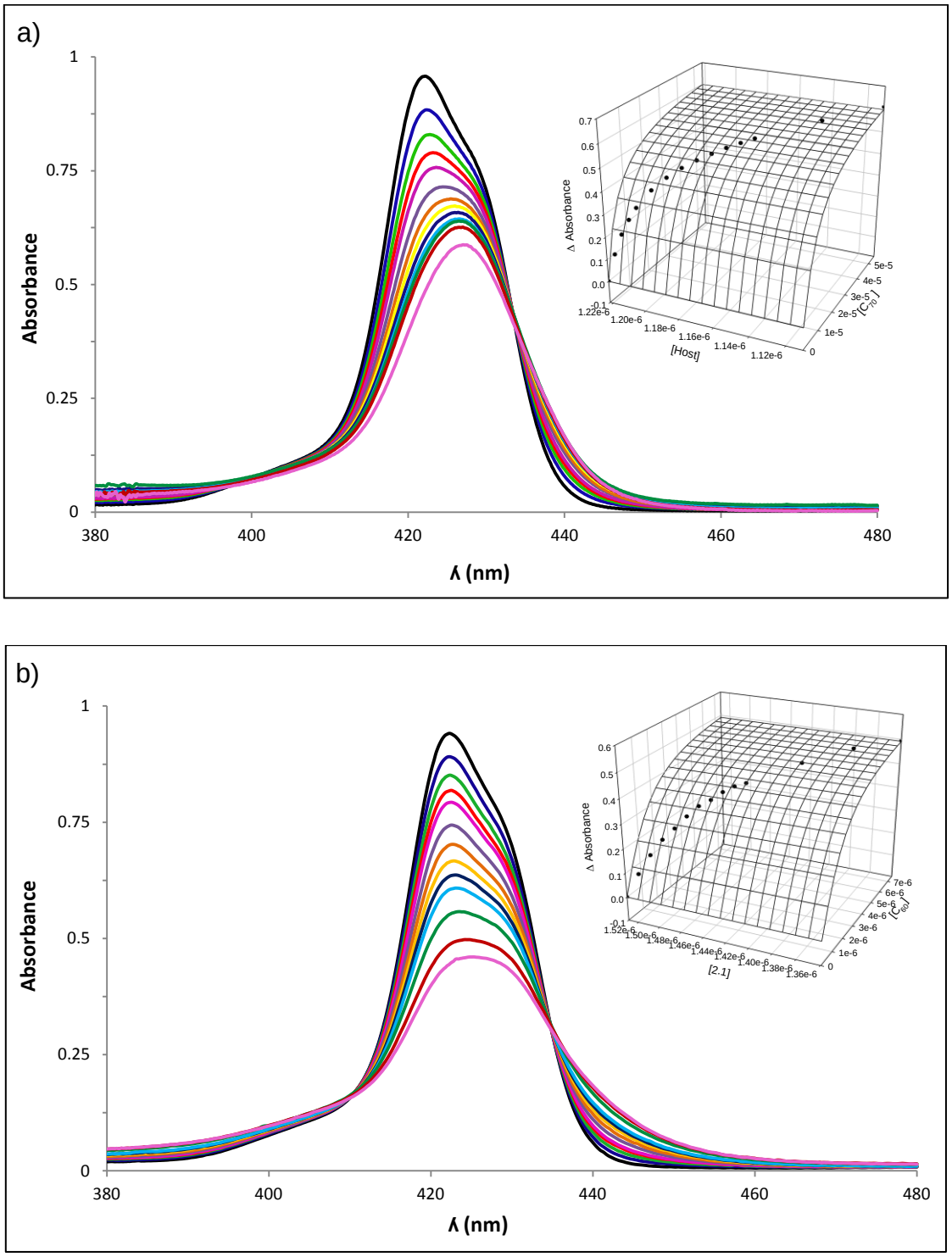

Figure 2.13: UV-visible titration of **2.1** (1.22×10^{-6} M) in toluene upon addition of a) C_{70} (0-20 Eq) and b) $Lu_3N@C_{80}$ (0-6 Eq). Insets; plot of the non-linear least square fit for the change in absorption at the Soret of **2.1** upon addition of fullerene.

Bis-porphyrin **2.2,** displays the highest binding constant for $C_{60,}$ with a K_a of 2.42 x10^4 M^{-1}. **2.2** displays the closest resemblance to the original host **1.36** because of CH-π interactions between the methoxy groups and the fullerene. Host **2.1** displays an association constant for C_{60} of 1.8 x10^4 M^{-1}, which is consistent with the removal of the CH-π interaction. Host **2.3** with no aromatic groups at the 15- *meso* position showed the lowest association with C_{60} and almost a third of binding shown by host **2.2** at 7.2 x10^3 M^{-1}. This difference in association could be due to the lack of CH-π interaction between the *ortho*-proton on the phenyl groups and the π system of the fullerene which has a estimated interaction energy of ~ 1.0 kcal mol^{-1} per CH-π interaction.[170] Association constants for the free base hosts are higher than that of the zinc derivative, which is been commonly observed in other supramolecular hosts for fullerenes and is ascribed to an electrostatic attraction between the electronegative 6:6 ring junction of the fullerene with the more electropositive H-N centre of the free base porphyrins.[171]

Binding constants for C_{70} are approximately an order of magnitude higher than that for C_{60} since C_{70} has a larger π surface due to the ellipsoidal shape of the fullerene and lower solubility. The hosts follow the same order of binding preference but not the same the trend in magnitude of binding, with host **2.2** demonstrating an association constant for C_{70} approximately 11 times higher than that for C_{60}, while **2.1** and **2.3** show binding for C_{70} approximately 8.5 times higher than C_{60}. Plots of the titration for **2.1** are shown in Figure 2.12 and Figure 2.13. The association constants for **2.1**-**2.3** are given in Table 2.3.

UV-visible titrations with bis-porphyrins **2.1, 2.2** and **2.3** were carried out with $Lu_3N@C_{80}$ to evaluate the effects of the change in size and polarization of the endohedral fullerenes relative to empty fullerenes. The UV-visible spectral changes due to the addition of $Lu_3N@C_{80}$ are similar to those described for the empty fullerenes. A red shift of the maximum of the Soret band of the complex, and a decrease in intensity are comparable with the changes observed for the empty fullerenes. However, the isosbestic point that is observed during the titration is shifted to the red with the endohedral fullerenes. On the basis of the titration data the association differs by approximately two orders of magnitude for the trimetallic endohedral fullerenes relative to C_{60}.

Table 2.3: Association constants for free base and zinc derivatives of host **2.1**, **2.2** and **2.3** with fullerenes C_{60}, C_{70} and $Lu_3N@C_{80}$.

	C_{60}($1x10^3$ M^{-1})	**C_{70}**($1x10^3$ M^{-1})	**$Lu_3N@C_{80}$**($1x10^3$ M^{-1})
2.1	18. (0.2)	157.5 (4.7)	1,446 (60)
Zn2.1	10.1 (0.3)	98.4 (2.5)	822 (41)
2.2	24.2 (0.5)	273.2 (5.9)	1,490 (33)
Zn2.2	14.8 (0.3)	159.9 (5.0)	789 (39)
2.3	7.2 (0.2)	59.4 (0.9)	467 (43)
Zn2.3	4.6 (0.1)	38.3 (0.8)	366.3 (68)

2.5.2 Fullerene Binding Studies of Bis-porphyrins 2.4 and 2.5

UV-visible titrations experiments for the bis-porphyrin complexes **2.4** and **2.5** were performed with both C_{60} and C_{70}. Upon addition of over 100 equivalence of either fullerene into a toluene solution of the bis-porphyrins, no significant decreases in the Soret bands occurred and there was no red shifting of the Soret band. This lack of spectral changes in the UV-visible spectrum is indicative of no association between the bis-porphyrins **2.4** and **2.5** and the fullerenes. This result was not surprising considering the large structural and energetic differences between the models of the host-guest complex and the free host and guest. Figure 2.14 and Figure 2.15 show the UV-visible spectra upon titration of C_{60} and C_{70} of **2.4** and **2.5** respectively.

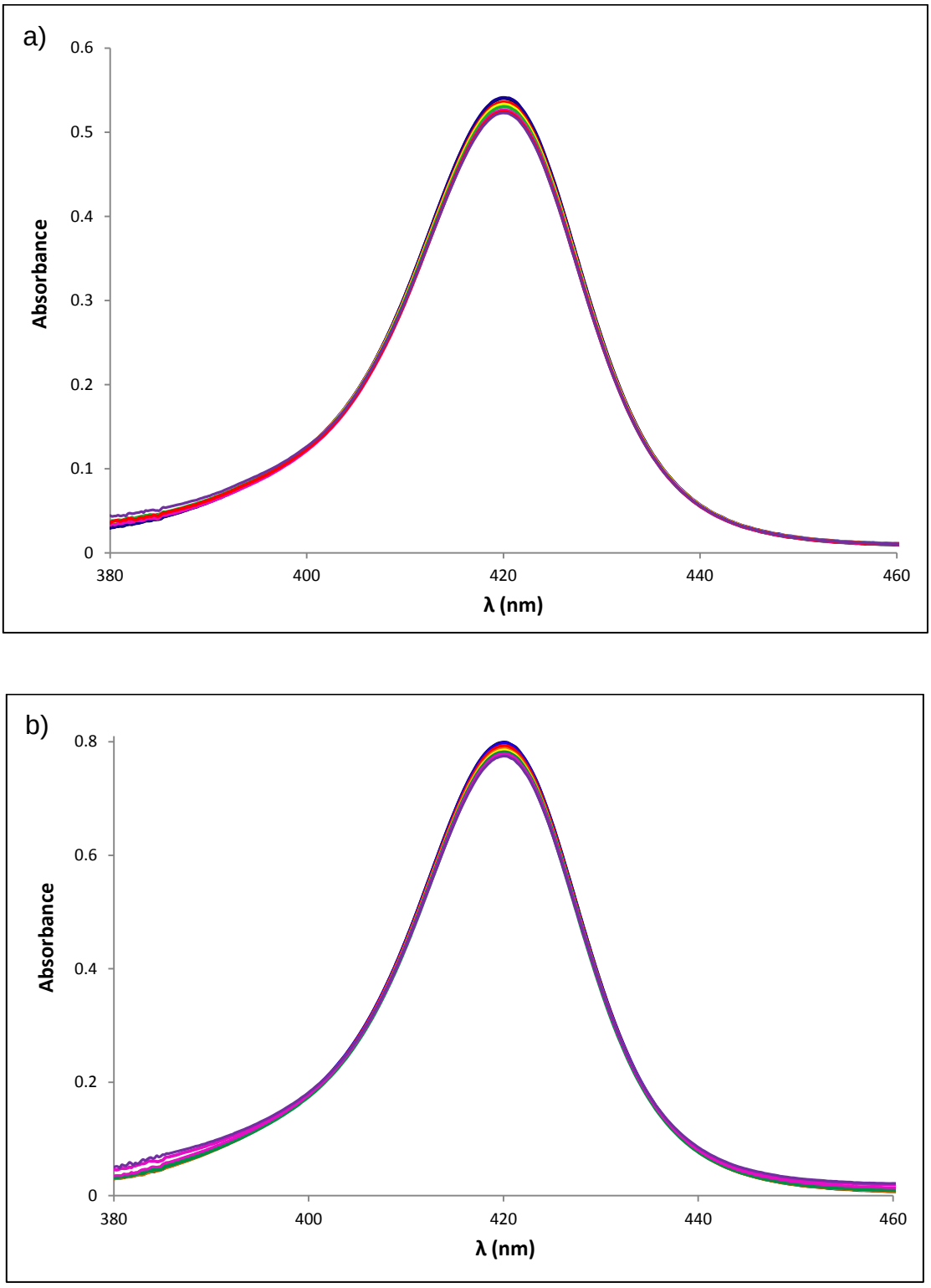

Figure 2.14: UV-visible titration of **2.4** (1.27×10^{-6} M) in toluene with addition of C_{60} (0-134 Eq.) and b) C_{70} (0-40 Eq.)

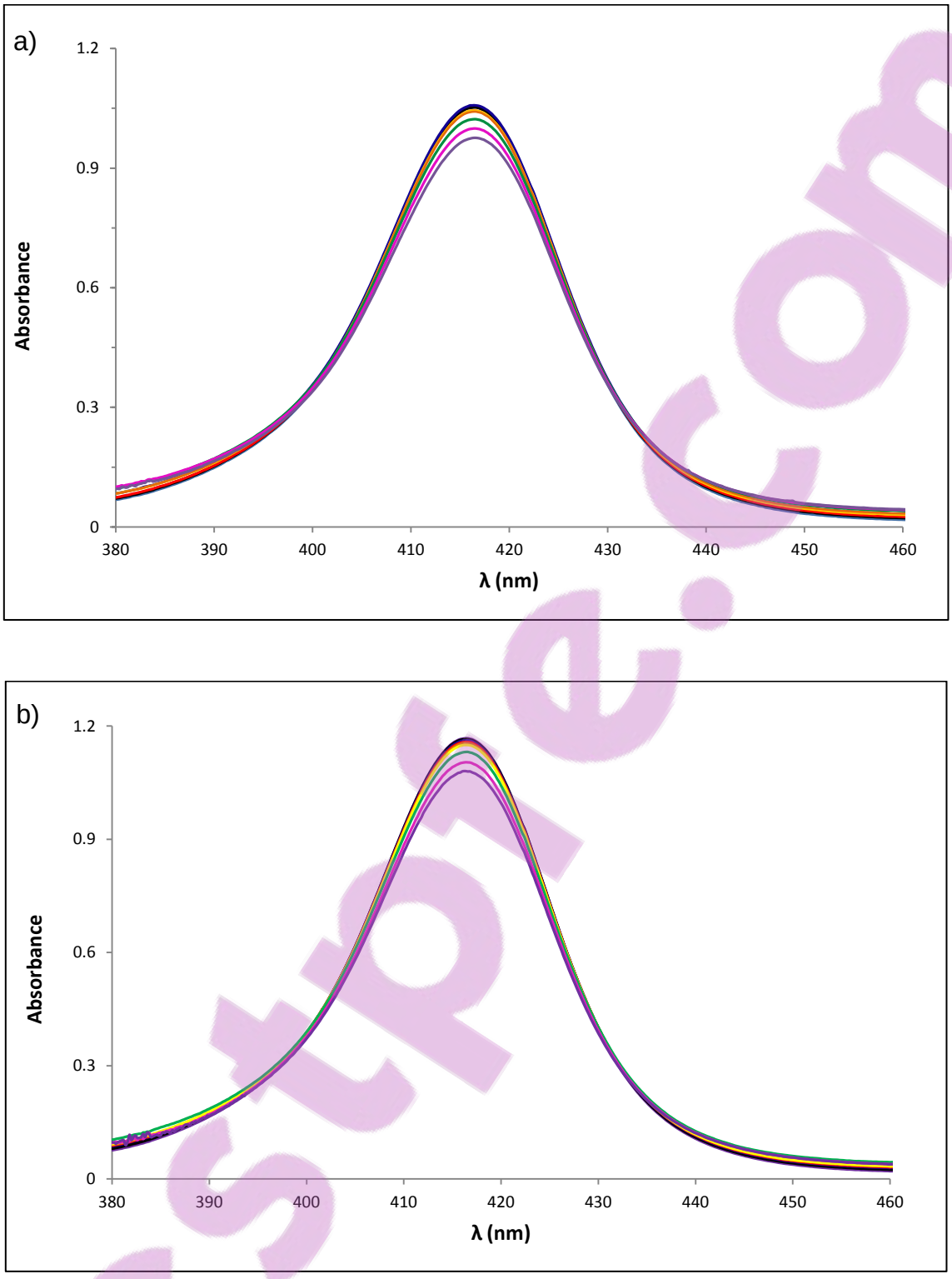

Figure 2.15 UV-visible titration of **2.5** (1.51×10^{-6} M) in toluene with addition of C_{60} (0-120 Eq) and b) addition C_{70} (0-35 Eq)

2.6 Porphyrin-Fullerene Co-Crystallates

Single crystals of porphyrins-fullerene co-crystallates have been grown to examine if the differences in the associations of **2.1-2.3** with fullerenes can be explained through X-ray structural data. Single crystal X-ray diffraction data was collected by Tania Groutso and the structure solved and refined by Associate Professor Peter Boyd. Crystal data for **Zn2.11.C_{60}.toluene, Zn2.11.2C_{70}**, and **Zn2.14.C_{60}.toluene** are shown Table 2.5, Table 2.6 and Table 2.7 respectively, located in the experimental section of this chapter.

2.6.1 Porphyrin-Fullerene Co-Crystallates Zn2.11.C_{60}.toluene and Zn2.11.2C_{70}

Di(tolyl)-bis-3,5-di-*tert*-butylphenyl porphyrin **2.11**, a side product (A_2B_2) from the Suzuki coupling of dibromo porphyrin **2.8** with 4-tolyl boronic acid and 4-acetamidophenyl boronic acid, was co-crystallized with C_{60} and C_{70}. The zinc analog **Zn2.11** co-crystallizes with C_{60} from toluene solution in a 1:1 ratio to give **Zn2.11.C_{60}.toluene.** Figure 2.16 shows a zigzag structural motif of alternating porphyrin and fullerene molecules with an interplanar angle between the porphyrin planes of 75.7°. This structure is typical of tetra aryl porphyrins and fullerenes.

The porphyrins display CH-π interactions between the tolyl group of one porphyrin and the 3,5-di-*tert*-butyl phenyl group, with a distance of 2.86 Å and another CH-π interaction between a methyl of a *tert*-butyl phenyl and a tolyl group with a distance of 2.98 Å. The fullerenes are centered over the porphyrin with the closest fullerene carbon atom to located 2.77 Å from the 24-atom porphyrin mean plane and 2.79 Å from the zinc metal. Four CH-π interactions between the *ortho* CH of the tolyl groups and 3,5-di *tert*-butyl phenyls and the fullerene occur on each side of the porphyrin. These distances range from 3.19-3.23 Å and have the potential to enhance the stability of the supramolecular structure.

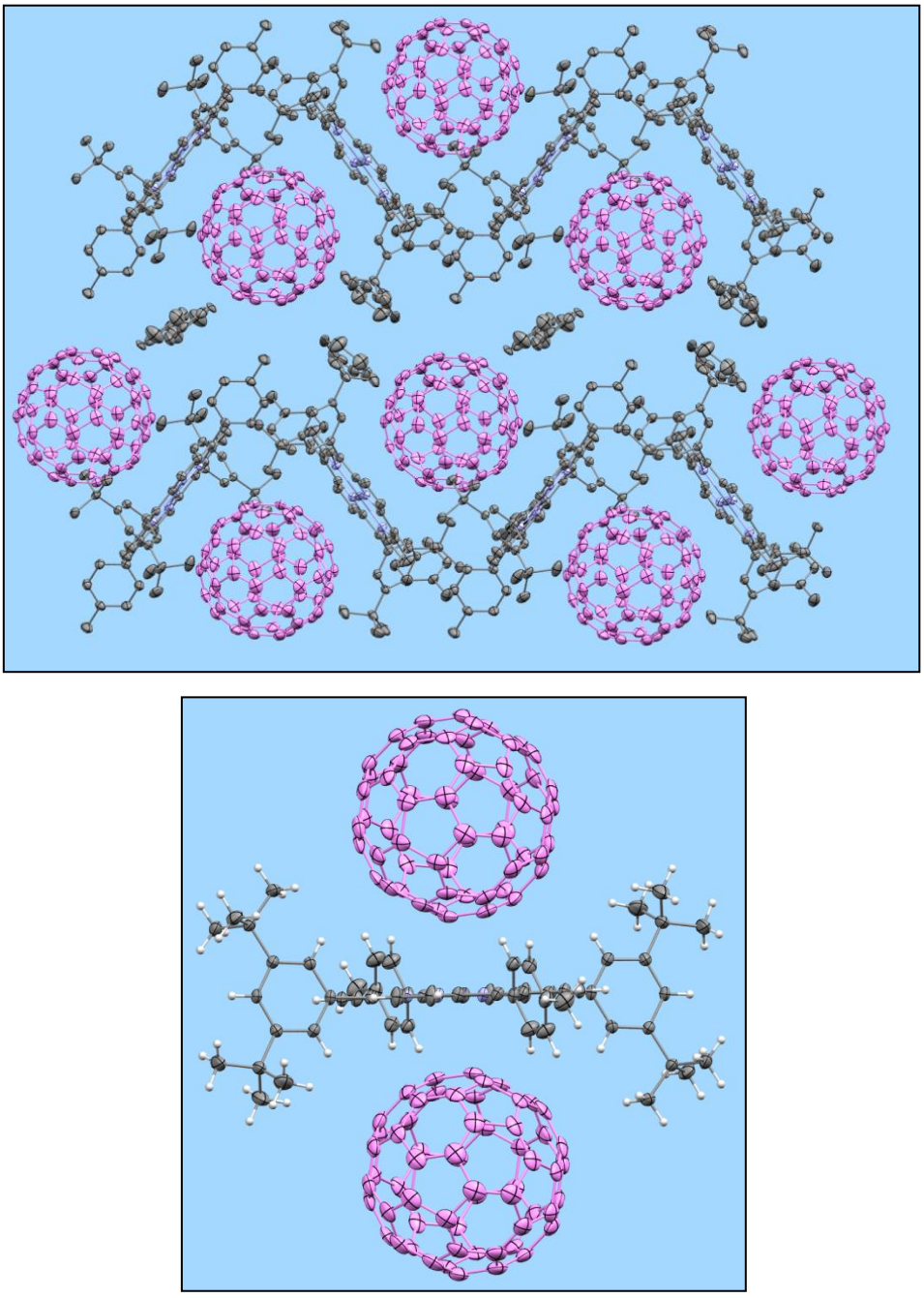

Figure 2.16: Co-crystallate packing structure (hydrogen atoms omitted for clarity) and the side view of the close contacts between the porphyrin and fullerene in **Zn2.11**.C_{60}.**toluene.** Represented with atomic displacement parameters shown as thermal ellipsoids at 50% probability.

Zn2.11 has been co-crystallized with C_{70} from a solution of toluene. This co-crystallate structure, shown in Figure 2.17, reveals a 1:2 porphyrin to fullerene ratio to give **2.11.2C_{70}.** The porphyrin is complexed by a pair of C_{70}, one on each side of the porphyrin. The 24-atom porphyrin mean plane to closest carbon distance is 2.78Å and the zinc to fullerene carbon distance is 2.79Å. The fullerene is centered side on over the porphyrin to maximize π-π interaction between the porphyrin and fullerene. The fullerene lies diagonally over the

porphyrin to maximize the *ortho* CH-π interactions from the tolyl and *tert*-butyl phenyls substituents. The *tert*-butyl methyls show CH-π interactions which range from 3.0-3.40 Å.

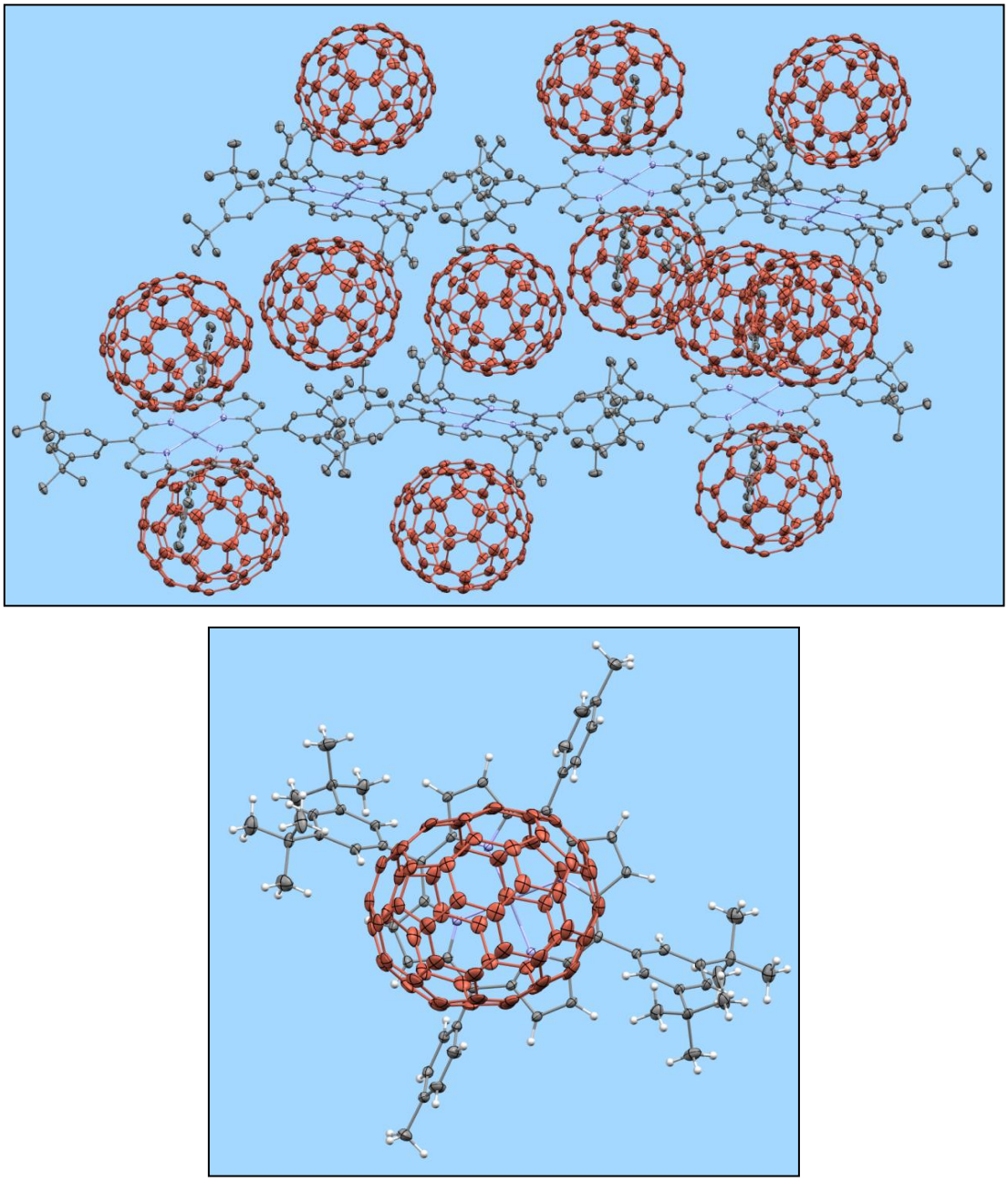

Figure 2.17: Co-crystallate packing structure (hydrogen atoms omitted for clarity) and the top view of the close contact between the porphyrin and fullerene for **Zn2.11.C_{70}** represented with atomic displacement parameters shown as thermal ellipsoids at 50% probability.

2.6.2 Porphyrin-Fullerene Co-Crystallate Zn2.14.3C_{60}.3toluene

Bis(3,5-dimethoxyphenyl)-di-3,5-*tert*-butylphenyl-porphyrin **2.14** was also prepared as a side product from the Suzuki coupling of dibromo porphyrin **2.8** and 3,5-dimethoxyphenyl boronic acid and 4-acetamidophenyl boronic acid. Single crystals of the zinc analog **Zn2.14** and C_{60} co-crystallates have been grown from toluene to give a 1:3 porphyrin to fullerene ratio to give **Zn2.14.3C_{60}.3toluene** (Figure 2.18). Each porphyrin is complexed by a pair of fullerenes with a distance of 2.87 Å, one on each side of the porphyrin. The fullerenes are offset from the centre of the porphyrin as there is a close contact with a third fullerene situated between two porphyrins at distance of 3.12-3.16 Å (shown in dark purple in Figure 2.13). The *ortho* protons on both the methoxy and the *tert*-butyl phenols display CH-π distances ranging from 2.85-3.07 Å. CH-π interactions between the methyl protons on the *tert*-butyl are present as well as one additional CH-π interaction from the methoxy groups on each side of the porphyrin. The methyls are orientated toward the fullerene, enhancing the number of close contacts between the porphyrin and the fullerene (Figure 2.19).

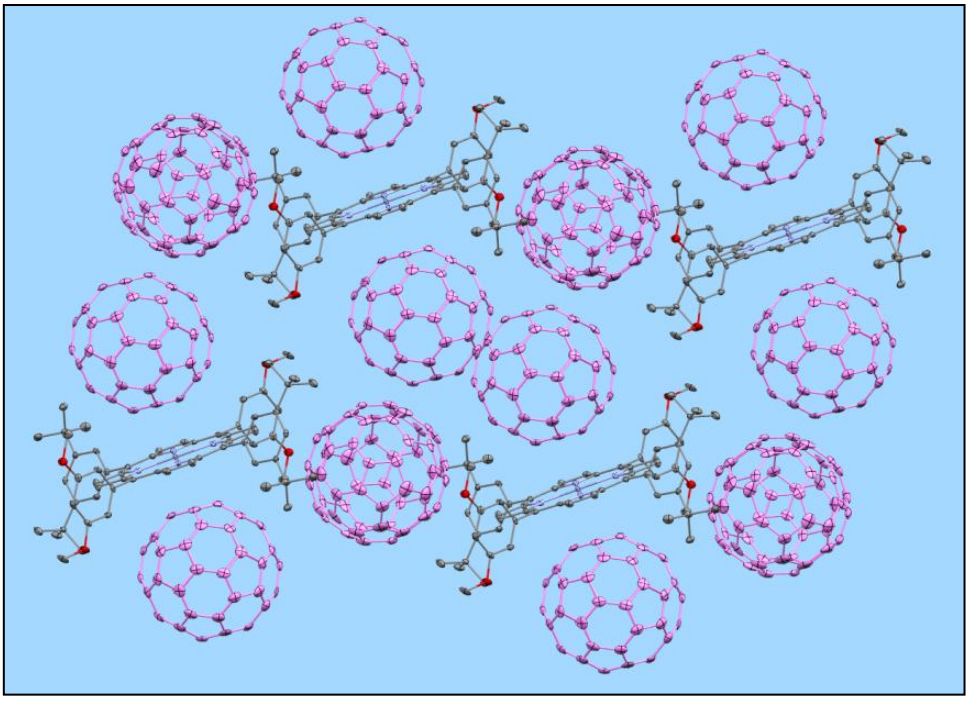

Figure 2.18: Co-crystallate packing structure for **Zn2.14.C_{60}.toluene**. Represented with atomic displacement parameters shown as thermal ellipsoids at 50% probability (hydrogens omitted for clarity).

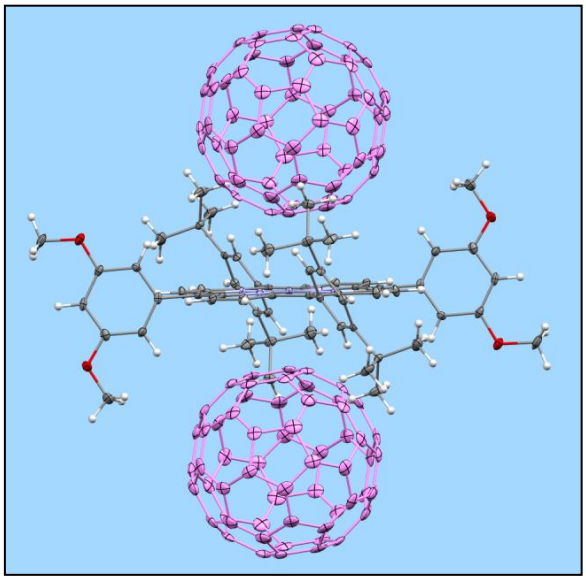

Figure 2.19: Side view of the close contacts between the porphyrin and fullerene for **Zn2.14.C_{60}.toluene**. Represented with atomic displacement parameters shown as thermal ellipsoids at 50% probability

2.6.3 Porphyrin-Fullerene Co-Crystallate 2.7.C_{60}

Single crystals of the 3,5-di-*tert*-butyl phenyl porphyrin **2.7** and C_{60} were grown by slow evaporation from toluene by Dr Dani Lyons. Single crystal X-ray diffraction data was collected by Tania Groutso and the structure solved and refined by Associate Professor Peter Boyd. Crystal data is shown in Table 2.8 located in the experimental section of this chapter.

Porphyrin **2.7** co-crystallizes with C_{60} from toluene solution in a 1:1 ratio to give **2.7.C_{60}.** Figure 2.20 shows a zigzag structural motif of alternating porphyrin and fullerene molecules with an interplanar angle between the porphyrin planes of 45.5°. There is a two-fold disorder in the C_{60}. The fullerene is centered directly above with a distance between the closest fullerene carbon atom to the 24-atom porphyrin mean plane of 2.56 Å. As there are only two 3,5-di-*tert* butyl phenyl groups on the porphyrin there are fewer CH-π interactions from the *ortho* protons. The porphyrins display two CH-π interactions between a 3,5-di-*tert*-butyl phenyl methyl group and a *tert*-butyl phenyl with a distance of 3.25 Å each.

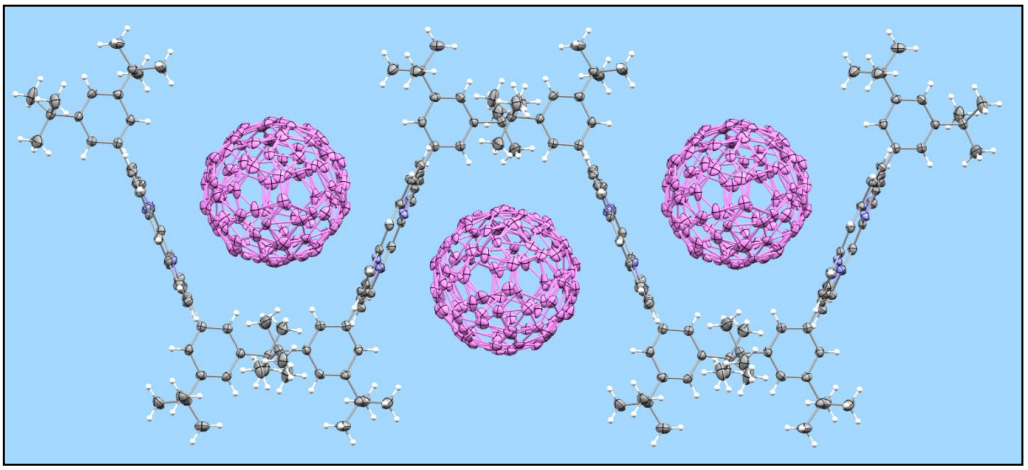

Figure 2.20: The zigzag arrangement between the porphyrins and fullerenes for **2.7**.$C_{60.}$ Represented with atomic displacement parameters shown as thermal ellipsoids at 50% probability.

The absence of phenyl substituents at the 10 and 20-positions of the **2.7** allow for an unconventional packing of the porphyrin and fullerenes. Figure 2.21 shows that the lack of a phenyl groups allows the C_{60} to form linear ribbons with short fullerene to fullerene distance of 2.96 Å. The porphyrin forms an offset stacking pattern with a porphyrin-porphyrin distance of 3.49 Å.

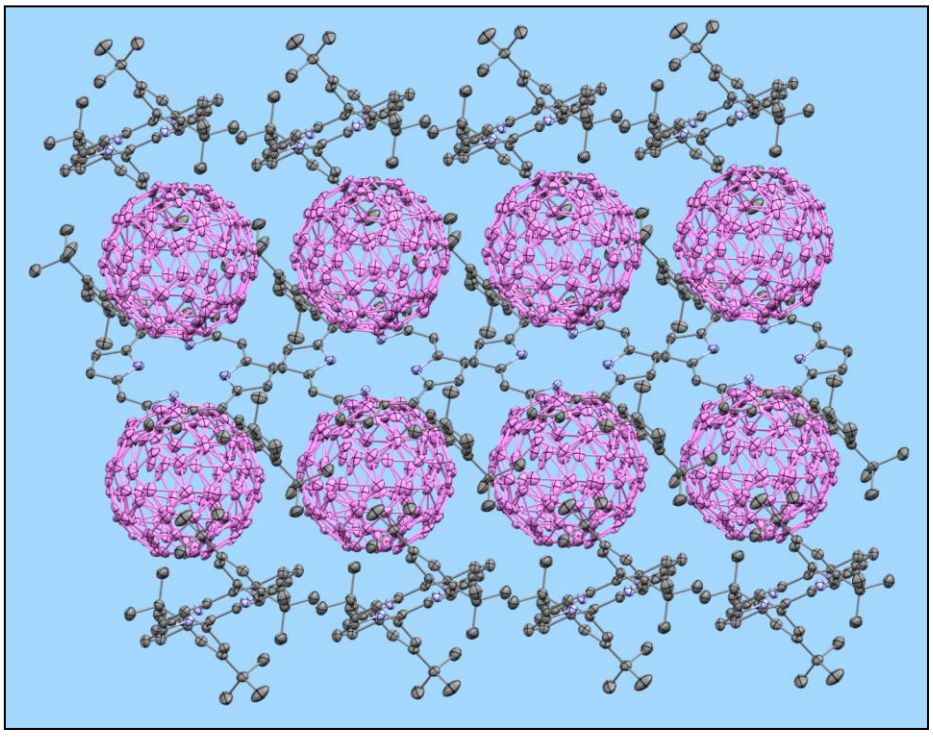

Figure 2.21: Co-crystallate packing structures of **2.7**.C_{60}, showing the linear packing of C_{60} and porphyrins. Represented with atomic displacement parameters shown as thermal ellipsoids at 50% probability (hydrogen atoms omitted for clarity).

The co-crystallate structures of porphyrins and fullerenes show how variation of the substituents on the *meso* positions of the porphyrin change the packing of the crystal and offer differing numbers of CH-π interactions. All phenyl groups offer CH-π interactions from the *ortho* protons. Substituents at *meta* position of the phenyl such as *tert*-butyl and methoxy groups increase the number of CH-π interaction to the fullerene from the methyl groups, with the *tert*-butyl groups the greatest number of CH-π interactions due to having a higher number of methyl groups.

2.7 Charge Transfer Bands

Photoexcitation of porphyrin electron donors, when in close proximity to electron acceptors such as fullerenes, may result in porphyrin to fullerene charge transfer transitions. These charge transfer transitions can sometimes be observed as bands with small extinction coefficients in the near infrared region of the absorption spectrum. Upon titration of bis-porphyrins **2.1**-**2.3** with fullerenes, the spectra show complex formation as indicated by a red shift and decrease in intensity of the Soret peak in the UV-visible spectra. A weak absorption band appears in the range of 700-760 nm which is attributable to the porphyrin-fullerene charge transfer band.

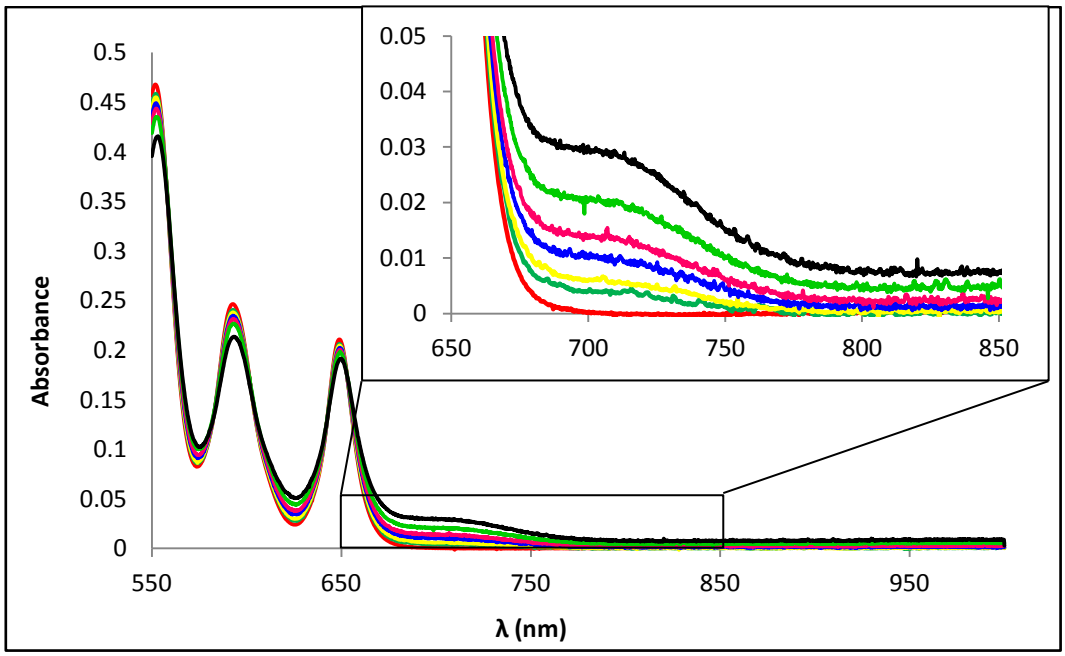

Figure 2.22: UV-visible absorption spectra of **2.1** [1.8 x10^{-5} M] in toluene upon addition of C_{60} (0-7 Eq.) showing the Q bands of the porphyrin and the emergence of the charge transfer band (inset magnified section of charge transfer band)

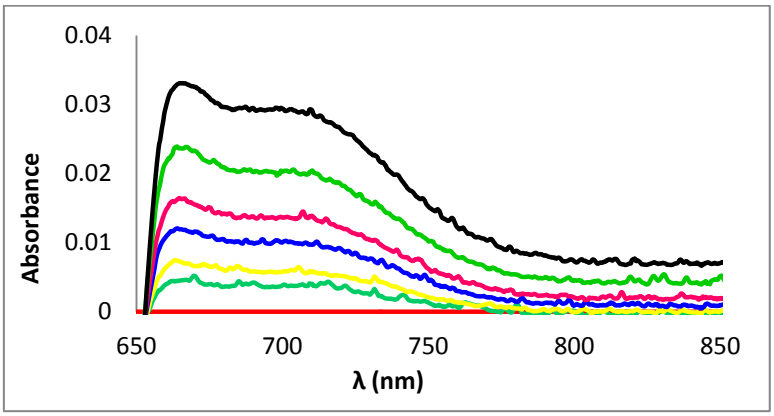

Figure 2.23: UV-visible absorption spectra of **2.1** [1.8 x10^{-5}] with C_{60} (0-7 Eq.) with the spectra of free **2.1** subtracted showing charge transfer band in toluene.

The charge transfer bands are of interest because information relevant to the rate of photoinduced electron transfer can be estimated from the wavelength, bandwidth and extinction coefficient of the band, as well as the inter-chromophore distance. The rate of electron transfer is proportional to the square of the electronic coupling constant (*V*) in the Marcus-Hush relationship for the rate of electron transfer (Equation 1.1).

$$k_{ET} = \left(\frac{4\pi^3}{h^2 \lambda k_B T}\right)^{1/2} V^2 \exp\left[-\frac{\left(\Delta G^0_{ET} + \lambda\right)^2}{4\lambda k_B T}\right]$$

Equation 1.1:

λ is the reorganisation energy upon electron transfer, *h* is Planck's constant, k_B is Boltzmann's constant, ΔG_{ET} is the free energy gap between the equilibrium nuclear configuration of the reactants and products, and T is the absolute temperature in K.

The charge transfer bands in the absorption spectra can be used to estimate the electronic coupling (V) between the porphyrin and the fullerene using Equation 2.2.

$$V = \frac{2.06 \times 10^{-2} \left(\varepsilon_{\max} \nu_{\max} \Delta\nu_{1/2}\right)^{1/2}}{R_{cc}}$$

Equation 2.2

where V is the electronic coupling in cm^{-1}, ε_{max} is the extinction coefficient of the charge transfer band at its maximum in mol^{-1} cm^{-1}, ν_{max} is the frequency of the charge transfer band in

cm^{-1}, $\Delta v_{1/2}$ full width at half height in cm^{-1} and R_{cc} is the porphyrin centre to fullerene distance in Å (which is taken as the common value for co-crystallates of 6.25 Å. [171])

Variation of the metal in the porphyrin core or alteration of the substituents on the porphyrin provides further evidence that this near IR band is a porphyrin to fullerene charge transfer transition. The energy of the band increases for C_{60} in the order; free base < Zn(II)< Cu (II) in the bis-porphyrin host **1.36** prepared by Hosseini.[122] This correlates with variation in the energies of the HOMO in the porphyrin, as calculated by DFT methods (Figure 2.24).[121,129] For example the charge transfer band for bis-porphyrin **1.36** is observed at 706 nm for the free base, when compared to 770 nm for the zinc derivative **Zn.1.36** which has a higher lying HOMO.

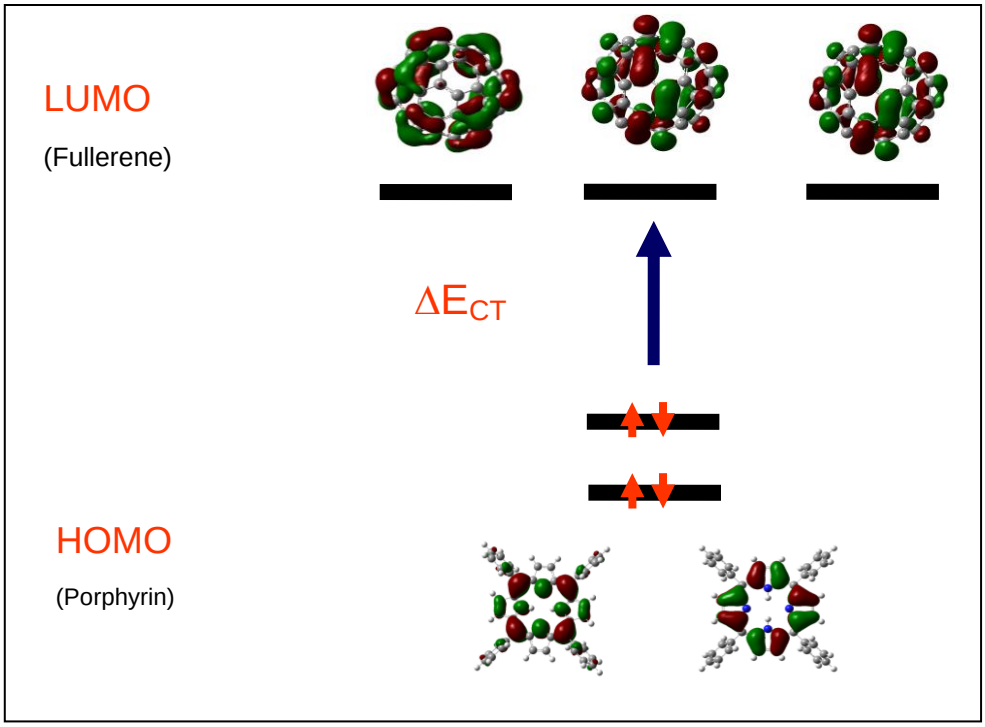

Figure 2.24: HOMO-LUMO gap of a porphyrin and fullerene.[121]

Table 2.4: Estimation of electronic coupling constants between the free base and zinc derivatives of bis-porphyrin hosts **2.1-2.3** and C_{60}

COMPLEX	**2.1**	**Zn2.1**	**2.2**	**Zn2.2**	**2.3**	**Zn2.3**
Binding Constant (K)	18,400	10,100	24,200	14,800	7,000	4,600
[Host] (M)	$1.85x10^{-05}$	$1.75x10^{-05}$	$1.49x10^{-05}$	$1.53x10^{-05}$	$1.39x10^{-05}$	$1.42x10^{-05}$
[C_{60}] (M)	$1.30x10_{-04}$	$1.30x10^{-04}$	$9.96x10^{-05}$	$9.96x10^{-05}$	$1.29x10^{-04}$	$1.37x10^{-04}$
[Complex] (M)	$1.2\ x10^{-05}$	$9.62x10^{-06}$	$1.02x10^{-05}$	$8.78x10^{-06}$	$6.48x10^{-05}$	$5.39x10^{-06}$
Absorbance height	0.028	0.023	0.023	0.021	0.130	0.011
V max (cm^{-1})	14060	12970	14100	12990	14530	13510
Δ V max (cm^{-1})	1600	2160	1720	2190	1780	2270
ε max	2200	2380	2190	2340	2010	2080
Rcc (Å)	6.25	6.25	6.25	6.25	6.25	6.25
V (cm^{-1})	**740**	**850**	**760**	**850**	**740**	**830**

Variation of the substituents, while having an effect on the ability of the bis-porphyrin to bind fullerenes, shows no real effect upon the electronic coupling. The zinc derivatives display higher electronic coupling than free base as the HOMO-LUMO gap is larger. This fact is reflected in the higher wavelength of the charge transfer bands of these derivatives. Both free base and zinc derivatives of **2.3** display a charge transfer band with slightly lower wavelengths when compared to **2.1** and **2.2**. This subtle change may be due to the lower association of C_{60} with the host, as higher concentrations for C_{60} are required to observe the band at the same absorbance. The difference in wavelength does not affect the electronic coupling between the two chromophores.

2.8 Summary

Several bis-porphyrins were prepared by modification of dibrominated porphyrins via Suzuki coupling and nickel catalyzed coupling. The effect of the porphyrin modification on binding of fullerenes has been explored.

New porphyrins have been prepared by Suzuki coupling of two different boronic acids to the dibrominated porphyrin, resulting in a statistical mixture of three differently substituted

porphyrins (A_2B_2,A_2BC, A_2C_2). Different substituents have been appended to the 15-position of the porphyrin. The substituents appended to the porphyrin are non substituted, tolyl or 3,5-dimethoxyphenyl. These porphyrins have been coupled to calixarene to give **2.1**-**2.3** respectively. Binding constants for these bis-porphyrins have been measured with C_{60}, C_{70} and $Lu_3N@C_{80}$. These hosts show that the type of substituent at the 15-position have a pronounced effect on the affinity of the bis porphyrin hosts for fullerenes. The highest association for fullerene was recorded with host **2.2** substituted with 3,5-dimethoxy phenyl groups. These functional group display binding similar of the 3,5-di-*tert*-butyl phenyl substituted host, due to the close CH-π interactions of the methoxy groups. Host **2.1**, with tolyl substituents displays a minor decrease in binding due to the removal of the CH-π interactions. Host **2.3,** bearing no aryl group, displays a dramatic decrease in binding. This has been attributed to the absence of the CH-π interaction of the of the aryl group *ortho* proton at the 15-position.

All hosts **2.1**-**2.3** display higher affinities for the larger fullerene C_{70} and the endohedral fullerene $Lu_3N@C_{80,}$ increasing by one and two orders of magnitude respectively. This has been attributed to the increased surface area which maximizes the π-π interactions between the fullerene and the porphyrin. Charge transfer bands have been observed for these bis-porphyrins and have shown that while variation of the substituents at the 15 position have an effect on the ability of the bis-porphyrin to bind fullerenes, no real effect on the electronic coupling between the porphyrin and fullerene is observed.

Phenoxyporphyrins prepared by a nickel catalyzed cross coupling between brominated porphyrins and substituted phenol, have been coupled to calixarenes to give bis-porphyrins **2.4** and **2.5**. While this coupling reaction shows great scope for increased functionalization of porphyrins, neither of these hosts displayed any affinity for either C_{60} or C_{70}. Reasons for the lack of association can be explained through computational modeling. Bis-porphyrin host **2.4** displays the potential to bind fullerenes with appropriate interplanar porphyrin angles and distances to accommodate fullerenes. However, the phenyls of the ether sterically hinder fullerene from accommodating the binding site. Bis-porphyrin **2.5** does not have a suitable geometry for the formation of a host-guest complex. The geometry of the free host orientates the porphyrin planes away from each other in the lower energy geometry. The host must undergo energetically unfavorable conformational changes in order to form a host-guest complex.

2.9 Experimental

2.9.1 General Experimental

All reactions were carried out in oven-dried glassware using standard Schlenk techniques. All commercial reagents were, unless otherwise noted, reagent grade and used without further purification. Air and moisture sensitive reagents were handled under an atmosphere of dry, oxygen free nitrogen unless otherwise noted. Solvents and liquid reagents were distilled under nitrogen. Dichloromethane, toluene and acetonitrile were distilled from calcium hydride. Methanol was dried with magnesium turnings and iodine. Tetrahydrofuran was distilled from sodium with benzophenone. Diethyl ether and hexane were dried using a MBRAUN MB SPS-800 solvent purifier. All solvent were distilled fresh or stored over molecular sieves and under an atmosphere of nitrogen. When used as a solvent or a reagent water was deionised.. Reactions were monitored by thin layer chromatography (TLC). Where compound were purified by chromatography, silica gel 0.032-0.063mm was used. Eluent mixtures described in text are v/v.

NMR spectra were recorded on either a Bruker DRX300 operating at 300 MHz for ^{1}H NMR for ^{1}H nuclei or with a either a Bruker AM-300 or a Bruker AM-400. NMR spectra were recorded in $CDCl_3$ containing TMS as reference, toluene or DMSO ^{1}H NMR data are reported as chemical shifts (δ) in parts per million (ppm) relative to TMS. ^{1}H NMR data are reported as chemical shifts relative to integral, multiplicity (s, singlet, d, doublet, t, triplet, q, quartet, m, multiplet), coupling constants (J, Hz) and assignments.

Mass spectrum samples were run on either a VG-7070 mass spectrometer at a nominal accelerating voltage of 70 eV for recording low resolution mass spectra, and fast atom bombardment (FAB^{+}) or a Bruker microQTOF coupled with a KD Scientific syringe pump.

2.9.2 General Procedure for UV-Visible Titrations

UV-Visible complexation titrations were recorded on a Perkin Elmer Lambda 35 UV-visible NIR Spectrophotometer. UV-Visible complexation titrations were performed by use of a dual

beam spectrometer with 1 cm path quartz curvettes running a spectrum of the host solution in toluene or acetonitrile at μM concentration and a blank of the corresponding solvent. The maximum absorption at the wavelength of Soret Band was recorded. To each curvettes, the desired fullerene (C_{60} C_{70} or $Lu_3N@C_{80}$) in toluene was added in incremental aliquots using a microlitre syringe. After each addition of guest a UV-visible spectrum was recorded and absorbance was measured at the wavelength of the free host Soret. The data was analyzed using SigmaPlot 11.0 and fit using a non linear least squares function Equation 2.1.

2.9.3 Computational Modeling Software and Calculations.

Gaussian 09, Revision A 1 was used for molecular modeling calculations.[172] Two-layer ONIOM optimizations were performed. DFT was utilized for modeling the high layer with the B3LYP hybrid functional and the 6-31g(d) basis set. Molecular mechanics was used for the low layer using a universal force field. In the molecular mechanics model atomic charges were estimated using the equalization method (Qeq) with electronic embedding. The opt=nomicro function was used to improve accuracy.

para-tert-butylcalixarene[105]

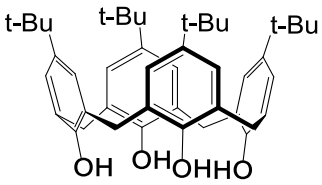

para-tert-butylphenol (100 g, 0.66 mmol) was heated with 40% formaldehyde (62 mL) and NaOH, (1.2 g, 0.03 mmol) in a 2 L three necked round bottom flask equipped with a mechanical stirrer. Contents were heated via a heating mantle for 1.5 hours at 110^{o}C during which time the mixture became yellow and viscous as water evaporates. The mixture can froth taking up the most of the volume of the flask. Warm diphenyl ether (500 mL) was added and the contents heated with a stream of nitrogen for 20 minutes to facilitate removal of water. The flask was fitted with a reflux condenser and refluxed for two hours during which time the contents turned dark brown in colour. The solution was then cooled, ethyl acetate (1 L) was added to precipitate out the product **1** and left to stir for 1 hour. The product was then filtered

and washed with ethyl acetate (2 x 100 mL), acetic acid (1 x 100 mL) and water (1 x 100 mL), 65g (65%).

^{1}H NMR (*400 MHz, $CDCl_3$*) ppm: 10.33 (s, 4H, ArO*H*), 7.04 (s, 8H, ArH), 4.25 (s, 4H, $ArCH_2Ar$), 3.47 (s, 4H, $ArCH_2Ar$), 1.21 (s, 72H, $C(CH_3)_3$)

FAB-MS: Calculated $[M]^+$: $C_{44}H_{56}O_4$ 648.4178, found 648.4182 *m/z*.

25,26,27,28-tetrahydroxycalixarene[111]

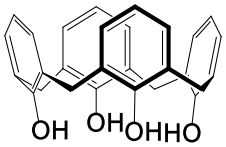

para-tert-butylcalixarene (25 g, 38.6 mmol) was dissolved in anhydrous toluene (500 mL) and heated to 90^{o}C for 30 minutes. The solution was cooled to 50^{o}C, $AlCl_3$ (25 g, 187 mmol) was added and stirred vigorously for 2 hours at 50-55^{o}C. The solution was cooled to 5^{o}C and stirred with HCl (1M, 250 mL) for 30 minutes. The organic phase was separated, washed with water (2 x 300) and the solvent removed via reduced pressure to leave an orange residue. Diethyl ether (1 L) was then added to the residue to precipitate the unsubstituted calixarene **19**. The product was then filtered off and recrystallized from chloroform/methanol as off white solid. Yield 9.1 g, (64%).

^{1}H NMR (*400 MHz, $CDCl_3$*) ppm: 10.19 (s, 4H, ArOH), 7.04 (d, 8H, J= 7.6 Hz, ArH), 6.71 (t, 4H, J= 7.5 Hz, ArH) 4.25 (s (br), 4H, $ArCH_2Ar$), 3.54 (s (br), 4H, $ArCH_2Ar$).

FAB-MS: Calculated $[M]^+$: $C_{28}H_{24}O_4$ 424. 1674, found 424.1675 *m/z*.

2.9.4 Synthetic Procedures for Porphyrin Modification Via Suzuki Coupling

Dipyrromethane (2.6)[161]

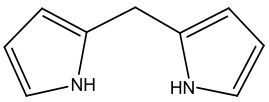

A solution of paraformaldehyde (1.0 g, 0.34mmol) in pyrrole (120 mL) was bubbled with N_2 for 30 minutes. Indium chloride (0.38 g, 1.7 mmol) was added and heated at 90°C for 2.5 hours. The solution was cooled and sodium hydroxide (2.04 g, 51.0 mmol) was added stirred for one hour at room temperature. The crude material was filtered through celite and the pyrrole was removed *in vacuo*. The crude material was extracted with ethyl acetate/hexane (4:1). The solvent was removed *in vacuo* to give **2.6** as a light brown solid, 4.1 g (91%).

^{1}H NMR (*400 MHz, $CDCl_3$*) ppm: 10.47 (s, NH, 2H), 6.57 (m, PyH, 2H), 5.87 (m, PyH, 2H), 5.72, (m, PyH, 2H), 3.79 and 3.65 (s, *meso*H, 2H).

3, 5-tert-butyl benzaldehyde[40]

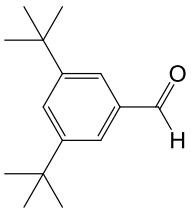

A solution of 3,5-di-tert-butyltoluene (60 g, 320 mmol) and N-bromosuccinimide (80 g, 0.450 mmol) in benzene (150 mL) was heated in a 2 L round bottom flask under visible light irradiation, during which time the reaction takes up most of the volume of the flask and the light must be periodically switched off. When the reaction ceased, the mixture was was then cooled, filtered and the benzene was removed under reduced pressure. The residue was added to a solution of hexamethylenetetramine (145 g, 900 mmol) in a 1:1 H_2O/EtOH mixture (150 mL). The solution was heated at reflux for 4 h, HCl was added (12M, 60 mL) and heating at reflux was continued for 30 min. The ethanol was removed under reduced pressure, and the remaining aqueous layer was extracted with ether. The ether layer was dried with magnesium sulphate and the solvent was removed *in vacuo*. Recrystallization from ethanol yielded the desired product as white crystals, 38g (60%).

5, 15-bis(3,5-di-*tert*-butylphenyl) Porphyrin (2.7)[163]

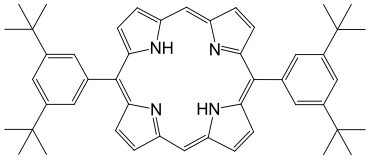

A solution of dipyrromethane **2.6**, (1.0 g, 6.84 mmol) and 3,5-di-*tert*-butyl benzaldehyde (1.49 g, 6.84 mmol) in dichloromethane (1.5 L) was bubbled with nitrogen for one hour. Trifluoroacetic acid (0.1 mL, 1.36 mmol) was added and the solution stirred for 18 hours. Chloranil (4.0 g, 16 mmol) was added to the reaction mixture and the solution refluxed for two hours. The solvent was removed *in vacuo* and the crude material passed thought a plug of silica eluting with hexane/dichloromethane (2:1), the solvent removed to give **2.7** as a purple solid, 0.820g (35%).

^{1}H-NMR (*$CDCl_3$, 300 MHz*): 10.31 (s, *meso*H, 2 H); 9.41 (d, H_β, J = 4.50, 4H); 9.15 (d, H_β, J = 4.50, 4H); 8.16 (d, ArH, J =1.80, 4H); 7.85 (t, ArH, J =1.80, 2H); 1.59 (s, $C(CH_3)_3$, 36H), -3.00 (s, NH, 2H).

5,15-bis(3,5-di-*tert*-butylphenyl) Porphyrin (Zn2.7)[163]

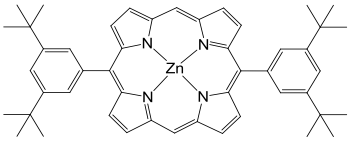

A saturated solution of zinc (II) acetate in methanol (40 mL) was added to a solution of porphyrin **2.**7 (3.30 g, 1 mmol) in dichloromethane (200 mL), the mixture was heated until no free base porphyrin was observed in the UV-visible spectrum. The solution was concentrated and purified by passing through a plug of silica eluting with dichloromethane/hexane (1:2) and the solvent evaporated to produce a magenta solid, 3.37g (94%).

^{1}H NMR (400 MHz, *CDCl3*) ppm: 9.46 (d, H_β, J = 4.50 Hz, 4H), 9.21 (d, H_β, J = 4.50 Hz, 4H), 8.15 (d, ArH, J = 1.70 Hz, 4H), 7.87 (m, ArH, J = 1.70 Hz, 2H), 1.57 (s, $C(CH_3)_3$, 36H).

HRMS (ESI-TOF-MS) Calculated: $[M+H]^+$: $C_{48}H_{52}N_4Zn$: 748.3478 m/z, found: 748.3480 m/z

5,15-Bis(3,5-di-*tert*-butylphenyl)-10,20-dibromoporphyrin (2.8)

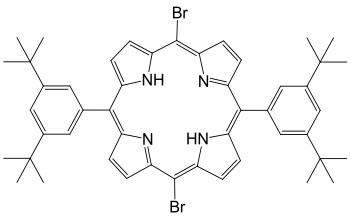

A solution of zinc porphyrin **Zn.7** (0.8 g, 1.07 mmol) and pyridine (3.5 mL) in dichloromethane (200 mL) was stirred at 0^{o}C under nitrogen. Recrystallized NBS (0.387 g, 2.19 mmol) was added and the solution turned green immediately. The solution was stirred for ten minutes and then was quenched with the addition of acetone (30 mL) the solution was diluted with methanol (50 mL) dichloromethane was removed *in vacuo*. The resulting precipitate was filtered and washed with methanol (3 x 50 mL). The purple solid was suspended in dichloromethane (20 mL) and washed with HCl (10 mL, 12M) and water: acetone (3:1). The solvent was removed in vacuo to produce a purple solid, 0.67 g, (81%).

^{1}H NMR (400 MHz, $CDCl_3$) ppm: 9.62 (d, H_β, J = 5.01 Hz, 4H), 8.88 (d, H_β, J = 5.01 Hz, 4H), 8.03 (d, ArH, J = 1.80 Hz 4H), 7.84 (t, ArH, J = 1.80 Hz 2H), 1.57 (s, $C(CH_3)_3$, 36H), -2.66 (s, NH, 2H)

5-(4-acetamidophenyl)-15-tolyl, 10,20-bis(3,5-di-*tert*-butylphenyl) porphyrin (2.10) (2.11) (2.12)

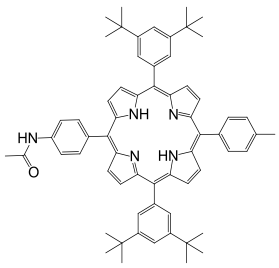

2.10

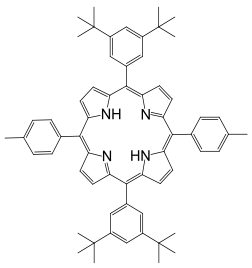

2.11

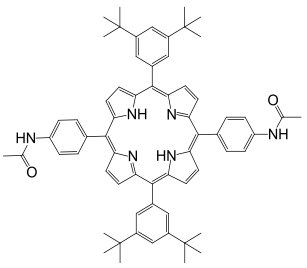

2.12

A suspension of dibromoporphyrin **2.8** (1.0 g, 1.18 mmol), tetrakis(triphenylphosphine) palladium (135 mg, 0.118 mmol), caesium carbonate (2.3 g, 7.1 mmol), 4-acetamidophenyl boronic acid (0.317 g 1.77 mmol), and 4-tolylboronic acid (0.177 g, 0.130 mmol) in

toluene/DMF (120 mL, 3:1) was taken through three freeze pump thaw cycles and heated at 90^{o}C for 16 hours. The solution was cooled, filtered through celite and the solvent removed *in vacuo*. The residue was purified via flash chromatography eluting with dichloromethane, dichloromethane/ethyl acetate (9:1), dichloromethane/ ethyl acetate (3:1). Three fraction were collected and evaporated, giving the ditolyl-porphyrin **2.11** as the first fraction, 0.205 g (20%), the mixed porphyrin **2.10** as the second fraction, 0.554 g, (54%), and the diacetamidophenyl **2.12** porphyrin as the third fraction, 0.150 g (15%).

2.10: ^{1}H NMR (300 MHz, *CDCl$_3$*) ppm: 8.86 (m, H$_\beta$ 8H), 8.19 (d, ArH, *J* = 7.8 Hz, 2H), 8.10 (d, ArH, *J* = 7.70 Hz, 2H), 8.08 (d, ArH, *J* = 1.80 Hz, 4H), 7.89 (d, ArH, *J* = 8.10 Hz, 2H), 7.80 (t, ArH, *J* = 1.80 Hz, 2H), 7.55 (d, *J* = 8.10 Hz, 2H), 7.48 (s, NH, 1H), 2.69 (s, CH$_3$, 3H), 2.36 (s, CH$_3$ 3H), 1.53 (s, C(CH$_3$), 36H), -2.72 (s, NH, 2H).

2.10: HRMS (ESI-TOF-MS) Calculated: [M+H]$^+$: $C_{63}H_{68}N_5O$: 910.5418 m/z, found: 910.5438 m/z.

2.11: ^{1}H NMR (300 MHz, *CDCl$_3$*) ppm: 8.87 (m, H$_\beta$ 8H), 8.10 (d, ArH, *J* = 7.70 Hz, 2H), 8.08 (d, ArH, *J* = 1.80 Hz, 4H), 7.81 (t, ArH, *J* = 1.80 Hz, 2H), 7.55 (d, ArH, J = 7.7 Hz, 2H 7.48 (d, ArH, *J* = 7.70 Hz, 2H), 2.69 (s, CH$_3$ 6H), 1.52 (s, C(CH$_3$), 36H), -2.72 (s, NH, 2H).
2.11: HRMS (ESI-TOF-MS) Calculated: [M+H]$^+$:$C_{62}H_{67}N_4$: 867.5288 m/z, found: 867.5286 m/z.
2.12: ^{1}H NMR (400 MHz, *CDCl$_3$*) ppm: 8.89 (d, H$_\beta$, *J* = 4.7 Hz, 4H) 8.85 (d, H$_\beta$, *J* = 4.7 Hz, 4H), 8.18 (d, ArH, *J* = 8.3 Hz, 4H), 8.08 (d, ArH, *J* = 1.80 Hz, 4H), 7.89 (d, ArH, *J* = 8.3 Hz, 4H), 7.79 (t, ArH, *J* = 1.80 Hz, 2H), 7.53 (s, ArH, 2H), 2.36 (s, C(O)CH$_3$, 6H), 1.53 (s, C(CH$_3$), 36H), -2.73 (s, NH, 2H).

2. 12: HRMS (ESI-TOF-MS) Calculated: [M+H]$^+$: $C_{64}H_{68}N_6O_2$: 953.5405 m/z, found: 952.5391 m/z.

5-(4-aminophenyl),15-tolyl, 10,20-bis(3,5-di-*tert*-butylphenyl) porphyrin (2.15)

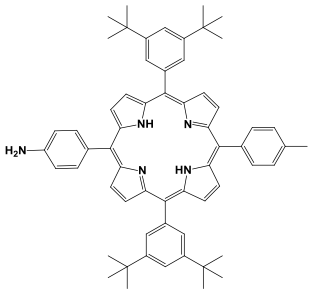

A suspension of the 4-acetamidophenyl porphyrin **2.10** (0.505 g, 0.528 mmol) in ethyl acetate (20 mL) and hydrochloric acid (12 M, 50 mL) was refluxed for three hours. The solution was then cooled, diluted with water (50 mL) and neutralized by slow addition of solid sodium bicarbonate. The aqueous solution was extracted with dichloromethane (200 mL), washed with brine, dried with sodium sulfate and concentrated. The residue was purified via flash chromatography, eluting with dichloromethane/hexane (19:1) and the solvent removed to give amino porphyrin **2.15** as a purple solid, 0.467 g (97%).

^{1}H NMR (400 MHz, *CDCl$_3$*) ppm: 8.93 (d, H$_\beta$, *J* = 4.7 Hz, 2H), 8.84 (m, H$_\beta$, 6H) , 8.10 (d, ArH, *J* = 7.80 Hz, 2H), 8.08 (d, ArH, *J* = 1.85 Hz, 4H), 8.00 (d, ArH, *J* = 8.30 Hz, 1H), 7.8 (t, ArH, *J* = 1.85, 2H), 7.54 (d, ArH, *J* = 8.30 Hz, 1H), 7.06 (d, ArH, *J* = 7.80 Hz, 1H), 2.72 (s, CH_3, 3H), 1.52 (s, $C(CH_3)_3$ 36H), -2.72 (s, NH, 2H).

HRMS (FAB-MS) Calculated: $[M+H]^+$: $C_{61}H_{66}N_5$: 868.5313 m/z, found: 868.5180 m/z.

25,27-bis[methoxy(4-amidophenyl)-15- tolyl-10,20-di-(3,5-di-*tert*-butylphenyl) porphyrin]-26-28-dihydroxycalix-[4]arene (2.1)

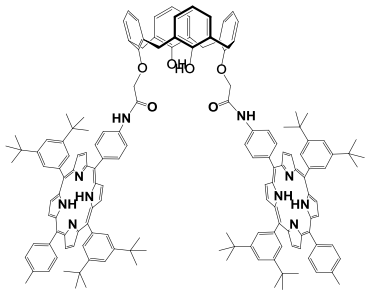

A solution of calixarene diacid **2.19** (0.055 g, 0.102 mmol), N,N'-dicyclohexylcarbodiimide (0.350 g, 1.71 mmol) and amino porphyrin **2.15** (0.15 g, 0.171 mmol) in dichloromethane (20 mL) was stirred for 16 hours. The solution was then concentrated and product was purified by flash chromatography eluting with chloroform/hexane (9:1) and the solvent evaporated to give the bis-porphyrin **2.1** as a purple solid, 0.110 g (58%). An analytically pure sample of **2.1** was prepared via recrystallization from chloroform/methanol at -4°C.

^{1}H NMR (300 MHz, *CDCl$_3$*) ppm: 11.04 (s, ArOH, 2H), 9.14 (d, H$_\beta$, *J* = 4.90 Hz, 4H), 8.89 (m, H$_\beta$, 4H), 8.80 (s, H$_\beta$, 8H), 8.28 (d, ArH, *J* = 2.20 Hz, 8H), 8.06 (d, ArH, *J* = 8.20 Hz, 4H), 8.00 (d, ArH, *J* = 1.80 Hz, 8H), 7.70 (t, ArH, *J* = 1.80, Hz, 4H), 7.50 (d, ArH, *J* = 8.20 Hz, 4H), 7.21 (d, ArH, *J* = 7.50 Hz, 4H), 7.15 (d, ArH, *J* = 7.50 Hz, 4H), 6.96 (t, ArH, *J* = 7.50 2H), 6.85 (t, ArH, *J* = 7.50, Hz, 2H), 4.96 (s, OCH$_2$C(O), 4H), 4.49 (d, ArCH$_2$Ar, *J* = 13.80 Hz, 4H), 3.73 (d, ArCH$_2$Ar, *J* = 13.80 Hz, 4H), 2.67 (s, CH$_3$, 6H), 1.54 (s, C(CH$_3$)$_3$ 72H), -2.77 (s, NH, 4H).

HRMS (ESI-TOF-MS), Calculated: [M+2H]$^+$: C$_{154}$H$_{156}$N$_4$: 2241.2209 m/z, found: 2241.2120 m/z.

25,27-bis[methoxy(4-amidophenyl)-15- tolyl-10,20-di-(3,5-di-*tert*-butylphenyl) Zn(II) porphyrin]-26-28-dihydroxycalix[4]arene (Zn2.1)

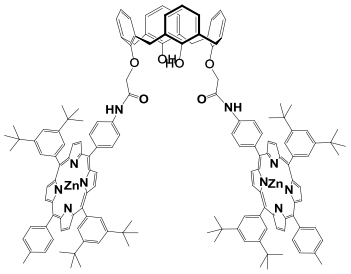

A saturated solution of Zn(II) acetate in methanol (5 mL) was added to a solution of bis-porphyrin **2.1** (0.030 g, 0.013 mmol) in chloroform (15 mL), the mixture was heated until no free base was observed in the UV-visible spectrum. The solution was washed with brine, dried with sodium sulfate and concentrated. The Zn(II) bis-porphyrin purified by flash chromatography eluting with dichloromethane/hexane (9:1) and the solvent evaporated to produced a pink solid, 0.030g, (97%). An analytically pure sample of **Zn2.1** was prepared via recrystallization from chloroform/methanol at -4°C

^{1}H NMR (400 MHz, *CDCl$_3$*) ppm: 11.03 (s, ArOH, 2H), 9.25 (d, H$_\beta$, *J* = 4.70 Hz, 4H), 9.02 (d, H$_\beta$, *J* = 4.70 Hz, 4H), 8.90 (s, H□, 8H), 8.29 (s, ArH, 8H), 8.06 (d, ArH, *J* = 8.00 Hz, 4H), 8.01 (s, ArH, 8H), 7.70 (s, ArH, 4H), 7.50 (d, *J* = 8.00 Hz, 4H), 7.25 (d, ArH, *J* = 7.40 Hz, 4H), 7.15 (d, ArH, *J* = 7.50 Hz, 4H), 7.00 (t, ArH, *J* = 7.40Hz, 2H), 6.86 (t, ArH, *J* = 7.50Hz, 2H), 4.96 (s, OCH$_2$C(O), 4H), 4.49 (d, ArCH$_2$Ar *J* = 13.30 Hz, 4H), 3.73 (d, ArCH$_2$Ar *J* = 13.30 Hz, 4H), 2.67 (s, CH$_3$, 6H), 1.42 (s, C(C<u>H</u>$_3$)$_3$ 72H).

HRMS (ESI-TOF-MS), Calculated: $[M+2H]^{2+}$: $C_{154}H_{152}N_4Zn_2$: 2365.2209 m/z, found: 2365.2108 m/z.

5-(4-acetamidophenyl),15-(3,5-di-methoxyphenyl),10,20-bis(3,5-di-*tert*-butylphenyl) porphyrin (2.13) + (2.14) + (2.12)

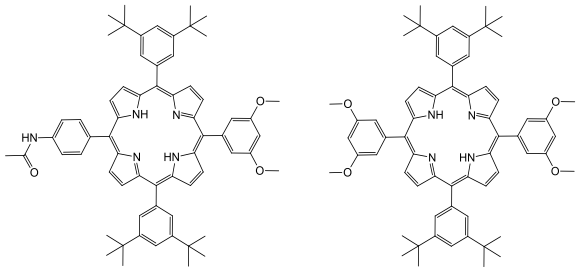

2.13 **2.14**

A suspension of dibromo porphyrin **2.8** (1.0 g, 1.18 mmol), tetrakis(triphenylphosphine) palladium (0.135 g, 0.118 mmol), caesium carbonate (2.3 g, 7.1 mmol), 4-acetamidophenyl boronic acid (0.463 g, 1.77 mmol), and 3,5-dimethoxyphenyl boronic acid (0.215 g, 1.18 mmol) in of toluene/DMF (120 mL, 3:1) was taken through three freeze pump thaw cycles and heated at 90^{o}C for 16 hours. The solution was cooled filtered through celite and the solvent removed by *in vacuo*. The residue was purified via flash chromatography eluting with dichloromethane, dichloromethane/ethyl acetate (9:1), dichloromethane/ethyl acetate (3:1), three fractions were collected and the solvent evaporated, giving di-3,5-methoxyphenyl-porphryin **2.14** as the first fraction, 0.210 g (19%), the mixed Suzuki porphyrin **2.13** as the second fraction, 0.564 g, (50%), and the diacetamidophenyl porphyrin **2.12** as the third fraction, 0.157 g (14%).

2.13 ^{1}H NMR (400 MHz, *CDCl$_3$*) ppm: 8.87 (d, H$_\beta$, *J* = 5.00 Hz, 4H), 8.81 (d, ArH, *J* = 2.25 Hz, 2H), 8.77 (d, H$_\beta$, *J* = 5.00 Hz, 4H), 8.10 (d, ArH, *J* = 8.10 Hz, 2H), 8.01 (d, ArH, *J* = 1.75 Hz, 4H), 7.80 (d, ArH, *J* = 8.10 Hz, 2H), 7.73 (t, ArH, *J* = 1.75, 2H), 7.41 (s, NH,1H), 7.34 (d, ArH, *J* = 2.25 Hz, 2H), 6.80 (m, ArH, 1H), 3.88 (s, OCH$_3$, 6H), 2.27 (s, CH$_3$, 3H), 1.46 (s, C(CH$_3$)$_3$ 36H), -2.81 (s, NH, 2H).

2.13 HRMS (ESI-TOF-MS) Calculated: [M+H]$^{+}$: $C_{64}H_{70}N_5O_3$: 956.5479 m/z, found: 956.5301 m/z.

2.14 ^{1}H NMR (400 MHz, *CDCl$_3$*) ppm: 8.87 (m, H$_\beta$, 8H), 8.07 (d, ArH, *J* = 1.75 Hz, 4H), 7.75 (t, ArH, *J* = 1.75, 2H), 7.32 (d, ArH, *J* = 2.20 Hz, 4H), 6.82 (m, ArH, 2H), 3.88 (s, OCH$_3$, 12H), 1.46 (s, C(CH$_3$)$_3$ 36H), -2.81 (s, NH, 2H).

2.14 HRMS. (ESI-TOF-MS) Calculated: $[M+H]^+$: $C_{64}H_{70}N_5O_3$: 959.5398 m/z, found: 959.5396 m/z.

5-(4-aminophenyl),15-(3,5-di-methoxyphenyl),10,20- bis(3,5-di-*tert*-butylphenyl) porphyrin (2.16)

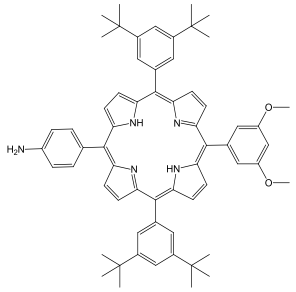

A suspension of the 4-acetamidophenyl porphyrin **2.13** (0.565 g, 0.565 mmol) in ethyl acetate (20 mL) and hydrochloric acid (12 M, 50 mL) was refluxed for three hours. The solution was then cooled, diluted with water (50 mL) and neutralized by slow addition of solid sodium bicarbonate. The aqueous solution was extracted with dichloromethane, washed with brine, dried with sodium sulfate and concentrated. The residue was purified via flash chromatography, eluting with dichloromethane and the solvent evaporated to give the amino porphyrin **2.16** as a purple solid, 0.519g (96%).

^{1}H NMR (300 MHz, *CDCl*$_3$) ppm: 8.97 (m, H_β, 6H), 8.91 (d, H_β, *J* = 4.75 Hz, 2H), 8.13 (d, ArH, *J* = 1.75 Hz, 4H), 8.02 (d, ArH, *J* = 8.20 Hz, 2H), 7.84 (t, ArH, *J* = 1.75 Hz, 2H), 7.46 (d, ArH, *J* = 2.25 Hz, 2H), 7.05 (d, ArH, *J* = 8.20 Hz, 2H), 6.92 ArH, (t, ArH, *J* = 2.25 Hz, 1H), 3.98 (s, OCH_3, 6H), 1.57 (s, $C(CH_3)_3$ 36H), -2.66 (s, NH, 2H).

HRMS (ESI-TOF-MS), Calculated: $[M+H]^+$: $C_{62}H_{68}N_5O_2$: 914.5368 m/z, found: 914.5217 m/z.

25,27-bis[methoxy(4-amidophenyl)-15-(3,5-di-methoxyphenyl) -10,20-di-(3,5-di-*tert*-butylphenyl) porphyrin]-26-28-dihydroxycalix[4]arene (2.2)

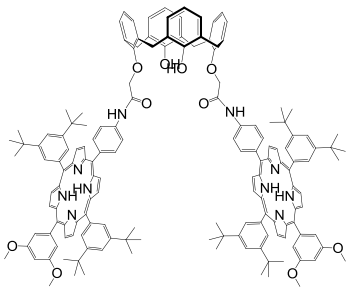

A solution of calixarene diacid **2.19** (0.044 g, 0.082 mmol), N,N'-dicyclohexylcarbodiimide (0.45 g, 2.20 mmol) and amino porphyrin **2.16** (0.10 g, 0.11 mmol) in dichloromethane (20 mL) was stirred for 16 hours. The solution was then concentrated and product was purified by flash chromatography, eluting with chloroform/hexane (9:1) and the solvent evaporated to give the bis-porphyrin **2.2** as a purple solid, 0.64 g (51%). An analytically pure sample of **2.2** was prepared via recrystallization from chloroform/methanol at -4°C

^{1}H NMR (400 MHz, *CDCl$_3$*) ppm: 11.06 (s, ArOH, 2H), 9.15 (d, H$_\beta$, *J* = 4.85 Hz, 4H), 8.95 (s, NH, 2H), 8.92 (d, H$_\beta$, *J* = 4.85 Hz, 4H), 8.89 (d, H$_\beta$, *J* = 4.85 Hz, 4H), 8.81 (d, H$_\beta$, *J* = 4.85 Hz, 4H), 8.24 (d, ArH, 8H), 8.01 (d, ArH, *J* = 1.75 Hz, 8H), 7.72 (s, 4H), 7.38 (d, *J* = 2.40 Hz, 4H), 7.25 (d, ArH, *J* = 7.65 Hz, 4H), 7.16 (d, ArH, *J* = 7.65 Hz, 4H), 6.98 (t, ArH, *J* = 7.5 Hz, 2H), 6.87 (m, ArH, 4H), 4.97 (s, OCH$_2$, 4H), 4.50 (d, ArCH$_2$Ar, *J* = 13.23 Hz, 4H), 3.93 (s, ArOCH$_3$, 12H), 3.75 (d, ArCH$_2$Ar, *J* = 13.46 Hz, 4H), 1.44 (s, C(CH$_3$)$_3$ 72H), -2.77 (s, NH, 4H).

HRMS (ESI-TOF-MS) Calculated: $[M+Na]^+$: $C_{156}H_{158}N_{10}NaO_{10}$: 2354.2094, found: 2354.2154.

25,27-bis[methoxy(4-amidophenyl)-15-(3,5-di-methoxyphenyl)-10,20-di-(3,5-di-*tert*-butylphenyl) Zn(II) porphyrin]-26-28-dihydroxycalix[4]arene (Zn.2)

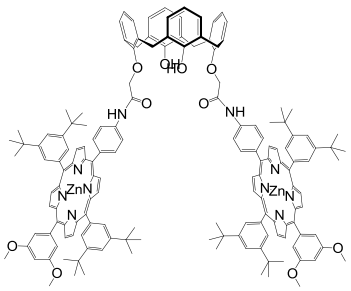

A saturated solution of zinc(II) acetate in methanol (5 mL) was added to a solution of bis-porphyrin **2.2** (0.030 g, 0.012 mmol) in chloroform (15 mL), the mixture was heated until no free base was observed in the UV-visible spectrum. The solution was washed with brine, dried with sodium sulfate and concentrated. The Zn(II) bis-porphyrin purified by flash chromatography, eluting with dichloromethane/hexane (9:1) and the solvent evaporated to produced a pink solid (0.029g, 92%). An analytically pure sample of **Zn2.2** was prepared via recrystallization from chloroform/methanol at -4°C

^{1}H NMR (400 MHz, *$CDCl_3$*) ppm: 11.03 (s, ArOH, 2H), 9.26 (d, H_β, *J* = 4.70 Hz, 4H), 9.02 (d, H_β, *J* = 4.65 Hz, 4H), 8.99 (d, H_β, *J* = 4.70 Hz, 4H), 8.94 (s, NH, 2H), 8.91 (d, H_β, *J* = 4.65 Hz, 4H), 8.29 (d, ArH, *J* = 2.26 Hz, 8H), 8.01 (d, ArH, *J* = 1.72 Hz, 8H), 7.71 (t, ArH, *J* = 1.72 Hz, 4H), 7.38 (d, ArH, *J* = 2.37 Hz, 4H), 7.24 (d, ArH, *J* = 7.70 Hz, 4H), 7.12 (d, *J* = *J* = 6.95Hz, 4H), 6.97 (t, *J* = 7.70 Hz, ArH, 2H), 6.86 (m, ArH, 4H), 4.96 (s,OCH_2, 4H), 4.49 (d,$ArCH_2Ar$, *J* = 13.41 Hz, 4H), 3.91 (s, $ArOCH_3$, 13H), 3.73 (d,$ArCH_2Ar$, *J* = 13.41 Hz, 1H), 1.42 (s, 72H).

HRMS (ESI-TOF-MS) Calculated: $[M+Na]^+$: $C_{156}H_{154}N_{10}NaO_{10}Zn_2$: 2478.03250 m/z, found: 2481.0165 m/z.

10,20-Bis(3,5-di-*tert*-butylphenyl)-5-bromoporphyrin. (2.9)

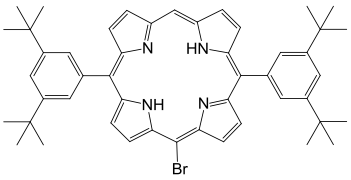

A solution of zinc porphyrin **Zn2.7** (0.626 g, 0.84 mmol) and pyridine (1 mL) in dichloromethane (65 mL) was cooled to 0°C. Recrystallized NBS (0.150 g, 0.84 mmol) was added and the solution immediately turned green. The solution was stirred for ten minutes and then was quenched with the addition of acetone (20 mL). The solution was diluted with methanol (30 mL) and dichloromethane was removed *in vacuo*. The resulting precipitate was filtered and washed with methanol (3 x 10 mL). The purple precipitate was suspended in dichloromethane (10 mL) and washed with HCl (12M, 10 mL) and water/acetone (3:1). The solvent was removed *in vacuo* to produce **2.9** as a purple solid, 0.475 g, (75%).

^{1}H NMR (400 MHz, *CDCl$_3$*) ppm 10.18 (s, mesoH, 1H), 9.75 (d, H$_\beta$, *J* = 4.75 Hz, 2H), 9.25 (d, H$_\beta$, *J* = 4.75 Hz, 2H), 9.01 (m, H$_\beta$,, 4H), 8.08 (d, *J*= 1.8 Hz, 4H), 7.83 (t, *J*= 1.8 Hz, 2H), 1.56 (s, C(CH$_3$)$_3$, 36H), -2.92 (s, NH 2H)

HRMS (ESI-TOF-MS) Calculated: [M+H]$^+$: $C_{48}H_{54}N_4Br$: 764.3433 m/z, found: 764.3454 m/z.

5-(4-acetamidophenyl), 10,20-bis(3,5-di-*tert*-butylphenyl) porphyrin (2.17)

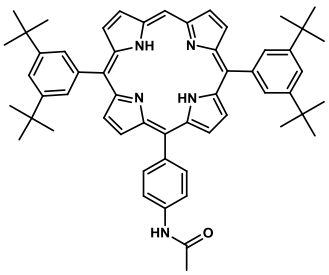

A suspension of mono-bromo porphyrin **2.9** (0.4 g, 0.52 mmol), tetrakis(triphenylphosphine) palladium (0.06 g, 0.052 mmol), caesium carbonate (1.02 g, 3.14 mmol), 4-acetamidophenyl boronic acid (0.197 g 1.09 mmol) in toluene/DMF (80 mL, 3:1) was taken through three freeze pump thaw cycles and heated at 90°C for 16 hours. The solution was cooled filtered through celite and the solvent removed by *in vacuo*. The residue was purified via flash chromatography,

eluting with dichloromethane/ethyl acetate (9:1) and the solvent evaporated to produce the acetamido-porphyrin **2.17** as a purple solid**,** 0.348 g (48%).

^{1}H NMR (300 MHz, *CDCl$_3$*) ppm: 10.20 (s, *meso*H, 1H), 9.35 (d, H$_\beta$, *J* = 4.67 Hz, 2H), 9.10 (d, H$_\beta$, *J* = 4.55 Hz, 2H), 8.98 (dd, H$_\beta$, *J* = 12.60, 4.70 Hz, 4H), 8.13 (d, ArH, *J* = 1.70 Hz, 4H), 8.01 (d, ArH, *J* = 8.25 Hz, 2H), 7.83 (t, ArH, *J* = 1.70Hz, 2H), 7.41 (s, NH,1H), 2.12 (s, CH_3, 3H) 1.57 (s, $C(CH_3)_3$, 36H), 2.89.

HRMS (ESI-TOF-MS) Calculated: $[M+H]^+$:$C_{56}H_{62}N_5O$: 819.4876 m/z, found: 819.4894 m/z.

5-(4-aminophenyl), 10,20-bis(3,5-di-*tert*-butylphenyl) porphyrin (2.18)

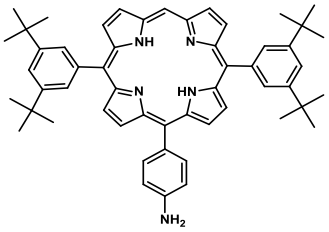

A suspension of the 4-acetamidophenyl porphyrin **2.17** (0.340 g, 0.418 mmol) in ethanol (20 mL) and hydrochloric acid (12 M, 20 mL) was refluxed for three hours. The solution was then cooled, diluted with water (50 mL) and neutralized by slow addition of solid sodium bicarbonate. The aqueous solution was extracted with dichloromethane, washed with brine, dried with sodium sulfate and concentrated. The residue was purified via flash chromatography, eluting with dichloromethane and the solvent evaporated to give amino porphyrin **2.18** as a purple solid, 0.290 g, (91%)

^{1}H NMR (400 MHz, *CDCl$_3$*) ppm: 10.20 (s, *meso*H, 1H), 9.34 (d, H$_\beta$, *J* = 4.67 Hz, 2H), 9.07 (d, H$_\beta$, *J* = 4.55 Hz, 2H), 8.97 (dd, H$_\beta$, *J* = 12.60, 4.70 Hz, 4H), 8.13 (d, ArH, *J* = 1.70 Hz, 4H), 8.01 (d, ArH, *J* = 8.25 Hz, 2H), 7.83 (t, ArH, *J* = 1.70Hz, 2H), 7.07 (d, ArH, *J* = 8.25 Hz, 2H), 1.57 (s, $C(CH_3)_3$, 36H), 2.89 (s, NH, 2H).

HRMS (ESI-TOF-MS), Calculated: $[M+H^+]$: $C_{54}H_{60}N_5$: 777.4770 m/z, found: 777.4793 m/z.

25,27-bis[methoxy(4-amidophenyl)-10,20-di-(3,5-di-*tert*-butylphenyl) porphyrin]-26-28-dihydroxycalix [4]arene (2.3)

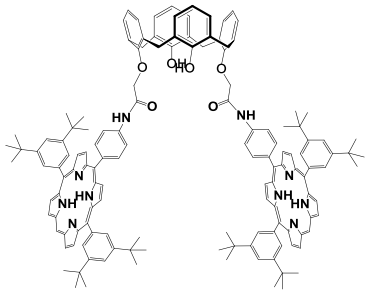

A solution of calixarene diacid **2.19** (0.041 g, 0.077 mmol), N,N'-dicyclohexylcarbodiimide (0.318 g, 1.54 mmol) and amino porphyrin **2.18** (0.120 g, 0.154 mmol) in dichloromethane (20 mL) was stirred for 16 hours. The solution was then concentrated and product was purified by flash chromatography, eluting with chloroform/hexane (9:1) and the solvent evaporated to give the bis-porphyrin **2.3** as a purple solid**,** 0.096 g (61%). An analytically pure sample of **2.3** was prepared via recrystallization from chloroform/methanol at -4°C.

^{1}H.NMR (400 MHz, *CDCl*$_3$) ppm 11.06 (s, ArOH, 2H), 10.16 (s, *meso*H, 2H), 9.29 (d, H$_\beta$, *J* = 4.70 Hz, 4H), 9.18 (d, H$_\beta$, *J* = 4.70 Hz, 4H), 8.99 (dd, H$_\beta$, *J* = 6.70, 4.70 Hz, 8H), 8.95 (s, NH, 2H), 8.30 (d, ArH, *J* = 1.80 Hz, 8H), 8.04 (d, ArH, *J* = 1.80 Hz, 1H), 7.73 (t, ArH,*J* = 1.77Hz, 1H), 7.25 (d, ArH, *J* = 7.63 Hz, 4H), 7.16 (d, ArH, *J* = 7.64 Hz, 4H), 7.01 (t, ArH, *J* = 7.60, Hz, 2H), 6.87 (t, ArH, *J* = 7.60 Hz, 2H), 4.97 (s, OCH$_2$C(O), 4H), 4.50 (d, ArCH$_2$Ar, *J* = 13.40 Hz, 4H), 3.74 (d, ArCH$_2$Ar, *J* = 13.40 Hz, 4H), 1.45 (s, C(CH$_3$)$_3$, 72H), -2.96 (s, 4H).

HRMS (ESI-TOF-MS) Calculated: $[M+H]^+$: $C_{140}H_{143}N_{10}O_6$: 2060.1103 m/z, found: 2061.1187 m/z, calculated: $[M+H+Na]^{2+}$: $C_{140}H_{143}N_{10}NaO_6$: 1041.552 m/z, found: 1041.5539 m/z.

25,27-bis[methoxy(4-amidophenyl)-10,20-di-(3,5-di-*tert*-butylphenyl) Zn(II) porphyrin]-26-28-dihydroxycalix[4]arene (Zn2.3)

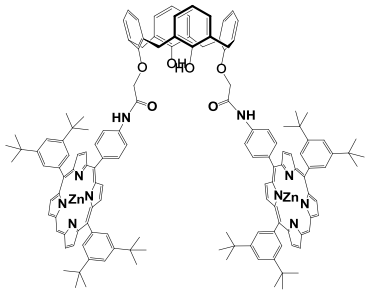

A saturated solution of zinc(II) acetate in methanol (5 mL) was added to a solution of bis-porphyrin **2.3** (0.040 g, 0.013 mmol) in chloroform (15 mL), the mixture was heated until no free base was observed in the UV-visible spectrum. The solution was washed with brine, dried with sodium sulfate and concentrated. The Zn(II)-bis-porphyrin purified by flash chromatography eluting with dichloromethane/hexane (9:1) and the solvent evaporated to produced a pink solid, 0.037 g, (90%). An analytically pure sample of **Zn2.3** was prepared via recrystallization from chloroform/methanol at -4°C.

^{1}H NMR (400 MHz, *CDCl*$_3$) ppm: 11.04 (s ArOH, 2H), 10.22 (s, *Meso*H, 2H), 9.36 (d, H$_\beta$, *J* = 4.60 Hz, 4H), 9.29 (d, H$_\beta$, *J* = 4.60 Hz, 1H), 9.08 (d, H$_\beta$, *J* = 4.60 Hz, 1H), 8.95 (s, NH, 2H), 8.30 (d, ArH, *J* = 3.20 Hz, 8H), 8.04 (d, ArH, *J* = 1.80 Hz, 8H), 7.74 (t, ArH, *J* = 1.80Hz, 4H), 7.24 (d, ArH, *J* = 7.60 Hz, 4H), 7.15 (d, ArH, *J* = 7.60 Hz, 4H), 7.03 (t, ArH, *J* = 7.60 Hz, 2H), 6.86 (t, ArH, *J* = 7.60 Hz, 2H), 4.96 (s, OCH$_2$C(O), 4H), 4.50 (d, ArCH$_2$Ar, *J* = 13.40 Hz, 4H), 3.74 (d, ArCH$_2$Ar, *J* = 13.40 Hz, 4H), 1.45 (s, C(C<u>H</u>$_3$)$_3$, 72H)).

HRMS (ESI-TOF-MS) Calculated: [M+Na]$^+$: $C_{140}H_{138}N_{10}O_6NaZn_2$: 2205.9276 m/z found: 2205.9193 m/z, and calculated: [M+H+Na]$^{2+}$: $C_{140}H_{139}N_{10}O_6NaZn_2$: 1103.4674 m/z, found: 1103.4665 m/z.

2.9.5 Synthetic Procedure for Porphyrin Modification Via Nickel Coupling

5,15-dibromo-10,20-bis(3,5-di-*tert*-butylphenyl) Ni(II) porphyrin (Ni2.7)

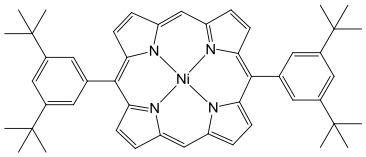

Porphyrin **2.**7 (2.0 g, 2.91 mmol) with nickel acetate (0.76 g, 4.37 mmol) in DMF (100 mL) was heated at 100°C for two hours. The solution was diluted with dichloromethane (300 mL), washed with water (3 x 300 mL), dried with sodium sulfate and the solvent removed *in vacuo*. The crude residue was purified by passing through a short plug of silica, eluting with dichloromethane and the solvent removed to give **Ni2.7** as a red solid, 1.77 g (82%).

^{1}H NMR (400 MHz, *CDCl$_3$*) ppm: 10.21 (s, *meso*H, 2H), 9.46 (d, H$_\beta$, *J* = 4.50 Hz, 4H), 9.21 (d, H$_\beta$, *J* = 4.50 Hz, 4H), 8.15 (d, ArH, *J* = 1.70 Hz, 4H), 7.87 (m, ArH, *J* = 1.70 Hz, 2H), 1.57 (s, C(CH$_3$)$_3$, 36H).

HRMS (ESI-TOF-MS) Calculated $[M+H]^+$ $C_{48}H_{52}N_4Ni$: 743.3640 m/z, found: 743.3618 m/z.

5,15-dibromo 10,20-bis(3,5-di-*tert*-butylphenyl) Ni(II) porphyrin (Ni2.8)

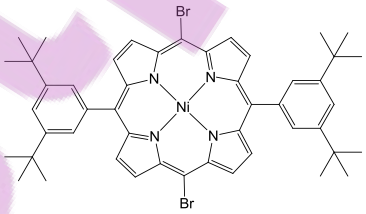

A solution of nickel porphyrin **2.8** (1.2 g, 1.617 mmol) and pyridine (20 mL) in dichloromethane (150 mL) was stirred at 0°C under nitrogen. Recrystallized NBS (0.7 g, 3.4 mmol) was added and the solution stirred for 20 minutes. The reaction was quenched with addition of acetone (20 mL) and the solvents were removed *in vacuo* and the solution filtered and washed with methanol (3 x 40 mL) to give **Ni2.8** as a red solid, 1.23 g (84%).

^{1}H NMR (400 MHz, *CDCl$_3$*) ppm: 9.45 (d, H$_{\beta,}$ *J* = 5.02 Hz, 1H), 8.77 (d, H$_\beta$ *J* = 5.00 Hz, 4 H), 7.80 (d, *J* = 1.70 Hz, 4H), 7.74 (t, ArH, *J* = 1.70 Hz, 2H), 1.49 (s, C(CH$_3$)$_3$, 36H).

HRMS (ESI-TOF-MS) Calculated: $[M+H]^+$:$C_{48}H_{50}$ Br_2N_4Ni: 898.1742 m/z, found: 898.1750 m/z.

5,15-bis(3-acetamidophexy)-10,20-bis(3,5-di-*tert*-butylphenyl) Ni (II) porphyrin (2.20)

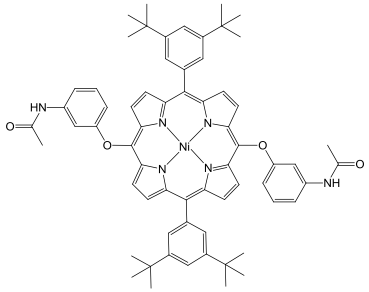

A suspension of dibromoporphyrin **Ni2.8** (0.7 g 0.77 mmol), nickel acetate (0.013 g, 0.08 mmol), 3-acetamido-phenol (0.471 g, 3.11 mmol) and potassium carbonate (0.430 g, 3.11 mmol) in dry DMF (100 mL) was heated at 130°C for ten hours. The reaction was cooled to room temperature, diluted with dichloromethane (100 mL) and washed with water (3 x100 mL). The organic layer was dried with sodium sulfate and the solvent removed *in vacuo*. The crude solid was then purified by flash chromatography eluting with dichloromethane/ethyl acetate (4:1) and the solvent evaporated to produce **2.20** as a red solid, 0.567 g (71%).

^{1}H NMR (300 MHz, *CDCl$_3$*) ppm: 9.18 (d, H$_{\beta,}$ *J* = 5.00 Hz, 4H), 8.77 (d, H$_{\beta,}$ *J* = 5.00 Hz, 4H), 7.84 (d, ArH, *J* = 1.8 Hz, 4H), 7.73 (t, ArH, *J* = 1.80Hz, 2H), 7.27 (d, ArH, *J* = 8.05 Hz, 2H), 7.15 (t, ArH, *J* = 8.08 Hz, 1H), 6.79 (s, ArH, 4H), 6.65 (d, ArH, *J* = 8.05 Hz, 2H), 1.93 (s, CH$_3$, 6H), 1.48 (s, C(CH$_3$)$_3$, 36H).

HRMS (ESI-TOF-MS) Calculated: $[M+H]^+$: $C_{64}H_{67}N_6NiO$: 1041.4499 m/z, found: 1041.4485 m/z.

5,15-bis(3-aminophenoxy) 10,20-bis(3,5-di-*tert*-butylphenyl) Ni (II) porphyrin (2.21)

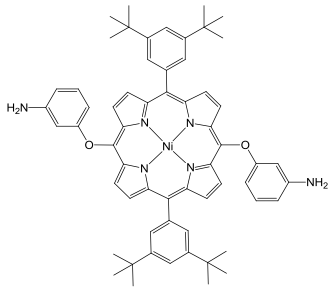

A suspension of the bis-3-acetamido-porphyrin **2.20** (0.50 g, 0.528 mmol) in ethyl acetate (50 mL) and hydrochloric acid (12 M, 50mL) was refluxed for three hours. The solution was then cooled to room temperature, diluted with water (100 mL) and neutralized by slow addition of solid sodium bicarbonate. The aqueous solution was extracted with dichloromethane (150 mL), washed with brine (3 x 50 mL), dried with sodium sulfate and concentrated *in vacuo*. The residue was purified via flash chromatography, eluting with dichloromethane/ethyl acetate (19:1) and solvent evaporated to give the diamino porphyrin **2.21** as a red solid, 0.467 g (97%).

^{1}H NMR (300 MHz, *CDCl$_3$*) ppm: 9.21 (d, H$_\beta$, *J* = 5.0 Hz, 4H), 8.75 (d, H$_\beta$, *J* = 5.0 Hz, 4H), 7.85 (d, ArH,*J* = 1.70 Hz, 4H), 7.73 (t, ArH, *J* = 1.70, Hz, 2H), 7.00 (t, ArH, *J* = 8.10 Hz, 2H), 6.37 (d, ArH, *J* = 8.10, Hz, 1H), 6.29 (d, ArH,*J* = 7.90 Hz, 1H), 6.04 (t ArH, *J* = 2.15 Hz, 2H), 1.47 (s, C(CH$_3$)$_3$ 36H)

HRMS (ESI-TOF-MS) Calculated: $[M+H]^+$: $C_{60}H_{61}N_6NiO_2$: 957.4288 m/z, found: 957.4280 m/z.

5-(3-aminophenoxy),15-(3-aminotrityl)-10,20 bis(3,5-di-*tert*-butylphenyl) Ni(II) porphyrin (2.22)

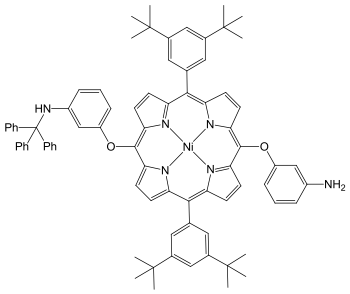

A solution of diamino poprhryin **2.21** (0.4 g, 0.418 mmol) and triethylamine (14 mL) in dichloromethane (400 mL) was cooled to 0°C under nitrogen. A solution of trityl bromide (0.148 g, 0.460 mmol) in dichloromethane (40 mL) was added drop wise over 30 minutes, and the solution was stirred for a further one hour. The solvent was removed *in vacuo* and the crude material was purified by column chromatography eluting with toluene, toluene/ethyl acetate (9:1) to give **2.22** as a red solid, (0.127 g, 53%).

^{1}H NMR (300 MHz, *CDCl*$_3$) ppm: 9.39 (d, H$_\beta$, *J* = 4.98 Hz, 2H), 8.93 (d, H$_\beta$, *J* = 4.98 Hz, 2H), 8.74 (d, H$_\beta$, *J* = 4.98 Hz, 2H), 8.65 (d, H$_\beta$, *J* = 4.98 Hz, 2H), 8.08 (m, ArH, 2H), 7.82 (d, ArH, *J* = 1.76 Hz, 1H), 7.68 (t, ArH, *J* = 1.76 Hz, 4H), 7.37 (d, ArH, *J* = 6.92 Hz, 2H), 6.99 (s, tritylH, 8H), 6.90 (t, ArH, *J* =8.32, 2H), 6.85-6.70 (m, tritylH, 32H), 6.31 (dd, ArH, *J* = 7.84, 2.33 Hz, 2H), 6.04 (dd, ArH, *J* = 7.59, 1.99 Hz, 2H), 5.96 (dd, ArH, *J* = 8.58, 1.84 Hz, 2H), 5.42 (s, ArH, 2H), 1.43 (s, C(CH$_3$)$_3$,72H)

HRMS (ESI-TOF-MS) Calculated: [M+H]$^+$: $C_{79}H_{77}N_6NiO_2$: 1199.5391 m/z, found: 1199.5383 m/z.

25,27-bis[methoxy (3-amidophenyl),15-(3- amino-trityl)-10,20 bis(3,5-di-*tert*-butyl-phenyl) Ni (II) porphyrin]-26-28-dihydroxycalix[4]arene (2.4)

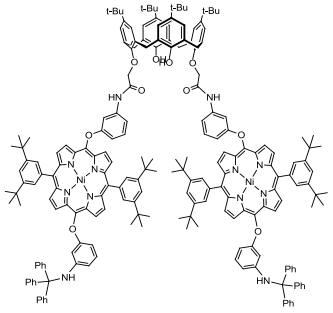

A solution of calixarene diacid **2.23** (0.07 g, 0.098 mmol) and DCC (0.27 g, 1.313 mmol) in dichloromethane (20 mL) was stirred for ten minutes. A solution of porphyrin **2.21** (0.15 g, 0.1313 mmol) in dichloromethane (10 mL) was added and the solution left to stir for four hours. The solution was concentrated and the crude product was purified by flash chromatography eluting with dichloromethane/hexane (9:1). The solvent was evaporated to give the bis-porphyrin **2.4** as a red solid, 0.080g (78%).

^{1}H NMR (300 MHz, *CDCl*$_3$) ppm: 10.72 (s, ArOH, 2H), 9.39 (d, H$_\beta$, *J* = 4.98 Hz, 4H), 8.93 (d, H$_\beta$, *J* = 4.98 Hz, 4H), 8.74 (d, H$_\beta$, *J* = 4.98 Hz, 4H), 8.65 (d, H$_\beta$, *J* = 4.98 Hz, 4H), 8.46 (s, NH, 2H), 8.08 (m, ArH, 2H), 7.82 (d, ArH, *J* = 1.76 Hz, 1H), 7.68 (t, ArH, *J* = 1.76 Hz, 4H), 7.37 (d, ArH, *J* = 6.92 Hz, 2H), 6.99 (s, tritylH, 8H), 6.90 (t, ArH, *J* =8.32, 2H), 6.85-6.70 (m, tritylH+ArH, 32H), 6.31 (dd, ArH, *J* = 7.84, 2.33 Hz, 2H), 6.04 (dd, ArH, *J* = 7.59, 1.99 Hz, 2H), 5.96 (dd, ArH, *J* = 8.58, 1.84 Hz, 2H), 5.42 (s, ArH, 2H), 4.82 (s, OCH$_2$, 2H), 4.21 (d, ArCH$_2$Ar, *J* = 13.33 Hz, 4H), 3.35 (d, ArCH$_2$Ar, *J* = 13.33 Hz, 4H), 1.43 (s, C(CH$_3$)$_3$,72H), 1.19 (s, C(CH$_3$)$_3$, 18H), 1.09 (s, C(CH$_3$)$_3$, 18H).

HRMS (ESI-TOF-MS) Calculated: [M+H]$^+$: $C_{206}H_{208}N_{12}Ni_2NaO_{10}$: 3148.4843 m/z, found: 3148.4741 m/z.

5-(4-nitrophenoxy)-10,20 bis(3,5-di-*tert*-butyl-phenyl) Ni (II) porphyrin (2.25)

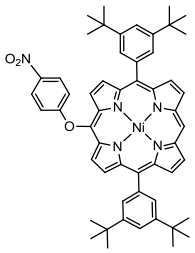

Ni2.8 (0.3g 0.33 mmol), nickel acetate (0.006 g, 0.033 mmol), 4-nitro-phenol (0.185 g, 1.336 mmol) and potassium carbonate (0.187 g, 1.336 mmol) were suspended in dry DMF (60 mL). The reaction mixture was heated to 130°C for three hours. The reaction was cooled to room temperature, diluted with dichloromethane (150 mL) and washed with water. The organic layer was dried with sodium sulfate and the solvent removed *in vacuo*. The crude solid was then purified by flash chromatography, eluting with dichlormethane/ethyl acetate (9:1) as the second fraction, and the solvent was evaporated to produce **2.25** as a red solid, 0.137 g (67%). the dinitrophenoxy porphryrin was isolated, 0. 11 g (49%).

^{1}H NMR (300 MHz, *CDCl*$_3$) ppm: 9.86 (s, *meso*H, 1H), 9.15 (m, H$_\beta$, 4H), 8.94 (d, H$_\beta$, *J* = 5.00 Hz, 2H), 8.87 (d, H$_\beta$, *J* = 5.00 Hz, 2H), 8.13 (d, ArH, *J* = 9.35 Hz, 2H), 7.90 (d, ArH, *J* = 1.80 Hz, 4H), 7.77 (t, ArH, *J* = 1.80 Hz, 2H), 6.96 (d, ArH, *J* = 9.35 Hz, 1H), 1.51 (s, C(CH$_3$)$_3$, 36H).

HRMS. (ESI-TOF-MS) Calculated: [M+H]$^+$: $C_{54}H_{56}N_5NiO_3$: 880.3742 m/z, found: 880.3737 m/z.

5-(4-aminophenyl)-10,20 bis(3,5-di-*tert*-butyl-phenyl) Ni (II) porphyrin (2.26)

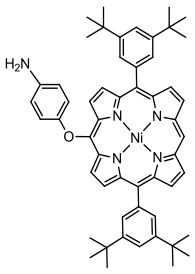

A suspension of 4-nitrophenoxy porphyrin **2.25** (0.205 g, 0.247 mmol), tin(II) chloride(0.56 g 2.47 mmol) in hydrochloric acid (30 mL, 12 M) and ethanol (30 mL) was refluxed for five hours under an atmosphere of nitrogen. The solution was neutralized by slow addition of ammonia (2 M) until a pH of 7 was reached. Dichloromethane was added to the solution and the organic phase decanted. The solvents were removed *in vacuo* and the crude material was purified by flash chromatography eluting with dichloromethane/hexane (19:1). The solvent was removed produce the amino porphyrin **2.26** as red solid, 0.163 g (85%).

^{1}H NMR (300 MHz, *CDCl$_3$*) ppm: 9.79 (s, *meso*H. 1H), 9.29 (d, H$_\beta$, *J* = 4.95 Hz, 2H), 9.10 (d, H$_\beta$, *J* = 4.8 Hz, 2H), 8.91 (d, H$_\beta$, *J* = 4.8 Hz, 2H), 8.81 (d, H$_\beta$, *J* = 4.95 Hz, 2H), 7.90 (d, ArH, *J* = 1.80 Hz, 4H), 7.76 (t, ArH, *J* = 1.80 Hz, 2H), 6.73 (d, ArH, *J* = 8.85 Hz, 2H), 6.53 (d, ArH, *J* = 8.85 Hz, 2H), 1.50 (s, C(CH$_3$)$_3$, 36H).

HRMS (ESI-TOF-MS) Calculated: [M+H]$^+$: $C_{54}H_{58}N_5NiO$:850.3989 m/z, found: 850.3880 m/z.

25,27-bis[methoxy (4-amidophenyl) 10,20 bis(3,5-di-tert-butyl-phenyl) Ni(II) porphyrin]-26-28-dihydroxycalix[4]arene (2.5)

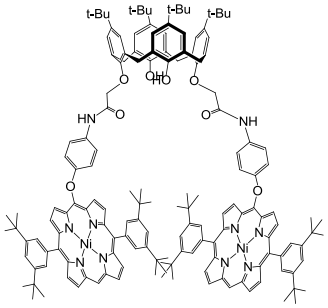

A solution of calixarene diacid **2.23** (0.70 g, 0.07 mmol) and DCC (0.291 g, 1.41 mmol) in dichloromethane (10 mL) was stirred under nitrogen for ten minutes. A solution of porphyrin **2.26** (0.12 g, 0.14 mmol) in dichloromethane (10 mL) was added and the solution left to stir for four hours. The solution was then concentrated and crude product was purified by flash chromatography eluting with dichloromethane. The solvent was removed *in vacuo* to give the bis-porphyrin **2.5** as a red solid, 0.12 g (70%).

^{1}H NMR (300 MHz, *CDCl$_3$*) ppm: 10.24 (s, *meso*H, 2H), 9.77 (s, ArOH, 2H), 9.27 (d, H$_\beta$, *J* = 5.00 Hz, 4H), 9.08 (d, H$_\beta$, *J* = 4.80 Hz, 4H), 8.90 (d, H$_\beta$, *J* = 4.80 Hz, 4H), 8.83 (d, H$_\beta$, *J* =

5.00 Hz, 4H), 8.02 (s, NH, 2H), 7.89 (d, ArH, *J* = 1.85 Hz, 8H), 7.72 (t, ArH, *J* = 1.85 Hz, 4H), 7.41 (d, ArH, *J* = 9.20 Hz, 4H), 6.94 (s, ArH, 4H), 6.88 (s, ArH 4H), 6.75 (d, ArH, *J* = 9.20 Hz, 4H), 4.43 (s, $OCH_2C(O)$, 4H), 4.01 (d, $ArCH_2Ar$, *J* = 13.30 Hz, 4H), 3.32 (d, $ArCH_2Ar$, *J* = 13.30 Hz, 4H), 1.47 (s, $C(CH_3)_3$, 72H), 1.15 (s, $C(CH_3)_3$, 18H), 1.02 (s, $C(CH_3)_3$, 18H)

HRMS (ESI-TOF-MS) Calculated: $[M+Na]^+$: $C_{156}H_{170}N_{10}Ni_2NaO_6$: 2451.1841 m/z, found: 2451.156 m/z.

2.9.6 General Information and Crystallographic Tables for Single Crystal X-ray Diffraction

Single crystal X-ray diffraction data for **Zn2.11.C$_{60}$, Zn2.11.2C$_{70}$, Zn2.14.3C$_{60}$.3toluene** and **2.7.C$_{60}$** were collected on a Bruker Smart APEX2 CCD diffractometer using graphite monochromated Mo Kα radiation. The structures were solved using direct methods (SHELXS-97) [173,174]. Non hydrogen atoms were refined anisotropically (SHELXL-97)[174] and H atoms were refined using a riding model, with C-H =0.93-0.97 Å and Ui_{so}(H)=1.2Ueq(C), $1.5U_{eq}$(methyl C) or $1.5U_{eq}$(O).

The program *PLATON* (Spek, 2009)[175] indicated solvent accessible void spaces for the structures of **Zn2.11.C$_{60}$** and **Zn2.11.2C$_{70}$** respectively. These solvent molecules in these voids are extensively disordered and could not be modeled. Their contribution was excluded in the final refinements of the two structures using the SQUEEZE procedure.[176]

Table 2.5: Crystal data and structure refinement for **Zn2.11.C_{60}.**

Empirical formula	C_{122} H_{64} C_{l0} N_4 Zn	
Formula weight	1651.14	
Temperature	89(2) K	
Wavelength	0.71073 Å	
Crystal system	Orthorhombic	
Space group	Pbcn	
Unit cell dimensions	a = 27.4609(4) Å	α= 90°.
	b = 17.8332(2) Å	β= 90°.
	c = 19.2884(3) Å	γ = 90°.
Volume	9445.8(2) $Å^3$	
Z	4	
Density (calculated)	1.161 Mg/m^3	
Absorption coefficient	0.313 mm^{-1}	
F(000)	3416	
Crystal size	0.32 x 0.28 x 0.26 mm^3	
Theta range for data collection	1.36 to 28.05°.	
Index ranges	-35<=h<=36, -23<=k<=23, -24<=l<=25	
Reflections collected	101291	
Independent reflections	11424 [R(int) = 0.0408]	
Completeness to theta = 28.05°	99.5 %	
Absorption correction	Semi-empirical from equivalents	
Max. and min. transmission	0.922 and 0.815	
Refinement method	Full-matrix least-squares on F^2	
Data / restraints / parameters	11424 / 0 / 635	
Goodness-of-fit on F^2	0.954	
Final R indices [I>2sigma(I)]	R1 = 0.0568, wR2 = 0.1355	
R indices (all data)	R1 = 0.0744, wR2 = 0.1441	
Largest diff. peak and hole	1.331 and -0.521 e.$Å^{-3}$	

Table 2.6: Crystal data and structure refinement for **Zn2.11.2C$_{70}$.**

Empirical formula	$C_{101}H_{32}C_{l0}NZn_{0.50}$	
Formula weight	1305.97	
Temperature	90(2) K	
Wavelength	0.71073 Å	
Crystal system	Monoclinic	
Space group	P21/n	
Unit cell dimensions	a = 14.0784(2) Å	α= 90°.
	b = 18.4147(3) Å	β= 90.4710(10)°.
	c = 22.8215(3) Å	γ = 90°.
Volume	5916.26(15) Å^3	
Z	4	
Density (calculated)	1.466 Mg/m^3	
Absorption coefficient	0.281 mm^{-1}	
F(000)	2668	
Crystal size	0.29 x 0.14 x 0.11 mm^3	
Theta range for data collection	1.42 to 27.89°.	
Index ranges	-18<=h<=18, -24<=k<=24, -29<=l<=29	
Reflections collected	105428	
Independent reflections	14119 [R(int) = 0.0777]	
Completeness to theta = 27.89°	99.8 %	
Absorption correction	Semi-empirical from equivalents	
Max. and min. transmission	0.970 and 0.833	
Refinement method	Full-matrix least-squares on F^2	
Data / restraints / parameters	14119 / 0 / 941	
Goodness-of-fit on F^2	1.053	
Final R indices [I>2sigma(I)]	R1 = 0.0489, wR2 = 0.1066	
R indices (all data)	R1 = 0.0771, wR2 = 0.1154	
Largest diff. peak and hole	0.463 and -0.568 e.Å^{-3}	

Table 2.7: Crystal data and structure refinement for **Zn2.14.3C_{60}.3toluene.**

Empirical formula	$C_{132.50}H_{42}N_2O_2Zn_{0.50}$	
Formula weight	1726.37	
Temperature	90(2) K	
Wavelength	0.71073 Å	
Crystal system	Triclinic	
Space group	P-1	
Unit cell dimensions	a = 13.3395(18) Å	α= 108.614(10)°.
	b = 17.137(3) Å	β= 97.846(10)°.
	c = 17.804(3) Å	γ = 99.969(9)°.
Volume	3717.8(9) $Å^3$	
Z	2	
Density (calculated)	1.542 Mg/m^3	
Absorption coefficient	0.247 mm^{-1}	
F(000)	1764	
Crystal size	0.35 x 0.09 x 0.05 mm^3	
Theta range for data collection	1.29 to 28.14°.	
Index ranges	-17<=h<=17, -22<=k<=22, -23<=l<=23	
Reflections collected	57288	
Independent reflections	16992 [R(int) = 0.1581]	
Completeness to theta = 28.14°	93.3 %	
Absorption correction	Semi-empirical from equivalents	
Max. and min. transmission	0.988 and 0.704	
Refinement method	Full-matrix least-squares on F^2	
Data / restraints / parameters	16992 / 0 / 1258	
Goodness-of-fit on F^2	1.113	
Final R indices [I>2sigma(I)]	R1 = 0.0990, wR2 = 0.2092	
R indices (all data)	R1 = 0.1642, wR2 = 0.2373	
Largest diff. peak and hole	1.046 and -0.633 $e.Å^{-3}$	

Table 2.8: Crystal data and structure refinement for **2.7.C_{60}.**

Empirical formula	C_{108} H_{54} N_4	
Formula weight	1407.55	
Temperature	93(2) K	
Wavelength	0.71073 Å	
Crystal system	Monoclinic	
Space group	C2/c	
Unit cell dimensions	a = 9.7022(4) Å	α= 90°.
	b = 30.7278(12) Å	β= 101.687(3)°.
	c = 22.9278(9) Å	γ = 90°.
Volume	6693.7(5) $Å^3$	
Z	4	
Density (calculated)	1.397 Mg/m^3	
Absorption coefficient	0.081 mm^{-1}	
F(000)	2920	
Theta range for data collection	1.61 to 27.90°.	
Index ranges	-12<=h<=12, 0<=k<=40, 0<=l<=29	
Reflections collected	7218	
Independent reflections	7218 [R(int) = 0.0000]	
Completeness to theta = 27.90°	90.0 %	
Refinement method	Full-matrix least-squares on F^2	
Data / restraints / parameters	7218 / 810 / 601	
Goodness-of-fit on F^2	0.942	
Final R indices [I>2sigma(I)]	R1 = 0.0748, wR2 = 0.1756	
R indices (all data)	R1 = 0.1738, wR2 = 0.2009	
Largest diff. peak and hole	0.434 and -0.462 e.$Å^{-3\backslash}$	

Chapter 3

Tetra-alkylated and Extended Linker Calixarene Bis-Porphyrins

3.1 Introduction

Studies on the effect of different meso of the substituents *trans* to the amide linker of porphyrins, demonstrate the importance of CH-π interactions in enhancing the associations between the bis-porphyrin hosts and fullerene guests. Modification of the porphyrin substituents through the introduction of an ether functionality resulted in a change in the geometry of the host that was not favorable for the association of fullerenes. In addition to variation of the porphyrin substituents, the calixarene scaffold and narrow rim linkers joining the calixarene to the porphyrin groups can be modified. This chapter describes the modification of the calixarene scaffold and linkers and examines how these changes effect the association of the bis-porphyrin with fullerenes.

3.1.1 Linker Flexibility versus Binding

A series of calixarene linked bis-porphyrin hosts with varying flexibility have been synthesized and their association with fullerenes studied.[122,128] The flexibility of the hosts has been varied by increasing the number of methylene groups between the calixarene and the porphyrin. Bis-porphyrin **3.1** was prepared by direct linkage of the two porphyrins to the phenolic groups via ester coupling. Two (*p*-COOH)-tris(tolyl) porphyrins coupled to alternate hydroxyl groups on the narrow rim of the calixarene using DCC and a catalytic amount of DMAP. Molecular mechanics indicate that the bis-porphyrin processed a suitable geometry for the formation of a host-guest complex with C_{60} with an interplanar angle between 40-60° and a distance between the porphyrins of 11-12.5 Å. The association constant for C_{60} was measured in toluene from fluorescence quenching titration studies.to be 2000 M^{-1} at 293 K

Bis-porphyrin **1.34** extended the linker by one methylene spacer. Based on molecular modeling, the increased flexibility of the linker allows the porphyrins to adopt a better geometry for fullerene binding which results in a significant increase in the association constant with C_{60} relative to bis-porphyrin **3.1**. The binding constants were measured by both fluorescence and ^{1}H NMR spectroscopy titrations to give a binding constant of 8,900 M^{-1} in toluene.

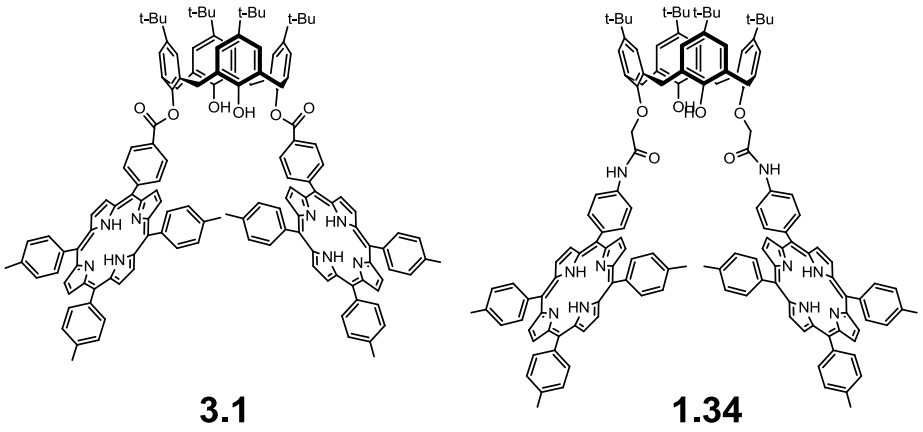

Figure 3.1: Directly substituted bis-porphyrin **3.1** and the methylene extended bis-porphyrin **1.35.**

The preparation of the dicarboxyethoxy-calixarene **3.3** was attempted in a similar fashion by the reaction of ethyl-α-bromopropionate in acetonitrile in presence of potassium carbonate as shown in Scheme 3.1.[128] This method failed to proceed, due to the elimination of HBr to form ethylacrylate.[177] The use of stoichiometric amounts of a bulkier base such as LDA at –78^{o}C, and 2,6-lutidine at room temperature in dry acetonitrile also afforded no reaction. Another approach for the formation of the dicarboxylic acid was oxidation of a primary alcohol derivative of the calixarene to the methyl ester . The diol **3.4** was prepared by the alkylation of the calixarene with 3-bromo-1-propanol in acetonitrile in the presence of potassium carbonate. The oxidation of primary alcohols to esters using trichloroisocyanuric acid as an oxidant have been described giving good yields under mild conditions.[178] The diol however, was not oxidised to the corresponding di-methyl ester under the same conditions.

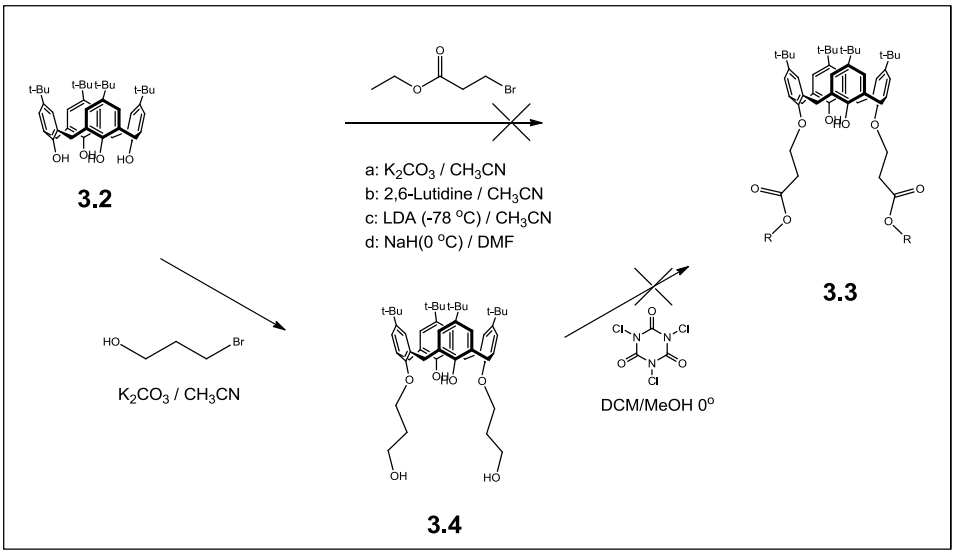

Scheme 3.1: Attempted synthesis of dicarboxyethoxy-calixarene.[128]

Synthesis of **3.5** with a three methylene spaced linker via alkylation with ethyl bromobutanoate was successful. Hydrolysis of the ester formed the diacid **3.6,** followed by coupling of the 5-mono-aminophenyl-10,15,20-tris-tolyl porphyrins to the calixarene diacid with DCC to give the desired bis-porphyrin **3.7**.

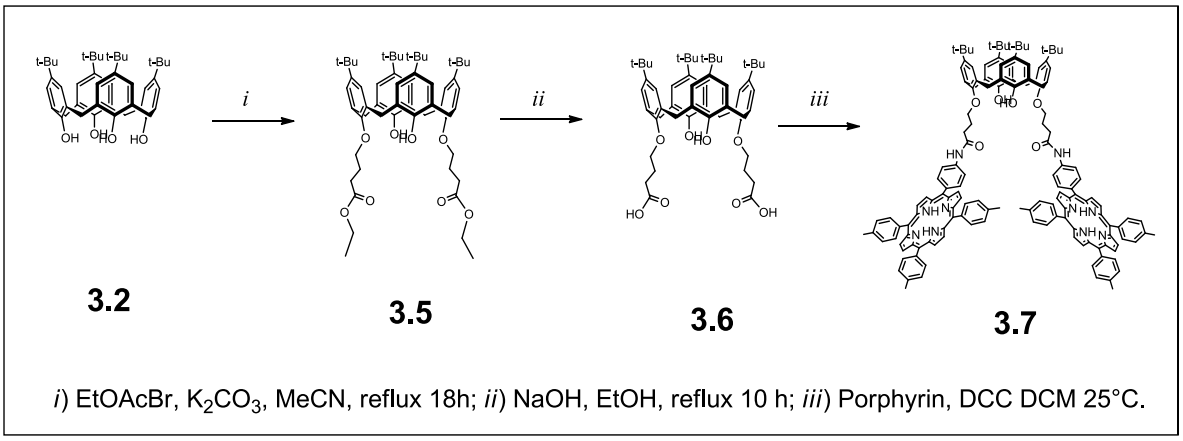

Scheme 3.2: Synthesis of three methylene spaced bis-porphyrin **3.7**[128]

Binding constants for bis-porphyrins are given in Table 3.1. Bis-porphyrin **1.35** displays the highest association constant with C_{60} compared to **3.1** and **3.7**. These results correlate to the increased flexibility and the ability for the host to better accommodate the fullerene. This work agreed with the findings of Aida and co-workers, with their macrocyclic hosts **1.24** and **1.25**, where the rigid, diynyl-linked bis-porphyrin host showed no interaction with C_{60} but the more flexible dihexyl-linked bis-porphyrin showed strong association for C_{60}.[179] Upon increasing the chain length, bis-porphyrin **3.7** showed that too much flexibility is unfavorable due an increase in the enthalpy of binding.

Table 3.1: Binding constants of bis-porphyrins with different flexibility.[122,128]

Linker	K_a C_{60} (M^{-1})
3.1 (n=0)	2,000
1.35(n=1)	8,900
3.7 (n=3)	2,900

3.1.2 Calixarenes as Scaffolds for Wide Rim Bis-Porphyrins

Dialkylated calixarenes have a preorganised geometry due to intramolecular hydrogen bonding on the narrow rim of the between the hydroxyl groups and the ether oxygen. This induces a pinched cone conformation commonly observed in X-ray crystal structures.[180] Alkylation of all the hydroxyl groups on the narrow rim the calixarene removes the hydrogen bonding, enhancing the flexibility of the calixarene and potentially allowing for symmetrical cone geometries. Several bis-porphyrins have been reported by various research groups with porphyrins attached to the wide rim of the calixarenes and either dialkylated or tetra-alkylated on the narrow rim.

Lhoták and co-workers synthesised bis-porphyrins **1.30** and **1.31** appended to the wide rim of the calixarene by urido linkers.[181] The narrow rim of the calixarene was fully alkylated, removing the intramolecular hydrogen bonding motif of the calixarene. These bis-porphyrins displayed an affinity for both C_{60} and C_{70} as the porphyrins are no longer held apart by the pinched cone conformation of the calixarene. Binding constants for fullerenes are not consistent with the different functional groups on the narrow rim. For **1.30** with propyl groups on the narrow rim the binding constants are 3,500 M^{-1} and 7,900 M^{-1} for C_{60} and C_{70} respectively. However for **1.31**, the narrow rim of the calixarene is functionalised with ester groups and shows a lower binding for C_{60} of 1,460 M^{-1}, while the binding C_{70} increases to 14,500 M^{-1}. This change in association for fullerenes can be attributed to the weak bonding interaction between the narrow rim esters holding the porphyrins wider apart.

Arimura *et al*. synthesised the wide rim calixarene bis-porphyrin host **1.32.** This bis-porphyrin was directly synthesised on the wide rim from an aldehyde functional group on the wide rim of the calixarene.[117] On the narrow rim the calixarene was dialkylated with n-propyl groups holding the porphyrins in a wide angle due to hydrogen bonding of the hydroxyl groups. The bis-porphyrin showed the ability to form host guest complexes with C_{70} but not C_{60}. It has been proposed that bis-porphyrin **1.32** displays a larger cavity size between the wide rim porphyrins which can accommodate C_{70} in a pole to pole orientation, but is too large to accommodate C_{60}.

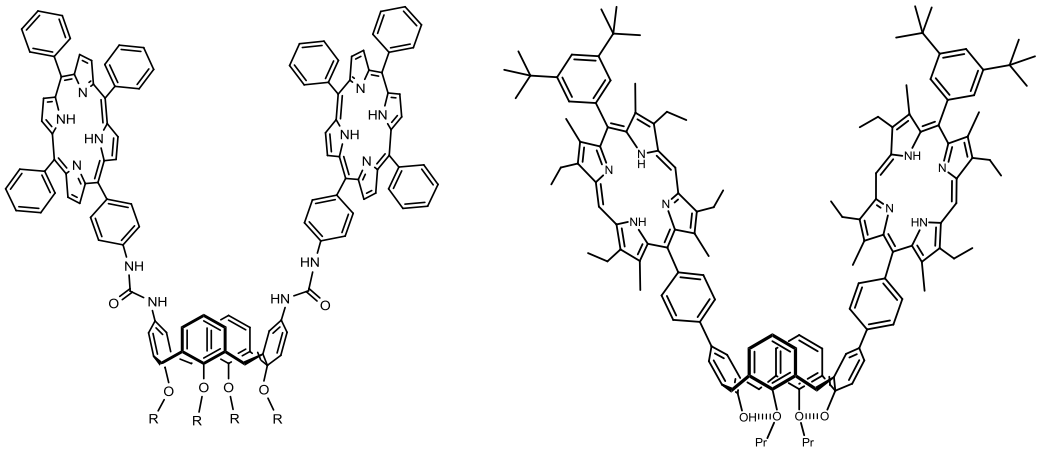

1.30 R= $(CH_2)_2CH_3$
1.31 R= CH_2COOEt

1.32

Figure 3.2: Wide rim calixarene bis-porphyrin hosts **1.35**, **1.36** and **1.37.** [117,181]

3.1.3 Synthesis and Conformation of Tetra-Alkylated Calixarenes

Narrow rim functionalization of the calixarene scaffold has been be accomplished by various methods.[104,111] The most well known method is the narrow-rim alkylation with alkyl and aryl halides. This method proceeds favorably and can be readily achieved with a variety of different alkyl or aryl halides to alkylate all or just some of the hydroxyl groups. If only two hydroxyl groups are functionalized, alkylation is directed in a 1,3 fashion due to the intramolecular hydrogen bonding on the narrow rim.[167] A second alkylation of the narrow rim remaining hydroxyl groups can be achieved with different groups to increase the functionality and the flexibility of the calixarene scaffold. Secondary alkylation presents a higher degree of complexity than the first alkylation as the removal of hydrogen bonding allows for rotation of one or both of the aryl rings during the reaction to give different cone conformations.

The choice of the base in secondary alkylation reactions is very important. Different bases will favor different calixarene conformations.[113] As calixarenes are good cations binders, and as such it is the cation which predominantly determines the conformation.[182-184] Larger metal cations such as caesium generally promote the 1,3 alternate isomer as the major isomer and potassium promotes a mixture of cone and 1,3 alternate geometries with the major isomer being the partial conformation. Sodium salts have been shown to give mixtures of 1,3-alternate and cone geometries, as well as selectively the cone geometry as the only isomer.

Both ^{1}H and ^{13}C NMR spectroscopy have been used to determine which isomers of calixarene are present and in what ratio. A study of the four different isomers of calixarene with functionalized with *tert*-butyl esters and *n*-butyl groups has been carried out by Park (Figure 3.3).[182] The different conformations can be determined by the signals arising from both the methylene bridges connecting the aryl rings as well as the methylene of the ester groups. In all the conformations, the methylene bridge protons (Ar$\underline{CH_2}$Ar) are locked in to different orientations, which means that they are chemically inequivalent and are shown as two sets of doublets in the region of 3.1-4.7 ppm with a coupling constant ranging between 12.8-14 Hz. The location and coupling varies depending on the isomer present. The methylene proton signals of the ester (-O$\underline{CH_2}$C(O)) should appear as a single singlet in the cone and 1,3 alternate isomers with different ppm values. The partial cone conformation shows two different signals as the methylenes are inequivalent. NMR data for the different conformations are shown in Table 3.2.

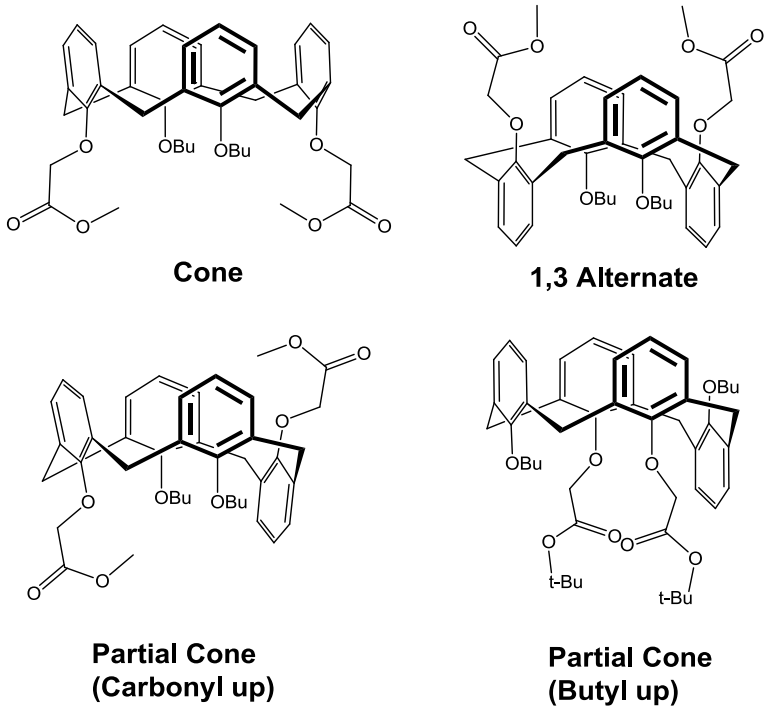

Figure 3.3: Different isomers of tetra-alkylated calixarene: cone; 1,3 alternate; partial cone (carbonyl up) and partial cone (butyl up).

Table 3.2: ^{13}C and ^{1}H NMR data for the bridging methylene and ester methylene groups.[182]

	ArCH$_2$Ar (ppm)		-OCH$_2$C(O)- (ppm)	
Isomer	$^{1}H^{a}$	$^{13}C^{a}$	$^{1}H^{a}$	$^{13}C^{a}$
Cone	3.21 (d, *J*=13.7 Hz) 4.66 (d, *J*=13.7 Hz)	31.2	4.75 (s)	70.46
Partial Cone (Butyl up)	3.09 (d, *J*=13 Hz) 3.64 (d, *J*=12 Hz) 3.86 (d, *J*=12 Hz) 4.15 (d, *J*=13 Hz)	31.1 35.1	4.24 (d, *J*=14.8 Hz) 4.27 (d, *J*=14.8 Hz)	72.22
Partial Cone (Carbonyl up)	3.15 (d, *J*=14 Hz) 3.68 (d, *J*=12.8 Hz) 3.78 (d, *J*=12.8 Hz) 4.32 (d, *J*=14 Hz)	31.7 35.1	3.94 (s) 4.39 (s)	66.67 70.06
1,3-Alternate	3.76 (d, *J*=15.3 Hz) 3.98 (d, *J*=15.3 Hz)	37.4	3.45 (s)	68.54

3.2 Aim and Strategy

This chapter describes modifications of the calixarene scaffold and linkers between the scaffold and porphyrin and examines how these changes affect the association of the bis-porphyrin with fullerenes. Bis-porphyrin **3.8** has been synthesized with two methylene spacers between the calixarene and the amide groups. This host has been prepared by an alternate method of inverting the amide bond used to connect the porphyrin to the calixarene linker. Of interest is the length of the chain linker and ability of the bis-porphyrin to bind fullerenes. Host **3.8** has been prepared with porphyrin carboxylic acid substituted at the other three *meso* positions with 3,5-di-*tert*-butyl phenyls, which provides additional close contacts to the bound fullerene via CH-π interactions that increase the porphyrin–fullerene association. This porphyrin offers a direct comparison to bis-porphyrin **1.36,** which displays a high affinity for both C_{60} and C_{70}.

Reported in this chapter is the synthesis of bis-porphyrin hosts **3.9** and **3.10**, which are tetra-alkylated on the narrow rim of the calixarene with methyl and *n*-butyl groups respectively. These bis-porphyrin hosts are of interest in terms of the conformational differences of the calixarene linker due to the lack of intramolecular hydrogen bonding among the two hydroxyl groups on the narrow rim. The calixarene scaffold should be conformationally labile and the no longer adopt the commonly observed pinched cone. Alkylation of the calixarene with alkyl

groups of different lengths is of interest as shorter chain alkyl groups provide increased flexibility of the calixarene than longer chains.

Bis-porphyrin **3.9** and **3.10** were prepared by alkylation the phenolic groups on the narrow rim of the calixarene scaffold with methyliodide and *n*-butyl iodide respectively. Introducion of these groups to the narrow rim via a second alkylation brings about a range of synthetic challenges. The order of alkylation, the type of cation used as base and the solvent used in the reaction can affect the calixarene conformation. This is important as the cone conformation is required for the preparation of the bis-porphyrins.

The amino porphyrin used in the synthesis of **3.9** and **3.10** was 5-(4-aminophenyl)-15-tolyl -10,20-bis-3,5-di-*tert*-butyl porphyrin **2.15**. **2.15** provides a good number of close contacts to bound fullerenes via CH-π interactions from the *tert*-butyl methyl groups which increase the porphyrin–fullerene association. The tolyl methyl is observed as singlet at 2.38 ppm and provides a good ^{1}H NMR fingerprint for the identification of the bis-porphyrin integrating for six protons.

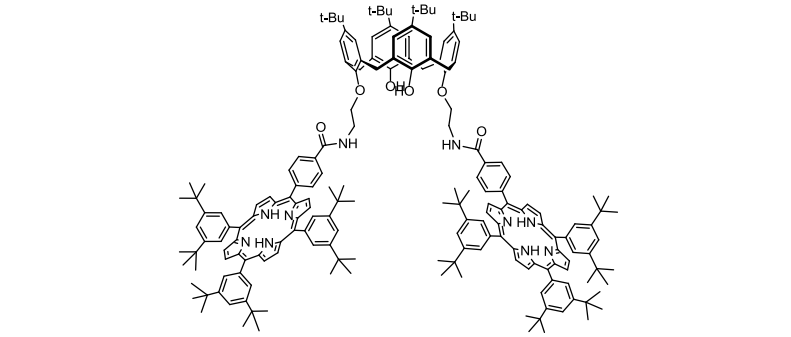

3.8

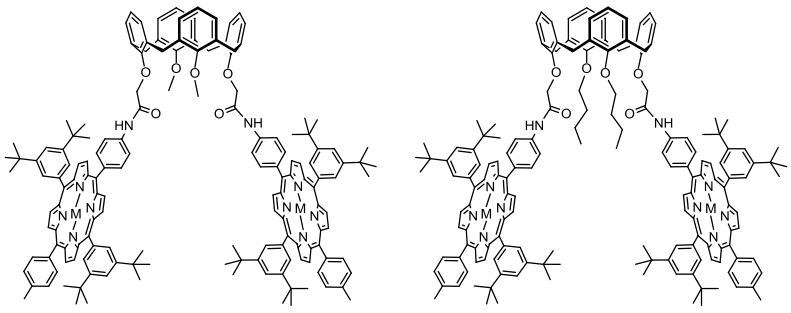

3.9 **3.10**

Figure 3.4: Hosts prepared in Chapter Three: **3.8**, **3.9** and **3.10**.

3.3 Computational Modeling of Bis-Porphyrins

In order to understand the possible differences in geometry of the structures, Hosts **3.8**, **3.9** and **3.10** were studied using molecular modeling. Geometry optimizations of the host-guest complex were carried out using a two layer ONIOM method described in Chapter Two. The calixarene scaffold and the amide linkers are modeled in the high layer by DFT with the B3LYP basis set with 6-31G(d), which adequately models the bond lengths and angles in organic molecules. The porphyrins and C_{60} are optimized in the low layer with molecular mechanics which more adequately describes the porphyrin-fullerene interaction. Nickel porphyrins were used in the computational modeling as the metalloporphyrins helps maintain planarity versus unmetallated porphyrin.

3.3.1 Computational Modeling of Bis-Porphyrin 3.8

There are two types of possible orientation for the amide linkers. *Syn*, where the amide oxygens are orientated outwards and *anti*, where the amide oxygens are orientated inwards. Based on previous modeling of bis-porphyrins, the *syn-syn* orientation of amide bond are more energetically favorable.[185]

x

In the optimized structure of the bis-porphyrin **3.8**, the calixarene adopts the typical pinched cone conformation observed for dialkylated calixarenes, due to the nature of the hydrogen bonding motif of the phenolic groups on the narrow rim. The interplanar angle of the phenol rings are approximately 88.9° while the interplanar angle of the functionalized phenyl rings are 35.4°. The hydrogen of the hydroxyl groups point toward the ether oxygen of an adjacent phenyl and the hydrogen bonding distance between phenol hydroxyl groups and ether oxygen are consistent between each host ranging from 1.76-1.80 Å. The extra methylene means that the amide NH groups are now too remote for hydrogen bonding. This allows the methylene linkers to be less restricted. The extra spacer also means that the linkers have increased flexibility to allow the porphyrins to orientate to fully wrap around the fullerene. The porphyrins are almost parallel to one another with an interplanar angle of approximately 4°. The center to center distance between the two porphyrins is 12.48 Å with the C_{60} arranged with 6:6 ring junctions centered over the porphyrin at distances of 2.82-2.94 Å. There are CH-π interactions from *ortho*-protons on the 10 and 20 phenyl substituents as well as the 15-position due to the parallel orientation of the porphyrins. CH-π interactions are present between the

methyl groups of the *tert*-butyl phenyls and the fullerene ranging from 2.7-3.3Å. The increased flexibility of the planes and the parallel arrangement of the porphyrins may allow for increased π-π interactions between the porphyrin and the fullerene as well as increasing the number of CH-π interactions between each phenyl substituent of the porphyrin to enhance the binding.

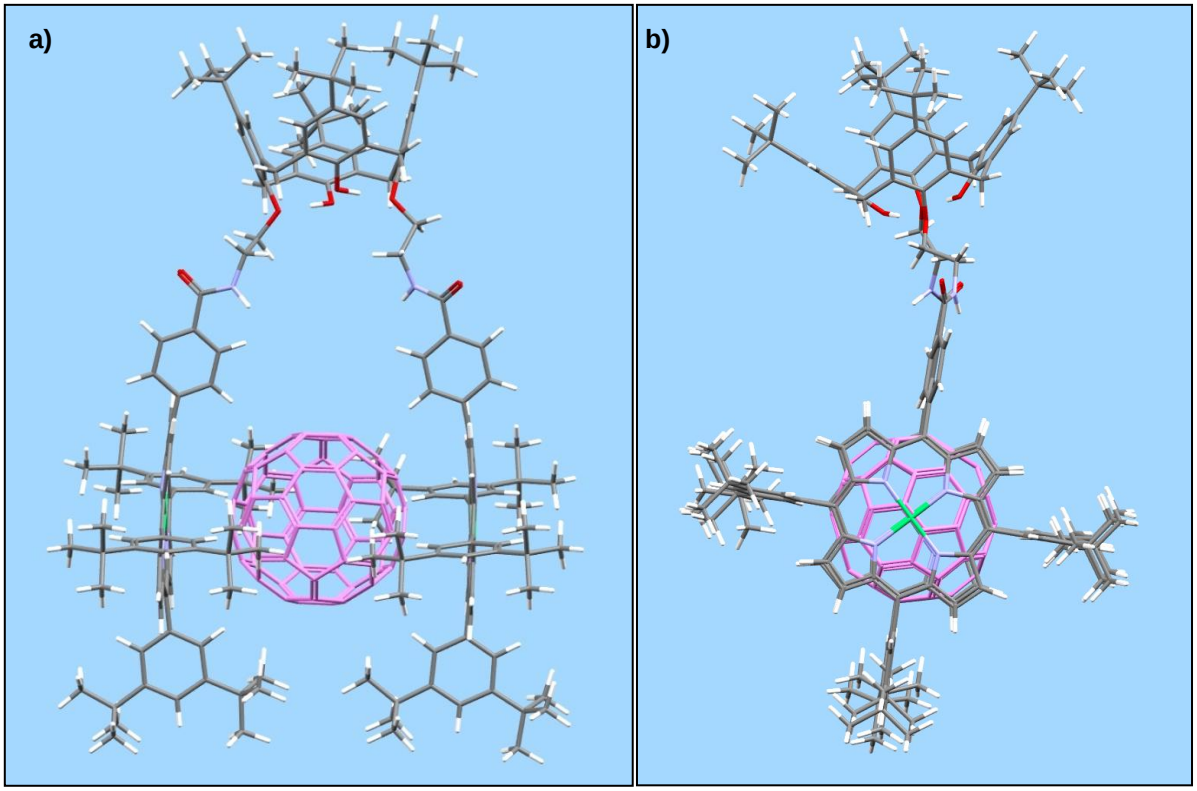

Figure 3.5: a) Front and b) side view of the calculated structure (ONIOM/B3LYP/6-31G(d);UFF) for the nickel(II) derivative of host–guest complex **3.8** with C_{60}.

With C_{60} removed and the structure of **3.8** reoptimized, the porphyrin planes twist and close up on each other. A similar but less extreme effect is observed with removal of C_{60} from hosts **2.1-2.3,** which show a small decrease in the angle of the porphyrin planes and center to center distances. This increase has been attributed to the increased flexibility of **3.8** which allows for movement of the linkers and porphyrins to adopt a lower energy conformation. With the increased distance and the reversal of the amide orientation, the absence of the hydrogen bonding motif between the amide NH and the hydroxyl groups reduces the level of preorganization within the host. The calculated structure of host **3.8** is shown in Figure 3.6.

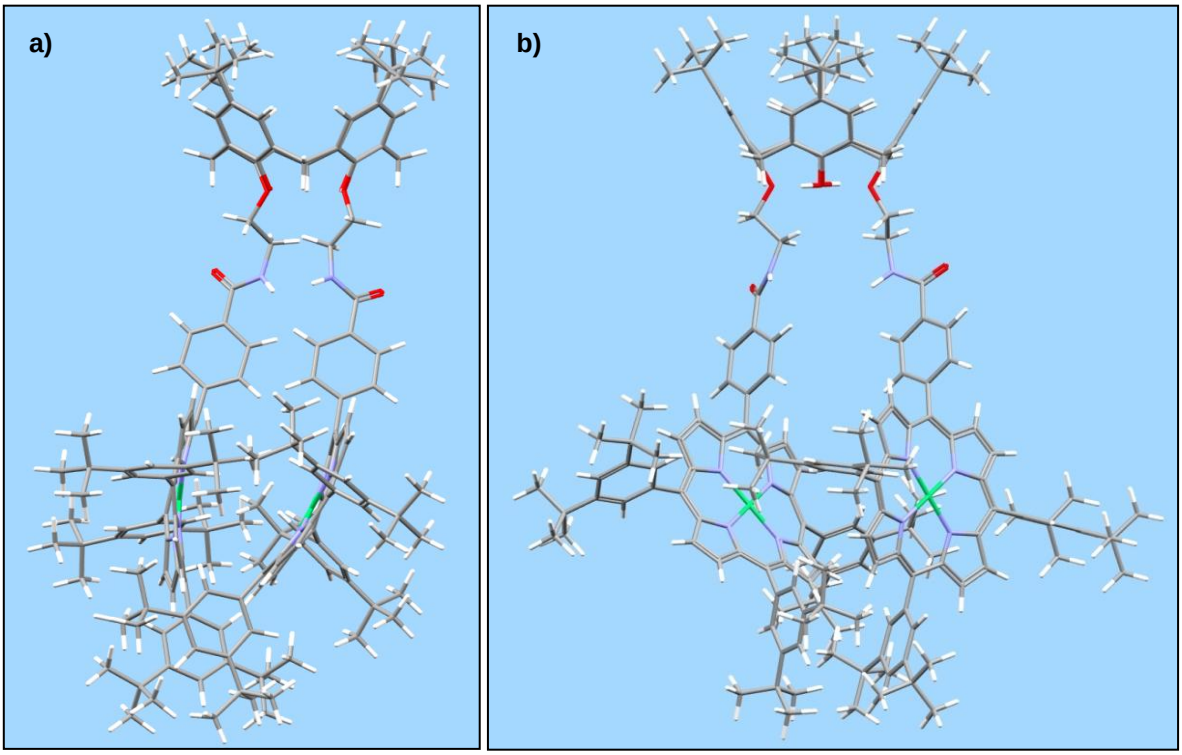

Figure 3.6: a) Front and b) side views of the calculated structure (ONIOM/B3LYP/6-31G(d);UFF) for the nickel(II) derivative of host **3.8**.

3.3.2 Computational Modeling of Bis-porphyrins 3.9 and 3.10

In the optimized structure of both tetra-alkylated host-guest complexes **3.9** and **3.10**, the calixarene scaffold still adopts a pinched cone conformation rather than forming a symmetric cone conformation. However with the removal of the hydrogen bonding and motif, the pinched nature of the calixarene is now reversed and the phenyl groups which are alkylated by methyl or *n*-butyl ethers are no longer tilted toward each other but are parallel with an interplanar angle of 13.3° for the methoxyphenyl rings and 5.5° for the *n*-butoxyphenyl rings. Unlike **2.1**, where the hydroxyl groups point toward the ether oxygen of an adjacent phenyl, the methoxy and *n*-butoxy groups orientate out away from the calixarene. The phenyl rings functionalized by the porphyrin substituents are now tilted toward each other with a wide interplanar angle of 73.1° for **3.9** and 80.0° for **3.10**. The wide angle between the aromatic rings can be attributed to the hydrogen bonding between the N-H of amide and the oxygen of the opposite ether. With the removal of the dominating phenolic hydrogen bonding, the amide NH-oxygen distance is slightly shorter being 2.26 Å and 2.27 Å for **3.9** and 2.27 Å and 2.22 Å for **3.10**.

The changes in the calixarene scaffold and the linking amide groups influence the porphyrin binding site geometry. In the tetra-alkylated bis-porphyrins, the amide phenyls at the

5-position of the porphyrin, which are relatively parallel in host **2.1,** are orientated toward each other at an angle of 57.9º for 60.2º. These phenyl rings show CH-π interactions between the proton *meta* to the porphyrin and the opposite amide phenyl with a distance of 2.679 and 2.65 Å for **3.9** and **3.10** respectively. The interplanar angles between two 24-atom mean porphyrin planes are narrower with **3.9** and **3.10** measuring 64.8° and 65.1° respectively. The center to center distance between the porphyrin planes increases to 10.67 Å for **3.9** and 10.66 Å for **3.10**. The distances between the porphyrin metal center and the fullerene 6:6 junction range from, 2.91-3.03 Å for **3.9**, and 2.84-3.00 Å for **3.10**. The calculated structures of the host guest **3.9** and **3.10** complexes are shown in Figure 3.7 and key geometric parameters for **3.9** and **3.10** as well as **2.1** are given in Table 3.3.

Table 3.3: Key geometric features of the molecular modeling (ONIOM/B3LYP/6-31G(d);UFF) for the nickel(II) derivative of host-guest complexes of A, **3.9** and **3.10** with C_{60}.

Bis-Porphyrin :C_{60}	**2.1**	**3.9**	**3.10**
Calixarene ester functionalized phenyl ring angle (°)	23.7	73.1	77.1
Calixarene phenol ring angle (°)	78.2	13.3	3.7
Hydrogen bonding distance phenol O-H ether O (Å)	1.90,1.95	-	-
Hydrogen bonding distance phenol N-H ether O (Å)	2.27, 2.40	2.28, 2.26	2.22, 2.25
Interplanar amide phenyl angle (°)	-	57.9	60.2
meta CH-π distance (Å)	-	2.879	2.849
Porphyrin center to center distance (Å)	9.93	10.67	10.66
Interplanar angle 24-atom mean porphyrin plane (°)	74.21	64.76	65.1
Porphyrin metal to fullerene 6:6 junction distance (Å)	2.81, 3.36 2.96, 3.03	3.03, 2.91 2.98, 2.88	2.84, 2.96 2.90, 3.00
CH-π interactions for *o*-protons and the CH-π interaction for methyl groups on the *tert*-butyls (Å)	2.72-3.31	2.81-3.47	2.73-3.47

The fullerene was removed and the host models recalculated. The reoptimized models of the bis-porphyrin hosts do not follow the same trend in the structural optimization as the dialkylated models. The calixarene scaffold maintains the same pinched cone conformation as the host complex with C_{60} and the angles of the cone do not change greatly, the angles between calixarene ether rings being 3.7° and 9.9° and 72.4° and 72.3° between the porphyrin functionalized phenyl rings for **3.9** and **3.10** respectively. Hydrogen bonding between the N-H of the amide and the oxygen of an ether also decreases only slightly as well with distances of 2.25 Å for **3.9** and 2.35 Å and 2.27 Å for **3.10**.

The optimized structure of **2.1** shows that the amide phenyls at the 5-position of the porphyrin remain relatively parallel to each other. The tetra-alkylated hosts **3.9** and **3.10** become further tilted by approx 5°. The CH-π interactions between the proton *meta* to the porphyrin and the opposite amide phenyl become stronger, with shorter distances of 2.56 and 2.76 Å for **3.9** and **3.10** respectively. The interplanar angle of the porphyrin planes increases to 83.1° and 81.5° for **3.9** and **3.10** respectively. The center to center distance of the porphyrins increases to 11.04 Å for **3.9** and 11.31 Å for **3.10**. CH-π interaction between methyl of *tert*-butyl group and the phenyl ring or a 3,5-di-*tert*-butyl on the other porphyrin CH-centroid are 2.70-2.74 Å. The calculated structures of the hosts **3.9** and **3.10** are shown in Figure 3.8 and key geometric parameters for **3.9** and **3.10** as well as **2.1** are given in Table 3.4.

Table 3.4: Key geometric features of the molecular modeling (ONIOM/B3LYP/6-31G(d);UFF) for the nickel(II) derivative of tetra-alkylated bis-porphyrins **3.9**, **3.10** and dialkylated porphyrin **2.1**.

Bis-Porphyrin Host	**2.1**	**3.9**	**3.10**
Calixarene ester functionalized phenyl ring angle (°)	17.62	72.48	74.53
Calixarene phenol ring angle (°)	75.5	13.67	7.29
Hydrogen bonding distance phenol O-H ether O (Å)	1.989, 2.001	-	-
Hydrogen bonding distance phenol N-H ether O (Å)	2.551, 2.505	2.251, 2.257	2.222, 2.253
Interplanar angle amide phenyl (°)	-	64.75	60.69
meta CH-π distance (Å)	-	2.560	2.548
Porphyrin center to center distance (Å)	8.254	11.035	11.020
Interplanar angle 24-atom mean porphyrin plane (°)	57.42°	83.12°	83.39°
CH-π interactions between methyl groups on the *tert*-butyl and *tert*-butyl phenyl second porphyrin.	2.934	2.761	2.764

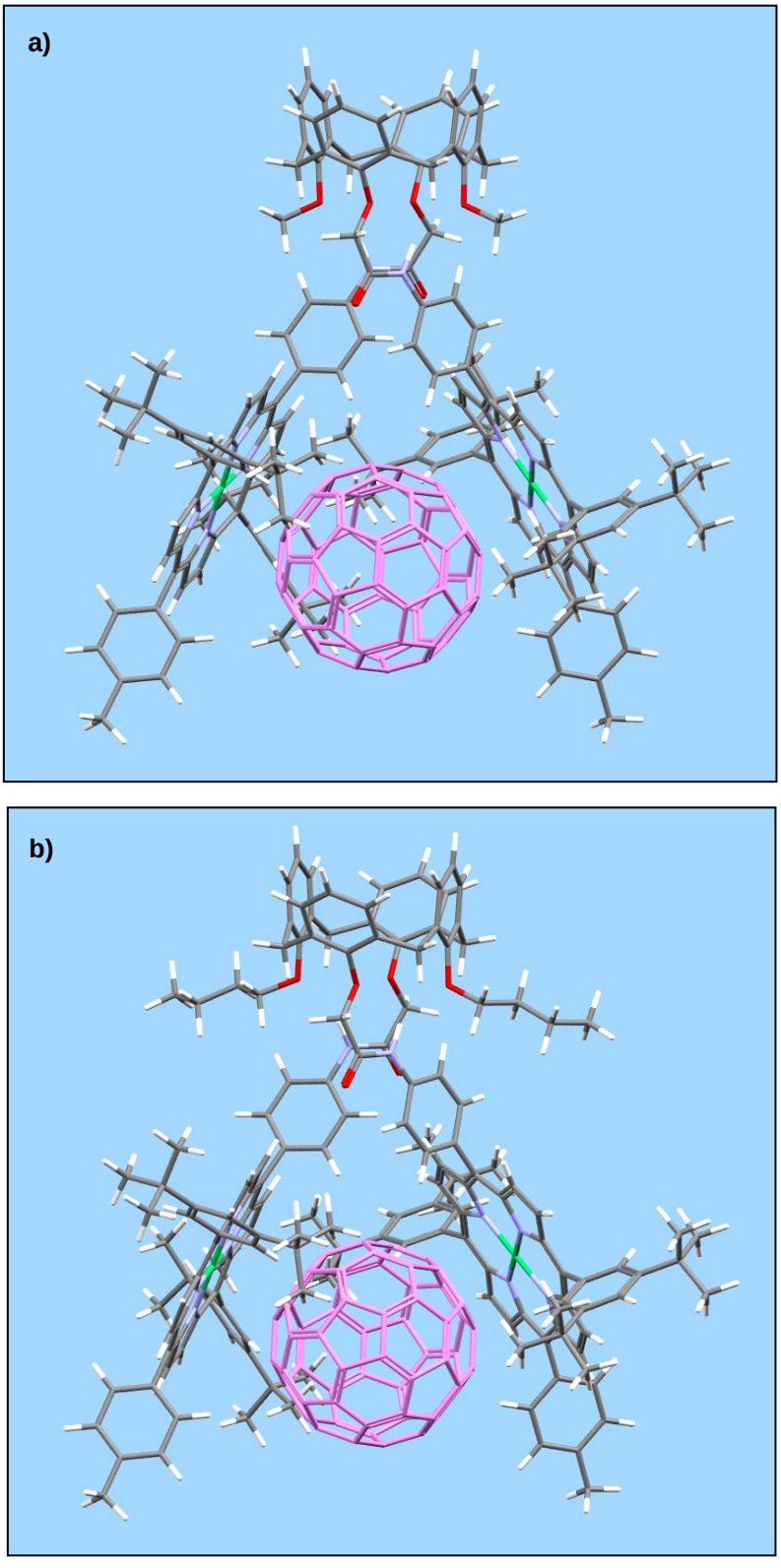

Figure 3.7 Calculated structures (ONIOM/B3LYP/6-31G(d);UFF) for the nickel(II) derivative of hosts–guest complex **3.9** with C_{60} and b) **3.10** with C_{60}.

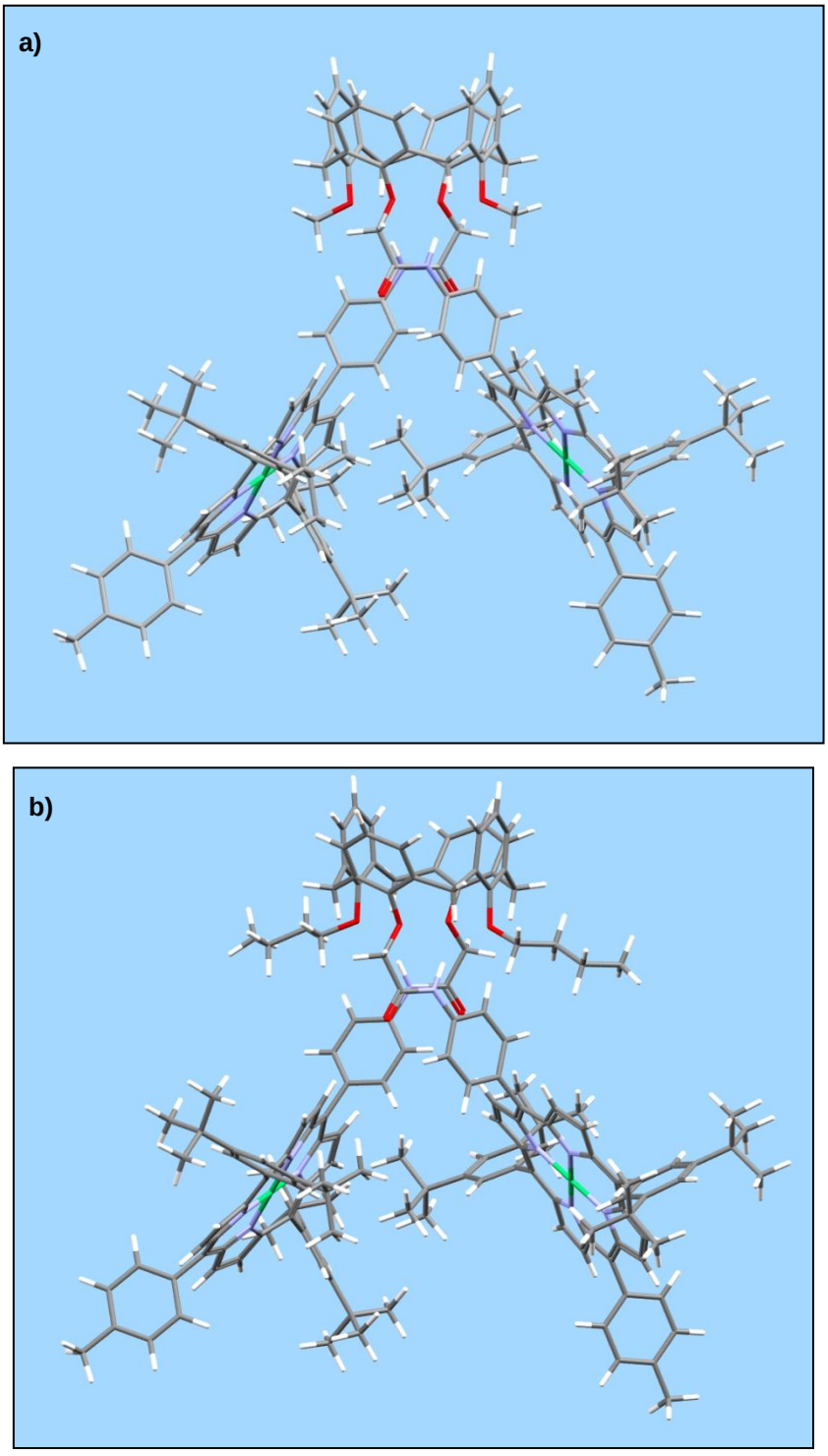

Figure 3.8: Calculated structures (ONIOM/B3LYP/6-31G(d);UFF) for the nickel(II) derivative of a) **3.9** and b) **3.10**.

The computational modeling of bis-porphyrins **3.8-3.10,** with and without C_{60}, show that all the hosts have the potential to bind fullerenes. Bis-porphyrin **3.8** shows a parallel arrangement of the porphyrin planes which may increase the binding constant for fullerenes through improved CH-π and π-π interactions. Hosts **3.9** and **3.10** show inverted cone conformations compared to

host **2.1**. Nevertheless the overall geometry between the porphyrin planes is relatively similar in terms of the angles and interplanar distances. It is expected that fullerene binding should be similar to that of **2.1.**

3.4 Synthesis of Bis-Porphyrins

3.4.1 Synthesis on Bis-Porphyrin 3.8

The synthetic route for the bis-porphyrin **3.8** is shown in Scheme 3.3. *Tert*-butyl calixarene **3.2** was alkylated by refluxing with two equivalents of bromoacetonitrile, sodium iodide and potassium carbonate in acetonitrile for 18 hours to give the 1,3 disubstituted compound in good yield.[186] Compound **3.11** showed the expected ^{1}H NMR pattern for the cone conformations with the presence of two sets of sharp doublets at 4.22 and 3.45 ppm with a coupling constant of 13.5 Hz corresponding to the methylene bridges and a singlet for the methylene of the acetonitrile groups. The dinitrile calixarene **3.11** was then refluxed with lithium aluminum hydride in dry THF to reduce the nitrile functionalities to the corresponding diamines,[187] giving **3.12** in almost quantitative yield. ^{1}H NMR spectra again showed that the cone conformation of the calixarene host was retained with the two methylene doublets at 4.33 and 3.37 ppm with a coupling constant of 12.9 Hz, as well as two sets of triplets at 4.07 and 3.28 ppm corresponding to the two methylene linkers of the amine groups.

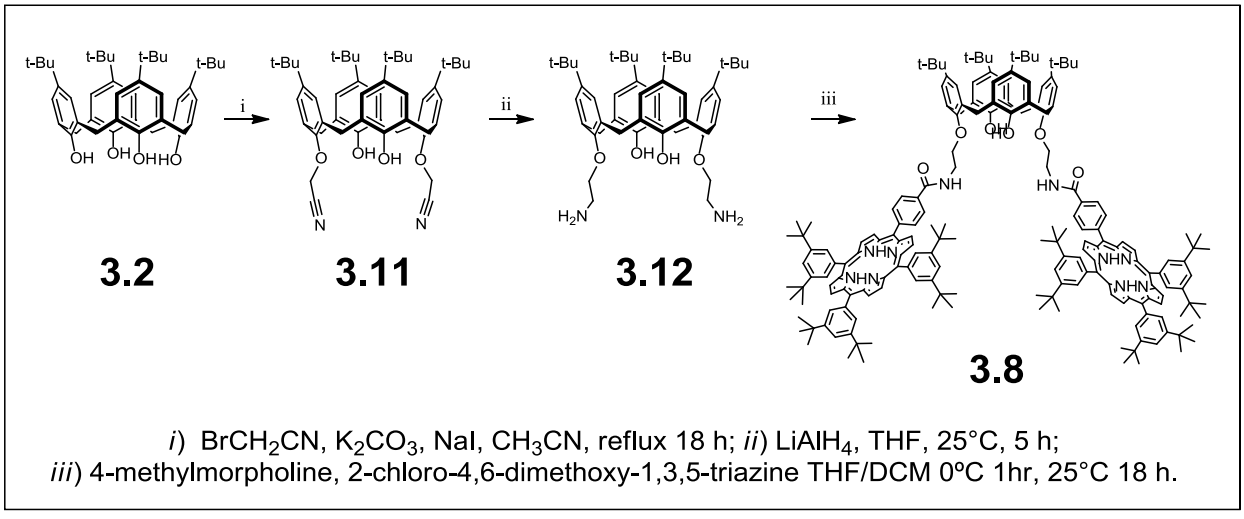

Scheme 3.3: Synthesis of bis-porphyrin **3.8**

The porphyrin employed for coupling to the calixarene diamine was the (4-carboxyphenyl)-10,15,20-tris(3,5-di-*tert*-butylphenyl)porphyrin **3.16**.[188] Porphyrin **3.16** was prepared by the method shown in Scheme 3.4. Reacting one equivalent of methyl 4-fomyl benzoate and three equivalents of 3,5 di-*tert*-butyl benzaldehyde with a catalytic amount of boron trifluoride diethyl etherate in high dilution. The mixture was then oxidized with chloranil to give a mixture of different substituted products which included tetrakis(3,5-di-*tert*-butyl)phenyl porphyrin **3.13**, the desired mono substituted porphyrin **3.14** and both cis (**3.cis-15**) and trans (**3.trans-15**) isomers of the di-substituted porphyrins. These porphyrins require separation from each other. Once isolated by flash chromatography the mono-substituted ester **3.14** was then hydrolyzed to the aromatic carboxylic acid **3.16** by refluxing in ethanol with a 10% sodium hydroxide solution. The preparation time as well the numerous chromatographical columns required for purification of the **3.16**, illustrates the superior versatility and practically of the Suzuki coupling method of porphyrin functionalization.

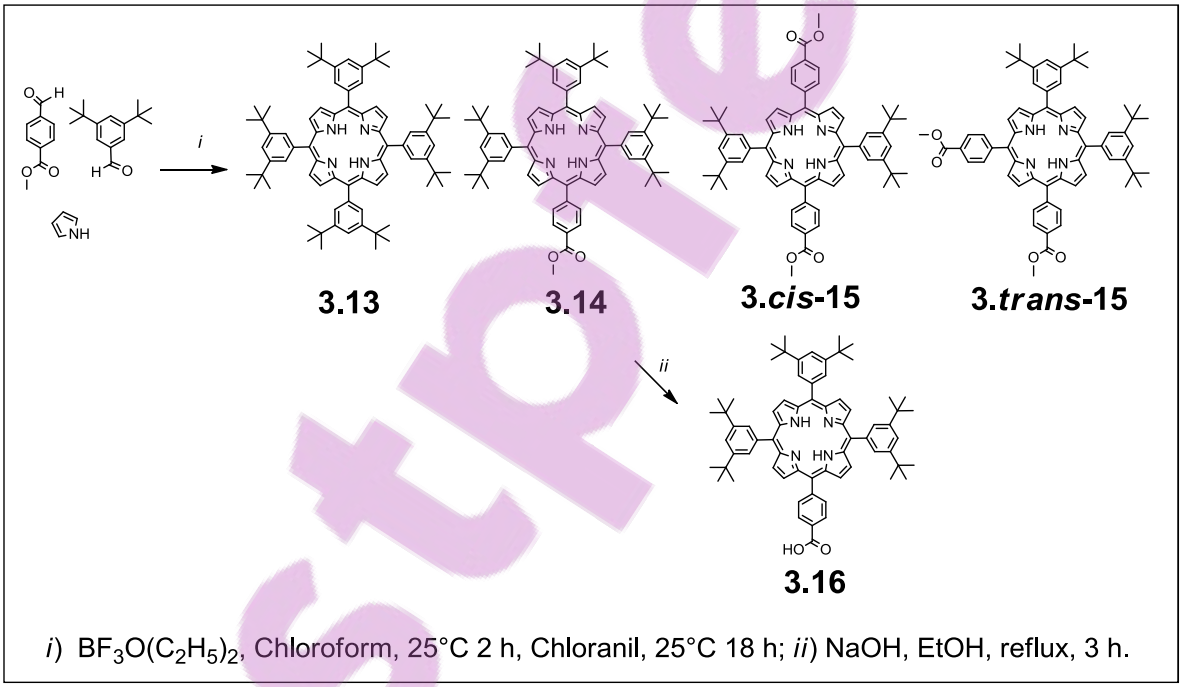

Scheme 3.4: Synthesis of porphyrin acid **3.16** via a statistical mixture;

The use of DCC is not best suited as coupling reagent for the calixarene diamine **3.12** to the porphyrin acid **3.16**. Different methods for the amide coupling reaction were investigated. Early attempts included the formation of an activated pentafluorophenol ester of **3.16** and coupling to calixarene **3.12**,[189] and the use of amide coupling reagents Hydroxybenzotriazole

(HOBt) and 1-[Bis(dimethylamino)methylene]-1*H*-1,2,3-triazolo[4,5-*b*]pyridinium 3-oxid hexafluorophosphate (HATU) which have been employed to couple aromatic acid to aromatic amines in polar solvents.[190,191] These methods however failed to produce any mono-porphyrin or bis-porphyrin.

Successful coupling was achieved by employing the method employed by Zink and Stoddart which has been used to prepare both porphyrin amides and esters in high yield.[192] The porphyrin acid **3.16** was converted to an activated ester by stirring 2-chloro-4,6-dimethoxy-1,3,5-triazine and 4-dimethylaminopyridine in the presence of *N*-methylmorpholine in THF. The formation of the activated ester was monitored by TLC through the formation of a less polar compound at the expense of the porphyrin acid and then the calixarene diamine was added and the reaction stirred overnight. Coupling of the porphyrin to the diamine occurred in almost quantitative yield with no starting porphyrin remaining. The bis-porphyrin **3.8** was purified by column chromatography eluting with dichloromethane/hexane.

The ^{1}H NMR spectrum of **3.8** revealed proton signals integrating for one calixarene and two porphyrins. The methylene bridges of the calixarene were shown as two sets of doublets at 4.41 and 3.45 ppm with a coupling constant of 13.0 Hz, corresponding to the cone conformation. Mass spectrometry confirmed the formation of the bis-porphyrin host **3.8**.

3.4.2 Synthesis of Bis-Porphyrin 3.9

It is possible to prepare **3.9** via two different methods. Alkylation of the calixarene with ethyl bromoacetate has been reported previously to form the precursor **2.19**.[167] This could be followed with a second alkylation of **3.17** with an excess of methyl iodide and sodium hydride in DMF. The other method would be to alkylate with methyl iodide and then follow with the second alkylation with ethyl bromoacetate.[167] Scheme 3.5 shows the synthetic approach chosen for the methyl derivative of the tetra-alkylated bis-porphyrin. The choice was made to alkylate using ethyl bromoacetate to the diethyl ester **3.17** first, then to follow this with a second alkylation using methyl iodide. This order of alkylation is preferred as the methyl groups are small pendant chains that could potentially allow interconversion of the calixarene to the undesired partial cone or 1,3 alternate conformations, whereas, the ethyl ester functional groups are larger and prevent interconversion.[193]

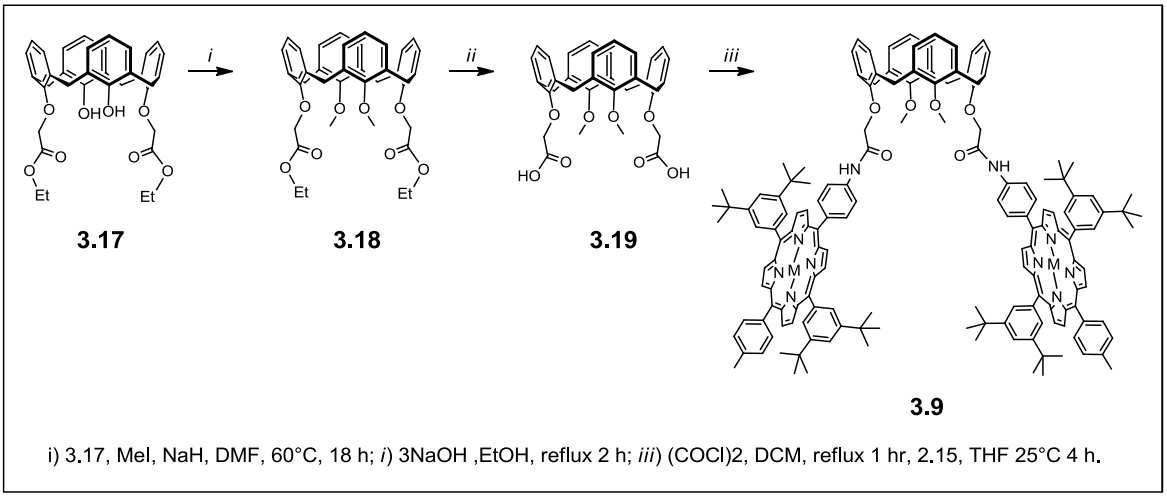

Scheme 3.5: Synthesis of bis-porphyrin **3.9**

The tetra-alkylated calixarene was prepared by taking sodium hydride dispersed in paraffin oil and washing with dry hexane three times under an atmosphere of nitrogen to remove all the paraffin oil. DMF was added and the solution was stirred for 30 minutes after which time a suspension of **3.17** in DMF was slowly added and the solution stirred for a further 30 minutes. Methyl iodide was added dropwise over ten minutes and the solution was then heated for 18 hours. The solution was quenched with slow addition of ethanol and diluted with dichloromethane. After aqueous workup, the solvent was removed to produce a brown oil. The crude material was then purified via column chromatography eluting with dichloromethane and ethyl acetate to give the methyl ester **3.18** as a light yellow oil. It should be noted that several research groups have reported **3.18** as either a yellow oil or a white solid.[194] However all attempts at producing **3.18** as a solid by purification either chromatography or recrystallization failed.

^{1}H NMR confirmed the second alkylation product. However, this was somewhat complicated by the appearance of broad shoulders in the methylene bridge doublets at 3.23 and 4.41 ppm. The ethyl ester signals were ambiguous as the quartet for the CH_2 of the ethyl ester appeared as a singlet at 4.04 ppm and the triplet corresponding to the CH_3 at 1.25 ppm was broadened. Evidence for the formation of **3.18** was given by the appearance of a clear singlet at 3.82 ppm that correspond to the six protons of the methoxy groups and the absence of the singlet at 7.63 ppm associated with the protons of the hydroxyl groups. There was an upfield shift in the signals corresponding to six protons for the aromatic rings *para* and *meta* to the methoxy

group. Confirmation of the product was achieved by mass spectrometry. These irregular features have been attributed to the increased flexibility of the cone conformation.

Hydrolysis of the ester was achieved by refluxing **3.18** with aqueous sodium hydroxide in ethanol to give calixarene diacid **3.19** as a white solid. In comparison with the ethyl ester, the ^{1}H NMR analysis of the acid was unambiguous with two characteristic doublets at 3.35 and 4.26 ppm corresponding to the bridging methylene groups. The coupling constants of the doublets were 13.2Hz and a lone singlet at 4.71 ppm for the carbonyl methylene both confirmed the cone conformation of the calixarene scaffold.

The amide coupling of the amino porphyrin **2.15** to the calixarene diacid **3.19** utilizing DCC as a coupling agent failed to yield the bis-porphyrin. Over several reactions varying the solvent, warming the reaction and by addition of DMAP, the mono coupled porphyrin was produced in about 20% yield and the bis-porphyrin isolated in extremely low yield, approximately 3%, which was enough for ^{1}H MNR and mass spectrometry but not for any photophysical and binding studies. An alternative method for coupling calixarene acids with porphyrins was demonstrated by Dudic for the preparation of calixarene linked tetra-porphyrins by utilizing oxalyl chloride to prepare the more reactive acid chloride and coupling with amino porphyrin.[120] Bis-porphyrin **3.9** was prepared by taking calixarene diacid **3.19** and refluxing with oxalyl chloride in anhydrous dichloromethane. The solvent was removed *in vacuo* and the calixarene redissolved in dichloromethane and the solvent distilled off to remove all traces of the oxalyl chloride. The acyl chloride was then dissolved in THF with three equivalents of amino porphyrin **2.15** and triethylamine, and the solution stirred for four hours. Upon aqueous workup the crude material was purified by column chromatography eluting with toluene/ethyl acetate to give the bis-porphyrin **3.9** as a purple solid in a yield of 20%. The host was recrystallized from chloroform and ethanol to give an analytically pure sample for binding studies.

In contrast to the ^{1}H NMR spectrum of the calixarene acid **3.19,** the proton signals of the methylene bridges and the methoxy groups of **3.8** appear as three broad bands which integrated to eight, four and six protons respectively. Although it was unlikely for the calixarene to invert during the coupling reaction, due to the broad signals in the ^{1}H NMR it was not possible to confirm the conformation of the host as solely the cone geometry. The signals which correspond to the protons *meta* and *para* to the ethers of the calixarene aryl rings were not as

broad but not the clearly define triplets and doublets seen in **2.1-2.3**. The porphyrin proton signals were affected by the increase in flexibility of the calixarene scaffold undergoing minor coalescence of the triplet and doublet in the *meso*-3,5 di *tert*-butyl phenyl rings. Mass spectrometry confirmed a bis-porphyrin host **3.8**.

3.4.3 Synthesis of Bis-Porphyrin 3.10

As with the synthesis of **3.9,** the order in which the alkylation of the calixarene can be performed to give the tetra-alkylated calixarene **3.21** can either be; 1) alkylation with *n*-iodobutane followed by a second alkylation with ethyl bromoacetate or 2) alkylation with ethyl bromoacetate followed by a second alkylation with *n*-iodobutane. Either method is practical as the suitable for the formation of the tetra-alkylated calixarene. The method for the preparation of **3.10** is given in Scheme 3.6.

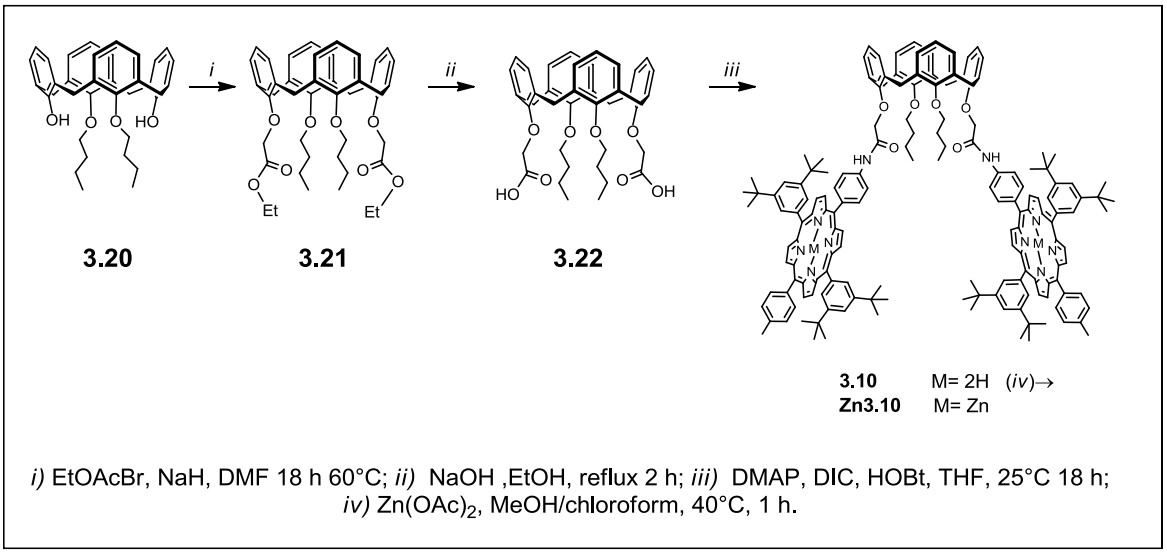

Scheme 3.6: Synthesis of bis-porphyrin **3.10**

Calixarene **3.20** was prepared by the method of Collins *et al.* The tetra-alkylated calixarene **3.21** was prepared by the same procedure as **3.18**.[167] To a hexane washed suspension of sodium hydride in DMF, a solution of **3.20** in DMF was added and the suspension stirred for a further 30 minutes. Ethyl bromoacetate was added dropwise over ten minutes and the solution heated for 18 hours. The reaction was quenched with slow addition of ethanol and diluted with dichloromethane. The after aqueous workup, the solvent was removed to give a yellow oil. The crude material was purified by column chromatography eluting with dichloromethane/ethyl

acetate. The solvent was removed, resulting in an oil which was recrystallized from chloroform/methanol to give **3.21** as a white solid.

^{1}H NMR spectrum of **3.21** was unambiguous compared to the methoxy analog **3.18**. Present was a singlet at 4.78 integrating to four protons corresponded methylene of the ester and a triplet and quartet at 1.29 and 4.21 ppm for the ethyl ester. An upfield shift of the triplet and doublet of the aryl ring functionalized by the butyl group to give a multiplet similar to the **3.18** was observed. Two doublets at 4.69 and 3.23 ppm corresponding to the methylene bridges with a coupling constant of J = 13.6 Hz gave clear evidence of the cone conformation. It should be noted that while every precaution was taken to exclude water from the reaction to prevent cleavage of the ester, upon workup of several reactions, the ^{1}H NMR of the crude material indicated that there was partial cleavage of the ethyl ester to produce a mixture of the diester and the mono acid. Even though the following step involves hydrolysis of the ester to form the diacid, it was decided that after aqueous workup of **3.21** the crude material should be redissolved in ethanol and 6 M hydrochloric acid and refluxed for one hour to re-esterify the acid groups. The crude material was then purified via chromatography. Hydrolysis of the ester **3.21** by refluxing with aqueous sodium hydroxide in ethanol resulted in a white solid of the calixarene diacid **3.22**. ^{1}H NMR spectroscopy confirmed the acid by the absence the triplet and doublet of the ethyl group. Cone conformation was maintained by the presence of the methylene bridge signals as doublets at 4.35 and 3.34 ppm which were still present with coupling constants of 13.4 Hz and a single carbonyl methylene singlet at 3.82 ppm.

As with the synthesis of the analogous **3.9**, the tetra-alkylated calixarene diacid **3.22** did not undergo amide coupling with the amino porphyrin **2.15** to give the bis-porphyrin host **3.10** when utilizing DCC as the coupling agent. Employing oxalyl chloride to form the more reactive acid chloride was successful in preparing the bis-porphyrin, however the yield was low and an alternative coupling reagent was utilized for the coupling of the diacid to the porphyrin. N,N'-Diisopropylcarbodiimide (DIC) and hydroxybenzotriazole (HOBt) and DMAP have been demonstrated in amide bond formation where DCC is not suitable. Diacid **3.22** and amino porphyrin **2.15** were stirred with DIC, HOBt and DMAP for 18 hours in THF.[195] The crude material was purified by column chromatography eluting with toluene/ethyl acetate and the solvent removed to give the bis-porphyrin **3.10** as a purple solid in a moderated yield of 60%. An analytically pure sample of **3.10** was prepared via recrystallization from chloroform/methanol. The zinc analog **Zn3.10** was prepared by standard metallation method

heating **3.10** with zinc acetate in a chloroform methanol solution until no free base was observed in the UV-visible spectrum.

The ^{1}H NMR of **3.10** was less ambiguous than the methoxy analog **3.9**. The ^{1}H NMR spectrum showed both the proton signals of the porphyrin substituents and the calixarene scaffold which integrated in a ratio 2:1 respectively. The conformation of the calixarene was shown to be in the cone conformation as shown by the two sets of doublets at 4.77 and 3.50 ppm with coupling constants of 14 Hz, corresponding to the methylene bridges, as well as a singlet corresponding methylene linker at 5.20 ppm. Mass spectrometry confirmed the host **3.10**.

3.5 Fullerene Binding Studies

3.5.1 Fullerene Binding Studies with Bis-Porphyrin 3.8

UV-visible titration studies were performed on bis-porphyrin **3.8.** Figure 3.9 shows the Soret band of UV-visible titrations experiments for the bis-porphyrin for both C_{60} and C_{70}. Upon addition of C_{60} (0-110 equivalents) into a toluene solution of the bis-porphyrin, no significant decrease in the Soret bands was observed due to complexation and there was no red shifting of the Soret band and no clear isosbestic point. For the titration of **3.8** with C_{70} (0-45 equivalents) the Soret bands show a small decrease in intensity and an isosbestic point is observed, but no significant red shifting of the band is observed. The association constants for C_{60} and C_{70} were calculated to be approximately 200 M^{-1} and 800 M^{-1}, respectively, which are similar in magnitude of the association of C_{60} and C_{70} to mono porphyrins such as TPP. Absence of major observable absorbance changes typical of porphyrin fullerene complexation and low association constants are indicative that there is no co-operative binding between the porphyrin units.

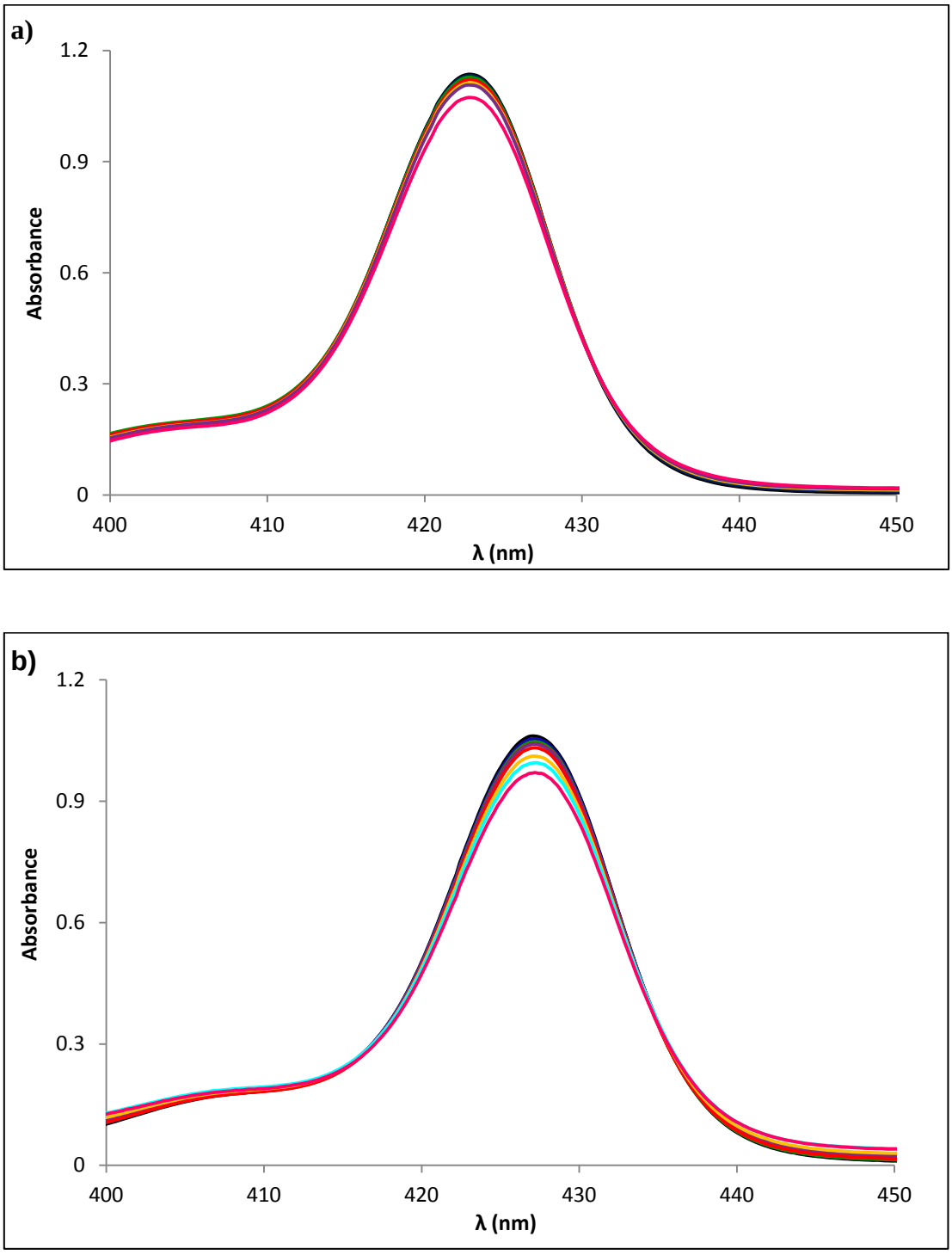

Figure 3.9: UV-visible titration of **3.8** (1.95 x10^{-6}M) in toluene with a) addition C_{60} (0-110 Eq.) and b) C_{70} (0-45 Eq.)

3.5.2 Fullerene Binding Studies with Bis-Porphyrin 3.9 and 3.10 in Toluene

UV-visible titration studies with tetra-alkylated bis-porphyrin hosts **3.9**, **3.10** and **Zn3.10** were performed. Upon addition of C_{60} with **3.9** (0-240 equivalents) there is a small decrease in the intensity of the Soret band and a minor amount of red shifting is observed. An isosbestic point is observed at 435 nm giving a good indication of a 1:1 complex being formed. Titrations of **3.9** and **3.10** with C_{70} (0-97 equivalents) displayed a significant decreases in the Soret band and a pronounced red shift. Binding constants were an order of magnitude lower for both bis-porphyrins **3.9** and **3.10** compared to host **2.1.** The association for **3.9** and **3.10** were both approximately 2.0 x 10^3 M^{-1} for C_{60}. The association for C_{70} with was higher with a value of 1.11 x 10^4 M^{-1} for **3.9** and 1.76 x 10^4 for **3.10.** Titrations of **Zn3.10** with fullerenes gave lower binding constants, consistent with trends for other calixarene linked bis-porphyrin hosts. Due to low yields of **3.9,** the zinc derivative was not prepared to perform binding studies. Association constants for **3.9** and **3.10** are given in Table 3.5 and the UV-visible absorption spectra of the Soret band for **3.9** and **3.10** in toluene are shown in Figure 3.10 and Figure 3.11, respectively.

Table 3.5: Association constants of hosts **3.9** and **3.10** with C_{60} and C_{70} in toluene.

K_a (M^{-1})	**3.9**	**3.10**	**Zn3.10**
C_{60} (x 10^3)	2.0 (0.1)	1.8 (0.10)	1.1 (0.12)
C_{70}(x 10^3)	11.1 (0.6)	17.6 (1.8)	6.7 (0.40)

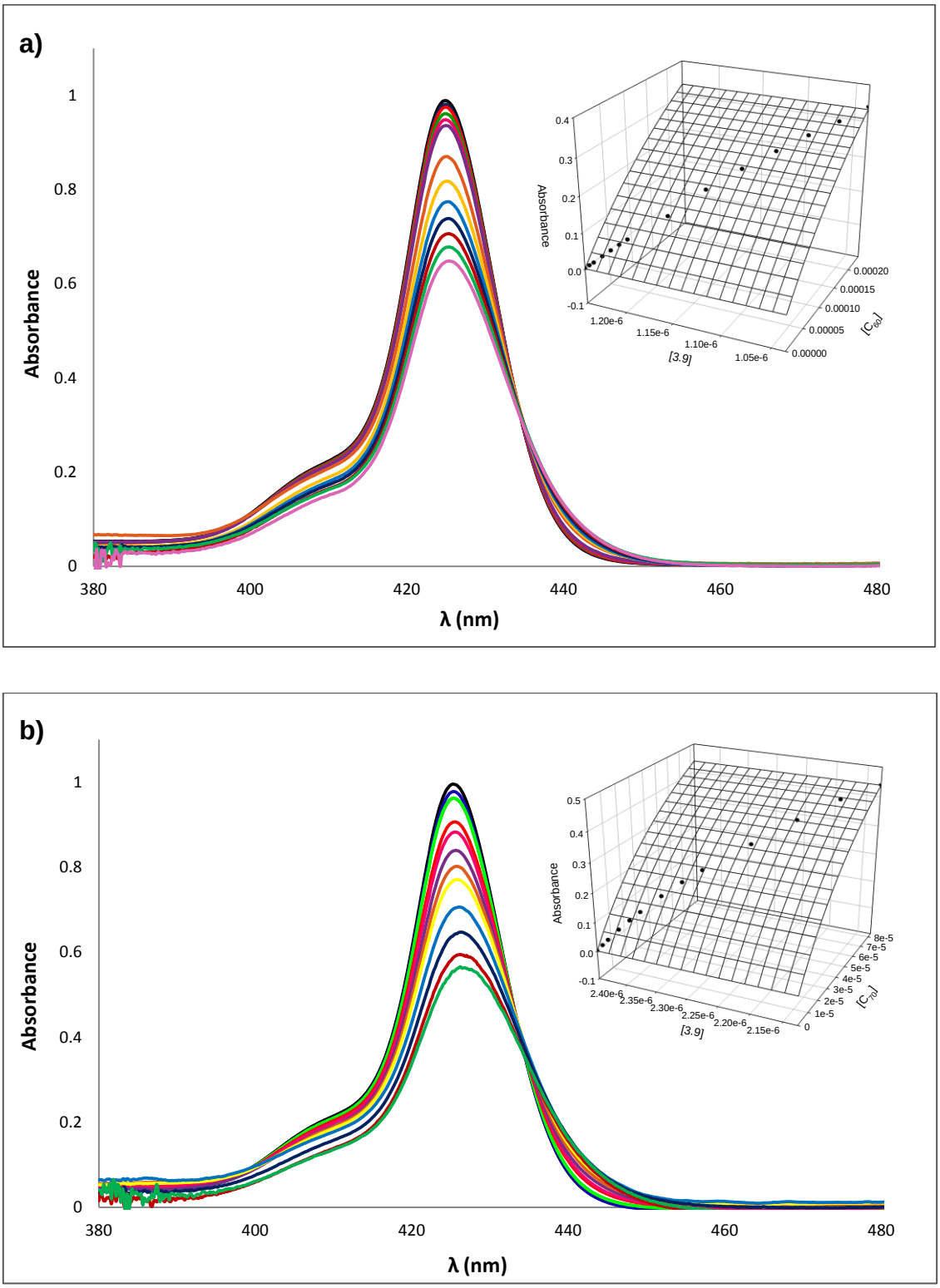

Figure 3.10 : UV-visible titration of **3.9** (1.2×10^{-6} M) in toluene with a) addition C_{60} (0-250 Eq.) and b) UV-visible titration of **3.9** with C_{70} (0-95 Eq.). Insets; plot of the non-linear least square fit for the change in absorption at the Soret of **3.9** upon addition of fullerene.

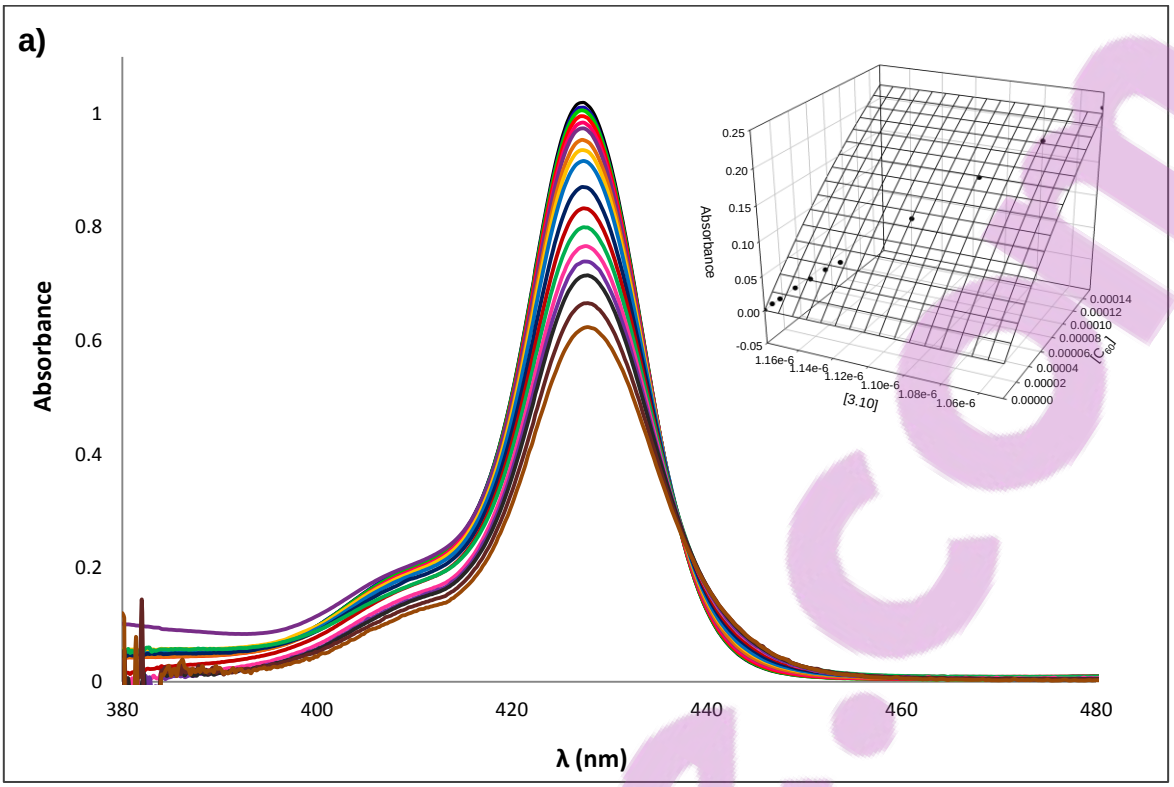

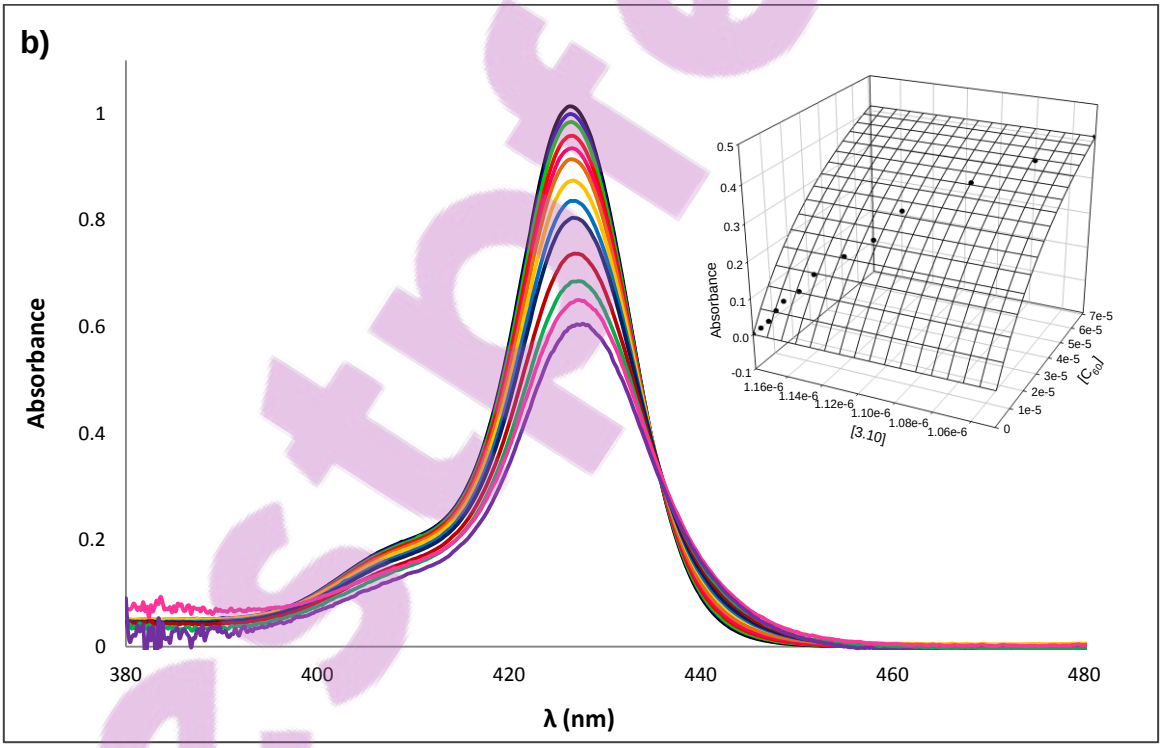

Figure 3.11 : UV-visible titration of **3.10** (1.2×10^{-6} M) in toluene with a) addition C_{60} (0-240 eq.) and b) C_{70} (85 Eq.). Insets; plot of the non-linear least square fit for the change in absorption at the Soret of **3.10** upon addition of fullerene.

3.5.3 Fullerene Binding Studies with Bis-Porphyrins 3.9 and 3.10 in Acetonitrile/Toluene (1:1)

Solvation of the species has a significant influence upon host-guest interactions. In solution, the energies of binding can be broken down into desolvation of the individual host and guest components, binding affinity between the host and guest and the resolvation of the host-guest complex. The formation of the host-guest complex will be favored in solvents where one or both of the host-guest components are weakly solvated or in which the complex is more solvated than the individual components. Fullerenes have low solubility in most solvents with the relative solubility of C_{60} decreasing in the order: 1,2-dichlorobenzene >> toluene > benzonitrile > dichloromethane > cyclohexane. A solution of C_{60} in toluene added to solutions of calixarene linked bis-porphyrin **1.36** in different solvents showed an increase in the binding constant to 5.0 $x10^3$ M^{-1} for benzonitrile compared to that of 2.5 $x10^3$ M^{-1} for toluene. Similar titrations in dichloromethane afforded an association constant of 9.0 $x10^3$ M^{-1}. Titrations carried out in cyclohexane displayed an increase in binding constant of 4.0 $x10^6$ M^{-1}. The binding constant of C_{60} in 1,2-dichlorobenzene in which it is more soluble was 1.8 $x10^2$ M^{-1}. The correlation between solvent and association for C_{60} suggests that desolvation of the fullerene is a dominant factor determining the energetics of host-guest formation.

Solvent mixtures can also be used to control the association constants. In acetonitrile/toluene mixtures the solubility of C_{60} decreases in a nonlinear fashion as the ratio of acetonitrile increases.[196] Solutions of **1.36** in ratios 1:1, 1:3, 1:9, and 1:19 acetonitrile/toluene, were prepared and association constants recorded. For a 1:1 mixture the solubility of C_{60} is comparable to that in cyclohexane and the association constant for C_{60} was measured to be 1.0 $x10^6$ M^{-1}, the same order of magnitude as cyclohexane. For lower ratios of acetonitrile, where the solubility of C_{60} is higher the binding constants decrease.

Acetonitrile/toluene 1:1 was used as a solvent for titrations of the tetra-alkylated bis-porphyrins **3.9** and **3.10,** as larger binding constants are required for the measurement of photophysical properties by transient absorption spectroscopy, due to the reduced interference processes arising from unbound fullerene. The UV-visible absorption spectra upon titration of fullerenes for **3.9** and **3.10** in acetonitrile/toluene 1:1 are shown in Figure 3.12 and Figure 3.13 respectively. These titrations show a greater reduction of the Soret band absorbance at a lower

concentration of C_{60} compared the same hosts in toluene alone. The red shifting of the Soret bands is pronounced and the isosbestic points are clearly defined at 434 nm.

Binding constants for **3.9** and **3.10** with C_{60} were approximately 2.0 $x10^3$ M^{-1} in toluene. Upon changing the solvent to 1:1 acetonitrile: toluene, the binding constants for **3.9** increased by a factor of around 25 for C_{60} to 4.7 $x10^4$ M^{-1}. Hosts **3.10** and **Zn3.10** displayed an increase in binding by two orders of magnitude for C_{60} which is consistent with changing the solvent mixture to acetonitrile/toluene 1:1. A similar trend was seen with C_{70} **3.9** increases by 33 times for C_{70}, giving moderated binding constants of 3.71 x 10^5 M^{-1} while **3.10** increases by over 50 times to 1.03 x 10^6 M^{-1}.

Table 3.6 : Association constants of bis-porphyrins **3.9** and **3.10** with C_{60} and C_{70} in toluene/acetonitrile (1:1).

K_a (M^{-1})	**3.9**	**3.1**	**Zn.3.10**
C_{60}($x10^3$)	47.4 (3.4)	144.0 (1.7)	117.0(6.0)
C_{70} ($x10^3$)	371.0 (5.7)	1,032.0 (38.2)	991.0 (49.0)

The small differences in the association constants of fullerenes in toluene alone are more accurately illustrated using solvent combinations where the fullerenes are less soluble. There is a significant difference in the association constants between **3.9** and **3.10** with the methoxy host **3.9**, showing less affinity for fullerenes. The lower biding constant for **3.9** can be attributed to the increased flexibility and the ability of the calixarene scaffold with the smaller methoxy groups to interconvert to the partial cone conformation.

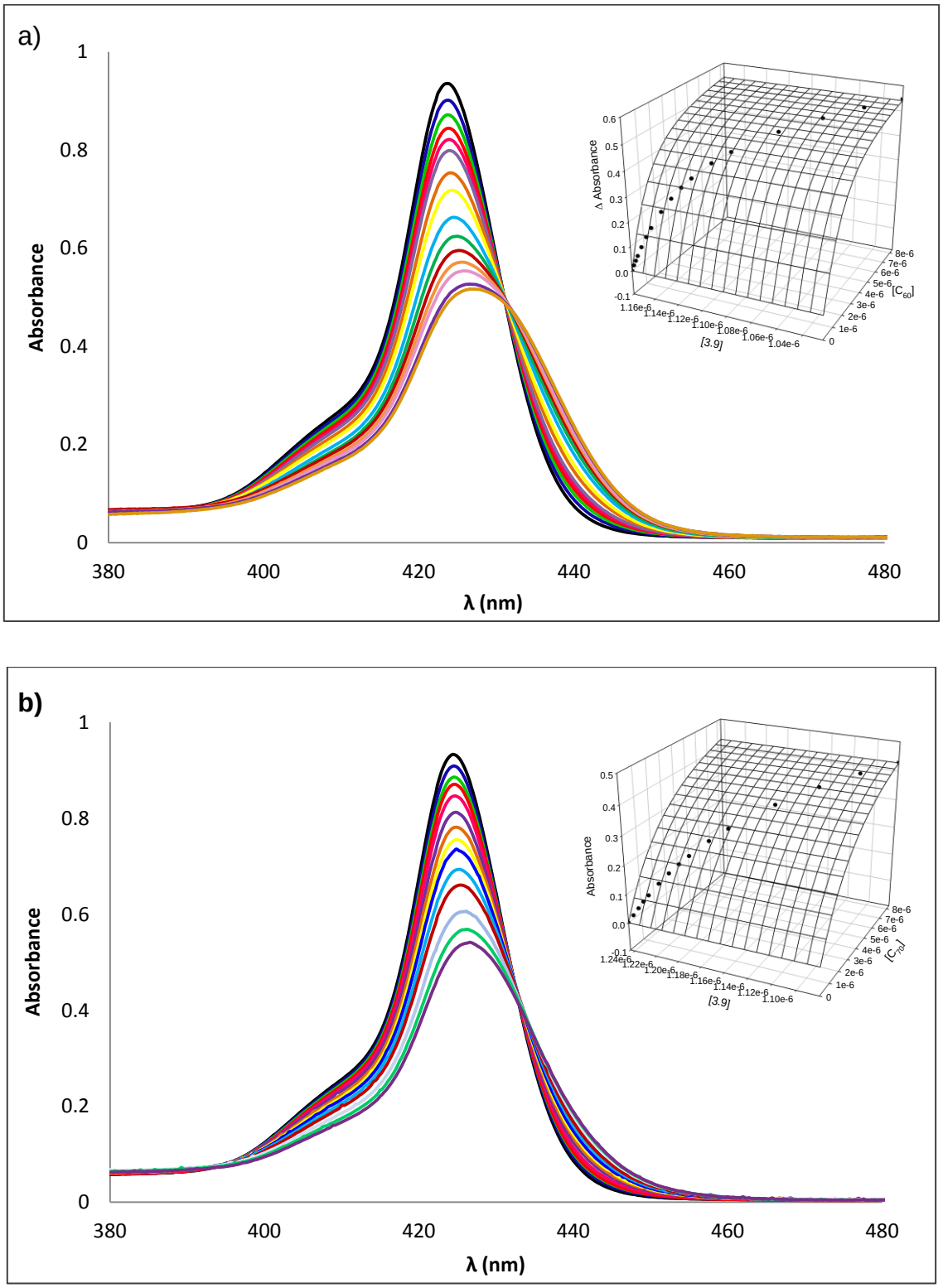

Figure 3.12: UV-visible spectra of titrations of **3.9** ($1.2x10^{-6}$ M) in toluene/acetonitrile (1:1) with a) C_{60} (0-39 Eq.)and b) C_{70} (0-20 Eq.). Inset; plot of the non-linear least square fit for the change in absorption at the Soret of **3.10** upon addition of fullerene.

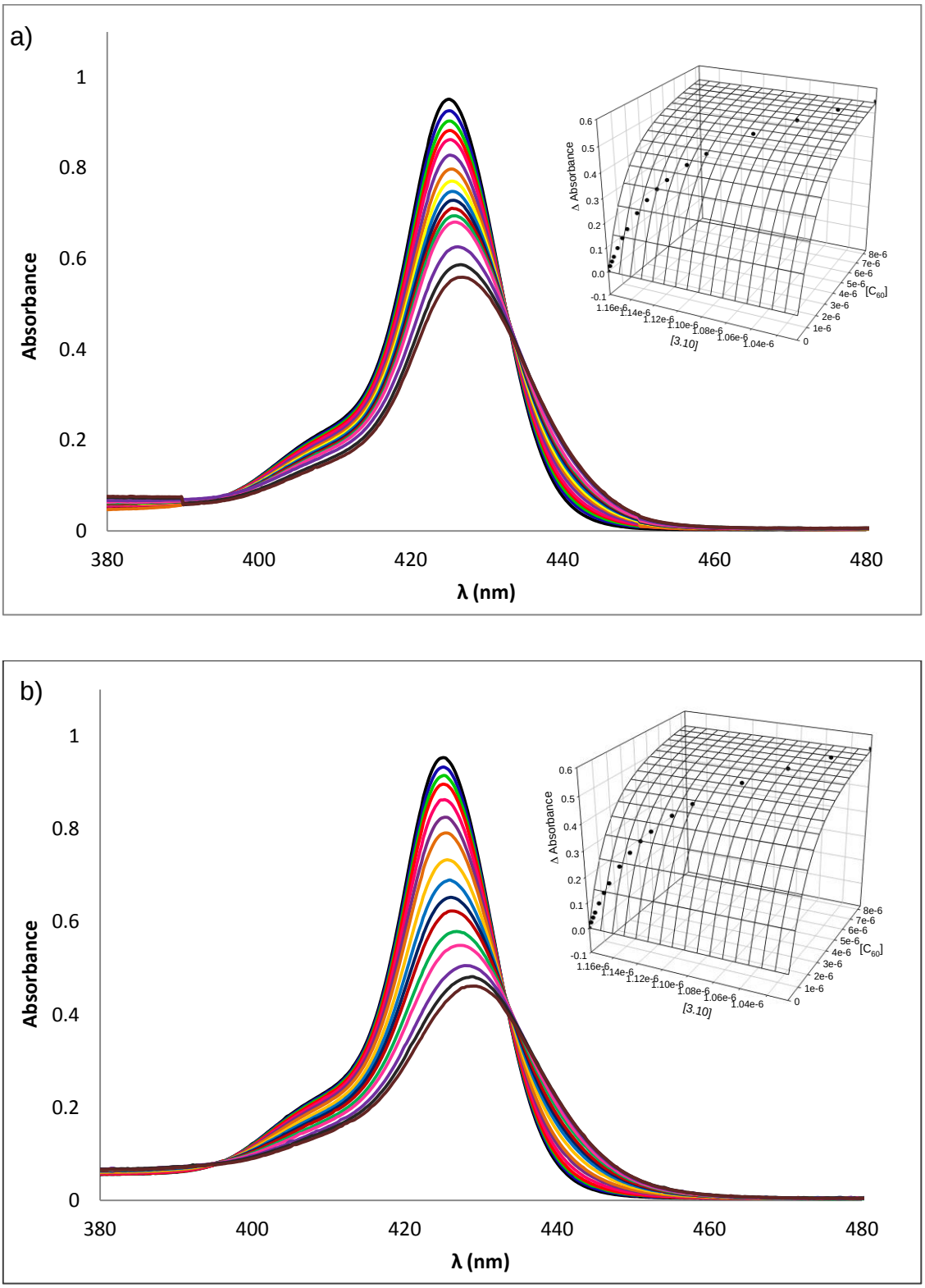

Figure 3.13: UV-visible spectra of titrations of **3.10** ($1.2x10^{-6}$ M) in toluene/acetonitrile (1:1) with a) addition C_{60} (0-37 Eq.) and b) C_{70} (0-18 Eq.) Inset; plot of the non-linear least square fit for the change in absorption at the Soret of **3.10** upon addition of fullerene.

3.6 Variable Temperature NMR studies

Like many macrocycles, calixarenes can have access to a number of stable conformations, with a preference for residing in those which minimize unfavorable steric and electronic effects. The signal broadening observed the ^{1}H NMR spectrum from the **3.9** suggests that there is a dynamic rotation process present within the calixarene due to the removal of the hydrogen bonding motif on the narrow rim.

Variable temperature ^{1}H NMR is commonly employed for studying dynamic processes.[197,198] This technique was used to determine that the spectra obtained with **3.9** were consistent with a single compound interconverting between conformational isomers, rather than a mixture of products. Variable temperature studies were performed with **3.10** and **2.1** as a method of gaining some insight into the conformation of the hosts and the differing binding ability.

3.6.1 NMR Spectra of Bis-Porphyrin Hosts 2.1, 3.9 and 3.10 at 300 K

The ^{1}H NMR spectrum of bis-porphyrins **2.1**-**2.3** display sharp proton signals and can all be assigned to a combination of calixarene and porphyrin. The ^{1}H NMR of bis-porphyrin host **2.1** is shown in Figure 3.15 and with a representation of the calixarene and porphyrin structure in Figure 3.14. The calixarene methylene bridge protons (marked as *) appear as two sharp doublets, indicating that on the NMR time scale the protons are inequivalent. The methylene linker (marked as ♦) connecting the calixarene to the porphyrin amide is observed as a sharp singlet and the calixarene aromatic proton signals (marked as ●) are given as two doublets and two triplets (one triplet omitted).

The porphyrin protons give sharp signals. The four doublets (marked as β) correspond to the β pyrrole protons. The aromatic substituents of the porphyrin (marked as ▼) consist of four doublets corresponding to the tolyl and the 4-amidophenyl substituents and a doublet and triplet for the 3,5-*tert*-butyl phenyl groups. Two singlets at 8.5 ppm and at the highly up field position of -2.09 ppm correspond to the amide proton (marked as ♠) and the central NH proton (marked as ♥), respectively. A singlet at 2.44 ppm is the tolyl CH_3 group (marked as ♣).

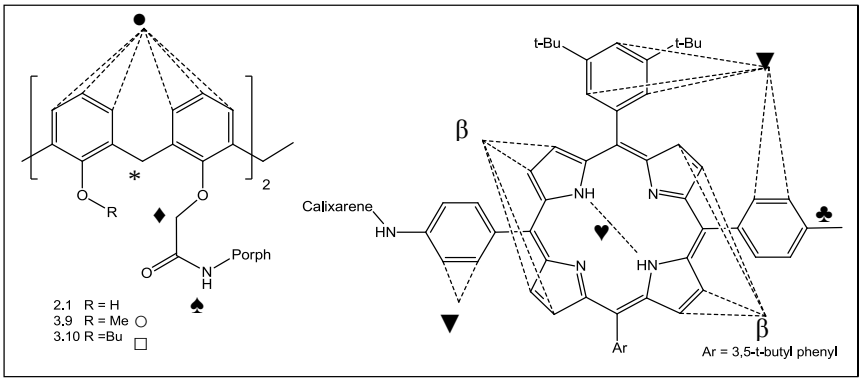

Figure 3.14: Calixarene and porphyrin with ^{1}H NMR markings.

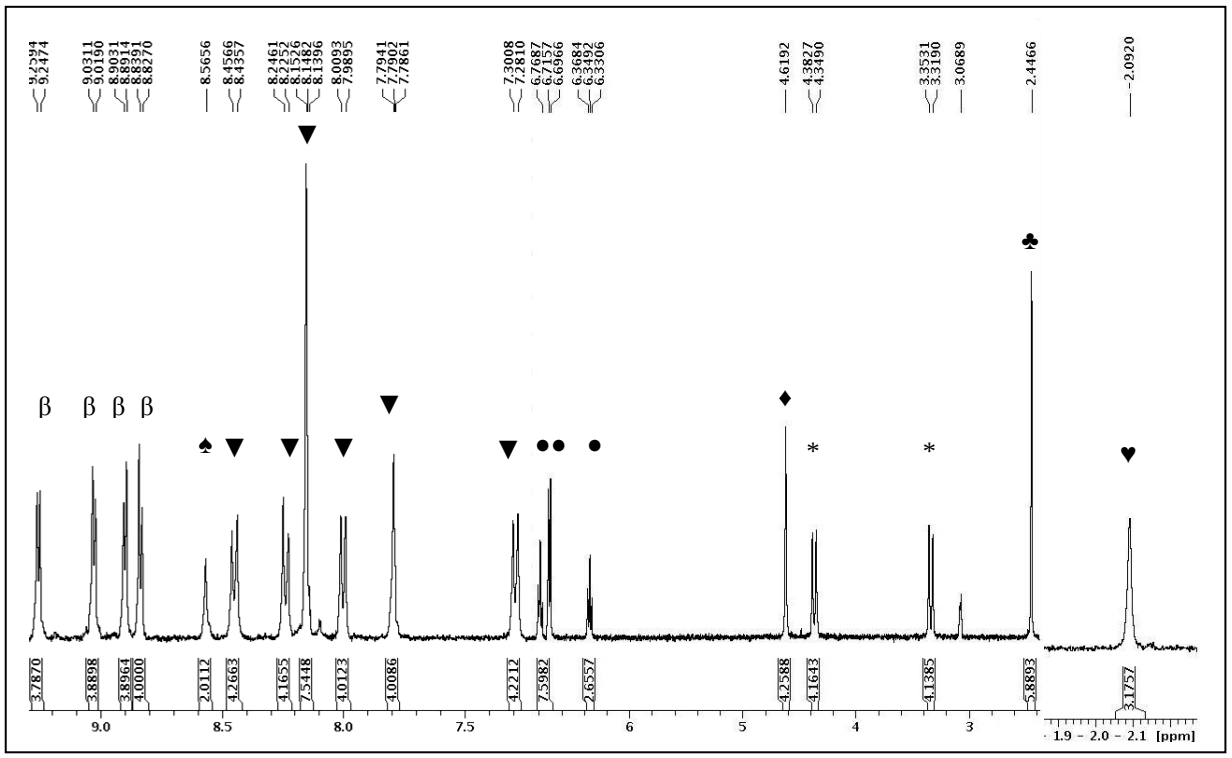

Figure 3.15: ^{1}H NMR spectra of **2.1** in D_8 toluene (solvent and *tert*-butyl protons signals omitted for clarity).

In the ^{1}H NMR spectrum of **3.9** (Figure 3.16), a different pattern of proton signals are observed, although the porphyrins and the calixarene scaffold are relatively similar to **2.1**. Both the porphyrin and calixarene signals occur at different positions and are broadened considerably. The β-pyrrole proton signals (β) are shown as two doublets at 8.92 and 8.97 ppm and a singlet at 8.88 ppm. The porphyrin aromatic substituent peaks (▼) are broadened with both the *ortho* and *para* protons signals for the 3,5-di-*tert*-butyl phenyl shown as singlets instead of a doublet and triplet. This broadening was observed in the central NH proton signal (♥) at

-2.17 ppm. The proton signals corresponding to the calixarene scaffold are further broadened indicating increased flexibility and equivalence of protons on the NMR time scale. In the region where there are usually two doublets for the methylene bridges (*) and two singlets correspond to the methoxy and methylene linker (♦), there are three broad bands at 3.45-4.15 ppm which in total integrate for 18 protons. A broad signal also occurs at 6.76 ppm, corresponding to the *para* protons of the aryl rings of the calixarene (●).

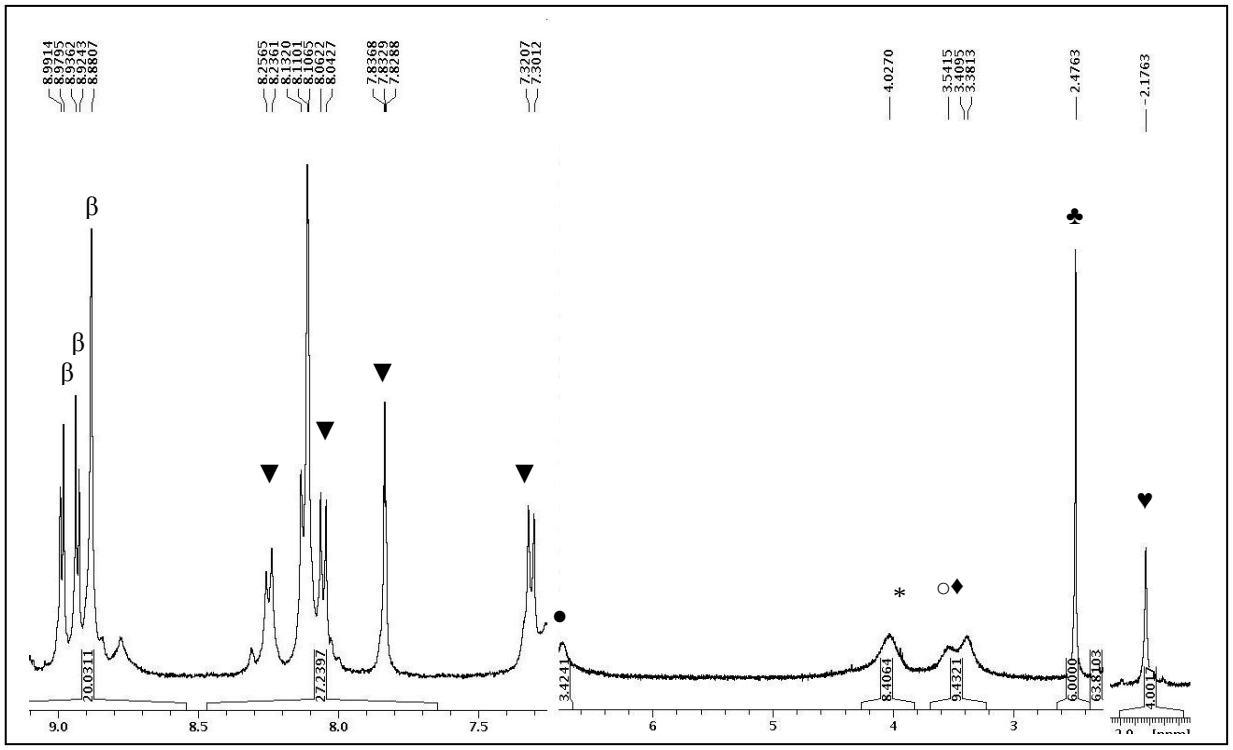

Figure 3.16: ^{1}H NMR Spectra of bis-porphyrin **3.9** in D_8 toluene (solvent and *tert*-butyl protons signals omitted for clarity).

The broadened signals in the ^{1}H NMR spectra of **3.9** are due to the increased flexibility of the calixarene scaffold is not seen in the spectra of **3.10**. Instead **3.10** displays sharp proton signals for both the porphyrin and calixarene similar to the dialkylated host **2.1** (Figure 3.17). Two doublets and a singlet (β) correspond to the β-pyrrole protons. Present are four doublets corresponding to the tolyl and the 4-amidophenyl substituents; a doublet and triplet for the 3,5 tert-butyl phenyl groups (▼); and a singlet at 8.5 ppm for the NH of amide (♠) and the central porphyrin NH proton (♥).

The calixarene methylene bridge protons (*) appear as two sharp doublets at 3.31 and 4.79 ppm indicating that on the NMR time scale the protons orientate toward the wide rim and those orientated toward the narrow rim are inequivalent. The methylene linker (♦) connecting the

calixarene to the porphyrin amide is observed as a sharp singlet at 5.09 ppm. A triplet at 3.84 ppm is observed corresponding to the first methylene of the *n*-butyl chain directly attached to oxygen (□). Evident in the aromatic region are two sharp sets of triplets and doublets (●).

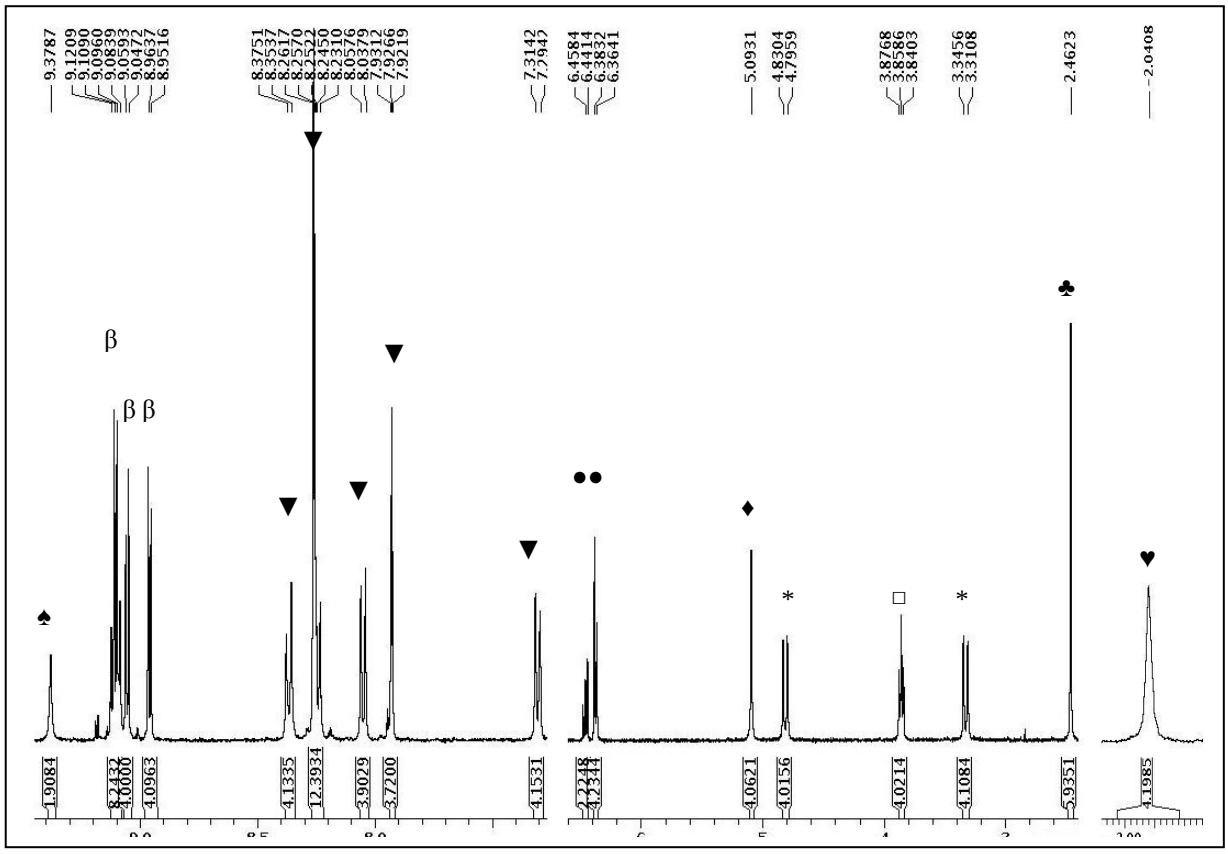

Figure 3.17: ^{1}H NMR spectra of bis-porphyrin **3.10** in D_8 toluene (solvent and *tert*-butyl protons signals omitted for clarity).

3.6.2 Variable Temperature ^{1}H NMR Studies of Bis-porphyrin 3.9

To determine if bis-porphyrin **3.9** is consistent with a single compound interconverting between conformational isomers, ^{1}H NMR spectra of **3.9** were obtained at a number of temperatures ranging from 365K-220 K in d_8.toluene and are shown in Figure 3.18 and Figure 3.19.

Upon heating, the host signals (Figure 3.18) begin to sharpen and separate. At 365 K, there are two sets of doublets 4.15 and 3.40 ppm for the methylene bridges and two singlet signals for the methylene linker at 4.22 ppm and the methoxy protons at 3.55 ppm. The signals at 6.76 and 6.90 ppm sharpen to give a sharp triplet and a broad doublet. The porphyrin proton signals (Figure 3.19) also sharpen, resulting in the splitting of the *para* and *ortho* protons of the 3,5-di-

tert-butyl to give a double and a triplet at 8.09 and 7.78 ppm, respectively. The two signals of the tolyl groups coalesce to give a single doublet integrating for four protons at 8.13 ppm. Observable at 365 K is a peak (♠) at 8.56 ppm integrating for two protons, corresponding to the NH of the amides. This variable temperature NMR experiment proved that the data was consistent with a single compound that undergoes increasingly rapid conformational changes

Upon Cooling **3.9** to 220 K, the ^{1}H NMR spectrum undergoes major changes and the emergence of several new bands at between 4.5 and 2.8 ppm are observed. The porphyrin β-pyrrole and aromatics proton signal broaden and three central NH signals around -2.2 ppm are observed indicating that the porphyrins are in more than one chemical environment. The number of different signals can be attributed to the presence are more than two conformations of the host. These conformations are the cone, partial cone, with interconversion of one methoxy groups and the 1,3-alternate with interconversion of both methoxy groups. As the signals are broadened it is difficult to distinguish which proton signals correspond to each of the different conformations of the calixarene at 220 K.

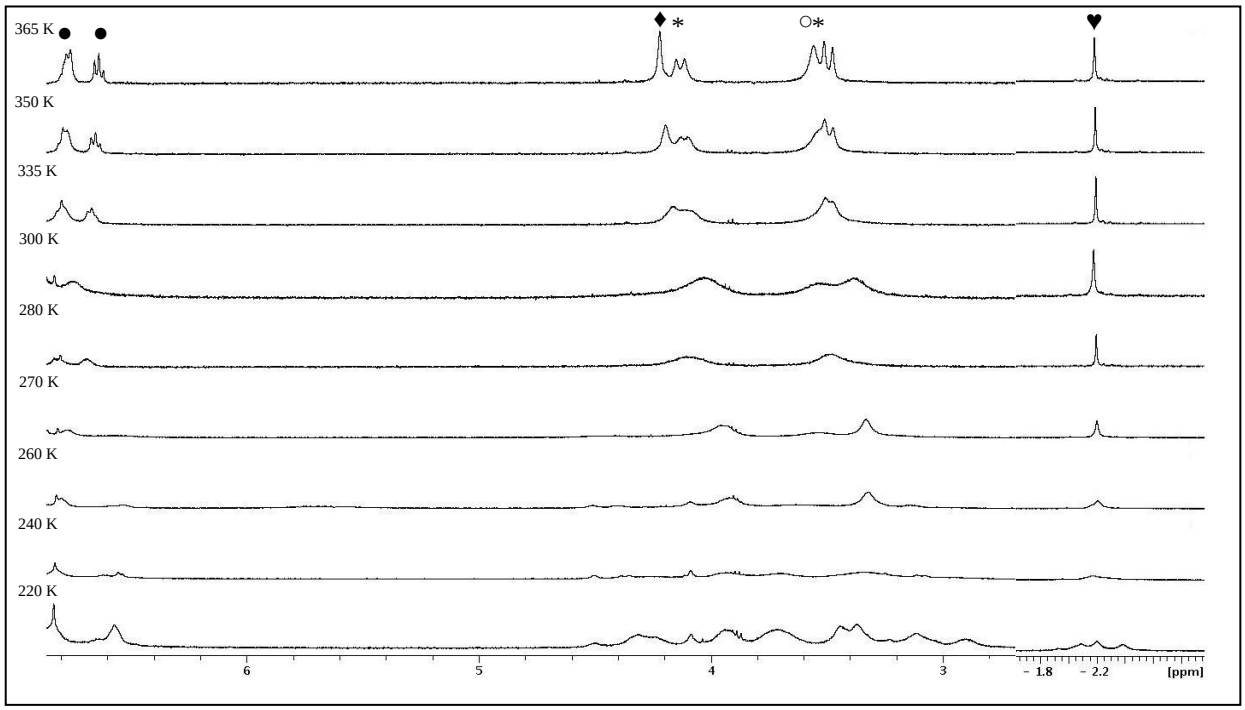

Figure 3.18: Variable temperature ^{1}H NMR of bis-porphyrin **3.9** ranging from 220-365K, illustrating the proton signals of the bridging methylenes (*), the amide linker methylene (♦), the methoxy CH_3 group (○) and the central porphyrin NH (♥).

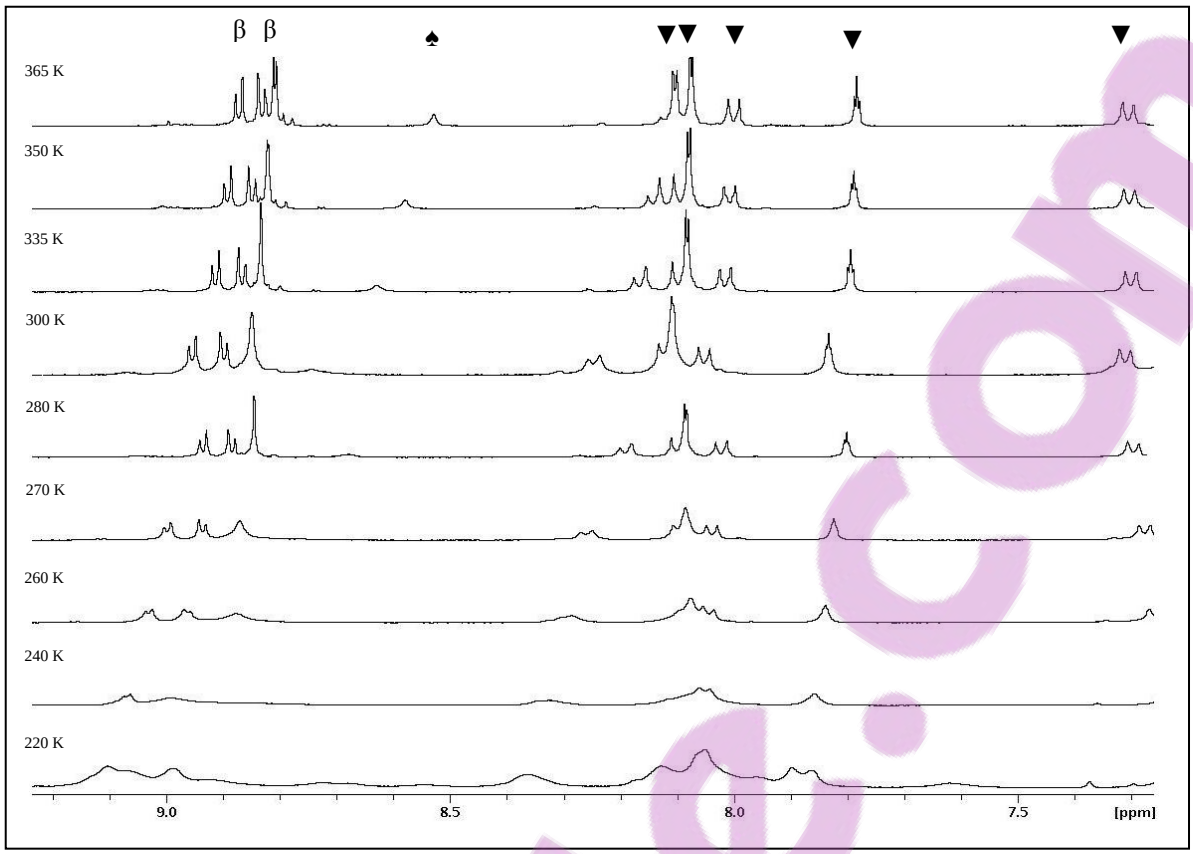

Figure 3.19: Variable temperature ^{1}H NMR of bis-porphyrin **3.9** ranging from 220-365K illustrating the broadening and shifting of the porphyrin proton signals, β pyrrole (β) and the aromatic substituents (▼).

3.6.3 Variable Temperature NMR Studies of Bis-porphyrin 2.1

At 300K, the ^{1}H NMR spectra of **2.1** displays sharp peaks for both the porphyrin and calixarene proton signals. Spectra were obtained at temperatures ranging from 300-220K in d_8 toluene. Upon cooling, the spectra begin to display broadening of the methylene and the methoxy proton signals to the point where at 260 K, the methylene bridges appeared as two broad bands at 3.22 and 4.22 ppm. Upon further cooling of **2.1** to 220K, the appearance of new broad bands are observed at 3.15, 3.25, 4.00, 4.15, 4.25 and 4.90 ppm indicative of multiple conformations for the bis-porphyrin, most likely the partial cone geometry. However, in comparison to **3.9** only one central porphyrin NH signal at -2.0 ppm is observed.

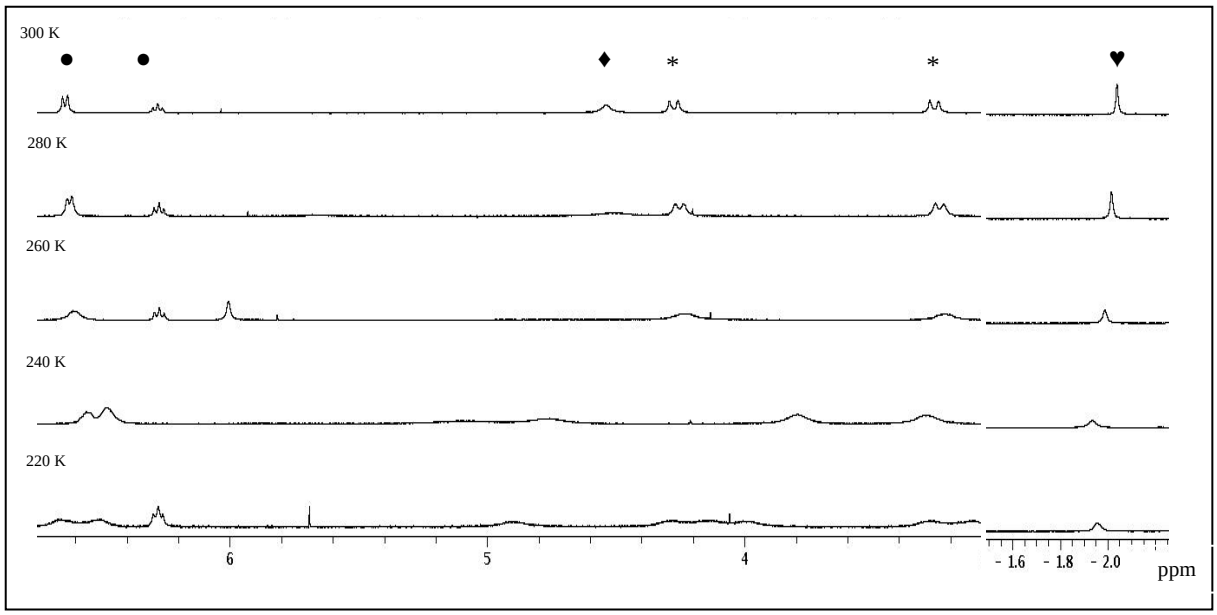

Figure 3.20: Variable temperature ^{1}H NMR spectra of bis-porphyrin **2.1** ranging from 220-300K illustrating the chemical shifts and broadening of the methylene bridges (*), the methylene amide linker (♦) and the porphyrin central NH protons (♥).

3.6.4 Variable Temperature NMR Studies of Bis-Porphyrin 3.10

At 300 K, the ^{1}H NMR spectrum of **3.10** displays sharp peaks for both the porphyrin and the calixarene protons. In order to investigate flexibility of **3.10** spectra were obtained at temperatures ranging from 300-240 K in d_8-toluene. Upon cooling, all proton signals begin to broaden. However this was not observed to the same extent as for the hosts **3.9** or **2.1,** which at 240 K, were beginning to show the appearance of several new bands between 3 and 6 ppm. On the contrary, at 240 K for **3.10** both methylene bridge doublets were still visible and the triplet of the first methylene of the n-butyl chain was also obseved. The aromatic proton signals of the calixarene occur as a double and a triplet. The bis-porphyrin showed no indication of any interconversion of the calixarene cone into different conformations. This has been attributed to the larger butyl groups on the narrow rim which prevent any interconversion and demonstrates that interconversion of rings in the calixarene must proceed via the narrow rim ether or hydroxyl groups passing through cavity of the macrocycle.

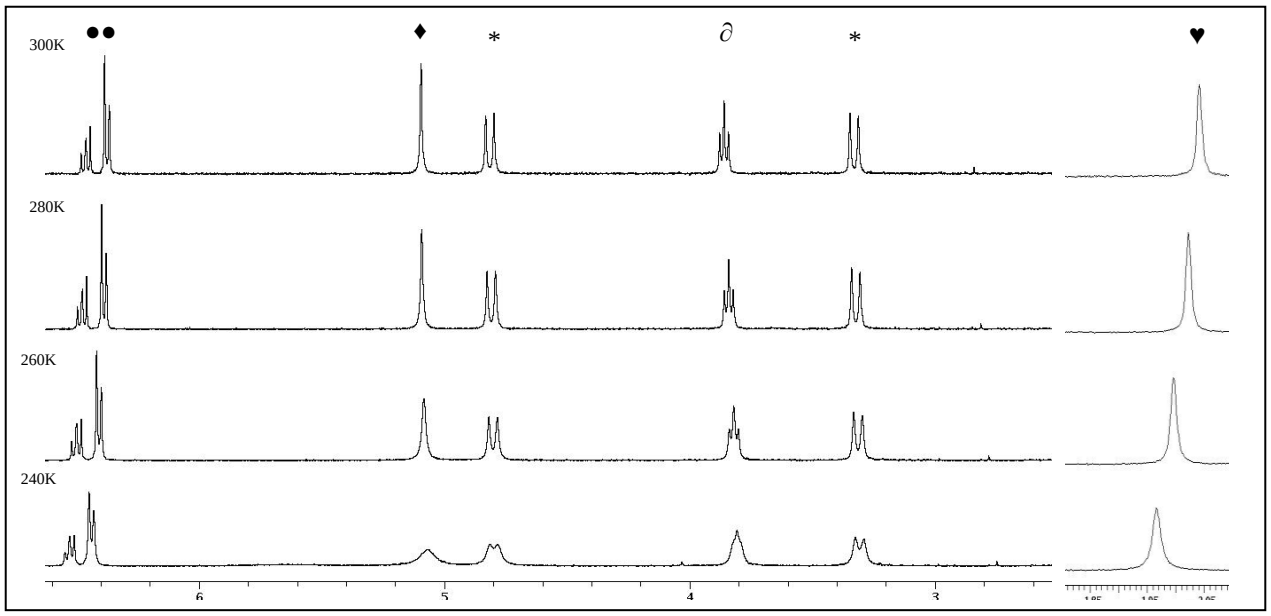

Figure 3.21: Variable temperature ^{1}H NMR of **3.10** showing the chemical shifts and broadening of the methylene bridges (*), the methylene amide linker (♦) and the porphyrin central NH protons (♥).

Variable temperature ^{1}H NMR has demonstrated that the smaller methoxy group allows the rotation of the aryl rings in the calixarene scaffold. Hydrogen bonding on the narrow rim in **2.1** lowers the conformational mobility of the scaffold but can still allow for potential interconversion of the calixarene. The fact that **3.10** cooled to 240 K still only displayed signals corresponding to the cone conformation demonstrates that no conversion to different conformations takes place as the butyl groups are too large to pass through the cavity of the macrocycle. ^{1}H NMR cannot give any information about the geometry of the aryl rings and how the removal of hydrogen bonding and appending the *n*-butyl groups affect the flexibility of the host **3.10** and why the association of fullerene is lower compared to bis-porphyrin **2.1**.

3.7 X-Crystal structures

3.7.1 X-Crystal structure of Bis-Porphyrin 3.8

Single crystals suitable for X-ray diffraction were successfully grown of bis-porphyrin **3.8** via slow evaporation from a toluene solution, producing purple needles. Single crystal X-ray diffraction data was collected by Tania Groutso and the structure solved and refined by Associate Professor Peter Boyd. The structure of **3.8** is shown in Figure 3.22 and Figure 3.23 Crystal data is shown in Table 3.8, located in the experimental section of this chapter.

The lack of association of C_{60} with bis-porphyrin **3.8** can be explained through the X-ray crystal structure, as this structure is considerably different from the computational model. In the crystal structure the calixarene maintains the pinched cone conformation, due to the hydrogen bonding between the hydroxyls of the phenol and the ether oxygens on the functionalized rings. The interplanar angles for the phenol rings on **3.8** are similar to the model of **1.36** with 86.8°, while the functionalized rings have a narrower angle of 21.0 °. Due to the extra methylene groups of the linker, the amide NHs becomes too remote from the ether oxygen to have hydrogen bonding interactions. The extra methylene results in the porphyrins planes being orientated away from each other instead of the desired face to face conformation. The crystal structure shows that these porphyrins have an interplanar porphyrin angle of 149.3º.

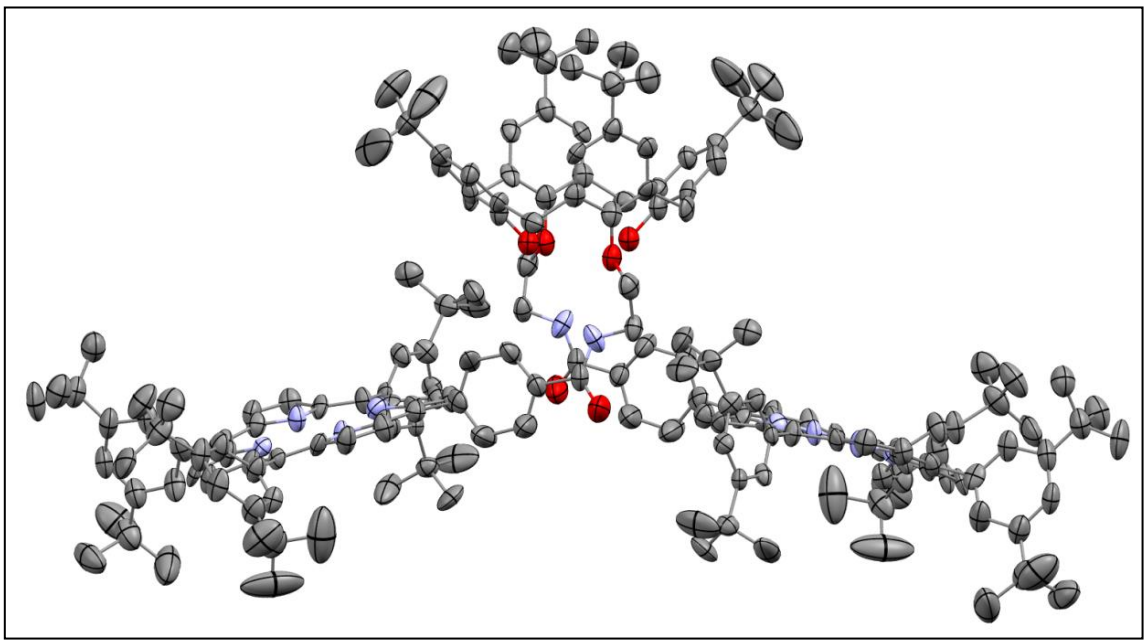

Figure 3.22: Side view of the X-ray crystal structures of bis-porphyrin **3.8,** represented with atomic displacement parameters shown as thermal ellipsoids at 50% probability (hydrogen atoms omitted for clarity).

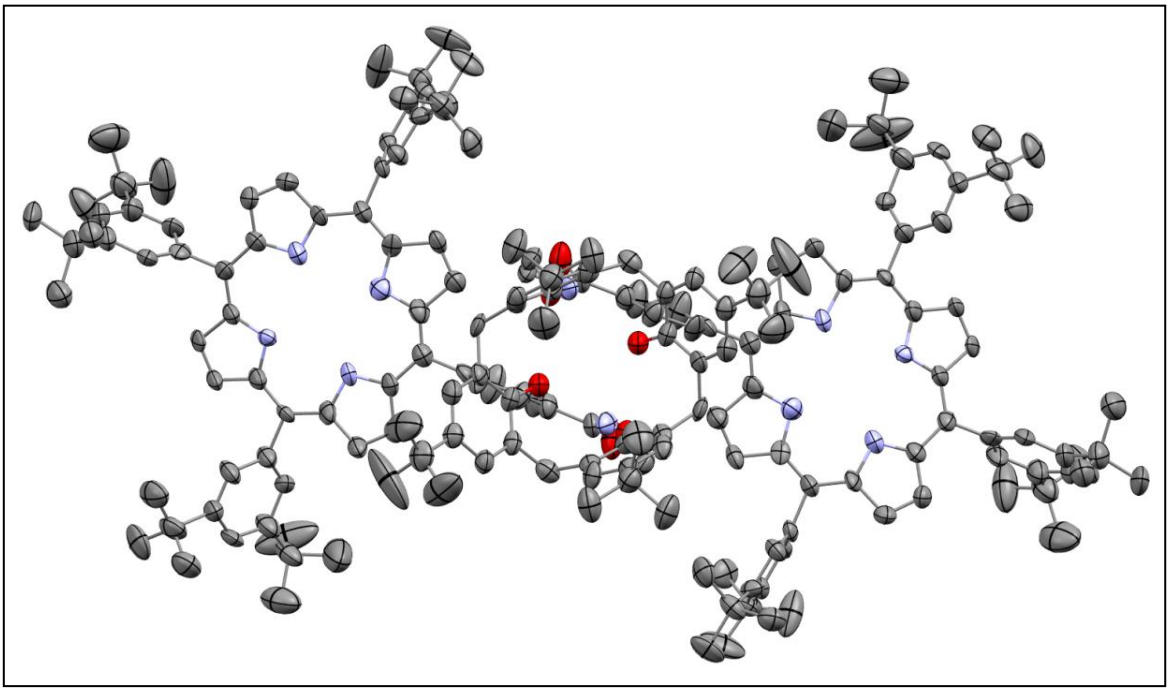

Figure 3.23: Top view of the X-ray crystal structures of bis-porphyrin **3.8**, represented with atomic displacement parameters shown as thermal ellipsoids at 50% probability (hydrogen atoms omitted for clarity).

The original computational modeling of **3.8** provided a structural geometry for the local energy minimum of the free host. Modeling of **3.8** based on the crystal structure where the porphyrin planes are rotated and facing away from each other gave a lower energy minimum for the host.

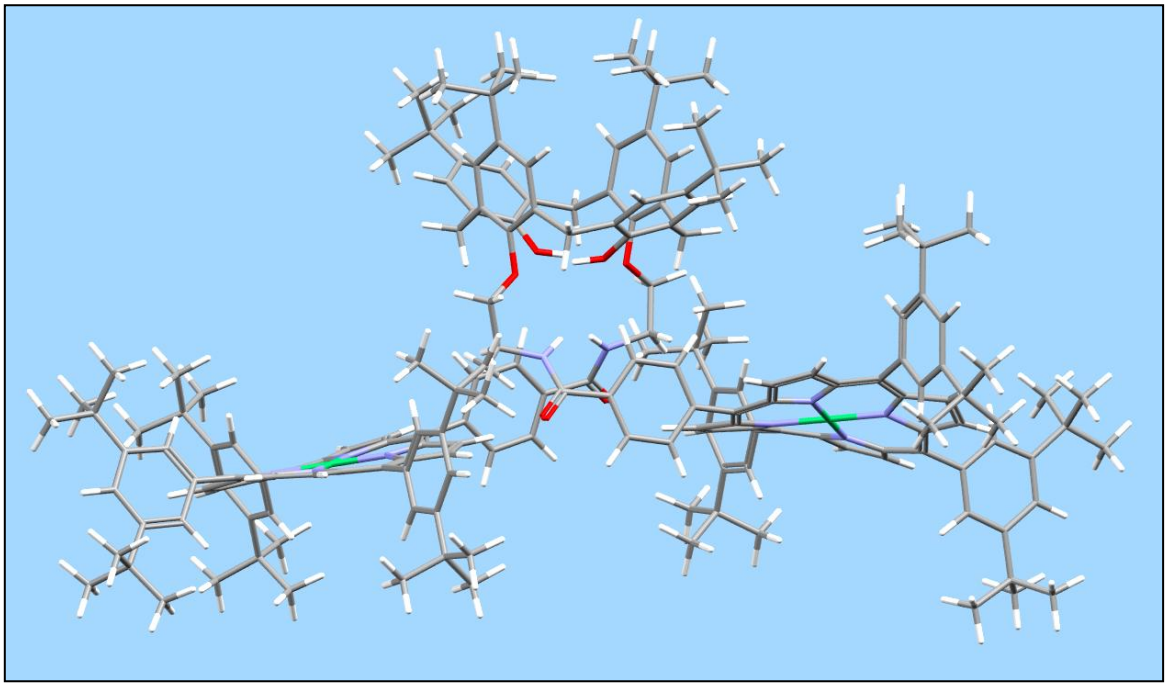

Figure 3.24: The recalculated model of the **3.8** based off the X-ray crystal structure. (ONIOM/B3LYP/6-31G(d);UFF) for the nickel(II)

3.7.2 X-Crystal Structure of Calixarene 3.21

Crystals of tetra-alkyalted diester **3.21** were grown for X-ray structural determination by slow evaporation of methanol into chloroform. Single crystal X-ray diffraction data was collected by Tania Groutso and the structure solved and refined by Associate Professor Peter Boyd. The structure of **3.21** is shown in Figure 3.25. Crystal data is shown in Table 3.8 and Table 3.9, located in the experimental section of this chapter.

During crystallization, trans-esterification of the ethyl ester by methanol occurred with half of the compound in solution to give a 1:1 co-crystallate of both the methyl and ethyl esters, as confirmed by ^{1}H NMR. Examination of the structure provides further evidence for the flexibility of the tetra-alkylated calixarenes and bis-porphyrin hosts, as the two different calixarene esters crystallize in opposite pinched cone orientations. The methyl ester calixarene crystallizes with the ester functionalized rings pinched into the cone with a wide angle of 107.9°. The aryl rings appended with the *n*-butyl groups show a parallel orientation with the wide rim sloping slightly towards each other with an interplanar angle of 24.3°. The ethyl ester calixarene displays the opposite orientation with *n*-butyl functionalized aryl rings pinched and pointing toward each other with a wide interplanar angle of 102.8° and the ethyl ester functionalized rings parallel to each other with an interplanar angle of 3.4°. The esters and *n*-butyl groups are orientated symmetrically within the structure.

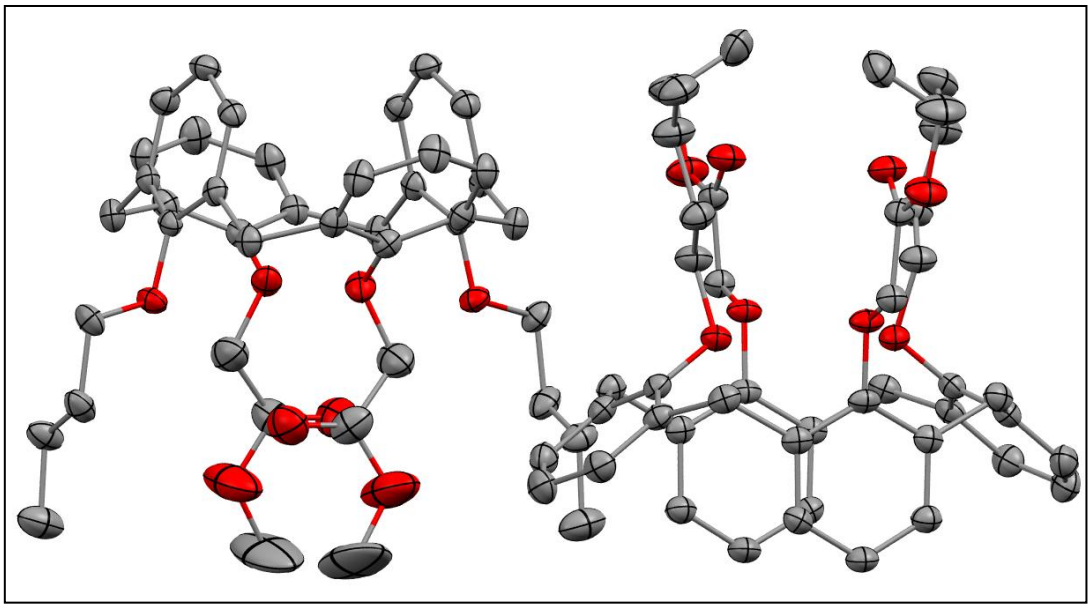

Figure 3.25: Crystal structure of the methyl and ethyl esters derivatives of **3.21** represented with atomic displacement parameters shown as thermal ellipsoids at 50% probability (hydrogen atoms omitted for clarity).

3.8 Charge Transfer Bands of 3.9 and 3.10 in Toluene.

Charge transfer bands were observed in the spectra of **3.10** and **Zn3.10** in both toluene and 1:1 acetonitrile:toluene. These charge transfer bands are observed in the range of 690-760 nm. Measurements were performed in order to estimate any changes in the electronic coupling due to the change in conformation of the host causing lower association for fullerenes. UV-visible spectra of **3.10** and **Zn3.10** and the subtracted absorption spectra displaying the charge transfer band are shown in Figure 3.26 and the estimation of electronic coupling between bis-porphyrin **3.10** with C_{60} is shown in Table 3.7.

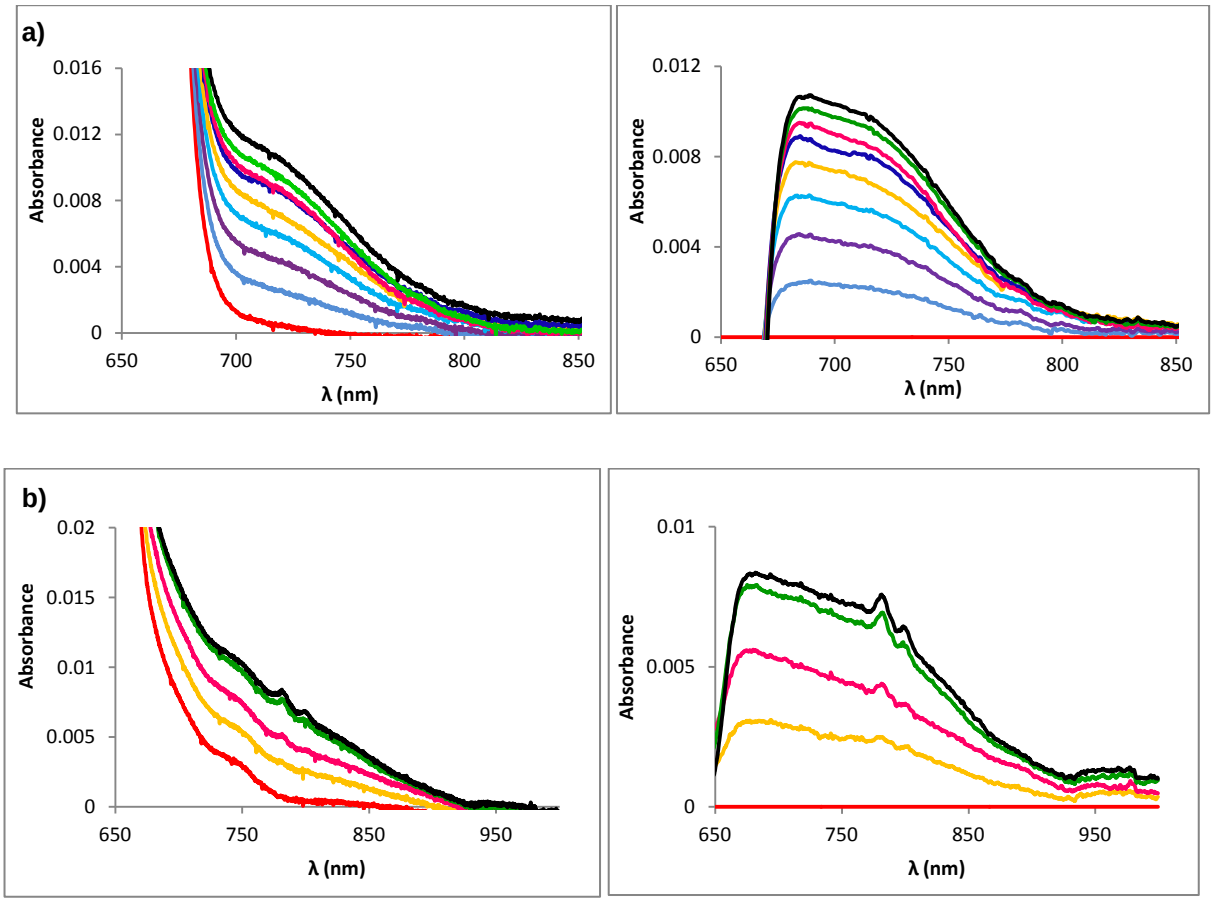

Figure 3.26: UV-visible spectra of a) **3.10** and b) **Zn3.10** in toluene displaying the emergence of the charge transfer band at 690 and 760 nm respectively with increasing concentration of C_{60} (Left)**.** The absorption spectra of **3.1** and **Zn3.1** with the free host subtracted giving a better visualization of the charge transfer band (right).

Table 3.7: Estimation of electronic coupling between the bis-porphyrin and fullerene based on the charge transfer band for **3.10** and **Zn 3.10.**

COMPLEX CONC	**3.10**	**Zn3.10**
Binding Constant (K)	1840	1100
[P] (M)	1.64E-05	1.56E-05
[C_{60}] (M)	2.38E-04	2.38E-05
[P-C_{60}] (M)	4.92E-06	3.20E-06
A	0.010	0.010
V max (cm^{-1})	14290	14030
Δ v max (cm^{-1})	2080	3200
ε max	2070	3100
Rcc	6.25	6.25
V(cm^{-1})	**820**	**1230**

Estimation of the band positions and absorbance height was difficult for hosts **3.10** and **Zn3.10** compared to **2.1**. The charge transfer band displayed a blueshift of approximately 20 nm, placing them partially under the last Q band of the porphyrin. The lower association of the bis-porphyrin hosts for fullerenes complicated the estimation the electronic coupling, as a higher concentration of fullerene was required to see significant changes in the height of the charge transfer bands.

Measuring the charge transfer band was attempted in a mixed solvent combination of toluene/acetonitrile (1:1) as the increase in association provides accurate measurement of the charge transfer band wavelength and absorbance. Changing the solvent may affect the position and energy of the charge transfer band due to difference in polarity. This has been observed by Guldi *et al.*[45] in parachute type porphyrin fullerene dyads when changing from toluene (ε_r = 2.4) to benzonitirile (ε_r = 20). It is less commonly observed when the solvent is changed to cyclohexane (ε_r = 2.0), as the polarity of the solvent is similar to toluene. Even though the polarity is not significantly different from acetonitrile (ε_r = 5.8). Estimation of the charge transfer bands in acetonitrile/toluene (1:1) has been difficult to determine as the charge transfer band blue shifts to a lower wavelength and as the last Q band red shifts, placing the maximum of the band under the last of Q band. Work is to be carried out measuring binding constants and charge transfer bands in cyclohexane which will allow the binding of fullerenes with a similar magnitude to acetonitrile/toluene (1:1) but will not shift the charge transfer band or Q bands significantly.

3.9 Summary

Three hosts have been prepared by increasing the number of methylene linkers connecting the calixarene to the porphyrin amide and by tetra-alkylation of the narrow rim of the calixarene scaffold.

It has been found that bis-porphyrin **3.8** displays no association with fullerenes. Absence of major observable absorbance changes typical of porphyrin fullerene complexation and low association constants indicated that there is no co-operative binding between the porphyrin units. This is supported by X-ray crystal structures of the bis-porphyrin. This structure shows that the host has the incorrect orientation of porphyrin planes and that binding of the fullerenes would be impossible. The attachment of porphyrins to the lower rim of a calixarene via an amide linker with a single methylene spacer has been shown to be the most suitable for the acceptance of a fullerene guest.

The tetra-alkylated calixarene bis-porphyrin hosts **3.9** and **3.10** have been prepared which differ by the length of the alkyl chain. These hosts display an association for fullerenes with increasing association increasing in the order C_{60}< C_{70}<$Lu_3N@C_{80}$. These bis-porphyrins however, show a significant decrease in association for fullerenes compared to **2.1**-**2.3**. The introduction of the alkyl chains and removal of the hydrogen bonding motif on the narrow rim has a detrimental effect on the preorganisation of the scaffold.

The length of the alkyl chains has a pronounced effect on the flexibility of the host. Smaller chains such as the methyl chain on **3.9** allows the aryl rings in the calixarene scaffold to interconvert to different conformations such as the partial cone and 1,3 alternate geometries. Larger chains can be controlled by changing chain lengths to give a butyl host.

3.10 Experimental

3.10.1 Synthetic Procedure for Bis-Porphyrin 3.8

5,11,17,23-*tert* -butyl-25,27-bis[(cyano-methyl)oxy]-26,28-dihydroxycalixarene (3.11)

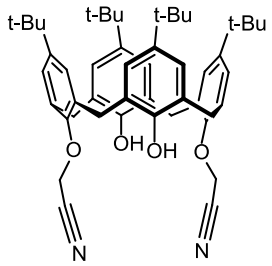

A suspension of *p-tert*-butylcalixarene **3.2** (1.0 g, 1.54 mmol), potassium carbonate (0.53 g, 3.8 mmol), sodium iodide (0.578 g, 3.8 mmol) and bromoacetonitrile (0.25 mL, 6.80 mmol) were refluxed in acetonitrile (50 mL) for 18 hours. The solution was filtered, the solvent removed *in vacuo* and the residue taken up in dichloromethane (75 mL), and then washed with hydrochloric acid (1 M, 50 mL), brine (2 x 50 mL) and dried with sodium sulfate. The solvent was concentrated and the residue was recrystallized by addition of methanol yielding **3.11** as a white solid, 0.56 g (73%).

^{1}H NMR (300 MHz, *CDCl$_3$*) ppm: 7.12 (s, ArH, 4H), 6.73 (s, ArH, 4H), 5.56(s, ArOH, 2H), 4.81 (s, OCH_2CN, 4H), 4.22 (d, $ArCH_2Ar$, J = 13.52 Hz, 4H), 3.45 (d, $ArCH_2Ar$, J = 13.52 Hz, 4H), 1.32 (s, $C(CH_3)_3$, 18H), 0.88 (s, $C(CH_3)_3$, 18H).

HRMS (FAB MS): Calculated: $[M]^+$: $C_{48}H_{58}N_2O_4$: 726.4396 m/z, found 726.4396 m/z.

5,11,17,23-tetra-*tert*-butyl-25,27-bis(aminoethoxy)-26,28-dihydroxycalixarene (3.12)

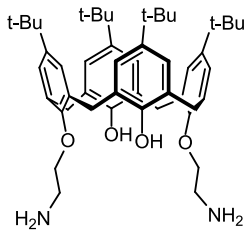

To a vigorously stirred solution of the **3.11** (0.56 g 0.77 mmol) in THF (50 mL), lithium aluminum hydride (0.25 g, 6.57 mmol) was added portionwise. The reaction mixture was then refluxed for five hours. The reaction was then immersed in an ice bath and the excess lithium aluminum hydride was quenched by slow addition of THF/water (50 mL, 9:1). The organic layer was decanted and the solvent removed *in vacuo*. The crude residue was dissolved in dichloromethane (50 mL), washed with brine and dried with sodium sulfate. The solvent was removed *in vacuo* to produce an off white solid **3.12** which was used without further purification, 0.54 g (96%).

^{1}H NMR (300 MHz, *CDCl$_3$*) ppm: 8.33 (s, ArOH, 2H), 7.04 (s, ArH, 4H), 6.97 (s, ArH, 4H), 4.33 (d, $ArCH_2Ar$, *J* = 12.91 Hz, 4H), 4.07 (t, OCH_2 *J* = 4.73 Hz, 4H), 3.37 (d, $ArCH_2Ar$, *J* = 12.94 Hz, 4H), 3.28 (t, OCH_2CH_2, *J* = 4.73 Hz, 4H), 1.25 (s, $C(CH_3)_3$, 18H), 1.09 (s, $C(CH_3)_3$, 18H).

HRMS (FAB MS): Calculated: $[M]^+$ $C_{48}H_{66}N_2O_4$: 735.5105 m/z ,found 735.5100 m/z.

5,11,17,23-tetra-*tert*-butyl-25,27-bis[(ethoxy(4-amidophenyl)-10,15,20-tris-(3,5-di-*tert*-butylphenyl)porphyrin]-]-26,28-dihydroxycalixarene (3.8)

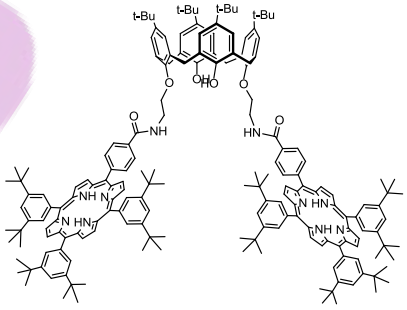

A solution of porphyrin **3.16** (0.150 g, 0.15 mmol) and 4-methylmorpholine (0.016 mL, 0.158 mmol) in THF/dichloromethane (2:1, 15 mL) solution was stirred at room temperature under nitrogen for ten minutes. The solution was cooled to 0° C and 2-chloro-4,6-dimethoxy-1,3,5-

triazine (0.002 g, 1.05 mmol) was added. The solution was stirred at 0° C for a further ten minutes before warming to room temperature and stirred for a further one hour. TLC of the solution showed the presence of a less polar compound (the active ester) at the expense of the acid. A solution of calixarene diamine **3.12** (0.055 g, 075mmol) in THF (20 mL) was added and the solution stirred for 18 hours. The solvent was removed *in vacuo* and the product purified via flash chromatography, eluting with dichloromethane/hexane (9:1) to give **3.8** as a purple solid, 0.145 g (72%).

^{1}H NMR (300 MHz, *CDCl$_3$*) ppm: 8.92 (s, H$_\beta$, 12H), 8.82 (d, H$_\beta$, J = 4.80 Hz, 4H), 8.76 (t, NH, J = 5.60 Hz, 2H), 8.54 (s, ArOH ,2H), 8.49 (d, ArH, J = 8.10 Hz, 4H), 8.30 (d, ArH, J = 8.10 Hz, 4H), 8.12 (d, ArH, J = 1.80 Hz, 8H), 8.09 (d, ArH, J = 1.80 Hz, 4H), 7.82 (d, 1.80 Hz, ArH, 4H), 7.79 (d, 1.80 Hz, ArH, 2H), 7.00 (s, ArH, 4H), 6.97 (s, ArH, 4H), 4.41 (d, ArCH$_2$, J = 13.00 Hz, 1H), 4.31 (t, OCH$_2$, J = 4.73 Hz, 4H), 4.12 (t, CH$_2$C<u>H</u>$_2$, J = 4.70 Hz, 4H), 3.45 (d, ArCH$_2$Ar, J = 13.0 Hz, 4H), 1.54 (m, C(CH$_3$)$_3$, 108H), 1.53 (s, C(CH$_3$)$_3$, 36H), -2.68 (s, NH, 4H).

HRMS (ESI-TOF-MS) Calculated: [M+Na+H]$^{2+}$: $C_{186}H_{219}NaN_{10}O_6$: 1355.8513 m/z, found: 1355.8529 m/z; calculated [M+2Na]$^{2+}$: $C_{186}H_{218}Na_2N_{10}O_6$: 1366.8423 m/z, found: 1366.8438 m/z; calculated [M+Na]$^+$: $C_{186}H_{219}NaN_{10}O_6$: 2710.6953 m/z, found: 2710.7115 m/z, [M+H]$^+$: $C_{186}H_{219}N_{10}O_6$: 2700.7134 m/z, found: 2700.7226 m/z;

3.10.2 Synthetic Procedure for Bis-Porphyrin 3.9 and 3.10

25,27-bis[(ethoxycarbonyl)-methoxy]-26,28-dimethoxycalixarene (3.18)

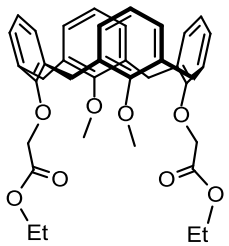

A solution of **3.17** (0.40 g, 0.67 mmol) in DMF (5 mL) was added drop wise to a suspension of hexane washed sodium hydride (0.26g, 6.7 mmol) in DMF (10 mL). The solution was stirred for 30 minutes at room temperature. Methyl iodide (1.07 mL, 3.35 mmol) was added to the solution and heated to 70^o C for 18 hours. The reaction was cooled and quenched by drop wise

addition of ethanol, diluted with dichloromethane and washed with hydrochloric acid (1 M) and water. The solvent was removed *in vacuo* and purified by flash chromatography eluting with dichloromethane/ethyl acetate (9:1) to produce **3.18** as a yellow oil, 0.252 g (59%).

^{1}H NMR (400 MHz, *CDCl$_3$*) ppm: 7.15 (d, ArH, *J* = 7.40 Hz, 4H), 6.94 (t, ArH, *J* = 7.40, 2H), 6.54 (t, ArH, 7.32 Hz, 2H), 6.34 (m, ArH, 4H), 4.44 (d, OC$\underline{H}_2$C(O)+ArCH$_2$Ar, 6H), 4.05 (s, C(O)OC$\underline{H}_2$CH$_3$ 4H), 3.83 (s, OCH$_3$, 6H), 3.22 (d, ArCH$_2$Ar, *J* = 13.21 Hz, 4H), 1.28 (t, C(O)OCH$_2$C$\underline{H}_3$, *J* = 7.19 Hz, 6H) .

HRMS (ESI-TOF-MS) Calculated. [M+H]$^+$ $C_{32}H_{42}O_8$: 625.2779 m/z, found: 625.2772 m/z.

25,27-bis(carbonyl-methoxy)-26,28-dimethoxycalixarene (3.19)

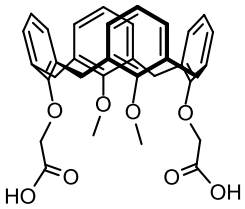

A suspension of tetra-alkylated calixarene **3.18** (0.2 g, 0.32 mmol) and 10% sodium hydroxide solution (10 mL) in ethanol (20 mL) was refluxed for two hours. Hydrochloric acid (6 M) was added until a pH of 1 was reached. The resulting suspension was extracted with chloroform (40 mL), washed with saturated ammonium chloride (40 mL) and dried with sodium sulfate. The solvent was removed *in vacuo* to produce **3.19** as an off white solid which was used without further purification, 0.170 g (95%).

^{1}H NMR (400 MHz, *CDCl$_3$*) ppm: 7.19 (d, ArH, *J* = 7.40 Hz, 4H), 7.03 (t, ArH, *J* = 7.40, 2H), 6.88 (t, ArH, *J* = 6.90, 2H), 6.53 (d, ArH, *J* = 6.90 Hz, 4H), 4.71 (s, OCH$_2$C(O), 4H), 4.29 (d, ArCH$_2$Ar, *J* = 13.25 Hz, 4H), 3.85 (s, OCH$_3$, 6H), 3.37 (d, ArCH$_2$Ar, *J* = 13.25 Hz, 4H).

HRMS (ESI-TOF-MS) Calculated [M+H]$^+$: $C_{34}H_{33}N_5O_8$: 569.2170 m/z, found: 569.2163 m/z; calculated [M+Na]$^+$: $C_{34}H_{32}N_5O_8Na$: 591.1978 m/z, found: 591.1989 m/ z.

25,27-bis[methoxy(4-amidophenyl)-15-tolyl-10,20-di-(3,5-di-*tert*-butylphenyl) porphyrin]-26-28-dimethoxycalixarene (3.9)

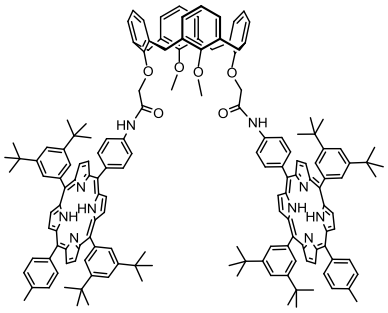

A solution of calixarene diacid **3.19** (0.045 g, 0.079 mmol), 4-dimethylaminopyridine (0.004 g, 0.032 mmol) and porphyrin **2.15** (0.1 g, 0.15 mmol) in THF (10 mL) was stirred at room temperature under nitrogen for ten minutes. DIC (0.1 mL, 0.63 mmol) was added in and the solution stirred for a further ten minutes. HOBt (0.085 g, 0.63 mmol) was added and the solution stirred for 18 hours. The solvent was removed *in vacuo* and the product purified via flash chromatography, eluting with toluene/ethyl acetate (9:1) and the solvent removed to give **3.9** as a purple solid, 0.048 g (35%). An analytically pure sample of **3.9** was prepared via recrystallization from chloroform/methanol at -4° C.

^{1}H NMR (400 MHz,$CDCl_3$) ppm: 8.99 (d, H_β, J = 4.75 Hz, 4H), 8.92 (d, H_β, J = 4.75 Hz, 4H), 8.81 (s, H_β, 8H), 8.76 (s, NH 2H), 8.24 (d, ArH, J = 8.15 Hz, 4H), 8.13 (d, J = 8.15 Hz, 4H), 8.11 (d, ArH, J = 1.75 Hz, 8H), 8.07 (d, ArH, J = 7.75 Hz, 4H), 7.83 (s, ArH, 4H), 7.30 (d, ArH, J = 7.75 Hz, 4H), 7.07 (s(br), ArH, 6H), 6.91 (s(br), ArH, 2H), 6.77 (s(br), ArH, 4H), 4.35 (s(br), $ArCH_2Ar$, 4H), 4.13 (s, OCH_3, 6H), 3.72 (s(br), $ArCH_2Ar$ 4H), 2.70 (s, $ArCH_3$, 6H), 1.37 (s, $C(CH_3)_3$, 72H), -2.83 (s, NH, 4H).

HRMS (ESI-TOF-MS) Calculated $[M+2H]^{2+}$: $C_{156}H_{160}N_{10}O_6$: 1135.1276 m/z, found 1135.1276 m/z; calculated $[M+H]^+$: $C_{156}H_{159}N_{10}O_6$: 2269.2678 m/z, found 2269.2370 m/z.

25,27-bis[ethoxycarbonyl-methoxy]-26,28-dibutoxycalixarene (3.21)

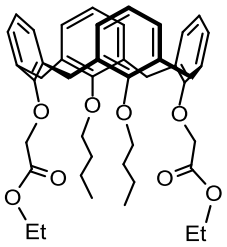

A solution of dibutoxy calixarene **3.20** (0.5 g, 0.93 mmol) in DMF (10 mL) was added drop wise to a suspension of hexane washed sodium hydride (0.56 g 13.98 mmol) in DMF (10 mL). The solution was stirred for 30 minutes at room temperature. Ethyl-bromoacetate (1.02 mL, 9.32 mmol) was added to the solution and heated to 70^{o}C for 18 hours. The reaction was cooled and quenched by drop wise addition of ethanol, diluted with dichloromethane (50 mL) and washed with hydrochloric acid (1 M, 30 mL) and water (30 mL). The solvent was removed *in vacuo* and the crude material resuspended in ethanol (50 mL) with hydrochloric acid (12 M, 5 mL) and refluxed for a further one hour. The solvent was removed and the crude product purified by flash chromatography eluting with dichloromethane/ethyl acetate (9:1). The solvent was removed and **3.21** was recrystallized from dichloromethane/hexane as a white solid, 0.39 g (58%).

^{1}H NMR (400 MHz, *CDCl$_3$*) ppm: 6.93 (d, ArH, *J* = 7.40 Hz, 4H), 6.78 (t, ArH, *J* = 7.40 Hz, 2H), 6.39 (t, ArH, *J* = 6.40 Hz, 2H), 6.33 (d, ArH, *J* = 6.40 Hz, 4H), 4.78 (s, OCH$_2$C(O), 4H), 4.69 (d, ArCH$_2$Ar, *J* = 13.60 Hz, 4H), 4.21 (q, C(O)OC$\underline{H}_2$CH$_3$, *J* = 7.20 Hz, 4H), 3.84 (t, OC$\underline{H}_2$CH$_2$, *J* = 7.10 Hz, 4H), 3.23 (d, ArCH$_2$Ar, *J* = 13.60 Hz, 4H), 1.87 (m, OCH$_2$C$\underline{H}_2$, 4H), 1.50 (m, C$\underline{H}_2$CH$_3$, 4H), 1.29 (t, C(O)OCH$_2$C$\underline{H}_3$ *J* = 7.20 Hz, 6H), 1.00 (t, CH$_2$C$\underline{H}_3$, *J* = 7.40 Hz, 6H).

HRMS (ESI-TOF-MS). Calculated [M+Na]$^{+}$: $C_{44}H_{53}NaO_8$: 731.3542 m/z, found 731.3554 m/z.

25,27-bis(carbonyl-methoxy)-26,28-dibutoxycalixarene (3.22)

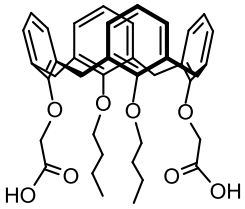

A suspension of tetra-alkylated calixarene **3.21** (0.35 g, 0.35 mmol) and 10% sodium hydroxide solution (10 mL) in ethanol (25 mL) was refluxed for one hour. The solution was cooled and hydrochloric acid (6 M) was added until a pH of 1 was reached. The resulting suspension was extracted with chloroform (60 mL) and washed with saturated ammonium chloride (50 mL), dried with sodium sulfate and evaporated to dryness to produce **3.22** as an off white solid which was used without further purification 0.29g (91%).

^{1}H NMR (400 MHz, *CDCl$_3$*) ppm: 7.20 (d, ArH, *J* = 7.45 Hz, 4H), 7.01 (t, ArH, *J* = 7.45 Hz, 2H), 6.38 (m, 6H), 4.71 (s, $OCH_2C(O)$, 4H), 4.35 (d, $ArCH_2Ar$,*J* = 13.45 Hz, 1H), 3.82 (t, $OC\underline{H}_2CH_2$, *J* = 7.08, 4H), 3.34 (d, $ArCH_2Ar$, *J* = 13.45 Hz, 4H), 1.88 (m, $OCH_2C\underline{H}_2$, 4H), 1.38 (m, $C\underline{H}_2CH_3$, 4H), 0.97 (t, $CH_2C\underline{H}_3$, 7.40 Hz, 6H).

HRMS (ESI-TOF-MS) Calculated: $[M+H]^+$: $C_{40}H_{45}O_8$: 653.3120 m/z, found 653.3109 m/z.

25,27-bis[(methoxy(4-amidophenyl)-15- tolyl-10,20-di-(3,5-di-*tert*-butylphenyl) porphyrin]-26-28-dibutoxycalixarene (3.10)

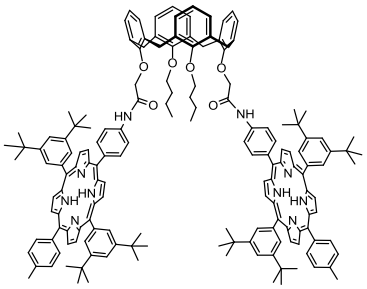

A solution of calixarene diacid **3.22** (0.037 g, 0.057), DMAP (0.003 g, 0.022 mmol) and porphyrin **2.15** (0.1 g, 0.15 mmol) in THF (10 mL) was stirred at room temperature under nitrogen for ten minutes. DIC (0.08 mL, 0.45 mmol) was added in and the solution stirred for a further ten minutes. HOBt (0.061 g, 0.45 mmol) was added and the solution stirred for 18 hours. The solvent was removed *in vacuo* and the product purified via flash chromatography, eluting with toluene/ethyl acetate (9:1). The solvent was removed to give **3.10** as a purple

solid, 0.069 g (48%). An analytically pure sample of **3.10** was prepared via recrystallization from chloroform/methanol at -4° C.

^{1}H NMR (400 MHz, *CDCl*$_3$) ppm: 9.74 (s, NH, 2H), 8.88 (m, H$_\beta$, 16H), 8.31 (d, ArH , *J* = 8.40 Hz, 4H), 8.14 (d, ArH, *J* = 8.40 Hz, 4H), 8.09 (d, ArH , *J* = 8.00 Hz, 4H), 8.06 (d, ArH, *J* = 1.90 Hz, 8H), 7.75 (t, ArH, *J* = 1.90 Hz, 4H), 7.54 (d, ArH, *J* = 8.00 Hz, 4H), 7.23 (d, ArH, *J* = 7.50 Hz, 4H), 7.06 (t, ArH, *J* = 7.50, 7.50 Hz, 2H), 6.42 (t, ArH, *J* = 7.70, 7.70 Hz, 2H), 6.28 (d, ArH, *J* = 7.75 Hz, 2H), 5.20 (s, $OCH_2C(O)$, 4H), 4.77 (d, $ArCH_2Ar$, *J* = 14.00 Hz, 4H), 3.94 (t, OCH_2CH_2, 7.50 Hz, 4H), 3.50 (d, $ArCH_2Ar$, *J* = 14.00 Hz, 4H), 2.69 (s, $ArCH_3$, 6H), 1.83 (m, OCH_2CH_2, 4H), 1.48 (s, $C(CH_3)_3$, 64H), 1.41 (m, CH_2CH_3, 4H), 0.92 (t, CH_2CH_3, *J* = 7.39Hz, 6H), -2.73 (s, NH, 4H).

HRMS (ESI TOF) Calculated $[M+2H]^{2+}$: $C_{162}H_{172}N_{10}O_6$: 1187.6632 m/z, found 1188.1646 m/z; calculated $[M+H]^+$: $C_{162}H_{171}N_{10}O_6$: 2352.3378 m/z, found 2353.3408 m/z; $[M+Na]^+$: $C_{162}H_{170}N_{10}NaO_6$: 2374.3197 m/z, found 2376.330 m/z.

25,27-bis(methoxy(4-amidophenyl)-15- tolyl-10,20-di-(3,5-di-*tert*-butylphenyl) porphyrin]-26-28-dibutoxycalixarene (Zn3.10)

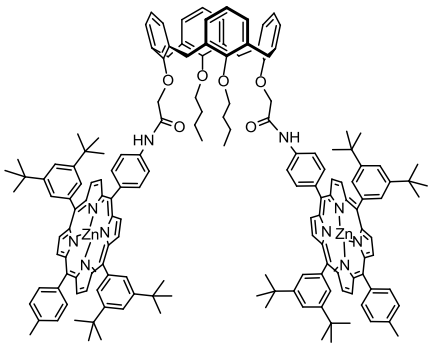

A saturated solution of zinc (II) acetate in methanol (5 mL) was added to a solution of bis-porphyrin **3.10** (0.020 g, 0.006 mmol) in chloroform (15 mL) and the mixture was heated until no free base was observed in the UV-visible spectrum. The solution was washed with brine, dried with sodium sulfate and concentrated. The Zn(II) bis-porphyrin was purified by flash chromatography eluting with dichloromethane/hexane (9:1) and the solvent evaporated to produced **Zn3.10** as a pink solid, 0.018 g (90%).

^{1}H NMR (300 MHz, *CDCl*$_3$) ppm: 9.72 (s, NH, 2H), 9.02 (d, H$_\beta$, *J* = 4.71 Hz, 4H), 8.97 (m, H$_\beta$, 12H), 8.31 (d, ArH, *J* = 8.50 Hz, 4H), 8.15 (d, ArH, *J* = 8.50 Hz, 4H), 8.10 (d, ArH, *J* =

7.85 Hz, 1H), 8.07 (d, ArH, *J* = 1.75 Hz, 8H), 7.75 (t, ArH, *J* = 1.75 Hz, 4H), 7.54 (d, ArH, *J* = 7.85 Hz, 4H), 7.22 (d, ArH, *J* = 7.50 Hz, 4H), 7.01 (m, ArH, 2H), 6.45 (t, ArH, *J* = 6.65 Hz, 2H), 6.30 (d, ArH, *J* = 7.50 Hz, 4H), 5.19 (s, $OCH_2C(O)$, 4H), 4.78 (d, $ArCH_2Ar$, *J* = 14.30 Hz, 4H), 4.00 (t, $COC\underline{H}_2CH_2$, *J* = 7.40, 4H), 3.51 (d, $ArCH_2Ar$, *J* = 14.30 Hz, 4H), 2.70 (s, CH_3, 6H), 1.81 (m, $COCH_2C\underline{H}_2$, 4H), 1.48 (s, $C(CH_3)_3$ 72H), 1.46-1.40 (m, $C\underline{H}_2CH_3$ 4H), 0.95 (t, $CH_2C\underline{H}_3$ *J* = 7.40 Hz, 6H).

HRMS (ESI TOF) Calculated $[M+2H]^{2+}$: $C_{162}H_{168}N_{10}O_6Zn_2$: 1238.1111 m/z, found 1238.1204 m/z; calculated $[M+H]^+$: $C_{162}H_{167}N_{10}O_6$: 2479.7655 m/z, found: 2479.7566 m/z; calculated $[M+Na]^+$: $C_{162}H_{166}N_{10}NaO_6Zn_2$: 2501.8475 m/z, found: 2501.8427 m/z.

3.10.3 General Information and Crystallographic Tables for Single Crystal X-ray Diffraction

Single crystal X-ray diffraction data for **3.8** and **3.21** were collected on a Bruker Smart APEX2 CCD diffractometer using graphite monochromated Mo Kα radiation. The structures were solved using direct methods (SHELXS-97) [173,174.]. Non hydrogen atoms were refined anisotropically (SHELXL-97)[173,174] and H atoms were refined using a riding model, with C-H =0.93-0.97 Å and $Ui_{so}(H)=1.2Ueq(C)$, $1.5U_{eq}$(methyl C) or $1.5U_{eq}(O)$.

Table 3.8: Crystal data and structure refinement for **3.8.**

Empirical formula	$C_{193}\ H_{269}N_{10}\ O_6$	
Formula weight	2825.18	
Temperature	93(2) K	
Wavelength	0.71073 Å	
Crystal system	Monoclinic	
Space group	C2/c	
Unit cell dimensions	a = 32.731(5) Å	α= 90°.
	b = 14.196(2) Å	β= 110.018(10)°.
	c = 41.995(8) Å	γ = 90°.
Volume	18334(5) $Å^3$	
Z	4	
Density (calculated)	1.024 Mg/m^3	
Absorption coefficient	0.061 mm^{-1}	
F(000)	6180	
Crystal size	0.25 x 0.1 x 0.05 mm^3	
Theta range for data collection	1.32 to 28.05°.	
Index ranges	-43<=h<=42, -18<=k<=17, -55<=l<=55	
Reflections collected	103517	
Independent reflections	22016 [R(int) = 0.3290]	
Completeness to theta = 28.05°	98.9 %	
Refinement method	Full-matrix least-squares on F^2	
Data / restraints / parameters	22016 / 953 / 934	
Goodness-of-fit on F^2	0.846	
Final R indices [I>2sigma(I)]	R1 = 0.1355, wR2 = 0.3173	
R indices (all data)	R1 = 0.4312, wR2 = 0.4030	
Largest diff. peak and hole	0.523 and -0.318 e.$Å^{-3}$	

Table 3.9: Crystal data and structure refinement for **3.21.**

Empirical formula	$C_{44}H_{52}O_8$	
Formula weight	708.86	
Temperature	97(2) K	
Wavelength	0.71073 Å	
Crystal system	Monoclinic	
Space group	C2/c	
Unit cell dimensions	a = 19.4147(8) Å	α= 90°.
	b = 20.3927(8) Å	β= 93.152(2)°.
	c = 18.9340(7) Å	γ = 90°.
Volume	7485.0(5) $Å^3$	
Z	8	
Density (calculated)	1.258 Mg/m^3	
Absorption coefficient	0.085 mm^{-1}	
F(000)	3040	
Crystal size	0.27 x 0.27 x 0.16 mm^3	
Theta range for data collection	1.45 to 27.87°.	
Index ranges	-13<=h<=25, -24<=k<=26, -24<=l<=24	
Reflections collected	35501	
Independent reflections	8766 [R(int) = 0.0661]	
Completeness to theta = 27.87°	98.0 %	
Refinement method	Full-matrix least-squares on F^2	
Data / restraints / parameters	8766 / 0 / 464	
Goodness-of-fit on F^2	1.135	
Final R indices [I>2sigma(I)]	R1 = 0.0659, wR2 = 0.1743	
R indices (all data)	R1 = 0.1061, wR2 = 0.1973	
Largest diff. peak and hole	0.719 and -0.823 e.$Å^{-3}$	

Chapter 4

Wide Rim Ferrocene Appended Bis-Porphyrins Prepared by Palladium Coupling Reactions.

12.1 Photoinduced Multistep Electron Transfer in Porphyrin-Fullerene Triads

Porphyrins and fullerenes have been shown to be excellent chromophores for the construction of covalent and supramolecular dyads for photoinduced charge separation. These covalently and supramolecularly coupled porphyrin-fullerene dyads however, do not have charge separated state lifetimes long enough for use in light harvesting devices. A number of research groups have prepared triads and tetrads of their corresponding dyads through addition of secondary donors or secondary acceptors.[67,70,199,200] This enables the system to undergo a multistep electron transfer process, spatially separating the charge separated state and increasing the lifetimes of the charge separated state. Multistep electron transfer is found in both photosystems I and II, to achieve longer lived charge separated state lifetimes for generation of ATP.[11,201]

The groups of Imahori and D'Souza have respectively prepared covalent and supramolecular triads based on a donor-sensitizer-acceptor model.[70,202] In this model the electron hole is moved by the transfer of an electron from a secondary donor to the sensitizer, and the electron charge remains on the acceptor. With the addition of a secondary electron donor such as ferrocene, dipyrrins, triphenylamines or metallated porphyrins to the original porphyrin fullerene dyads, the electron hole can be moved by the transfer of an electron from the secondary donor to the porphyrin. While this electron transfer process results in a loss of energy within the system, the resulting distantly separated radical ion pair attenuates the electronic coupling significantly, thereby prolonging the lifetime of the final charge-separated state.

Imahori *et al.* has prepared a ferrocene (Fc), free base porphyrin (P), fullerene (C_{60}) triad **1.13** and zinc porphyrin (ZnP), free base porphyrin (P) fullerene (C_{60}) triad **1.14** by covalently connecting the chromophores by amide bonds.[67,72,77,78] In the triad **1.13**, photoexcitation of porphyrin, results in a primary electron transfer from the porphyrin to the fullerene, generating a charge separated state Fc-$P^{\bullet+}$-$C_{60}^{\bullet-}$. The triad then undergoes a secondary electron transfer process from the ferrocene to the porphyrin to generate the $Fc^{\bullet+}$- P- $C_{60}^{\bullet-}$ charge separated state. The spatial distance separating the radical ion pair results in a significantly longer lifetime of charge separated state of up to 16 μs. Upon excitation of **1.14**, the zinc porphyrin (ZnP) transfers its singlet energy to the energetically lower lying free base porphyrin (P).[72,77] This energy transfer is then followed by sequential electron transfer from the generated singlet excited state of the free base porphyrin to the fullerene to yield ZnP-$P^{\bullet+}$-$C_{60}^{\bullet-}$ followed by a

subsequent electron transfer from the ZnP to the $H_2P^{\bullet+}$ to yield $ZnP^{\bullet+}$-H_2P-$C_{60}^{\bullet-}$ with a lifetime of 21μs.

D'Souza has reported a supramolecularly assembled ferrocene-porphyrin-fullerene triad **1.22**,[92] by axial co-ordination of an imadazole functionalized fullerene to a ferrocene functionalized zinc porphyrin. Transient absorption studies have shown that photoexcitation of the zinc porphyrin was followed by electron transfer to the fullerene to yield Fc-$ZnP^{\bullet+}$-$ImC_{60}^{\bullet-}$. This was followed by transfer of an electron from the ferrocene to the zinc porphyrin resulting in $Fc^{\bullet+}$-ZnP-$ImC_{60}^{\bullet-}$, with a charge separated state lifetime of 10 ns.

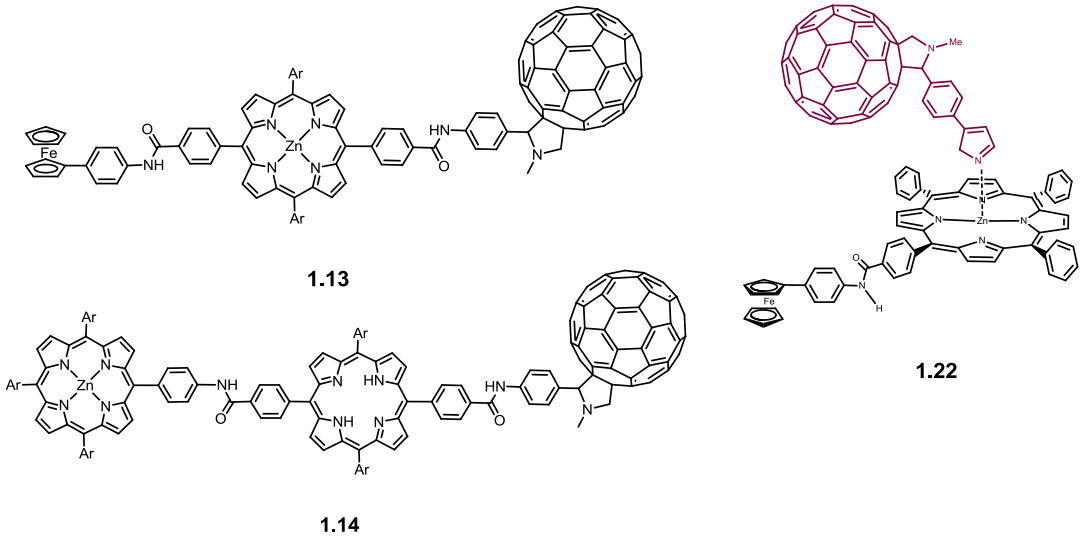

Figure 12.1: Covalent triads **1.13** and **1.14**[72,77] and supramolecular triad **1.22**.[92]

12.1.1 Porphyrin Appended Ferrocene Calixarene Bis-Porphyrin

The calixarene linked bis-porphyrin host **1.36** with C_{60} has been shown to produce lifetimes for the charge separated state ranging from 910 to 1480 ps.[122,127,128] As with other dyads the charge separated state lifetime is too short to produce a photovoltaic device with high efficiency. A calixarene linked bis-porphyrin functionalized by direct attachment of ferrocene to the porphyrins has been synthesized by Lyons *et al*. which, when complexed with C_{60}, forms a supramolecular porphyrin-ferrocene-fullerene triad.[165] The porphyrin used for the bis-porphyrin was prepared using a Suzuki coupling reaction with 4-ferrocene-phenyl boronic acid and 4-acetamidophenyl boronic acid, to form an A_2BC type porphyrin, functionalized with ferrocene the 15-position. Binding constants of **4.1** with C_{60} and C_{70} were determined by UV-

visible titrations in toluene and are comparable to the tolyl functionalized bis-porphyrin **2.1**. Binding constants of **4.1** and **Zn4.1** in toluene are 1.70 x 10^4 and 1.06 x 10^4 M^{-1} respectively for C_{60} and 1.49 x $10^5$and 7.0 x 10^4 M^{-1} for C_{70}.

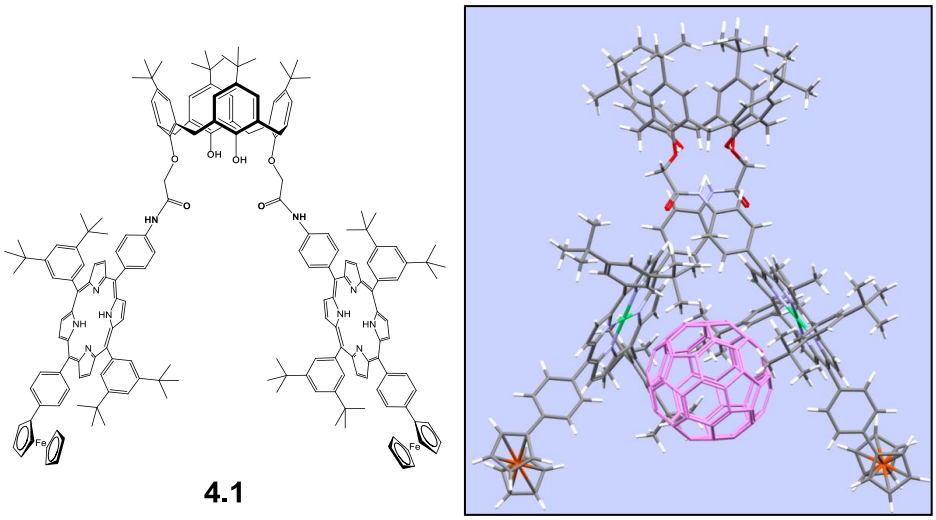

4.1

Figure 12.2 Host 4.1 and the calculated structure (ONIOM/B3LYP/6-31G(d);UFF) for the nickel(II) derivative of hosts–guest complex **4.1** with C_{60}.[165]

Both the free base and the zinc derivatives of the ferrocene appended hosts **4.1** and **Zn4.1** display UV-visible and fluorescence spectra which were identical in shape and position to those of the individual free-base and zinc derivative of *meso*-tetraphenyl porphyrins.[203] The fluorescence intensities, however, were about 25-30 times lower than the analogous ferrocene free hosts **1.36**. The porphyrin quenching has been attributed to energy transfer from the lowest singlet excited states centered on the porphyrin moieties, to the low lying triplet of ferrocene.[204] Charge separated state life times of the triad were not significantly increased. Instead of acting as an electron donor transferring an electron to the porphyrin, the active role of the ferrocene groups in the photoinduced process was observed as deactivation of the porphyrin singlet levels through photoinduced energy transfer. This has been accredited to the ferrocene groups being located too close to the porphyrins and is further reinforced by the strong quenching of the porphyrin fluorescence in the supramolecular adducts compared to the free **4.1** and **Zn4.1** bis-porphyrin hosts with appended ferrocene.

12.2 Aims and Strategy

This chapter describes the synthesis of calixarene bis-porphyrins functionalized with ferrocene groups on the wide rim of the calixarene through palladium catalyzed reactions. The remote distance of the ferrocene groups from the porphyrin sensitizers is expected to promote electron transfer and retard energy transfer. Irradiation of the bis-porphyrin-C_{60} complex excites the porphyrin to a higher singlet energy state The porphyrin can then undergo an electron transfer to the fullerene to generate a charge separated state with the porphyrin radical cation and fullerene radical anion. From there the ferrocene can transfer an electron through to the porphyrin to increase the spatial distance between the two charges and therefore increase the lifetime of the charge separated state.

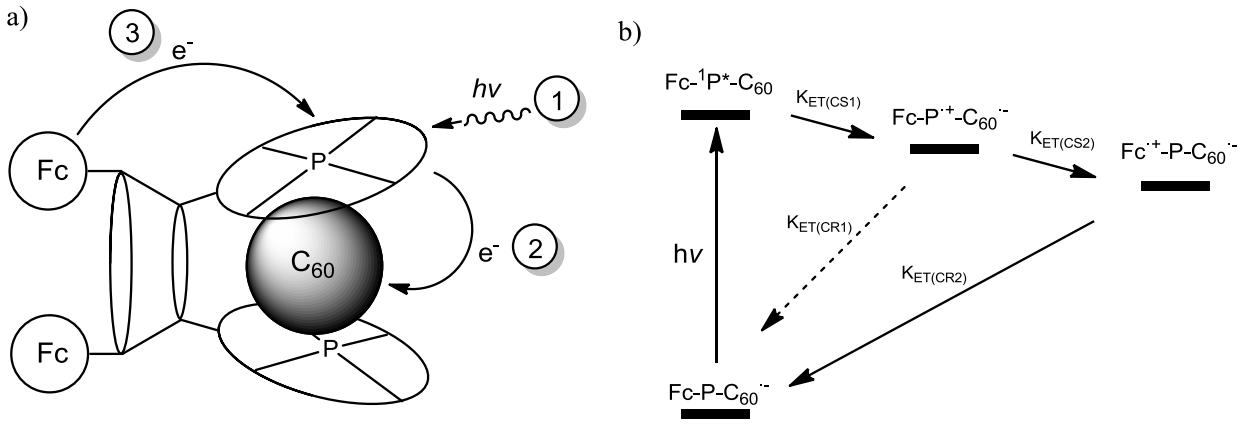

Figure 12.3: a)Photoexcitation (1) and primary electron transfer (2) followed by secondary electron transfer (3). b) Reaction scheme and energy level diagram for ferrocene functionalized calixarene bis-porphyrin.

Two different palladium catalyzed reactions have been employed for the functionalization of calixarenes on the wide rim with ferrocene. The first reaction type is Sonogashira coupling reaction,[141] which has been used to prepare bis-porphyrins **4.2** and **4.3**. Bis-porphyrins **4.2** and **4.3** have been prepared from ethynyl ferrocene and *para*-ethynyl phenyl ferrocene respectively. Addition of a phenyl groups increases the distance between the ferrocene groups and porphyrins by approximately four angstroms and are of interest in terms of what effect the different spatial distances between the chromophores will have on the lifetimes of the charge separated state.

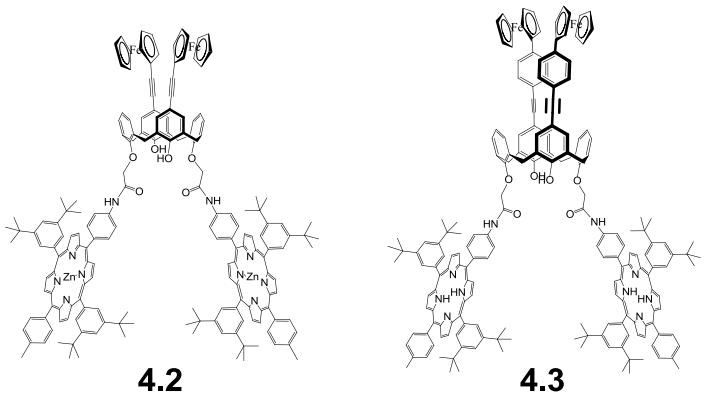

Figure 12.4: Hosts **4.2** and **4.3** prepared via Sonogashira coupling in Chapter Four.

The second reaction used for preparation of wide rim ferrocene functionalized bis-porphyrins was Suzuki coupling.[138] The initial synthetic route for the preparation of the ferrocene functionalized bis-porphyrin **4.4**, was with a dialkylated bromo-calixarene analogous to the iodo calixarene used into the Sonogashira coupling. The Suzuki coupling proved difficult however and all attempts at coupling ferrocene to the wide rim of the dialkylated calixarene failed. This is briefly discussed in the synthetic section of this chapter. It was decided that a second alkylation of the remaining hydroxyl groups would be employed as these groups can interfere with wide rim chemistry. While a second alkylation of the calixarene decreases the association of the bis-porphyrin host with fullerenes due to a change in the calixarene conformation, it provides the opportunity to modify the order of alkylation and in turn the final position of the ferrocene in the functionalized bis-porphyrin.

Two reaction pathways for alkylation of the calixarene have been developed to for Suzuki coupling ferrocene to the wide rim of the calixarene. These pathways differ in the order of alkylation with ethyl bromoacetate and iodobutane. Bis-porphyrin **4.5** was prepared by alkylation of the calixarene with ethyl bromo acetate, followed by bromination of the wide rim of the calixarene with bromine *para* to the phenol. A second alkylation of the phenol *para* to the bromo groups with iodobutane and coupling of ferrocene via a Suzuki reaction ultimately results in the ferrocene groups being appended to the aryl rings of the calixarene *para* to the *n*-butyl chains. In bis-porphyrin **4.6**, the order of alkylation is reversed and the first alkylation of the calixarene is with *n*-iodobutane. Subsequent bromination *para* to the phenol hydroxyl groups with bromine and then secondary alkylation with ethyl bromo acetate and Suzuki coupling of ferrocene ultimately results in the ferrocene groups being appended to the aryl rings of the calixarene *para* to the porphyrin amides. It is hoped that the associated changes in

the location of ferrocene groups on the wide rim of the calixarene may lead to different lifetimes of the multistep charge separated state.

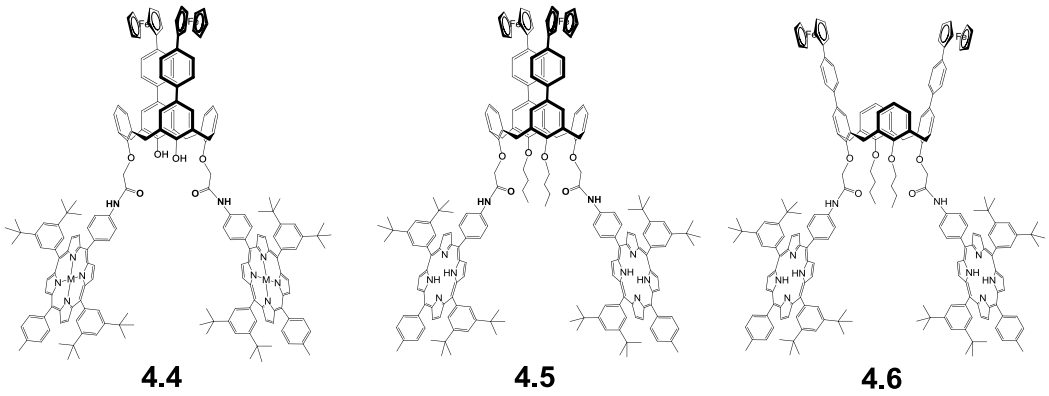

Figure 12.5: Attempted ferrocene functionalized bis-porphyrin host **4.4** and hosts made **4.5** and **4.6** in Chapter Four.

The amino porphyrin used in the synthesis of **4.2, 4.3, 4.5** and **4.6** were 5-(4-aminophenyl)-15-tolyl -10,20-bis(3,5-di-*tert*-butylphenyl) porphyrin **2.15**. Porphyrin **2.15** provides a number of close contacts to bound fullerenes via CH-π interactions from the *tert*-butyl methyl groups which increase the porphyrin–fullerene association in comparison to tetra-phenyl porphyrins. The tolyl methyl observed as a singlet at approximately 2.38 ppm provide a good ^{1}H NMR fingerprint for the identification of the bis-porphyrin, integrating for six protons. In **4.5** and **4.6** *n*-iodobutane was chosen as the reagent for the second alkylation, as the longer chain butyl prevents the aryl rings of the calixarene from interconverting to different conformations.

Computational modeling of bis-porphyrins has been employed to investigate if the changes in geometry off the calixarene scaffold upon appending ferrocene to the wide rim. Binding constant measurements have been carried out using UV-visible titrations in toluene and acetonitrile/toluene (1:1) Estimation of the electronic coupling between the porphyrin and fullerene has been determined from charge transfer transitions. Fluorescence spectra have been recorded for the ferrocene appended hosts to investigate if there is any fluorescence quenching of the porphyrin from the ferrocene.

12.2.1 Computational Modeling of Bis-Porphyrins

In order to investigate spatial distances between the ferrocene groups and the porphyrin sensitizers, as well as any significant differences in geometry of the bis-porphyrins, computational modeling of the host-guest complexes **4.2, 4.3, 4.5** and **4.6** with C_{60} were employed using the two layer ONIOM method described in Chapter Two. The calixarene, the amide linkers groups as well as the appended ferrocenes were modeled in the high layer using DFT with the B3LYP hybrid functional and a 6-31G(d) basis set. The porphyrins and C_{60} were modeled in the low layer with molecular mechanics which adequately describes the porphyrin-fullerene interaction. Nickel porphyrins were used in the computational modeling to help maintain planarity of the porphyrin versus unmetallated porphyrins.

12.2.2 Modeling of Bis-Porphyrins 4.2 and 4.3 with C_{60}

Both **4.2** and **4.3** display a pinched cone conformation similar to the non-ferrocene substituted bis-porphyrin **2.1** due to the narrow rim hydrogen bonding motif. Hydrogen bonding distances are consistent between both hosts ranging from 1.89 to 1.92 Å. Hydrogen bonding between the amide NH and the ether oxygen show distances of 2.33 and 2.40 Å for **4.2** and **4.3**. The interplanar angles between the phenol rings are relatively unchanged for the both hosts **4.2** and **4.3** with angles of approximately 78°. The porphyrin amide functionalized rings do vary slightly, with angles of 22.6° and 24.7° for **4.2** and **4.3** respectively. The porphyrins are tilted slightly towards each other due to CH-π interactions between the methyl groups of one *tert*-butyl phenyl and a *tert*-butyl phenyl ring on the second porphyrin. The interplanar porphyrin angles and center to center porphyrin distances for **4.2** are 73.8° and 9.71 Å, and for **4.3** are 73.8 ° and 9.71 Å. The C_{60} is arranged with 6:6 ring junctions centered over the porphyrin at distances of 2.87-3.15 Å, several CH-π interactions from *ortho*-protons on the 10 and 20 phenyl substituents and the fullerene and a number of CH-π interactions between the methyl groups of the *tert*-butyl groups and the fullerene.

The key differences between the triads are the distance between the ferrocene secondary donors and the porphyrin sensitizers. The center to center distance of the ferrocene to the porphyrin in **4.2** is 16.02-16.15 Å .With the addition of the phenyl ring the center to center distance in **4.3** extends to 19.65-19.99 Å. Optimized structures for **4.2** and **4.3** are shown in

Figure 12.6. A table of key structural characteristics for hosts **4.2** and **4.3** as well as the non-ferrocene functionalized host **2.1** are given in Table 12.1

Table 12.1: Key geometric features of the computational modeling (ONIOM/B3LYP/6-31G(d);UFF) for the nickel(II) derivative of host-guest complexes of **2.1**, **4.2** and **4.3** with C_{60}.

Host:C_{60} Complex	**2.1**	**4.2**	**4.3**
Calixarene ester functionalized phenyl ring angle (°)	23.8	22.6	24.7
Calixarene phenol ring angle (°)	78.2	78.3	78.6
Hydrogen bonding distance phenol O-H ether O (Å)	1.90, 1.95	1.90, 1.92	1.89, 1.88
Hydrogen bonding distance amide N-H ether O (Å)	2.27, 2.400	2.36, 2.40	2.33, 2.31
Porphyrin center to center distance (Å)	9.94	9.71	10.17
Interplanar angle for the 24 atom porphyrin mean planes (°)	74.2	73.8	70.4
Porphyrin metal to fullerene 6:6 junction distance (Å)	2.81, 3.36 2.96, 3.03	2.87, 2.96 2.88, 3.06	2.83, 3.24 2.82, 3.15
Ferrocene to porphyrin Center to Center distance(Å)	n/a	16.02, 16.15	19.99, 19.65

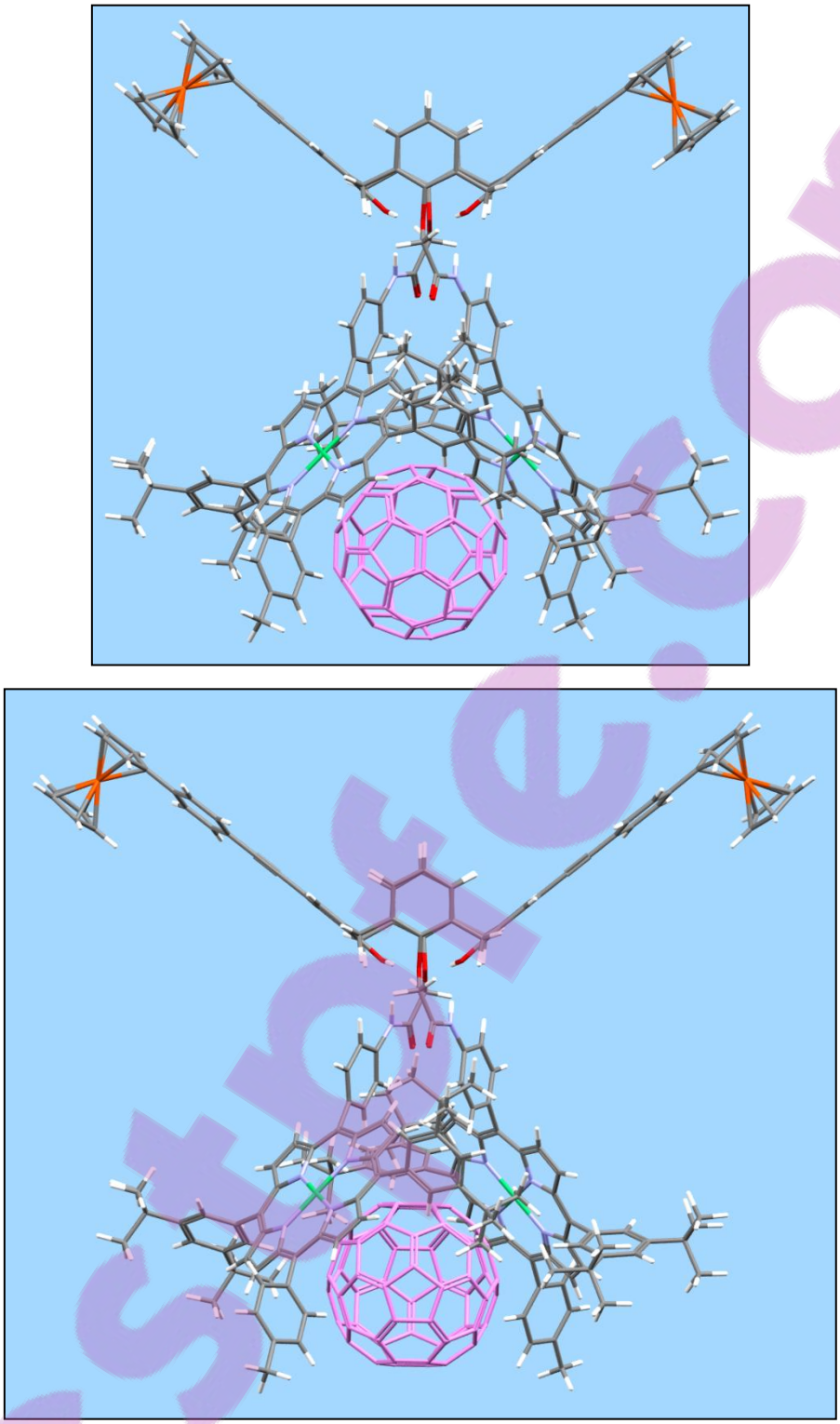

Figure 12.6: Calculated structures (ONIOM/B3LYP/6-31G(d);UFF) for the nickel(II) derivative of hosts–guest complexes a) **4.2** and b) **4.3** with C_{60}.

12.2.3 Computational Modeling of Bis-Porphyrins 4.5 and 4.6 with C_{60}

Optimized models of **4.5** and **4.6** have the same pinched cone orientation as the non ferrocene functionalized host **3.10**. The porphyrin amide functionalized aryl ring adopts the wide orientation with angles of 73.7° and 82.0° for **4.5** and **4.6** respectively. The *n*-butyl functionalized rings take a parallel orientation with angles of 9.5° for **4.5** and 1.1° for **4.6**. There are differences in this calixarene scaffold angle which can be attributed to steric effects the ferrocene phenyl groups on **4.5.** In this isomer the appended ferrocenes are on the *n*-butyl functionalized aryl rings and widen to minimize steric interactions. In **4.6** the ferrocene phenyl groups are appended to wide angle aryl rings and are significantly separated from each other. As with the non-functionalized tetra-alkylated hosts **3.9** and **3.10** the hydrogen bonding between the N-H of amide and the oxygen of the opposite ether is shorter than the dialkylated hosts being 2.20 Å and 2.25 Å for **4.5** and 2.16 and 2.46 Å for **4.6**.

As in the tetra-alkylated bis-porphyrin **3.10**, the amide phenyls at the 5-position of the porphyrin are orientated toward each other at an angle of 59.0° for **4.5** and 51.7° for **4.6**. These changes translate to the geometry of the porphyrins, which become tilted towards each other than in the di-alkylated host. The interplanar porphyrin angles and center to center porphyrin distances for **4.5** is 65.3° and 10.65 Å, and for **4.6** are 62.1° and 10.78 Å. The C_{60} is arranged with 6:6 ring junctions centered over the porphyrin at distances of 2.87-3.15 Å, CH-π interactions from *ortho*-protons on the 10 and 20-phenyl substituents and the fullerene and between the methyl groups of the *tert*-butyls groups and the fullerene. In host **4.5** the ferrocene groups are located directly above the porphyrin groups with a ferrocene-porphyrin center to center distance of 20.77 and 21.27 Å. In **4.6** both ferrocene groups are situated between the two porphyrin planes with distances ranging from 19.25 to 20.91 Å and 21.93 to 22.75 Å. Optimized structures for **4.5** and **4.6** are shown in Figure 12.7 and Figure 12.8 respectively. Key structural characteristics for hosts **4.5** and **4.6** and the non ferrocene functionalized host **3.10** are given in Table 12.2.

Table 12.2: Key geometric features of the computational modeling (ONIOM/B3LYP/6-31G(d);UFF) for the nickel(II) derivative of host-guest complexes of **3.10**, **4.5** and **4.6** with C_{60}.

Complex:C_{60}	**3.10**	**4.5**	**4.6**
Calixarene ester functionalized phenyl ring angle (°)	77.1	73.7	82.0
Calixarene n-butyl phenyl ring angle (°)	3.7	9.5	1.1
Hydrogen bonding distance amide N-H ether O (Å)	2.22, 2.25	2.20, 2.25	2.16, 2.46
Interplanar amide phenyl angle (°)	60.2	59.0	51.7
meta CH-π distance (Å)	2.85	2.62	2.71
Porphyrin center to center distance (Å)	10.66	10.65	10.78
Interplanar angle porphyrin 24 mean plane (°)	65.1	65.3	62.1
Porphyrin metal to fullerene 6:6 junction distance(Å)	2.84, 2.96 2.90, 3.00	2.84,2.98 2.91, 3.04	2.87,2.91 2.88,3.00
Ferrocene to porphyrin Center to Center distance(Å)	n/a	20.77, 21.27	19.25, 20.91 21.93,22.75

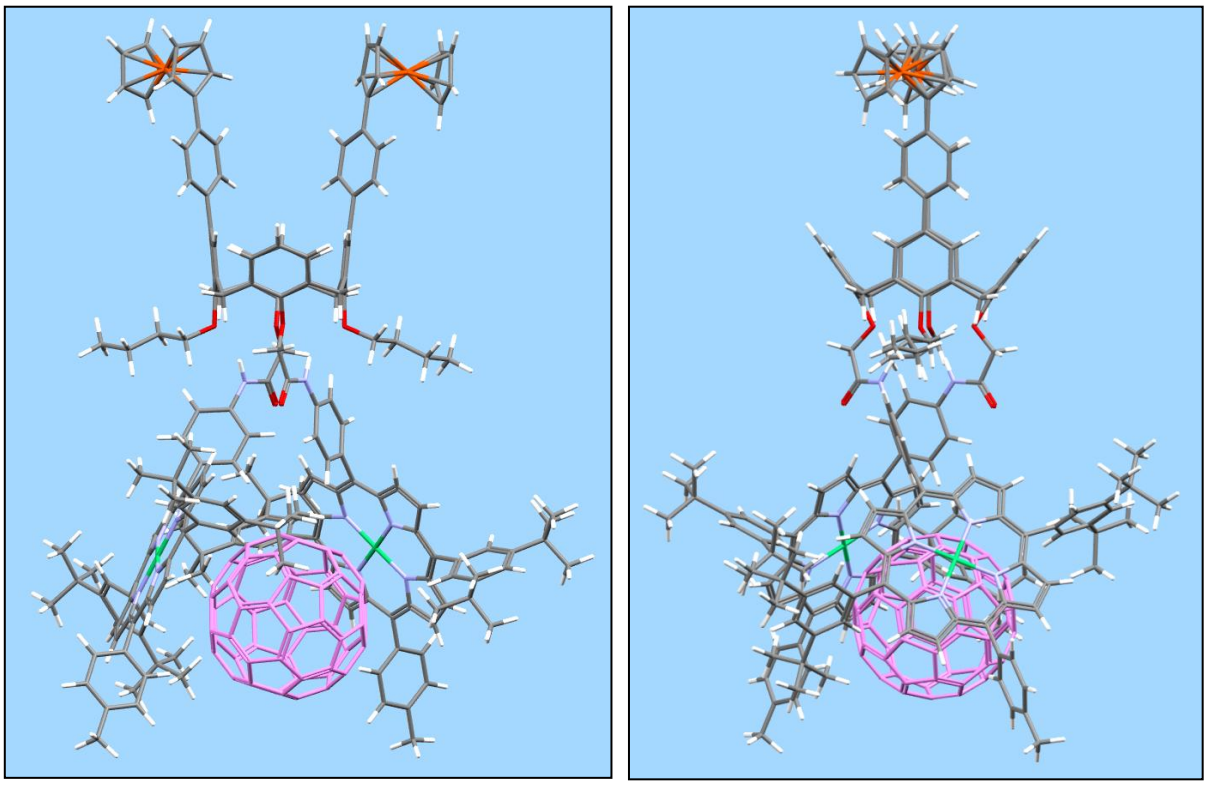

Figure 12.7: Calculated structures (ONIOM/B3LYP/6-31G(d);UFF) for the nickel(II) derivative of hosts–guest complex **4.5** with C_{60}.

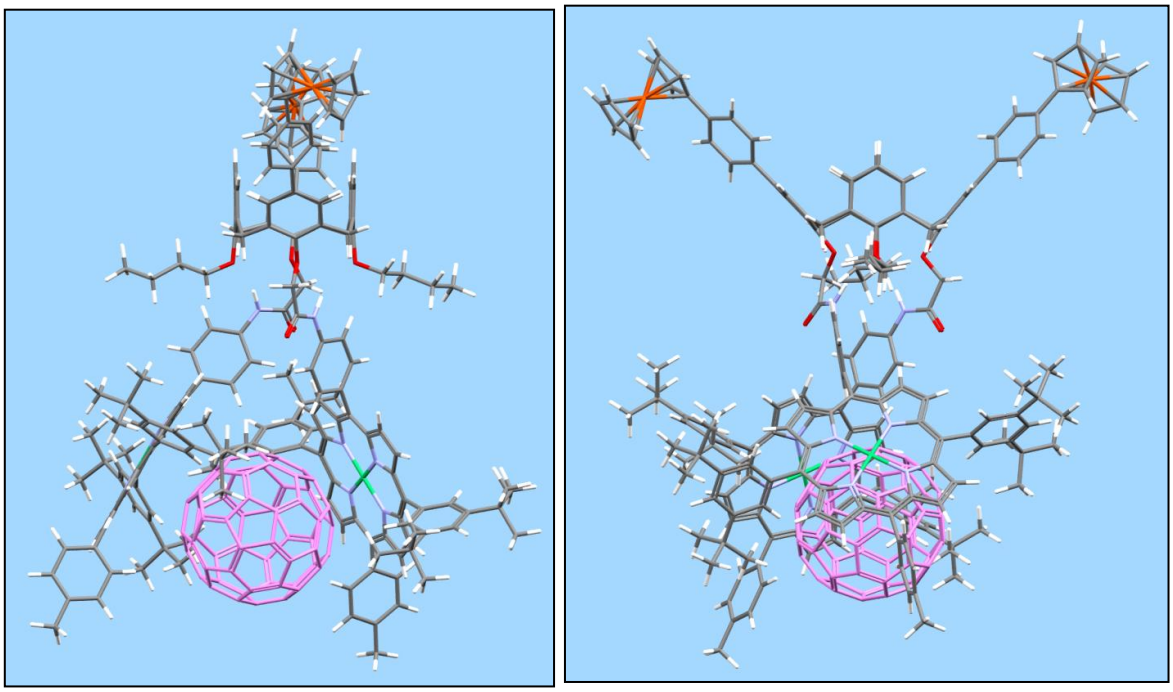

Figure 12.8: Calculated structures (ONIOM/B3LYP/6-31G(d);UFF) for the nickel(II) derivative of hosts–guest complex **4.6** with C_{60}.

Computational models of the ferrocene functionalized bis-porphyrins **4.2** and **4.3** do not display any significant changes in the calixarene scaffold and porphyrin moieties when compared to the non-ferrocene functionalized bis-porphyrin host **2.1**. The ferrocene groups are appended on the aryl rings in the wide orientation and display a spatial distance of 16 Å and 20 Å away from the porphyrins in **4.2** and **4.3** respectively. Bis-porphyrins **4.5** and **4.6** show similar geometries to the non-ferrocene functionalized bis-porphyrin **3.10**. Key differences in these two hosts lie in which aryl ring of the ferrocene groups are appended. In bis-porphyrin **4.5** the ferrocene groups are appended to the phenyl ring in the parallel orientation. This alters the calixarene angle slightly due to steric repulsion of the phenyl ferrocene groups. The average distance of the ferrocene from the porphyrin sensitizers is 21 Å. Bis-porphyrin **4.6** has the ferrocene groups in the wide orientation, with the ferrocene groups angled the away from each other with an average distance of 21 Å from the porphyrin sensitizers.

12.3 Synthesis of Ferrocene Appended Bis-Porphyrins

12.3.1 Synthesis of Bis Porphyrin 4.2

The synthesis of the ferrocene functionalized calixarene bis-porphyrin **4.2** is shown in Scheme 4.1. Iodination of the *tert*-butyl ester calixarene **4.7** was achieved by stirring trimethylbenzyl ammonium iodine dichloride ($BTMA.ICl_2$) with calcium carbonate in an anhydrous chloroform/methanol solution (2:1) for 18 hours.[205,206] The reaction was quenched by addition of concentrated HCl and decolorized by addition of sodium thiosulfite. After aqueous workup the solution was concentrated and a pure sample of **4.8** was crystallized by slow addition of ethanol as a yellow solid in almost quantitative yield. ^{1}H NMR confirmed the iodated calixarene with a singlet at 7.83 ppm corresponding to the proton *ortho* to the iodine groups at the cost of the triplet and doublet. The cone conformation was confirmed by the presence of two doublets at 4.39 and 3.31 ppm corresponding the methylene bridges and a lone singlet corresponding to the methylene of the ester at 4.55 ppm.

Coupling of the ethynyl ferrocene to the wide rim of the calixarene was accomplished by a Sonogashira coupling utilizing the method reported by Gunther.[207] The iodo-calixarene **4.8** was stirred with three equivalents of ethynyl ferrocene, 10 mol% dichloro(bistriphenylphosphine) palladium(II) and copper iodide suspended in a solution of DMF/TEA (1:1). The solvent was degassed by taking the mixture through three freeze pump thaw cycles and the solution was heated at 100°C for 40 hours, over which time the initially orange solution turned dark. The reaction mixture was extracted into dichloromethane and washed with hydrochloric acid and brine. The crude material was purified by column chromatography eluting with dichloromethane/ethyl acetate to give **4.9** in a moderate yield of 63%.

The ^{1}H NMR spectrum for **4.9** displayed a combination of substituted ferrocene and calixarene proton signals in a 2:1 ratio. A singlet was observed at 4.24 ppm integrating for ten protons corresponded to the two unsubstituted cyclopentadiene rings and two triplets located at 4.44 and 4.20 ppm corresponding to the substituted cyclopentadiene rings. A shift in the *ortho* proton singlet from 7.83 to 7.24 ppm upon changing from an iodine to an acetylene on the calixarene phenol ring was observed. The cone conformation was maintained with two sets

doublets at 4.40 and 3.35 ppm and the singlet for the methylene of the ester. Mass spectrometry confirmed the ferrocene calixarene as the sodium adduct.

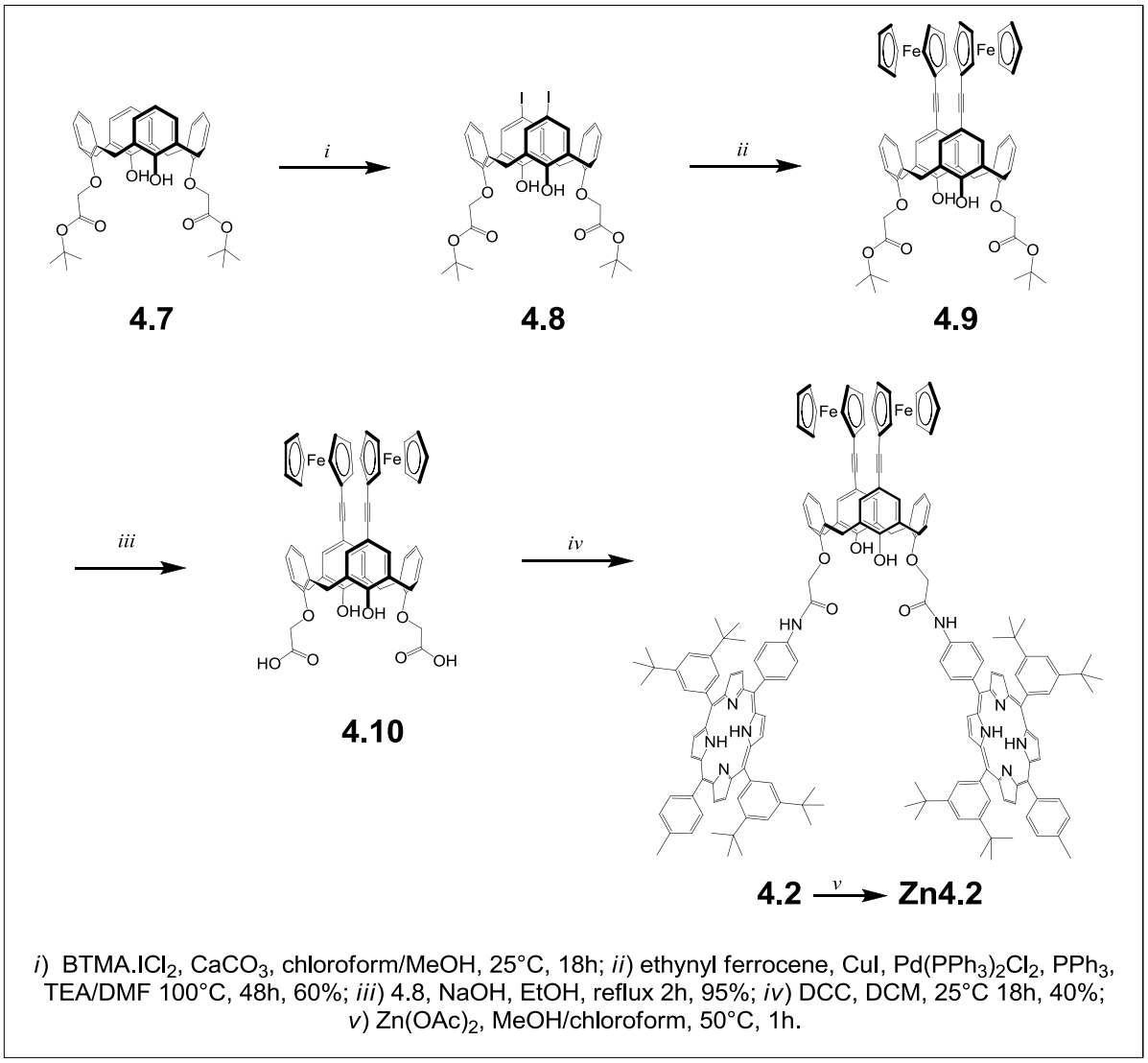

Scheme 12.1: Synthesis of bis-porphyrin **4.2** and **Zn4.2**

Hydrolysis of the *tert*-butyl ester was accomplished by refluxing **4.9** with aqueous sodium hydroxide in ethanol. This resulted in an orange solid for the calixarene diacid **4.10** in almost quantitative yield. Coupling of two equivalents amino porphyrin **2.15** to the calixarene diacid **4.10** was accomplished with excess of DCC as the coupling agent to give the bis-porphyrin host **4.2**. The ferrocene functionalized bis-porphyrin was purified by column chromatography eluting with dichloromethane/ethyl acetate, giving the host as a purple solid in a moderate yield of 40%. The ^{1}H NMR spectra of **4.2** showed the clear presence of signals corresponding to the ferrocenes, calixarene and the porphyrins which integrated in a ratio of 2:1:2, respectfully. The

methylene bridges of the calixarene were shown as two sets of doublets at 3.72 and 4.45 ppm and one singlet at 4.95 ppm for the methylene amide linker, which confirmed the cone conformation of the calixarene. Mass spectrometry confirmed the synthesis of **4.2** as both the mono and disodium cations. **Zn4.2** was prepared by heating **4.2** in a saturated solution of zinc(II)acetate in methanol/chloroform until no free base host was observed in Bis-porphyrin **4.2** and **Zn4.2** were recrystallized from chloroform/ethanol to prepare an analytical sample for titration reactions.

12.3.2 Synthesis of Bis-Porphyrin 4.3

The ethynyl phenyl ferrocene used for the synthesis of **4.3** was prepared from the method reported by Ambroise *et al.*[208] Treatment of ferrocene with a two-fold excess of the diazonium salt of 4-iodoaniline afforded 4-iodophenylferrocene **4.12** in 30% yield. This was then reacted further via a palladium-mediated Sonogashira coupling with trimethylsilylacetylene (TMS) to give the TMS-protected 4-ethynylphenyl ferrocene **4.13** in 92% yield. The TMS group was then cleaved using potassium carbonate to give **4.14**.

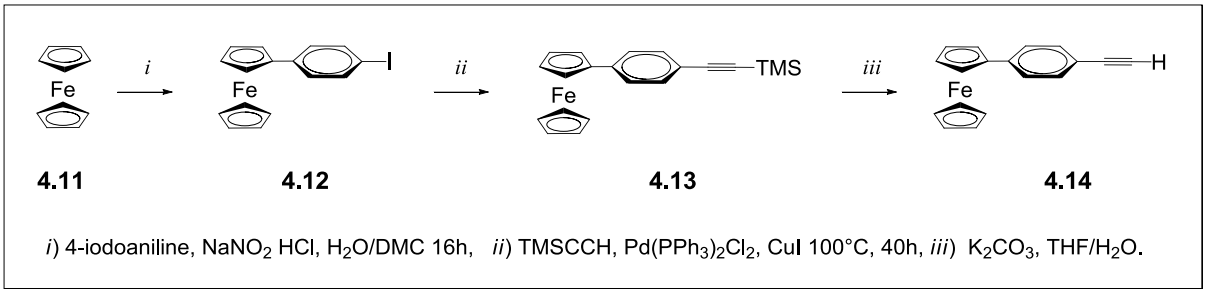

Scheme 12.2: Synthesis of 4-ethynyl phenyl ferrocene.

Coupling of the ethynyl phenyl ferrocene **4.14** to iodo-calixarene **4.8** proceeded under similar conditions to the coupling of ethynyl ferrocene. A solution of iodo-calixarene **4.8,** three equivalents of **4.14**, 10 mol% bis(triphenylphosphine) palladium dichloride and copper iodide in DMF/TEA (1:1) was degassed by freeze-pump-thawing and heated at 100°C for 40 hours. The mixture was extracted into dichloromethane, washed with hydrochloric acid and then purified by column chromatography, eluting with dichloromethane/ethyl acetate and evaporated to give **4.15** as an orange solid in 55% yield.

Hydrolysis of the ester was again accomplished by refluxing **4.15** with aqueous sodium hydroxide in ethanol resulting in an orange solid for the calixarene diacid **4.16**. Coupling of two equivalents amino porphyrin **2.15** to the calixarene diacid **4.16** was accomplished with excess of DCC as the coupling agent to give the bis-porphyrin host **4.3**. The bis-porphyrin was purified by column chromatography eluting with dichloromethane/ethyl acetate, giving the host as a purple solid

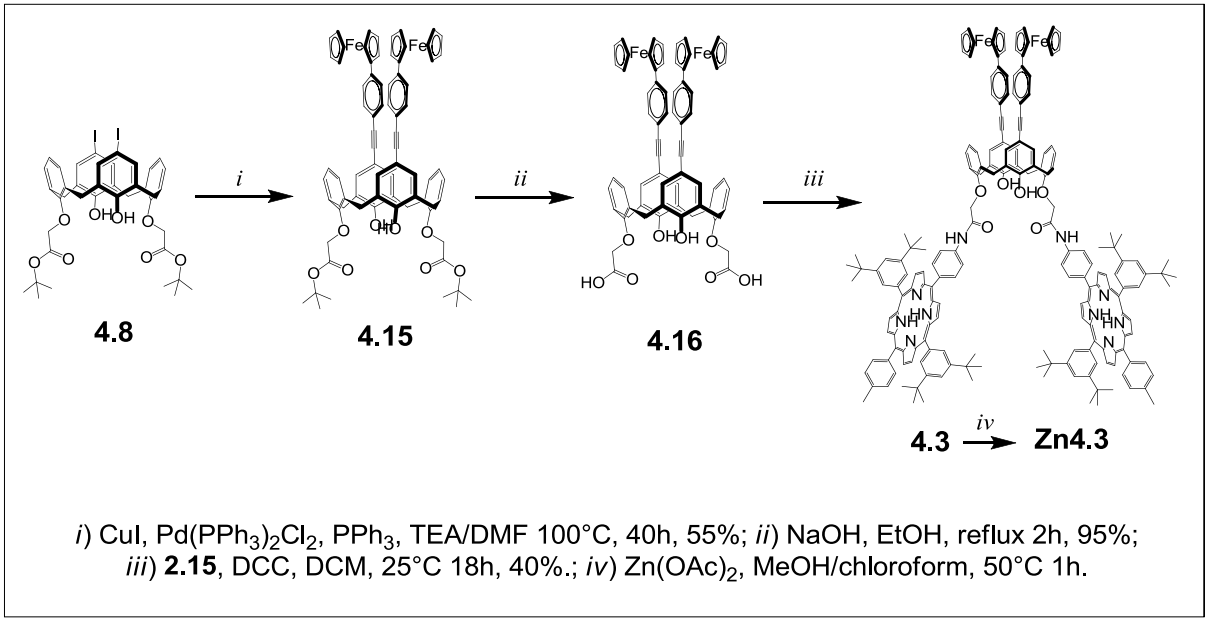

Scheme 12.3: Synthesis of bis-porphyrin **4.3** and **Zn4.3**.

The ^{1}H NMR spectrum of **4.3** was almost analogous to **4.2.** Proton signals corresponding to the ferrocene, the calixarene and the porphyrins integrated in a ratio of 2:1:2. The methylene bridges of the calixarene were shown as two sets of doublets corresponding to the cone conformation. Apart from a signal shift in the positions on the proton signals, the only difference in the spectrum was a shift of the phenol proton signal *ortho* to the acetylene linker from 7.71 to 7.48 ppm and a singlet at 7.45 ppm integrating for eight protons of the phenyl spacer between the ferrocene and the acetylene.

12.3.3 Attempted Synthesis of Bis-Porphyrin 4.4

The attempted route for the preparation of a ferrocene functionalized bis-porphyrin **4.4** via Suzuki coupling reactions with the brominated disubstituted calixarene **4.17** is shown in Scheme 12.4. Bromination of the wide rim of the calixarene has been reported by a number of groups with bromine using various functional groups on the narrow rim to give tetra-

brominated and di-brominated calixarenes.[209] Bromination of the ethyl ester **3.17** in chloroform by slow addition of bromine resulted in the di-bromo calixarene **4.17** as an off white solid with the bromines *para* to the activating hydroxyl.

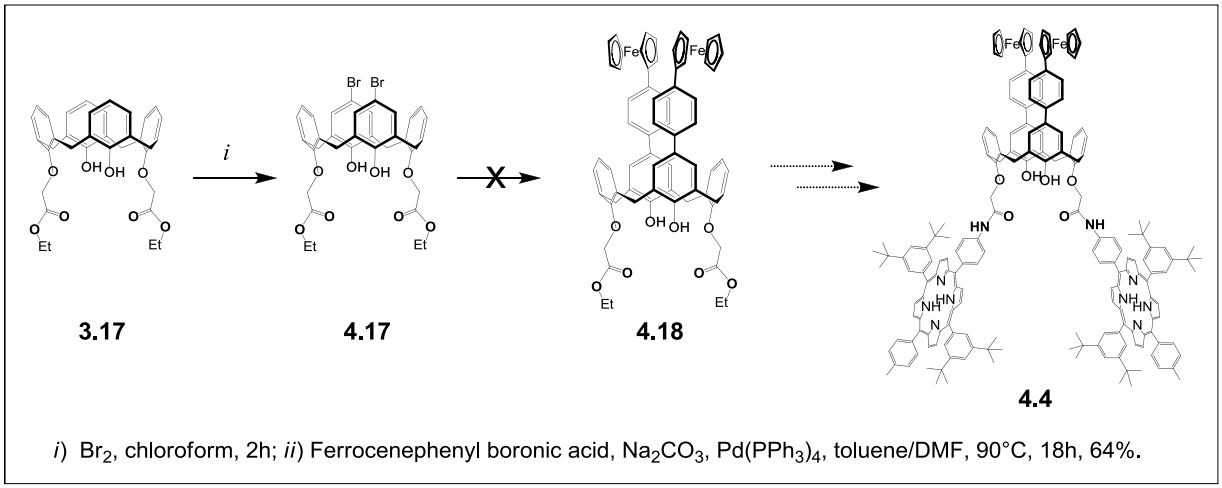

Scheme 12.4: Attempted synthesis of bis-porphyrin **4.4;**

Suzuki coupling with disubstituted calixarenes has been reported with n-propyl and crown ether functionalized calixarenes in good yield by reacting with tetrakis(triphenylphosphine) palladium(0) catalyst in toluene and aqueous sodium carbonate as base.[210,111] Attempts were made to repeat this procedure with the ethyl ester derivative **4.17**. However, under these conditions the ester groups hydrolyzed to the diacids, complicating the reaction. Attempts with anhydrous sodium carbonate failed to yield any substituted ferrocene functionalized calixarene **4.18**. The main product for these reactions was self coupled ferrocene phenyl boronic acid giving 4,4'di-ferrocenyl-1,1'biphenyl.

Potassium and caesium carbonate have been employed for Suzuki coupling calixarene in anhydrous conditions with di- and tetra-alkylated calixarenes.[212] However the use of larger bases with dialkylated calixarenes has an effect on the conformation of the calixarene and will give the 1,3-alternate conformation in most cases. As the cone conformation is the conformation required for the preparation of **4.4,** these conditions are not suitable. The use of $Pd(dppf)Cl_2$ and $Pd(PPh_3)_2Cl_2$ were also investigated for several reactions, however these failed to yield the ferrocene coupled product.

12.3.4 Synthesis of Bis-Porphyrin 4.5

With attempts at appending a secondary donor to the wide rim of the dialkylated calixarene **4.17** being unsuccessful, it was decided to alkylate the hydroxyl groups on the narrow rim *para* to the bromine with iodobutane. This synthetic route was initially avoided as the tetra-alkylated hosts **3.9** and **3.10** showed decreased association of fullerenes due to removal of the preorganised hydrogen bonding motif. Alkylation with iodobutane as the larger butyl groups does not allow interconversion of the aryl groups of the calixarene and thus it will be easier to maintain the cone conformation. This results in sharper signals in the ^{1}H NMR spectra. The synthetic route for the preparation of bis-porphyrin **4.5** is shown in Scheme 12.5.

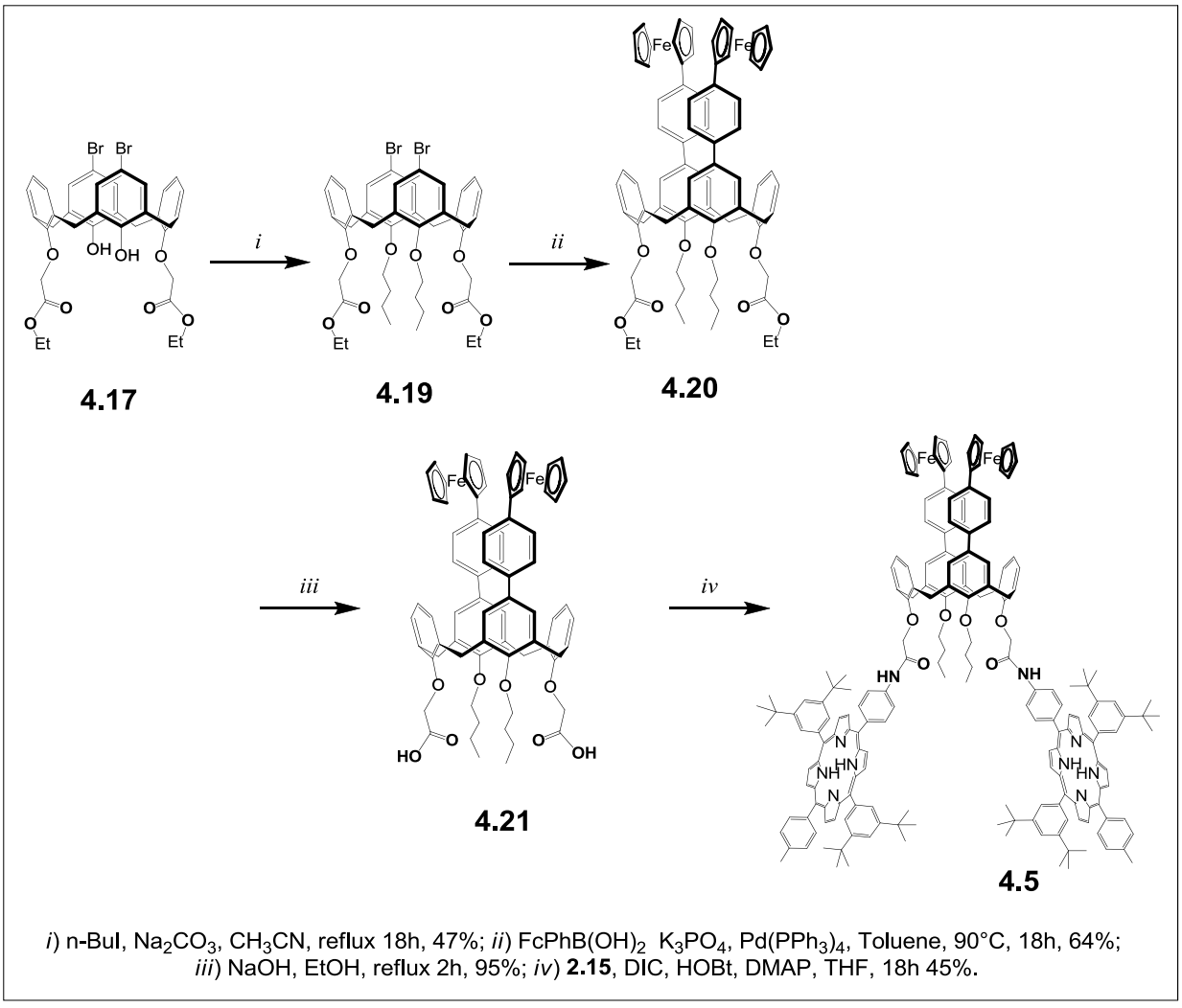

Scheme 12.5: Synthesis of bis-porphyrin **4.5**.

The second alkylation of the dibrominated ethyl ester **4.17** was initially performed by the same method as the non-brominated calixarene **3.17** by using hexane washed sodium hydride as the base and heating with iodobutane in DMF at 60° for 18 hours. This method gave a relatively

low yield for the tetra-alkylated product. An alternative method for alkylation as reported by Tongraung *et al.* enables alkylation of the deactivated nitro calixarenes was employed.[213] The tetra-alkylated calixarene **4.19** was prepared by refluxing iodobutane and **4.17** in anhydrous acetonitrile with an excess of anhydrous sodium carbonate for 40 hours. The product was then filtered though celite to remove the excess base and refluxed again in ethanol with HCl. The product was then purified by column chromatography eluting with ethyl acetate and dichloromethane to give **4.19** in 62% yield. ^{1}H NMR confirmed the tetra-alkylated calixarene with a triplet at 3.79 ppm, two multiplets at 1.81 and 1.47 ppm and a final triplet at 0.98 ppm corresponding to the *n*-butyl chain. The spectra confirmed the cone conformation with the two methylene doublets at 4.64 and 3.18 ppm and a lone singlet at 4.73 ppm.

Suzuki coupling ferrocene phenyl boronic acid to the wide rim of the dibromo calixarene was achieved using the method reported by Liu *et al.*[214] The dibromo calixarene **4.19** was heated to 100° C for 18 hours with ferrocene phenyl boronic acid and tri potassium phosphate in with tetrakis(triphenylphosphine)palladium(0) catalyst in degassed toluene. This method utilized anhydrous potassium phosphate as the base instead of the typical a carbonate base. At this point the use of the potassium salt is practical as the tetra alkylated calixarene cannot be interconverted without cleavaging of one of the narrow rim ethers. Purification of the product on silica eluting with dichloromethane and ethyl acetate yielded **4.20** in a moderate yield of 68%.

The ^{1}H NMR spectrum of **4.20** displays a combination of calixarene and ferrocene signals in a ration of 1:2. A singlet at 4.01 ppm integrating for ten protons corresponds to the unsubstituted cyclopentyldiene rings and two triplets at 4.56 and 4.20 ppm correspond to the substituted cyclopentyldiene ring. The cone conformation was confirmed with doublets present at 4.70 and 3.30 ppm and single methylene ester signal at 4.20 ppm. Hydrolysis of the ester groups to the corresponding carboxylic acid was achieved by refluxing **4.20** with 10% sodium hydroxide in THF for three hours. The solvent was removed in vacuo to give an orange solid, **4.21**. ^{1}H NMR confirmed the synthesis of the carboxylic acid through the absence of the triplet and quartet of the ethyl ester.

As with the synthesis of tetra substituted bis-porphyrins **3.9** and **3.10**, the calixarene diacid **4.21** did not undergo amide coupling with amino-porphyrin **2.15** when using DCC as the coupling agent. Successful coupling was achieved by stirring calixarene **4.21** and amino

porphyrin **2.15 at** room temperature for 18 hours with DIC, DMAP and HOBt. The solvent was removed and the crude material purified by column chromatography with toluene/ethyl acetate the eluent. The solvent was removed to give a purple solid in a moderate yield of 48%. An analytically pure sample of **4.5** was prepared via recrystallization from chloroform/methanol.

Confirmation of the ferrocene functionalized bis-porphyrin **4.5** was achieved by ^{1}H NMR. Signals corresponding to the calixarene, the porphyrins and the ferrocene groups which were all identified and integrated in a ratio of 2:1:2 respectively. The methylene bridges of the calixarene were shown as two sets of doublets at 4.48 and 3.56 ppm and one singlet at 5.04 ppm for the methylene amide linker corresponding to the cone conformation. Mass spectrometry was able to confirm **4.5** which was detected as the disodium cation.

12.3.5 Synthesis of Bis-Porphyrin 4.6

An additional benefit of the second alkylation of the calixarene scaffold is that it allows the opportunity to modify the order of alkylation and in turn the final position of the ferrocene in the functionalized bis-porphyrin. By alkylation of the narrow rim first with iodobutane, followed with bromination of the wide rim at the position *para* to the hydroxyl groups, the second alkylation with ethyl bromoacetate occurs *para* to the bromines. The subsequent Suzuki coupling reactions mean that the appended phenyl ferrocenes will be on the same aryl ring functionalized with porphyrin amide. Once the tetra-alkylated calixarene **4.23** is prepared the synthetic strategy is analogous to that of bis-porphyrin **4.5**. The synthesis of bis-porphyrin **4.6** is shown in Scheme 4.4.

The calixarene **3.20** was brominated by the same method used to prepare the dibromo-ethyl ester **4.17**. The di-bromo calixarene **4.22** was alkylated with ethyl bromoacetate in the presence of sodium carbonate in anhydrous acetonitrile to give the tetra-alkylated cone diester **4.23**. Purification of **4.23** was accomplished by column chromatography eluting with dichloromethane and ethyl acetate, followed by recrystallization from dichloromethane and methanol.

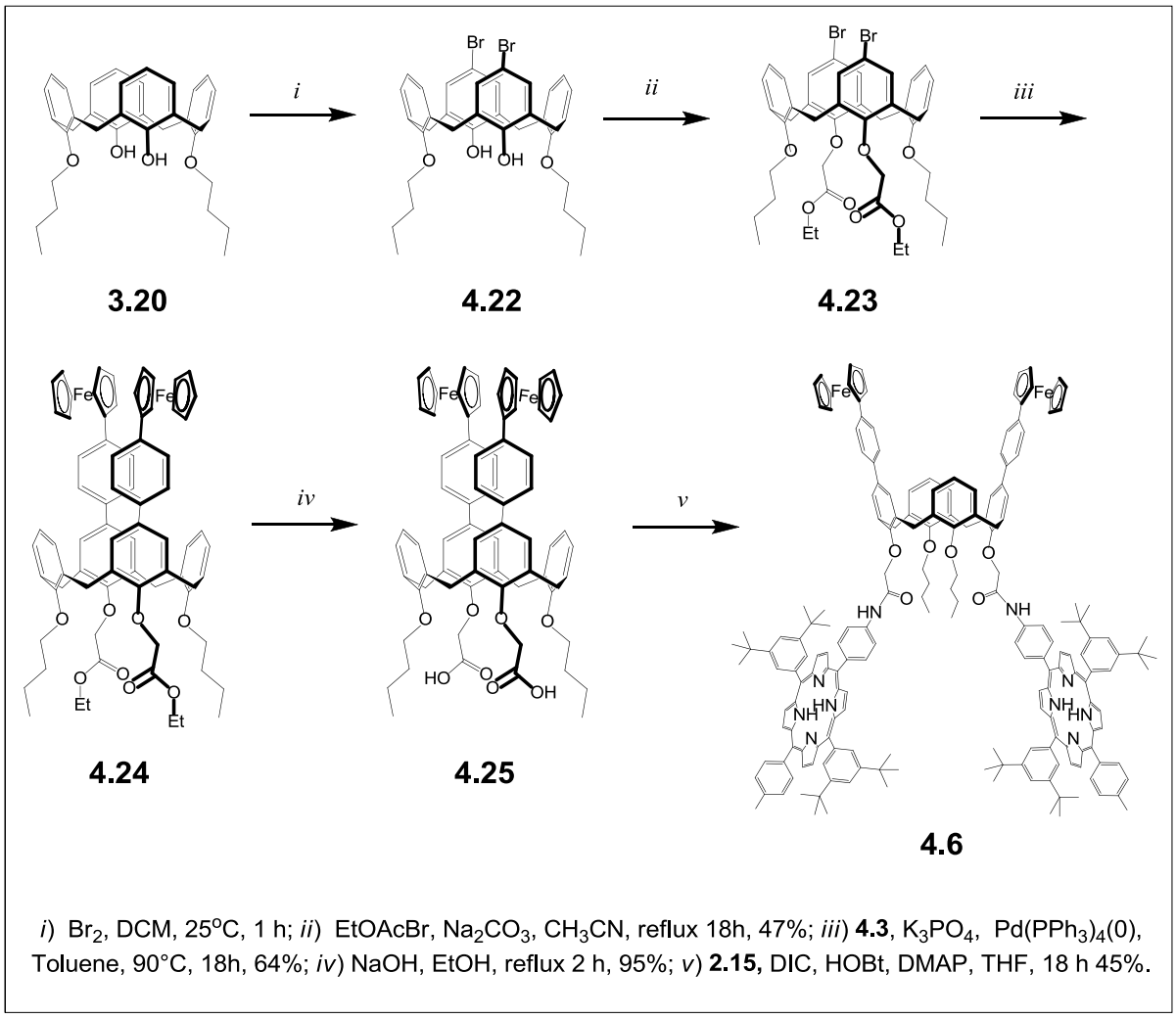

Scheme 12.6: Synthesis of bis-porphyrin **4.6.**

The ^{1}H NMR spectrum of the tetra alkylated scaffold is almost analogous to its isomer **4.19**. The ^{1}H NMR spectra of the two isomers are shown in Figure 12.9. The only significant difference between **4.19** and **4.23** is in the aromatic region. The multiplet and doublet corresponding to the *para* and *meta*-proton signals (marked as •) of the non brominated phenyl rings and the singlet for the protons *ortho* to the bromine exchange positions due to the electron withdrawing nature of the ester. The singlet shifts downfield from 6.52 ppm in **4.19** to 7.20 ppm for **4.23** and the multiplet and double-shift upfield from 6.93 and 6.86 ppm in **4.19** to 6.39 and 6.33 ppm in **4.23**.

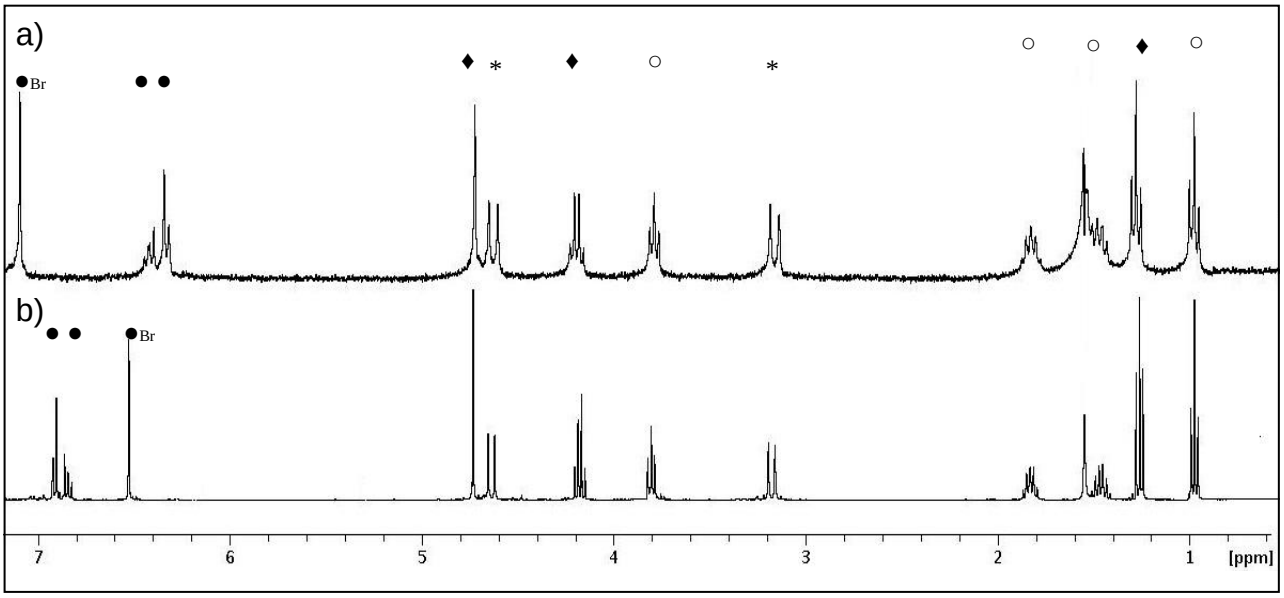

Figure 12.9: ^{1}H NMR of bromocalixrenes a) **4.23** and b) **4.19**, showing proton signals of the phenyl rings (●), the methylene linker ethyl ester (♦), the methylene bridges (*)and the *n*-butyl chains (○).

Coupling of the ferrocene phenyl boronic acid was achieved though by the same method used for **4.20. 4.23,** potassium phosphate, the boronic acid and tetrakis(triphenylphosphine)palladium(0) catalyst in degassed toluene were heated to 100°C for 18 hours followed by purification by column chromatography eluting with dichloromethane/ethyl acetate to give the **4.24** as an orange solid.

The ^{1}H NMR spectra of both ferrocene phenyl functionalized calixarene isomers **4.20** and **4.24** is shown in Figure 12.10. Unlike the brominated calixarene isomers, these two isomers exhibit divergent proton signals due to the bulkier ferrocene phenyl groups. The flexibility of the calixarene allows the cone conformation adjusts to minimize steric interactions on the wide rim. This can be seen in the singlet of the methylene ester and the methylene triplet of the *n*-butyl groups (marked as ○) as well as a shift in the positions of the ferrocene cyclopentadiene signals (ↄ). Two doublets occur at 7.31 and 7.19 ppm for the phenyls of the ferrocene (▼) in **4.20,** while it is the same proton signals that appear as a single doublet at 7.55 ppm in **4.24**. There is a downfield shift in the singlets of the both *ortho* protons for the substituted calixarene ring upon the removal of the bromine groups. The singlet occurs at 7.39 ppm while the multiplet remains relatively unchanged.

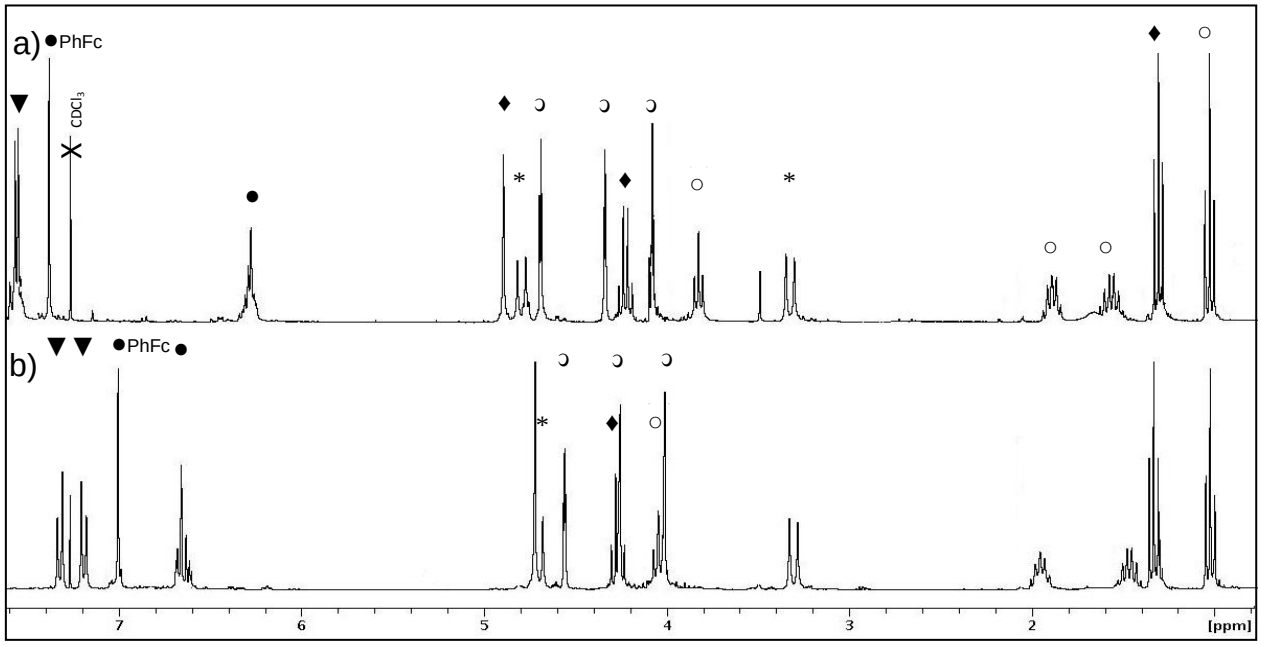

Figure 12.10: ^{1}H NMR of ferrocene functionalized calixarenes **4.24** and **4.20**; showing proton signals of the ferrocene (ɔ), the phenyl rings (●), methylene linker ethyl ester (♦),methylene bridges (*) and n-butyl chain (○).

Hydrolysis of the ethyl ester was achieved by refluxing **4.24** in THF and 10% sodium hydroxide. The diacid **4.25** was confirmed through the absence of the ethyl ester quartet and triplet at 4.28 and 1.29 ppm respectively. As with the other tetra-alkylated calixarene acids, coupling with amino porphyrin **2.15** was achieved using the coupling reagent DIC with HOBt and DMAP to give the bis porphyrin **4.6.** The host was purified by column chromatography with silica, eluting with toluene/ethyl acetate. An analytically pure sample was prepared through recrystallization from chloroform and methanol.

The bis-porphyrin **4.6** was characterized by both ^{1}H NMR and mass spectrometry. In the ^{1}H NMR, the key difference between the isomers **4.6** and **4.5** lies in the aromatic proton region. In **4.6** the doublet and multiplet for the unsubstituted calixarene phenyl rings lies further upfield at 6.33 and 6.46 ppm. The same protons signals in the unsubstituted ring of **4.5** appear as multiplets at 6.95 ppm with a number of other aromatic signals of the porphyrin. The singlet corresponding to the *ortho* protons of the substituted phenyl ferrocene in **4.6** lie at 7.62 ppm and in **4.5** they lie at 7.0 ppm.

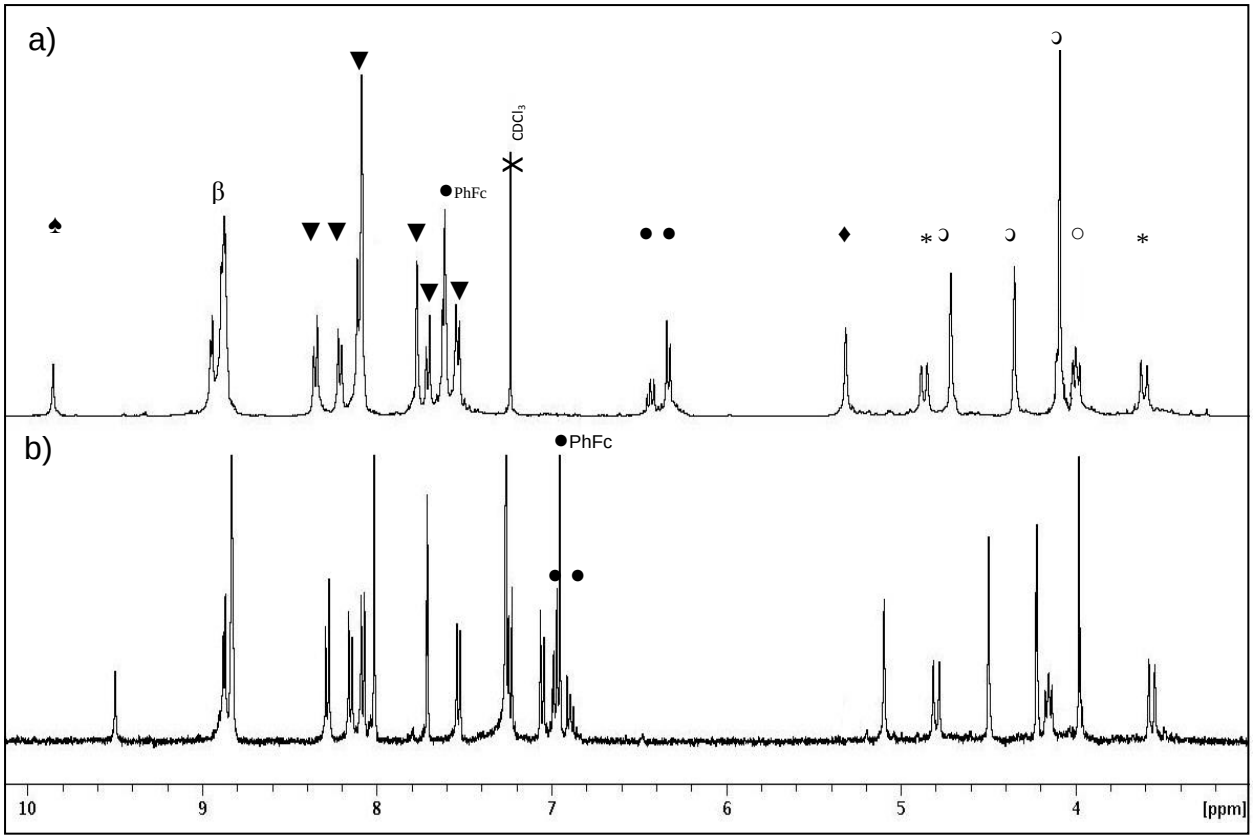

Figure 12.11 ^{1}H NMR of ferrocene functionalized bis-porphyrin a) **4.6** and b) **4.5**, showing proton signals of the phenyl rings (●),the ferrocene (ɔ) the methylene linker ethyl ester (♦), methylene bridges (*) and *n*-butyl chains(○).

12.4 Fullerene Binding Studies with Bis-Porphyrins

Binding constants for fullerenes with ferrocene functionalized bis-porphyrins **4.2**, **4.3, 4.5** and **4.6** were determined by UV-visible titrations using the method outlined in Chapter Two. The optical absorption of the ferrocene functionalized hosts was found to be similar to the corresponding non ferrocene functionalized bis-porphyrins **2.1** and **3.10**; that is, they exhibited an intense Soret band and less intense Q bands. No new peaks corresponding to the appended ferrocene were observed due to the low absorptivity of the ferrocene in comparison to the porphyrins (ca. 96 M^{-1} cm^{-1}).[215]

12.4.1 Fullerene Binding Studies with Bis-Porphyrins 4.2 and 4.3

Association constants for fullerenes were determined for free base and zinc derivatives of **4.2** and **4.3** in toluene. Upon addition of fullerene to a solution of the host in toluene, a clear decrease in the intensity of the Soret band at 421 nm as well as a red shift occurs. Titrations produce a clear isosbestic point at 429 nm with larger volumes of C_{60} and C_{70}.

The binding constants of **4.2** and **4.3** with C_{60} have both been calculated to be approximately 1.8. x 10^4 M^{-1}. The zinc derivatives **Zn4.2** and **Zn4.3** display lower association with 1.0 x 10^4 M^{-1}. The binding constants are an order of magnitude higher for C_{70} with 1.60 x 10^5 M^{-1} for the free base and 1.0 x $10^5 M^{-1}$ for the zinc derivatives. Binding constants for $Lu_3N@C_{80}$ are two orders of magnitude higher than C_{60} with 1.42 x 10^6 M^{-1} for **4.2** and 1.17 x 10^6 M^{-1} for **4.3**. These binding constants are of the same size and magnitude as the non-ferrocene substituted host **2.1**. Such small differences between association constants between **4.2, 4.3** and **2.1** demonstrate that there is little or no effect on the binding due to the functional groups on the wide rim for dialkylated hosts. The ferrocene groups are appended to the phenol rings which adopt the wide interplanar angle due to the hydrogen bonding motif present on the narrow rim. A table of calculated binding constants for **4.2** and **4.3** as well as **2.1** is shown in Table 4.4 and the UV-visible absorption spectra of the Soret band for **4.2** with C_{60} and C_{70} in toluene are shown in Figure 12.12 and with $Lu_3N@C_{80}$ in Figure 12.13.

Table 12.3: Association constants of free base and zinc(II)derivatives of **4.2, 4.3** and **2.1** with C_{60}, C_{70} and $Lu_3@C_{80}$ in toluene.

Host	C_{60} ($x10^4$ M^{-1})	C_{70}($x10^5$ M^{-1})	$Lu_3N@C_{80}$($x10^6$ M^{-1})
2.1	1.80 (0.02)	1.57 (0.05)	1.44 (0.06)
Zn2.1	1.01 (0.03)	0.98 (0.03)	0.82 (0.04)
4.2	1.81 (0.02)	1.57 (0.03)	1.42 (0.09)
Zn4.2	1.40 (0.01)	0.95 (0.05)	0.89 (0.05)
4.3	1.87 (0.05)	1.61 (0.03)	1.17 (0.04)
Zn4.3	0.92 (0.01)	1.07 (0.03)	0.83(0.03)

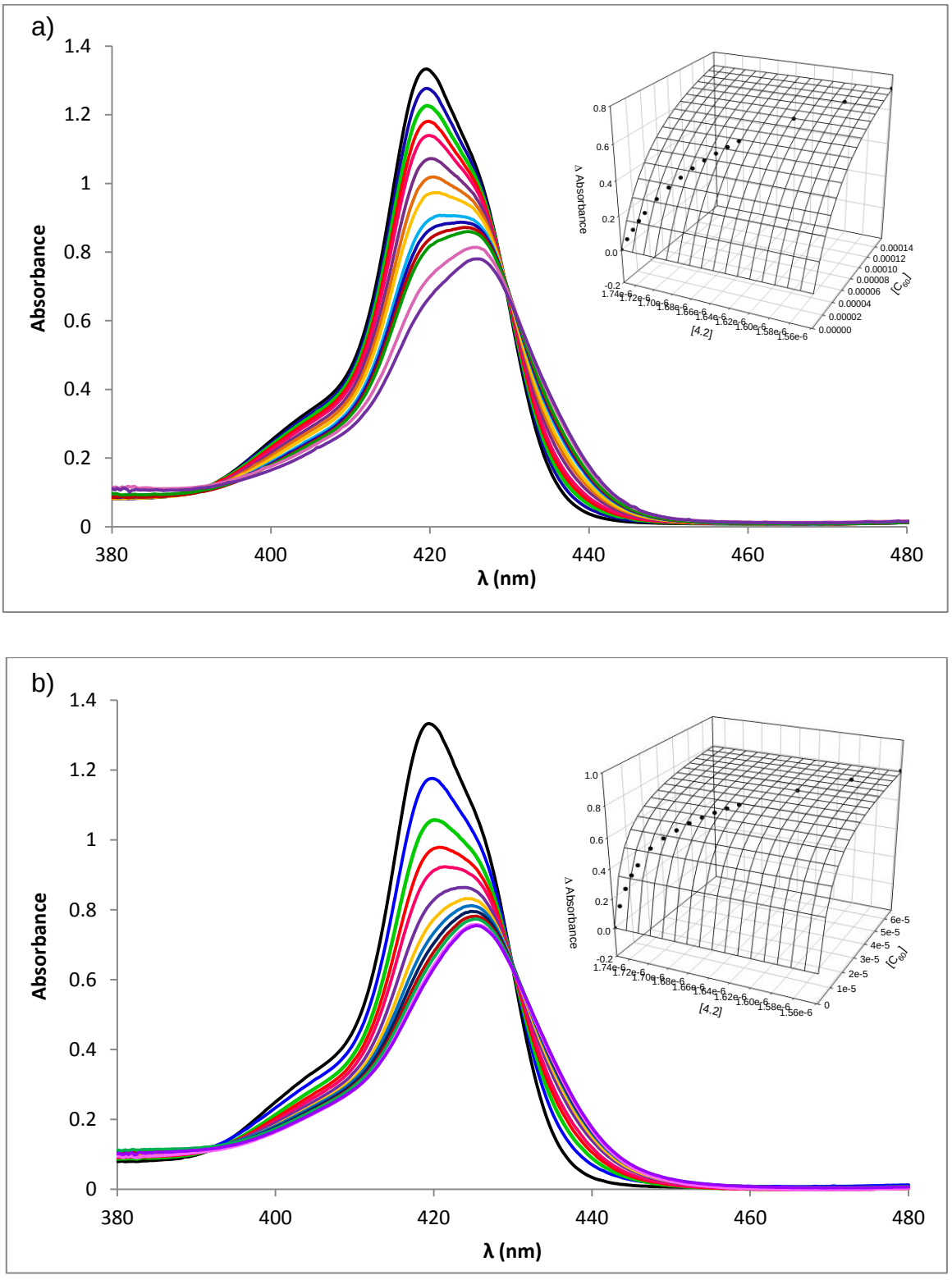

Figure 12.12: UV-visible titration of **4.2** (1.75×10^{-6} M) in toluene with a) addition C_{60} (0-120 Eq.) and b) C_{70} (0-45 Eq.). Insets; plot of the non-linear least square fit for the change in absorption at the Soret of **4.2** upon addition of fullerene.

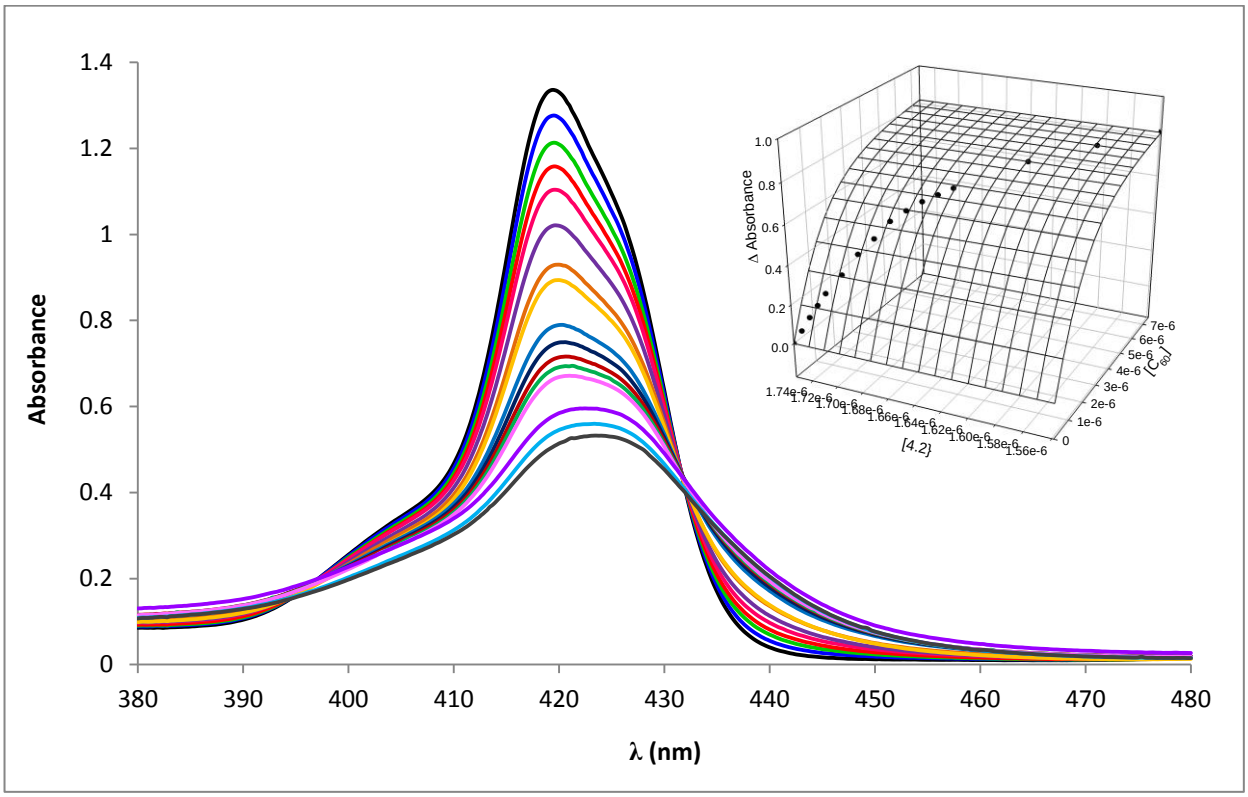

Figure 12.13: UV-visible titration of **4.2** (1.75×10^{-6} M) in toluene with addition $Lu_3N@C_{80}$ (0-4.9 Eq.). Inset; plot of the non-linear least square fit for the change in absorption at the Soret of **4.2** upon addition of fullerene.

12.4.2 Fullerene Binding Studies of Bis-porphyrins 4.5 and 4.6 in Toluene

The UV-visible absorption spectra for **4.5** showing the Soret band in toluene is shown in Figure 12.14. Upon addition of C_{60} (0-550 equivalents) and C_{70} there is a modest decrease in the intensity of the Soret band and a minor amount of red shifting. An isosbestic point is observed at 435 nm giving a good indication of a 1:1 complex being formed. For both the **4.5** and **4.6**, the association constants for C_{60} have been calculated to be 1,600 and 1,300 M^{-1} respectively and 15.0×10^3 and 13.5×10^3 for C_{70}. These association constants are approximately the same as the non-ferrocene functionalized host **3.10**. Calculated binding constants for **4.5**, **4.6** and **3.10** are shown in Table 4.4.

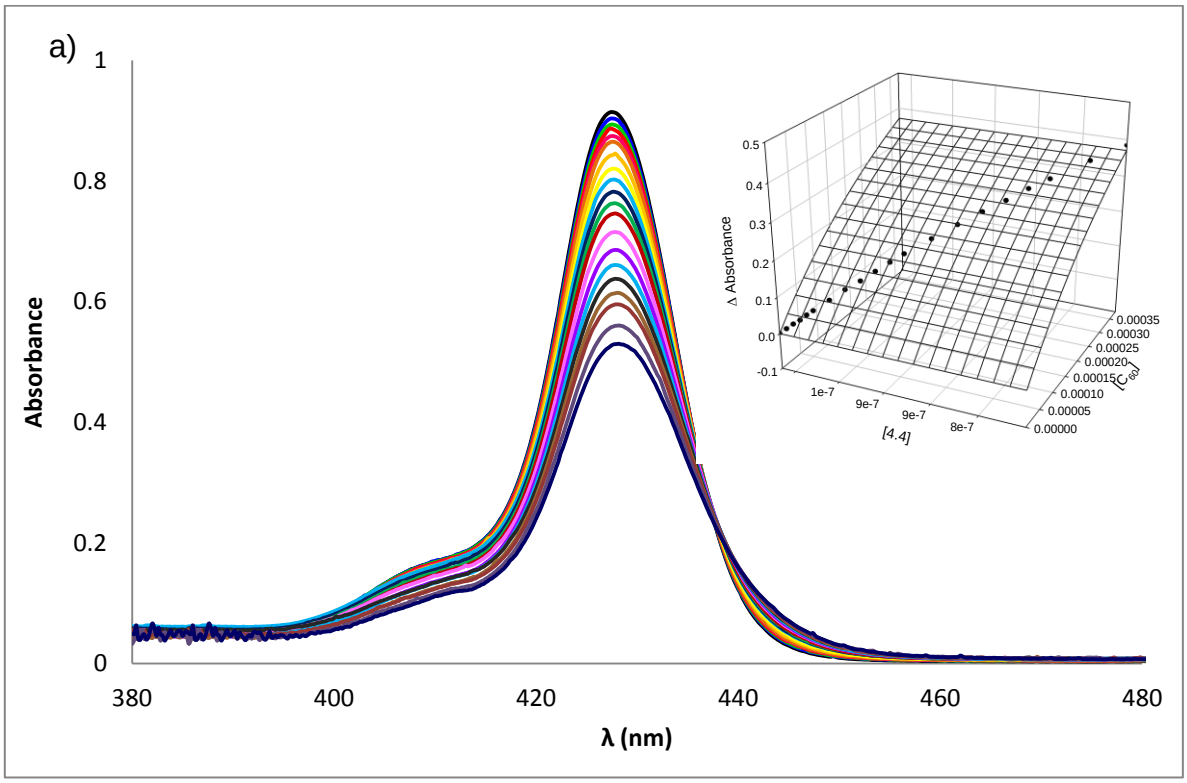

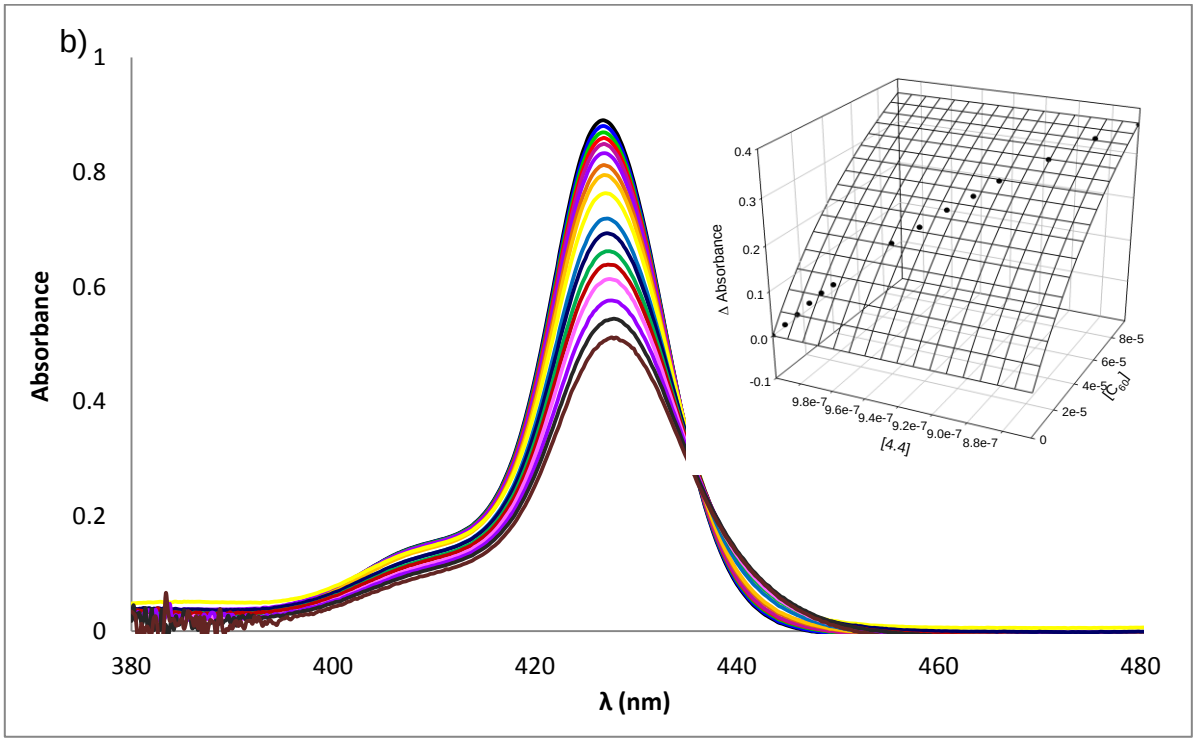

Figure 12.14: UV-visible titration of **4.5** (1.28×10^{-6} M) in toluene with a) addition C_{60} (0-550 Eq.) and b) C_{70} (0-95 Eq.) Insets; plot of the non-linear least square fit for the change in absorption at the Soret of **4.5** upon addition of fullerene.

Table 12.4: Association constants of hosts **4.5**, **4.6** and **3.10** with C_{60} and C_{70} in toluene.

Host	C_{60} ($1x10^3M^{-1}$)	C_{70} ($1x10^3M^{-1}$)
3.10	1.8(0.2)	17.6 (4.7)
4.5	1.6 (0.1)	15.0 (2.7)
4.6	1.3 (0.1)	13.5 (1.3)

12.4.3 Fullerene Binding studies of Bis-porphyrins 4.5 and 4.6 Acetonitrile/Toluene (1:1)

Given that the binding constants were low for the hosts **4.5** and **4.6** binding constants were measured in a solvent mixture of acetonitrile/toluene (1:1). In this solvent mixture the binding constants for C_{60} and C_{70} are higher compared to than in toluene alone. This is illustrated by the UV-visible spectra showing greater reduction of the Soret band absorbance upon addition of C_{60} and C_{70}. The red shifting of the Soret bands are pronounced and the isosbestic point are clearly defined. Upon changing the solvent to acetonitrile/toluene (1:1) the binding constants increased by two order of magnitude for C_{60} and C_{70}. The association constants have been calculated for both the **4.5** and **4.6** in acetonitrile/toluene (1:1) and are shown in Table 12.5.

Table 12.5: Association constants of hosts **4.4**, **4.5** and **3.10** with C_{60} and C_{70} in acetonitrile/toluene (1:1).

Host	C_{60} ($1x10^3M^{-1}$)	C_{70} ($1x10^3M^{-1}$)
3.10	144.0 (1.7)	1,032 (14)
4.5	146.0 (2.0)	1,382 (18)
4.6	135.0 (1.7)	1,243 (17)

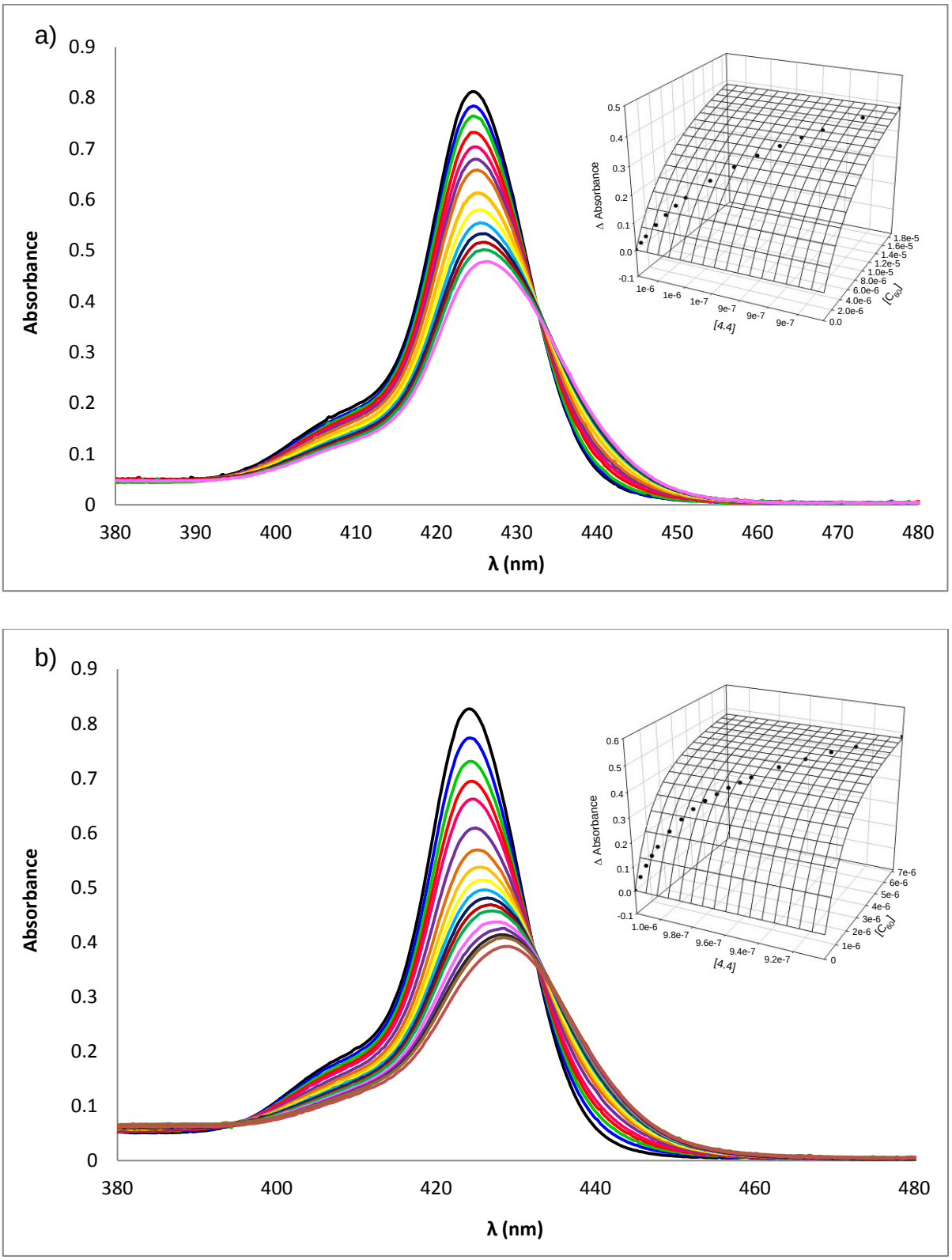

Figure 12.15: UV-visible titration of **4.5** (1.28×10^{-6} M) in acetonitrile/toluene (1:1) with a) addition C_{60} (0-20 Eq.) and b) C_{70} (0-5 Eq.). Insets; plot of the non-linear least square fit for the change in absorption at the Soret of **4.5** upon addition of fullerene

12.5 Fluorescence of Bis-Porphyrins

The absorption spectra of the ferrocene functionalized bis-porphyrins are nearly identical to the non functionalized hosts and no new additional bands were observed, which indicated that there is weak or little ground state electronic interaction between the porphyrins and ferrocene moieties. Fluorescent properties of the hosts were studied. As ferrocene has an oxidation potential of +0.50V (SCE) it can undergo either energy or electron transfer to the porphyrin resulting in the fluorescence of the porphyrin being quenched by this intramolecular energy/electron transfer. As the ferrocene moieties are at significant distance (ca. 16-20 Å) from the porphyrins, the level of fluorescent quenching will be reduced. Fluorescence spectra were measured for **4.2-4.5** and compared to the two non ferrocene functionalized hosts **2.1** and **3.10.** All were measured at the same concentration to determine the level of quenching from the secondary electron donor to the porphyrin.

12.5.1 Fluorescence of Bis-porphyrins 2.1, 4.2 and 4.3

At the same concentration (1.2×10^{-6} M), the Soret band are observed at the same wavelength and has the same intensity for **2.1, 4.2** and **4.3**. The solutions of bis-porphyrins in toluene were excited at the Soret band, which were 420 nm for the free base derivatives and 422 nm for the zinc derivatives. The fluorescence spectra of the zinc and free base derivatives of **4.2** and **4.3** are shown in Figure 12.16.

Porphyrin hosts **2.1**, **4.2** and **4.3** show emission bands centered at 653 and 718 nm. The relative intensities of fluorescence for **4.2** and **4.3** compared to the non ferrocene bis-porphyrin **2.1** are 0.83 and 0.85 respectively. The decrease in fluorescence intensity is attributed to the appended ferrocene moieties. The zinc derivatives display similar emission bands at 600 and 645 nm and the relative intensities of the ferrocene bis-porphyrins are 0.83 and 0.85 for **Zn4.2** and **Zn4.3** respectively. In comparison to the porphyrin functionalized ferrocene bis-porphyrin **4.1** prepared by Lyons, which displayed a relative intensity of fluorescence of about 0.03-0.04, the porphyrin fluorescence of **4.2** and **4.3** are higher. The differences in porphyrin fluorescence intensities between the two hosts is minor considering that the distance between ferrocene and the porphyrins host in **4.3** is 25% larger than **4.2**. This may be attributed to conjugation within the phenyl and acetylene.

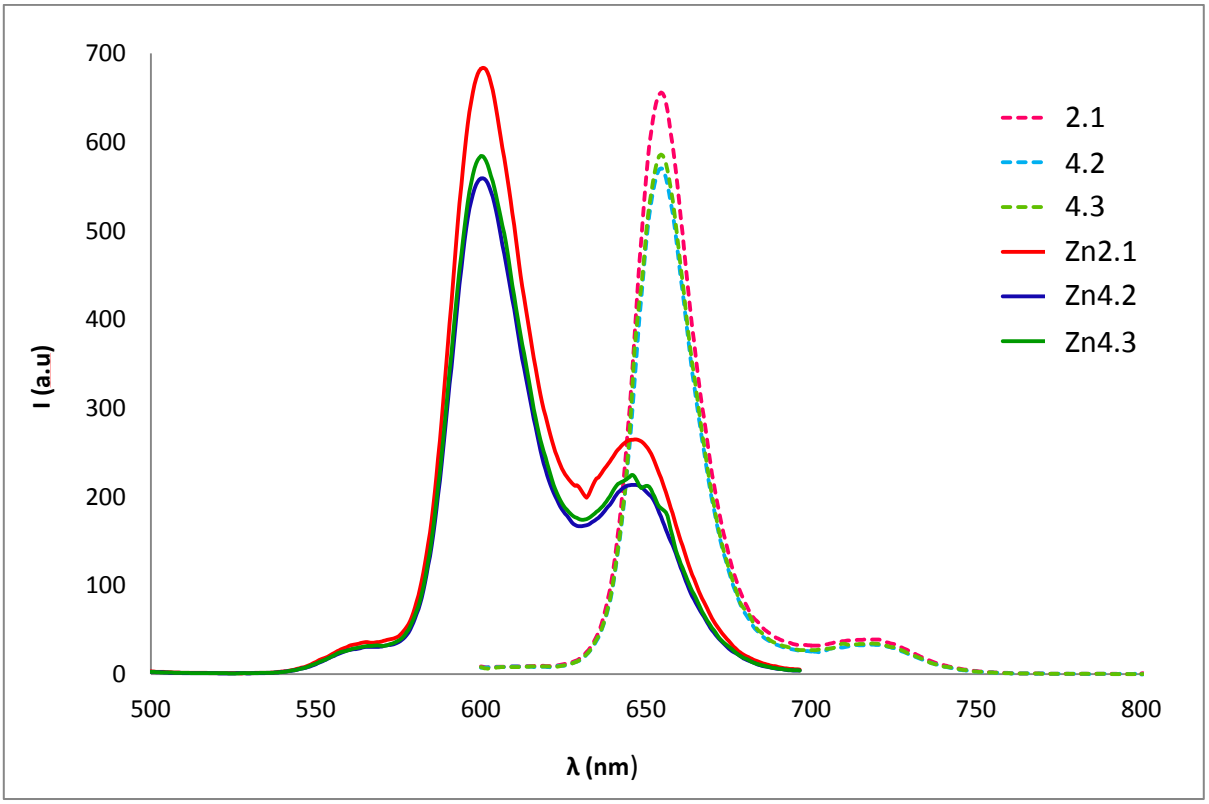

Figure 12.16 Fluorescence spectra of the free base (1.2 x 10^{-6} M) and zinc derivatives of **4.4** and **4.5** compared to the non ferrocene functionalized bis-porphyrin **3.10**.

12.5.2 Fluorescence of Bis-porphyrins 3.10, 4.5 and 4.6

The Soret band occurs at the same wavelength and intensity for **3.1**, **4.5** and **4.6** at a concentration of 1.2 x10 $^{-6}$ M. The bis-porphyrins were excited at 419 nm. The fluorescence spectra of **4.5, 4.6** and **3.10** are shown in Figure 12.16.

All bis-porphyrin hosts **3.1**, **4.5** and **4.6** show emission bands centered at 653 and 718 nm. The relative intensities of fluorescence compared to the non ferrocene bis-porphyrin **3.10** are 0.95 for both **4.5** and **4.6**. In comparison to **4.2** and **4.3**, there is almost no reduction in the fluorescence emission given experimental error, even though the distance between the porphyrin and secondary donor differs.

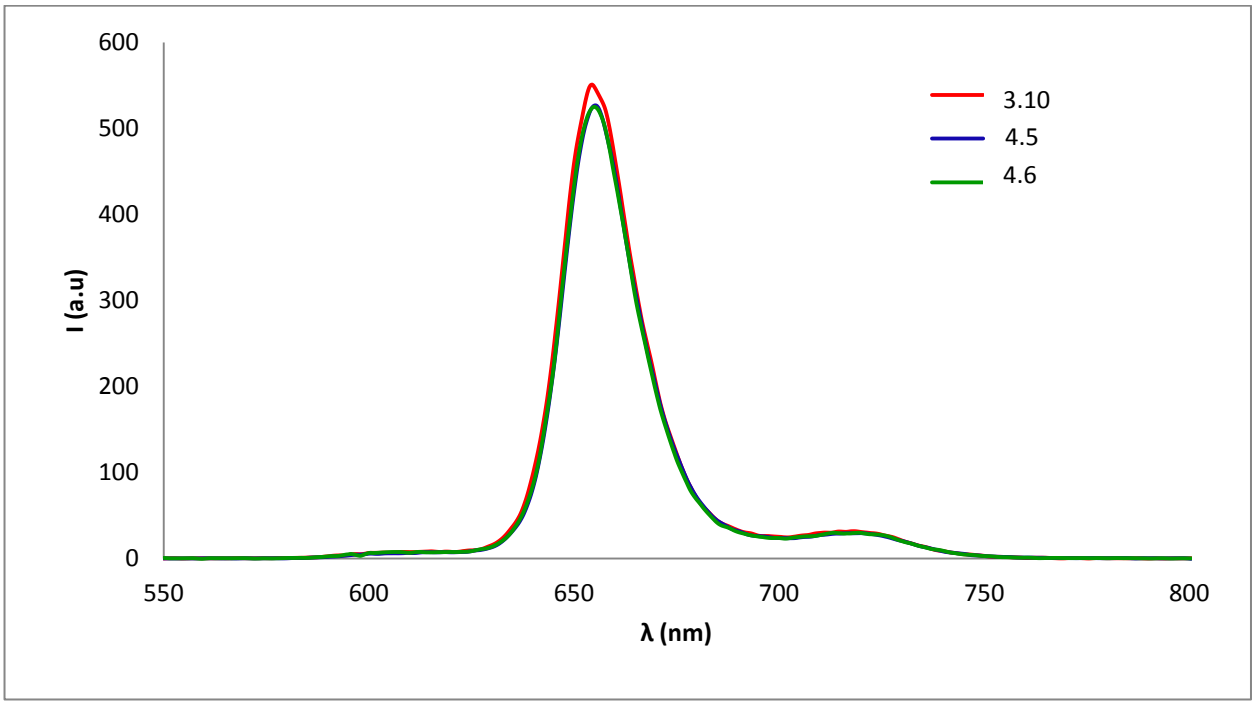

Figure 12.17: Fluorescence Quenching of **4.5** and **4.6** compared to the non ferrocene functionalized bis-porphyrin **3.10**.

The small decrease in fluorescence of the functionalized hosts **4.2** and **4.3** and the lack of fluorescence quenching of **4.5** and **4.6** demonstrate that the ferrocene units and linkers are at a remote distance to the porphyrins. It is believed that the lesser quenching is favorable for future transient absorption studies, which will show an increase in the lifetime of the charge separated state.

12.6 X-Ray Crystal Structures

12.6.1 X-Ray Crystal Structure of Calixarene 4.9

Crystals of **4.9** were grown by slow diffusion of methanol and a solution of **4.9** in chloroform. Single crystal X-ray diffraction data was collected and the structure solved and refined by Associate Professor Peter Boyd. The structure of **4.9** is shown Figure 12.18 and crystal data is shown Table 12.8, located in the experimental section of this chapter.

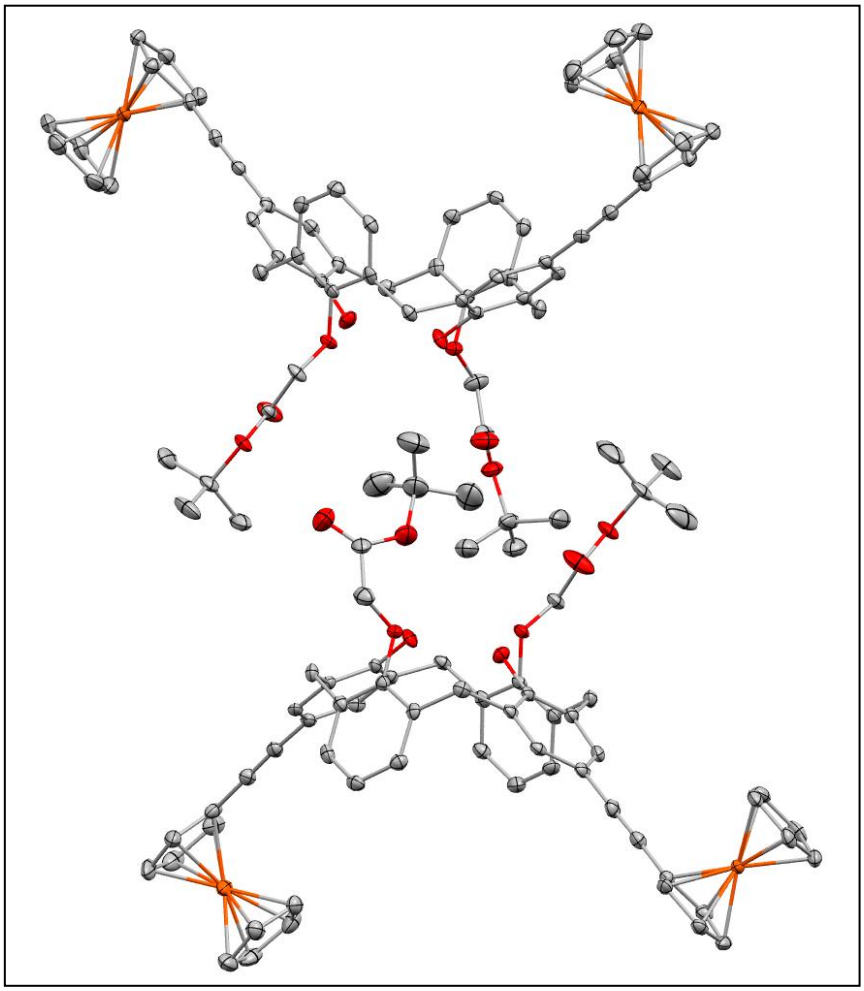

Figure 12.18: X-ray structure of **4.9** represented with atomic displacement parameters shown as thermal ellipsoids at 50% probability (hydrogen atoms omitted for clarity).

The structure of **4.9** shows the calixarene in the pinched cone conformation, which is commonly observed for dialkylated calixarenes due to the intramolecular hydrogen bonding of the hydroxyl group and the ether oxygens. The hydrogen bonding distances between the oxygen of the ether and the oxygen of the hydroxyl group average at 2.28 Å. The wide interplanar angle of the phenol rings functionalized on the wide rim with the ferrocene acetylene groups is 76.19°. The alternate aryl rings functionalized with *tert*-butyl esters adopt a parallel angle of 27.8°. The crystal structure displays a reasonable comparison with the calixarene scaffold in the modeling of the host-guest complex of **4.2.** The calixarene adopts similar interplanar angles in the calixarene of 78.3° and 22.6° for the respective rings. Distances between the calixarene aryl rings and the ferrocene groups are 4.06 Å. The same distance as depicted in the computational models.

12.6.2 X-Ray Crystal Structure of Calixarene 4.23

Crystals were successfully grown for the dibromo tetraalkylated calixarene, **4.23** were grown by slow diffusion of methanol and a solution of **4.23** in chloroform. Single crystal X-ray diffraction data was collected and the structure solved and refined by Andrew Dalebrook. The structure of **4.23** is shown in Figure 12.19 and crystal data is shown in Table 12.9, located in the experimental section of this chapter.

The X-ray structure of **4.23** reveals the calixarene in the cone conformation, the interplanar angles of the rings bearing the ethyl ester and bromines tilting away from the calixarene cavity with a dihedral angle of 71.5°. The opposite rings substituted with butyl groups are tilted inward toward each other with an angle of 21.3°. The pendent groups are asymetrially disposed about the macrocycle.

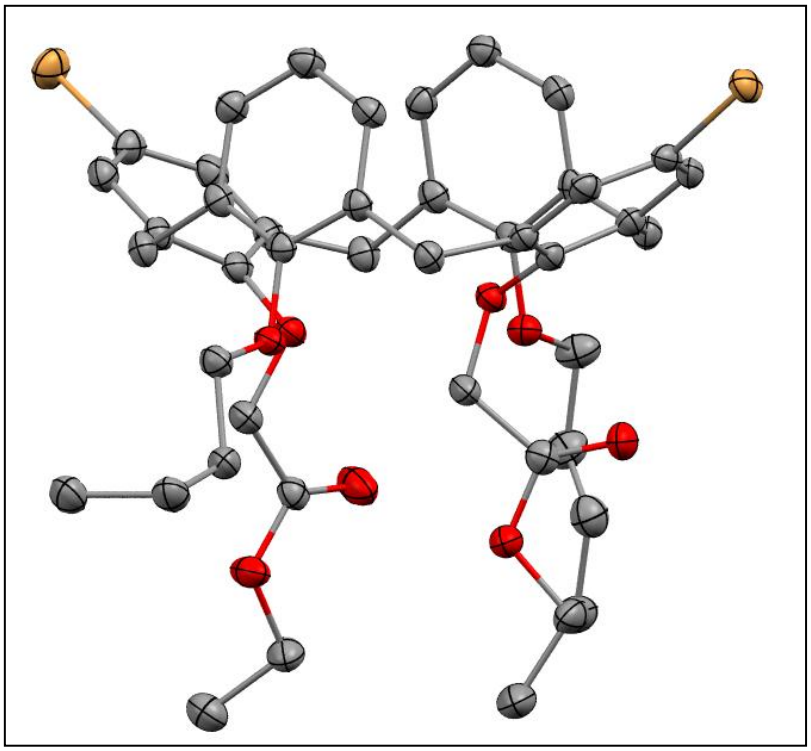

Figure 12.19: X-ray structure of **4.23** represented with atomic displacement parameters shown as thermal ellipsoids at 50% probability (hydrogen atoms omitted for clarity).

12.6.3 X-ray Structure of Calixarene 4.24

Crystals of **4.24** were successfully grown by slow evaporation of methanol into benzene. Single crystal X-ray diffraction data was collected and the structure solved and refined by Andrew Dalebrook. The structure of **4.24** is shown in Figure 12.20 and crystal data is shown in Table 12.10, located in the experimental section of this chapter.

In comparison with the bromocalixarene **4.23,** the calixarene displays higher symmetry. The aryl ring functionalized on the wide rim with ferrocene with ethyl ester on the narrow rim adopts a wider interplanar angle of 81.8° and the ring substituted with n-butyl groups is parallel with an angle of 2.4°. The substituents on the narrow rim are symmetrically orientated.

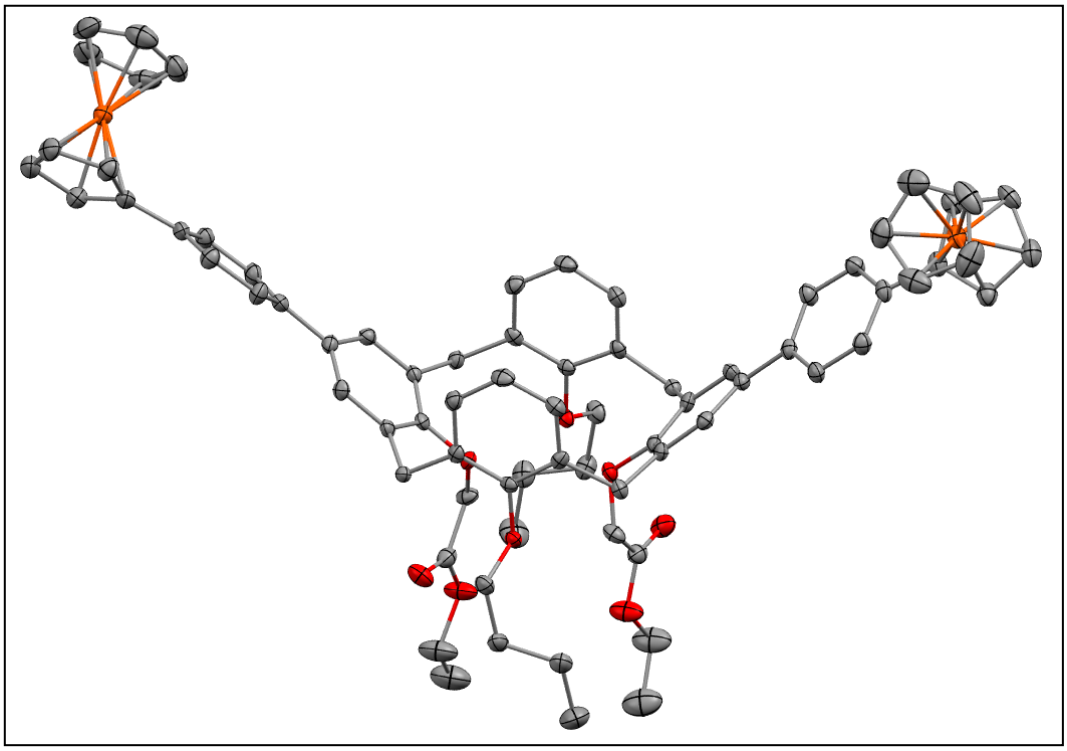

Figure 12.20: X-ray structure of **4.24** represented with atomic displacement parameters shown as thermal ellipsoids at 50% probability (protons omitted for clarity).

12.7 Porphyrin-Fullerene Charge Transfer Bands

As with the non ferrocene substituted hosts, charge transfer bands were observed in the spectra of **4.2**, **4.3, 4.5** and **4.6** with C_{60} in the range of 690-760 nm. UV-visible titrations measurements with higher concentration host solutions were performed in order to estimate any changes in electronic coupling due to the presence of the appended ferrocene moieties.

12.7.1 Charge Transfer and Electronic Coupling in Bis-Porphyrins 4.2 and 4.3

The electronic coupling estimations between the porphyrins and fullerene in both the free base and zinc derivatives of **4.2** and **4.3** are higher than the analogous non ferrocene bis-porphyrins. Changes of about 70-100 cm^{-1} indicated that the ferrocene groups have an effect on the electronic coupling between the hosts and fullerenes. UV-visible spectra of **4.2** and absorption spectra with the free host subtracted showing the CT Band is given in Figure 12.21. Estimation of electronic coupling between bis-porphyrin hosts **4.2**, **4.3** and **2.1** with C_{60} are shown in Table 12.6.

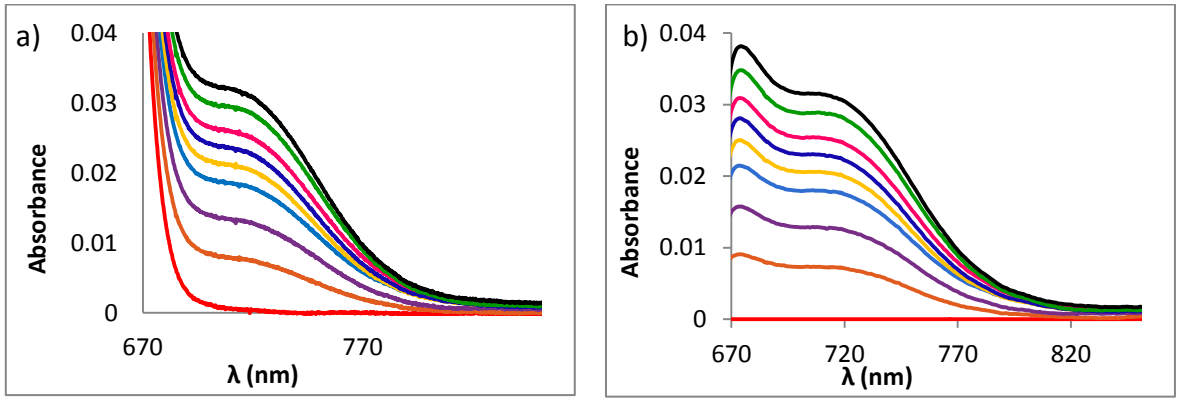

Figure 12.21: a) UV- visible spectra of **4.2** in toluene displaying the emergence of the charge transfer band at 715 nm with increasing concentration of C_{60} and b) the absorption spectra of **4.2** with the free host subtracted giving a better visualization of the charge transfer band.

Table 12.6: Estimation of electronic coupling constants between free base and zinc bis-porphyrin hosts **4.2, 4.3** and **2.1** and C_{60}.

COMPLEX	**2.1**	**Zn2.1**	**4.2**	**Zn4.2**	**4.3**	**Zn4.3**
Binding Constant (K)	18400	10100	18,100	10400	18700	9200
[Host]	1.85E-05	1.75E-05	1.95E-05	1.89E-05	1.46E-05	1.41E-05
[C_{60}]	1.30E-04	1.30E-04	1.58E-05	1.58-05	1.55E-04	1.58E-04
[Complex]	1.27E-05	9.62E-06	1.40E-05	1.13E-05	1.06E-05	8.14E-06
Absorbance height	0.0270	0.0223	0.032	0.028	0.026	0.023
V max (cm^{-1})	14060	12970	14180	13070	14180	13020
D V max (cm^{-1})	1600	2160	1950	2330	1950	2180
ε max	2200	2380	2220	2460	2450	2120
Rcc (Å)	6.25	6.25	6.25	6.25	6.25	6.25
V (cm^{-1})	**730**	**850**	**830**	**900**	**860**	**930**

12.7.2 Charge Transfer and Electronic Coupling in Bis-Porphyrins 4.5 and 4.6

Charge transfer bands were observed in the spectra of **4.5** and **4.6** with C_{60}**.** As with host **3.10**, estimation of the band positions and absorbance height was difficult. CT bands showed a blueshift in wavelength placing them partially under the last Q-band of the porphyrin. The lower association of the bis-porphyrin hosts for fullerenes made it difficult to estimate the electronic coupling of the pair, as a higher concentration of fullerene is required to see significant changes in the intensity of the charge transfer band. UV-visible spectra of **4.5** and the corrected absorption spectra showing the CT Band is shown in Figure 12.22 Estimation of electronic coupling between bis-porphyrins **4.5**, **4.6** as well as **3.10** with C_{60} are shown in Table 12.7.

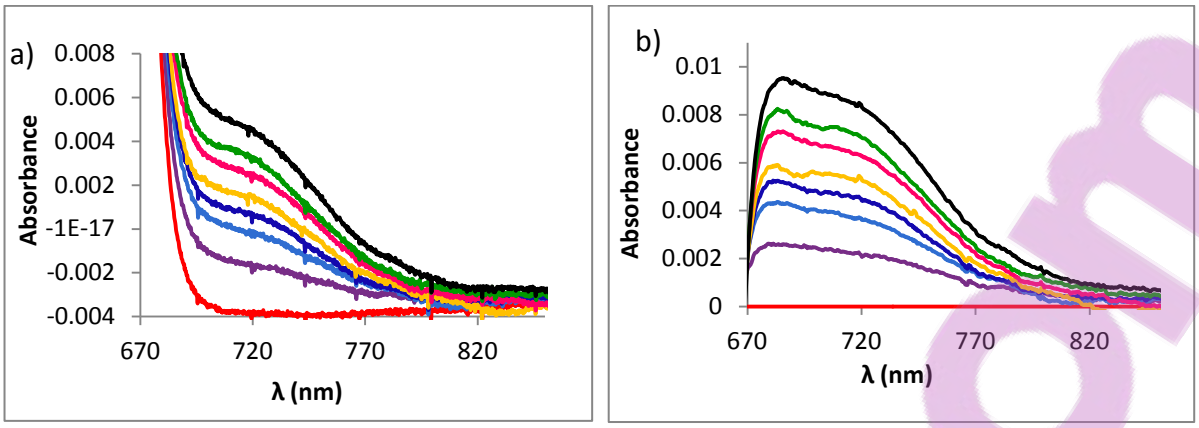

Figure 12.22: a) UV- visible spectra of **4.5** in toluene displaying the emergence of the charge transfer band at 710 nm with increasing concentration of C_{60} and b) the absorption spectra of **4.5** with the free host subtracted giving a better visualization of the charge transfer band.

The estimated electronic coupling between the bis-porphyrins **4.5** and **4.6** and C_{60} are higher than the analogous non ferrocene bis-porphyrin **3.10** by about 200 cm^{-1}. This indicates that the ferrocene groups have an effect on the electronic coupling between the hosts and the fullerenes.

Table 12.7: Estimation of electronic coupling constants between bis-porphyrin host **3.10**, **4.5** and **4.6** with C_{60}

COMPLEX	**3.10**	**4.5**	**4.6**
Binding Constant (K)	1840	1300	1700
[Host] (mol L^{-1})	1.64E-05	1.45E-05	1.17-5
[C_{60}] (mol L^{-1})	2.38E-04	2.13E-04	2.38E-04
[Complex] (mol L^{-1})	4.92E-06	3.1-06	3.34E-06
Absorbance height	0.0105	0.009	0.104
V max (cm^{-1})	14290	14330	14340
D V max (cm^{-1})	2080	2200	2240
ε max	2070	2900	2990
Rcc (Å)	6.25	6.25	6.25
V (cm^{-1})	**820**	**990**	**1020**

12.8 Summary

Four bis-porphyrins functionalized with ferrocene on the wide rim of the calixarene have been prepared by two different methods using palladium catalyzed coupling reactions. These have

been developed as a host for the complexation of fullerene to form supramolecular triads which can act as light harvesting dyes for solar energy conversion.

Bis-porphyrins **4.2** and **4.3** were prepared through coupling of acetylene functionalized ferrocene groups to iodocalixarenes via a Sonogashira reaction. Molecular modeling of the host shows no significant differences in the geometry of the calixarene and the porphyrin binding cavity upon appending the ferrocene groups but vary by the distance between the secondary donors and the porphyrins sensitizers. For host **4.2,** the distance between the ferrocene and porphyrin is approximately 16 Å. Though the addition of a phenyl rings as spacers in **4.3**, this distance increases to 21 Å. Bis-porphyrins **4.2** and **4.3** display binding constants with $C_{60,}$ C_{70} and $Lu_3N@C_{80}$ similar to that of the non-ferrocene functionalized bis-porphyrin host **2.1**. The ferrocene groups are appended to the aryl rings held in the wide angle by hydrogen bonding on that the narrow rim therefore no steric interactions between the ferrocenes groups can occur. Fluorescence spectra of the ferrocene hosts decrease by approximately 15% compared to **2.1**, demonstrating that there is an interaction between the secondary donor and the porphyrin sensitizer. The remote distance between ferrocene groups and the porphyrins suggests that the process of electron transfer will occur over energy transfer. Charge transfer bands have been observed for both **4.2** and **4.3** upon addition of C_{60}. Estimations of the electronic coupling between the porphyrin and the fullerene are higher by 80 cm^{-1} than the non ferrocene functionalized host.

Bis-porphyrins have been prepared through Suzuki coupling of ferrocene phenyl boronic acid to the wide rim bromo tetra-alkylated calixarenes. Two different isomers of the ferrocene functionalized bis-porphyrin host have been prepared by changing the order of alkylation before and after the bromination of the calixarene scaffold. The two isomers of the bis-porphyrin vary according to which aryl ring the secondary donor ferrocene is appended. Bis-porphyrin **4.5** has the ferrocene appended to the aryl ring alkylated on the narrow rim with *n*-butyl groups while **4.6** has the ferrocene appended on the aryl ring alkylated with the porphyrin amide. This change in the geometry of the ferrocene groups in the host may affect the process of secondary electron transfer within the triad system which will in turn affect the lifetime of the charge separated state.

From computational modeling, the ferrocene hosts display similar geometries to the non-ferrocene functionalized host **3.10**. There is a minor change in the calixarene scaffold in **4.5** where the aryl rings in the parallel orientation are functionalized with ferrocene. A slight

widening of the interplanar angle is observed which removes possible steric interactions between the ferrocene phenyl groups. The ^{1}H NMR of the two hosts are similar, with differences only in the proton signals of the substituted and unsubstituted aryl rings which shift downfield when *para* to the porphyrin amide. Such similarities between the proton signals on the calixarene scaffold, alkyl chain and porphyrins suggest that the calixarene adopt similar cone conformations, which is possible given the increased flexibility due to the tetra alkylation of the calixarene.

The UV-visible and fluorescence spectroscopy studies of **4.5** and **4.6** in toluene show the binding constants to be similar to **3.10.** Changing the solvent to a mixture of acetonitrile/toluene (1:1), increases the association of **4.5** and **4.6** with fullerenes by almost two orders of magnitude. The fluorescence intensities of **4.5** and **4.6** are similar to **3.10**, showing little quenching of the porphyrin emission due to the ferrocene donors. Porphyrin to fullerene charge transfer bands has been observed in the UV-visible spectra for both **4.5** and **4.6.** In a similar manner to **4.2** and **4.3,** the estimation of the electronic coupling between the two chromophores is higher than the unsubstituted host **3.10**.

12.9 Experimental

12.9.1 Synthetic Procedure for Bis-Porphyrins 4.2 and 4.3

5,17-Diiodo-25,27-bis[(tert-butoxycarbonyl)-methoxy]-26,28-dihydroxycalixarene (4.8)

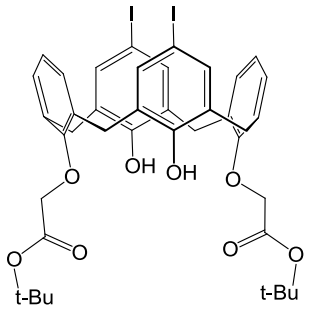

A solution of **4.7** (2.0 g, 3.06 mmol) and BTMA.ICl_2 (2.33 g, 6.75 mmol) in dichloromethane/methanol (200 mL: 80 mL) was stirred for 30 minutes. Calcium carbonate (1.50 g, 15.33 mmol) was added and the solution stirred at 25°C for 24 hours. The reaction was quenched with hydrochloric acid (12 M, 10 mL) and stirred with sodium thiosulfate (10%, 50 mL). The organic layer was washed with brine (3 x 50 mL), dried with sodium sulfate and the solvent removed *in vacuo*. The residue was recrystallized by dichloromethane/methanol to give **4.8** as a yellow solid, 2.08g, (75 %).

^{1}H NMR (400 MHz, $CDCl_3$) ppm: 7.35 (s, ArOH, 2H), 7.83 (s, ArH, 4H), 6.90 (d, ArH, J = 7.5 Hz, 4H), 6.81 (dd, ArH, J = 8.10, 6.8 Hz, 2H), 4.55 (s, O*C*H_2C$(CH_3)_3$, 4H), 4.39 (d, ArCH_2Ar J = 13.20 Hz, 4H), 3.31 (d, ArCH_2Ar, J = 13.20 Hz, 4H), 1.56 (s, C$(CH_3)_3$, 18H).

HRMS (ESI-TOF-MS) Calculated: $[M+Na]^+$: $C_{40}H_{42}I_2O_8Na$: 927.0861 m/z, found: 927.0735 m/z.

5,17-Di(ferrocene ethynyl)-25,27-bis[(tert-butoxycarbonyl)-methoxy]-26,28-dihydroxycalixarene (4.9)

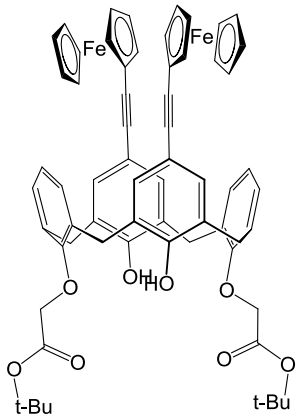

Iodocalixarene **4.8** (0.390 g, 0.43 mmol) and ethynyl ferrocene (0.200 g, 0.95 mmol) were dissolved in a mixture of DMF/triethylamine (1:1, 6 mL). The solution was degassed by three freeze-pump-thaw cycles and Pd(II)$(PPh_3)_2Cl_2$, copper iodide and triphenyl phosphine (5 mol % per iodo group) was added to the solution and backfilled with nitrogen three times. The mixture was stirred at 80°C for 36 hours. Dichloromethane was added to the solution and was washed with saturated ammonium chloride (3 x 50 mL). The organic layers were combined, dried with sodium sulfate and concentrated *in vacuo*. The crude material was then purified via column chromatography eluting with dichloromethane/ethyl acetate (3:1) to give **4.9** as an orange solid, 0.290 g (63%).

^{1}H NMR (400 MHz, $CDCl_3$) ppm: 7.87 (s, ArOH, 2H), 7.24 (s, ArH, 4H), 6.93 (d, ArH, J = 7.6 Hz, 4H), 6.70 (m, ArH, 2H), 4.55 (s, $OCH_2C(CH_3)_3$, 4H), 4.44 (m, CpH, 4H), 4.40 (d, $ArCH_2Ar$, J = 13.30 Hz, 4H), 4.24 (s, CpH, 10H), 4.20 (m, CpH, 4H), 3.35 (d, $ArCH_2Ar$, J = 13.30 Hz, 4H), 1.57 (s, $C(CH_3)_3$, 18H),

HRMS (ESI-TOF-MS): Calculated $[M+Na]^+$: $C_{64}H_{60}Fe_2NaO_8$: 1091.2885 m/z, found 1091.2847 m/z.

5,17-Di(ferrocene-ethynyl)-25,27-bis(carbonylmethoxy)-26,28-dihydroxycalixarene (4.10)

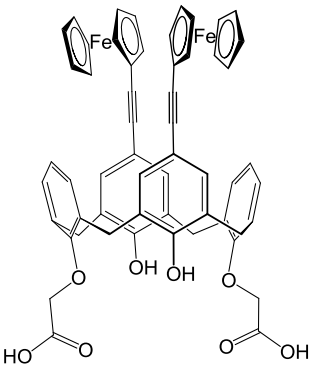

A solution of ester **4.9** (0.30 g, 0.28 mmol) and 10% sodium hydroxide (10 mL) in ethanol (50 mL) was refluxed for three hours. After cooling, the solution was acidified to pH 1 with hydrochloric acid (2 M) and extracted into dichloromethane (80 mL). The organic layer was washed with brine (3 x 50 mL) and dried with sodium sulfate. The solvent was removed *in vacuo* to give **4.10** as a orange solid, 0.244 g (91%).

^{1}H NMR (400 MHz, $CDCl_3$) ppm:7.27 (s, ArH, 4H),7.06 (d, ArH, J = 7.85 Hz, 4H), 6.94-6.89 (m, ArH, 2H), 4.72 (s, $OCH_2C(CH_3)_3$, 4H), 4.49 (s, Cp, 4H), 4.25 (s, Cp, 10H), 4.24 (s, Cp, 4H), 3.52 (d, $ArCH_2Ar$, J = 13.30 Hz, 4H), 4.14 (d, $ArCH_2Ar$, J = 13.30 Hz, 1H).

HRMS (ESI-TOF-MS): Calculated $[M+Na]^+$: $C_{56}H_{44}Fe_2NaO_8$: 979.1633 m/z, found: 979.1660 m/z.

5,17-Di(ferrocene-ethynyl)-25,27-bis[methoxy(4-amidophenyl)-15-tolyl-10,20-di-(3,5-di-tert-butylphenyl) porphyrin]-26-28-dihydroxycalixarene (4.2)

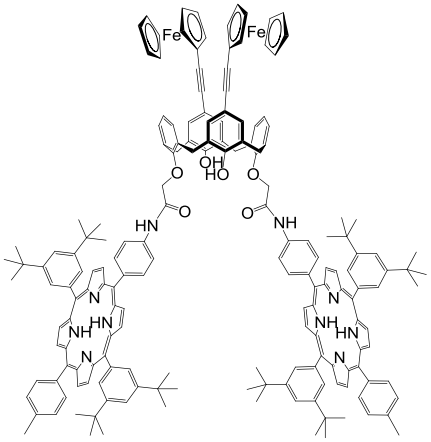

A solution of **4.10** (0.12 g, 0.125 mmol) and DCC (0.517 g, 0.2.51 mmol) in dry dichloromethane (25 mL) was stirred for 10 minutes. Amino-porphyrin **2.15** (0.22 g, 0.25 mmol) in dichloromethane (10 mL) was added. The mixture was stirred overnight and concentrated *in vacuo*. The residue was purified via flash chromatography, eluting with chloroform/hexane (19:1) and the solvent evaporated to give the bis-porphyrin **4.2** as a purple solid, 0.12 g (60%).

^{1}H NMR (400 MHz, $CDCl_3$) δ ppm: 10.92 (s, ArOH, 2H), 9.13 (d, H_β, J = 4.60 Hz, 4H), 9.08 (s, NHCO, 2H), 8.92 (d, H_β, J = 4.60 Hz, 4H), 8.81 (s, H_β, 8H), 8.30 (d, ArH, J = 8.65 Hz, 4H), 8.22 (d, ArH, J = 8.65 Hz, 4H), 8.06 (d, ArH, J = 8.00 Hz, 4H), 8.01 (s, ArH, 8H), 7.71 (s, ArH, 4H), 7.50 (m, ArH, 8H), 6.98 (d, *m*-ArH, J = 7.45 Hz, 4H), 6.68 (s, *p*-ArH, 2H), 4.95 (s, $OCH_2C(CH_3)_3$, 4H), 4.52 (t, Cp, J = 1.80, 1.80 Hz, 4H), 4.45 (d, $ArCH_2Ar$, J = 13.40 Hz, 4H), 4.22 (m, Cp, 14H), 3.72 (d, $ArCH_2Ar$, J = 13.40 Hz, 4H), -2.77 (s, NH, 4H)

HRMS (ESI-TOF-MS): Calculated $[M+2Na]^{2+}$: $C_{178}H_{170}Fe_2N_{10}Na_2O_8$: 1350.5896 m/z, found: 1350.5875 m/z., $[M+Na+H]^{2+}$: $C_{178}H_{171}Fe_2N_{10}NaO_8$: 1339.5990 m/z; Found: 1339.6870 m/z, $[M+2H]^{2+}$: $C_{178}H_{172}Fe_2N_{10}O_8$: 1328.6076 m/z; Found: 1328.6003 m/z, $[M+Na]^+$: $C_{178}H_{170}Fe_2N_{10}NaO_6$: 2678.1869 m/z, found: 2678.1297 m/z.

5,17-Di(ferrocene-ethynyl)-25,27-bis[methoxy(4-amidophenyl)-15-tolyl-10,20-di-(3,5-di-tert-butylphenyl) Zn(II) porphyrin]-26-28-dihydroxycalixarene (Zn4.2)

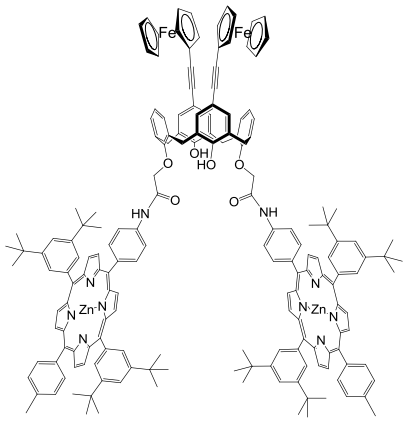

A saturated solution of zinc(II) acetate in methanol (0.5 mL) was added to a solution of bis porphyrin **4.2** (0.06 g, 0.075 mmol) in chloroform (20 mL) and the mixture was heated until no free-base porphyrin was observed in the UV-visible spectrum. The solvent was removed *in vacuo* and the residue was purified via flash chromatography, eluting with dichloromethane. The solvent was evaporated to give the zinc bis-porphyrin **Zn.4.2** as a purple solid, 0.058 g (95%).

^{1}H NMR (400 MHz, $CDCl_3$) ppm: 10.84 (s, ArOH, 2H), 9.17 (d, H_β, J = 4.8 Hz, 4H), 9.00 (s, NHCO, 2H), 8.95 (d, H_β, J = 4.8 Hz, 4H), 8.86-8.81 (m, H_β, 8H), 8.24 (d, ArH, J = 8.6 Hz, 4H), 8.16 (d, ArH, J = 8.6 Hz, 4H), 7.99 (d, ArH, J = 8.00 Hz, 4H), 7.94 (m, ArH, 8H), 7.63 (m, ArH, 4H), 7.43 (d, ArH, J = 8.00 Hz, 4H), 7.39 (s, ArH, 4H), 7.00 (d, ArH, J = 7.53 Hz, 4H), 6.76 (t, ArH, J = 7.21, 7.21 Hz, 2H), 4.88 (s, $OCH_2C(CH_3)_3$, 4H), 4.44 (m, Cp, 4H), 4.38 (d, $ArCH_2Ar$, J = 13.4 Hz, 4H), 4.16 (s, Cp, 10H), 4.16-4.14 (m, Cp, 4H), 3.65 (d, $ArCH_2Ar$, J = 13.4 Hz, 4H)

HRMS (ESI-TOF-MS): Calculated $[M+Na+H]^{2+}$: $C_{178}H_{166}Fe_2N_{10}O_8Zn_2$: 1389.5142 m/z, found: 1389.5109 m/z.

4-Iodophenylferrocene (4.12) [208]

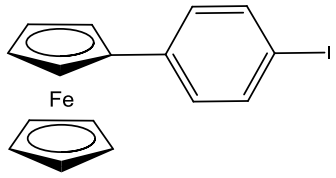

4-Iodoaniline (8.75g, 40.15 mmol) was suspended in a mixture of hydrochloric acid (24 mL) and water (100 mL), was cooled to 0 °C in an ice bath. The suspension was treated dropwise with a solution of sodium nitrite (6.04 g, 87.6 mmol) in water maintaining the temperature at 5 °C and stirred for a further 30 minutes. The aqueous solution slowly added to a solution of ferrocene (6.79 g, 36.5 mmol)) in dichloromethane (180 mL) at 0 °C. The reaction was stirred at 0 °C for one hour and then allowed to warm to room temperature with stirring for 16 hours. The aqueous layer was separated and washed with dichloromethane. The organic layers were combined washed with brine (3 x 100 mL) and dried with magnesium sulphate. The crude material was purified via column chromatography eluting with dichloromethane/hexane (1:1) and the solvent removed in vacuo to give and orange solid, 4.51 g (31%).

^{1}H NMR (400 MHz, $CDCl_3$) ppm: 7.58 (d, ArH, J= 8.10 Hz, 2H), 7.21(d, ArH, J= 8.10 Hz, 2H), 4.60 (t, CpH, J= 1.50 Hz, 2H), 4.32 (t, CpH, J= 1.50 Hz, 2H), 4.03 (s, CpH , 5H),

HRMS (FAB MS) Calculated $[M]^+$: $C_{16}H_{13}FeI$: 387.9411 m/z, found: 387.9420 m/z.

4-[2-(Trimethylsilane)ethynyl]phenyl ferrocene (4.13) [208]

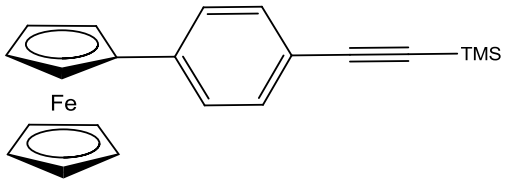

4.12 (1.8 g, 4.63 mmol), $Pd(PPh_3)_2Cl_2$ (0.04 g, 0.046mmol), copper iodide (0.01 g, 0.052 mmol) and trimethylsilylacetylene (0.78 mL, 5.56 mmol) in triethylamine/DMF (10 mL, 1:1) were taken through three freeze pump thaw cycles. The reaction mixture was heated at 90 °C for 16 hours. the reaction mixture was diluted with dichloromethane (100 mL), washed with water and dried with magnesium sulphate. The crude product was purified via column chromatography eluting with dichloromethane/hexane (1:10). The solvent was removed *in vacuo.* to give **4.13** as an orange solid, 1.58 g (90%).

^{1}H NMR (400 MHz, $CDCl_3$) ppm: 7.40 (4, ArH, 4H), 4.65 (t, CpH, J= 2.10 Hz, 2H), 4.34 (t, CpH, J= 2.10 Hz, 2H), 4.01 (s, CpH , 5H),0.26 (s, TMS, 4H)

HRMS (FAB MS) Calculated $[M]^+$: $C_{21}H_{22}FeSi$: 358.0840 m/z, found: 358.0851 m/z.

4-Ethynylphenyl ferrocene (4.14)[208]

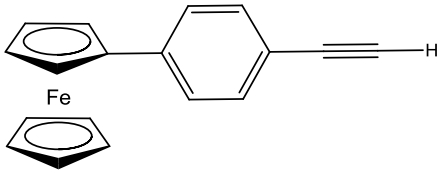

A mixture of **4.13** (1.56 g, 4.1 mmol) and potassium carbonate (2.0 g, 14.3 mmol) in methanol/water (12 ml, 5:1) was stirred at 25 °C for one hour. The reaction mixture was diluted with dichloromethane and wash with brine. The organic layer was dried and concentrated. The crude material was purified by column chromatography eluting with dichloromethane and the solvent removed *in vacuo* to give **4.14** as an orange solid, 1.4 g (95%).

^{1}H NMR (400 MHz, $CDCl_3$) ppm: 7.42 (s, ArH, 4H), 4.65 (s, CpH, 2H), 4.34 (s, 2H), 4.03 (s, CpH , 5H), 3.10(s, C≡CH, 1H).

HRMS (FAB MS) Calculated $[M]^+$: $C_{18}H_{14}Fe$: 286.0445 m/z, found: 286.0460 m/z.

5,17-Di[(4-ferrocenylphenyl)ethynyl]-25,27-bis[(tert-butoxycarbonyl)-methoxy]-26,28-dihydroxycalixarene (4.15)

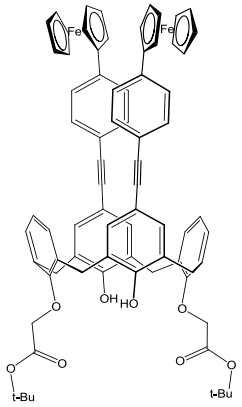

Iodocalixarene **4.8** (0.430 g, 0.61 mmol) and 4-ferrocenylphenyl acetylene **4.14** (0.40 g, 1.39 mmol) were dissolved in a mixture of DMF/triethylamine (1:1, 6 mL). The solution was degassed by three freeze-pump-thaw cycles and tetrakis(triphenylphosphine)palladium(0), copper iodide and triphenylphosphine (10 mol %) were added to the solution and backfilled with nitrogen three times. The mixture was stirred at 80°C for 36 hours and after this time dichloromethane (100 mL) was added to the solution and washed with saturated ammonium chloride (3 x 50 mL). The organic layers were dried with sodium sulfate and concentrated *in vacuo*. The crude material was then purified via column chromatography (dichloromethane/ethyl acetate (3:1) to give **4.15** as an orange solid, 0.427 g (55%).

^{1}H NMR (400 MHz, $CDCl_3$) δ ppm: 7.96 (s, ArOH, 2H), 7.43 (s, ArH, 8H), 7.30 (s, ArH, 4H), 6.93 (d, ArH, J = 7.6 Hz, 4H), 6.74 (m, ArH, 2H), 4.65 (m, Cp, 4H), 4.44 (d, $ArCH_2Ar$, J = 13.30 Hz, 4H), 4.57 (s, $OCH_2C(CH_3)_3$, 4H), 4.33 (s, Cp, 4H), 4.04 (s, Cp, 10H), 3.39 (d, $ArCH_2Ar$, J = 13.30 Hz, 4H), 1.57 (s, $C(CH_3)_3$, 18H).

HRMS (ESI-TOF-MS): Calculated $[M+Na]^+$: $C_{77}H_{68}Fe_2NaO_8$: 1243.3515 m/z, found 1243.3525 m/z.

5,17-Di[(4-ferrocenylphenyl)-ethynyl]-25,27-bis(carbonylmethoxy)-26,28-dihydroxycalixarene (4.16)

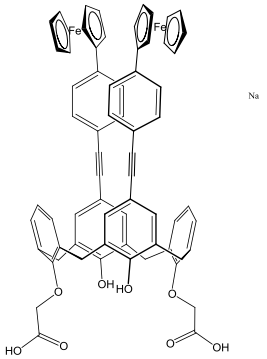

A solution of ester **4.15** (0.420 g, 0.349 mmol) and 10% sodium hydroxide (20 mL) in ethanol (60 mL) was refluxed for 3 hours. After cooling the solution was acidified to pH 1 with hydrochloric acid (2 M) and extracted into dichloromethane. The organic layer was washed with brine and dried with sodium sulfate and evaporated *in vacuo* to give **4.16** as a orange solid, 0.342 g (89%).

^{1}H NMR (400 MHz, $CDCl_3$) δ ppm: 7.43 (s, ArH, 8H), 7.34 (s, ArH, 4H), 7.03 (d, ArH, J = 7.40 Hz, 4H), 6.86 (t, ArH, J = 6.90 Hz, 2H), 4.73 (s, $OCH_2C(CH_3)_3$, 4H), 4.67 (s, CpH, 4H), 4.36 (s, CpH, 4H), 4.15 (d, $ArCH_2Ar$, J = 13.60 Hz, 4H), 4.05 (s, CpH, 10H), 3.52 (d, $ArCH_2Ar$, J = 13.34 Hz, 4H).

HRMS (ESI-TOF-MS): Calculated $[M+Na]^+$: $C_{68}H_{52}Fe_2NaO_8$: 1131.2287 m/z; found 1131.2294 m/z.

5,17-Di[(4-ferrocenylphenyl)-ethynyl]-25,27-bis[methoxy(4-amidophenyl)-15-tolyl-10,20-di-(3,5-di-tert-butylphenyl) porphyrin]-26-28-dihydroxycalixarene (4.3)

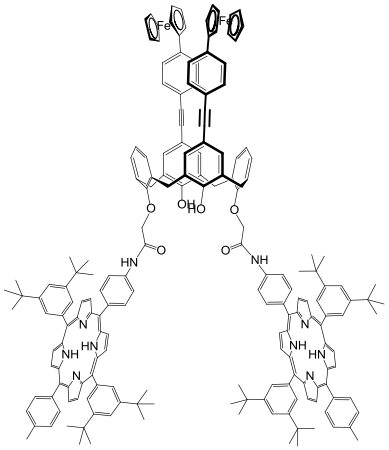

A solution of **4.16** (0.089 g, 0.08 mmol) and DCC (0.329 g, 1.6 mmol) in dry dichloromethane (10 mL) was stirred for ten minutes. Amino porphyrin **2.15** (0.140 g, 0.16 mmol) in dichloromethane (5 mL) was added. The mixture was stirred overnight and then concentrated *in vacuo*. The residue was purified via flash chromatography, eluting with chloroform/hexane (19:1) and solvent the evaporated to give the bis-porphyrin **4.3** as a purple solid, 0.096 g (43%).

^{1}H NMR (400 MHz, $CDCl_3$) δ ppm: 10.92 (s, ArOH, 2H), 9.12 (m, H_β, 4H), 8.91 (d, H_β, J = 4.80 Hz, 4H), 8.81 (s, H_β,8H), 8.31 (d, ArH, J = 8.60 Hz, 4H), 8.24 (d, ArH, J = 8.60 Hz, 4H), 8.06 (d, ArH, J = 8.80 Hz, 4H), 8.00 (d, ArH, J = 1.85 Hz, 8H), 7.70 (t, ArH, J=1.85 Hz, 4H), 7.51 (d, J = 8.80 Hz, 4H), 7.48 (s, ArH, 4H), 7.45 (s, ArH, 8H), 7.21 (d, ArH, J = 7.60 Hz, 4H), 7.04 (t, ArH, J = 7.60 Hz, 2H), 4.98 (s, $OCH_2C(O)$, 4H), 4.66 (t, CpH, J = 1.85 Hz, 4H), 4.48 (d, $ArCH_2Ar$, J = 13.60 Hz, 4H), 4.35 (t, CpH,J = 1.85 Hz, 4H), 4.04 (s, CpH, 10H), 3.76 (d, $ArCH_2Ar$,J = 13.60 Hz, 4H), 2.67 (s, 6H), 1.42 (s, $C(CH_3)_3$, 72H) -2.77 (s, NH, 4H).

HRMS (ESI-TOF-MS): Calculated $[M+Na+H]^{2+}$: $C_{190}H_{179}Fe_2N_{10}NaO_6$: 1438.1220 m/z; found: 1438.3480 m/z, $[M+Na]^+$ $C_{190}H_{178}Fe_2N_{10}NaO_6$: 2830.2530 m/z, found 2830.1895 m/z.

5,17-Di[(4-ferrocenylphenyl)-ethynyl]-25,27-bis[methoxy(4-amidophenyl)-15-tolyl-10,20-di-(3,5-di-tert-butylphenyl) Zn(II) porphyrin]-26-28-dihydroxycalixarene (Zn4.3)

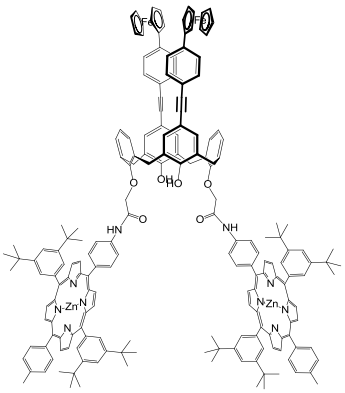

A saturated solution of zinc(II) acetate in methanol (0.5 mL) was added to a solution of bis porphyrin **4.2** (0.04 g, 0.075 mmol) in chloroform (20 mL) and the mixture was heated until no free-base porphyrin was observed in the UV-visible spectrum. The solvent was removed *in vacuo* and the residue was purified via flash chromatography, eluting with dichloromethane. The solvent was evaporated to give the zinc bis-porphyrin **Zn.4.2** as a purple solid, 0.038 g (92%).

^{1}H NMR (400 MHz, $CDCl_3$) δ ppm 10.92 (s, ArOH, 2H), 9.26 (d, H_β,*J* = 4.75 Hz, 4H), 9.14 (s, NH, 2H), 9.04 (d, H_β, *J* = 4.75 Hz, 4H), 8.92 (s, H_β,8H), 8.33 (d, ArH, *J* = 8.65Hz, 4H), 8.27 (d, ArH, *J* = 8.65 Hz, 4H), 8.08 (d, ArH, *J* = 7.95 Hz, 4H), 8.02 (d, ArH, *J* = 1.85 Hz, 8H), 7.71 (t, *J* = 1.85 Hz, 4H), 7.52 (d, ArH, *J* = 7.95 Hz, 4H), 7.50 (s, ArH, 4H), 7.46 (s, 8H), 7.21 (d, ArH, *J* = 7.60 Hz, 4H), 7.04 (t, ArH, *J* = 7.60 Hz, 2H), 4.99 (s, $OCH_2C(O)$, 4H), 4.68 (t, CpH, *J* = 1.80Hz, 4H), 4.49 (d, *J* = 13.60 Hz, 4H), 4.37 (t, CpH, *J* = 1.80Hz, 4H), 4.05 (s, CpH,10H), 3.77 (d, *J* = 13.60 Hz, 4H), 2.68 (s ,$ArCH_3$, 6H), 1.43 (s, $C(CH_3)_3$, 72H).

HRMS (ESI-TOF-MS): Calculated $[M+2Na]^{2+}$: $C_{190}H_{174}Fe_2N_{10}Na_2O_6Zn_2$: 1488.5354 m/z; found: 1488.5288 m/z, $[M+Na]^{2+}$ $C_{190}H_{175}Fe_2N_{10}NaO_6Zn_2$: 2954.0792 m/z, found 2954.1036 m/z.

12.9.2 Synthetic Procedure for Bis-Porphyrins 4.5 and 4.6

5,17-Dibromo-25,27-bisbutoxy-26,28-di[(ethoxycarbonyl)-methoxy]calixarene (4.19)

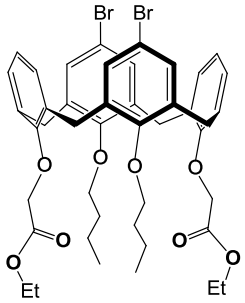

A solution of **4.17** (1.0 g, 1.32 mmol) and sodium carbonate (2.38 g, 13.3 mmol) in acetonitrile (60 mL) was stirred at room temperature for one hour. iodobutane (1.58 mL, 8.94 mmol) was then added and the mixture was refluxed for 40 hours. The mixture was allowed to cool to room temperature and sodium carbonate was removed by filtration through celite. The solvent was removed *in vacuo* and the residue was redissolved in ethanol (50) and concentrated HCl (5 mL) and the solution refluxed for a further two hours. Dichloromethane (40 mL) was then added and the organic phase was washed with saturated ammonium chloride (3 x 30 mL). The organic layer was dried over anhydrous sodium sulphate and concentrated. The product was purified by column chromatography eluting with dichloromethane/hexane 4:1. The solution was then evaporated to give **4.19** as a white solid, 0.72 g (62%).

^{1}H NMR (300 MHz, $CDCl_3$) δ ppm: 6.93 (d, ArH, J = 7.40 Hz, 4H), 6.86 (t, ArH, J = 7.40 Hz,2H), 6.52 (s, ArH, 4H), 4.73 (s, $OCH_2C(O)$, 4H), 4.64 (d, $ArCH_2Ar$, J = 13.70 Hz, 1H), 4.18 (q, $C(O)OC\underline{H}_2CH_3$, J = 7.10, 4H), 3.81 (t, $OC\underline{H}_2CH_2$, J = 7.0 Hz, 4H), 3.18 (d, $ArCH_2Ar$, J = 13.70 Hz, 4H), 1.83 (m, $OCH_2C\underline{H}_2$, 4H), 1.47 (m, $C\underline{H}_2CH_3$, 4H), 1.26 (t, $C(O)OCH_2C\underline{H}_3$, J = 7.10, 6H), 0.98 (t, $CH_2C\underline{H}_3$, J = 7.40 Hz, 6H).

HRMS (ESI-TOF-MS): Calculated $[M+Na]^+$: $C_{44}H_{50}NaBr_2O_8$: 899.1765 m/z, found: 899.1731 m/z.

5,17-Bis-4-phenylferrocenyl-25,27-bisbutoxy-26,28-bis[(ethoxycarbonyl)-methoxy]-calixarene (4.20)

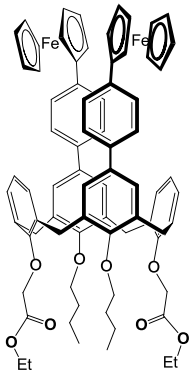

A mixture of tri-potassium phosphate (0.488 g, 2.31 mmol), tetrakis(triphenyl phosphine) palladium(0) (0.053 g, 0.046 mmol), **4.19** (0.200 g, 0.231 mmol) and ferrocenephenyl boronic acid (0.198 g, 0.648 mmol) in DMF (25 mL) was taken through three freeze pump thaw cycles. The solution was heated at 100°C for 16 hours. The reaction mixture was diluted with dichloromethane (60 mL), washed with water saturated ammonium chloride (3 x 30 mL) and dried with sodium sulphate. The solvent was removed *in vacuo* and the residue was purified via flash chromatography, eluting with dichloromethane. The solvent was evaporated to give **4.20** as an orange solid, 0.194 g (68%).

^{1}H NMR (300 MHz, *CDCl$_3$*) δ ppm: 7.31 (d, ArH, *J* = 8.20 Hz, 4H), 7.19 (d, ArH, *J* = 8.20 Hz, 4H), 7.00 (s, ArH, 4H), 6.56 (m, ArH, 6H), 4.70 (d, $ArCH_2Ar$ + $OCH_2C(O)$, *J* = 13.40 Hz, 8H), 4.56 (t, CpH, 1.80 Hz, 4H), 4.20 (m, CpH+ $C(O)OC\underline{H}_2CH_3$, 8H), 4.05 (t, $OC\underline{H}_2CH_2$, *J* = 7.70Hz, 4H), 4.01 (s, CpH 10H), 3.30 (d, $ArCH_2Ar$, *J* = 13.40 Hz, 4H), 1.95 (m, 4H), 1.46 (m, 4H), 1.33 (t, $C(O)OCH_2C\underline{H}_3$, 7.10 Hz, 6H), 1.02 (t, $CH_2C\underline{H}_3$, *J* = 7.40 Hz, 6H).

HRMS (ESI-TOF-MS): Calculated $[M+Na]^+$: $C_{76}H_{76}Fe_2NaO_8$: 1251.4107 m/z, found: 1251.4096 m/z.

5,17-Bis-4-phenylferrocenyl-25,27-bisbutoxy-26,28-bis(carbonyl-methoxy)calixarene (4.21)

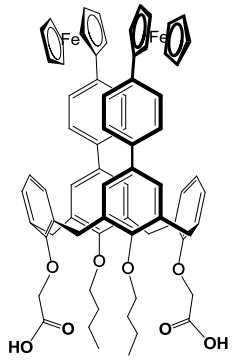

A solution of calixarene **4.20** (0.190 g, 0.157 mmol) and 10% sodium hydroxide (3mL) in tetrahydrofuran (20 mL) was refluxed for one hour. After cooling the solution was diluted dichloromethane (20 mL) washed with saturated ammonium chloride (3 x 15 mL). The organic layer was dried with sodium sulfate and evaporated *in vacuo* to give **4.21** as an orange solid, 0.136 g (86%).

^{1}H NMR (300 MHz, *CDCl$_3$*) δ ppm 7.24 (d, ArH, *J* = 8.20 Hz, 4H), 7.14 (d, ArH, *J* = 8.31 Hz, 4H), 7.11-7.06 (m, ArH, 2H), 6.72 (d, ArH, *J* = 8.30 Hz, 4H), 6.62 (s, ArH, 4H), 4.76 (s, $OCH_2C(O)$, 4H), 4.42 (m, CpH+ $ArCH_2Ar$, 8H), 4.21-4.18 (m, CpH, 4H), 3.98 (d, $OC\underline{H}_2CH_2$, *J* = 7.77 Hz, 4H), 3.94 (s, CpH, 10H), 3.41 (d, $ArCH_2Ar$ *J* = 13.30 Hz, 4H), 1.99-1.84 (m, $OCH_2C\underline{H}_2$ 4H), 1.40 (m,$C\underline{H}_2CH_3$, 4H), 0.99 (t, $CH_2C\underline{H}_3$*J* = 7.35 Hz, 6H).

HRMS (ESI-TOF-MS): Calculated: $[M+Na]^+$:$C_{72}H_{68}$ Fe_2O_8Na: 1195.3509 m/z, found: 1195.3528 m/z.

5,17-Bis-4-phenylferrocenyl-25,27-bisbutoxy-26,28-dimethoxy-(4-amidophenyl)-15-tolyl-10,20-di-(3,5-di-*tert*-butylphenyl)-porphyrin-calixarene (4.5)

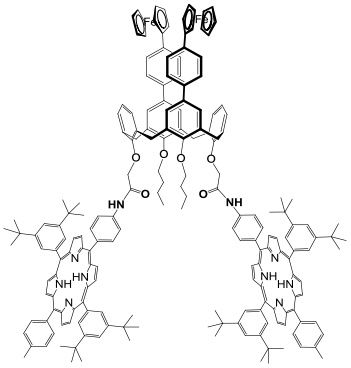

A solution of diacid **4.21** (0.037 g, 0.057), DMAP (0.003 g, 0.022 mmol) mmol and porphyrin **2.15** (0.10 g, 0.15 mmol) in THF (10 mL) was stirred at room temperature under nitrogen for ten minutes. DIC (0.08 mL, 0.45 mmol) was added and the solution stirred for a further ten minutes. HOBt (0.061 g, 0.45 mmol) was added and the solution stirred for 18 hours. The solvent was removed *in vacuo* and the product purified via flash chromatography, eluting with toluene/ethyl acetate (9:1) and the solvent removed to give **4.5** as a purple solid, 0.069 g (48%).

^{1}H NMR (400 MHz, *CDCl$_3$*) δ ppm 9.50 (s, NH, 2H), 8.87 (d, H$_\beta$, *J* = 4.90 Hz, 4H), 8.85-8.81 (m, H$_\beta$, 12H), 8.28 (d, ArH, *J* = 8.40 Hz, 1H), 8.15 (d, ArH, *J* = 8.40 Hz, 4H), 8.08 (d, ArH, *J* = 7.90 Hz, 4H), 8.01 (d, *J* = 1.75 Hz, 8H), 7.71 (t, *J* = 1.74Hz, 4H), 7.53 (d, ArH, *J* = 7.90 Hz, 4H), 7.14 (d, ArH, *J* = 8.40 Hz, 4H), 6.99-6.95 (m, ArH, 6H), 6.86 (s, ArH, 4H), 5.04 (s, $OCH_2C(O)$, 4H), 4.80 (d, ArCH2Ar, *J* = 13.70 Hz, 4H), 4.48 (m, CpH, 4H), 4.22 (m, CpH, 4H), 3.98-3.97 (m, CpH +O$\underline{CH_2}CH_2$, 14H), 3.56 (d, ArCH2Ar, *J* = 13.70 Hz, 4H), 2.69 (s, $ArCH_3$, 6H), 2.04-1.95 (m, OCH_2CH_2, 4H), 1.43 (s, $C(CH_3)_3$ +CH_2CH_3, 76H), 0.98 (t CH_2CH_3, J=7.40, 6H),-2.76 (s, NH, 4H).

HRMS (ESI-TOF-MS): Calculated: $[M+2Na]^{2+}$: $C_{194}H_{194}Fe_2N_{10}Na_2O_6$: 1458.6838 m/z, Found: 1458.6870 m/z; $[M+Na+H]^{2+}$: $C_{194}H_{194}Fe_2N_{10}NaO_6$: 1448.6925 m/z, Found:1448.7021 m/z.

5,17-Dibromo-25,27-bis[(ethoxycarbonyl)-methoxy]-26,28-dibutoxy-calixarene (4.23)

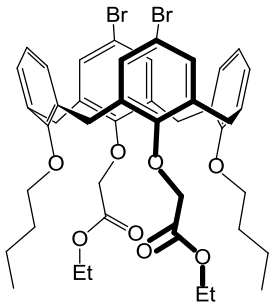

A solution of **4.22** (1.2 g, 1.73 mmol) and sodium carbonate (3.03 g, 17.34 mmol) in acetonitrile (80 mL) was stirred at room temperature for one hour. Ethyl bromoacetate (2.78 mL, 11.27 mmol) was then added and the mixture was refluxed for 40 hours. The mixture was allowed to cool to room temperature and sodium carbonate was removed by filtration through celite. The solvent was removed *in vacuo* and the residue was redissolved in ethanol (50 mL) and concentrated HCl (5 mL) and the solution refluxed for a further two hours. Dichloromethane (60 mL) was then added and the organic phase was washed with saturated ammonium chloride (3 x 30 mL). The organic layer was dried over anhydrous sodium sulphate and concentrated. The product was purified by column chromatography eluting with dichloromethane/hexane 4:1. The solution was then evaporated to give **4.23** as an off white solid, 0.58 g (59%).

^{1}H NMR (300 MHz, *CDCl$_3$*) δ ppm: 7.10 (s, ArH, 4H), 6.40 (m, ArH, 2H), 6.33 (d, ArH, *J* = 7.40 Hz, 4H), 4.73 (s, $OCH_2C(O)$, 4H), 4.63 (d, $ArCH_2Ar$, *J* = 13.70 Hz, 5H), 4.20 (q, $C(O)OC\underline{H}_2CH_3$, *J* = 7.10 Hz, 4H), 3.79 (t, $OC\underline{H}_2CH_2$, *J* = 7.0 Hz, 4H), 3.17 (d, $ArCH_2Ar$, *J* = 13.70 Hz, 4H), 1.76 (m, $OCH_2C\underline{H}_2$, 4H), 1.47 (m, $C\underline{H}_2CH_3$, 4H), 1.28 (t, $C(O)OCH_2C\underline{H}_3$, 7.10 Hz, 6H), 0.98 (t, $CH_2C\underline{H}_3$, 7.40 Hz, 6H).

HRMS (ESI-TOF-MS): Calculated: $[M+Na]^+$: $C_{44}H_{50}NaBr_2O_8$: 899.1765 m/z ,found: 899.1744 m/z.

5,17-Bis-4-phenylferrocenyl-25,27-bis[(ethoxycarbonyl)-methoxy]-26,28-dibutoxy-calixarene (4.24)

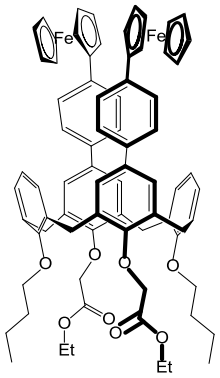

A mixture of **4.23** (0.200 g, 0.231 mmol), tri-potassium phosphate (0.488 g, 2.31 mmol), tetrakis(triphenyl phosphine) palladium(0) (0.053 g, 0.046 mmol) and ferrocenephenyl boronic acid (0.198 g, 0.648 mmol) in DMF (25 mL) was taken through three freeze pump thaw cycles. The solution was heated at 100°C for 16 hours. The reaction mixture was diluted with dichloromethane (60 mL), washed with water saturated ammonium chloride (3 x 30 mL) and dried with sodium sulphate. The solvent was removed *in vacuo* and the residue was purified via flash chromatography, eluting with dichloromethane. The solvent was evaporated to give **4.24** as an orange solid, 0.194 g (68%).

^{1}H NMR (400 MHz, $CDCl_3$) δ ppm: 7.55 (dd, ArH, *J* = 16.64, 8.05 Hz, 8H), 7.37 (s, ArH, 4H), 6.27 (m, ArH 6H), 4.88 (s, $OCH_2C(O)$, 4H), 4.78 (d, $ArCH_2Ar$, *J* = 13.40 Hz, 4H), 4.68 (s, Cp, 4H), 4.33 (s, Cp, 4H), 4.21 (q, $C(O)OC\underline{H}_2CH_3$, *J* = 7.0 Hz, 1H), 4.05 (s, Cp, 10H), 3.81 (t, $OC\underline{H}_2CH_2$, *J* = 6.70 Hz, 4H), 3.31 (d, $ArCH_2Ar$, *J* = 13.40 Hz, 4H), 1.83 (m, $OCH_2C\underline{H}_2$, 4H), 1.54 (m, $C\underline{H}_2CH_3$, 4H), 1.30 (t, $C(O)OCH_2C\underline{H}_3$, *J* = 7.20 Hz, 6H), 1.01 (t, $CH_2C\underline{H}_3$, *J* = 7.40 Hz, 6H).

HRMS (ESI-TOF-MS): Calculated: $[M+H]^+$ $C_{76}H_{76}Fe_2O_8$: 1228.4257 m/z, found 1228.4238 m/z, $[M+Na]^+$ $C_{76}H_{75}Fe_2NaO_8$: 1251.4136 m/z ,found 1251.4096 m/z.

5,17-Bis-4-phenylferrocenyl-25,27-bis-(carbonyl-methoxy)-26,28-dibutoxy-calixarene (4.25)

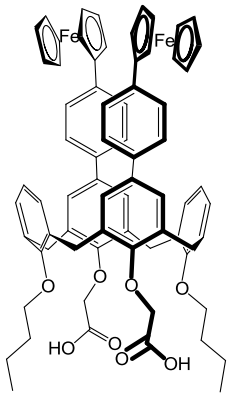

A solution of calixarene **4.24** (0.190 g, 0.157 mmol) and 10% sodium hydroxide (3mL) in tetrahydrofuran (20 mL) was refluxed for one hour. After cooling the solution was diluted dichloromethane (20 mL) washed with saturated ammonium chloride (3 x 15 mL). The organic layer dried with sodium sulfate and evaporated *in vacuo* to give **4.25** as an orange solid, 0.136 g (86%).

^{1}H NMR (300 MHz, *$CDCl_3$*) δ ppm 7.59 (s, ArH, 8H), 7.47 (m, ArH, 4H), 6.46 (s, ArH, 4H), 4.77 (s, $OC\underline{H}_2C(O)$, 4H), 4.74-4.65 (m, CpH, 4H), 4.42 (d, $ArC\underline{H}_2Ar$, J = 13.30 Hz, 4H), 4.36 (s, CpH, 4H), 4.08 (s, CpH, 10H), 3.99-3.90 (m, $OC\underline{H}_2CH_2$, 1H), 3.42 (d, $ArC\underline{H}_2Ar$, J = 13.40 Hz, 4H), 1.99-1.82 (m, $OCH_2C\underline{H}_2$, 4H), 1.41 (m, $C\underline{H}_2CH_3$, 4H), 0.99 (t, $CH_2C\underline{H}_3$, J = 7.35 Hz, 6H).

HRMS (ESI-TOF-MS): Calculated: $[M+Na]^+$:$C_{72}H_{68}$ Fe_2O_8Na: 1195.3509 m/z, found: 1195.3589 m/z.

5,17-Bis-4-phenylferrocenyl-25,27-bis- [methoxy(4-amidophenyl)-15-tolyl-10,20-di-(3,5-di-*tert*-butylphenyl) porphyrin]-26,28-dibutoxy-calixarene (4.6)

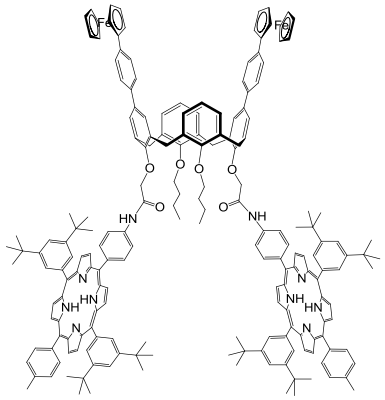

A solution of calixarene diacid **4.26** (0.037 g, 0.057), DMAP (0.003 g, 0.022 mmol) and porphyrin **2.15** (0.10 g, 0.15 mmol) in THF (10 mL) was stirred at room temperature under nitrogen for 10 minutes. DIC (0.08 mL 0.45 mmol) was added in and the solution stirred for a further ten minutes. HOBt (0.061 g, 0.45 mmol) was added and the solution stirred for 18 hours. The solvent was removed *in vacuo* and the product purified via flash chromatography, eluting with toluene/ethyl acetate (9:1) and the solvent removed to give **4.5** as a purple solid, 0.069 g (48%).

^{1}H NMR (400 MHz, *$CDCl_3$*) δ ppm 9.85 (s, NH, 2H), 8.95 (d, H_β, J = 4.70 Hz, 4H), 8.92-8.83 (m, H_β, 12H), 8.34 (d, ArH, J = 8.40, Hz, 4H), 8.21 (d, ArH, J = 8.40 Hz, 4H), 8.10 (d, ArH, J = 8.15 Hz, 4H), 8.07 (d, ArH, J=1.85Hz, 8H) 7.77 (t, ArH, J=1.85Hz, 4H), 7.71(d, ArH, J= 4.30 Hz , 4H), 7.62 (m ,ArH , 8H), 7.54 (d, ArH, J = 7.90 Hz, 4H), 6.46-6.40 (m, ArH, 2H), 6.33 (d, ArH,J = 7.60 Hz, 4H), 5.32 (s, $OCH_2C(O)$, 4H), 4.87 (d, $ArCH_2Ar$, J = 13.85 Hz, 1H), 4.71 (s, 1H), 4.35 (s, Cp, 4H), 4.09 (s, Cp 10H), 4.02-3.98 (m, OCH_2CH_2, 4H), 3.61 (d, $ArCH_2Ar$, J = 13.85 Hz, 1H), 2.69 (s,CH_3, 6H), 1.90-1.81 (m, $OCH_2C\underline{H_2}$ 1H), 1.50 (s, $C(CH_3)_3$ +$\underline{CH_2}CH_3$, 78H), 0.96 (t, $CH_2C\underline{H_3}$, J = 7.40 Hz, 6H), -2.71 (s, NH, 4H).

HRMS (ESI-TOF-MS): Calculated: $[M+2Na]^{2+}$: $C_{194}H_{194}Fe_2N_{10}Na_2O_6$: 1458.6835 m/z. found: 1458.6797 m/z, : $[M+Na]^+$: $C_{194}H_{194}Fe_2N_{10}NaO_6$: 2894.377 m/z. found: 2894.3733 m/z,

12.9.3 General Information and Crystallographic Tables for Single Crystal X-ray Diffraction

Single crystal X-ray diffraction data for **4.9, 4.23** and **4.24** were collected on a Bruker Smart APEX2 CCD diffractometer using graphite monochromated Mo Kα radiation. The structures were solved using direct methods (SHELXS-97).[173,174] Non hydrogen atoms were refined anisotropically (SHELXL-97) [174] and H atoms were refined using a riding model, with C-H =0.93-0.97 Å and Ui_{so}(H)=1.2Ueq(C), 1.5U_{eq}(methyl C) or 1.5U_{eq}(O).

Table 12.8: Crystal data and structure refinement for **4.9**.

Empirical formula	$C_{134.50}\ H_{122.50}\ C_{l20}\ Fe_4\ O_{16}$	
Formula weight	2927.22	
Temperature	98(2) K	
Wavelength	0.71073 Å	
Crystal system	Triclinic	
Space group	P-1	
Unit cell dimensions	a = 14.4762(3) Å	α= 96.0260(10)°.
	b = 16.6587(3) Å	β= 92.8300(10)°.
	c = 29.1870(6) Å	γ = 107.4310(10)°.
Volume	6654.0(2) $Å^3$	
Z	2	
Density (calculated)	1.461 Mg/m^3	
Absorption coefficient	0.892 mm^{-1}	
F(000)	3003	
Crystal size	0.33 x 0.1 x 0.07 mm^3	
Theta range for data collection	0.70 to 28.06°.	
Index ranges	-19<=h<=19, -22<=k<=21, -38<=l<=38	
Reflections collected	121698	
Independent reflections	31498 [R(int) = 0.0936]	
Completeness to theta = 28.06°	97.5 %	
Absorption correction	Semi-empirical from equivalents	
Max. and min. transmission	0.939 and 0.716	
Refinement method	Full-matrix least-squares on F^2	
Data / restraints / parameters	31498 / 0 / 1605	
Goodness-of-fit on F^2	1.027	
Final R indices [I>2sigma(I)]	R1 = 0.0691, wR2 = 0.1612	
R indices (all data)	R1 = 0.1413, wR2 = 0.1956	
Largest diff. peak and hole	2.236 and -1.260 e.$Å^{-3}$	

Table 12.9: Crystal data and structure refinement for **4.23**.

Empirical formula	$C_{44}\ H_{50}\ Br_2\ O_8$	
Formula weight	866.6821	
Temperature	93(2) K	
Wavelength	0.71073 Å	
Crystal system	Monoclinic	
Space group	C2/c	
Unit cell dimensions	a = 20.476(5) Å	α= 90.000(5)°.
	b = 20.604(5) Å	β= 114.477(5)°.
	c = 20.763(5) Å	γ = 90.000(5)°.
Volume	7972(3) $Å^3$	
Z	8	
Density (calculated)	1.444 Mg/m^3	
Absorption coefficient	2.087 mm^{-1}	
F(000)	3584	
Crystal size	0.45 x 0.38 x 0.38 mm^3	
Theta range for data collection	1.47 to 27.92°.	
Index ranges	-26<=h<=26, -27<=k<=26, -27<=l<=27	
Reflections collected	72694	
Independent reflections	9530 [R(int) = 0.0458]	
Completeness to theta = 27.92°	99.8 %	
Absorption correction	Semi-empirical from equivalents	
Max. and min. transmission	0.452 and 0.407	
Refinement method	Full-matrix least-squares on F^2	
Data / restraints / parameters	9530 / 0 / 491	
Goodness-of-fit on F^2	1.038	
Final R indices [I>2sigma(I)]	R1 = 0.0351, wR2 = 0.0854	
R indices (all data)	R1 = 0.0601, wR2 = 0.1009	
Largest diff. peak and hole	1.766 and -0.422 $e.Å^{-3}$	

Table 12.10: Crystal data and structure refinement for **4.24**

Empirical formula	C_{88} H_{88} Fe_2 O_8	
Formula weight	1385.28	
Temperature	93(2) K	
Wavelength	0.71073 Å	
Crystal system	Monoclinic	
Space group	C2/c	
Unit cell dimensions	a = 35.1454(11) Å	α= 90°.
	b = 11.3064(3) Å	β= 107.980(2)°.
	c = 18.5404(5) Å	γ = 90°.
Volume	7007.6(3) $Å^3$	
Z	4	
Density (calculated)	1.313 Mg/m^3	
Absorption coefficient	0.474 mm^{-1}	
F(000)	2928	
Crystal size	0.12 x 0.09 x 0.02 mm^3	
Theta range for data collection	1.90 to 28.03°.	
Index ranges	-46<=h<=46, -14<=k<=14, -24<=l<=24	
Reflections collected	58895	
Independent reflections	8449 [R(int) = 0.1832]	
Completeness to theta = 28.03°	99.6 %	
Absorption correction	Semi-empirical from equivalents	
Max. and min. transmission	0.991 and 0.950	
Refinement method	Full-matrix least-squares on F^2	
Data / restraints / parameters	8449 / 12 / 437	
Goodness-of-fit on F^2	1.001	
Final R indices [I>2sigma(I)]	R1 = 0.0689, wR2 = 0.1371	
R indices (all data)	R1 = 0.1592, wR2 = 0.1725	
Largest diff. peak and hole	0.635 and -0.511 e.Å	

Chapter 5

Wide Rim Appended Ferrocene Bis-Porphyrins Prepared by Amide Coupling

5.1 Introduction

Palladium catalyzed reactions are an excellent method for carbon-carbon bond formation and for the direct connection of ferrocene to the wide rim of the calixarene. Attachment of the ferrocene groups to the wide rim of the calixarene places the secondary donors a significant distance from the porphyrin sensitizers, allowing a multistep electron transfer to take place. The remote distance of the ferrocene from the porphyrin should prevent energy transfer from the ferrocene to the porphyrin and promote electron transfer. This will increase the life time of the charge separated state required for solar energy conversion.

An alternative method for appending ferrocene functional groups to the wide rim of calixarenes is through coupling of ferrocene carboxylic acid derivatives to wide rim amino functionalized calixarenes via the formation of an amide bond. Several wide and narrow rim ferrocene and cobaltocenium amide coupled calixarenes have been reported in literature.[106,109,187,216-219] Beer and co workers have prepared a number of wide rim amide calixarenes to investigate anion recognition.[106,218,219] Wide-rim bis-cobaltocenium/ferrocene calixarene receptors **5.1, 5.1b** and **5.2** as well as a cobaltocenium-bridged calixarene derivative **5.3** have been prepared. These calixarene hosts have been shown to form complexes with carboxylate anions, dihydrogen phosphate and halide anions to different extents based upon the degree of preorganization of the wide-rim anion recognition site. The level of preorganization of the calixarene scaffold is dictated by intramolecular hydrogen bonding on the narrow rim of the calixarene by the relative positioning of narrow-rim tosyl substituents.

Tomapatanaget *et al*. has prepared ferrocene bridged calixarenes **5.4a-c** on a tetra alkylated calixarene scaffold to act as an ion-pair receptor and sensor.[220,194] The narrow rims are alkylated with ethyl esters which act as a cation binding sites, while the wide rim amide units act as anion receptors. A bridging ferrocene attached to the amides act as an electrochemical sensor. The variation of the pendant chains on the narrow rim of the calixarene allows for increased flexibility of the calixarene rings. Problems do arise with tetra-alkylation on the narrow rim as the conformational flexibility of the calixarene increases due to removal of the hydrogen bonding motif. Alkylation with methyl groups has shown the calixarene to interconvert from cone to partial cone conformation, while tetra-alkylation with ethyl esters prevented phenyl ring rotation.

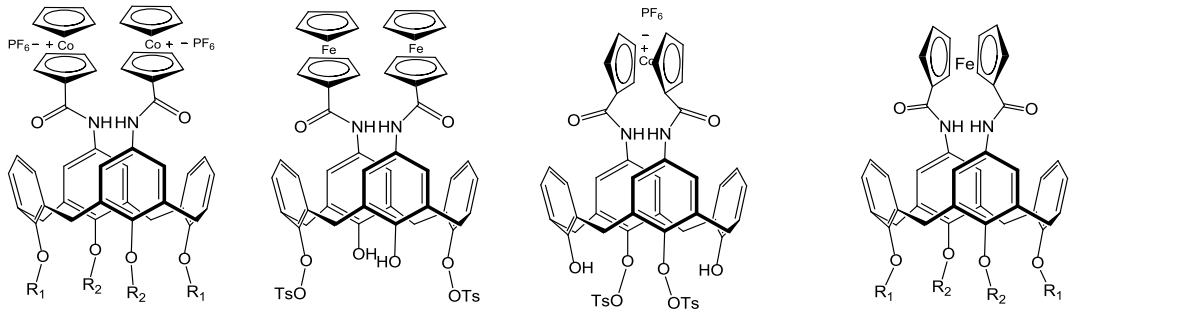

5.1a R_1= H , R_2= Ts
5.1b R_1= Ts , R_2= H

5.2

5.3

5.4a R_1= CH_3 , R_2= CH_3
5.4b R_1= CH_3 , R_2= CH_2COOEt
5.4c R_1= CH_2COOEt, R_2= CH_2COOEt

Figure 5.1: Various wide rim ferrocene amide functionalized calixarenes prepared for anion and cation sensing

5.2 Aims and Strategy

This chapter describes the synthesis of bis-porphyrins appended with ferrocene groups on the wide rim of the calixarene via an amide bond. Reported first in this chapter is the attempted synthesis of ferrocene appended calixarene bis-porphyrin, **5.5.** This host is dialkylated on the narrow rim and has unprotected hydroxyl groups *para* to the amides. Several methods for the reduction of the nitro substituents *para* to the hydroxyl groups were attempted and were successful in the formation of the amino calixarene. The instability of the amino calixarene however, resulted in decomposition during aqueous workup.

In an attempt to overcome problems in the stability of the amino calixarenes it was decided that protection of the phenolic hydroxyl groups on the narrow rim would be required. A secondary alkylation of the hydroxyl groups was performed prior to the reduction of the two *para* nitro groups. Tetra-alkylation of the calixarene with different groups allows for the opportunity to change the of the order of alkylation and in turn the final position of the appended ferrocene in the bis-porphyrin host. This change in final position of the ferrocene groups on the wide rim of the calixarene may lead to different lifetimes of the multistep charge separated state.

Two reaction pathways have been developed for the synthesis of the wide rim amide functionalized ferrocene bis-porphyrins. These pathways differ in the order of addition of the alkyl groups in a similar manor to the dibrominated calixarene scaffolds **4.4** and **4.5**. Bis-porphyrin **5.6** was prepared by alkylation of the calixarene first with ethyl bromo acetate which

is followed by nitration and a second alkylation with iodobutane, which results in the ferrocene amide being appended to the aryl ring of the calixarene *para* to the *n*-butyl groups. Bis porphyrin **5.7** was alkylated in the opposite order which resulted in the ferrocene amide being appended to the aryl ring of the calixarene *para* to the porphyrin amide.

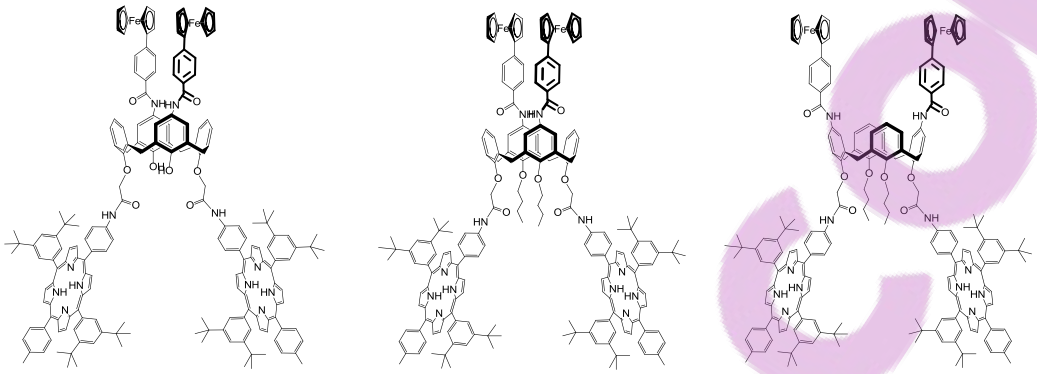

5.5 **5.6** **5.7**

Figure 5.2: Attempted ferrocene functionalized bis-porphyrin host **5.5** and the hosts **5.6** and **5.7** made in Chapter Five

The amino porphyrin employed in the synthesis of **5.6** and **5.7** was the 5-(4-aminophenyl)-15-tolyl-10,20-bis(3,5-di-*tert*-butylphenyl)porphyrin **2.15**. Porphyrin **2.15** provides a number of close contacts to bound fullerenes via CH-π interactions from the *tert*-butyl methyl groups which increase the porphyrin–fullerene association in comparison to tetra-phenyl porphyrins. The tolyl methyl observed as singlet at 2.38 ppm provides a good ^{1}H NMR fingerprint for the identification of the bis-porphyrin, integrating for six protons.

Computational models of bis-porphyrins have been employed to investigate possible changes in the geometry of the calixarene scaffold due to the appending of ferrocene groups to the wide rim. Binding constant measurements have been carried out using UV-visible titrations in toluene and acetonitrile/toluene (1:1) and are reported. Fluorescence spectra have been recorded for the ferrocene appended host to see if there are any changes in the porphyrin fluorescence from energy or electron transfer to the ferrocene.

5.3 Computational Modeling of Bis-Porphyrins 5.6 and 5.7

Hosts **5.6** and **5.7** were studied using computational molecular modeling in order to understand possible differences in geometry and determine the spatial distance between the secondary

electron donor, ferrocene and the porphyrin sensitizer. Geometry optimizations of the host-guest complex were carried out using a two layer ONIOM method as described in Chapter Two. The calixarene scaffold, and the amide linkers and the ferrocene groups were modeled in the high layer by the DFT model with the B3LYP functional and a 631-G(d) basis set. The porphyrins and C_{60} were described in the low layer with molecular mechanics, which more adequately models the porphyrin-fullerene interaction. Nickel porphyrins were utilized in the computational modeling to help maintain planarity of the porphyrin versus unmetallated porphyrins.

As with the previous hosts **4.4** and **4.5**, the amide coupled hosts still maintain the same pinched cone conformation as the non substituted host **3.10.** However in comparison to **4.4** and **4.5** there are no significant differences in the calixarene cone angles. In both **5.6** and **5.7**, the porphyrin amide functionalized rings adopts a pinched cone orientation with a wide angle of 68° and the *n*-butyl functionalized ring being in a parallel orientation with an angle of 15°.

The amide phenyls at the 5-position of the porphyrin are orientated towards each other at an angle of 64° for both **4.4** and **4.5**. These changes translate in the porphyrins geometry with the porphyrins tilted towards each other in comparison to the in di-alkylated host. The interplaner angles of the porphyrins and the centre to centre porphyrin distances for **5.6** and **5.7** are 62° and 10.67 Å, respectively. The C_{60} is arranged with the 6:6 ring junctions centered over the porphyrin at distances of 2.87-3.15 Å.

The distances between the secondary donor and the porphyrin sensitizer are about two angstroms longer for **5.6** and **5.7** than they are for the biphenyl hosts **4.2** and **4.3** due to the addition amide linker between the calixarene and the phenyl ring. Centre to centre distances between the secondary donor and the porphyrin are 22.58 Å and 22.63 Å for **5.6** as the ferrocene groups are situated directly above the porphyrins. In **5.7** the ferrocene groups are situated between the two porphyrin planes placing them on average one angstrom further away from the porphyrins with distances ranging from 21.82 to 24.47 Å. Optimized structures for **5.6** and **5.7** are shown in Figure 5.3 and Figure 5.4, respectively. A table of key structural characteristics for hosts **5.6** and **5.7** as well as the non-ferrocene functionalized host **3.10** is given in Table 5.1.

Table 5.1: Key geometric features of the molecular modeling (ONIOM/B3LYP/6-31G(d);UFF) for the nickel(II) derivative of functionalized bis-porphyrin hosts of **5.6** and **5.7** and non functionalized bis-porphyrin host **3.10**.

Host:C_{60}	**3.10**	**5.6**	**5.7**
Calixarene ester functionalized phenyl ring angle (°)	77.1	69.0	68.3
Calixarene n-butyl phenyl ring angle (°)	3.7	15.1	15.0
Hydrogen bonding distance amide N-H ether O (Å)	2.22, 2.25	2.29, 2.46	2.23, 2.46
Interplaner amide phenyl angle (°)	60.17	64.85	64.03
meta CH-π distance (Å)	2.849	2.719	2.697
Porphyrin centre to centre distance (Å)	10.66 Å	10.67	10.67
Interplaner angle porphyrin 24 mean plane (°)	65.1	62.3	62.7
Porphyrin metal to fullerene 6:6 junction distance(Å)	2.84, 2.96 2.90 3.00	2.85,2.94 2.91, 2.95	2.85,2.95 2.90,2.97
Ferrocene to porphyrin Centre to Centre distance(Å)	-	22.58, 22.63	21.82,23.83 23.88,24.47

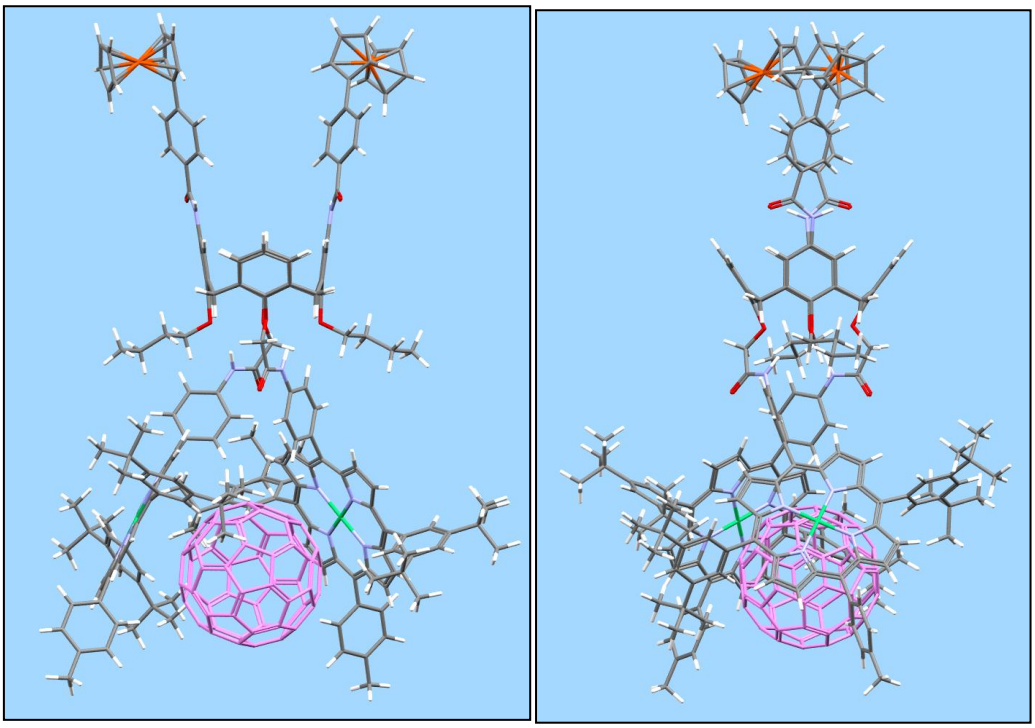

Figure 5.3: Calculated structures (ONIOM/B3LYP/6-31G(d);UFF) for the nickel(II) derivative of host–guest complex **5.6** with C_{60}.

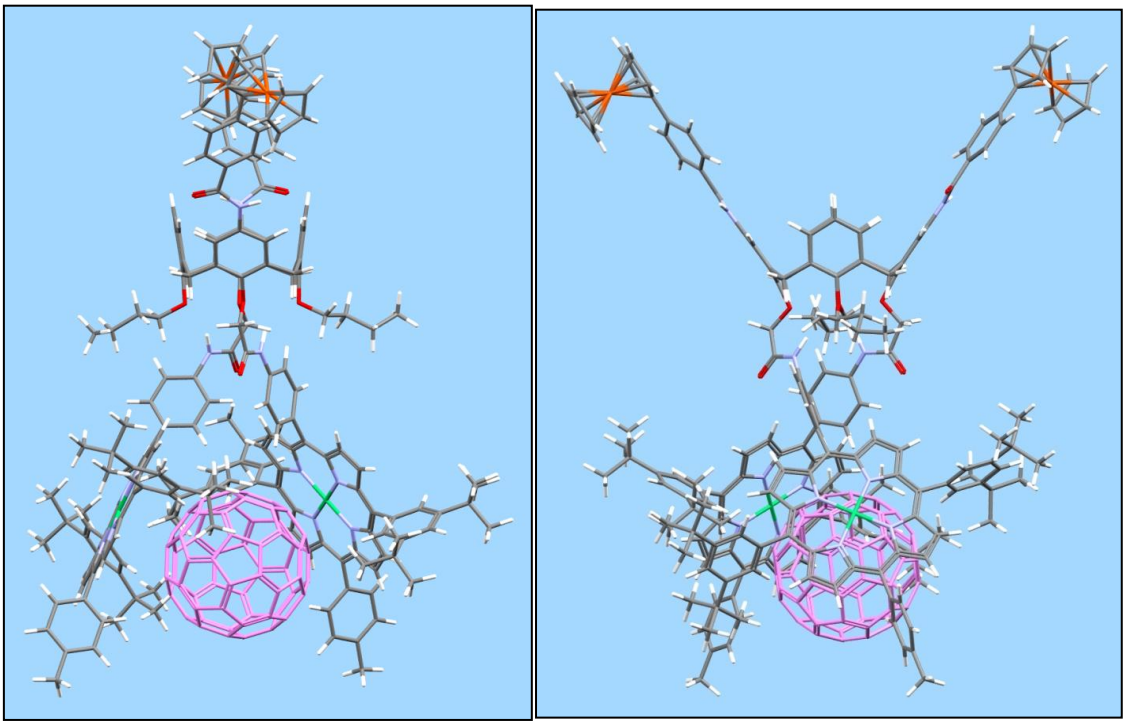

Figure 5.4: Calculated structures (ONIOM/B3LYP/6-31G(d);UFF) for the nickel(II) derivative of host–guest complex **5.7** with C_{60}.

5.4 Synthesis of Ferrocene Appended Bis-Porphyrins

5.4.1 Attempted Synthesis of Bis-Porphyrin 5.5

Initial attempts at preparing ferrocene functionalized bis-porphyrin **5.5** were made via amide coupling reactions with the disubstituted ethyl ester calixarene scaffold as shown in Scheme 5.1. Nitration of the wide rim of unsubstituted calixarenes has been reported by a number of groups with various functional groups on the narrow rim. Various nitration methods include addition of neat nitric acid or nitric acid and acetic acid.[209,211,222,223] Dinitro calixarene **5.7** was prepared by a catalytic nitration reaction of the diethyl ester **2.19**.[220,224] A solution of **2.19** in dichloromethane was stirred with an aqueous solution of sodium nitrate, hydrochloric acid and lanthanum nitrate as a catalyst for 18 hours. After aqueous workup and removal of the solvent a pure sample of **5.7** was obtained through recrystallization from dichloromethane and methanol. This method is appropriate as it only results in calixarene with nitro substituents on the *para* position to the phenol rings.

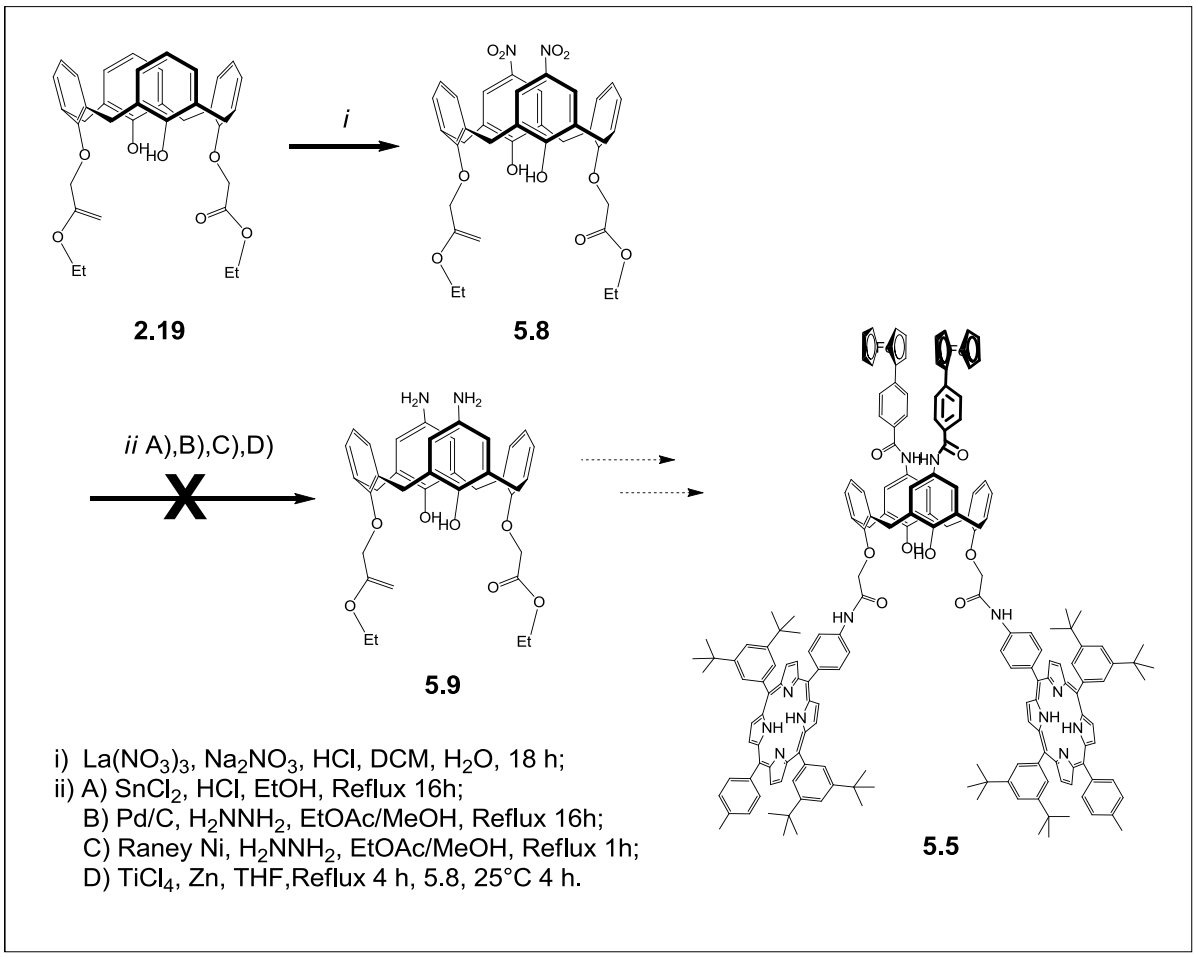

Scheme 5.1: Original synthesis of amide functionalized bis-porphyrin **5.11**.

During the preparation of the wide rim amide calixarenes, it has been observed that calixarenes substituted with amino groups *para* to the phenols are relatively unstable and decompose over time; this has been reported in literature.[110] Methods A-D were attempted for the reduction of the nitro functionality of **5.8.** While they have successfully reduced the nitro functionality to the corresponding amino calixarene **5.9**, side reactions and decomposition of the product during work up was common.

The dinitro calixarene **5.8** underwent reduction via Method A with tin (II) chloride in ethanol and hydrochloric acid to give the dialkylated amine **5.9**.[110] During aqueous workup and neutralization of the reaction mixture, a precipitate of the tin hydroxide salt resulted in the aqueous phase. Attempts to extract the product from the aqueous layer resulted in low yields of **5.8**. The retained aqueous phase would over time result in the precipitate changing to a pink solution indicating, the **5.9** was lost in the precipitate.

In an effort to avoid the loss of product through the tin hydroxide precipitate, reduction Method B was employed using hydrazine hydrate with palladium on carbon catalyst in ethanol/ethyl acetate.[225] Upon addition of hydrazine to a solution of **5.8**, the solution changed to an intense yellow colour. The solution was refluxed and the colour dissipated overnight, indicating that no starting material remained. The catalyst was filtered off and the organic layer was washed, dried and concentrated to dryness to afford an off white solid. The product was identified in the ^{1}H NMR by an upfield shift in the aromatic *ortho* proton signal from 8.05 to 6.42 ppm. Also observed in the ^{1}H NMR was the absence of the triplet and quartet of the ethyl ester, indicating that the groups had cleaved to form the diacid. Reflux of the solid in ethanol under nitrogen with hydrochloric acid was attempted to re-esterify the acid, however aqueous workup resulted in a sticky red solid.

Alternative reaction conditions were employed in Method C to reduce the nitro groups to amines without the cleavage of the ester functionality through the use of hydrazine and Raney nickel catalyst. It was found that the yellow colour of the solution dissipated within an hour compared to the overnight reaction using palladium on carbon catalyst. However when the catalyst was filtered off, and the solvent removed, the crude material became a deep red in colour over a short time.

Method D utilized low valent titanium, which has been used for reductive coupling of carbonyls and nitro groups as well as a reducing agent for nitro functionalities.[226] Titanium tetrachloride was added to a suspension of zinc metal in dry THF under nitrogen. After reflux and cooling to 25°C, **5.8** was added dropwise to the low valent titanium reagent and stirred at room temperature. Neutralization of the reaction mixture by addition of potassium carbonate resulted in a rapid colour change to a pink solution as a sign of degradation of the product. Upon removal of solvent this once again gave the red sticky solid.

5.4.2 Synthesis of Bis-porphyrin 5.6

Reduction of the dialkylated nitro calixarene has been accomplished; however the instability of the resulting diamine results in decomposition before the ferrocene acid can be coupled to the calixarene. It was decided that a second alkylation of remaining hydroxyl groups on the narrow rim *para* to the nitro groups with iodobutane prior to the reduction would increase the stability

of the amine and allow for successful coupling of the ferrocene groups. The synthesis of the tetra-alkylated bis-porphyrin **5.6** is shown in Scheme 5.2.

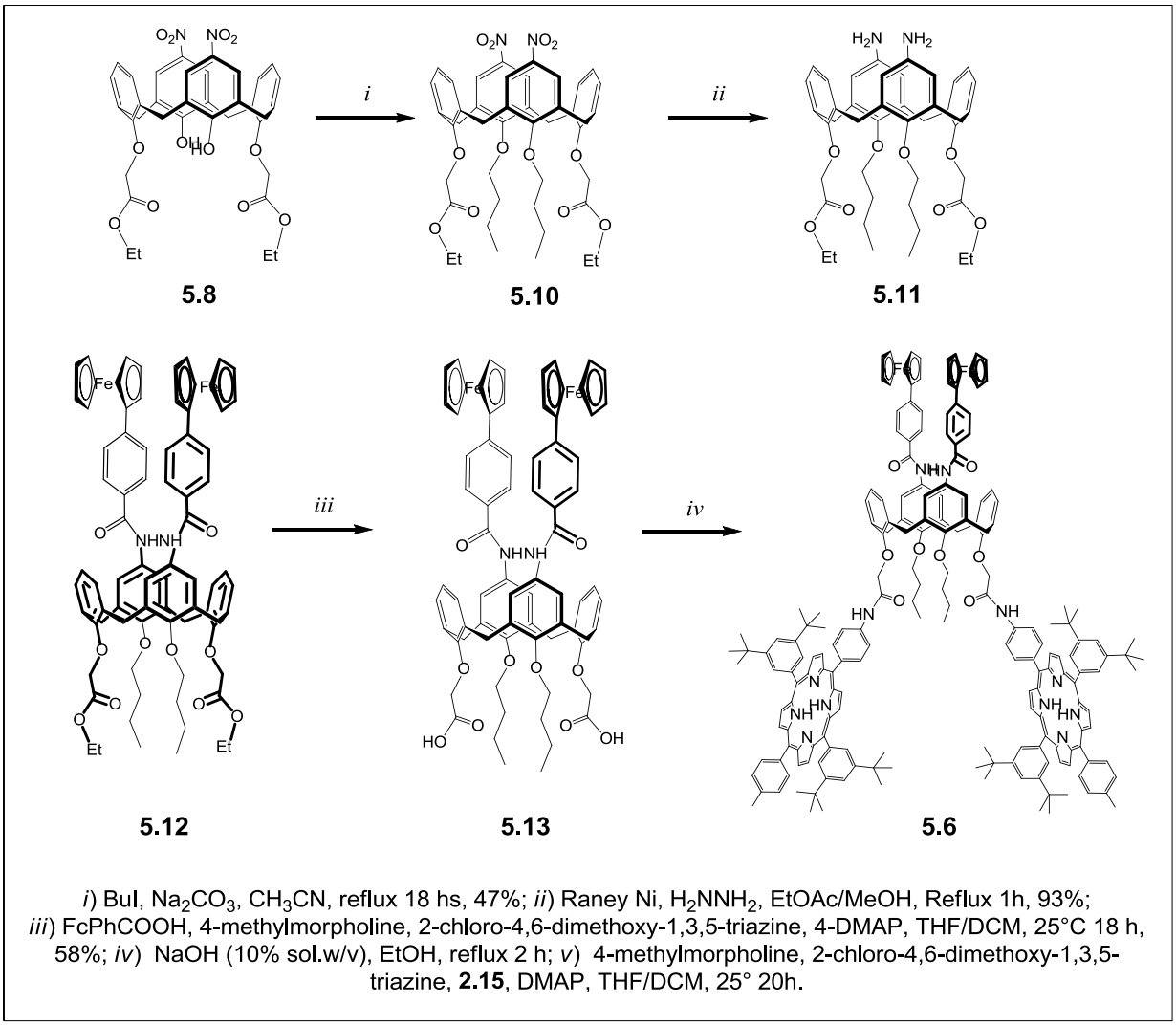

Scheme 5.2: Synthesis of bis-porphyrin **5.6**.

The second alkylation of the nitro calixarene **5.8** with iodobutane to give **5.10** is analogous to the procedure described in Chapter Four for the alkylation of the dibrominated calixarene. **5.8** was refluxed with iodobutane and in anhydrous acetonitrile with an excess of anhydrous sodium carbonate for 40 hours. Over this time the intense yellow colour of the nitro phenol of the calixarene decolorized to pale yellow. The product was then filtered though celite to remove the excess base and refluxed again in ethanol with hydrochloric acid. The crude material was then purified by column chromatography eluting with ethyl acetate and dichloromethane to give the tetra-alkylated calixarene **5.10**. The ^{1}H NMR spectrum confirmed the tetra-alkylated calixarene with the absence of the hydroxyl protons at 8.91 ppm and four

signals including a triplet at 3.93, multiplets at 1.86 and 1.49 ppm and a triplet at 0.99 ppm integrating for two *n*-butyl groups. The two methylene doublets and a lone singlet for the methylene of the ester linker indicated that the calixarene scaffold retained the cone conformation.

Reduction of the dinitro tetra-alkylated calixarene **5.10** to the corresponding amine **5.11** was achieved via a Raney nickel catalyzed reduction using hydrazine hydrate in ethyl acetate and methanol (1:1). The catalyst was removed by filtration and the reaction mixture washed with ammonium chloride. The solvent was removed giving an off white solid which was used without further purification. ^{1}H NMR confirmed the successful reduction by the upfield shift of the protons *ortho* on the substituted ring from 7.20 to 5.68 ppm as well as the quartet and triplet of the ethyl ester at 4.18 and 1.32 ppm. No changes in the calixarene scaffold conformation were observed.

Successful coupling of the ferrocene benzoic acid to the wide rim of the amino calixarene **5.11** was successfully achieved via the formation of an active ester with 2-chloro-4,6-dimethoxy-1,3,5-triazine and 4-methylmorpholine.[192] Ferrocene benzoic acid was dissolved in THF and dichloromethane and cooled to 0^{o}C. 4-methylmorpholine was added and the solution stirred for ten minutes, triazine was the added and the mixture stirred for four hours while warming to room temperature. During this time the formation of the active ester was monitored by TLC and was observed as a less polar orange compound at the expense of the ferrocene benzoic acid which remained at the baseline. The diamine **5.11** in dichloromethane was added to the ferrocene solution and the mixture was stirred for 18 hours. After aqueous workup, the solvent was removed and the crude material purified by column chromatography eluting with dichloromethane and ethyl acetate (9:1).

The ^{1}H NMR spectrum of the ferrocene amide **5.12** exhibited the calixarene signals corresponding to the cone conformation as well as the presence of six signals of the ferrocene phenyl amide. These signals were two triplets of the substituted cyclopentadiene at 4.56 and 4.32 ppm integrating for four protons each, a singlet of unsubstituted rings of the ferrocene at 3.95 ppm integrating for 10 protons. The aromatic region showed two doublets at 7.49 and 7.24 ppm for the phenyl linkers integrating for four protons each as well as a singlet at 7.56 ppm corresponding to the amide integrating for two protons. Hydrolysis of the ester groups to the corresponding acid was achieved by refluxing **5.12** with 10% sodium hydroxide in THF for

three hours. The solvent was removed *in vacu.* to give an orange solid. ^{1}H NMR confirmed the acid **5.13** through the absence of the triplet and quartet of the ethyl ester and was used without further purification.

As with the synthesis of other tetra substituted bis-porphyrins, the calixarene diacid **5.13** did not undergo amide coupling with porphyrin **2.15** using DCC as the coupling agent. Coupling of the tetra-alkylated calixarene diacid **5.13** to the porphyrin **2.15** was achieved by utilization of the same coupling method used to append the ferrocene benzoic acid to the wide rim. This method had been previously attempted as an alternative to DCC coupling with dialkylated hosts **2.1-2.3,** however coupling was unsuccessful due to side reactions with the free hydroxyl groups on the narrow rim.

The calixarene acid **5.13** was dissolved in THF and dichloromethane and cooled to 0^{o}C. 4-methyl morpholine was added and the reaction stirred for ten minutes. Triazine added and the mixture stirred for eight hours, warming to room temperature. As with the ferrocene benzoic acid the reaction was monitored by TLC and over this time the formation of a less polar orange compound was observed at the expense of the diacid. A solution of porphyrin **2.15** and DMAP in dichloromethane was added and the reaction stirred for 18 hours. After this time aqueous workup and purification by column chromatography with toluene/ethyl acetate was carried out to give a purple solid in a moderate yield of 48%. An analytically pure sample of **5.6** was prepared via recrystallization from chloroform/methanol.

^{1}H NMR of the ferrocene functionalized bis-porphyrin **5.6** displayed proton signals corresponding to the porphyrins, calixarene and ferrocene integrating in a ratio of 2:1:2 respectively. The spectra confirmed that the cone conformation was retained by the two doublets of methylene bridges at 4.84 and 3.55 ppm and one singlet at 5.29 ppm for the methylene amide linker. Mass spectrometry confirmed **5.6,** which was detected as the disodium cation.

5.4.3 Synthesis of Bis-Porphyrin 5.7

As with the functionalized bis-porphyrins **4.4** and **4.5,** reversing the order of alkylation of the calixarene before and after the nitration of calixarene scaffold allows for the synthesis of the isomer of the tetra-alkylated calixarene scaffold **5.10**. Alkylation of the calixarene with

iodobutane, followed by nitration and a second alkylation with ethyl bromoacetate, results in the nitro groups being *para* to the ethyl esters. Subsequent reduction of the nitro groups and amide coupling of ferrocene and porphyrins to the calixarene scaffold result in the ferrocene groups being appended *para* to the aryl ring bearing the porphyrin substituents. The synthesis of **5.7** is shown in Scheme 5.3.

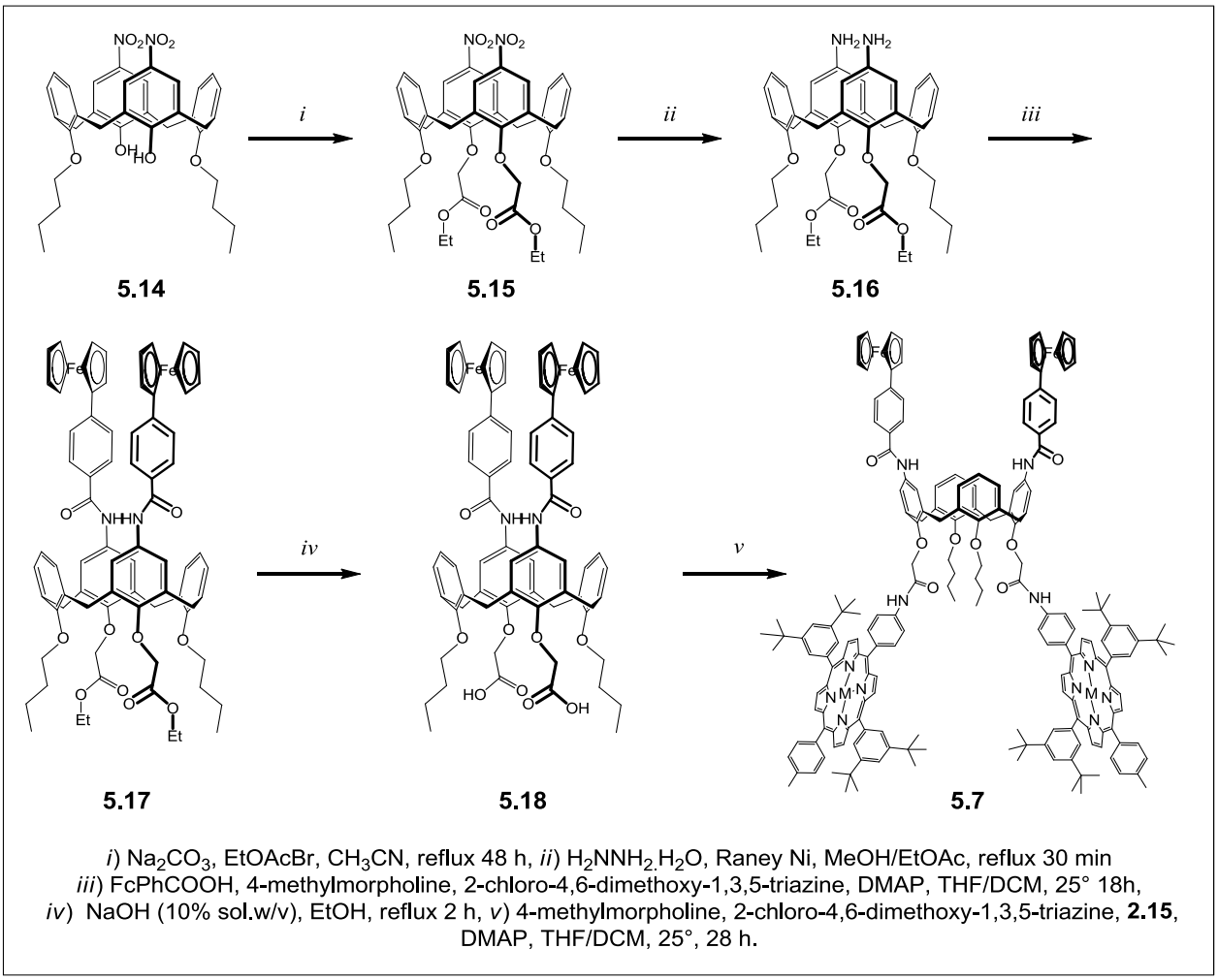

Scheme 5.3: Synthesis of bis-porphyrin **5.7**.

The calixarene **5.14** was prepared by the same method employed to make the nitro ethyl ester calixarene **5.10**. A solution of dibutyl calixarene **3.20** in dichloromethane was stirred with an aqueous solution of sodium nitrate, hydrochloric acid and catalytic amount of lanthanum nitrate to give **5.14**. A second alkylation of **5.15** with ethyl bromoacetate and sodium carbonate base in anhydrous acetonitrile followed by reflux with hydrochloric acid in ethanol resulted in the tetra-alkylated diester **5.15** in the cone conformation. Purification was accomplished by column chromatography eluting with dichloromethane and ethyl acetate.

The ^{1}H NMR spectrum of the tetra alkylated scaffold **5.15** is almost analogous to its isomer **5.10**. The spectra of the two isomers are shown in Figure 5.5. The narrow rim groups (ethyl ester and *n*-butyl chains marked as ♦ and ○ respectively) and the methylene bridges (*) display the same chemical shifts and splitting patterns. Differences are only observed in the aromatic signals (●), where the proton signals of the aryl ring *para* and *meta* to the with the ethyl ester are shifted further downfield compared to the ring functionalized with the *n*-butyl groups. This is observed as the singlet for the protons *ortho* to the nitro groups in **5.15** at 7.88 ppm and the triplet and doublet of the unsubstituted ring at 6.48 and 6.34 ppm while in **5.10** and the singlet occurs at 7.20 ppm and the doublet and triplet are shifted downfield to 6.99 and 6.90 ppm.

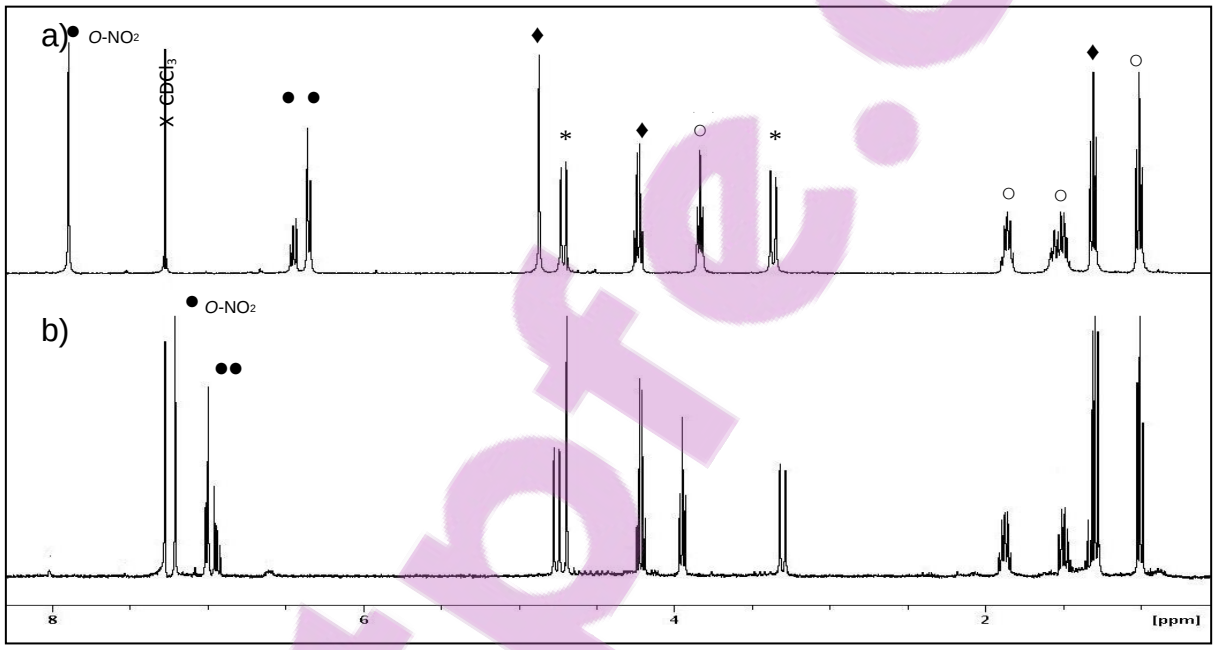

Figure 5.5: ^{1}H NMR of nitro functionalized calixarenes a) **5.15** and b) **5.10**, showing proton signals of the phenyl rings (●), methylene linker ethyl ester (♦), methylene bridges (*) and the n-butyl chain (○).

Reduction of the di-nitro tetra-alkylated calixarene **5.15** to the corresponding diamine **5.16** was achieved via a Raney nickel catalyzed reduction using hydrazine hydrate in ethyl acetate/methanol (1:1). ^{1}H NMR confirmed the successful reduction of the nitro groups by an upfield shift of the *ortho* protons to the amine on the substituted ring. The ^{1}H NMR of the two isomers of the amines **5.16** and **5.11** shown in Figure 5.6 display similar chemical shifts in the narrow rim pendent groups and the methylene bridges. Key differences in the ^{1}H NMR remain in the aryl ring proton signals, the aryl ring functionalized, with the ethyl ester being shifted

downfield compared to the ring functionalized with the *n*-butyl groups. Observed in **5.16** is the coalescence of the multiplet of the unsubstituted aryl ring at 6.41 ppm.

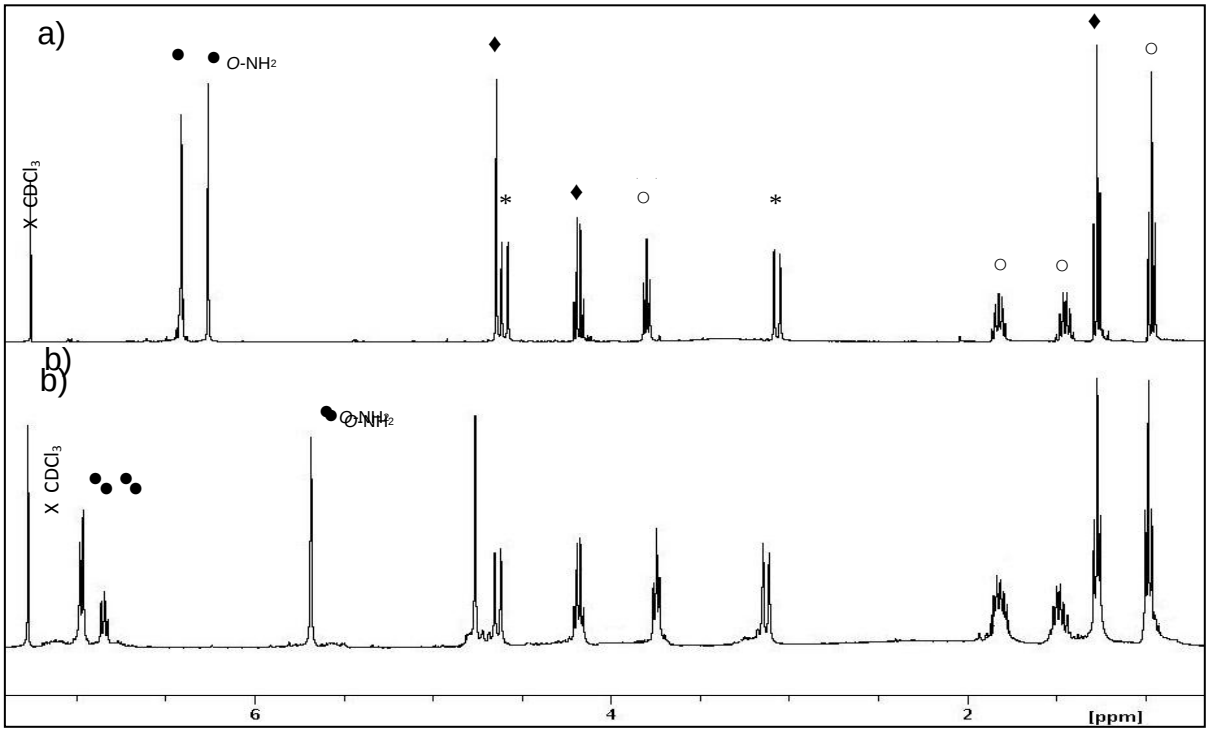

Figure 5.6: ^{1}H NMR of amino functionalized calixarenes a) **5.16** and b) **5.11** showing proton signals of the phenyl rings(●), the methylene linker ethyl ester (♦), methylene bridges (*) and *n*-butyl chains(○).

Condensation of ferrocene benzoic acid to the wide rim of the amino calixarene **5.16** was achieved through the formation of an activated ester of the ferrocene benzoic acid. Ferrocene benzoic acid was stirred with 2-chloro-4,6-dimethoxy-1,3,5-triazine and 4-methylmorpholine in THF and DCM at 0^{o}C. The diamine **5.16** in dichloromethane was added to the ferrocene solution and the mixture stirred for 18 hours. The mixture was then purified by column chromatography eluting with dichloromethane/ethyl acetate (9:1) to give the ferrocene coupled calixarene **5.17** as the third band.

The ^{1}H NMR spectra of the two isomers show some minor differences in the positions of the proton signals. In isomer **5.17** there are overlaps of the proton signals for one of the triplets of a substituted cyclopentyldiene ring with the methylene bridge doublet at 4.64 ppm. The multiplets of the unsubstituted phenyl ring still coalesce into a singlet at 6.52 ppm in **5.17** while the no such coalesce is observed for the multiplets at 6.95 and 7.04 ppm in **5.12.**

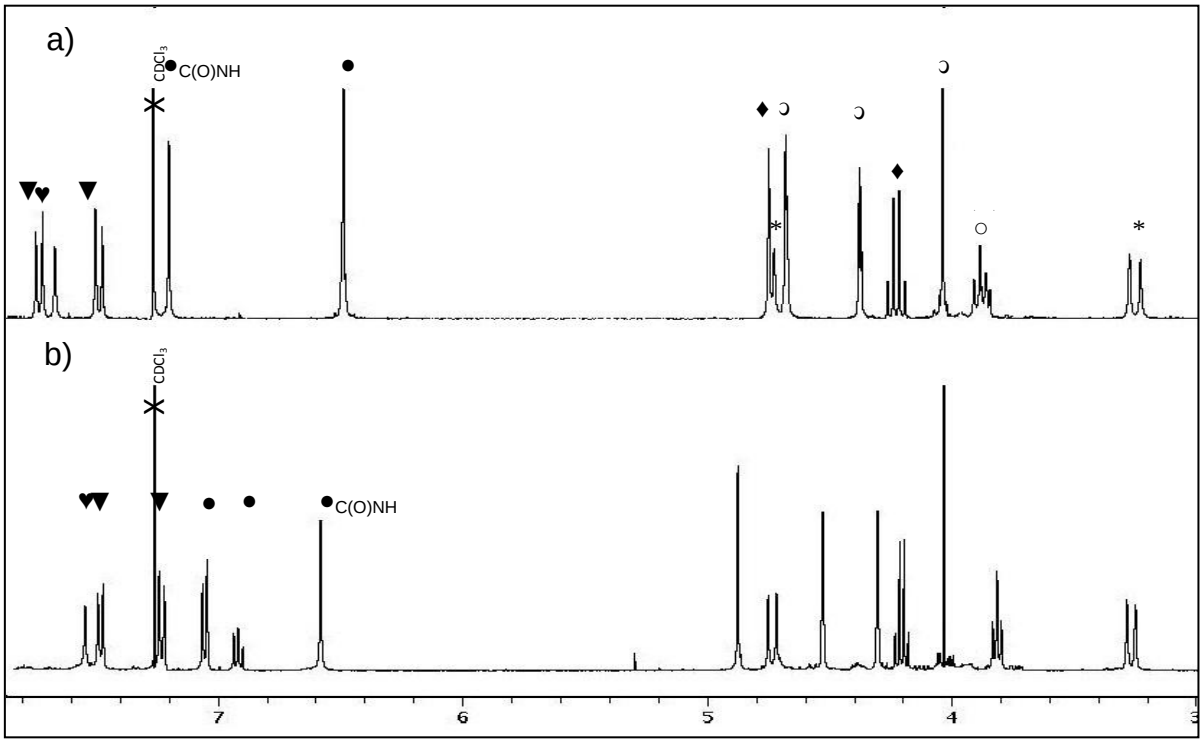

Figure 5.7: ^{1}H NMR of ferrocene functionalized calixarenes a) **5.17** and b) **5.12** showing proton signals of the phenyl rings (●), the ferrocene (ɔ) the methylene linker ethyl ester (♦), methylene bridges (*) and *n*-butyl chains (○).

Hydrolysis of the ester groups to the corresponding acid was achieved by refluxing **5.17** with 10% sodium hydroxide in THF for three hours. The solvent was removed *in vacuo* to give an orange solid, **5.18**. ^{1}H NMR confirmed the acid through the absence of the triplet and quartet of the ethyl ester and was used without further purification.

The diacid **5.18** was coupled to the amino porphyrin **2.15** using the same method reported for the synthesis of **5.6**. The calixarene acid **5.18** was dissolved in THF and dichloromethane and cooled to 0^{o}C. 4-methylmorpholine was added and the reaction mixture was stirred for ten minutes. 2-chloro-4,6-dimethoxy-1,3,5-triazine and then added and the mixture stirred for ten hours warming to room temperature. Porphyrin **2.15** and DMAP in dichloromethane was then added and the reaction stirred for a further 18 hours. Aqueous workup and purification by column chromatography with toluene/ethyl acetate, gave of **5.7** as a purple solid in a moderate yield of 54%. An analytically pure sample was prepared via recrystallization from chloroform/methanol.

In the ^{1}H NMR spectra, the key differences between the isomers **5.6** and **5.7** lie in the chemical shifts of the aryl rings of the calixarene. The doublet and multiplet for the unsubstituted

calixarene phenyl rings lie further upfield at 6.33 and 6.46 ppm in **5.7**. The same protons signals in the unsubstituted ring of **5.6** appear as multiplets at 7.14 ppm. The singlets corresponding to the *ortho* protons of the aryl rings substituted by the amide lie at 7.62 ppm in **5.7** and at 6.65 ppm for **5.6**.

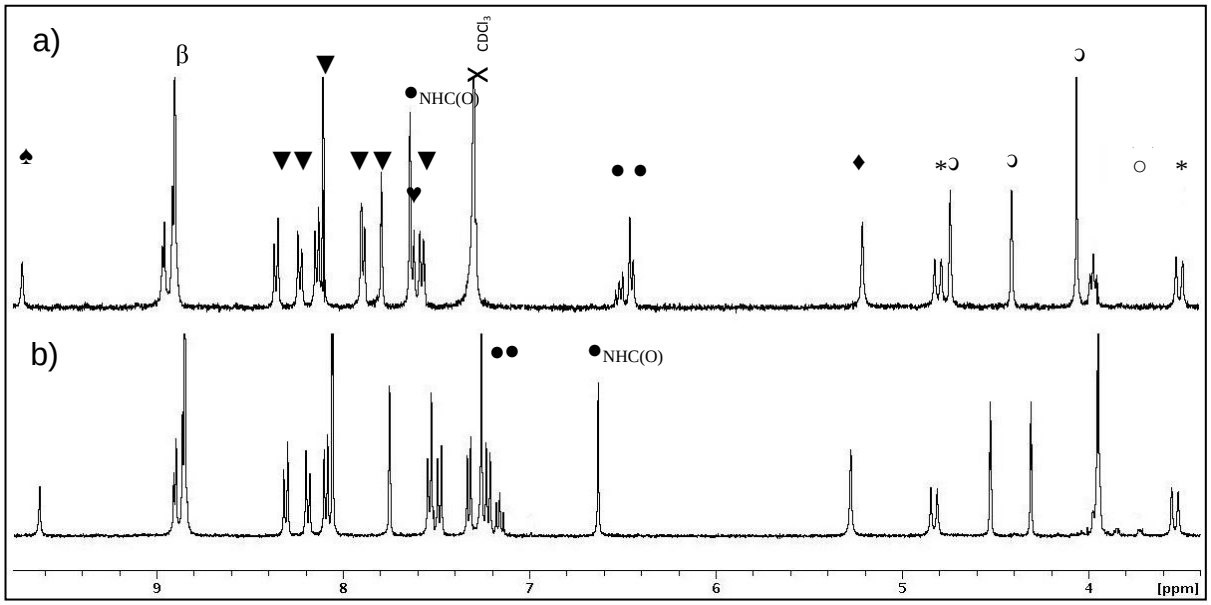

Figure 5.8: ^{1}H NMR of ferrocene functionalized bis-porphyrin a) **5.7** and b) **5.6,** showing proton signals of the phenyl rings (●), the ferrocene (ɔ), the methylene linker ethyl ester (♦), methylene bridges (*) and *n*-butyl chains (○).

The ^{1}H NMR of the isomers of the calixarenes and bis-porphyrin hosts are similar, with the only differences being in the proton signals of the substituted and unsubstituted aryl rings which shift downfield when *para* to the ethyl esters and the porphyrin amides. The proton signals for the remainder on the calixarene, alkyl chain and porphyrins remain relatively unchanged. It is expected that the calixarenes adopt similar cone conformations, which is possible given the increased flexibility due to the tetra alkylation of calixarene.

5.5 Fullerene Binding Studies with Bis-Porphyrins 5.6 and 5.7

Binding constants for fullerenes with ferrocene functionalized bis-porphyrins **5.6** and **5.7** were determined by UV-visible titration using the method outlined in Chapter Two. The optical absorption of the hosts were found to be similar to **4.4**, **4.5** and **3.10**; that is they exhibited an intense Soret band and less intense Q bands.

5.5.1 Fullerene Binding studies with Bis-porphyrins 5.6 and 5.7 in Toluene

As with **4.4** and **4.5**, upon addition of C_{60} (0-550 equivalents) or C_{70} (0-95 equivalents) to a solution of **5.6** or **5.7** in toluene there is a decrease in the absorption intensity of the Soret band with a small red shift, resulting in an isosbestic point at 435 nm. For **5.6** and **5.7**, the association constants for C_{60} have been calculated to be 1.9 $x10^3$ and 1.7 $x10^3$ M^{-1} respectively. For C_{70} the association constants are 1.7 $x10^4$ and 1.64 $x10^4$ M^{-1}, respectively. These association constants are approximately the same as the non-ferrocene functionalized host **3.10**. Calculated binding constants for **5.6** and **5.7**, and as well as **3.10** are shown in Table 5.2 and the UV-visible absorption spectra of **5.6** in toluene is shown in Figure 5.9.

Table 5.2: Association constants for bis-porphyrins **5.6**, **5.7** and **3.10** in toluene.

Host	C_{60} ($1x10^3$ M^{-1})	C_{70} ($1x10^4$ M^{-1})	$Lu_3N@C_{80}$ ($1x10^6$ M^{-1})
3.10	1.8 (0.2)	1.76 (0.5)	1.12 (0.14)
5.6	1.9 (0.3)	1.70 (0.12)	1.10 (0.11)
5.7	1.7 (0.2)	1.64 (0.1)	0.87 (0.17.)

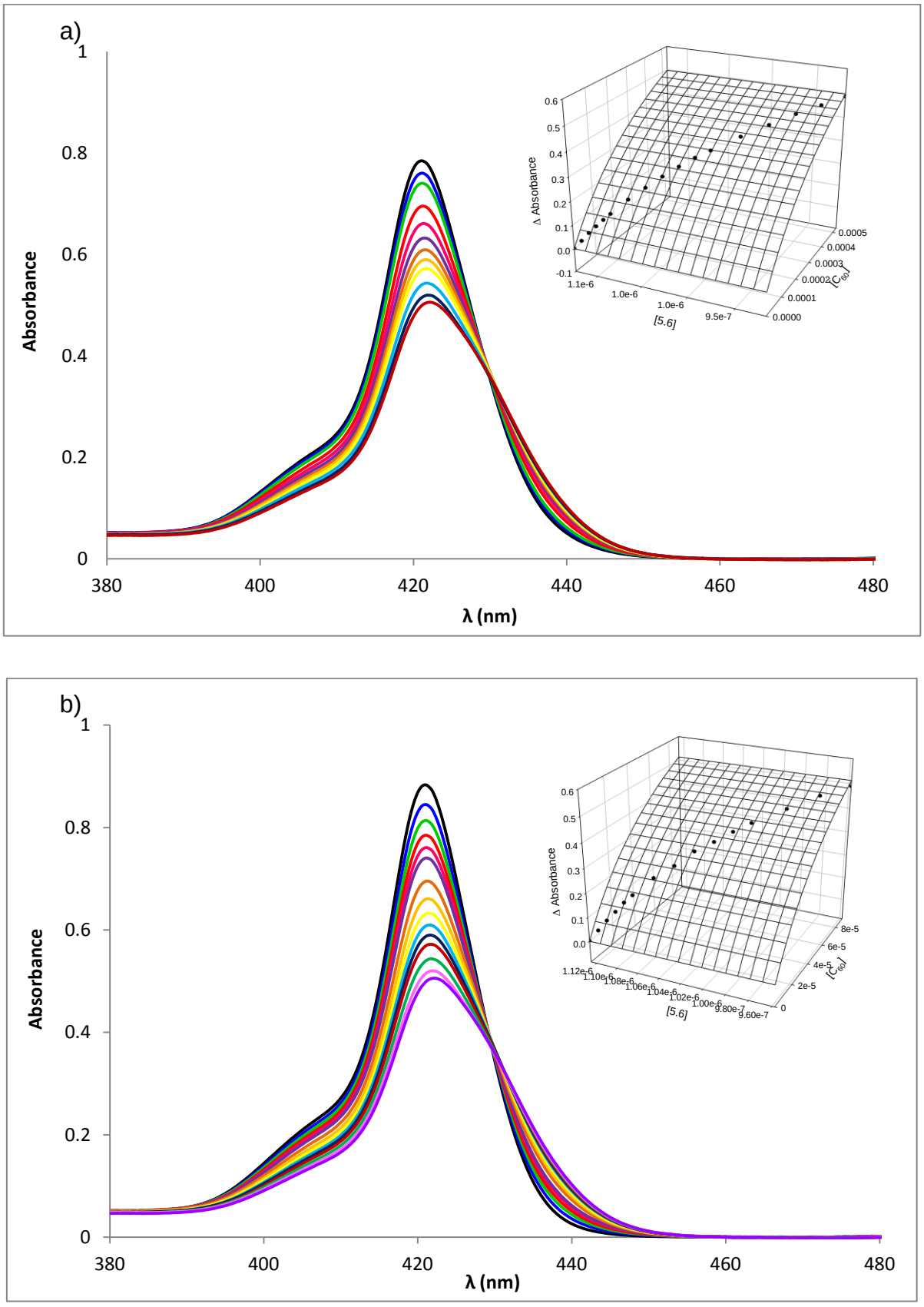

Figure 5.9: UV-visible titration of **5.6** 1.28x10^{-6} M) in toluene with a) addition C_{60} (0-490 Eq.) and b) C_{70} (0-95 Eq.): Insets; plot of the non-linear least square fit for the change in absorption at the Soret band of **5.6** upon addition of fullerene.

5.5.2 Fullerene Binding studies with Bis-porphyrins 5.6 and 5.7 Acetonitrile/Toluene (1:1)

Binding constants for bis-porphyrin hosts **5.6** and **5.7** were determined in a solvent mixture of acetonitrile/toluene (1:1). In this solvent mixture the binding constants for C_{60} and C_{70} are higher compared to than in toluene alone. The spectra displayed a greater reduction of the Soret band absorbance upon titration of fullerenes as well as a pronounced red shifting of the Soret band. The isosbestic points were clearly defined at 430 nm. The UV-visible spectra of titration of **5.6** with C_{60} and C_{70} in acetonitrile/toluene (1:1) are shown in Figure 5.10.

Upon changing the solvent to acetonitrile/toluene (1:1), the binding constants increased by almost two orders of magnitude for both C_{60} and C_{70}. The association constants have been calculated for **5.6** and **5.7**, as 1.25 $x10^5$ and 1.36 $x10^5$ M^{-1} for C_{60} and 1.12 $x10^6$ and 1.25 $x10^6$ M^{-1} for C_{70}, respectively. Such a small decrease in the association constants signifies that functionalization of the wide rim with secondary donors such as ferrocene has little effect on the binding of fullerenes. Calculated binding constants for **5.6**, **5.7** and **3.10** in acetonitrile/toluene (1:1) are shown in Table 5.3.

Table 5.3: Association constants for bis-porphyrins **5.6**, **5.7** and **3.10** in acetonitrile/toluene (1:1).

	C_{60} ($1x10^3M^{-1}$)	**C_{70}** ($1x10^3M^{-1}$)
3.10	144.0 (1.7)	1,032 (38)
5.6	125.8 (4.6)	1,116 (62)
5.7	136.6 (3.8)	1,246 (54)

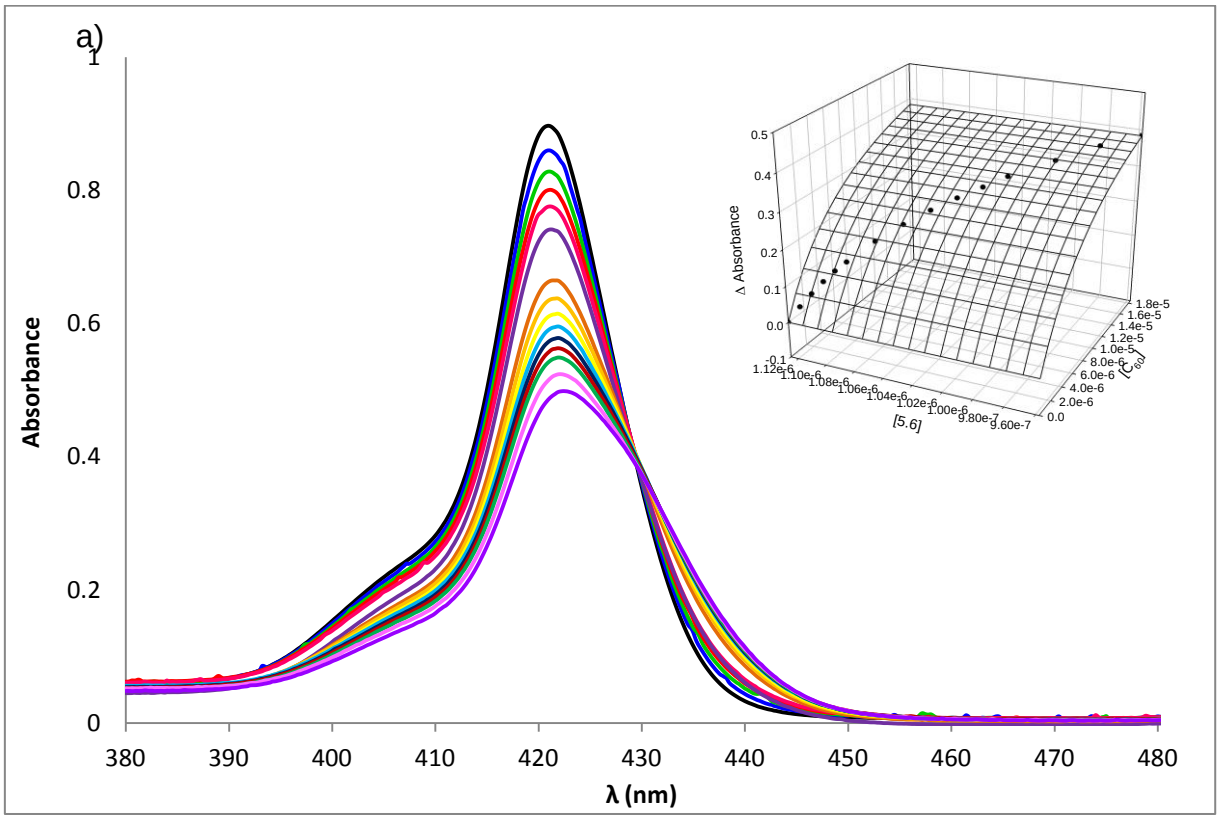

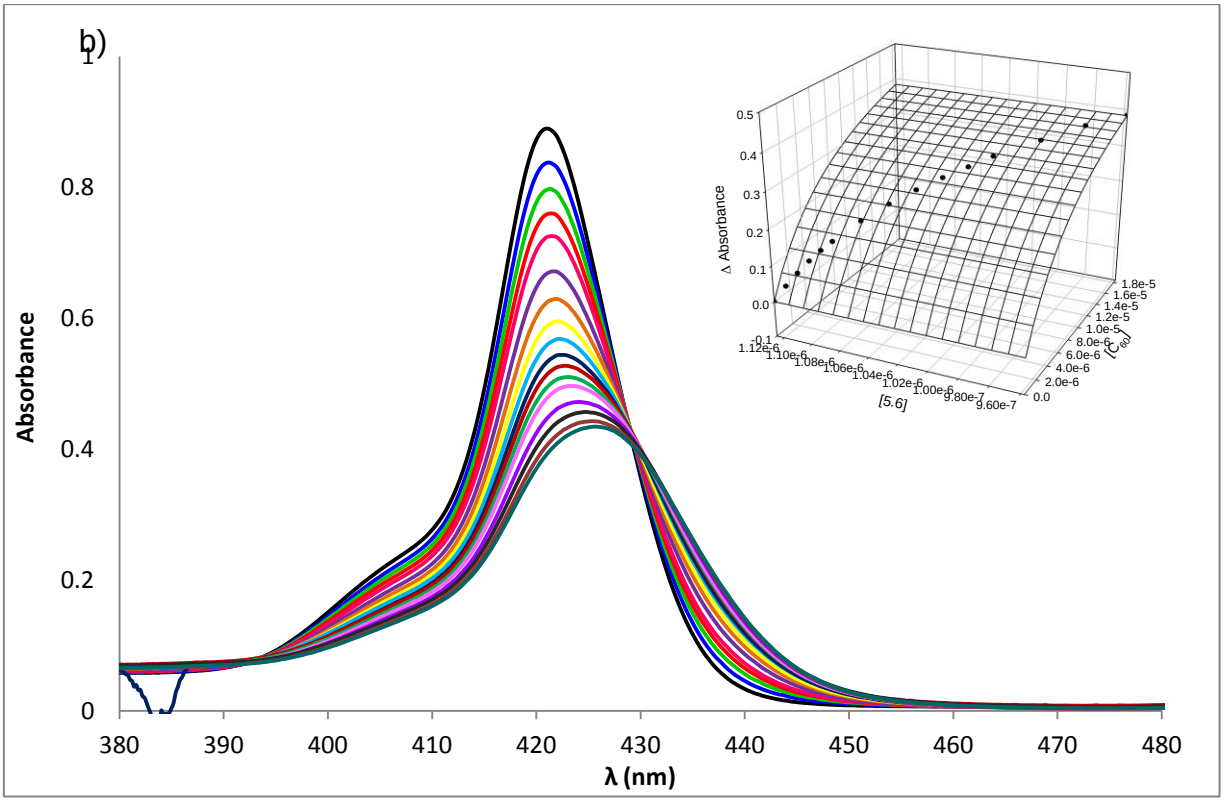

Figure 5.10: UV-visible titration of **5.6** (1.28×10^{-6} M) in acetonitrile/toluene (1:1) with a) addition C_{60} (0-20 Eq.) and b) C_{70} (0-5 Eq.) Insets; plot of the non-linear least square fit for the change in absorption at the Soret band of **5.6** upon addition of fullerene.

5.6 Fluorescence of Bis-Porphyrins 3.10, 5.6 and 5.7

The absorption spectra of the ferrocene functionalized bis-porphyrins **5.6** and **5.7** are nearly identical to the non functionalized host **3.10** and no additional bands were observed which indicated that there is weak or little ground state electronic interaction between the two moieties. Fluorescence spectra were measured for **5.6** and **5.7** and compared to the non ferrocene functionalized host **3.10** to determine the level of quenching from the secondary electron donor to the porphyrin.

At the same concentration the Soret band occurs at the same wavelength and has the same intensity in **3.10**, **5.6** and **5.7.** The bis-porphyrins were excited at the Soret band at 419 nm. Bis-porphyrin hosts **3.10**, **5.6** and **5.7** display emission bands centered at 653 and 718 nm. The relative intensities of fluorescence for **5.6** and **5.7** compared to the non ferrocene bis-porphyrin **3.10** are 0.98 for both **5.6** and **5.7**. The fluorescence spectra of **5.6**, **5.7** and **3.10** are shown in Figure 5.11.

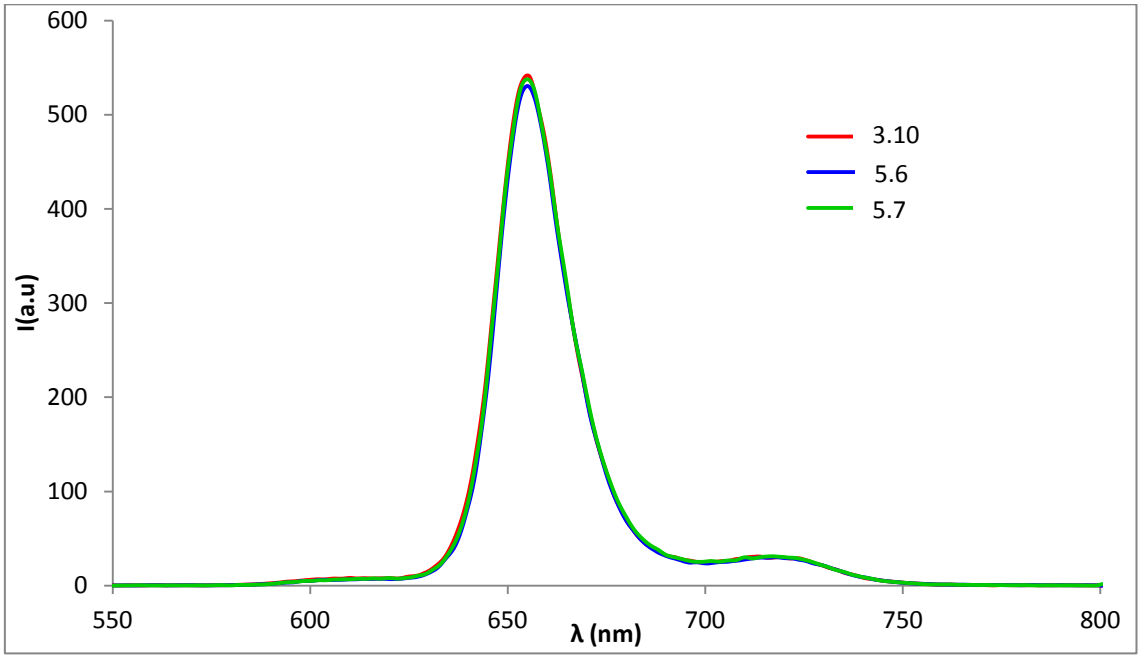

Figure 5.11: Fluorescence emission spectra of **5.6** and **5.7**, compared to the non ferrocene functionalized bis-porphyrin **3.10** (1.2x10-4 M)

5.7 Charge Transfer Bands

Charge transfer bands were observed in the UV-visible spectrum of **5.6** and **5.7** with increasing concentration of C_{60}. As with host **3.10,** estimation of the band positions and absorbance height was difficult. Charge transfer bands exhibited a significant blueshift, placing the band partially under the last Q band of the porphyrin. The lower association of the bis-porphyrin hosts for fullerenes made it difficult to estimate the electronic coupling of the pair, as a higher concentration of fullerene was required to see significant changes in the height of the charge transfer band. The UV-visible spectra of **5.6** and the subtracted absorption spectra revealing the charge transfer band are shown in Figure 5.12.

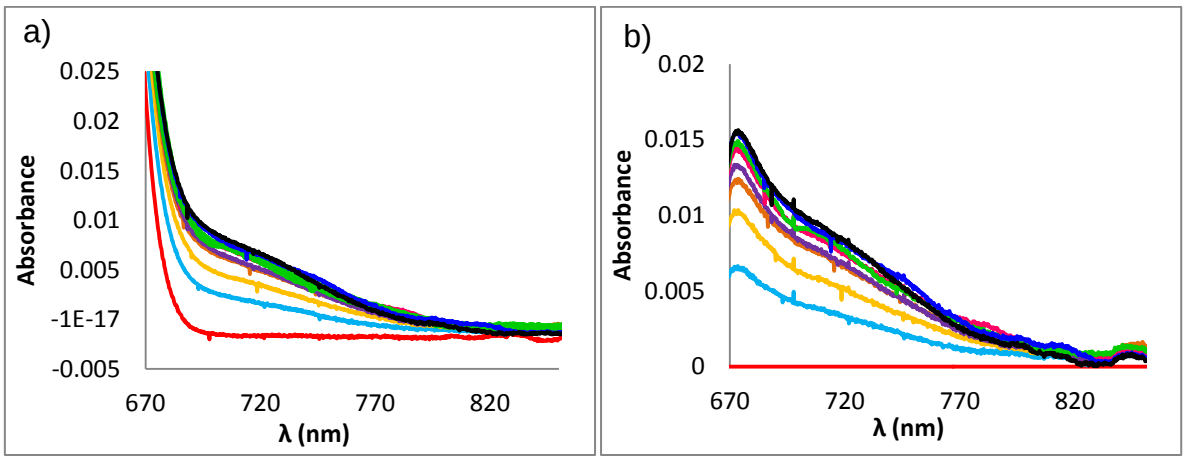

Figure 5.12: a) UV-visible spectra of **5.6** in toluene displaying the emergence of the charge transfer band at 700nm with increasing concentration of C_{60} and b) the absorption spectra of **5.6** with the free host subtracted giving a better visualization of the charge transfer band.

An accurate estimation of the electronic coupling between the porphyrin and fullerenes in hosts **5.6** and **5.7** has been attempted, however due to difficulties in viewing the intensity and wavelength of the charge transfer bands this has not been possible. A general estimation of the electronic coupling of the porphyrin and fullerenes is between 800 and 1,150 cm^{-1}.

5.8 Summary

The synthesis of two ferrocene appended bis-porphyrin hosts **5.6** and **5.7** has been reported for use as light harvesting dyes in solar energy conversion. These hosts have been prepared through amide coupling of ferrocene benzoic acid to wide rim amino groups of tetra-alkylated calixarenes. The two bis-porphyrins vary by which aryl ring the secondary donor ferrocene is appended. Bis-porphyrin **5.6** has the ferrocene appended to the aryl ring alkylated on the narrow rim with *n*-butyl groups while **5.7** has the ferrocene appended on the aryl ring alkylated with the porphyrin amide.

The ^{1}H NMR of the two hosts are similar, with differences only in the proton signals of the substituted and unsubstituted aryl rings which shift downfield when *para* to the porphyrin amide. Such similarities between the proton signals on the calixarene scaffold, alkyl chain and porphyrins suggest that the calixarenes adopt similar cone conformations, which is possible given the increased flexibility due the tetra alkylation of the calixarene.

The UV-visible and fluorescence spectroscopy studies of **5.6** and **5.7** in toluene show the binding constants to be similar to **3.10** and the ferrocene appended hosts **4.4** and **4.5.** Using a solvent mixture of acetonitrile/toluene (1:1), the hosts display slightly lower association for the fullerenes compared to **3.10**. The fluorescence intensities of **5.6** and **5.7** are similar to **3.10**, indicating that no quenching of the porphyrin emission is occurring from the ferrocene donors due to the two chromophores being remote. Porphyrin to fullerene charge transfer bands have been observed in the UV-visible spectra for both **5.6** and **5.7.** General estimation of the electronic coupling between the two chromophores is higher than in the unsubstituted host **3.10**.

5.9 Experimental

5.9.1 Synthetic Procedure for Bis-Porphyrins 5.6 and 5.7

5,17-Dinitro-25,27-bis[(ethoxycarbonyl)-methoxy]-26,28-dibutoxycalixarene (5.10)

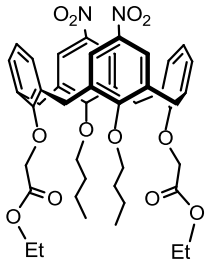

A suspension of dinitro calixarene **5.7** (1.50 g, 2.18 mmol) and anhydrous sodium carbonate (2.31 g, 21.86 mmol) in acetonitrile (50 mL) was stirred under an atmosphere of nitrogen for 10 minutes. iodobutane (4.02 mL, 21.86 mmol) was added to the solution which was refluxed for 18 hours. The reaction was cooled, diluted with dichloromethane (50 mL) and washed with 1 M hydrochloric acid and water. The organic phase was dried with sodium sulfate. The solvent was removed *in vacuo* to give a brown oil. The crude material was re-dissolved in ethanol (30 mL) and hydrochloric acid (5 mL) and refluxed for one hour. The ethanol was removed and washed with sodium carbonate (2 x 10 mL), extracted into dichloromethane (3 x 10 mL) and the solvent removed. The crude product was passed though a plug of silica, eluting with dichloromethane. The solution was concentrated and **5.10** was precipitated by slow addition of hexane as an off white solid, 1.32 g (76%).

^{1}H NMR (400 MHz, *CDCl$_3$*) ppm 7.20 (s, ArH, 4H), 6.99 (d, ArH, *J* = 6.70 Hz, 4H), 6.95-6.90 (m, ArH, 2H), 4.74 (d, $ArCH_2Ar$, *J* = 14.00 Hz, 4H), 4.68 (s, $OCH_2C(O)$, 4H), 4.20 (q, $C(O)OC\underline{H}_2CH_3$, *J* = 7.10 Hz, 4H), 3.93 (t, $OC\underline{H}_2CH_2$, *J* = 7.05 Hz, 4H), 3.28 (d, , $ArCH_2Ar$, *J* = 14.00 Hz, 4H), 1.86 (m, $OCH_2C\underline{H}_2$, 4H), 1.49 (m, $C\underline{H}_2CH_3$, 4H), 1.28 (t, $C(O)OCH_2C\underline{H}_3$, *J* = 7.05 Hz, 6H), 0.99 (t, $CH_2C\underline{H}_3$, *J* = 7.33 Hz, 6H)

HRMS (ESI-TOF-MS) Calculated: $[M+Na]^+$: $C_{44}H_{50}N_2NaO_{12}$: 821.3130 m/z, found: 821.3211 m/z.

5,17-Diamino-25,27-bis[(ethoxycarbonyl)-methoxy]-26,28-dibutoxycalixarene (5.11)

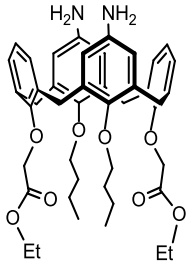

dinitro-calixarene **5.10** (0.2 g, 0125 mmol) and methanol washed Raney nickel was suspended in 1:1 ethyl acetate/methanol (20 mL). Hydrazine monohydrate (0.2 mL, 1.25 mmol) was added and the solution refluxed under nitrogen for one hour. The solution was filtered, the solvent was removed under reduced pressure and the residue was dissolved in dichloromethane (25 mL) and then washed with water (3 x 25 mL). The organic phase was separated, dried with sodium sulfate and the solvent removed to produce **5.11** as an off white solid, yield 0.166 g (91%).

^{1}H NMR (300 MHz, *CDCl$_3$*) δ ppm 6.97 (d, ArH, *J* = 7.35 Hz, 4H), 6.88-6.81 (m, ArH, 2H), 5.68 (s, ArH, 4H), 4.76 (s, C(O)OC$\underline{H}_2$CH$_3$, 4H), 4.63 (d, ArC$\underline{H}_2$Ar, *J* = 13.60 Hz, 4H), 4.18 (q, *J* = 7.10 Hz, 4H), 3.74 (t, OC$\underline{H}_2$CH$_2$, *J* = 6.94 Hz, 4H), 3.21 (d, ArC$\underline{H}_2$Ar, *J* = 13.60 Hz, 4H), 2.97 (s(Br), NH$_2$, 4H), 1.89-1.74 (m, OCH$_2$C$\underline{H}_2$, 4H), 1.56-1.39 (m, C$\underline{H}_2$CH$_3$, 4H), 1.32 (t, C(O)OCH$_2$C$\underline{H}_3$, J=7.10 Hz 6H), 0.98 (t, CH$_2$C$\underline{H}_3$, *J* = 7.35 Hz, 6H).

HRMS (ESI-TOF-MS) Calculated: $[M+H]^+$: $C_{44}H_{54}N_2O_8$: 739.3953 m/z, found 739.3975 m/z.

5,17-di-4-amidophenylferrocene-25,27-bis[(ethoxycarbonyl)-methoxy]-26,28-dibutoxycalixarene (5.12)

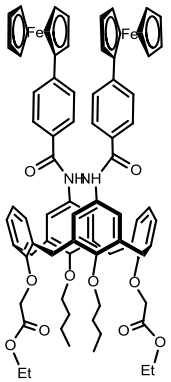

Ferrocene benzoic acid was prepared via the method publish by Savage.[227] Ferrocene benzoic acid (0.20 g, 0.337 mmol) was dissolved in a mixture of THF (6 mL) and dichloromethane (14 mL) and stirred under nitrogen. 4-methylmorpholine (0.074 mL, 0.676 mmol) was added and the solution stirred at room temperature for ten minutes. The solution was then cooled to 0^{o}C and 2-chloro-4,6-dimethoxy-1,3,5-triazine(0.12 g, 0.67 mmol) was added and the solution stirred for a further ten minutes before being warmed to room temperature where the solution was maintained at the temperature for one hour. *di*amino-calixarene **5.11** (0.165 g, 0.112 mmol) and DMAP (0.2 g, 0.9 mmol) in dichloromethane (20 mL) was added to the mixture and stirred for four hours. The solvent was removed under reduced pressure and purified by flash chromatography eluting with dichloromethane:ethyl acetate (4:1). The solvent was removed *in vacuo* to produce **5.12** as an orange solid, yield 0.181 g (62%).

^{1}H NMR (400 MHz, *CDCl$_3$*) ppm 7.56 (s, C(O)NH, 2H), 7.49 (d, ArH, *J* = 8.35 Hz, 4H), 7.24 (d, ArH, *J* = 8.35 Hz, 4H), 7.07 (d, ArH, *J* = 7.45 Hz, 4H), 6.96-6.90 (m, ArH, 2H), 6.59 (s, ArH, 4H), 4.89 (s, OCH$_2$C(O), 4H), 4.75 (d, ArCH$_2$Ar,*J* = 13.50 Hz, 4H), 4.56-4.52 (m, CpH, 4H), 4.32-4.30 (m, CpH, 4H), 4.21 (q, C(O)OC<u>H$_2$</u>CH$_3$ *J* = 7.05, Hz, 4H), 3.95 (s, CpH, 10H), 3.82 (t, O<u>CH$_2$</u>CH$_2$, 4H *J* = 7.00, Hz, 4H), 3.28 (d, ArCH$_2$Ar,*J* = 13.50 Hz, 4H), 1.93-1.83 (m, OCH$_2$<u>CH$_2$</u>, 4H), 1.52 (m, <u>CH$_2$</u>CH$_3$ 4H), 1.30 (t, C(O)OCH$_2$C<u>H$_3$</u>, *J* = 7.15, Hz, 6H), 1.01 (t, CH$_2$<u>CH$_3$</u>*J* = 7.40 Hz, 6H).

HRMS (ESI-TOF-MS) Calculated: [M+Na]$^{+}$:$C_{78}H_{78}$ $Fe_2N_2NaO_{10}$: 1337.4252 m/z, found: 1337.4194 m/z.

5,17-Di-4amidophenylferrocene-25,27-bis-carbonyl-methoxy-26,28-dibutoxycalixarene (5.13)

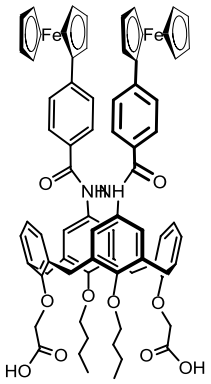

A suspension of calixarene **5.12** (0.181 g, 0.138 mmol) and 10% sodium hydroxide (5 mL) in ethanol was refluxed for two hours. The solution was then cooled and hydrochloric acid (2 M) was added until a pH of 1 was reached. The resulting suspension was extracted with chloroform and then washed with saturated ammonium chloride, dried with sodium sulfate and evaporated to dryness to produce **5.13** as an orange solid which was used without further purification, 0.167 g (94%).

1H NMR (400 MHz, *$CDCl_3$*) ppm: 7.57 (s, C(O)NH, 2H), 7.53 (d, ArH, *J* = 7.40 Hz, 4H), 7.30 (d, ArH, *J* = 7.40 Hz, 4H), 7.25 (s, ArH, 4H), 7.16-7.07 (m, ArH, 2H), 6.68 (s, ArH, 4H), 4.75 (s, $OCH_2C(O)$, 4H), 4.59-4.56 (s, CpH, 4H), 4.44 (d, $ArCH_2Ar$, *J* = 13.20 Hz, 4H), 4.34 (s, CpH, 4H), 3.96 (s, CpH, 10H), 3.92 (m, $O\underline{CH_2}CH_2$, 4H), 3.39 (d, $ArCH_2Ar$, *J* = 13.20 Hz, 4H), 1.88 (m, $OCH_2\underline{CH_2}$,4H), 1.40 (m, $\underline{CH_2}CH_3$, 4H), 0.99 (t, $CH_2\underline{CH_3}$, *J* = 7.35 Hz, 6H).

HRMS (ESI-TOF-MS) Calculated: $[M+Na]^+$: $C_{74}H_{70}Fe_2N_2NaO_{10}$: 1281.3626 m/z; found: 1281.3693 m/z.

5,17-Di-4-amidophenylferrocene-25,27-bis-[(methoxy(4-amidophenyl)-15-tolyl-10,20-di-(3,5-di-*tert*-butylphenyl) porphyrin]26,28-dibutoxycalixarene (5.6)

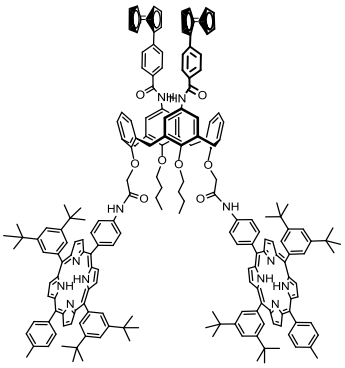

Calixarene diacid **5.13** (0.058 g, 0.457 mmol) was dissolved in a mixture of THF (3 mL) and dichloromethane (7 mL) and stirred under nitrogen. 4-methylmorpholine (0.009 mL, 0.091 mmol) was added and the solution stirred at room temperature for 10 minutes. The solution was then cooled to 0^{o}C and 2-chloro-4,6-dimethoxy-1,3,5-triazine (0.0031 g, 0.091 mmol) was added and the solution stirred for ten minutes before being warmed to room temperature at which temperature the solution was maintained for one hour. Porphyrin **2.15** (0.08 g, 0.091 mmol) and DMAP (0.002 g, 0.009 mmol) in dichloromethane (10 mL) was added to the mixture and a stirred for four hours. The solvent was removed under reduced pressure and purified by flash chromatography with eluting toluene/ethyl acetate (9:1). The solvent was removed *in vacuo* to produce **5.6** as a purple solid, yield, 0.071 g (54%).

^{1}H NMR (400 MHz, *CDCl$_3$*) ppm: 9.65 (s, C(O)NH, 2H), 8.92 (d, H$_\beta$, *J* = 4.80 Hz, 4H), 8.87 (d, H$_\beta$, *J* = 5.00 Hz, 12H), 8.32 (d, ArH, *J* = 8.50 Hz, 4H), 8.21 (d, ArH, *J* = 8.40 Hz, 4H), 8.11 (d, *J* = 7.91 Hz, 4H), 8.07 (d, ArH, *J* = 1.80 Hz, 8H), 7.76 (t, ArH, *J* = 180 Hz, 4H), 7.55 (d, ArH + C(O)NH, *J* = 5.95 Hz, 6H), 7.50 (d, ArH, *J* = 8.35 Hz, 4H), 7.33 (d, ArH, *J* = 7.50 Hz, 4H), 7.24 (d, ArH, *J* = 8.35 Hz, 4H), 7.17 (t, ArH, *J* = 7.43, Hz, 2H), 6.65 (s, ArH, 4H), 5.29 (s, OCH$_2$C(O), 4H), 4.84 (d, ArCH$_2$Ar, *J* = 13.70 Hz, 4H), 4.54 (t, CpH, *J* = 1.85 Hz, 4H), 4.32, (t, CpH, *J* = 1.85 Hz, 4H), 3.96 (m, CpH +O<u>CH$_2$</u>CH$_2$, 14H), 3.55 (d, ArCH$_2$Ar, *J* = 13.70 Hz, 4H), 2.70 (s, ArCH$_3$, 6H), 1.90 (m, OCH$_2$CH$_2$, 4H), 1.49 (s, C(CH$_3$)$_3$, 1H), 1.45 (m, C<u>H$_2$</u>CH$_3$, 4H), 0.97 (t, CH$_2$C<u>H$_3$</u>, *J* = 7.40 Hz, 6H), -2.72 (s, NH, 4H).

HRMS (ESI-TOF-MS) Calculated: [M+2H]$^{2+}$: $C_{196}H_{198}Fe_2O_8N_{12}$: 1480.7111 m/z, found: 1480.7002 m/z; [M+Na+H]$^{2+}$:$C_{196}H_{197}$ $Fe_2O_8N_{12}Na$: 1491.7003 m/z, found 1491.6900 m/z; [M+2Na]$^{2+}$: $C_{196}H_{196}$ $Fe_2O_8N_{12}Na_2$: 1502.6930 m/z, found: 1502.6827 m/z.

11,23-Dinitro-25,27-bis[(ethoxycarbonyl)-methoxy]-26,28-dibutoxycalixarene (5. 15)

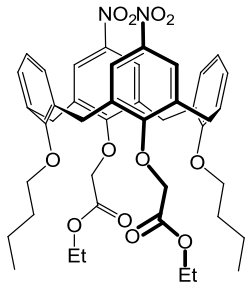

A solution of **5.14** (2.0 g, 2.91 mmol) and sodium carbonate (3.06 g, 29.15 mmol) in acetonitrile (80 mL) was stirred at room temperature for one hour. Ethyl bromoacetate (7.4 mL, 29.15 mmol) was then added and the mixture was refluxed for 40 hours. The mixture was allowed to cool to room temperature and the sodium carbonate was removed by filtration through celite. The solvent was removed *in vacuo* and the residue was redissolved in ethanol (50 mL) and concentrated HCl (5 mL) and the solution refluxed for a further two hours. Dichloromethane (60 mL) was then added and the organic phase was washed with saturated sodium carbonate (3 x 30 mL). The organic layer was dried over anhydrous sodium sulphate and concentrated. The product was purified by column chromatography eluting with dichloromethane/hexane 4:1. The solution was then evaporated to give **5.15** as an off white solid, 1.39 g (67%).

^{1}H NMR (400 MHz, *CDCl$_3$*) ppm: 7.88 (s, ArH, 4H), 6.48-6.40 (m, ArH, 2H), 6.34 (d, ArH, *J* = 7.50 Hz, 4H), 4.86 (s, C(O)OC$\underline{H}_2$CH$_3$, 1H), 4.70 (d, ArCH_2Ar, *J* = 13.90 Hz, 4H), 4.22 (q, *J* = 7.15 Hz, 4H), 3.82 (t, OC$\underline{H}_2$CH$_2$, *J* = 7.02, 7.00 Hz, 4H), 3.35 (d, ArCH_2Ar, *J* = 13.90 Hz, 4H), 1.90-1.79 (m, OC$\underline{H}_2$CH$_2$, 4H), 1.54-1.43 (m, C$\underline{H}_2$CH$_3$, 4H), 1.26 (t, C(O)OCH$_2$C$\underline{H}_3$, *J* = 7.15 Hz, 6H), 1.00 (t, C$\underline{H}_2$CH$_3$, *J* = 7.35 Hz, 6H).

HRMS (ESI-TOF-MS) Calculated: $[M+H]^+$: $C_{44}H_{51}N_2O_{12}$: 799.3437 m/z, found: 799.3439 m/z; $[M+Na]^+$: $C_{44}H_{50}N_2O_{12}Na$: 821.3256 m/z, found: 821.3130 m/z.

11,23-Diamino-25,27-bis[(ethoxycarbonyl)-methoxy]-26,28-dibutoxycalixarene (5.16)

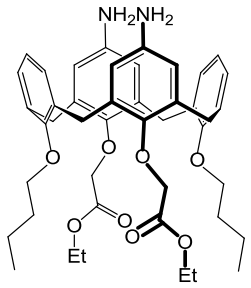

*di*nitro-calixarene **5.15** (0.2 g, 0.251 mmol) and methanol washed Raney nickel was suspended in ethyl acetate/methanol (20 mL, 1:1). Hydrazine monohydrate (0.314 mL, 25.1 mmol) was added and the solution refluxed under nitrogen for one hour. The solution was filtered, the solvent was removed under reduced pressure and the residue was dissolved in dichloromethane (25 mL) and then washed with water (2 x 25 mL). The organic phase was separated, dried with sodium sulfate and the solvent removed to produce **5.16** as an off white solid.

^{1}H NMR (400 MHz, $CDCl_3$) ppm: 6.41 (s, ArH, 6H), 6.26 (s, ArH, 4H), 4.64 (s, ArH, 4H), 4.60 (d, $ArCH_2Ar$, J = 13.55 Hz, 4H), 4.18 (q, $C(O)OC\underline{H}_2CH_3$, J = 7.18 Hz, 4H), 3.80 (t, $OC\underline{H}_2CH_2$, J = 7.12 Hz, 4H), 3.07 (d, $ArCH_2Ar$, J = 13.55 Hz, 4H), 1.83 (m, $OCH_2C\underline{H}_2$, 4H), 1.45 (m, $CH_2C\underline{H}_3$, 4H), 1.27 (t, $C(O)OCH_2C\underline{H}_3$, J = 7.16Hz, 6H), 0.97 (t, $CH_2C\underline{H}_3$, J = 7.37, 6H),

HRMS (ESI-TOF-MS) Calculated: $[M+H]^+$: $C_{44}H_{54}N_2O_8$: 739.3953 m/z, found 739.4012 m/z.

11,23-Di-4-amidophenylferrocene-25,27-bis[(ethoxycarbonyl)-methoxy]-26,28-dibutoxycalixarene (5.17)

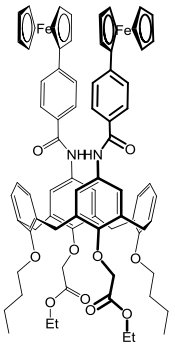

Ferrocene benzoic acid (0.20 g, 0.337 mmol) was dissolved in a mixture of THF (6 mL) and dichloromethane (14 mL) and was stirred under nitrogen. 4-methylmorpholine (0.074 mL, 0.676 mmol) was added and the solution stirred at room temperature for ten minutes. The solution was then cooled to 0^{o}C and 2-chloro-4,6-dimethoxy-1,3,5-triazine (0.12 g, 0.67 mmol) was added and the solution stirred for ten minutes before being warmed to room temperature where the solution was maintained for one hour. diamino-calixarene **5.16** (0.165 g, 0.112 mmol) and DMAP (0.2 g, 0.9 mmol) in dichloromethane (20 mL) was added to the mixture and stirred for four hours. The solvent was removed under reduced pressure and purified by flash chromatography eluting with dichloromethane:ethyl acetate (4:1). The solvent was removed *in vacuo* to produce **5.17** as an orange solid, 0.170 g (58%).

^{1}H NMR (300 MHz, $CDCl_3$) ppm: 7.73 (d, ArH, J = 8.45 Hz, 4H), 7.67 (s, C(O)NH, 2H), 7.49 (d, ArH, J = 8.45 Hz, 4H), 7.23-7.17 (s, ArH, 4H), 6.51-6.41 (m, ArH, 6H), 4.75 (s, $OCH_2C(O)$, 4H), 4.73-4.64 (m, $ArCH_2Ar$ + CpH, 8H), 4.39-4.35 (m, CpH, 4H), 4.22 (q, $C(O)OCH_2$, J = 7.10 Hz, 4H), 4.03 (s, CpH, 10H), 3.88 (t, $OC\underline{H}_2CH_2$, J = 8.40 Hz, 4H), 3.25 (d, $ArCH_2Ar$, J = 13.60 Hz, 4H), 1.89 (m, $OCH_2C\underline{H}_2$, 4H), 1.50 (m, $C\underline{H}_2CH_3$, 4H), 1.31 (t, $OC\underline{H}_2CH_3$, J = 7.10 Hz, 6H), 1.00 (t, $CH_2C\underline{H}_3$, J = 7.37 Hz, 6H).

HRMS (ESI-TOF-MS) Calculated: $[M+Na]^+$: $C_{78}H_{78}Fe_2O_{10}N_2Na$: 1337.4127 m/z found: 1337.4114 m/z.

11,23-Di-4-amidophenylferrocene-25,27-bis-carbonyl-methoxy-26,28-dibutoxycalixarene (5.18)

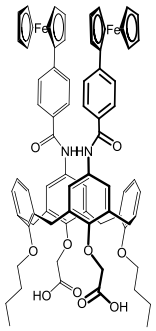

A suspension of calixarene **5.17** (0.170 g, 0.121 mmol) and 10% sodium hydroxide (5 mL) in ethanol was refluxed for two hours. The solution was then cool and hydrochloric acid (2 M) was added until a pH of 1 was reached. The resulting suspension was extracted with chloroform and then washed with saturated ammonium chloride, dried with sodium sulfate and evaporated to dryness to produce **5.18** as an orange solid which was used without further purification, 0.156 g (94%).

^{1}H NMR (400 MHz, $CDCl_3$) ppm 8.03 (s, C(O)NH, 2H), 7.87 (s, ArH, 4H), 7.58 (s, ArH, 8H), 6.51 (s, ArH, 4H), 6.43 (d, *J* = 7.93 Hz, 2H), 4.73 (s, $OCH_2C(O)$, 4H), 4.70 (s, CpH, 4H), 4.41 (s, CpH, 4H), 4.36 (d, $ArCH_2Ar$, *J* = 13.31 Hz, 4H), 4.06 (s, CpH, 10H), 3.91-3.84 (m, OCH_2CH_2, 4H), 3.33 (d, $ArCH_2Ar$,*J* = 13.31 Hz, 4H), 1.92-1.81 (m, OCH_2CH_2, 4H), 1.38-1.30 (m, CH_2CH_3,4H), 0.95 (t, OCH_2CH_3, *J* = 7.29Hz, 4H)

HRMS (ESI-TOF-MS) Calculated: $[M+Na]^+$: $C_{74}H_{70}Fe_2O_{10}N_2Na$: 1281.3278 m/z found: 1281.3612 m/z.

11,23-Di-4-amidophenylferrocene-25,27-bis-[(methoxy(4-amidophenyl)-15-tolyl-10,20-di-(3,5-di-*tert*-butylphenyl) porphyrin]26,28-dibutoxycalixarene (5.7)

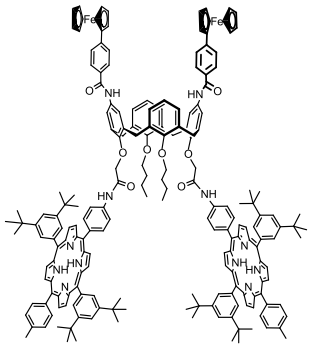

Calixarene diacid **5.18** (0.051 g, 0.457 mmol) was dissolved in a mixture of THF (3 mL) and dichloromethane (7 mL) and was stirred under nitrogen. 4-methylmorpholine (0.009 mL, 0.091 mmol) was added and the solution stirred at room temperature for ten minutes. The solution was then cooled to 0^{o}C and 2-chloro-4,6-dimethoxy-1,3,5-triazine (0.0031 g, 0.091 mmol) was added and the solution was then stirred for ten minutes before being warmed to room temperature, at which temperature solution was maintained for one hour. Porphyrin **2.15** (0.07 g, 0.091 mmol) and DMAP (0.002 g, 0.009 mmol) in dichloromethane (10 mL) was added to the mixture and stirred for four hours. The solvent was removed under reduced pressure and purified by flash chromatography, eluting with toluene/ethyl acetate (9:1). The solvent was removed *in vacuo* to produce **5.7** as a purple solid. Yield 0.069g. (60%).

^{1}H NMR (400 MHz, *CDCl$_3$*) ppm 9.69 (s, C(O)NH, 2H), 8.91 (d, H$_\beta$, J = 4.7 Hz, 4H), 8.86 (d, J = H$_\beta$, 5.00 Hz, 12H), 8.31 (d, ArH, J = 8.30 Hz, 4H), 8.19 (d, ArH, J = 8.30 Hz, 4H), 8.09 (d, ArH, J = 7.70 Hz, 4H), 8.05 (t, ArH, J =1.85 Hz, 1H), 7.90 (d, ArH + C(O)NH, 6H), 7.86 (d, J = 8.32 Hz, 4H), 7.75 (t, J= 1.85, 4H), 7.59 (m, ArH+ArH, 8H), 7.53 (d, ArH, 4H), 6.51-6.39 (m, ArH, 6H), 5.16C(s, OCH$_2$C(O), 4H), 4.75 (d, ArCH$_2$Ar, J = 14.00, 4H), 4.73 (m, CpH, 4H), 4.41-4.37 (m, CpH, 4H), 4.05 (s, CpH, 10H), 3.96 (t, O<u>CH$_2$</u>CH$_2$, J = 7.35 Hz, 4H), 3.50 (d, ArCH$_2$Ar,J = 14.00 Hz, 4H), 2.69 (s, ArCH$_3$, 6H), 1.85 (m, OCH$_2$CH$_2$, 4H), 1.48 (s, C(CH$_3$)$_3$ +CH$_2$CH$_3$, 76H), 0.95 (t, CH2CH3, J = 7.40 Hz, 6H), -2.73 (s, NH, 4H).

HRMS (ESI-TOF-MS) Calculated: [[M+Na+H]$^{2+}$:C$_{196}$H$_{197}$ Fe$_2$O$_8$N$_{12}$Na: 1490.6983 m/z, found 1490.6932 m/z; M+2Na]$^{2+}$: C$_{196}$H$_{196}$Fe$_2$O$_8$N$_{12}$Na$_2$: 1501..6893 m/z, found: 1501.6859 m/z; [M+Na]$^{+}$: C$_{196}$H$_{196}$ Fe$_2$O$_8$N$_{12}$Na: 2980.3893 m/z, found: 2980.4096 m/z.

Summary and Future Work

This thesis presents several new calixarene linked bis-porphyrins as hosts for fullerenes. UV-visible spectroscopic titrations have demonstrated that the bis-porphyrins most suitable for the association of fullerenes are the di-alkylated bis-porphyrins **2.1** and **2.2.** The hydrogen bonding motif present on the narrow rim maintains a level of preorganization within the calixarene scaffold and orientates the porphyrin plane in a geometry most suited for binding fullerenes. These hosts also reveal the importance of CH-π interactions for increasing the association of porphyrins and fullerenes. Hosts **3.9** and **3.10** demonstrate that removal of this hydrogen bonding motif increases the flexibility of the calixarene, so the scaffold can adopt different cone geometries which adversely affect the fullerene binding site. The association constants of these host for fullerenes with have been enhanced by varying the solvent to one in which fullerenes are less soluble.

Several bis-porphyrins with extended linkers have been prepared and display no association with fullerenes. It is believe that the extension of the linkers for these bis-porphyrins results in the porphyrin planes being in the incorrect orientation and that binding of the fullerenes would be impossible. The attachment of a single methylene spacer has been shown to be the most suitable linker for the acceptance of a fullerene guest.

A number of ferrocene functionalized bis-porphyrins have been prepared. Transient absorption spectroscopy of these bis-porphyrin hosts are to be employed to further probe the photophysical processes of the host-guest complexes to determine how the secondary electron donor extends the lifetime of the charge separated state of the radial ion pair.

Future synthetic work will focus on appending other secondary donors such as zinc porphyrins to the wide rim of the calixarene through palladium catalyzed and amide reactions. The attachment of multiple donor chromophores is also of interest for the construction of supramolecular tetrads which can further enhance the lifetime of the photoinduced charge separated state.

References

(1) IEA *Key World Energy Statistics*, 2011.
(2) Oreskes, N. *Science* **2004**, *306*, 1686.
(3) Kamat, P. V. *J. Phys. Chem. C* **2007**, *111*, 2834.
(4) Lewis, L. S.; Nocera, D. G. *PNAS* **2006**, *103*, 15729.
(5) Programme, U. N. D. *World Energy Assessment: Energy and the challange of Sustainablity*, 2003.
(6) El Chaar, L.; lamont, L. A.; El Zein, N. *Renewable and Sustainable Energy Reviews* **2011**, *15*, 2165.
(7) Green, M. A.; Emery, K.; Hishikawa, Y.; Warta, W.; Dunlop, E. D. *Progress in Photovoltaics: Research and Applications* **2012**, *20*, 12.
(8) O'Regan, B.; Gratzel, M. *Nature* **1991**, *353*, 737.
(9) Bai, Y.; Cao, Y.; Zhang, J.; Wang, M.; Li, R.; Wang, P.; Zakeeruddin, S. M.; Gratzel, M. *Nat Mater* **2008**, *7*, 626.
(10) Campbell, W. M.; Jolley, K. W.; Wagner, P.; Wagner, K.; Walsh, P. J.; Gordon, K. C.; Schmidt-Mende, L.; Nazeeruddin, M. K.; Wang, Q.; Graetzel, M.; Officer, D. L. *J. Phys. Chem. C* **2007**, *111*, 11760.
(11) Gregry, R. P. F. *Photosynthesis*; Chapman and Hall: New York, 1989.
(12) Gregry, R. P. F. *Biochemistry of Photosynthesis*; John Wiley and Sons, 1989.
(13) Gust, D.; Moore, T. A. *Adv. Photochem.* **1991**, *16*, 1.
(14) Milgrom, L. R. *The Colours of Life*; Oxford University Press, 1997.
(15) Gouterman, M. *J. Mol. Spectros.* **1961**, *6*, 138.
(16) Gouterman, M.; Wagnière, G. H.; Snyder, L. C. *Journal of Molecular Spectroscopy* **1963**, *11*, 108.
(17) Anderson, H. L. *Chem. Commun.* **1999**, 2323.
(18) Osuka, A.; Morikawa, S.; Maruyama, K.; Hirayama, S.; Minami, T. *Chem. Commun.* **1987**, 359.
(19) Tsue, H.; Higashida, S.; Sakata, Y. *Mem. Inst. Sci. Ind. Res., Osaka Univ.* **1993**, *50*, 55.
(20) Wasielewski, M. R. *Chem. Rev.* **1992**, *92*, 435.
(21) Kroto, H. W.; Heath, J. R.; O'Brien, S. C.; Curl, R. F.; Smalley, R. E. *Nature* **1985**, *318*, 162.
(22) Hirsch, A.; Brettreich, M. In *Fullerenes*; Wiley-VCH Verlag GmbH & Co. KGaA: 2005, p 383.
(23) Hawkins, J. M.; Meyer, A.; Lewis, T. A.; Loren, S.; Hollander, F. J. *Science* **1991**, *252*, 312.
(24) Bürgi, H.-B.; Blanc, E.; Schwarzenbach, D.; Liu, S.; Lu, Y.-j.; Kappes, M. M.; Ibers, J. A. *Angew. Chem., Int. Ed.* **1992**, *31*, 640.
(25) Montellano Lopez, A.; Mateo-Alonso, A.; Prato, M. *J. Mater. Chem.* **2011**, *21*, 1305.
(26) Haddon, R. C. *Science* **1993**, *261*, 1545.
(27) Haddon, R. C.; Brus, L. E.; Raghavachari, K. *Chem. Phys. Lett.* **1986**, *125*, 459.

(28) Hirsch, A. *The chemistry of the fullerenes* New York, 1994.
(29) Echegoyen, L.; Echegoyen, L. E. *Acc. Chem. Res.* **1998**, *31*, 593.
(30) Ohsawa, Y.; Saji, T. *Chem. Commun.* **1992**, 781. (31) Delgado, J. L.; Guldi, D. M.; Martín, N. In *Supramolecular Soft Matter*; John Wiley & Sons, Inc.: 2011, p 429.
(32) Accorsi, G.; Armaroli, N. *J. Phys. Chem. C* **2010**, *114*, 1385.
(33) Liddell, P. A.; Sumida, J. P.; Macpherson, A. N.; Noss, L.; Seely, G. R.; Clark, K. N.; Moore, A. L.; Moore, T. A.; Gust, D. *Photochem. Photobiol.* **1994**, *60*, 537.
(34) Kuciauskas, D.; Lin, S.; Seely, G. R.; Moore, A. L.; Moore, T. A.; Gust, D.; Drovetskaya, T.; Reed, C. A.; Boyd, P. D. W. *J. Phys. Chem.* **1996**, *100*, 15926.
(35) Sun, Y.; Drovetskaya, T.; Bolskar, R. D.; Bau, R.; Boyd, P. D. W.; Reed, C. A. *J. Org. Chem.* **1997**, *62*, 3642.
(36) Fukuzumi, S.; Ohkubo, K.; Imahori, H.; Shao, J.; Ou, Z.; Zheng, G.; Chen, Y.; Pandey, R. K.; Fujitsuka, M.; Ito, O.; Kadish, K. M. *J. Am. Chem. Soc.* **2001**, *123*, 10676.
(37) Bell, T. D. M.; Smith, T. A.; Ghiggino, K. P.; Ranasinghe, M. G.; Shepard, M. J.; Paddon-Row, M. *Chem. Phys. Lett.* **1997**, *268*, 223.
(38) Tamaki, K.; Imahori, H.; Nishimura, Y.; Yamazaki, I.; Shimomura, A.; Okada, T.; Sakata, Y. *Chem. Lett.* **1999**, 227.
(39) Yamada, K.; Imahori, H.; Nishimura, Y.; Yamazaki, I.; Sakata, Y. *Chem. Lett.* **1999**, 895.
(40) Schuster, D. I.; MacMahon, S.; Guldi, D. M.; Echegoyen, L.; Braslavsky, S. E. *Tetrahedron* **2006**, *62*, 1928.
(41) Imahori, H.; Hagiwara, K.; Akiyama, T.; Taniguchi, S.; Okada, T.; Sakata, Y. *Chem. Lett.* **1995**, *24*, 265.
(42) Imahori, H.; Hagiwara, K.; Aoki, M.; Akiyama, T.; Taniguchi, S.; Okada, T.; Shirakawa, M.; Sakata, Y. *J. Am. Chem. Soc.* **1996**, *118*, 11771.
(43) Guldi, D. M.; Luo, C.; Prato, M.; Dietel, E.; Hirsch, A. *Chem. Commun.* **2000**, 373.
(44) Armaroli, N.; Marconi, G.; Echegoyen, L.; Bourgeois, J.-P.; Diederich, F. *Chem. Eur. J.* **2000**, *6*, 1629.
(45) Guldi, D. M.; Hirsch, A.; Scheloske, M.; Dietel, E.; Troisi, A.; Zerbetto, F.; Prato, M. *Chem. Eur. J.* **2003**, *9*, 4968.
(46) Schuster, D. I. *Carbon* **2000**, *38*, 1607.
(47) Schuster, D. I.; Cheng, P.; Jarowski, P. D.; Guldi, D. M.; Luo, C.; Echegoyen, L.; Pyo, S.; Holzwarth, A. R.; Braslavsky, S. E.; Williams, R. M.; Klihm, G. *J. Am. Chem. Soc.* **2004**, *126*, 7257.
(48) Marcus, R. A.; Sutin, N. *Biochim. Biophys. Acta* **1985**, *811*, 265.
(49) Marcus, R. A. *Angew. Chem., Int. Ed.* **1993**, *32*, 1111.
(50) Hiroshi, I.; Kiyoshi, H.; Tsuyoshi, A.; Masanori, A.; Seiji, T.; Tadashi, O.; Masahiro, S.; Yoshiteru, S. *Chem. Phys. Lett.* **1996**, *263*, 545.
(51) Guldi, D. M. *Chem. Commun* **2000**, 321.
(52) Imahori, H.; Tkachenko, N. V.; Vehmanen, V.; Tamaki, K.; Lemmetyinen, H.; Sakata, Y.; Fukuzumi, S. *J. Phys. Chem. A* **2001**, *105*, 1750.
(53) Imahori, H.; Mori, Y.; Matano, Y. **.** *J. Photochem. Photobiol. C: Photochem. Rev.* **2003**, *4*, 51.

(54) Akasaka, T.; Nagase, S. *Endofullerenes: a new family of carbon clusters*; Kluwer Academic Publishers: Dordrecht, The Netherlands, 2002.
(55) Chaur, M. N.; Melin, F.; Ortiz, A. L.; Echegoyen, L. *Angew. Chem., Int. Ed.* **2009**, *48*, 7514.
(56) Stevenson, S.; Rice, G.; Glass, T.; Harich, K.; Cromer, F.; Jordan, M. R.; Craft, J.; Hadju, E.; Bible, R.; Olmstead, M. M.; Maitra, K.; Fisher, A. J.; Balch, A. L.; Dorn, H. C. *Nature* **1999**, *401*, 55.
(57) Ling, Y.; Stevenson, S.; Zhang, Y. *Chem. Phys. Lett.* **2011**, *508*, 121.
(58) Cardona, C. M.; Elliott, B.; Echegoyen, L. *J. Am. Chem. Soc.* **2006**, *128*, 6480.
(59) Lu, X.; Akasaka, T.; Nagase, S. *Chem. Commun.* **2011**, *47*, 5942.
(60) Ross, R. B.; Cardona, C. M.; Guldi, D. M.; Sankaranarayanan, S. G.; Reese, M. O.; Kopidakis, N.; Peet, J.; Walker, B.; Bazan, G. C.; Van, K. E.; Holloway, B. C.; Drees, M. *Nat. Mater.* **2009**, *8*, 208.
(61) Liedtke, M.; Sperlich, A.; Kraus, H.; Baumann, A.; Deibel, C.; Wirix, M. J. M.; Loos, J.; Cardona, C. M.; Dyakonov, V. *J. Am. Chem. Soc.* **2011**, *133*, 9088.
(62) Kooistra, F. B.; Knol, J.; Kastenberg, F.; Popescu, L. M.; Verhees, W. J. H.; Kroon, J. M.; Hummelen, J. C. *Organic Letters* **2007**, *9*, 551.
(63) Rodriguez-Fortea, A.; Balch, A. L.; Poblet, J. M. *Chem. Soc. Rev.* **2011**, *40*, 3551.
(64) Feng L.; Gayathri Radhakrishnan, S.; Mizorogi, N.; Slanina, Z.; Nikawa, H.; Tsuchiya, T.; Akasaka, T.; Nagase, S.;Martin,, N.; Guldi, D. M. *J. Am. Chem. Soc.* **2011**, null.
(65) Imahori, H.; Fukuzumi, S. *Adv. Funct. Mater.* **2004**, *14*, 525.
(66) Imahori, H.; Tamaki, K.; Yamada, H.; Yamada, K.; Sakata, Y.; Nishimura, Y.; Yamazaki, I.; Fujitsuka, M.; Ito, O. *Carbon* **2000**, *38*, 1599.
(67) Imahori, H.; Guldi, D. M.; Tamaki, K.; Yoshida, Y.; Luo, C.; Sakata, Y.; Fukuzumi, S. *J. Am. Chem. Soc.* **2001**, *123*, 6617.
(68) Lee, S.-H.; Larsen, A. G.; Ohkubo, K.; Cai, Z.-L.; Reimers, J. R.; Fukuzumi, S.; Crossley, M. J. *Chemical Science* **2012**, *3*.
(69) Li, Y.; Gan, Z.; Wang, N.; He, X.; Li, Y.; Wang, S.; Liu, H.; Araki, Y.; Ito, O.; Zhu, D. *Tetrahedron* **2006**, *62*, 4285.
(70) Fujitsuka, M.; Ito, O.; Imahori, H.; Yamada, K.; Yamada, H.; Sakata, Y. *Chem. Lett.* **1999**, 721.
(71) Curiel, D.; Ohkubo, K.; Reimers, J. R.; Fukuzumi, S.; Crossley, M. J. *Phys. Chem. Chem. Phys.* **2007**, *9*, 5260.
(72) Luo, C.; Guldi, D. M.; Imahori, H.; Tamaki, K.; Sakata, Y. *J. Am. Chem. Soc.* **2000**, *122*, 6535.
(73) Liddell, P. A.; Sumida, J. P.; Macpherson, A. N.; Noss, L.; Seely, G. R.; Clark, K. N.; Moore, A. L.; Moore, T. A.; Gust, D**.** *J. Photochem. Photobiol. B: Biol.* **1994**, *60*, 537.
(74) Liddell, P. A.; Kuciauskas, D.; Sumida, J. P.; Nash, B.; Nguyen, D.; Moore, A. L.; Moore, T. A.; Gust, D. *J. Am. Chem. Soc.* **1997**, *119*, 1400.
(75) Liu, J.-Y.; El-Khouly, M. E.; Fukuzumi, S.; Ng, D. K. P. *Chem. Eur. J.* **2011**, *17*, 1605.
(76) D'Souza, F.; Gadde, S.; Islam, D. M. S.; Wijesinghe, C. A.; Schumacher, A. L.; Zandler, M. E.; Araki, Y.; Ito, O. *J. Phys. Chem. A* **2007**, *111*, 8552.

(77) Imahori, H.; Guldi, D. M.; Koichi, T.; Yoshida, Y.; Lou, C.; Sakata, Y.; Fukuzumi, S. *J. Am. Chem. Soc.* **2001**, *123*, 6617.
(78) Imahori, H.; Tamaki, K.; Guldi, D. M.; Luo, C.; Fujitsuka, M.; Ito, O.; Sakata, Y.; Fukuzumi, S. *J. Am. Chem. Soc.* **2001**, *123*, 2607.
(79) Imahori, H.; Norieda, H.; Yamada, H.; Nishimura, Y.; Yamazaki, I.; Sakata, Y.; Fukuzumi, S. *J. Am. Chem. Soc.* **2001**, *123*, 100.
(80) Imahori, H.; Sekiguchi, Y.; Kashiwagi, Y.; Sato, T.; Araki, Y.; Ito, O.; Yamada, H.; Fukuzumi, S. *Chem. Eur. J.* **2004**, *10*, 3184. (81) Steed, J. W.; Atwood, J. L. *Supramol.Chem.*; Wiley, 2000.
(82) Steed, J. W.; Turner, D. R.; Wallace, K. J. *Core Concepts in Supramolecular Chemsitry and Nanochemistry*; Wiley, 2007.
(83) Sessler, J. L.; Jayawickramarajah, J.; Gouloumis, A.; Torres, T.; Guldi, D. M.; Maldonado, S.; Stevenson, K. J. *Chem. Commun.* **2005**, 1892.
(84) D'Souza, F.; Chitta, R.; Gadde, S.; Zandler, M. E.; McCarty, A. L.; Sandanayaka, A. S. D.; Araki, Y.; Ito, O. *Chem. Eur. J.* **2005**, *11*, 4416.
(85) Solladié, N.; Walther, M. E.; Herschbach, H.; Leize, E.; Dorsselaer, A. V.; Duarte, T. M. F.; Nierengarten, J.-F. *Tetrahedron* **2006**, *62*, 1979.
(86) Da Ros, T.; Prato, M.; Guldi, D.; Alessio, E.; Ruzzi, M.; Pasimeni, L. *Chem. Commun.* **1999**, 635.
(87) D'Souza, F.; Rath, N. P.; Deviprasad, G. R.; Zandler, M. E. *Chem. Commun.* **2001**, 267.
(88) D'Souza, F.; Deviprasad, G. R.; Zandler, M. E.; Hoang, V. T.; Klykov, A.; VanStipdonk, M.; Perera, A.; El-Khouly, M. E.; Fujitsuka, M.; Ito, O. *J. Phys Chem. A* **2002**, *106*, 3243.
(89) Da Ros, T.; Prato, M.; Carano, M.; Ceroni, P.; Paolucci, F.; Roffia, S.; Valli, L.; Guldi, D. *J. Organomet. Chem.* **2000**, *599*, 62.
(90) Da Ros, T.; Prato, M.; Guldi, D. M.; Ruzzi, M.; Pasimeni, L. *Chem.--Eur. J.* **2001**, *7*, 816.
(91) D'Souza, F.; Smith, P. M.; Zandler, M. E.; McCarty, A. L.; Itou, M.; Araki, Y.; Ito, O. *J. Am. Chem. Soc.* **2004**, *126*, 7898.
(92) D'Souza, F.; Smith, P. M.; Gadde, S.; McCarty, A. L.; Kullman, M. J.; Zandler, M. E.; Itou, M.; Araki, Y.; Ito, O. *J. Phys. Chem. B* **2004**, *108*, 11333.
(93) Boyd, P. D. W.; Reed, C. A. *Acc. Chem. Res.* **2004**, *38*, 235.
(94) Boyd, P. D. W.; Hodgson, M. C.; Rickard, C. E. F.; Oliver, A. G.; Chaker, L.; Brothers, P. J.; Bolskar, R. D.; Tham, F. S.; Reed, C. A. *J. Am. Chem. Soc.* **1999**, *121*, 10487.
(95) Olmstead, M. M.; Costa, D. A.; Maitra, K.; Noll, B. C.; Phillips, S. L.; Van Calcar, P. M.; Balch, A. L. *J. Am. Chem. Soc.* **1999**, *121*, 7090.
(96) Tashiro, K.; Aida, T.; Zheng, J.; Kinbara, K.; Saigo, K.; Sakamoto, S.; Yamaguchi, K. *J. Am. Chem. Soc.* **1999**, *121*.
(97) Zheng, J.-Y.; Tashiro, K.; Hirabayashi, Y.; Kinbara, K.; Saigo, K.; Aida, T.; Sakamoto, S.; Yamaguchi, K. *Angew. Chem.* **2001**, *113*, 1909.
(98) Hernandez L. P.; -Eguia L Escudero- Adan, E. C.; Pinzon, J. R.; Echegoyen, L.; Ballester, P. *J. Org. Chem.***2011**, *76*, 3258.
(99) Nobukuni, H.; Shimazaki, Y.; Tani, F.; Naruta, Y. *Angewandte Chemie International Edition* **2007**, *46*, 8975.

(100) Shelnutt, J. A. *In The Porphyrin Handbook*; Academic:: New York, 2000; Vol. 7.
(101) Nobukuni, H.; Shimazaki, Y.; Uno, H.; Naruta, Y.; Ohkubo, K.; Kojima, T.; Fukuzumi, S.; Seki, S.; Sakai, H.; Hasobe, T.; Tani, F. *Chem. Eur. J.* **2010**, *16*, 11611.
(102) Sun, D.; Tham, F. S.; Reed, C. A.; Chalker, L.; Boyd, P. D. W. *J. Am. Chem. Soc.* **2002**, *124*, 6604.
(103) Gutsche, C. D. *Calixarenes*; The Royal Society of Chemistry, 1989.
(104) Gutsche, C. D. *Calixarenes Revisited*; The Royal Society of Chemistry, 1998.
(105) Gutsche, C. D.; Dhawan, B.; No, K. H.; Muthukrishnan, R. *J. Am. Chem. Soc.* **1981**, *103*, 3782.
(106) Beer, P.; Hesek, D.; Nam, K.; Drew, M. G. B. *Organometallics* **1999**, *18*, 3933.
(107) Shaabani, B.; Shaghaghi, Z. *Tetrahedron* **2010**, *66*, 3259.
(108) Gutsche, C. D.; See, K. A.; Fronczek, F. R.; Watson, W. H.; Kashyap, R. P. *J. Org. Chem.* **1991**, *56*, 7256.
(109) Cooper, J. B.; Drew, M. G. B.; Beer, P. D. *J. Chem. Soc., Dalton Trans.* **2000**, 2721.
(110) Creaven, B. S.; Gernon, T. L.; McGinley, J.; Moore, A.-M.; Toftlund, H. *Tetrahedron* **2006**, *62*, 9066.
(111) Gutsche, C. D.; Pagoria, P. F. *J. Org. Chem.* **1985**, *50*, 5795.
(112) Sliwa;, W.; Deska, M. *ARKIVOC* **2011**, 496
(113) Ikeda, A.; Shinkai, S. *Chem. Rev.* **1997**, *97*, 1713.
(114) Davis, F.; Higson, S. In *Macrocycles*; John Wiley & Sons, Ltd: 2011, p 77.
(115) Dudic, M.; Lhoták, P.; Stibor, I.; Dvoráková, H. Lang K Proškova, P. *Org. Lett* **2003**, *5*, 149.
(116) Dudic, M.; Lhoták, P.; Stibor, I.; Petrícková, H.; Lang, K. *New. J. Chem.* **2004**, *28*, 85.
(117) Arimura, T.; Nishioka, T.; Suga, Y.; Murata, S.; Tachiya, M. *Mol. Cryst. Liq. Cryst.* **2002**, *379*, 413.
(118) Dudic, M.; Lhoták, P.; Stibor, I.; Dvoráková, H.; Lang, K. *Tetrahedron* **2002**, *58*, 5475.
(119) Dudic, M.; Lhotak, P.; Stibor, I.; Petrickova, H.; Lang, K. *New J. Chem.* **2004**, *28*, 85.
(120) Dudic, M.; Lhoták, P.; Stibor, I.; Dvoráková, H.; Lang, K. *Tetrahedron* **2002**, *58*, 5475.
(121) Hosseini, A., University of Auckland, 2006.
(122) Hosseini, A.; Taylor, S.; Accorsi, G.; Armaroli, N.; Reed, C. A.; Boyd, P. D. W. *J. Am. Chem. Soc.* **2006**, *128*, 15903.
(123) Hosseini, A.; Hodgson, M. C.; Tham, F. S.; Reed, C. A.; Boyd, P. D. W. *Cryst. Growth Des.* **2005**, *6*, 397.
(124) Ishii, T.; Kanehama, R.; Aizawa, N.; Yamashita, M.; Matsuzaka, H.; Sugiura, K.-i.; Miyasaka, H.; Kodama, T.; Kikuchi, K.; Ikemoto, I.; Tanaka, H.; Marumoto, K.; Kuroda, S.-I. *Journal of the Chemical Society, Dalton Transactions* **2001**, 2975.
(125) van Paauwe, J. D., The University of Auckland, 2005.
(126) Jung, S.; van, P. J. D.; Boyd, P. D. W.; Shin, S. K. *Phys. Chem. Chem. Phys.* **2011**, *13*, 20248.
(127) Grimm, B.; Schornbaum, J.; Cardona, C. M.; van Paauwe, J. D.; Boyd, P. D. W.; Guldi, D. M. *Chem. Sci.* **2011**.
(128) Hosseini, A. PhD, The University of Auckland, 2006.

(129) Hosseini, A.; Taylor, S.; Accoursi, G.; Armaroli, N.; Reed, C. A.; Boyd, P. D. W. *J. Am. C Chem. Soc.* **2006**, *128*, 15903.
(130) Adler, A. D.; Longo, F. R.; Finarelli, J. D.; Goldmacher, J.; Assour, J.; Korsakoff, L. *J. Org. Chem.* **1967**, *32*, 476.
(131) Lindsey, J. S.; Schreiman, I. C.; Hsu, H. C.; Kearney, P. C.; Marguerettaz, A. M. *J. Org. Chem.* **1987**, *52*, 827.
(132) Gryko, D. T.; Tasior, M. *Tetrahedron Lett.* **2003**, *44*, 3317.
(133) Paul-Roth, C. O.; Williams, J. A. G.; Letessier, J.; Simonneaux, G. *Tetrahedron Lett.* **2007**, *48*, 4317.
(134) Rao, P. D.; Dhanalekshmi, S.; Littler, B. J.; Lindsey, J. S. *J. Org. Chem.* **2000**, *65*, 7323.
(135) Vaz, B.; Alvarez, R.; Nieto, M.; Paniello, A. I.; de Lera, A. R. *Tetrahedron Lett.* **2001**, *42*, 7409. 286
(136) Stürmer, R.; Negishi, E.; de Meijere, A. *Adv. Synth. Catal.* **2003**, *345*, 1032.
(137) Sergeeva, N. N.; Senge, M. O.; Ryan, A. In *Handbook of Porphyrin Science Vol. III*; Kadish, K. M., Smith, K. M., Guilard, R., Eds.; World Scientific/Imperial College Press: 2010, p 325.
(138) Miyaura, N.; Suzuki, A. *Chem. Rev.* **1995**, *95*, 2457.
(139) Senge, M. O.; Fazekas, M.; Pintea, M.; Zawadzka, M.; Blau, W. J. *Eur. J. Inorg. Chem.* **2011**, *2011*, 5797.
(140) Shinokubo, H.; Osuka, A. *Chem. Commun.* **2009**, 1011.
(141) Sonogashira, K. *Metal-catalyzed Cross-coupling Reactions*; Wiley-VCH, 1998.
(142) Fazekas, M.; Pintea, M.; Senge, M. O.; Zawadzka, M. *Tetrahedron Lett.* **2008**, *49*, 2236.
(143) Kozaki, M.; Akita, K.; Suzuki, S.; Okada, K. *Org. Lett.* **2007**, *9*, 3315.
(144) Kozaki, M.; Tujimura, H.; Suzuki, S.; Okada, K. *Tetrahedron Lett.* **2008**, *49*, 2931.
(145) Poon, K.-W.; Liu, W.; Chan, P.-K.; Yang, Q.; Chan, T. W. D.; Mak, T. C. W.; Ng, D. K. P. *J. Org. Chem.* **2001**, *66*, 1553.
(146) Locos, O. B.; Arnold, D. P. *Org. Biomol. Chem.* **2006**, *004*, 902.
(147) Odobel, F.; Suzenet, F.; Blart, E.; Quintard, J.-P. *Org. Lett.* **1999**, *2*, 131.
(148) Sergeeva N. N.; Scala A.; Bakar M. A.; O'Riordan, G.; O'Brien, J. Grassi, G.; Senge, M. O. *J. Org.Chem.* **2009**, *74*, 7140.
(149) Liu, C.; Shen, D.-M.; Chen, Q.-Y. *J. Org. Chem.* **2007**, *72*, 2732.
(150) Dapprich, S.; Komáromi, I.; Byun, K. S.; Morokuma, K.; Frisch, M. J. *Journal of Molecular Structure: THEOCHEM* **1999**, *461-462*, 1.
(151) Vreven, T.; Byun, K. S.; Komáromi, I.; Dapprich, S.; Montgomery, J. A.; Morokuma, K.; Frisch, M. J. *J. Chem. Theory Compu.* **2006**, *2*, 815.
(152) Parr, R. G.; Yang, W. *Density-Functional Theory of Atoms and Molecules*; Oxford University Press., 1989.
(153) Becke, A. D. *J. Chem. Phys.* **1993**, *98*, 5648.
(154) Rassolov, V. A.; Pople, J. A. *J. Chem. Phys.* **1998**, *109*, 1223.
(155) Rassolov, V. A.; Ratner, M. A.; Pople, J. A.; Redfern, P. C.; Curtiss, L. A. *J.Comput. Chem.* **2001**, *22*, 976.

(156) Atkins, P. W.; Friedman, R. *Molecular Quantum Mechanics 4th Ed.*; Oxford University Press, 2005.
(157) Rappe, A. K.; Casewit, C. J. *Molecular Mechanics Across Chemistry*; University Science Books,: Sausalito, 1997.
(158) Rappe, A. K.; Casewit, C. J.; Colwell, K. S.; Goddard, W. A.; Skiff, W. M. *J. Am. Chem. Soc.* **1992**, *114*, 10024.
(159) Laha, J. K.; Dhanalekshmi, S.; Taniguchi, M.; Ambroise, A.; Lindsey, J. S. *Org. Process Res. Dev.* **2003**, *7*, 799.
(160) Clezy, P.; Smythe, G. *Aust. J.Chem.* **1969**, *22*, 239.
(161) Littler, B. J.; Miller, M. A.; Hung, C.-H.; Wagner, R. W.; O'Shea, D. F.; Boyle, P. D.; Lindsey, J. S. *J. Org. Chem.* **1999**, *64*, 1391.
(162) Temelli, B.; Unaleroglu, C. *Tetrahedron* **2006**, *62*, 10130.
(163) Bonifazi, D.; Accorsi, G.; Armaroli, N.; Song, F.; Palkar, A.; Echegoyen, L.; Scholl, M.; Seiler, P.; Jaun, B.; Diederich, F. *Helv. Chim. Acta* **2005**, *88*, 1839.
(164) Arnold, D. P.; Bott, R. C.; Eldridge, H.; Elms, F. M.; Smith, G.; Zojaji, M. *Aus. J. Chem.* **1997**, *50*, 495. 287
(165) Lyons, D. M.; Mohanraj, J.; Accorsi, G.; Armaroli, N.; Boyd, P. D. W. *New J. Chem.* **2011**, *35*, 632.
(166) Cheng, F.; Zhang, S.; Adronov, A.; Echegoyen, L.; Diederich, F. *Chem. Eur. J.* **2006**, *12*, 6062.
(167) Collins, E. M.; McKervey, M. A.; Madigan, E.; Moran, M. B.; Owens, M.; Ferguson, G.; Harris, S. J. *J. Chem. Soc., Perkin Trans. 1* **1991**, 3137
(168) Behloul, C.; Guijarro, D.; Yus, M. *Synthesis* **2004**, 1274.
(169) Fery-Forgues, S.; Le Bris, M. T.; Guette, J. P.; Valeur, B. *J. Phys. Chem.* **1988**, *92*, 6233.
(170) Wang, Y.-B.; Lin, Z. *J. Am. Chem. Soc.* **2003**, *125*, 6072.
(171) Boyd, P. D. W.; Reed, C. A. *Acc. Chem. Res.* **2005**, *38*, 235.
(172) Gaussian 09, R. A., Frisch, M. J.; Trucks, G. W.; Schlegel, H. B.; Scuseria, G. E.; Robb, M. A.; Cheeseman, J. R.; Scalmani, G.; Barone, V.; Mennucci, B.; Petersson, G. A.; Nakatsuji, H.; Caricato, M.; Li, X.; Hratchian, H. P.; Izmaylov, A. F.; Bloino, J.; Zheng, G.; Sonnenberg, J. L.; Hada, M.; Ehara, M.; Toyota, K.; Fukuda, R.; Hasegawa, J.; Ishida, M.; Nakajima, T.; Honda, Y.; Kitao, O.; Nakai, H.; Vreven, T.; Montgomery, Jr., J. A.; Peralta, J. E.; Ogliaro, F.; Bearpark, M.; Heyd, J. J.; Brothers, E.; Kudin, K. N.; Staroverov, V. N.; Kobayashi, R.; Normand, J.; Raghavachari, K.; Rendell, A.; Burant, J. C.; Iyengar, S. S.; Tomasi, J.; Cossi, M.; Rega, N.; Millam, N. J.; Klene, M.; Knox, J. E.; Cross, J. B.; Bakken, V.; Adamo, C.; Jaramillo, J.; Gomperts, R.; Stratmann, R. E.; Yazyev, O.; Austin, A. J.; Cammi, R.; Pomelli, C.; Ochterski, J. W.; Martin, R. L.; Morokuma, K.; Zakrzewski, V. G.; Voth, G. A.; Salvador, P.; Dannenberg, J. J.; Dapprich, S.; Daniels, A. D.; Farkas, Ö.; Foresman, J. B.; Ortiz, J. V.; Cioslowski, J.; Fox, D. J. Gaussian, Inc., Wallingford CT, 2009.
(173) SHELX97 [Includes SHELXS97, S., CIFTAB (and SHELXA?)] - Programs for Crystal Structure Analysis (Release 97-2). Sheldrick, G.M., Institüt für Anorganische Chemie der Universität, Tammanstrasse 4, D-3400 Göttingen, Germany, 1998. .

(174) Sheldrick, G. *Acta Cryst. Section A* **2008**, *64*, 112.
(175) PLATON - (a) Spek, A. L. A. C. A., C34. (b) Spek, A. L. (1998) PLATON, A Multipurpose Crystallographic Tool, Utrecht University, Utrecht, The Netherlands.
(176) van der Sluis, P.; Spek, A. L. *Acta Cryst. Section A* **1990**, *46*, 194.
(177) Bitter, I.; Grün, A.; Tóth, G.; Balázs, B.; Horváth, G.; Tõke, L. *Tetrahedron* **1998**, *54*, 3857.
(178) Heigel, G. A.; Gilley, C. B. *Synthetic Commun* **2003**, *33*, 2003.
(179) Tashiro, K.; Aida, T.; Zheng, J.-Y.; Kinbara, K.; Saigo, K.; Sakamoto, S.; Yamaguchi, K. *J. Am. Chem. Soc.* **1999**, *121*, 9477.
(180) Barbour, J.; Atwood, L., *Chem. Commun.* **1998**, 1901.
(181) Kás, M.; Lang, K.; Stibor, I.; Lhoták, P. *Tetrahedron Lett.* **2007**, *48*, 477.
(182) Park, C.; Chun, S.; Bartsch, R. *J. Inclusion Phenom. Macrocyclic Chem.***2010**, *66*, 95.
(183) Talanova, G. G.; Talanov, V. S.; Gorbunova, M. G.; Hwang, H.-S.; Bartsch, R. A. *J. Chem. Soc., Perkin Trans. 2* **2002**.
(184) Talanov, V. S.; Bartsch, R. A. *J. Chem. Soc., Perkin Trans. 1* **1999**, 1957.
(185) Boyd, P. D. W., Personal Communication.
(186) Schazmann, B.; O'Malley, S.; Nolan, K.; Diamond, D. *Supramol. Chem.* **2006**, *18*, 515.
(187) Szemes, F.; Hesek, D.; Chen, Z.; Dent, S. W.; Drew, M. G. B.; Goulden, A. J.; Graydon, A. R.; Grieve, A.; Mortimer, R. J.; Wear, T.; Weightman, J. S.; Beer, P. D. *Inorg. Chem.* **1996**, *35*, 5868.
(188) Luo, C.; Guldi, D. M.; Imahori, H.; Tamaki, K.; Sakata, Y. *J. Am. Chem. Soc.* **2000**, *122*, 6535.
(189) Morosini, V.; Frochot, C.; Barberi-Heyob, M.; Schneider, R. *Tetrahedron Lett.* **2006**, *47*, 8745.
(190) Zhu, J.; Lin, J.-B.; Xu, Y.-X.; Jiang, X.-K.; Li, Z.-T. *Tetrahedron* **2006**, *62*, 11933.
(191) Benoiton, N. L.; Begley, T. P. In *Wiley Encyclopedia of Chemical Biology*; John Wiley & Sons, Inc.: 2007.
(192) Sourav, S.; Erik, J.; Amar, H. F.; Hsian-Rong, T.; Jeffrey, I. Z.; Stoddart, J. F. *Chemistry - A European Journal* **2005**, *11*, 6846.
(193) Harvey, P. D. *Coord. Chem. Rev.* **2002**, *233–234*, 289.
(194) Tomapatanaget, B.; Tuntulani, T.; Chailapakul, O. *Org. Lett.* **2003**, *5*, 1539.
(195) Kahn, G. S., The University of Auckland, 2010.
(196) Beck, M. T.; Mándi, G. *Fullerene Science and Technology* **1997**, *5*, 291.
(197) Zhang, H. Y.; Wang, H.; Liu, Y. *ARKIVOC* **2003**, 92.
(198) Loeber, C.; Matt, D.; Briard, P.; Grandjean, D. *J. Chem. Soc., Dalton Trans.* **1996**, 513.
(199) Fukuzumi, S. *Eur. J. Inorg. Chem.* **2008**, *2008*, 1351.
(200) Imahori, H.; Umeyama, T.; Ito, S. *Acc. Chem. Res.* **2009**, *42*, 1809.
(201) Nelson, N.; Yocum, C. F. *Annual Review of Plant Biology* **2006**, *57*, 521.
(202) D'Souza, F.; Gadde, S.; Schumacher, A. L.; Zandler, M. E.; Sandanayaka, A. S. D.; Araki, Y.; Ito, O. *J. Phys. Chem. C* **2007**, *111*, 11123.
(203) Ventura, B.; Flamigni, L.; Marconi, G.; Lodato, F.; Officer, D. L. *New J. Chem.* **2008**, *32*.
(204) Araki, Y.; Yasumura, Y.; Ito, O. *J. Phys. Chem. B* **2005**, *109*, 9843.

(205) Kajigaeshi, S.; Kakinami, T.; Yamasaki, H.; Fujisaki, S.; Kondo, M.; Okamoto, T. *Chemistry Letters* **1987**, *16* 2109.
(206) Klenke, B.; Friedrichsen, W. *J. Chem. Soc., Perkin Trans. 1* **1998**, 3377
(207) Gunther, H.; Ma Teresa, M.; Pilar, P.; Hassan, A.-S.; Abdelmeneim, E.-D.; David , W. T.; Julie, C.; Paris , E. G.; Ayele, T.; Inge, A.; Koen, C. *Chem. Eur. J* **2007**, *13*, 7753.
(208) Ambroise, A.; Wagner, R. W.; Rao, P. D.; Riggs, J. A.; Hascoat, P.; Diers, J. R.; Seth, J.; Lammi, R. K.; Bocian, D. F.; Holten, D.; Lindsey, J. S. *Chem. Mater.* **2001**, *13*, 1023.
(209) Van Loon, J. D.; Arduini, A.; Coppi, L.; Verboom, W.; Pochini, A.; Ungaro, R.; Harkema, S.; Reinhoudt, D. N. *J. Org. Chem* **1990**, *55*, 5639.
(210) Guillon, J.; Leger, J.-M.; Dapremont, C.; Denis, L. A.; Sonnet, P.; Massip, S.; Jarry, C. *Supramol. Chem.* **2004**, *16*, 319.
(211) Smukste, I.; House, B. E.; Smithrud, D. B. *J. Org. Chem.* **2003**, *68*, 2559.
(212) Sun, X. H.; Chan, C. S.; Wong, M. S.; Wong, W. Y. *Tetrahedron* **2006**, *62*, 7846.
(213) Tongraung, P.; Chantarasiri, N.; Tuntulani, T. *Tetrahedron Lett.* **2003**, *44*, 29.
(214) Liu, J.; Tonigold, M.; Bredenkötter, B.; Schröder, T.; Mattay, J.; Volkmer, D. *Tetrahedron Lett.* **2009**, *50*, 1303.
(215) Bozak, R. E. In *Advances in Photochemistry*; John Wiley & Sons, Inc.: 2007, p 227.
(216) Beer, P. D.; Gale, P. A.; Hesek, D. *Tetrahedron Lett.* **1995**, *36*, 767.
(217) Gale, P. A.; Chen, Z.; Drew, M. G. B.; Heath, J. A.; Beer, P. D. *Polyhedron* **1998**, *17*, 405.
(218) Beer, P. D.; Hesek, D.; Kingston, J. E.; Smith, D. K.; Stokes, S. E.; Drew, M. G. B. *Organometallics* **1995**, *14*, 3288.
(219) Beer, P. D.; Drew, M. G. B.; Hesek, D.; Shade, M.; Szemes, F. *Chem. Commun.* **1996**, 2161.
(220) Tomapatanaget, B.; Tuntulani, T. *Tetrahedron Lett.* **2001**, *42*, 8105.
(221) Verboom, W.; Durie, A.; Egberink, R. J. M.; Asfari, Z.; Reinhoudt, D. N. *J. Org. Chem.* **2002**, *57*, 1313.
(222) Dozol, H.; Asfari, Z.; Vicens, J.; Thuéry, P.; Nierlich, M.; Dozol, J.-F. *Tetrahedron Lett.* **2001**, *42*, 8285.
(223) Hudecek, O.; Curinova, P.; Budka, J.; Lhoták, P. *Tetrahedron* **2011**, *67*, 5213.
(224) Yang, G.; Jin, C.; Li, Y.; Hong, J.; Miao, R.; Zhao, C.; Guo, Z.; Zhu, L. *J. Inclusion Phenom. Macrocyclic Chem.* **2005**, *52*, 119.
(225) Arduini, A.; Secchi, A.; Pochini, A. *J. Org. Chem.* **2000**, *65*, 9085.
(226) Shi, D.; Zhao, H.; Wang, X.; Yao, C.; Zhou, L. *Synth. Commun.* **2002**, *32*, 3311.
(227) Savage, D.; Gallagher, J. F.; Ida, Y.; Kenny, P. T. M. *Inorg. Chem. Commun.* **2002**, *5*, 1034